Enhanced topical delivery of chlorhexidine digluconate for improved skin antisepsis

Melissa Kirkby

A thesis submitted to Keele University for the degree of

Doctor of Philosophy

June 2020

Abstract

Chlorhexidine digluconate (CHG) is a cationic bisbiguanide that has been used extensively for the past half century as a topical antiseptic, due to its ability to effectively kill surface bacteria with minimal reports of resistance. However, bacteria are understood to reside in deeper skin layers, skin furrows and follicular appendages that harbour the ability to cause skin and soft tissue infections (SSTIs), particularly where the *stratum corneum* barrier is compromised, such as at the site of a surgical incision. CHG permeates poorly into human skin due to its physicochemical properties, which lie outside of the "ideal" limits for topical and transdermal drug delivery and therefore it is unlikely to be able to target bacteria in deeper skin layers without permeation enhancement.

The purpose of this thesis was to enhance the depth permeation of CHG into skin for enhanced topical skin antisepsis. Both chemical and physical methods of permeation enhancement were explored. Previously it had been found that a topical skin pre-treatment with a G3 PAMAM-NH_2 dendrimer significantly enhanced the permeation of CHG *in vitro*. This thesis began by creating a physically stable and clinically acceptable topical gel formulation that co-formulated CHG and a G3 PAMAM-NH_2 dendrimer together in a one-step application for practicality purposes. This co-formulation (containing 4% CHG and 1 mM G3 PAMAM-NH_2) was found to significantly enhance the depth permeation of CHG within porcine skin compared to the commercial benchmark Hibiscrub® (contains 4% w/v CHG; $p < 0.05$). Permeation enhancement was initially characterised using Franz-type diffusion cell and tape stripping studies, considered the "gold standard" technique for quantifying dermal drug penetration. The systematic creation, characterisation and successful co-formulation of the drug and dendrimer within a topical gel formulation are novel developments.

The potential disadvantages of the tape stripping technique utilised in Chapter 3 were explored and the results from the tape stripping studies were confirmed by repeating *in vitro* studies and visualising treated skin samples using Time-of-Flight Secondary Ion Mass Spectrometry (ToF-SIMS) in Chapter 4. This method has been used to image topical drug distribution and co-localisation of the drug with endogenous skin components. The method was developed further by transforming the data semi-quantitatively, which reduced the subjectivity of image interpretation. The study found that CHG, when combined with a G3 PAMAM-NH_2 dendrimer was able to permeate past the superficial *stratum corneum* skin barrier and was able to reside within deeper skin layers without significant permeation through full thickness porcine skin.

The mechanism of action of the PAMAM dendrimer mediated enhancement of CHG within the co-formulation was explored. Results from this study indicated that occlusive effects and a reduction in surface tension were the likely mechanistic contributions of the G3 PAMAM-NH_2 dendrimer. It appears as though the PAMAM dendrimer exerted its enhancement effects within the co-formulation without altering the *stratum corneum* barrier. This may correlate to a lack of skin irritation, which is advantageous when considering irritation has prevented the commercial use of many chemical permeation enhancers.

A physical method of CHG permeation enhancement was explored for the first time. A solid microneedle 10 second pre-treatment (750 µm, 36 needle array) was found to enhance the depth permeation of CHG within porcine skin. This permeation enhancement effect was considered to be equivalent to the enhancement effect provided by the 4% CHG-1 mM PAMAM co-formulation regarding CHG depth permeation, however equivalence did not align when considering homogeneity of drug distribution across the skin.

In conclusion, the permeation of CHG was successfully enhanced using both a chemical and physical method of permeation enhancement. The gel formulation improved CHG delivery

compared to the commercial Hibiscrub® solution, even without the addition of the chemical enhancer, indicating the significance of vehicle effects on the ability to enhance drug permeation into skin. This enhancement effect was statistically significant with the addition of the PAMAM dendrimer at clinically relevant concentrations ($p < 0.05$). The results from this thesis suggest that a reduction in surface tension and an increase in occlusion were predominant in CHG mediated permeation enhancement, which has significantly positive implications when considering the clinical acceptability of this formulation compared to chemical permeation enhancers used in the past, which exhibit unacceptable levels of skin irritation.

Acknowledgements

This experience would not have been possible without the support of those surrounding me during this journey. I would firstly like to thank my supervisors Dr. Gary Moss and Prof. Stephen Chapman, for their assistance and guidance throughout the PhD. Their advice and supervision has undoubtedly shaped me into the researcher I am today. I would also like to express my sincere gratitude to Dr. David Scurr, not only for allowing me to make use of Nottingham University's ToF-SIMS, but also for introducing me to his Nottingham research group; Akmal, Nichola and Jatin. Akmal particularly, thank you for your assistance with the cryostat and the inspiration you provided to explore the world of microneedles. I would also like to thank Rebecca Harrison for her expert assistance in the microbiology laboratory at Keele University, and to Rachel Gater for teaching me how to use the OCT. Thank you also to Dr. Richard Darton and Dr. Chris Hawes from the Keele University Chemistry Department for analysing my drug-dendrimer precipitate using XRD.

To my Jack Ashley best friends – Mark, Liam, Rachel and Clare – thank you so much for your support, I could not have done it without you. Mark – thank you for spending endless Friday afternoons helping me figure out what was wrong with the HPLC, I'll never forget your patience! Clare – you have been a wonderful friend. You are an inspiration for women in science and have inspired me to never give up on my dreams, no matter the obstacle. Rachel, thanks for keeping me sane during the endless late nights of thesis writing, for being a great friend and for introducing me to "your" (-now my-) friends!

Thank you to my mum and dad. You have supported me through everything and have always been proud of me, and reminded me to take time to be proud of my achievements before moving onto the next challenge. I couldn't have done this without your unwavering support. To

my wonderful friends Chris, Sophie, Tasha, and Ayasha, thank you for your advice, encouragement and laughs when needed! The distance between us as we carve our own paths has never stopped us from supporting each other throughout the years, and I thank you all for that.

A thousand thank you's must go to my soon to be husband, William. Your patience, support and kindness have helped me move forward even when I never thought I could. Every day is special with you and I am so thankful you want to continue this journey with me, Harry, Schrank, and the many other dogs we will inevitably adopt over the years.

"You are braver than you believe, stronger than you seem, and smarter than you think. But the most important thing is, even if we're apart… I'll always be with you"

Christopher Robin to Winnie the Pooh

Grandad, Auntie Kathy – this is for you.

Contents

Abstract ..... **i**

Acknowledgements ..... **iv**

List of Figures ..... **x**

List of Tables ..... **xvii**

List of Abbreviations ..... **xxi**

1 Chapter One - General Introduction **22**

1.1 Skin Structure and Function 22

1.1.1 Subcutis 23

1.1.2 Dermis 23

1.1.3 Epidermis 24

1.1.4 *Stratum Corneum* 26

1.2 Bacterial composition of the skin 29

1.3 Drug transport and routes of permeation into and through skin 32

1.4 Physicochemical properties which affect percutaneous absorption 36

1.5 Fick's Laws of diffusion 39

1.6 Thermodynamic activity 42

1.7 *In vitro* permeation studies 43

1.8 Drug-skin deposition imaging techniques 49

1.8.1 Time of Flight Secondary Ion Mass Spectrometry (ToF-SIMS) 51

1.9 Skin infections and the rise of antibacterial resistance 55

1.10 Chlorhexidine (CHX) and chlorhexidine digluconate (CHG) 58

1.11 Active strategies to enhance topical and transdermal drug delivery 65

1.12 Polyamidoamine (PAMAM) dendrimers 68

1.12.1 Percutaneous Penetration enhancement mediated by PAMAM dendrimers 72

1.12.2 Mechanisms of PAMAM dendrimer mediated drug delivery enhancement 75

1.12.3 Safety of PAMAM dendrimers 78

1.13 Microneedle-mediated drug delivery into and across skin 80

1.14 Aims of the thesis 84

2 Chapter Two – Formulation of an antimicrobial formulation containing CHG 86

2.1 Introduction 86

2.2 Aims and Objectives 88
2.3 Materials and Methods 89
2.3.1 Materials 89
2.3.2 Methods 89
2.3.3 Formulation development 90
2.3.4 Characterising experimental gel formulations 92
2.3.5 Statistical analysis of data 94
2.4 Results 95
2.4.1 CHG adsorption onto glass surfaces 95
2.4.2 Co-formulation Development 96
2.5 Discussion 104
2.6 Conclusion 116
3 Chapter Three - Co-formulation of CHG with G3 PAMAM-NH2 dendrimer 117
3.1 Introduction 117
3.2 Aims and Objectives 118
3.3 Materials and Methods 119
3.3.1 Materials 119
3.3.2 Methods 119
3.3.3 *In vitro* diffusion cell studies and tape stripping protocols 120
3.3.4 Investigating the interactions between CHG and PAMAM dendrimers using light microscopy, infra-red (IR) and X-ray diffraction (XRD) 124
3.4 Results 131
3.4.1 Analysis of CHG by HPLC 131
3.4.2 Effect of HEC concentration in gels on the *in vitro* skin permeation of CHG 132
3.4.3 Effect of CHG concentration in gels on the *in vitro* skin permeation of CHG 135
3.4.4 Effect of G3 PAMAM-NH_2 concentration in gels on the *in vitro* skin permeation of CHG 139
3.4.5 Commercial benchmark – *in vitro* permeation studies 141
3.4.6 Comparative Data 145
3.4.7 Investigating the interactions between CHG and PAMAM dendrimers using light microscope and infra-red (IR) 149
3.4.8 X-ray diffraction (XRD) analysis of unknown precipitate 158
3.5 Discussion 159

3.6 Conclusion 178

4 Chapter Four – Characterisation of skin deposition of CHG by Time-of-Flight Secondary Ion Mass Spectrometry (ToF-SIMS) 179

4.1 Introduction 179

4.2 Aims and Objectives 182

4.3 Materials and Methods 184

4.3.1 Materials 184

4.3.2 Methods 184

4.4 Results 192

4.4.1 Identification of fragment ions characteristic of G3-PAMAM-NH_2 dendrimer 192

4.4.2 ToF-SIMS analysis of CHG treated porcine tape strips 196

4.4.3 Ion intensity analysis of CHG treated porcine tape strips 205

4.4.4 ToF-SIMS analysis of CHG treated porcine cryosections 208

4.5 Discussion 218

4.6 Conclusion 231

5 Chapter 5 – Investigating the mechanism of G3 PAMAM-NH_2 dendrimer skin permeation enhancement 233

5.1 Introduction 233

5.2 Aims and Objectives 237

5.3 Materials and Methods 238

5.3.1 Materials 238

5.3.2 Methods 238

5.4 Results 242

5.4.1 TEWL Measurements 242

5.4.2 Optical Coherence Tomography (OCT) to determine time-dependent interactions between G3 PAMAM-NH_2 dendrimers and porcine skin 245

5.4.3 G3 PAMAM-NH_2 surface tension measurements 250

5.4.4 CHG experimental formulation with Tween and Span surfactants in a water-PG/water-ethanol 50:50 vehicle 255

5.5 Discussion 263

5.6 Conclusion 286

6 Chapter 6 – Investigating the use of microneedles as a physical method of drug permeation enhancement 287

6.1 Introduction 287

6.2 Aims and Objectives 289
6.3 Materials and Methods 290
6.3.1 Materials 290
6.3.2 Methods 290
6.4 Results 293
6.4.1 Homogeneity of MN depth penetration – gentian violet study 293
6.4.2 Homogeneity of MN diameter and depth penetration – Parafilm® study 296
6.4.3 Permeation of CHG from gel formulations following MN pre-treatment 299
6.4.4 Permeation of CHG from experimental gel formulations following MN pre-treatment – tape strip study analysed using ToF-SIMS 305
6.4.5 Permeation of CHG from gel formulations following MN pre-treatment – cross section study analysed using ToF-SIMS 311
6.4.6 Horizontal cross sections 316
6.4.7 Comparisons of a chemical (G3 PAMAM-NH_2 dendrimer) and physical (12A/36A solid MN pre-treatment) as a method of enhancing the dermal deposition of CHG within porcine skin 321
6.5 Discussion 327
6.6 Conclusion 344
7 General Conclusion 345
7.1 Implications of research and future work 347
References 350

List of Figures

Figure 1.1. *Human skin and its appendages, with particular focus on the epidermal layer. 22*

Figure 1.2. *A refined "bricks and mortar" representation of the stratum corneum. 26*

Figure 1.3. *Schematic of skin histology viewed in cross-section with bacteria and skin appendages. Replicated from Grice and Segre (2011) 31*

Figure 1.4. Routes of penetration through skin. 33

Figure 1.5. *Franz type diffusion cell apparatus. Type A is a typical "static" diffusion cell, type B is jacketed for temperature control. 44*

Figure 1.6. Schematic of the ToF-SIMS analysis of a porcine tape strip by ToF-SIMS. 53

Figure 1.7. Chemical structure of chlorhexidine digluconate (CHG), a commonly used salt of chlorhexidine (CHX). 59

Figure 1.8. Active strategies to enhance topical and transdermal drug delivery. 66

Figure 1.9. *Structure of a G3-PAMAM-NH_2 dendrimer. (A) indicates the core of the structure, (B) indicates the interior branching of the structure and (C) indicates the peripheral functional groups. The asterisk (*) illustrates an interior void which may potentially host encapsulated drugs. 68*

Figure 2.1. Preparation of experimental gel formulations. 91

Figure 2.2. *Apparent viscosity measurements of experimental and commercial formulations with increasing spindle speed ± SE. n=20 ± SE. 99*

Figure 2.3. *Ionisation states of CHX in A. basic and B. acidic conditions. CHG has two pK_a values representing the monocation and dication, 2.2 and 10.8 respectively (Hugo and Longworth 1964). 111*

Figure 3.1. *Evidence of drug-dendrimer interactions. A – 20% w/v CHG in water, B – 20% w/v PAMAM in methanol, C – 0.5 mL of 20% w/v PAMAM added to 0.5 mL of 20% w/v CHG, D – 0.5 mL 20% w/v PAMAM in methanol and 0.5 mL of 20% w/v CHG stabilised in a water-ethanol 50:50 solution. 126*

Figure 3.2. *Appearance of candidate formulations following a 24 hr application onto a silicone membrane. The formulation retains the shape set by the donor chamber at the start of the experiment. A. 4% CHG gel*

formulation; B. 4% CHG-1 mM PAMAM gel formulation; C. and D. Appearance of 4% CHG gel / 4% CHG -1 mM PAMAM gel following donor chamber removal indicating ability of the gel to hold its own shape. 127

Figure 3.3. *Images of a 4% CHG-1 mM PAMAM gel co-formulation illustrating the formulation of a pearlescent white precipitate at the end of a 24 hr diffusion cell experiment..... 128*

Figure 3.4. *Schematic diagram of the requirements for each statistical test type utilised within this thesis. 130*

Figure 3.5. *Example chromatogram obtained from a tape strip containing porcine skin material and CHG, allowed to leach from the tape into mobile phase over a 24hr period – 4% CHG-1 mM PAMAM, tape strip 4-6. ..... 132*

Figure 3.6. *Concentration profile of CHG detected on tape strips 1-21 following treatment with an experimental 1% CHG gel formulation with varying concentrations of HEC (0.5-4%). n=6 ± SE..... 133*

Figure 3.7. *Concentration profile of CHG detected on tape strips 1-21 following treatment with an experimental gel formulation with varying concentrations of CHG (1-4%). n=9 ± SE. 136*

Figure 3.8*. Concentration profile of CHG detected on tape strips 1-21 following treatment with an experimental gel formulation with varying concentrations of PAMAM dendrimer. n=13 ± SE. 140*

Figure 3.9. *Concentration profile of Hibiscrub® 4% detected on tape strips 1-21 following a 2 min or 24 hr application time following 24hrs. n=4 for Hibiscrub® 4%, n= 9 for 4% CHG, ± SE. 143*

Figure 3.10*. Comparative data of concentration of CHG permeated onto tape strips 1-21 from various experimental and commercial formulations. n=4 for Hibiscrub® 4%, n=9 for 4% CHG, n=13 for 4% CHG-0.5mM PAMAM and 4% CHG-1mM PAMAM, ± SE. 146*

Figure 3.11*. Photograph of shard crystals produced on addition of 0.5 mM PAMAM dendrimer to 4% CHG after 24hr A. 4 × magnification, B. 40 × magnification. 150*

Figure 3.12. *Photograph of shard crystals produced on addition of 4% CHG to 1 mM PAMAM dendrimer after 24hr A. 4 × magnification, B. 40 × magnification. 150*

Figure 3.13. *IR spectra of CHG 20% w/v in water. 151*

Figure 3.14. *IR spectra of G3 PAMAM-NH_2 PAMAM 20% w/v in methanol. 152*

Figure 3.15. *IR spectra of 4% CHG-1 mM PAMAM crystals. 153*

Figure 3.16. *Annotated diagram indicating functional groups indicative of CHG. 154*

Figure 3.17. *Annotated diagram indicating function groups indicative of G3-PAMAM NH_2. Note that this figure does not include the entirety of the G3 PAMAM-NH_2 structure, but includes a branch that allows identification of the groups indicated by IR. 155*

Figure 3.18. *Chemical structure obtained from XRD analysis of a single crystal of the unknown precipitate. 158*

Figure 4.1*. Images of skin samples A. in the process of freezing in liquid nitrogen, B. skin samples following partial embedding in OCT material. 186*

Figure 4.2. *ToF-SIMS corneocyte image data; ion intensity processing (following CN^- thresholding) to produce four 2 mm × 2 mm regions of interest (ROI). 189*

Figure 4.3. *Image illustrating how the CHG ion intensity changes across the cross section (section manually chosen indicated by the red box). Intensity of CHG ion spikes indicating CHG resides mainly in the stratum corneum. 190*

Figure 4.4. *Illustration of the "Measurement Editor" feature using the IONTOF software. Depth permeation of the $C_7H_4N_2Cl^-$ ion within porcine skin cross sections are measured manually and are illustrated by the green line. 191*

Figure 4.5. *m/z values of interest, A. 26.01 and B. 101.08. All mass spectra represent tape strip 3 from porcine skin. 193*

Figure 4.6*. m/z values of interest, C. 179.06 and D. 241.22 All mass spectra represent tape strip 3 from porcine skin. 194*

Figure 4.7. *Theoretical mass fragmentation sites of the G3 PAMAM-NH_2 dendrimer and the associated m/z values. 195*

Figure 4.8. *Mass spectra images indicating specificity of $C_7H_4N_2Cl^-$ ion to CHG. 197*

Figure 4.9. *Tape strip images indicating specificity of $C_7H_4N_2Cl^-$ ion to CHG. Each image represents a 4 mm × 4 mm area. 198*

Figure 4.10. *Tape strip images indicating ion intensity of PO_3^- on the same tape strips of different treatment groups. Each image represents a 4 mm × 4 mm area. 200*

Figure 4.11. *CHX ion $C_7H_4N_2Cl^-$ ion intensity across Hibiscrub® 4%, formulations 1-4% CHG, 4% CHG-0.5 mM PAMAM and 4% CHG-1 mM PAMAM. Each image represents a 4 mm × 4 mm area. 203*

***Figure 4.12**. Quantified $C_7H_4N_2Cl^-$ ion intensity values for tape strips 1, 2, 3, 6, 9, 12, 15, 18, 21 from treatment groups 1-4% CHG, Hibiscrub™ 4%, 4% CHG-0.5 mM PAMAM and 4% CHG-1 mM PAMAM. Areas normalised by total ion intensity, n=4 ± SE. 206*

***Figure 4.13.** Histology analysis of a 20µm thick porcine skin cross section prior to ToF-SIMS analysis and associated ToF-SIMS analytical image of the unique CHG fragment ion. 208*

***Figure 4.14.** Comparative ion intensity overlaid chemical distribution maps illustrating the chemical distribution of $C_7H_4N_2Cl^-$ (drug, green) PO_3^- (phosphite, red) and $C_{27}H_{45}SO_4^-$ (cholesterol sulphate, blue), n=3. ..... 210*

***Figure 4.15.** Magnified image of A. 4% CHG treatment group and B. 4% CHG-1 mM PAMAM treatment group. $C_7H_4N_2Cl^-$ ion indicative of CHG (green colour) has permeated past the stratum corneum in the 4% CHG-1 mM PAMAM treatment group. 212*

***Figure 4.16.** Suggestion of a sweat gland, apparent from the total ion count and phosphite ion chemical distribution map indicated by the white arrows. There appears to be no evidence of the CHG ion ($C_7H_4N_2Cl$) within the gland. 213*

***Figure 4.17.** Suggestion of a hair follicle, apparent from the phosphite ion and cholesterol sulphate ion chemical distribution map, indicated by the white arrows. There appears to be no evidence of the CHG ion ($C_7H_4N_2Cl^-$) within the hair follicle shaft. 213*

***Figure 4.18.** Suggestion of a skin furrow, apparent from the CHG ion ($C_7H_4N_2Cl^-$) chemical distribution map indicated by the white arrow. The CHG ion ($C_7H_4N_2Cl^-$) appears to accumulate within the furrow..... 214*

***Figure 4.19.** Line scan images illustrating the changes in ion intensity with depth permeation (mm) of CHG within porcine skin from various skin treatments, n=3. ..... 215*

***Figure 4.20.** Depth permeation of CHG ($C_7H_4N_2Cl^-$ ion) according to the "Measurement Editor" software from various formulations. The translucent grey box indicates the 400-700 µm depth target of CHG permeation (Selwyn and Ellis 1972, Touitou et al. 1998, Grice and Segre 2011, Nakatsuji et al. 2013), n=20 ± SE. 217*

***Figure 5.1.** Measurement of skin barrier integrity, as determined by TEWL, over the course of 24 hr, following dosing with G3 PAMAM-NH_2 dendrimer (A) solutions and (B) gels, n=3. Mean temperature 19.7 ± 0.4 ^oC; mean humidity 35.50 ± 2.50%, n=3 ± SE. 243*

Figure 5.2. *Measurement of skin barrier integrity, as determined by TEWL, before and after dosing with G3 PAMAM-NH_2 dendrimer solutions and gels, n=3 ± SE. Mean temperature 19.7 ± 0.4 ^oC; mean humidity 35.50 ± 2.50%. 244*

Figure 5.3. *OCT images of untreated porcine ear skin at A. 30 min and B. 24 hr. Red line 250 µm scale bar. 246*

Figure 5.4. *OCT images of porcine ear skin dosed with a either 1%, 2%, 3% 4% CHG gel formulation or 4% CHG-0.5 mM or 4% CHG-1 mM PAMAM gel co-formulation taken over a 24 hr time period. Red line - 250 µm scale bar..... 248*

Figure 5.5. *PAMAM-dendrimer-mediated change in surface tension, n=20 ± SE..... 251*

Figure 5.6*. Scatter plot illustrating the change in surface tension with increasing surfactant concentration, n=10 ± SE..... 253*

Figure 5.7. *Concentration profile of CHG detected on tape strips 1-21 following treatment with a CHG 4% in a water-PG 50:50 vehicle. Concentrations are presented following gravimetric analysis. n=4 ± SE.... 256*

Figure 5.8. *Concentration profile of CHG detected on tape strips 1-21 following treatment with CHG 4%-Tween 40 formulations containing various concentrations of surfactant (05%-5%) in a water-PGl 50:50 vehicle. Concentrations are presented following gravimetric analysis. n=4 ± SE. ……..257*

Figure 5.9. *Concentration profile of CHG detected on tape strips 1-21 following treatment with CHG 4%-Tween 80 formulations containing various concentrations of surfactant (05%-5%) in a water-PG 50:50 vehicle. Concentrations are presented following gravimetric analysis. n=4 ± SE. ……..258*

Figure 5.10. *Concentration profile of CHG detected on tape strips 1-21 following treatment with CHG 4%-Tween 85 formulations containing various concentrations of surfactant (05%-5%) in a water-PG 50:50 vehicle. Concentrations are presented following gravimetric analysis. n=4 ± SE. ……..259*

Figure 5.11*. Concentration profile of CHG detected on tape strips 1-21 following treatment with CHG 4%-Span 80 formulations containing various concentrations of surfactant (05%-5%) in a water-PG 50:50 vehicle. Concentrations are presented following gravimetric analysis. n=4 ± SE. ……..260*

Figure 5.12. *Comparative tape strip data, including controls (CHG 4% in water, CHG 4% in water-PG 50:50 and treatment groups, n=4± SE ……261*

Figure 6.1. *A. Appearance of skin samples following application of various MN devices. B. Appearance of gentian violet stained MN channels following application of various MN devices. n=3. ..... 294*

Figure 6.2. *Depth penetration of MN channels from various MN devices, MN depth settings and MN arrays. "Zero" value is considered to be the outermost layer of skin, the stratum corneum n=10 ± SE. 295*

Figure 6.3. *Visualisation of a MN channel viewed using light microscope at 10 × magnification. The inner diameter was measured (153.0 mm) for the graphs created for Figure 6.4. Inner diameters were measured from the widest point. MN channel from a Dermapen®, 750 µm, 12A, PF sheet 1. ..... 296*

Figure 6.4. *MN diameter measurements on each PF layer from a Dermapen® MN device with varying needle length. A. 250 µm, B. 500 µm, C. 750 µm, D. 1000 µm, n=4 ± SE. 297*

Figure 6.5. *Comparative graphical data illustrating the concentration of CHG found in tape strips 1-21 from treatment groups 1% and 4% CHG, Hibiscrub 4%. Data compares the CHG concentration from porcine skin treated with formulation only, formulation following a 12A 750 µm solid MN pre-treatment or formulation following a 36A 750 µm solid MN pre-treatment, n=4 ± SE. 301*

Figure 6.6*. Distribution of ions $C_7H_4N_2Cl^-$ (drug), PO_3^- (phosphite) and $C_{27}H_{45}SO_4^-$ (cholesterol) in untreated skin. Images were rebuilt to account for stratum corneum material only and the ion intensity was normalised to the total ion within the region of interest to ensure ion intensity was representative of stratum corneum material. 307*

Figure 6.7. *CHX ion $C_7H_4N_2Cl^-$ ion intensity across porcine skin treated with either experimental 1% or 4% CHG formulations, or the commercial benchmark Hibiscrub. Data compares the CHG ion intensity from porcine skin treated with formulation only, formulation following a 12A 750 µm solid MN pre-treatment or formulation following a 36A 750 µm solid MN pre-treatment. 309*

Figure 6.8. *Quantified mean ion intensity values for tape strips 1, 2, 3, 6, 9, 12, 15, 18, 21 from treatment groups 1% and 4% CHG, Hibiscrub 4%. Areas normalised by total ion intensity. Data compares the CHG ion intensity from porcine skin treated with formulation only, formulation following a 12A 750 µm solid MN pre-treatment or formulation following a 36A 750 µm solid MN pre-treatment, n=4± SE. 310*

Figure 6.9*. ToF-SIMS images of CHG ($C_7H_4N_2Cl^-$, green colour), phosphite (PO_3^-, red colour) and cholesterol ($C_{27}H_{45}SO_4^-$, blue colour) overlaid to indicate CHG depth permeation within porcine skin treated following various 24 hr formulation treatments with and without the use of solid MNs as a skin pre-treatment. 313*

Figure 6.10. *Porcine skin treated with 4% CHG following a 36A solid MN pre-treatment. Figure indicates inconsistent CHG permeation in deeper skin layers.* *314*

Figure 6.11*. Histological examination of porcine skin following 12A solid MN pre-treatment (MN channels shown in red circles). Red scale bar - 150µm.* *317*

Figure 6.12*. ToF-SIMS images of horizontal porcine skin cross sections. Images indicate the bores created by the Dermapen® using the ion indicative of cholesterol ($C_{27}H_{45}SO_4^-$) and the drug using the unique CHG fragment ion ($C_7H_4N_2Cl^-$).* *318*

Figure 6.13*. ToF-SIMS image of CHG diffusion within a porcine skin cross section, illustrating higher ($C_7H_4N_2Cl^-$) ion intensity in the area immediately surrounding the MN bore.* *319*

Figure 6.14. *Example ToF-SIMS image of CHG distribution within porcine skin treated with 4% CHG following a 12A solid MN pre-treatment. Area indicated on ToF-SIMS images provides an example of the ion intensity values plotted to compare CHG ion distribution between groups A. area immediately surrounding the MN bore, B. 1 mm × 1 mm area in "bulk" skin. All values normalised for total ion intensity, n=3 ± SE.* *320*

Figure 6.15. *Graphical illustration of the tabulated data found in Table 6.5. Concentration of drug adjusted per mg of stratum corneum material (µg/mg) detected using HPLC on tape strips 1-21 from various treatment groups. All formulations contained 4% CHG and permeation enhancement was detected by chemical methods (co-formulation with a G3 PAMAM-NH_2 dendrimer) or by physical methods (solid MN pre-treatment)- Concentration of drug adjusted per mg of stratum corneum material (µg/mg) detected using HPLC on tape strips 1-21 from various treatment groups. All formulations contained 4% CHG and permeation enhancement was detected by chemical methods (co-formulation with a G3 PAMAM-NH_2 dendrimer) or by physical methods (solid MN pre-treatment), n=6 for 4% CHG, n=13 for 4% CHG-0.5mM PAMAM and 4% CHG-1mM PAMAM, n=4 for 4% CHG 12A and 4% CHG 36A, ± SE.* *324*

Figure 6.16. MN channels created from a. Dermaroller®; b. Dermapen®. *328*

List of Tables

***Table 1.1**. Illustration of the linear increase in molecular weight, diameter and surface groups of PAMAM dendrimers as a function of generation (Dendritech 2017).* *69*

***Table 2.1.** Experimental gel formulations created with the aim of enhancing delivery of CHG into porcine skin. 0.35% and 0.69% G3 PAMAM-NH_2 dendrimer is equivalent to 0.5mM and 1mM dendrimer respectively.* *90*

***Table 2.2.** Percentage recovery of a CHG solution and experimental CHG gels from untreated and silanised glassware, n=3 ± SE.* *95*

***Table 2.3.** Viscosity measurements (±SE) of various experimental and commercial formulations – spindle 63 (lowest available), n=20 ± SE.* *98*

***Table 2.4.** Measured pH for experimental formulations with and without the addition of PAMAM dendrimer following a 1:50 dilution using purified water. n=3 ± SE.* *100*

***Table 2.5.** CHG recovery from experimental formulations after dissolving 1mL of formulation to create a 10µg/mL solution - n=3/4 ± SE depending on formulation, see table.* *101*

***Table 2.6.** Zone of inhibition of experimental formulations and commercial benchmarks against Gram positive S. aureus at 37 ^oC after 24 hr, n = 3 ± SE.* *102*

***Table 2.7**. Zone of inhibition of experimental formulations and commercial benchmarks against Gram negative E. coli at 37 ^oC after 24 hr, n = 3 ± SE.* *102*

***Table 2.8.** One-Way ANOVA data analysis to determine whether formulations with and without PAMAM dendrimer, and the commercial benchmark Hibiscrub significantly affect the zone of inhibition following 24hr incubation with S. aureus or E. coli. Pairwise comparisons are arranged so that the formulation which developed the highest concentration of CHG is given first. OWA – One-Way ANOVA, n=3.* *103*

***Table 3.1.** Analytical tests chosen to determine whether formulations with differing concentration of HEC (0.5-4%) significantly affect the depth permeation of CHG within porcine skin and the resulting pairwise comparisons which resulted in a statistically significant result ($p < 0.05$). Pairwise comparisons are*

arranged so that the formulation which developed the highest concentration of CHG is given first (F1). KW – Kruskal Wallis; OWA – One-Way ANOVA, n=6. ..... *135*

Table 3.2. *Analytical tests chosen to determine whether formulations with differing concentration of CHG (1-4%) significantly affect the depth permeation of CHG within porcine skin and the resulting pairwise comparisons which resulted in a statistically significant result (p <0.05). Pairwise comparisons are arranged so that the formulation which developed the highest concentration of CHG is given first (F1). KW – Kruskal Wallis; OWA – One-Way ANOVA, n=9.* *138*

Table 3.3. *Analytical tests chosen to determine whether the duration of application of the commercial benchmark significantly affected the depth permeation of CHG within porcine skin and the resulting pairwise comparisons which resulted in a statistically significant result (p <0.05). Pairwise comparisons are arranged so that the formulation which developed the highest concentration of CHG is given first (F1). KW – Kruskal Wallis; OWA – One-Way ANOVA, n=4 for Hibiscrub® 4%, n= 9 for 4% CHG.* *144*

Table 3.4. *Analytical tests chosen to determine whether formulations with and without PAMAM dendrimer, and with the commercial benchmark Hibiscrub® significantly affect the depth permeation of CHG within porcine skin. The table reports the resulting pairwise comparisons which resulted in a statistically significant result (p <0.05). Pairwise comparisons are arranged so that the formulation which developed the highest concentration of CHG is given first. KW – Kruskal Wallis; OWA – One-Way ANOVA. n=4 for Hibiscrub® 4%, n=9 for 4% CHG, n=13 for 4% CHG-0.5mM PAMAM and 4% CHG-1mM PAMAM.* *148*

Table 3.5. *IR spectroscopy absorptions and associated functional groups of CHG (20% w/v in water).* . *154*

Table 3.6. *IR spectroscopy absorptions and associated functional groups of G3 PAMAM-NH_2 (20% w/v in methanol)*..... *155*

Table 3.7. *IR spectroscopy absorptions and associated functional groups of CHG (20% w/v in water)-G3 PAMAM-NH_2 (20% w/v in methanol) mixture.* *156*

Table 3.8. *Table indicating shifts in IR frequency (cm^{-1}) upon mixing 20% w/v CHG and 20% w/v PAMAM dendrimer together.* *156*

Table 3.9. *Crystal data obtained from XRD analysis.* *158*

Table 5.1. *Hydrophilic-Lipophilic Balance (HLB) values for surfactants used in this study.* *240*

Table 5.2. *Cricical micellar concentrations (CMCs) of surfactants utilised in this study. 241*

Table 5.3. *CHG-surfactant formulation ingredients. The vehicle used for formulations containing Tween surfactant was water-PG 50:50; the vehicle used for the formulation containing Span surfactant was water-ethanol 50:50. ..... 241*

Table 5.4. *Surface tension measurements of various co-formulations with and without the addition of a G3 PAMAM-NH_2 dendrimer at clinically relevant concentrations, n = 20 ± SE. Mean temperature 20.0 ± 2 ^oC..... 250*

Table 5.5. *Surface tension measurements of various co-formulations with and without the addition of a non-ionic surfactant at clinically relevant concentrations, n=10 ± SE. Mean temperature 20.5 ±2 ^oC. ... 252*

Table 5.6. *Analytical tests chosen to determine wither formulations with differing concentrations of Tween 40 (0.5-5%) significantly affects the depth permeation of CHG within porcine. Pairwise comparisons are arranges so that the formulation which delivered the highest concentration of CHG is given first (F1). KW - Kruskal Wallis; OWA - One Way ANOVA, n=4……257*

Table 5.7. *Analytical tests chosen to determine wither formulations with differing concentrations of Tween 80 (0.5-5%) significantly affects the depth permeation of CHG within porcine. Pairwise comparisons are arranges so that the formulation which delivered the highest concentration of CHG is given first (F1). KW - Kruskal Wallis; OWA - One Way ANOVA, n=4……258*

Table 5.8. *Analytical tests chosen to determine wither formulations with differing concentrations of Tween 85 (0.5-5%) significantly affects the depth permeation of CHG within porcine. Pairwise comparisons are arranges so that the formulation which delivered the highest concentration of CHG is given first (F1). KW - Kruskal Wallis; OWA - One Way ANOVA, n=4……259*

Table 5.9. *Analytical tests chosen to determine wither formulations with differing concentrations of Span 80 (0.5-5%) significantly affects the depth permeation of CHG within porcine. Pairwise comparisons are arranges so that the formulation which delivered the highest concentration of CHG is given first (F1). KW - Kruskal Wallis; OWA - One Way ANOVA, n=4……260*

Table 5.10. *Pairwise comparisons between CHG-surfactant formulations which provided a statistically significant result (p <0.05), n=4……279*

Table 5.11. *Table indicating the log P and aqueous solubility of – CHG (Farkas et al. 2007, Sigma Aldrich 2019b), diazepam (Newton et al. 1981, Kempe, Metz and Mäder, 2008), lidocaine (Nakano 1979, Padula et al 2013) and lorazepam (Nokhodchi et al. 2003, van der Vossen et al. 2017, PubChem 2019c)……..280*

Table 6.1. *Skin treatments for determining the effect of MN length and array on penetration. n=3. .... 293*

Table 6.2*. Approximate depth permeation of 12A and 36A MNs of differing lengths (250-1000µm) according to the number of PF layers permeated, assuming a single PF layer is equal to 127µm thickness, n=4. ..... 298*

Table 6.3. *Depth permeation of 12A and 36A MNs of differing lengths (750-1000 µm) – comparison of gentian violet dyed porcine skin and the eight layer PF study, assuming a single PF layer is equal to 127 µm thickness, n=4. ..... 299*

Table 6.4. *Analytical tests chosen to determine whether formulations significantly affect the depth permeation of CHG within porcine skin – HPLC data – comparing no MN, 12A MN and 36A MN treatment groups and reporting the resulting pairwise comparisons which resulted in a statistically significant result (p <0.05). Pairwise comparisons are arranged so that the formulation which developed the highest concentration of CHG is given first. KW – Kruskal Wallis; OWA – One-Way ANOVA, n=4..... 302*

Table 6.5. *Concentration of drug adjusted per mg of stratum corneum material (µg/mg) detected using HPLC on tape strips 1-21 from various treatment groups. All formulations contained 4% CHG and permeation enhancement was detected by chemical methods (co-formulation with a G3 PAMAM-NH_2 dendrimer) or by physical methods (solid MN pre-treatment), n=6 for 4% CHG, n=13 for 4% CHG-0.5mM PAMAM and 4% CHG-1mM PAMAM, n=4 for 4% CHG 12A and 4% CHG 36A, ± SE. 323*

Table 6.6. *Analytical tests chosen to determine whether formulations significantly affect the depth permeation of CHG within porcine skin – HPLC data – comparing CHG without permeation enhance, CHG-PAMAM co-formulation and CHG with MN pre-treatment, and reporting the resulting pairwise comparisons which resulted in a statistically significant result (p <0.05). Pairwise comparisons are arranged so that the formulation which developed the highest concentration of CHG is given first. KW – Kruskal Wallis; OWA – One-Way ANOVA, n=6 for 4% CHG, n=13 for 4% CHG-0.5mM PAMAM and 4% CHG-1mM PAMAM, n=4 for 4% CHG 12A and 4% CHG 36A 325*

List of Abbreviations

5FU	**5-Fluorouracil**
ADR	Adverse drug reaction
CHG	Chlorhexidine digluconate
CHX	Chlorhexidine
CLSM	Confocal laser scanning microscopy
CMC	Critical micellar concentration
EUCAST	European Committee on Antimicrobial Susceptibility Testing
HLB	Hydrophilic-lipophilic balance
HPLC	High performance liquid chromatography
IPM	Isopropyl myristate
IQR	Interquartile range
IR	Infra-red
LoD	Limit of detection
LoQ	Limit of quantification
m/z	Mass to charge ratio
MALDI	Matrix assisted laser desorption ioninsation
MHRA	Medicines and Healthcare products Regulatory Agency
MIC	Minimum inhibitory concentration
MO	Mineral oil
n	Number of samples
NICE	National Institute for Health and Care Excellence
NMF	Natural moisturising factor
OCT material	Optimum cutting temperature
OCT instrument	Optical coherence tomography
OECD	The Organisation for Economic Co-operation and Development
p	Significance level
PAMAM	Polyamidoamine
PBS	Phosphate buffer saline
PG	Propylene glycol
SE	Standard error
PF	Parafilm®
SSTI	Skin and soft tissue infection
TEER	Transepithelial electric resistance
TEWL	Transepidermal water loss
ToF-SIMS	Time of flight-secondary ion mass spectrometry
w/v	Weight by volume
w/w	Weight by weight
WHO	World Health Organisation
XRD	X-ray diffraction

1 Chapter One - General Introduction

1.1 Skin Structure and Function

Skin is the largest organ in the human body, accounting for 16% of a person's total body weight and covering a mean surface area of 1.8 m^2 (Fenner and Clark 2016). This complex and diverse structure has numerous roles, including temperature regulation, mechanical support and sensation transmission (Proksch *et al.* 2008). Furthermore, the barrier regulates water ingress and egress, and prevents the entry of exogenous chemicals and microbes (Harding 2004). This organ can be subdivided into three main histological layers. These are, from innermost to outermost – the subcutis, the dermis (0.1-0.5 cm thick [Barry, 1983]) and the epidermis, further separated into (from innermost to outermost layer) *stratum basale, stratum spinosum, stratum granulosum, stratum lucidum* and *stratum corneum*, defined by their level of cell differentiation. The epidermis is 0.06-0.8 mm thick and varies dependent on body site, age and between individuals (Williams, 2003c). Figure 1.1 illustrates the structure of human skin and appendages, with a particular focus on the epidermis.

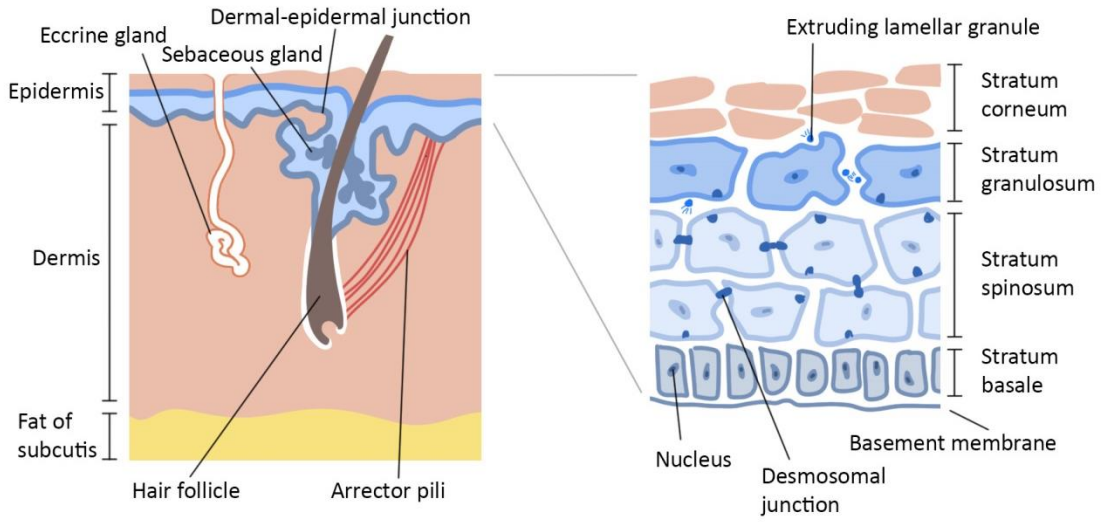

Figure 1.1. Human skin and its appendages, with particular focus on the epidermal layer.

1.1.1 Subcutis

The subcutaneous fat layer (subcutis) is the innermost layer of skin, comprised of adipose cells and is embedded within connective tissue. This layer functions to insulate the body, act as protection for internal organs against mechanical shock and to provide a region for energy storage (Walters and Roberts 2002). A dense microcirculation exists within this layer to supply oxygen and nutrients to the upper skin layers (Fenner and Clark 2016).

1.1.2 Dermis

The dermis lies immediately above the subcutis and is composed of a complex network of collagen fibres and elastic tissue embedded within a mucopolysaccharide matrix (Williams, 2003c). Approximately 70% of the dermis contains collagen fibres, which increase in density towards the subcutis (Fenner and Clark 2016). The collagen fibres provide tensile strength to the skin and the elastic tissue provides flexibility and resistance to mechanical injury (Moss 2015). A scarce cellular population exists within this layer and includes fibroblasts (which produce precursors to connective tissue), mast cells (involved in the immune response), and melanocytes (responsible for skin pigment [Benson, 2012]). Embedded within the dermis are nerve tissues, various skin appendages and vascular and lymphatic systems. Blood vessels branch from arteries in the subcutis and rise almost parallel to the dermal-epidermal junction (Odland 1991), Capillaries provide the nutritional requirements of skin for its maintenance and wound repair, and the rich blood flow also acts as a means of drug removal from the skin. This establishes an effective concentration gradient between a penetrant applied to the skin and the skin layers below. The lymphatic system within the skin has also been attributed to drug clearance and systemic uptake (Supersaxo *et al.* 1990, Jepps *et al.* 2013), particularly with larger molecules such as interferon (a type of signalling protein primariliy released from host cells in response to

viral stimuli [Cross and Roberts 1993]), and so should not be overlooked when considering drug binding and clearance into the systemic circulation.

The number and distribution of skin appendages varies between individuals and body site, but generally accounts for 0.1% of the skin surface (Schaefer and Redelmeier 1996, Otberg *et al.* 2004b). This equates to 40-70 hair follicles and 200-250 sweat ducts/cm^2 (Moss 2015). Hairs are formed from compacted keratinocytes and extend to a depth of 400-700 µm (Touitou *et al.* 1998). The sebaceous gland is attached to the hair follicle and secretes sebum, a mixture of free fatty acids and triglycerides which lubricates the skin and may help maintain the skin surface at a pH of approximately 5 (Surber, Smith, *et al.* 1999). The secretion of sebum onto the skin may impede delivery of drugs via the hair follicle, firstly via the upward flow of sebum, and secondly by retarding permeation of largely water soluble drugs (which are thought to use the transcellular and transappendageal route (Section 1.3), by creating a lipid rich environment. Thus, sebum may be considered the first barrier to permeation prior to contact with the *stratum corneum*, but can be removed easily via skin washing (Mavon *et al.* 1998).

1.1.3 Epidermis

The epidermal layer is the outer, avascular layer of the skin. It is comprised primarily of keratinocytes which are secreted from stem cells associated with the *stratum basale* and undergo several stages of differentiation as they migrate towards the outer environment, eventually becoming flattened, anucleate cells in the *stratum corneum* (Roberts and Walters 1998, Baroni *et al.* 2012). This process is under constant renewal, whereby dead skin cells are sloughed off the *stratum corneum* into the external environment and are replaced with cells from the layers below, termed desquamation (Milstone 2004). This process maintains the barrier to the outside world.

Keratinocytes originate within the *stratum basale*, are mitotically active and are connected to the basal membrane via hemidemosomes. The *stratum basale* contains three further specialised cell types: melanocytes, which synthesise melanin, essential for protection against UV radiation; Merkel cells, which are involved in touch sensation (Maricich *et al.* 2009); and Langerhans cells, which present antigens to pathogens invading the skin (Williams 2003a). In the *stratum spinosum*, cells change shape from columnar to polygonal. Anchoring junctions named desmosomes secure the cells to one another, forming a scaffold to provide further mechanical strength to the structure (Haake *et al.* 2001, Green and Simpson 2007). In the *stratum granulosum*, layers of cells flatten in shape and two types of granules are formed within the keratinocytes. Keratohyalin granules are responsible for the granular appearance of the cell and may be involved in keratin production (Moss 2015). Lamellar granules are discharged into the intercellular space and play an important role in creating *stratum corneum* lipids, a large contributor to the barrier function of human skin (Harding 2004). Enzymes present in the upper region of this layer degrade cellular components, which facilitates the terminal differentiation of keratinocytes into anucleate corneocytes which are present in the *stratum corneum*. The *stratum lucidum* is only seen clearly in areas of the body where skin is thickest, and is often grouped together with the *stratum corneum* and considered to be a lower level of this layer. It is comprised of a flattened layer of dead keratinocytes that have a thicker outer membrane (than keratinocytes in the *stratum corneum*) and secrete large amounts of keratin, to potentially increase the skin's barrier function (Tortora and Derrickson 2012). The epidermal skin layers which sit below the *stratum corneum* are often termed the "viable epidermis" because the cells are still able to replicate, unlike the anucleate cells in the *stratum corneum*, and are able to renew epidermal tissue (Micali *et al.* 2001).

1.1.4 *Stratum Corneum*

The *stratum corneum* is the outermost layer of the skin, comprised of numerous layers of terminally differentiated keratinocytes, termed corneocytes due to their cornified structure. This layer is approximately 10-20 µm thick comprising of 10-15 layers of cells (Williams, 2003a), although thickness can vary with body site (Holbrook and Odland 1974) and skin hydration (Bouwstra *et al.* 2003).The *stratum corneum* is considered to be the main barrier to exogenous penetrants due to its complex structure (Scheuplein and Blank 1971), which provides an effective interface between the human body and external environment and is considerably more hydrophobic than the lower epidermal layers.

One of the most popular descriptors of the *stratum corneum* originated from Elias (1983), who compared the structure to "bricks and mortar". The intricacies of the barrier were described further by Rawlings (2010), who defined the structure as "a continuous structure of varying thickness, where natural moisturising factor (NMF) containing keratin sponges are tightly interconnected by corneodesmosomes; interspersed between a continuous highly ordered and largely orthorhombically packed lipid phase".

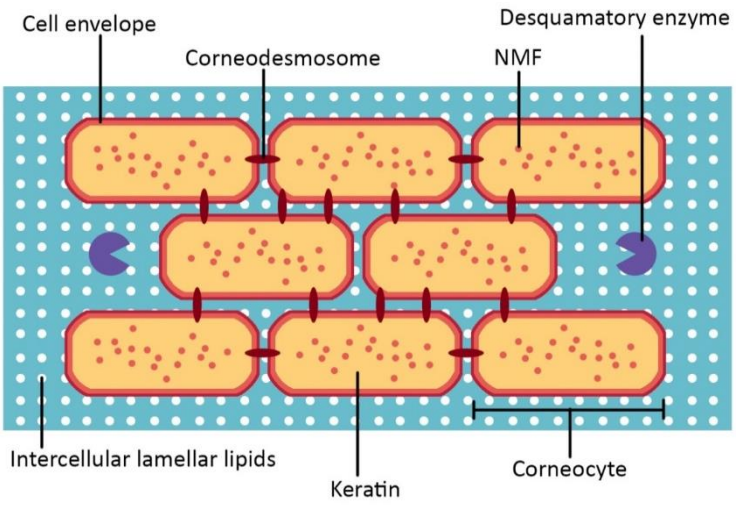

Figure 1.2. A refined "bricks and mortar" representation of the stratum corneum.

Corneocytes have a thickness of 0.3-0.5 µm (Voegeli and Rawlings 2013) and consist of 75% protein, the majority of which is arranged into a highly ordered keratin filament matrix (Downing 1992) flattened by the presence of filaggrin, which causes the cell to compact (Sandilands *et al.* 2009) as well as serving as scaffolding for the attachment of covalently bound lipids (Palmer *et al.* 2006). NMF in corneocytes is comprised of amino acids and their derivatives (Harding *et al.* 2000, Rawlings and Harding 2004), and plays a large role in preventing water loss from the skin by acting as a humectant (Rawlings and Matts 2005). The corneocyte "bricks" are enveloped by a cornified cell envelope, which is insoluble, approximately 15 nm thick (Jarnik *et al.* 1998, Voegeli and Rawlings 2013) and comprised of both proteins and lipids. This structure provides an interface between the hydrophilic proteins of the cell envelope and the hydrophobic lipids which produce the "mortar" structure of the *stratum corneum*.

Lipids are derived from lamellar bodies which are secreted into the *stratum granulosum-stratum corneum* interface (Menon and Ghadially 1997, Menon 2002). The major lipid classes in the *stratum corneum* are ceramides, free fatty acids and cholesterol (Proksch *et al.* 2008) in an approximate 1:1:1 ratio (Wertz and Norlén 2003). Phospholipids, whilst a common feature of typical keratinocyte membranes, are largely absent from the *stratum corneum* but in increase in percentage weight with increasing epidermal depth (Lampe *et al.* 1983). The lipid components of the *stratum corneum* are subsequently modified and arranged into highly organised lipid bilayers which constitute the majority of the skin barrier. X-ray diffraction studies have identified three types of lamellar phases. These are, in increasing order of organisation, liquid, hexagonal and orthorhombic (Elias *et al.* 1983; Garson *et al.* 1991). Bouwstra *et al.* (1991a) found evidence using X-ray diffraction (XRD) of two different lipid phases present in the *stratum corneum,* characterised by a repeating unit distance of 6.4 nm and 13.4 nm, thus providing evidence of differential lipid packing within the *stratum corneum* which may influence its barrier function.

Corneodesmosomes are protein structures which act as rivets between neighbouring corneocytes, provide the main cohesive force in the *stratum corneum* and are able to resist shearing forces to give stability to the physical barrier (Jonca *et al.* 2002). It is through corneodesmosome degradation that the terminally differentiated corneocytes are sloughed from the skin surface into the external atmosphere (Ekholm *et al.* 2000, Bernard *et al.* 2003). Degradation of corneodesmosomes is regulated by proteolytic cleavage of their extracellular portions, viakallikrein-regulated peptidases and cathepsins (Kitajima 2015).

The *stratum corneum* may be further divided into two distinct layers: the *stratum compactum* and the *stratum disjunctum*. The *stratum compactum* is defined as "the lower region of the *stratum corneum* in which adjacent corneocytes are held firmly by competent corneodesmosomes". The *stratum dysjunctum* is defined as "the outermost region of the *stratum corneum* in which adherence between adjacent corneocytes has been weakened by proteolytic cleavage of corneodesmosomes" (Wakefield 2008).

In summary, the *stratum corneum* is considered the major barrier to drug permeation into and across the skin because of the number and size of corneocytes; the cell envelope surrounding the corneocytes; the presence of tightly packed lipid bilayers; corneodesmosomes, long chain ceramide "rivets" which anchor and hold the structure together and the presence of several lipid and aqueous phases through which a drug must traverse. Advancements in *stratum corneum* characterisation continue to be made with the development of more sophisticated techniques, proposing the existence of a "single gel phase" and "sandwich" model to describe the *stratum corneum* lipids (Bouwstra *et al.* 2000, Norlén 2001), a major component of the barrier.

1.2 Bacterial composition of the skin

Approximately 1 million bacteria inhabit each square centimetre of skin, including its many folds and appendages (Grice and Segre 2011). For the most part, bacteria exhibits a symbiotic relationship with the host, unable to cause infection without infiltrating a compromised skin barrier. The composition of skin flora varies dependent on skin site, environmental and endogenous host factors and bacterial growth is perpetuated by providing a warm environment and nutrition through sweat, sebum and dead corneocytes on the outer skin surface (Gibbs and Stuttard 1967).

When considering the diversity of skin flora, skin sites can be divided into three categories; “dry”, “moist” and “sebaceous” (Grice *et al.* 2009). Dry sites include the inner forearm, palm and buttock; moist sites include areas with skin folds such as toe webs, genital creases and the axillary region; and sites rich in sebaceous glands include the face and back. The skin microbiome is highly dependent on the microenvironment of these sites. *Staphylococcus* and *Corynebacterium* spp. are the most abundant organisms colonizing moist areas given the high humidity (Costello *et al.* 2009, Grice *et al.* 2009), *Propionibacterium* spp. dominates sebaceous areas, associated with the pilosebaceous unit, thus the bacterium has been investigated in the pathogenesis of acne vulgaris (Puhvel *et al.* 1975, Bojar and Holland 2004). Dry sites harbour the most diverse skin bacteria, including Actinobacteria, Proteobacteria, Firmicutes and Bacteriodetes (Gao *et al.* 2007, Grice *et al.* 2008, 2009).

Environmental factors which may affect the skin microbiome include clothing, external temperature and applied cosmetic or pharmaceutical products (McBride *et al.* 1977, Lee *et al.* 2018). Factors specific to the host which may affect the skin microbiome include age (Somerville 1969, Leyden *et al.* 1975), sex (Marples 1982, Fierer *et al.* 2008) and the host genotype which

may predispose them to skin disease (such as a filaggrin mutation which has been associated with an increased risk of atopic dermatitis [Palmer *et al.* 2006; O'Regan *et al.* 2008]).

Bacteria are understood to reside not only on the skin surface, but deep within the epidermis and these bacteria has recently been found to consistently reside within the dermis (Zeeuwen *et al.* 2012, Nakatsuji *et al.* 2013). These recent discoveries are due to the development of techniques such as skin biopsies, scrapes and scrubs used to identify the bacteria, as traditional techniques such as skin swabbing has failed to reach these deeper bacteria (Fahlén *et al.* 2012, Kong *et al.* 2017). Sample detection and processing, for example DNA extraction, quantitative PCR, Gram staining, immunofluorescence and *in situ* hybridisation, has also improved (Kong *et al.* 2017). For example, Nakatsuji *et al.* (2013) detected DNA encoding for bacterial 16S rRNA genes below the maximal depth of follicles in facial skin (3.0 mm), and below the eccrine glands in palm skin (1.5 mm). PCR amplification, Gram staining, immunostaining and *in situ* hybridisation was performed to identify the bacterial class and phylum. Bacteria was understood to be diverse, with high proportions of Proteobacteria present across all samples. *S. epidermidis* was routinely detected below the epidermal basement membrane, and *Pseudomonas spp.* was readily detected in the dermis outside of appendageal structures. The authors concluded that the presence of microbes within the dermis allows physical contact between bacteria on the skin surface and bacteria subepidermally, suggesting that normal commensal bacterial communities communicate with the host to change in response to changes in the external environment.

In addition to their presence below the epidermis, bacteria are understood to reside in skin folds and appendages (Bolon 2016). The idea that bacteria is present in deeper layers in addition to the skin surface was initially suggested by Lovell (1945) who determined by sectioning skin that a significant proportion of bacteria (*S. epidermidis*) which were situated so deeply within appendages that they could not reasonably be removed without damaging the skin. A study

completely by Lange-Asschenfeldt *et al.* (2011) found that 85% of bacteria on participant's forearm were found within the first six corneocyte layers, and 25% of bacteria were found within and aggregating around hair follicles, sweat and sebaceous glands. Grice *et al*. (2008) found that the number of bacteria increased with increasing depth of skin. This "hidden" flora (inaccessible by traditional skin sampling methods) is estimated to be present at a depth of 400-700 µm (Touitou *et al.* 1998), the depth of hair follicles. Therefore a topically applied antimicrobial must reach this depth to efficiently remove bacteria which may cause infection. Figure 1.3 illustrates the topography of bacteria in human skin.

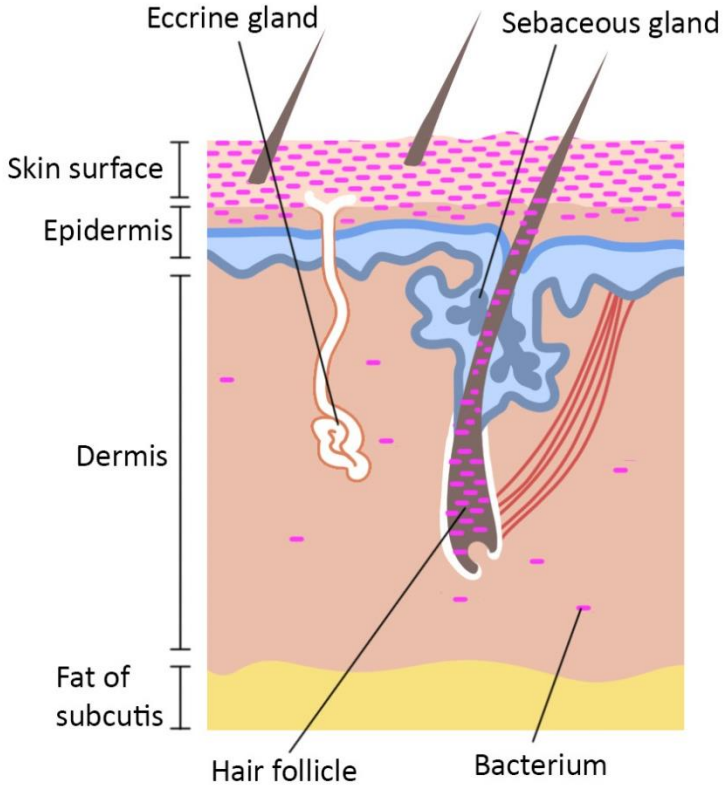

Figure 1.3. Schematic of skin histology viewed in cross-section with bacteria and skin appendages. Replicated from Grice and Segre (2011)

1.3 Drug transport and routes of permeation into and through skin

The structure of skin presents a complex barrier and any topically applied permeant must diffuse through these layers to reach the deeper tissues and systemic circulation. The first partition step is that which occurs from the topically applied formulation into the *stratum corneum*. Following *stratum corneum* partitioning, the permeant must diffuse and partition across the numerous skin layers in order to reach the systemic circulation. Partitioning occurs between the *stratum corneum* and viable epidermis, between the viable epidermis and dermis, and finally between the dermis and blood vessels located in this layer for systemic uptake. Throughout this tortuous diffusion pathway to reach the systemic circulation, the permeant may bind to structural elements of the tissue according to its physicochemical properties (Walter and Kurz 1988, Banning and Heard 2002), and the drug may also be metabolised by enzymes present in the skin (Nacht *et al.* 1981). Esterases in particular exhibit high activities within this tissue (Williams 2003a).

Skin provides three main pathways in which transdermal permeants may move across skin: the transcellular, intercellular and transappendageal route. Each route may be used in conjunction with another, which varies depending on the physicochemical properties of the penetrant.

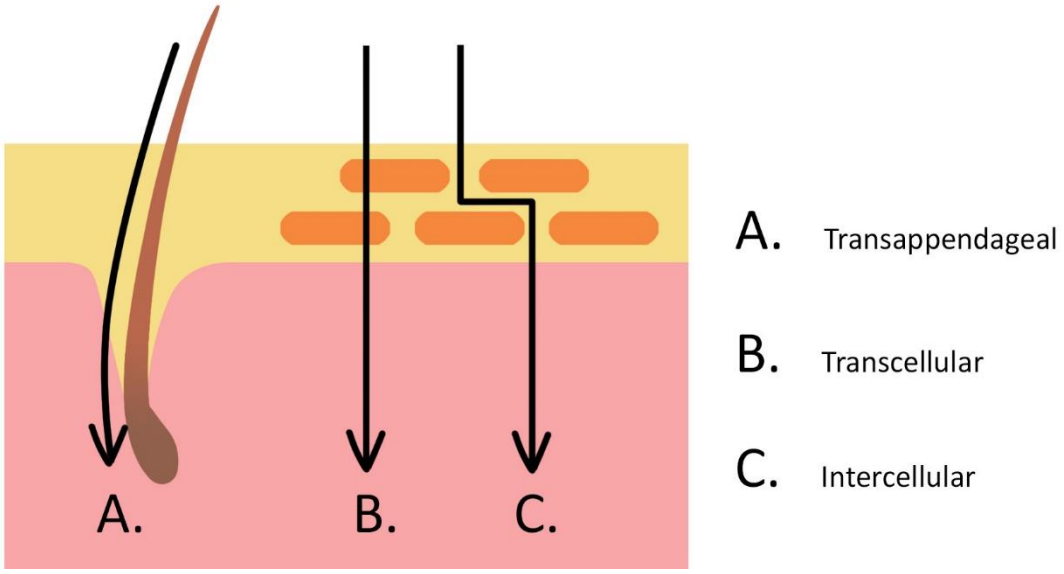

Figure 1.4. Routes of penetration through skin.

The intercellular route of permeation is preferred for compounds which exhibit lipophilic properties, because diffusion occurs through the continuous (yet tortuous) lipid matrix (Elias and Friend 1975, Elias 1983). Although tortuous in length, this route avoids the hydrophilic corneocytes and therefore is preferable for the minimal number of partitioning steps compared to the route traversed by compounds which exhibit hydrophilic properties. Hydrophilic molecules prefer the transcellular route, as partitioning occurs through the aqueous corneocytes. However, permeation via this route also involves repeated partitioning between the corneocytes across the lipid corneocyte cell envelope into the lipid phase of the *stratum corneum.* It is possible for hydrophilic molecules to use the thin layer of water between polar head groups of the lipid lamellae to diffuse through the *stratum corneum* barrier to minimise diffusion through the lipid moieties (Roberts *et al.* 1995).

The transappendageal route is described as a transdermal delivery route across skin appendages - hair follicles, sweat and sebaceous glands. This route is largely cited as providing a delivery route for large polar molecules that cross the intact *stratum corneum* with difficulty (Barry 2002b). However, as is clear in Figure 1.1 and Figure 1.4, the *stratum corneum* and epidermal

layers extend into follicular invaginations (Knorr *et al.* 2009), therefore polar molecules attempting to diffuse via this route must also contend with the lipophilic regions of the epidermis extending into the appendage. Thus, the popular cited surface area of appendages (0.1% [Schaefer and Redelmeier, 1996; Otberg *et al.* 2004b]) that is often used to discard the route as a viable route of drug delivery may also be consdiered inaccurate. Furthermore, appendageal structures are generally lined with cornified cells and so diffusion from the follicle into the dermis is still subject to the same barrier layer as is present on the skin surface. Nonetheless, this route continues to be explored, particularly for the delivery of drug-encapsulated particles (e.g. niosomes, liposomes) which may aggregate within follicular openings (Mura *et al.* 2007, Patzelt *et al.* 2011, Venuganti *et al.* 2011, Patzelt and Lademann 2013). There is potential for drugs to act as depots within appendages as permeation within this area is not subject to desquamation like bulk skin (Weigmann *et al.* 2001). Of particular interest is the bulge region of the hair follicle (in the outer root sheath, near the arrector pili muscle) which is understood to contain keratinocyte stem cells (Ohyama *et al.* 2006) and has been investigated as a site for hair follicle regeneration in patients with alopecia (Stenn and Cotsarelis 2005).

Immunisation via the follicular route has also been investigated. For example, Baleeiro *et al.* (2013) developed a microparticle-based topical vaccine, 1 µm SiO_2 particles consisting of an influenza matrix peptide. After 24 hours, an average penetration depth of 259.1 ± 92.7 µm was found for the particles and 631.2 ± 182.4 µm for the peptide. The difference in depth detection was attributed to the change in pH with increasing depth, triggering peptide release. Mittal *et al.* (2013) delivered polymeric nanoparticles containing ovalbumin (183.6 ± 2.71 nm) into porcine hair follicles. Encapsulation of ovalbumin into nanoparticles significantly enhanced follicular uptake of ovalbumin by a factor of 2-3 compared to ovalbumin solution. Penetration enhancement of the nanoparticles was able to stimulate efficiently murine dendritic cells and subsequently antigen-specific CD4+ and CD8+ T-cells for an improved immune response.

When a drug is applied to the skin, it is clear that the diffusion pathway into and across skin is not straightforward, with numerous partitioning steps and the potential for drug binding to protein and lipid structures (Walter and Kurz 1988), reducing the bioavailability of the topically applied compound. Where dermal delivery is a priority, the homogeneity of drug permeation across the intended skin site is a concern, as a lack of homogeneity may result in delivery of sub-therapeutic levels of drug to the intended site, which may in turn have consequences for the efficacy of the drug. Studies which have measured the lateral diffusion of a drug in conjunction with skin penetration are few (Johnson *et al.* 1996, 1997, Jacobi *et al.* 2004, Schicksnus and Müller-Goymann 2004, Gee *et al.* 2012). These studies appear to show that the extent of horizontal diffusion is dependent on log P, with hydrophilic drugs more likely to spread laterally than hydrophobic drugs (Gee *et al.* 2012). Formulation excipients have also been understood to contribute towards the extent of lateral diffusion; Gee *et al.* (2014) found ibuprofen was more likely to diffuse laterally when applied in an octisalate vehicle than a propylene glycol (PG) vehicle. Raufast and Mavon (2006) confirmed that the preferred route of linoleic acid permeation was via the transfollicular route using microautoradiography. More recently, techniques such as Fourier-transform infrared spectroscopy (FTIR) and Confocal Laser Scanning Microscopy (CLSM) have been used to image lateral drug diffusion (Zhang *et al.* 2014, Nguyen *et al.* 2018).

1.4 Physicochemical properties which affect percutaneous absorption

The permeation of a molecule cannot be predicted successfully without an understanding of the physicochemical factors which can affect and define percutaneous absorption (Guy and Hadgraft 1987). It is clear from Section 1.3 that an understanding of the permeant's properties is required to understand how it will traverse into and through the various skin structures. It should be emphasised that the physicochemical properties which are desirable for topical and transdermal drug delivery do not necessarily mean that permeants with properties outside the "ideal" parameters (Naik *et al.* 2000) cannot be delivered topically or transdermally, but other strategies may be required to assist percutaneous penetration (explored further in Section 1.11). Similarly, a single parameter within the "ideal" range does not necessarily make the candidate ideal for topical and transdermal drug delivery, hence all parameters and their influence should be considered simultaneously.

1.4.1.1 Partition Coefficient

The partition coefficient is a measure of the distribution of molecules between two phases such as water and octanol, often described as log P. A log P between 1-3 is described as the ideal range for topical and transdermal drug delivery (Naik *et al.* 2000) and this figure can be used to predict the route of permeation into and through the skin (i.e. transcellular, intercellular or transappendageal). Simplistically, hydrophilic molecules will interact preferentially with hydrated corneocytes and lipophilic molecules will interact preferentially with lipid bilayers. The most favourable diffusion pathway through the *stratum corneum* is through the continuous lipid bilayers (intercellular route), as this reduces the number of partition steps required to be undertaken by the penetrant. Because of this, lipid solubility is conducive to percutaneous

absorption (Williams 2003b). However, drugs which are delivered via the transdermal route require both hydrophilic and lipophilic domains in order to transverse the highly lipidic *stratum corneum* as well as partition through the aqueous dermis into the systemic circulation. If a drug is highly lipophilic (log P >3), it is likely to be retained within the lipid layers of the *stratum corneum* without further depth permeation into deeper, hydrophilic skin tissues such as the dermis. If a drug is highly hydrophilic (log P <1), the drug is unlikely to partition into the *stratum corneum* at a concentration required for efficacious effects without assistance from permeation enhancers. Ultimately, a balance is required for optimal drug partitioning into and across skin (Benson 2012).

1.4.1.2 Molecular weight

The molecular weight of the permeant is understood to influence the ability of the permeant to diffuse into and across the *stratum corneum* (Bunge and Cleek 1995, Potts and Guy 1995, Pugh *et al.* 1996). Molecules with a molecular weight of <500 g/mol are known to be better able to permeate into the *stratum corneum* (Crank 1975, Bos and Meinardi 2000) than those above this threshold as smaller molecules are able to diffuse faster than larger molecules, and are better able to diffuse between the tightly packed, orthorhombic packed lipid bilayers.

1.4.1.3 Applied Concentration

It is generally understood that increasing the applied concentration of drug increases the amount of drug absorbed across the skin (Maibach and Feldmann 1969, Barry 1983) in accordance with Fick's Law (Equation 1). Increasing the surface area for topical absorption has also been shown to increase the amount of drug absorbed across skin (Crank 1975, Wester and Noonan 1980). Increasing the concentration of drug available in a formulation decreases the

amount of formulation required for skin application to provide an efficacious effect, which is an important practical consideration, though not necessarily cost effective.

1.4.1.4 Solubility and melting point

The aqueous solubility, alongside the partition coefficient, greatly influences the penetration of a molecule into skin. A drug must be sufficiently soluble in the vehicle applied to the skin to form a reasonable concentration gradient to direct flux into the skin (Ostrenga *et al.* 1971). If a drug is not sufficiently soluble in the vehicle, it may permeate away from the vehicle and onto the skin, but without sufficient concentration to create a suitable concentration gradient needed for diffusion into the systemic circulation. For example, if a lipophilic drug is delivered from an aqueous vehicle, it is unlikely to be present at saturated concentration and thus the concentration will only diminish as diffusion progresses. The drug may readily permeate into the lipophilic *stratum corneum* due to its partition coefficient, however once the drug partitions across the dermal-epidermal junction, there is a depleted concentration, coupled with the hydrophilic environment of the dermis, which is likely to limit systemic uptake of the drug.

There is generally an inverse relationship between solubility and melting point of a chemical – penetrants with high aqueous solubilities are more likely to have low melting points and vice versa. A high melting point indicates that intermolecular forces between molecules are strong, as a large amount of energy is required to break the bonds. Therefore, the addition of a solvent is unlikely to be able to break these intermolecular bonds. Thus, solubility of the drug is likely to be low. However, most melting points are not recorded with sufficient accuracy to be used as a single parameter for predicting percutaneous penetration, and often a melting point range is given for a specific drug rather than a definitive value (Jorgensen and Duffy 2002, Delaney 2005).

1.4.1.5 Ionisation state

The pH partition hypothesis is applicable to drug delivery into and across skin. As the *stratum corneum* is highly lipophilic, the unionised form of a drug is more likely to permeate (Shore *et al.* 1957). Lipophilic structures are understood to act as barriers to ionised species, however ionised species may pass through pores (Shore *et al.* 1957, Swarbrick *et al.* 1984), therefore permeation via the transappendageal route may be possible by ionised drugs. However one must consider the limitations of the transappendageal route described in Section 1.3, namely the fact that appendages cover 0.1% of the skin surface area (Schaefer and Redelmeier, 1996; Otberg *et al.* 2004b). Ionisation does not always prevent permeation into and through skin (Swarbrick *et al.* 1984, Obata *et al.* 1993). The drugs pK_a and the environmental pH should be considered alongside the other physicochemical parameters discussed when investigating percutaneous penetration, as alteration of these paramaters will change the ratio of unionised:ionised form of the drug, therefore altering the rate of drug penetration (Siddiqui *et al.* 1985, Neubert 1989, Valenta *et al.* 2000, Moss 2015).

1.5 Fick's Laws of diffusion

Fick's First and Second Laws are often used to explain and predict how a molecule may diffuse across the skin. Diffusion is defined as "movement of molecules through a domain, from high concentration to low concentration, by random molecular movement" (Williams 2003b). Diffusion across the *stratum corneum* relies on a passive method and is influenced by the physicochemical properties of the permeant and the nature of the membrane. Thus, application of compounds that change the nature of the membrane will also change the rate of diffusion. The epidermis, dermis and subcutis all have their own diffusion coefficient, but all layers other

than the *stratum corneum* are generally treated as one as their function as a barrier is considered negligible.

Flux (J) is defined as the amount of material diffusing through a unit area per unit time (e.g. μg/cm^2/hr) and is commonly used as a measurement of permeation through skin (Crank 1975).

$$J = -D \frac{\delta c}{\delta x} \quad \textbf{(1)}$$

Where

D is the diffusion coefficient

$\frac{\delta c}{\delta x}$ is the concentration gradient

The diffusion coefficient is expressed negatively as this reflects that flux is in the direction of decreasing concentration (Florence and Attwood 2006a). Fick's First Law indicates that increasing the concentration gradient increases flux, as discussed in Section 1.4.1.3, and the law assumes steady state conditions. However, topical application of a drug, unless applied as an infinite dose, will deplete over time as diffusion occurs. Thus, Fick's Second Law considers the change in concentration of the applied permeant over time

$$\frac{\boldsymbol{\delta M}}{\boldsymbol{\delta t}} = \frac{\boldsymbol{DC_O}}{\boldsymbol{h}} \quad \textbf{(2)}$$

Where

$\frac{\delta M}{\delta t}$ is the mass "M" of permeant that diffuses through the membrane per unit area in time "t"

C_o is the concentration of the permeant at layer "0", the first layer of skin

"h" is the thickness of the membrane

From Equations 1 and 2, it can be assumed that to increase flux, one must either increase the diffusion coefficient (increasing diffusivity), increase partitioning into the skin, increase the concentration of the drug applied to the skin, or decrease the thickness of the membrane. Increasing diffusivity and partitioning is due to interactions between the vehicle and skin, whereas increasing drug concentration in the vehicle is due to interactions between the drug and vehicle (Moser *et al.* 2001). Membrane thickness may be altered by application of the formulation to a thinner skin site; however this is not always practical. Where the drug is saturated in the vehicle, flux is predicted to be equal, presuming the vehicle does not interact with the barrier in any respect (Higuchi 1960). However, topical application of a vehicle is highly likely to exert an effect on the membrane. Even simple vehicles such as water have shown evidence of permeation enhancement effects (Behl *et al.* 1980, Roberts and Walker 1993, Williams and Barry 2012), altering the membrane and in doing so enhancing passive diffusion into the skin.

Fick's Laws make several assumptions in order to maintain their simplicity. In addition to the assumptions provided above (*stratum corneum* is considered the "main" barrier and is not altered by vehicle application), the laws also assume that permeation via the transappendageal route is minimal, the diffusion coefficient is independent of concentration, time or distance, diffusion occurs through a homogeneous membrane, and that diffusion is unidirectional (Williams 2003b). These assumptions may not be considered accurate if, for example, a highly lipophilic molecule is applied to the skin or the vehicle changes the nature of the skin barrier. *In vitro* and *in vivo* experiments quantify topical and transdermal permeation of the specific formulation applied to the skin.

1.6 Thermodynamic activity

Fick's laws place a large focus upon the role of concentration in the ability of a permeant to diffuse across the skin. As is clear from Equations 1 and 2, Fick's laws state that increasing the concentration of a permeant increases flux. However, Fick's laws do not take into account interactions between the permeating molecules and the surrounding medium, which is imperative when considering how a molecule may transfer from an applied vehicle into the *stratum corneum*. Nor does it take into account how that same molecule may diffuse from the *stratum corneum* into the deeper structures, either for localised delivery or for uptake into the systemic circulation via the dermal microcirculation. The first instance, diffusion out of the vehicle into the skin, is dependent on a thermodynamic equilibrium. Diffusion across the *stratum corneum* into deeper structures is dependent on a thermodynamic gradient (Pugh and Chilcott 2008).

The *stratum corneum* is comprised of both hydrophilic and lipophilic domains (Figure 1.2), though it is considered primarily as a lipophilic layer. Therefore, in the context of skin permeation, it is important to consider that the partition coefficient will affect the thermodynamic gradient and thus permeant diffusion across the *stratum corneum* into the skin layers below. This is discussed further in Section 1.4.1.1, but can be described by the term fugacity, i.e. the tendency of a molecule to leave a particular environment. For example, a lipophilic molecule in an aqueous vehicle with display a greater fugacity than a hydrophilic molecule when it is brought into contact with the lipophilic environment of the *stratum corneum* (Pugh and Chilcott 2008). This tendency to partition away from one environment to another is not considered by either of Fick's laws and therefore should be used with the understanding that several assumptions are made to maintain the simplicity of the equations.

The importance of the relevance of thermodynamics is clearly illustrated when applying Higuchi's principle (Section 1.5). The saturated concentration of a lipophilic permeant dissolved in a lipophilic vehicle is likely to be greater than the saturated concentration of the same permeant dissolved in an aqueous vehicle. Thus, if the principles of concentration were applied, one would assume that flux would be greatest from the lipophilic vehicle, as the concentration of permeant in this vehicle is greatest. However, as the permeant is saturated in both vehicles, thermodynamic activity, therefore flux, is equal. This clearly illustrates the need to consider thermodynamic activity for skin permeation, rather than solely relying on concentration gradient, as is apparent from Fick's laws of diffusion.

1.7 *In vitro* permeation studies

Diffusion cell studies are the most common method of measuring the permeation of an externally applied product through the skin. The most widely used diffusion cell type in modern literature is described by Franz (1975), though diffusion cells have existed since the 1940s (Pendlington 2008). Diffusion cell studies are specifically requested to measure *in vitro* diffusion by the Organisation for Economic Cooperation and Development (OECD 2004a). The simple apparatus and method can be used on a large scale to rapidly provide information on the initial delivery of drugs within a specific experimental formulation across skin. This method is a fast and reproducible way of assessing the permeation of topically applied compounds, particularly where their safety *in vivo* cannot yet be assured and when formulations require development before testing *in vivo*.

A model membrane is mounted between a glass donor phase and receptor phase. Formulation is placed in the donor phase and at specific time points, receptor phase samples are removed via the sampling arm and are analysed primarily using a chromatographic technique. Plotting

drug concentration as a function of time creates a permeation profile. Experiments typically last 24 hr as this allows adequate characterisation of the permeation profile (OECD 2004a). Diffusion cell apparatus is versatile – the size of the receptor compartment can be changed where appropriate to ensure the permeant is detectable using analytical equipment with ease, and the donor chamber can be covered to mimic occluded conditions.

Several types of diffusion cells are available for use in *in vitro* testing of chemical absorption. The most common types are illustrated in Figure 1.5.

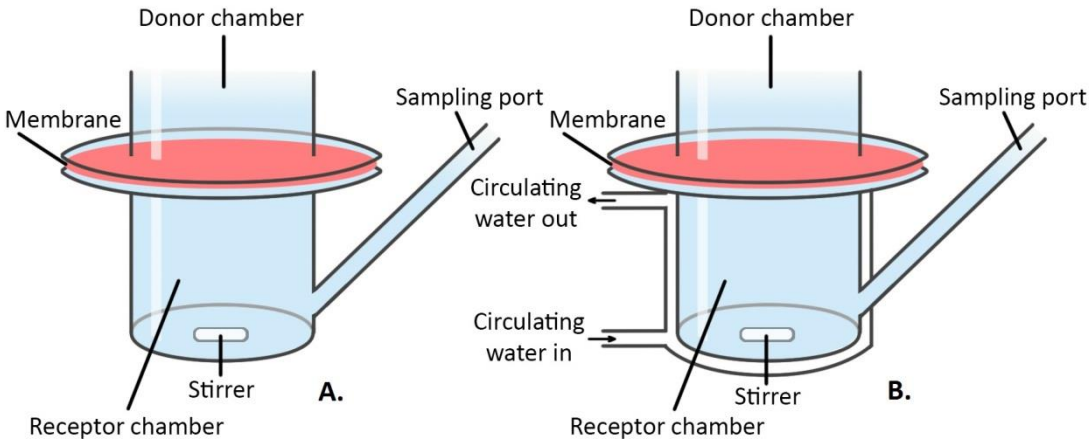

Figure 1.5. Franz type diffusion cell apparatus. Type A is a typical "static" diffusion cell, type B is jacketed for temperature control.

Static, upright cells are typically used and are the type of cell employed throughout this thesis. Horizontal "side-by-side" cells are also available, but for topical and transdermal delivery, vertical cells are preferred. "Flow though" cells mimic systemic blood supply by providing a continuous flow of receptor fluid, rather than static cells that rely on the need for the researcher to manually remove and replace receptor fluid over the course of the experiment. Despite this advantage, static cells are often preferred as flow through cells must be interconnected, thus improper experimental setup would affect the entire batch of cells.

Ex vivo human skin is obviously the best model for determining the permeation profile of drugs intended for delivery in humans (Bronaugh *et al.* 1986). However, the difficulties associated with obtaining human skin, variability between samples and the large numbers of studies required to assess and develop formulations for topical and transdermal drug delivery mean that animal models are often used as a viable alternative. Generally, rodent skin is deemed unsuitable as a human skin surrogate, as rodent skin is thinner than human skin with a large variation in hair follicle density and this generally results in an overestimation of drug permeability (Bond and Barry, 1988a; Bond and Barry, 1988b; Barbero and Frasch, 2009). Furthermore, rodent skin has a muscular layer, the *panniculus carnosus* that human skin does not. Snake skin has been utilised as a human skin surrogate because the ability of snakes to shed their skin means that the animal does not need to be sacrificed (Megrab *et al.* 1995a). However, shed snake skin differs in structure to human skin in terms of lipid composition and the "hinge-and-scale" structure which increases flexibility of the structure as the snake moves (Williams 2003c). Porcine skin is considered to be the most viable alternative to human skin due to the similarities in total and individual skin thickness (Jung and Maibach 2015), epidermal lipids (Gray and Yardley 1975), follicular distribution and density (Bronaugh *et al.* 1982), and permeability properties (Simon and Maibach 2000, Jacobi *et al.* 2007, Barbero and Frasch 2009). Furthermore, Barbero and Frasch (2009) reported a low intra-species variation in porcine skin samples compared to human skin.

OECD (2004a) suggests that either full thickness or split thickness membranes may be considered for use in *in vitro* diffusion cell experiments. Split thickness skin is usually produced by using a dermatome which is able to produce skin sections of reproducible thickness. As the *stratum corneum* barrier is considered to be the main barrier to penetration into and through human skin, the use of epidermal membranes without the underlying tissue is considered acceptable. However, a later study (Heard and Screen 2008) has questioned the accuracy of

using split thickness skin, finding that the permeation of mefenamic acid was different when comparing full thickness skin, heat separated epidermis and heat separated dermis, questioning the relative accuracy of utilising split-thickness skin as a model for human skin.

The integrity of a suitable skin sample should be tested prior to commencing diffusion cell studies to remove any damaged skin from the batch which may skew permeation profile results. OECD (2004a) recommends using transepithelial electrical resistance (TEER), transepidermal water loss (TEWL) or tritiated water flux (TWF) to measure barrier integrity. TEWL and TEER are quick, convenient methods of measuring the barrier integrity of the skin (Wilson and Maibach 1989, Levin and Maibach 2005, Srinivasan *et al.* 2015) as opposed to TWF, which requires measurement of tritiated water permeation and thus is more time consuming.

Further considerations for diffusion cell studies include the receptor fluid, temperature, finite vs infinite dosing and duration of the experiment (OECD 2004a). The permeant must be sufficiently soluble in the receptor phase and ideally sink conditions should be maintained as to not diminish the concentration gradient, the driving force for drug permeation into the skin. Sink conditions are maintained as long as the concentration of the drug in receptor phase does not exceed 10% of its saturated solubility (Ng *et al.* 2010). Typically, saline solutions with a pH of approximately 7.4 are used for water soluble drugs, as this mimics physiological conditions. Organic solvents must be used in the receptor phase for lipophilic compounds to ensure their solubility; however this may compromise the skin barrier and so must be used with the understanding that permeation may be overestimated (OECD 2004a). In static diffusion cells, agitation of the receptor fluid using a magnetic stirrer bead prevents accumulation of the concentration gradient over the course of the experiment (Ng *et al.* 2010).

The temperature of the apparatus is typically 37 ^{o}C, this gives a skin surface temperature of 32 ^{o}C ± 1 ^{o}C which is reflective of physiological conditions and is acheived via placing the cell in a water

bath or by encasing the cell in a jacket through which water flows (OECD 2004a, Schaefer *et al.* 2008; Figure 1.5B).

The OECD guidelines (2004a) state that the quantity of formulation applied should be justified by the expected use conditions. For example, the formulation applied should typically replicate "in use" conditions in terms of dose applied and duration of exposure, however infinite dosing may be appropriate in cases such as where toxicity information is required, or where large volumes of formulation are expected to be used. Although finite dosing aims to replicate "real life" use of products, the donor chamber in diffusion cell experiments is often small and may not be considered representative of the actual skin area intended for formulation application. Furthermore, application of a finite dose may make detection by HPLC difficult, due to the low doses applied and analytical quantification limits (Selzer *et al.* 2013). Particularly where permeation through skin is understood to be poor, infinite doses may be required to reach the limits of HPLC detection. This issue may be overcome with the addition of radiolabels (Van De Sandt *et al.* 2004).

Where knowledge of the permeation into (rather than across) skin is required, for example, for drugs intended to be delivered topically, and for calculating drug recovery, it is necessary to quantify dermal absorption into the skin. There are several methods utilised to measure dermal absorption of topically applied compounds, such as vasoactive assays, skin biopsies and tape stripping. Non-invasive techniques may also be used. Vasoactive assays using skin blanching are well established (Montenegro *et al.* 1996, Haigh *et al.* 1997), but are limited to investigating permeants which act on the vasculature (Williams 2003c). Several types of biopsies are available - punch biopsies allow drug permeation to be detected within the *stratum corneum,* viable epidermis, dermis and subcutaneous fat; shave biopsies allow detection of permeant within the *stratum corneum*, viable epidermis and some dermal tissue; and suction blisters may be used to

detect permeant within the *stratum corneum* and viable epidermis (Surber *et al.* 1993; Williams, 2003c). Biopsies are invasive and require specialist training to complete successfully.

The most popular technique used to determine dermal deposition of permeants is tape stripping. Tape stripping is the "gold standard" technique for determining the penetration of exogenous chemicals into the skin (Kezic 2008, Ho *et al.* 2016). The procedure is a robust, minimally invasive and simple way of quantifying drug permeation into the skin that uses adhesive tape to sequentially remove layers of skin cells. Complete *stratum corneum* removal is apparent when the skin appears shiny which indicates the presence of interstitial fluid from viable epidermal layers (Lavrijsen *et al.* 1994). Drug is then extracted from the tape and analysed to provide the concentration of drug on the specific tape strip. As differing amounts of *stratum corneum* material can be removed from each tape, the concentration of drug on each tape should be normalised to the mass of *stratum corneum* removed from the skin sample (Reddy *et al.* 2002, Jacobi *et al.* 2005).

The number and depth of corneocytes removed from a sample may be influenced by numerous parameters, such as site of application (Machado *et al.* 2010), vehicle (Jacobi *et al.* 2003, Lademann *et al.* 2009), adhesive strength (Jui-Chen *et al.* 1991), presence of sebum and interstitial fluid (Weigmann *et al.* 1999) and velocity of tape removal (Loffler, Dreher and Maibach, 2004). In order to more accurately quantify the amount of drug in each tape strip, the drug concentration on each tape strip can be adjusted to account for the weight of *stratum corneum* removed (Reddy *et al.* 2002), but this method assumes that the same tape strip number removes corneocytes of equal depth between skin samples.

Although the technique is simple and quick to use without the requirement of complex apparatus and provides quantitative data, the limitations of the technique do not allow specific depth permeation measurements of drug within skin, as is a requisite for determining the depth

permeation of drugs for topical use. Drug-skin deposition imaging techniques have been utilised as an alternative to this technique, which are able to map the distribution of topically applied drugs.

1.8 Drug-skin deposition imaging techniques

Several imaging techniques are currently available which can map the distribution of exogenous chemicals. CLSM is routinely used for imaging fluorescently labelled biological samples (Rajadhyaksha *et al.* 1995; Alvarez-Román *et al.* 2004) and has been used to image carboxyfluorescein separation from liposomes (Verma *et al.* 2003), bacitracin enhancement from ethosomes (Godin and Touitou 2004) and nanoparticles (Campbell *et al.* 2012, Zhang and Monteiro-Riviere 2012). However, compounds must either auto-fluoresce or be fluorescently labelled for CLSM imaging, limiting the number of compounds which can be imaged. Furthermore, labelling drugs using fluorescent tags will impact the physicochemical parameters of the drug, which in turn will affect the deposition and localisation within skin. Specific tissues within skin naturally fluoresce, and whilst this has been useful to understand natural effects on skin such as ageing and skin disease (Kollias *et al.* 1998, González *et al.* 2000), this has the potential to overwhelm any fluorescence exhibited by the drug whose deposition is being mapped.

Autoradiography is a technique that allows visualisation of a radiolabelled material within histological compartments of skin (Fabin and Touitou 1991, Solon *et al*. 2010). It may be applied in conjunction with quantitative methods to allow production of quantitative datasets in each histological compartment targeted (Gupta and Trivedi 2018). This technique allows radiolabelled drug to be visualised throughout the entirety of skin tissue, therefore localisation

of drug within specific compartments, such as hair follicles, is possible. The disadvantages associated with this technique include the cost and small amounts of radiolabels available, which may be technically challenging. Furthermore, the position of the label needs careful consideration – if a drug is likely to be metabolised in skin, the radiolabel may be attached to the parent molecule and thus detection of the metabolite via autoradiography would not be possible. Finally, radiolabels may only be used under licence in specific areas with stringent safety processes in place (Pendlington 2008).

Infrared (IR) and Raman are two types of non-destructive, vibrational spectroscopy techniques which have gained popularity for imaging deposition within skin, for example liposomes, dimethyl sulfoxide (DMSO) and sodium dodecyl sulfate (SDS) (Mendelsohn *et al.* 2006, Mao *et al.* 2012). Neither technique requires drugs to be fluorescently labelled and therefore is more advantageous than CLSM. IR microscopy provides detailed molecular information, with an entire spectrum for each pixel of the sample analysed and has a high sensitivity (Mendelsohn *et al.* 2006). However, IR has a poor spatial resolution of 5-10 µm and the high water content in corneocyte cells is likely to produce a broad IR peak, potentially obscuring other essential IR peaks indicative of the compound of interest.

In contrast, Raman has a much lower spatial resolution of <1 µm and does not suffer from signal interference by water. Raman has been utilised in the field of topical skin penetration enhancement to image the depth permeation of SDS (Mao *et al.* 2012) as well as its interactions with human *stratum corneum* (Anigbogu *et al.* 1995), UV absorbers from sunscreens (Adlhart and Baschong 2011), flufenamic acid (Pyatski *et al.* 2016), hyaluronic acid (Essendoubi *et al.* 2016) and ketoprofen and ibuprofen (Saar *et al.* 2011). Six key disadvantages of Raman imaging are provided by Smith *et al.* (2015). Those which are most important to consider for pharmaceutical applications are a lack of Raman signal produced by the permeating drug and skin fluorescence which may obscure a Raman signal.

Matrix assisted laser desorption ioninsation (MALDI) is an ionisation technique which has been used to image the depth profile of various pharmaceuticals (Bunch *et al.* 2004, Enthaler *et al.* 2012, Sørensen *et al.* 2017, Bonnel *et al.* 2018). The technique involves mixing the sample of interest with a suitable matrix. The sample-matrix mixture is crystallised in a vacuum, then irradiated using a short laser pulse to produce gaseous ions. MALDI is typically combined with mass spectrometry (i.e. MALDI-ToF), to separate ions according to their m/z ratio. A matrix is required to adsorb energy from the applied laser, which is then transferred to the sample, resulting in ionisation of the sample. The matrix additionally serves to prevent aggregation of the analyte molecules (Karas and Hillenkamp 1988). Thus, the matrix is specific to the analyte and must be able to transfer energy from the laser pulse to the analyte. The advantages of MALDI-ToF include a high mass detection and high spatial resolution (Benabdellah *et al.* 2010, Zavalin *et al.* 2015). As a result, large endogenous skin components such as protein and peptides can be characterised (Hart *et al.* 2011, Enthaler *et al.* 2013, Mess *et al.* 2013). However, matrix ions may impede the appearance of smaller ions, thus applications for this type of analysis may be somewhat limited.

1.8.1 Time of Flight Secondary Ion Mass Spectrometry (ToF-SIMS)

ToF-SIMS is an analytical technique which can simultaneously provide a mass spectrum of the sample and images of a high spatial resolution (<1 µm; [Bich, Touboul and Brunelle, 2015]) without the need for matrix deposition prior to sample analysis (Sjövall *et al.* 2018). Furthermore, the technique has a wide mass range, an additional improvement on the MALDI technique; and all secondary ions of the same polarity can be identified simultaneously with the ability to detect secondary ions retrospectively. Therefore, the spatial distribution of drugs can be detected alongside native skin components to provide information on the depth permeation

of a drug and how it may diffuse through the *stratum corneum* barrier. Other advantages of ToF-SIMS include minimal sample preparation, a lower limit of detection than HPLC thereby allowing for individual tape strip analysis from deeper skin layers, decreased sample contamination, high mass resolution (>10,000) and overlay of several ions of interest allowing a chemical distribution map to be created (Belu *et al.* 2003). Where the mechanism of action of a drug or permeation enhancer is not fully understood, the identification of a unique fragment indicative of the permeation enhancer may aid in the elucidation of its mechanism of action. There are many potential applications of ToF-SIMS which are still in their infancy.

ToF-SIMS uses a high energy, pulsed primary ion beam to bombard a sample surface *in vacuo*. This causes a collision cascade, resulting in liberation of "secondary" particles from the sample surface (~1 nm; [Amstalden van Hove, Smith and Heeren, 2010]). The secondary ions may contain whole molecules, molecular fragments or atoms, and occur due to processes such as fragmentation, gaining of protons, loss of protons or less frequently due to molecular re-arrangement. Fragments will be in the positive or negative polarity depending on the ionisation efficiencies (Grams *et al.* 2007). These liberated secondary particles are then accelerated into the drift field of a time-of-flight analyser, and are separated according to their mass to charge (m/z) ratio. This produces an individual mass spectrum for each region analysed and associated images, providing information on the chemical composition and distribution of a sample (Sodhi 2004). The charge build-up caused by discharge of charged ions requires neutralisation, which is undertaken by an electron flood gun following sample analysis.

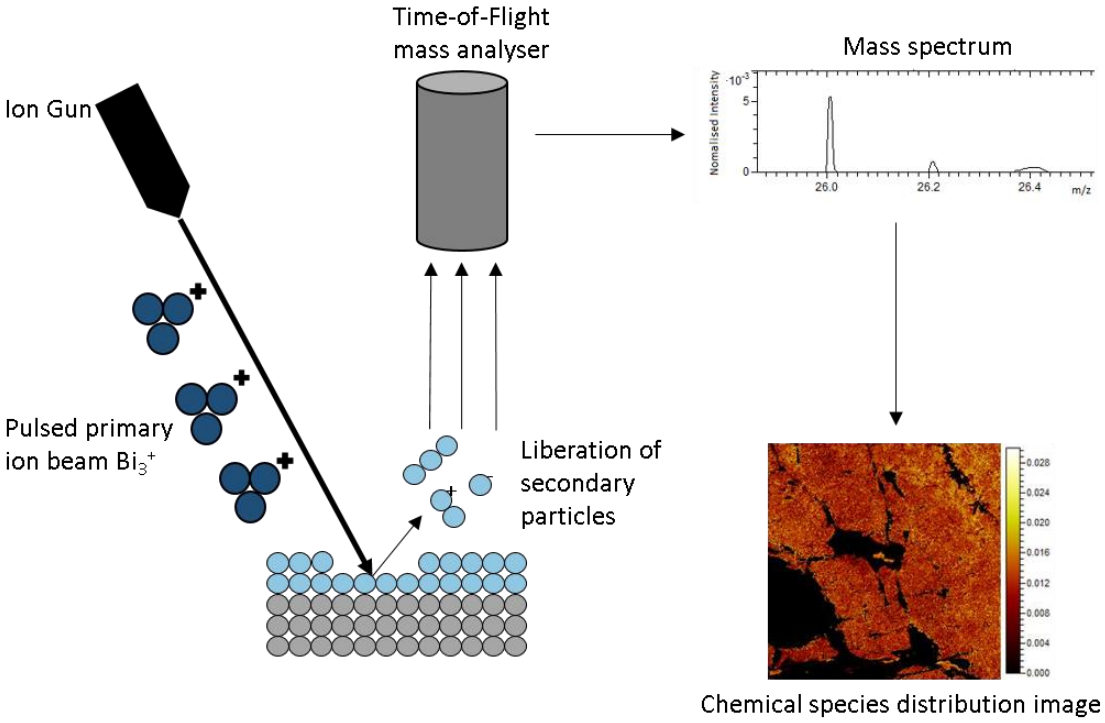

Figure 1.6. Schematic of the ToF-SIMS analysis of a porcine tape strip by ToF-SIMS.

Limitations of the ToF-SIMS technique include its inability to provide fully quantitative data due to matrix effects. The matrix is defined as the components of the sample, other than the ion of interest, and matrix effects are those effects caused by all other components of the sample, except for the specific compound to be quantified (Gilmore and Seah 2002, Sodhi 2004). Within this thesis, the compound of interest is the CHG ion ($C_7H_4N_2Cl^-$), and the surrounding matrix is the porcine skin to which the CHG formulation is applied. As the process of ionisation of CHG occurs close to the emission of particles from the skin surface, ionisation efficiency (of the CHG ion in this instance) will depend on interactions with the surrounding skin, resulting in a variation of both ion formation and yield. Skin is not a homogeneous structure, therefore liberation of secondary ions from the sample surface is greatly affected by species in the surrounding sample (Jones *et al.* 2007). Ultra-high vacuum conditions must be maintained throughout sample analysis to allow the ion beam to operate consistently, to avoid ion collision with gas phase molecules and to reduce the chance of sample contamination (Vickerman 2009). The use of a

vacuum is unsuitable if samples are to be analysed in real time and thus this limits the sample types available for analysis. The use of cryo-preparation of samples prior to ToF-SIMS analysis has increased in popularity with a view of retaining features of a solid-liquid interface in biological samples (Piwowar *et al.* 2011).

ToF-SIMS has been utilised to view native skin components, particularly the lipids which are thought to make up the majority of the skins barrier function (Lu *et al.* 2011, Bich *et al.* 2014). Many studies have also identified the differences between healthy (Nygren *et al.* 2004, 2005, Starr *et al.* 2016) and diseased (Touboul *et al.* 2007, Sjövall *et al.* 2008, Lazar *et al.* 2013) tissue.

Studies that utilise ToF-SIMS to image drug deposition within skin are currently few. Sjövall *et al.* (2014) utilised ToF-SIMS alongside scanning electron microscopy (SEM) to image the distribution of roflumilast, tofacitinib and ruxolitinib within mouse ear skin. Whilst the use of mouse skin should be criticised due to the lack of similarities with human skin (Wester and Maibach 1993), the use of SEM aided in identification of the different skin layers so the depth permeation of the drug could not be overestimated. The distribution of fatty acids acting as permeation enhancers into human skin was mapped by Kezutyte *et al.* (2013). When treating the skin with a 10% fatty acid solution, oleic and lauric acids were found to exhibit the greatest skin penetration depth, with lauric acid appearing to accumulate within the dermis. ToF-SIMS 3D chemical profiling as a method of visualising vitamin C permeation into porcine skin from supramolecular hydrogels was investigated by Starr *et al.* (2019). The use of 3D chemical profiling in this instance allowed accurate visualisation of drug on each individual skin layer laterally and as a function of depth. Significant permeation was visualised from a supramolecular gel formulation, and the breakdown of ascorbyl glucoside into ascorbic acid was also illustrated, which elucidated that the hydrogel formulation was able to prevent this conversion until the targeted epidermal layer was reached.

The permeation of a 2% w/v CHG solution into porcine skin has also been visualised using ToF-SIMS (Judd *et al.* 2013b). This study confirmed previous studies which have illustrated its poor permeation of CHG into the skin (Karpanen *et al.* 2008a), with ToF-SIMS images illustrating permeation into the upper *stratum corneum* only, with little permeation into deeper skin tissues. The study concluded that the poor CHG permeation may lead to an inefficient reduction of bacteria in the deeper skin strata, justifying the use of permeation enhancers or alternative topical antiseptics to provide a more comprehensive skin micro flora reduction below the *stratum corneum*. This thesis builds upon this study by utilising the CHG specific ion that the authors found to determine whether co-formulating CHG with a G3 PAMAM-NH_2 dendrimer is able to enhance CHG depth permeation within porcine skin for potential improved antisepsis effects.

In summary, the use of ToF-SIMS has been recognised as a useful technique for mapping the distribution of topically applied drugs to provide information of depth permeation and co-localisation with native skin components. The HPLC data will provide quantitative results, and the high sensitivity of ToF-SIMS allows CHG permeation into deeper skin layers to be better estimated. Furthermore, the production of ToF-SIMS images allows the spatial distribution of the drug to be viewed, which can be co-localised to endogenous skin components.

1.9 Skin infections and the rise of antibacterial resistance

In Section 1.2 the skin microbiome was described. Although bacteria reside on the skin surface which can exist symbiotically with the host, damage to the skin barrier may allow resident bacteria to become pathogenic and infect the site of impaired barrier function (Roth and James 1988, Grice *et al.* 2008). Typically, it is the host's own resident microbial flora that invades and causes infection (Dryden 2009). Physical damage to the barrier, such as a surgical site incision,

largely increases the risk of infection. Surgical site infections are defined as infections occurring up to 30 days after surgery, or up to one year after surgery in patients receiving implants (Hibbard *et al.* 2002, Crosby *et al.* 2009). The risk of developing a surgical site infection is further influenced by the wound type, microorganism and the strength of the patient's immune system (Fry 2006). They are a common post-operative complication, with 5% of patients developing one (NICE, 2019). Surgical site infections affect up to one third of patients following a surgical procedure and are the second most common cause of a healthcare associated infection in the UK and USA (WHO 2018a). Public Health England (2018b) reported a high incidence of obese patients being referred for surgery, and commented that if the level of obesity continues to rise, so too will conditions such as osteoarthritis and coronary heart disease, increasing the need for surgery and thus increasing the risk of skin and soft tissue infections (SSTIs; [Lamagni, Elgohari and Harrington, 2015; Thelwall *et al.* 2015]).

Surgical site infections have remained a major cause of poor outcomes for patients, increasing morbidity and mortality as well as increasing the financial burden of the healthcare provider, despite improvements in infection control (Kirkland *et al.* 1999, Mangram *et al.* 1999, Leaper *et al.* 2015, Badia *et al.* 2017).

The obvious strategy to combat skin infections is to use antibiotics. However, the rise of antibiotic resistance has significantly reduced the numbers of available drugs which are able to effectively combat infections. *Staphylococcus aureus* was initially highly susceptible to the majority of antibiotics available: in 1994, over 94% of *Staphylococcus aureus* strains were susceptible to penicillin (Livermore 2000), but an increase in the number of resistant strains has emerged over time, firstly in the hospital setting and eventually in the community. Reports of resistance occurred as early as 1961 (Jevons 1961) and in 2012, it was estimated that 70% of *Staphylococcus aureus* strains are resistant to methicillin (Stefani *et al.* 2012). Public Health England (2018a) reported that there were 12,784 cases of *Staphylococcus aureus* bacteraemia

in the year 2017/18, an increase of 3.7% compared to 2016/17 and a 29.4% increase from 2011/12, indicating the gradual rise of infections.

Two strategies to prevent the increasing rate of bacterial resistance are to create new efficacious and safe antibiotics, and to maximise the potential of current antibiotics and antimicrobials that have, to date, shown little evidence of resistance at present. Although technologies for identifying potential antibacterial chemical entities have vastly improved since the discovery of penicillin in 1928, a lack of return for antibiotic investments prevents pharmaceutical companies in assigning money to antibiotic drug discovery, preferring to place the money elsewhere for a higher chance of a safe investment return (Walsh 2000, Wenzel 2004). Numerous factors influence this lack of investment, for example pharmaceutical companies gain greater profits from drugs which are used to treat chronic conditions, rather than antibiotics, which should only be used short term and are often curative (Piddock 2012, Gould and Bal 2013). Health care professionals have also been advised against inappropriate and over-use of antibiotics in recent years in an attempt to combat the antibiotic resistance crisis, only using the newer drugs as a last effort to combat infection where all previous drugs fail (Piddock 2012). Resistance to new antibiotic drugs is almost inevitable, although it is not easy to predict when, consequently pharmaceutical companies may find a sudden and premature lack of return once signs of antibiotic resistance appear (Ventola 2015).

The second option is to maximise the efficacy of antibacterials that are already established, and have shown few patterns of resistance. This pool of drugs is also small; however enhancing the efficacy of drugs that are widely used is likely to take less time than creating a new antimicrobial entity. Furthermore, capitalising on recognised antimicrobials prevents the use of “end of line” drugs that can only be used where all other strategies fail, with no further treatment available if resistance patterns emerge. Improving the efficacy of current antimicrobials may hold off the

looming “antibiotic crisis” which is one of the biggest threats to global health according to the World Health Organisation (WHO 2018b).

1.10 Chlorhexidine (CHX) and chlorhexidine digluconate (CHG)

Chlorhexidine (CHX) is a cationic bisbiguanide, first synthesised in 1950 (Denton 2001). Its positive charge allows binding to occur on the negatively charged cell surface of both Gram positive and Gram negative bacteria. More specifically, the drug binds to phosphate containing compounds within the cell membrane (Jones 1997), causing leakage of low molecular weight cell components (such as potassium ions), resulting in eventual cell death (Russell and Path 1986). At lower concentrations, the structural changes are minor and recoverable, at higher concentrations, structural changes are far greater and the bacteria are unable to recover (Kuyyakanond and Quesnel 1992). Karpanen *et al.* (2008b) reported minimum inhibitory concentrations (MIC) and minimum bactericidal concentrations (MBC) of CHG for two strains of *S. epidermidis* (RP62A and TK1). MIC was reported as 2 mg/L for both strains, and MBC was reported as 4 mg/L for both strains. For *S. aureus* and *E. coli,* two common skin pathogens, Denton (2001) reported the MIC as 1.6 mg/L and 4 mg/L respectively.

Activity has also been shown against viruses and mycobacteria (McDonnell and Russell 1999). In addition to a wide range of antibacterial activity, Denton (2001) reported that the drug exhibits low mammalian toxicity and a high affinity for skin binding and as such the drug is well suited for skin antisepsis. CHX is practically insoluble in water and therefore a more soluble salt form of the drug is more commonly used (Figure 1.7).

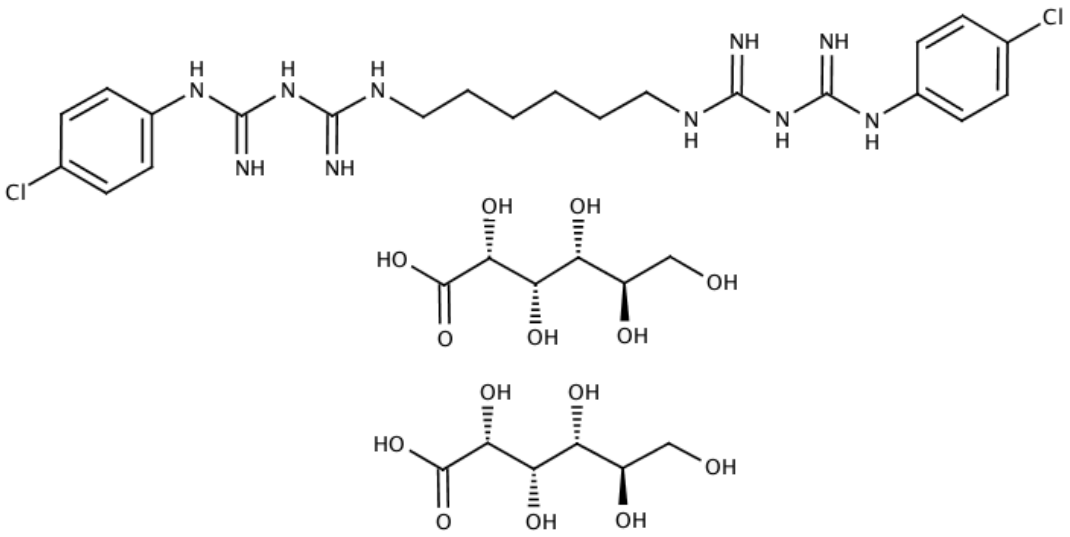

Figure 1.7. Chemical structure of chlorhexidine digluconate (CHG), a commonly used salt of chlorhexidine (CHX).

Since it was first synthesised in 1950, CHX has established itself as the antiseptic of choice in healthcare. Its uses are wide ranging, from skin antisepsis to the prevention and treatment of oral disease. In 2009 WHO published guidelines on hand hygiene in health care. The guidelines stated that alcohol-based hand rubs were the gold standard for hand hygiene in health care following the consideration of logistic, economic, safety, cultural and religious factors. However, the guidelines acknowledged that alcohol-based hand antiseptics had no residual activity due to the sub-lethal effect alcohols have on some skin bacteria, which can be rectified with the addition of CHX (Rotter 1999), thus providing significantly longer lasting antiseptic effects (Lowbury, Lilly and Ayliffe, 1974; Aly and Maibach, 1979). Furthermore, the most active agent used for surgical hand antisepsis is CHG and the drug is not affected by the presence of bodily fluids such as blood, unlike other antimicrobial compounds, for example povidone iodine (Darouiche *et al.* 2010). The National Institute for Health and Care Excellence (NICE) guidelines for prevention and treatment of surgical site infections (NICE, 2019) name an alcohol-based solution of CHX as the first choice antiseptic. If the surgical site is next to a mucous membrane then an aqueous solution of CHX is indicated. Povidone iodine is only indicated when CHX is

contraindicated (NICE, 2019). This recommendation is supported by other studies which have consistently found CHX to lower skin flora to a greater extent than other products available (Lowbury and Lilly, 1973; Lowbury, Lilly and Ayliffe, 1974; Vernon *et al.* 2006) and due to successful implementations of CHX into existing hospital protocols (Zywiel *et al.* 2011, Johnson *et al.* 2013). Daily CHX bathing has been shown to reduce the incidence of multidrug-resistant organisms in some cases (Kassakian *et al.* 2011, Climo *et al.* 2013), although the significance of this protocol has been disputed (Noto *et al.* 2015, Bui *et al.* 2018), depending on the type of bacteria investigated. Such extended use of CHX and its commonly used salts confirms this drug as a widely used, commercially accepted biocide.

Reports of adverse reactions and resistance have been relatively few when considering the long term, widespread use of CHX, and particularly when discussing its use as a topical antiseptic. Adverse events include contact dermatitis, photosensitivity, toxicity due to an accidental application to the inner ear through a perforated membrane, and hypersensitivity reactions in very rare cases (Krautheim *et al.* 2004, Lim and Kam 2008). Mucosal irritation can occur when CHX is ingested, however systemic toxicity is rare due to a lack of absorption from the gastrointestinal tract. Direct contact with brain tissue and the meninges should also be avoided (Martindale: The Complete Drug Reference 2010). CHX has been used to coat catheters in an attempt to reduce the incidence of bacterial colonisation and catheter related infections, however the Medicines and Healthcare products Regulatory Agency (MHRA) released a medical device alert in 2012 regarding medical devices and products containing CHX, stating that an awareness of patients allergies was required due to a number of incidences where CHX containing products were used on patients with CHX allergies (MHRA 2012). In 2015, the MHRA issued a drug safety update which reminded healthcare professionals to be mindful of the risk of chemical burn injuries in premature infants from CHX (MHRA 2015).

Resistance to antimicrobial compounds is one of the biggest issues threatening global healthcare today. CHX is not immune to resistance, however the drug has outlived numerous other antimicrobial compounds that were synthesised later, and resistance to this drug is still comparatively rare. Resistance from *Pseudomonas* strains is becoming increasingly common, including reports of *Pseudomonas stutzeri* resistance to chlorhexidine diacetate when the strain was exposed to gradually increasing concentrations of the antibacterial (Tattawasart *et al.* 1999), and strains of multidrug-resistant *Pseudomonas aeruginosa* and methicillin-resistant *Staphylococcus aureus* (MRSA) located from the surface of soap dispensers containing 2% CHX (Brooks *et al.* 2002). Furthermore, a study by Fritz *et al*. (2013) found that 0.9% of 1089 patients with a community onset SSTI carried CHX resistance *Staphylococcus aureus*. Of two patients prescribed CHX who carried a CHX resistance *Staphylococcus aureus* strain, 50% remained colonised at one month after treatment. The researchers noted that the prevalence of CHX resistance in *Staphylococcus aureus* is low, and eradication efforts were more successful in patients carrying a CHX resistant *Staphylococcus aureus* strain than patients carrying a mupirocin resistant *Staphylococcus aureus* strain, another topical antimicrobial compound. Kampf (2016) reported that CHG resistance is rarely found in *E. coli* or *S. aureus*, two of the most common pathogens associated with skin infections (Grice *et al.* 2008).

Although CHX is able to provide skin surface antisepsis to an acceptable standard, its physicochemical properties are undesirable for suitable permeation into deeper layers of the skin, where it has been established that hidden flora reside, able to cause SSTIs in high risk groups and when the skin barrier has been compromised. The salt form of the drug is typically used when applied to the skin due to reduced solubility associated with the free drug. The hydrophilicity of the drug (log P 0.0133; [Farkas, Kiss and Zelko, 2007]), whilst practical for creating suitable aqueous formulations, is not ideal for diffusion across the highly lipid *stratum corneum*. Furthermore, the drug is incompatible with numerous materials which may be

incorporated into topical and transdermal formulations, including anionic materials such as soaps, insoluble powders, insoluble compounds of zinc, magnesium and calcium and suspending agents such as tragacanth and alginates (McCarthy 1969, Yousef *et al.* 1973, McCarthy and Myburgh 1974). This limits the number of topical formulations that can incorporate CHX for topical antisepsis. The high molecular weight of CHG (897.8g/mol) also far exceeds the ideal limit proposed by (Naik *et al.* 2000) of 500g/mol, limiting its potential for diffusion into the skin.

A study by Karpanen *et al.* (2008a) found that following application of a 2% w/v CHG solution to full thickness human skin, poor permeation was observed after two and 30 min and levels were less than 0.002µg/mg tissue below 300µm. After 24 hours, there was 7.88µg/mg tissue (±1.37µg) within the top 100µm of skin, but there was <1µg/mg tissue below 300µm, and there was no detection of CHX through the full-thickness skin. A further study compared penetration of aqueous and alcohol-based formulations of CHG (2% w/v) through full thickness human skin (Karpanen *et al.* 2009). After two and 30 min, skin penetration was poor for both formulations. The amount of CHG residing in the top 100 µm was significantly less for the alcohol than for the aqueous formulation after 2 min, but there was no statistically significant difference between the depth permeation of CHG from both formulations after 30 min. Neither of the Karpanen *et al.* studies detected CHG in the receptor chamber when permeation was measured through full thickness human skin. Lafforgue *et al.* (1997) studied the percutaneous absorption of a 5% w/v CHG solution across the abdominal skin of hairless rats. The study found that after 48 hr, 0.00403 ± 0.0006 mg/cm^2 CHG was present in the receptor chamber, and 0.02663 ± 0.01317 mg/cm^2 CHG was present in the whole skin. Tape stripped skin resulted in a higher degree of permeation of the drug into and through skin (0.23865 ± 0.04633 mg/cm^2 and 0.34241 ± 0.04633 mg/cm^2 respectively). The results from the Lafforgue *et al*. study should be viewed with caution due to the use of hairless rat skin, rather than an alternative, such as porcine skin, which is more representative of human skin (Section 1.7).

Numerous methods have been employed in an attempt to enhance the permeation of CHG. Lboutounne *et al.* (2002, 2004) investigated the release of CHG from PCL nanocapsules. The earlier study (Lboutounne *et al.* 2002) found that concentrations of CHG released from nanocapsules onto porcine ear skin was equivalent to a CHG aqueous solution when considering minimum inhibitory concentrations against several bacteria, and that the PCL nanoparticles mediated a prolonged and more direct contact between the drug and bacteria, skin surface and skin follicles. This was attributed to the use of CHX rather than chlorhexidine salts, thus using an unionised drug with a higher lipophilicity which is more able to transverse the *stratum corneum* barrier, improving the vehicle/*stratum corneum* partition coefficient and facilitating bioadhesion of the drug carrier onto the porcine skin surface allowing for a prolonged period of administration. Additionally, the use of a surfactant in the nanocapsule improved attachment to the target bacteria. The later study (Lboutounne *et al.* 2004) investigated the transport of CHX loaded nanoparticles through hairless rat skin and conversely found that drug encapsulation reduced percutaneous absorption through tape stripped skin, attributed to nanocapsule aggregation within appendages thus reducing the amount of drug available for permeation across the membrane.

Essential oils, termed “terpenes” have been investigated as potential permeation enhancers (Williams and Barry 1991, Cornwell and Barry 1993). Eucalyptus oil has penetration enhancing properties (Williams and Barry 1989) and also acts as a mild antiseptic, therefore combining the two has the potential to not only enhance the deposition of CHX, but also provide an additive antimicrobial effect. Karpanen *et al* completed two studies which investigated the permeation of CHX in combination with essential oils (Karpanen *et al.* 2008b; Karpanen *et al.* 2010). The earlier study (Karpanen *et al.* 2008b) compared the efficacy of CHX in combination with eucalyptus oil, tea tree oil and thymol against *Staphylococcus epidermidis* in a suspension and biofilm. In this study it was found that eucalyptus oil reduced the minimum inhibitory

concentration by 28-60 g/L. The drug and oil combination also demonstrated synergistic effects against the *Staphylococcus epidermidis* biofilm. The later study (Karpanen *et al.* 2010) explored the penetration of CHX through human skin when combined with eucalyptus oil. The study found 5% v/v eucalyptus oil facilitated the greatest CHG permeation into skin layers below 300 µm, and 10% v/v eucalyptus oil facilitated the greatest CHG permeation into skin layers within the upper 900 µm. A study by Hendry *et al.* (2009) also investigated the antimicrobial efficacy of eucalyptus oil in combination with CHG and the results supported the Karpanen *et al.* (2008b) study, concluding that synergistic antimicrobial effects were present when combining the drug and essential oil.

Bako *et al.* (2006) designed nanocomposite hydrogel systems, comprised of different molar ratios of biocompatible monomers hydroxyethyl methacrylate (HEMA) and polyethylene glycol dimethacrylate (PEGDMA). Nanoparticles were formed from copolymerisation of these monomers. The highest drug release rate was observed for CHG in the nanoparticles and hydrogel matrix, rather than matrix or nanoparticles alone A further study synthesised and tested nanocomposite biocompatible hydrogels with the aim to sustain the release of CHX (Bako *et al.* 2008). The study found that the nanocomposite hydrogels allowed sustained release of CHX over 48 hr, compared to the control hydrogel (24 hr release). Furthermore, 60% of the loaded CHX was released and the nanocomposite hydrogels were described as flexible and soft, suitable for implantation into the periodontal pockets or for application as a surface film on infected gums. This could be translated to topical use for sustained CHX delivery**.** Some studies have also investigated CHX loaded hydrogels for ophthalmic use (Paradiso *et al.* 2014, Pimenta *et al.* 2016). Fewer studies have investigated CHX based hydrogels for topical application (Kiremitçi *et al.* 2007, Brazdaru *et al.* 2015) but there appears to be no studies which investigated the permeation of CHX from hydrogels using *in vitro* diffusion cells and tape stripping.

In summary, CHG is a well-tolerated, first line topical antiseptic which provides suitable skin surface antisepsis. It is desirable for the skin penetration of this drug to be improved so that it is able to target bacteria in deeper skin layers which harbour the ability to cause SSTIs. This may be achieved via formulating the drug with chemical or physical permeation enhancers. However, a balance must be established between enhancing drug permeation within skin without increasing drug permeation across skin, as uptake of the drug within the systemic circulation may increase the risk of adverse events.

1.11 Active strategies to enhance topical and transdermal drug delivery

The highly efficient barrier of the *stratum corneum* provides an effective barrier to the external environment, therefore permeation of drugs is often limited, particularly when considering that many drugs were principally designed for the oral and or parenteral route (Moss 2015). Therefore, modification of either the barrier or the formulation is required to maximise skin permeation.

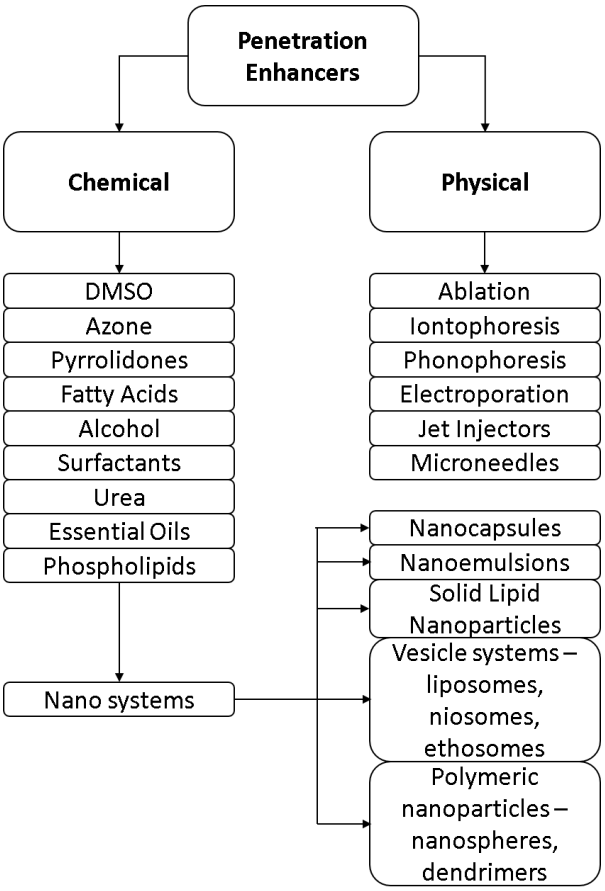

Figure 1.8. Active strategies to enhance topical and transdermal drug delivery.

Methods of penetration enhancement are generally classified as chemical or physical (Figure 1.8). A catalogue of chemical permeation enhancers exist which may enhance the deposition of the target drug into the skin. The mechanisms of permeation enhancement are numerous and an enhancer may use utilise several mechanisms to achieve the desired penetration enhancement effect. For example, the enhancer may directly interact with the *stratum corneum* barrier via disruption of the lipid bilayers. Alternatively, the enhancer may have effects on the permeant in the vehicle, modifying the thermodynamic activity of the permeant, increasing the driving force for the permeant to diffuse out of the vehicle into the skin (Moser *et al.* 2001). Mechanisms of specific permeation enhancers are often not well understood, but increasing this knowledge would be beneficial as it would allow drugs and penetration enhancers to be more successfully

paired with a higher chance of a resulting enhancement effect. A list of ideal properties of permeation enhancers can be found from Katz and Poulsen (1972), but no permeation enhancers which currently exist exhibit all of these ideal properties –

(i) Non-toxic, non-irritating and non-allergenic

(ii) Rapidly effective, with a predictable activity and duration which is reproducible

(iii) No systemic pharmacological activity

(iv) Unidirectional activity

(v) Barrier properties of the skin should return to normal following removal of the permeation enhancer

(vi) Compatible with numerous excipients and drugs to allow for formulation into diverse topical preparations

(vii) Cosmetically acceptable to the consumer (Barry 1983)

In addition to chemical permeation enhancers, physical methods such as iontophoresis, phonophoresis and microneedles have emerged which have been investigated as methods of transdermal permeation enhancement. The use of such physical methods of permeation enhancement may be useful when chemical methods have failed, or are deemed clinically unacceptable, for example due to skin irritation, sensitisation or a lack of stability between the drug and permeation enhancer. The physical methods essentially circumvent the *stratum corneum*, thus avoiding the main barrier to drug permeation, particularly where partitioning into the *stratum corneum* is considered the rate limiting step, i.e. hydrophilic permeants. The main chemical and physical methods of permeation enhancement utilised within this thesis (G3 PAMAM-NH_2 dendrimer and microneedles) are described in the following text.

1.12 Polyamidoamine (PAMAM) dendrimers

PAMAM dendrimers are highly branched polymer structures which have only recently been utilised in the field of percutaneous permeation enhancement, having previously been successful in the field of anti-cancer drug delivery, gene delivery and magnetic resonance imaging (Stiriba *et al.* 2002, Boas and Heegaard 2004, Majoros *et al.* 2006). The structure of the G3 PAMAM-NH_2 dendrimer utilised within this study can be found in Figure 1.9.

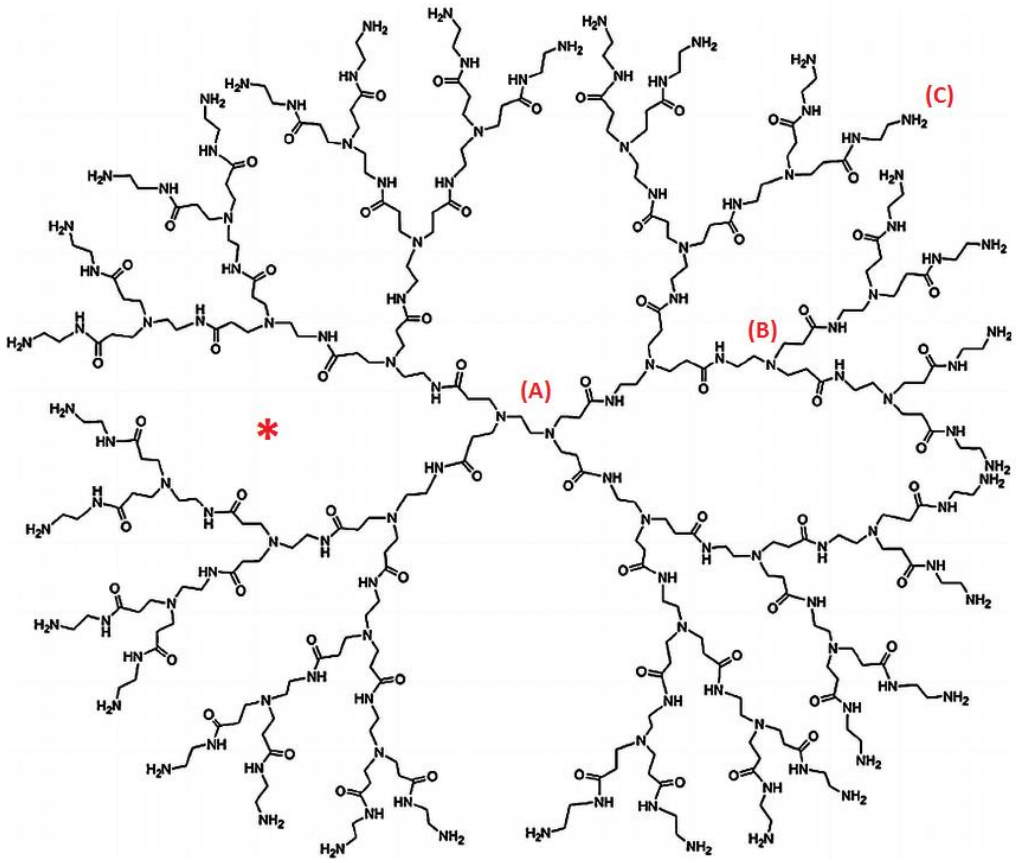

Figure 1.9. Structure of a G3-PAMAM-NH_2 dendrimer. (A) indicates the core of the structure, (B) indicates the interior branching of the structure and (C) indicates the peripheral functional groups. The asterisk (*) illustrates an interior void which may potentially host encapsulated drugs.

All PAMAM dendrimers contain a diamine core, "arms" extending from the core and the terminal periphery groups (Tomalia *et al.* 1985), which are commonly carboxylic acid, amine and hydroxyl functional groups. The shape of the dendrimer varies from an elliptical shape at lower

generation numbers (G0-G4) and a globular shape at higher generation numbers (G5-G10, [Taghavi Pourianazar, Mutlu and Gunduz, 2014]). Dendrimers increase in generation via addition of branches to the outer shell of the dendrimer, linearly increasing its molecular weight, measured diameter and number of surface groups (Esfand and Tomalia 2001). The structure of dendrimers differs from that of linear polymers by offering a uniform, controlled structure (illustrated in Table 1.1), which allows a high density of functional groups to be placed in close proximity to one another without chain entanglement (Kannan *et al.* 2007). Thus, these functional groups are available to interact with guest molecules with may become entrapped within the dendrimer core (Figure 1.9*), or may interact with peripheral functional groups (Figure 1.9C). Factors that may influence drug-dendrimer interactions are discussed in further detail in Section 1.12.2.

Table 1.1. Illustration of the linear increase in molecular weight, diameter and surface groups of PAMAM dendrimers as a function of generation (Dendritech 2017).

Generation	Molecular Weight	Measured Diameter (nm)	Surface Groups
0	517	1.5	4
1	1430	2.2	8
2	3256	2.9	16
3	6909	3.6	32
4	14215	4.5	64
5	28826	5.4	128
6	58048	6.7	256
7	116493	8.1	512
8	233383	9.7	1024
9	467162	11.4	2048
10	934720	13.5	4096

The use of PAMAM dendrimers in the biomedical field has increased dramatically since they were first synthesised in the 1980's. They are the most popular dendrimer to be investigated

within the literature, owing to their unique physicochemical properties which make PAMAM dendrimers desirable for clinical use for enhancing drug delivery (Jang *et al.* 2009) –

(i) Uniform molecular weight

(ii) Stepwise synthesis produces a structure of uniform size and shape. There is a systematic size increase with increasing generation number

(iii) Stepwise synthesis allows for site specific functionalities. Peripheral functionalities may be altered to enhance solubility where necessary

(iv) Ability to accommodate small molecules in the dendrimer core and or complex drugs to the PAMAM surface. This may protect degradable drugs and modify and extend drug release

PAMAM dendrimers exhibit highly ordered branching, increasing their reproducibility and uniformity of drug delivery, unlike more readily available, irregular branched, polymers. This potentially makes dendrimers ideal for commercial use if efficacy and safety can be assured. PAMAM dendrimers are biocompatible, nonimmunogenic, and water soluble (Patri et al, 2002) and therefore possess many qualities that would be useful for aiding drug delivery. The potential for enhancement of permeant solubility has been proven to be of particular use when required for increased bioavailability (Gautam *et al.* 2015). Their large molecular weight (6909 Da [Dendritech 2017]) and surface charge make them unlikely to permeate into the skin, limiting the risk of adverse events associated with systemic uptake of the dendrimer, whilst still being able to enhance drug penetration into the skin (Sun *et al.* 2012).

One may postulate that the G3 PAMAM-NH_2 dendrimer used in this study, at a size of 3.6 nm (Dendritech 2017), may be able to penetrate between the corneocytes for deposition into the skin. However, this does not take into account the lipid packing within the *stratum corneum*. The distribution of hydrocarbon chains within the lipid lamellae are 0.46 nm, 0.41 nm and

0.37 nm for liquid, hexagonal and orthorhombically packed chains respectively, as described by Bouwstra and Ponec (2006). PAMAM dendrimers may be able to penetrate superficially into the *stratum dysjunctum*, because adherence between corneocytes in this layer has been weakened by proteolytic cleavage of corneodesmosomes. However, even if this were the case, sloughing of corneocytes due to desquamation would presumably also remove any PAMAM dendrimer that was able to permeate to this depth. The evidence provided by Bouwstra and Ponec (2006) certainly suggests stearic hindrance would occur even in the more mobile, "liquid" packing of specific regions of lamellar lipids, preventing permeation of PAMAM dendrimers into viable skin tissue. Furthermore, this does not take into account the ionisation state and aqueous solubility of the dendrimer, both of which will likely hinder the extent of permeation into the skin, as described in Section 1.4.

PAMAM dendrimers in particular may be a useful permeation enhancer to link with CHG and other antimicrobial drugs as some studies have found that PAMAM dendrimers exhibit antimicrobial activity (Calabretta *et al.* 2007, Cheng *et al.* 2007, Wang *et al.* 2010). A study completed by Cheng *et al.* (2007) found that quinolones can be successfully carried by PAMAM dendrimers whilst still exhibiting antimicrobial activity. This study, however, did not attempt to deliver quinolones transdermally. The results of a study conducted by Holmes *et al.* (2019) indicate that the antimicrobial efficacy of PAMAM dendrimers is dependent on generation number, concentration and terminal functionalities. Increasing the number of amine groups on the dendrimer surface decreased the 50% minimum inhibitory concentration (MIC_{50}). Furthermore, PAMAM dendrimers were found to be more effective against Gram-negative than Gram-positive bacteria, thought to be due to the ability of the cationic dendrimer to electrostatically bond with the bacteria outer membrane.

1.12.1 Percutaneous Penetration enhancement mediated by PAMAM dendrimers

There is a wide variety of literature that has explored drug delivery enhancement using PAMAM dendrimers, though those that focus on topical and transdermal delivery are comparatively small. Those that do use differing generations of dendrimer, differing vehicles and apply the drug either after pre-treatment with the dendrimer, or in a co-formulation where the drug and dendrimer are applied together in the same vehicle. Furthermore, many of the studies utilising PAMAM dendrimers in topical and transdermal drug delivery do not utilise a suitable human skin substitute. Therefore a lack of similarity between rodent and human skin (Wester and Noonan 1980, Bronaugh *et al.* 1982) and snake and human skin (Wester and Maibach 1993; Section 1.7) may limit the value of these studies in estimating dendrimer-mediated drug delivery into or across human skin. However, the current numbers of studies which investigate dendrimer-mediated drug permeation enhancement are few and so they should not be discounted altogether.

Percutaneous absorption of furfural through rat skin was studied in the presence of a G5 PAMAM dendrimer. Drug permeation was decreased in a concentration dependent manner (× 4-12 in co-treatment study, × 2.3 in pre-treatment study; [Moghimi, Varshochian *et al.* 2010]). This study, unlike many others that follow, desired a reduction in permeation with the PAMAM dendrimer because the drug was used as a model toxicant.

Chauhan *et al.* (2003) investigated transdermal permeation of indomethacin through rat skin via co-formulation with a G4 dendrimer with varying surface groups (-OH, -NH_2 and –COOH). The highest increase in flux observed was from the G4-NH_2 dendrimer at a 0.2% w/v concentration, increasing drug permeation 4.5 × more than the drug alone.

Delivery of ketoprofen and diflunisal through excised rat skin was significantly enhanced after 24 hr when the drug was co-formulated with a G5 PAMAM dendrimer. The bioavailability of the ketoprofen-PAMAM complex and diflusinal-PAMAM complex was 2.73 × and 2.48 × higher than the drug delivered without G5 PAMAM dendrimer co-formulation (Yiyun *et al.* 2007).

Penetration of tamsulosin hydrochloride was studied through snake skin *via* PAMAM dendrimer pre-treatment for 24 hours following the development of a novel polymeric drug delivery matrix using polyhydroxyalkanoate (PHA) (Wang *et al.* 2003b). No enhancement was observed when drug and dendrimer were applied as a co-treatment, but weak enhancement was observed when the drug was applied after dendrimer pre-treatment of the skin. The lack of permeation enhancement when delivered as a co-formulation was thought to be due to interactions between the drug and dendrimer, preventing drug permeation into the skin. Drug enhancement was detected however, when the dendrimer was first mixed with the PHA matrix before skin application.

Two studies completed by Venuganti and Perumal; (2008, 2009) investigated the effects of PAMAM dendrimers on the permeation of 5-fluorouracil (5FU). The studies investigated the effects of both types of applications – pre-treatment and co-treatment, and three different vehicles: water, isopropyl myristate (IPM) and mineral oil (MO). The study concluded that a significant enhancement of 5FU was observed in both the pre-treatment and co-treatment group, but only with the IPM and MO vehicles. The second study examined the influence of surface charge, dendrimer generation and concentration of PAMAM dendrimer on the skin permeation of 5FU and found that increasing dendrimer concentration did not proportionally increase the skin permeation of the drug; lower generation cationic dendrimers were more effective in enhancing hydrophilic drug permeation and that the permeation of 5FU was enhanced mostly by G4-NH_2, followed by G4-OH and G3.5-COOH. Consequently, it appears that the properties of the PAMAM dendrimer (generation, surface charge), drug in question, skin

type, drug vehicle and dose application type (pre-treatment or co-treatment) may affect the dendrimers ability to improve transdermal permeation.

The permeation of riboflavin was studied when applied to the skin with both full and half generation dendrimers. The results of the study concluded that the dendrimers weakly enhanced solubility of the drug, with earlier generations of dendrimer enhancing solubility to a greater extent than later generation dendrimers (Filipowicz and Wołowiec 2011).

A study by Venuganti, *et al.* (2015) investigated whether a PAMAM dendrimer could carry a gene silencer across the skin with the aid of iontophoresis for the potential treatment of skin cancer. Delivery of the gene silencer was limited to 20 µm depth (*stratum corneum* localised) without the addition of iontophoresis which was not statistically significant. The addition of anodal iontophoresis increased the depth permeation of the gene silencer to 100 µm.

Borowska *et al.* (2012) investigated the use of G3 and G4 PAMAM dendrimers as permeation enhancers of 8-methoxypsoralene (8-MOP). 8-MOP is used as a photochemotherapy agent, however when administered orally gastrointestinal side effects are common as well as the increased risk of serious complications, and permeation from topical creams, emulsions and solutions could be improved. The results of this study indicate that the dendrimer significantly enhanced the permeation of 8-MOP compared to a standard 8-MOP solution without PAMAM dendrimer. The authors also noted that the G4-PAMAM was a more effective permeation enhancer than the G3-PAMAM dendrimer.

1.12.2 Mechanisms of PAMAM dendrimer mediated drug delivery enhancement

The studies above illustrate that PAMAM dendrimers are able to enhance the delivery of various drugs into and across the skin. Permeation enhancement is not limited to a specific "type" of drug, i.e. the permeation of both hydrophilic (Venuganti and Perumal 2008, 2009) and lipophilic (Chauhan *et al.* 2003, Yiyun *et al.* 2007) drugs have been enhanced by pre-treatment or co-formulation with a PAMAM dendrimer. The extent of dendrimer enhancement may be altered by using different concentrations, generations and charge of dendrimers (Venuganti and Perumal 2009). The precise mechanism of PAMAM-mediated permeation enhancement, however, is poorly understood.

A comprehensive review of drug-dendrimer interactions was published by (D'Emanuele and Attwood 2005). Broadly, there appears to be two potential types of interactions between drug and dendrimers that may result in permeation enhancement. Firstly, a drug may become entrapped within the dendritic architecture. Numerous studies have illustrated the ability of drug molecules to be encapsulated within the dendrimer core (Jansen *et al.* 1995, Boas *et al.* 2001, Beezer *et al.* 2003). The density of the dendrimers increases with increasing generation number (Inoue 2000) and the flexibility of the dendrimer decreases with increasing generation number (Maiti *et al.*2004), which may affect their ability to host guest molecules.

The second postulated mechanism of drug-dendrimer interaction involves the drug electrostatically or covalently interacting with the surface of the dendrimer. Whilst factors such as the size and density of the dendrimer may affect their ability to host guest molecules, the loading capacity of the dendrimer may be increased by complexation of a drug on the dendrimer surface. With increasing generation number, the number of surface groups doubles and therefore so does the opportunities for drug complexation. Several studies have found that the

drug loading and drug solubility increases following complexation with a PAMAM dendrimer (Chauhan *et al.* 2003, Kolhe *et al.* 2003, Wang *et al.* 2012). A review by Svenson (2009) provided numerous examples of drug-dendrimer interactions and suggested that small organic molecule drugs are often encapsulated within the dendrimers interior void, whereas larger biomolecules adsorb onto the dendrimer surface. There is no data currently available on the method of CHG binding to a G3-PAMAM-NH_2 dendrimer. The molecular size of CHG (897.76 g/mol) is larger than those which are encapsulated by the dendrimer according to Svenson (typically between 200-400 g/mol), and the lower generation number of the dendrimer used in this thesis alludes to a smaller internal void space. However, both the dendrimer used within this thesis and the drug are cationic and so drug conjugation with the dendrimer surface may be pH-dependent.

More recently, Chauhan (2018) reviewed the use of dendrimers in drug delivery. The author discussed the fact that currently, there no tools to predict the entrapment potential of a dendrimer for any drug, so one must systematically perform entrapment studies with differing surface functional groups, generations and concentrations to determine the most suitable dendrimer for any specific drug. Current trends suggest entrapment occurs most successfully at higher dendrimer generations (alluding to a greater void space, Figure 1.9*), and when the drug and interior of the dendrimer are fully ionised. In relation to CHG, the likelihood of entrapment within a G3 PAMAM-NH_2 dendrimer is discussed further in Chapter 5.

Either by encapsulation or surface interaction, the mechanism of PAMAM-mediated enhancement of drug delivery to the skin is still not well understood. Sun *et al.* (2012) proposed three potential mechanisms for dendrimer mediated enhancement of drug delivery to the skin. Firstly, the authors proposed that the dendrimer is able to increase drug saturation in the vehicle via increasing drug solubility in the dendrimer core. Once applied to the skin it is theorised that rapid release of drug from the dendrimer would result in a greater drug concentration on the skin surface than if the drug was applied alone, thus increasing the thermodynamic activity

(Section 1.6) of the drug in the vehicle required to drive drug delivery into the skin. This was the mechanism postulated for the increase in indomethacin delivery (Chauhan *et al.* 2003) across rat skin.

Secondly, the authors postulated that the dendrimer may cause permeation enhancement when coupled with a vehicle understood to disrupt the *stratum corneum* barrier. The vehicle acts as a permeation enhancer in its own right, disrupting the lipid phase of the *stratum corneum* and by doing so, allowing the dendrimer to permeate deeper into the *stratum corneum* than before. Upon entering the *stratum corneum*, the cationic dendrimer is able to cause lipid fluidisation, polarity alteration, phase separation or lipid extraction (Barry 2004) before releasing the drug into the compromised skin barrier, enhancing drug permeation. This is the mechanism suggested for permeation enhancement of 5FU in the presence of a PAMAM dendrimer with a IPM/MO vehicle, but not a water vehicle (Venuganti and Perumal 2008). One may suggest that this permeation enhancement effect is more dependent on the vehicle than the dendrimer itself.

The third postulated mechanism is via hair follicles. The ability of compounds to be attached to the surface groups of PAMAM dendrimer allows for numerous modification strategies which could optimise the dendrimers for targeted follicular delivery (D'Emanuele and Attwood 2005). This has been supported by a study from Alvarez-Román *et al.* (2004) who demonstrated that polystyrene nanoparticles have the ability to accumulate in follicular openings in a time-dependent manner. The study found that found that 20 nm polystyrene particles penetrated deeper than 200 nm particles in porcine skin in skin follicles and furrows. Increasing the hydrophilicity of nanoparticles has been shown to increase drug partitioning into hair follicles (Wu *et al.* 2009). Increasing the hydrophilicity of the drug increases the likelihood of diffusion into the skin via the transcellular or transappendageal routes (Section 1.3).

In addition to the three proposed mechanisms by Sun *et al.* (2012), surfactant like behaviour has also been attributed to PAMAM dendrimers, particularly lower generation dendrimers as the focal point of larger dendrimers are shielded within the inside of the dendrimer and therefore, is not accessible by water for a reduction in surface tension to take effect (Saville *et al.* 1993, Sayed-Sweet *et al.* 1997). Kirton *et al.* (1998) found that nitrile and ester surface groups resulted in thinner film formation, increased affinity for the water surface and more spreading across the surface. Despite this research, there has yet to be studies which investigate the effects of dendrimers at the skin interface, and whether a reduction in surface tension may be the mechanism for drug enhancement into human skin. According to the studies above, a G3 (low generation) dendrimer with NH_2 surface groups could be an ideal candidate for enhancing drug permeation due to surface effects.

PAMAM dendrimers are highly hygroscopic (Uppuluri *et al.* 1998) and are able to extract water from the surrounding environment. Judd (2013b) stated that "hydration caused by the occlusion of the SC surface by viscous PAMAM dendrimers and an increase in wettability and reduction of surface tension due to the presence of PAMAM dendrimers should also be considered as a possible contributing penetration enhancing effect." Hence, an occlusive effect may also contribute to the mechanism of PAMAM dendrimers-mediated drug permeation enhancement. A number of mechanisms may also work in conjunction with one another to create this enhancement effect.

1.12.3 Safety of PAMAM dendrimers

Utilising PAMAM dendrimers for the enhancement of topical and transdermal drug delivery raises the question whether the PAMAM dendrimer itself may be able to permeate into the skin, as this may have toxicity implications. *In vitro* toxicity studies have demonstrated that

cytotoxicity appears dependent on concentration and generation of the dendrimer (Mukherjee and Byrne 2013), and that cationic dendrimers are more toxic than anionic dendrimers (Duncan and Izzo 2005). The exact *in vitro* toxic concentrations reported differ between studies. For example, Malik *et al.* (2000) reported that full generation dendrimers > G1 are haemolytic at concentrations > 1mg/mL, whereas Labieniec *et al.* (2008) reported that a G4 PAMAM dendrimers showed no evidence of haemolysis up to 10 µM/L. When tested *in vivo*, it was reported that PAMAM dendrimers (up to G5) were non- toxic when injected into mice at a concentration of 10 mg/kg (Roberts *et al.* 1996, Bourne *et al.* 2000, Boas and Heegaard 2004). Chauhan, Jain and Diwan (2010) found that G4-NH_2 and G4-OH dendrimers were non-toxic in mice at low (4.75 mg/kg/day), medium (9.5 mg/kg/day) and high (19 mg/kg/day) concentrations.

Permeation of PAMAM dendrimers through skin seems unlikely, as the physicochemical properties of the dendrimer make it unsuitable for delivery into the skin (high molecular weight, surface ionisable groups and high aqueous solubility). It should also be noted that the tortuous pathway a drug must take to pass through the *stratum corneum* would also apply to the PAMAM dendrimer, therefore free movement of the nanoparticle is likely to be impeded without the use of an external driving force (Sun *et al.* 2012). There have been few studies demonstrating lower generation dendrimers ability to permeate into the skin. G4 PAMAM dendrimers were found to be limited to the *stratum corneum* following topical application (Venuganti *et al.* 2011) and deposition was only improved using iontophoresis for 2 hr. Currently there are no regulatory documents that could be found that specify “safe” concentrations of PAMAM dendrimers.

1.13 Microneedle-mediated drug delivery into and across skin

Microneedle arrays consist of multiple micro-projections assembled on one side of a supporting base, ranging in height from 25-900 μm and are a minimally invasive method of bypassing the *stratum corneum* barrier. This is achieved by creating small channels through the layer which drugs can be delivered through. The damage created by MNs is thought to be reversible (Gupta *et al.* 2011), with evidence of faster healing at the injection site than with a traditional hypodermic needle. In addition to this, further advantages include reduced pain when compared to a traditional hypodermic needle (Gill *et al.* 2008), or in some cases pain free drug administration (Kaushik *et al.* 2001, Haq *et al.* 2009) as needles should not penetrate deeply enough to make contact with nerves. Another advantage of MNs is their ability to target specific skin sites for drug administration, administration of large molecules, and long term tolerability. Certain types of MN devices such as dissolving MNs also eliminate the potential for needle misuse as the needles are made of a biocompatible dissolving material which dissolves in the skin once applied. This is of course in addition to general advantages of topical drug delivery, such as avoidance of first pass metabolism and the potential for dose reduction due to enhanced efficacy via MN delivery. Furthermore, there is the potential for self-administration of MNs (Donnelly *et al.* 2014; Norman *et al.* 2014; Alkilani, McCrudden and Donnelly, 2015; Ripolin *et al.* 2017) when manufactured into a transdermal patch or when using a MN roller or pen, both of which are inexpensive to produce and are simple for patients to use without extensive training required.

Numerous factors can be altered in order to create a MN which maximises the efficacy of the drug intended for topical and transdermal delivery, whilst still maintaining safety. The manufacturing material, MN length, tip radius, shape and needle density can all be tailored for the intended drug, depth and safety criteria. For example, the material used to fabricate the MN

should consider the force of application required for successful insertion into the skin, whilst still retaining some flexibility to counteract skin elasticity (Donnelly *et al.* 2012b). MNs were initially manufactured from silicone (Hashmi *et al.* 1995), but have since been made from materials such as stainless steel (Verbaan *et al.* 2007), silk (Tsioris *et al.* 2012) and various polymers (McAllister *et al.* 2003, Park *et al.* 2005). MNs with an increased length will increase the risk of pain as the needle is more likely to come into contact with nerves present in the dermis, and should deliver the compound of choice deeper into the skin, which may encourage systematic uptake. The size and geometry of the MN may impact the concentration of drug able to coat the needle or be delivered through a hollow MN. Theoretically, increasing the needle density would increase the concentration of drug delivered to the skin, however there is the potential for a "bed of nails" effect whereby a higher MN density may counteract the piercing ability of the MNs due to different pressures at the tip, reducing the piercing properties (Verbaan *et al.* 2008).

The field of MN use for enhanced topical and transdermal drug delivery is growing rapidly. The literature is extensive and too large to be covered fully in this chapter, however a review by Kim, Park and Prausnitz (2012) documents the ever growing body of literature surrounding MNs and their use in drug and vaccine delivery. The permeability of low molecular weight drugs such as naltrexone (Banks *et al.* 2010) and 5-aminolevulinic acid ([Donnelly *et al.* 2008]; used for photodynamic therapy of skin tumours) was found to be increased following skin pre-treatment with solid MNs. Initially solid MNs were preferred for these drugs as larger doses are able to be administered compared to a transdermal patch. However, more recently, improvements in drug loading of dissolving MNs has allowed low molecular weight drugs to be delivered through dissolving MNs (Katsumi *et al.* 2012, McCrudden *et al.* 2014), eliminating the need for a solid MN pre-treatment step.

Larger biomolecules such as DNA (Pearton *et al.* 2012) and insulin (McAllister *et al.* 2003, Martanto *et al.* 2004, Ito *et al.* 2012) have been targeted for MN mediated drug delivery as this

eliminates the requirement of hypodermic injections, the method by which the majority of these large molecules are delivered given their difficulty for oral or transdermal delivery.

Vaccines are perhaps the most widely investigated use of MNs due to the potential advantages of simplified vaccine distribution, potential for self-administration and increased compliance as well as vaccine targeting to the skin, which holds immunological advantages due to the potency of antigen presenting cells compared to the traditional intramuscular injection route (Prausnitz *et al.* 2009). MN vaccines have been developed for a number of microorganisms and have had particular success targeting influenza (Van Damme *et al.* 2009, Sullivan *et al.* 2010).

There are several types of MNs which have been utilised in the studies cited (Prausnitz, 2004; Alexander *et al.* 2012; Alkilani, McCrudden and Donnelly, 2015). Solid MNs are used as a skin pre-treatment, after which the drug is applied before the skin can repair itself. Coated MNs are coated with the drug formulation intended for drug delivery into the skin, removing the need for a two-step process. However, the amount of drug able to be delivered into the skin is limited by the size of the MN. Dissolving MNs eliminate the need to remove MNs following application to the skin as they are made from a dissolving biodegradable material. Hollow MNs are able to deliver drug solutions through the hollow inner pore into the skin. More recently, Donnelly *et al.* (2012a) created a novel MN system which used hydrogel-forming materials to produce a continuous channel into the skin which remains in place and may allow prolonged transdermal drug administration.

The clinical safety of MNs has logically required investigation due to the physical nature of creating holes in the skin. Within the scope of this thesis, where preventing infection is the primary concern, it is important to establish the safety profile of MNs to justify their use in this context. Donnelly, Singh and Woolfson (2010) summarised the studies used to inform the safety profile of MNs. Alongside several studies report minimal pain and reversible irritation (Sivamani

et al. 2005, Bal *et al.* 2008, Gupta *et al.* 2009), the authors reported that creating holes in the skin through the use of MNs provides opportunities for microorganisms to traverse through. However, the risk of infection was assessed to be less than the risk posed by hypodermic needle use (Donnelly *et al.* 2009, 2013). Considering the drug to be applied in this study exhibits antimicrobial properties, it is unlikely that the risk of infection posed by MN insertion is significant. Furthermore, the authors state that safety may be enhanced by sterile manufacturing techniques and by creating MNs which dissolve after use to prevent inappropriate or repeat use.

There are, however, as with all methods of percutaneous permeation enhancement, some limitations associated. Whilst the use of MNs has garnered huge interest over the past decade, there are still some challenges which must be overcome before widespread clinical use can be implemented. Several studies have investigated drug permeation alongside MN use, however studies are limited to short term use and therefore the long term risk of irritation, pain and inadequate barrier repair has yet to be quantified. This risk is less concerning within the parameters of this study, as skin disinfection prior to surgery is unlikely to be required long term or in the same area of skin. Nonetheless, for widespread use of MNs and for delivery of drugs for chronic diseases, the safety profile of MNs should be further established.

The skin is an elastic barrier with many furrows and folds. Additionally, the thickness of skin changes depending on body site (Sandby-Møller and Wulf 2003). With these two facts in mind, there are valid concerns regarding the ability of MNs to deliver a consistent dose of drug into the skin at the correct depth. Further concerns relate to the regulation of MN manufacture, such as product sterility, appropriate packing and the choice of biomaterial to ensure the needle retains enough strength and flexibility to pierce the skin without breaking (Davis *et al.* 2004; Alkilani, McCrudden and Donnelly, 2015).

1.14 Aims of the thesis

Antimicrobial resistance is one of the greatest threats to global health and the economy through medical costs and higher mortality rates (WHO 2018b). Surgical site infections are the most frequent type of hospital acquired infection reported hospital-wide in low and middle income countries and is the second most frequent type of hospital acquired infection in Europe and the USA (WHO 2018a).

The rise of antibiotic resistance has reduced the pool of new drugs available for combating bacterial resistance, and the pharmaceutical industry is less inclined to allocate money for the development of new antimicrobials when a lack of economic return is likely as the drug is used acutely (rather than for chronic conditions); and the looming threat of resistance may cut the market life of the drug short (Walsh 2000, Wenzel 2004). It is imperative to enhance the efficacy of drugs currently used and accepted clinically to maximise their efficiency for killing bacteria which harbour the ability to cause infections.

The primary aim of this thesis is to enhance the dermal deposition of CHG within porcine skin. Chemical and physical methods of permeation enhancement are to be investigated, firstly by co-formulating the drug with a G3 PAMAM-NH_2 dendrimer, a development of a previous study (Holmes *et al.* 2017) which found dendrimer pre-treatment of the skin enhanced CHG deposition. Secondly, permeation enhancement of CHG is to be explored by utilising MNs. The most appropriate device, needle length and array for topical delivery of CHG is to be determined. The two methods are to be compared to determine whether they provide comparative enhancement effects.

A further aim of this study is to assess the methods used for drug quantification in porcine skin, due to the limitations of the “gold standard” tape stripping technique. A qualitative method of

visualising drug distribution (ToF-SIMS) is utilised in the hope that this will provide a complimentary method of assessing drug permeation into skin and support the quantitative data provided by the *in vitro* diffusion cell studies.

ToF-SIMS is able to provide quantitative drug distribution data that may allude to a drugs mechanism of action. An objective of this study is to determine the mechanism of action of the PAMAM dendrimer using ToF-SIMS and other methods, specifically its ability to enhance drug distribution within skin when applied as a co-formulation. Determining the mechanism of action of permeation enhancers may allow for specific pairings with drugs for a guaranteed permeation enhancement effect.

2 Chapter Two – Formulation of an antimicrobial formulation containing CHG

2.1 Introduction

The unique physicochemical properties of PAMAM dendrimers which make them acceptable for clinical use have been summarised in Section 1.12 (Jang *et al.* 2009). For topical and transdermal formulations, dendrimers have been increasingly investigated due to several desirable properties which are summarised below.

(i) Potential to enhance the topical and transdermal delivery of drugs (Wang *et al.* 2003a, 2003b; Venuganti and Perumal, 2008, 2009; Filipowicz and Wołowiec, 2011)

(ii) Potential to increase drug solubility and bioavailability (Devarakonda *et al.* 2004, Venuganti and Perumal 2008)

(iii) Exhibits antimicrobial properties (Cheng *et al.* 2007, Holmes *et al.* 2019)

(iv) Evidence of reduced irritation through binding to anionic surfactants (Derici *et al.* 2010)

(v) Compatible in both aqueous solutions and organic solvents (Liu and Fréchet 1999)

(vi) Good adhesion to biological surfaces (Vandamme and Brobeck 2005)

A previous study (Holmes *et al.* 2017) found that pre-treatment of porcine skin with a G3 PAMAM-NH_2 dendrimer significantly increased the amount and depth permeation of CHG within porcine skin. This chapter focuses on the development of this study; formulating the drug and dendrimer into a one-step application. A one-step application is likely to be more convenient with the potential to enhance patient adherence to treatment, where adherence is defined as "the extent to which a person's behaviour – taking medication, following a diet, and/or

executing lifestyle changes, corresponds with agreed recommendations from a health care provider" (Chakrabarti 2014).

Furthermore, the type of formulation should be considered and properties aligned with clinically available formulations and suitable guidance where appropriate, for example, the British Pharmacopeia (2019a). Tests include viscosity, uniformity of content, sterility and stability. A lack of stability in a formulation may cause the drug to precipitate out, rendering it unavailable for topical and transdermal drug delivery (Williams, 2003d). CHG has numerous incompatibilities (Section 1.10), reducing the number of potential excipients that CHG may be co-formulated with and thus the potential for permeation enhancement effects via excipient-*stratum corneum* interactions. Whilst flux is considered equal from all chemicals when saturated (Higuchi 1960), vehicles and excipients are able to disrupt the *stratum corneum* barrier and thus vehicle components and their ability to act as penetration enhancers should be considered alongside formulation stability and clinical acceptance.

The type of preparation must be considered as some of the major formulation based factors resulting in patient non-adherence include the cosmetic "feel" of the formulation (i.e. greasiness or stickiness, including whether the formulation results in adherence to patients clothing), its appearance and smell, and the convenience and time taken to apply the formulation (Augustin *et al.* 2011). Without patient adherence, there is an increased risk of poor patient outcomes, increased patient morbidity and increased costs to the healthcare provider (Osterberg and Blaschke 2005). Medication adherence rates for topical treatment are lower than for systemic treatment (Storm *et al.* 2008, Zschocke *et al.* 2014) and were reported as low as 32% in a study completed by Krejci-Manwaring *et al.* (2007). It is clear that patient acceptance is an important factor to consider when creating a topically applied formulation.

2.2 Aims and Objectives

The aim of this chapter was to create a formulation containing both CHG and a G3 PAMAM-NH_2 dendrimer, which could be considered comparable to commercially available antimicobiral formulations when considering its appearance, stability, rheology, antimicrobial activity and ease of use for the consumer. The aim was to create such a formulation that would be physically stable and acceptable to the patient in the event that the CHG-PAMAM dendrimer co-formulation successfully enhanced CHG depth permeation within porcine skin. The objectives to complete this aim were:

1. Determine the type of formulation required following consideration of formulation types available for the topical delivery of CHG.
2. Develop a range of candidate formulations with potential for enhanced delivery of CHG into the skin.
3. To characterise the following properties of a range of candidate formulations, benchmarked against suitable commercially available antimicrobial products in accordance (where appropriate) with the British Pharmacopoeia (2019a).
    a. Appearance, including consistency and physical stability
    b. Rheology
    c. pH
    d. Uniformity of content
    e. Ability to be withdrawn from a suitable container
4. To characterise the candidate formulations by their ability to inhibit bacteria when compared to a commercially available CHG containing product using European Committee on Antimicrobial Susceptibility Testing (EUCAST) guidelines (2019).

2.3 Materials and Methods

2.3.1 Materials

The following products were purchased from Sigma Aldrich - 2-hydroxyethyl cellulose (HEC, molecular weight ~1300000); G3-PAMAM-NH_2 dendrimer (molecular weight 6909g/mol, 20% w/v in methanol) and dichlorodimethylsilane (DMDCS). Chlorhexidine digluconate (CHG, 20% w/v in H_2O) was purchased from Alfa Aesar. Ethanol absolute was purchased from VWR. Glycerol was purchased from Acros Organics. pH standard buffer solutions were purchased from Fisher Scientific (pH 4, pH 7 and pH 10).

2.3.2 Methods

2.3.2.1 Adsorption of CHG into glass

CHG is known to adsorb into glass surfaces (Pinzauti *et al.* 1984, Denton 2001). However, a previous study had found silanising glassware to be of no benefit for reducing drug adsorption into glass (Holmes *et al.* 2017). The extent of glass adsorption was quantified from glass beakers with and without silanasation in this study to confirm the results of the study completed by Holmes *et al* (2017).

Glass beakers were either left untreated or were silanised using a method produced by Restek Corporation (2013) whereby the glass was placed in 5% v/v DMDCS solution for 15 min, rinsed with toluene, placed in methanol for 15 min, rinsed with methanol again and left to dry.

Following glassware treatment, a CHG solution and CHG gel formulation in the presence and absence of dendrimer was created in the untreated and silanised beaker. The formulations were

left for 24 hr (duration of a Franz-type diffusion cell experiment), then diluted appropriately using distilled water for HPLC analysis of CHG content.

2.3.3 Formulation development

Table 2.1 and Figure 2.1 illustrate the components of each formulation and the order of addition of these components required to create stable formulations.

Table 2.1. Experimental gel formulations created with the aim of enhancing delivery of CHG into porcine skin. 0.35% and 0.69% G3 PAMAM-NH_2 dendrimer is equivalent to 0.5mM and 1mM dendrimer respectively.

1. **Altering Ethanol Concentration**					
CHG (%)	**Glycerol (%)**	**Ethanol (%)**	**HEC (%)**	**G3 PAMAM-NH_2 dendrimer (%)**	**Water**
1	1	**50**	2	-	To 100%
1	1	**60**	2	-	To 100%
1	1	**65**	2	-	To 100%
1	1	**70**	2	-	To 100%
1	1	**75**	2	-	To 100%
1	1	**80**	2	-	To 100%
1	1	**90**	2	-	To 100%
1	1	**100**	2	-	To 100%
2. **Altering HEC Concentration**					
1	1	60	**0.5**	-	To 100%
1	1	60	**1**	-	To 100%
1	1	60	**2**	-	To 100%
1	1	60	**3**	-	To 100%
1	1	60	**4**	-	To 100%
3. **Altering CHG Concentration**					
1	1	60	0.5	-	To 100%
2	1	60	0.5	-	To 100%
3	1	60	0.5	-	To 100%
4	1	60	0.5	-	To 100%
4. **4. Altering PAMAM Concentration**					
4	1	60	2	**0.35**	To 100%
4	1	60	2	**0.69**	To 100%

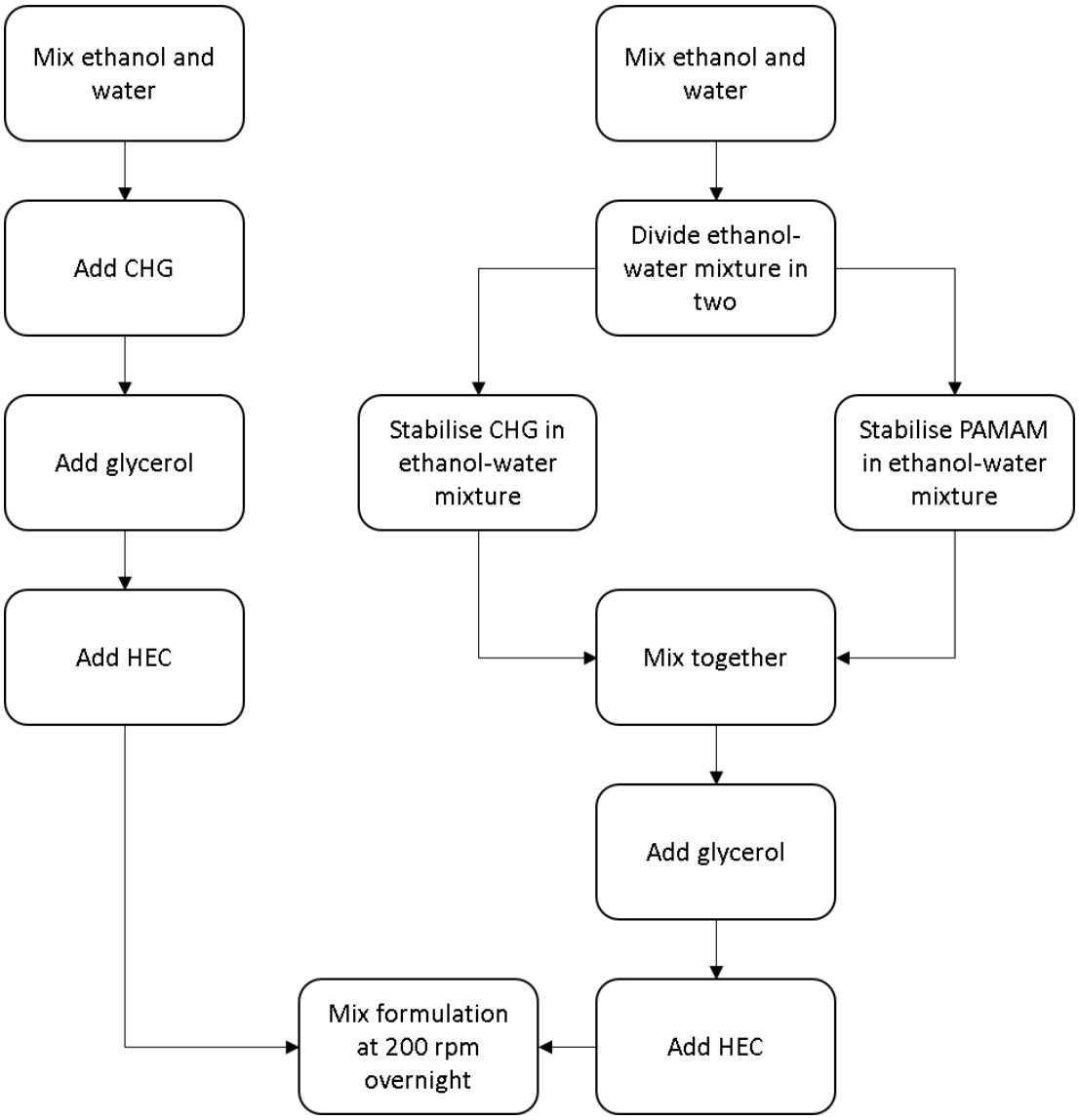

Figure 2.1. Preparation of experimental gel formulations.

2.3.3.1 Determination of apparent viscosity of formulations

The apparent viscosity of formulations with differing concentrations of HEC was measured using a Brookfield DV-E Rotary Viscometer (Fisher Scientific. Model: LVDVE, serial number: E6509621 using spindle 63 (lowest available). The British Pharmacopeia (2019a) requests that "defined rheological properties are fulfilled" and thus the apparent viscosity was compared to commercially available antimicrobial formulations. Apparent viscosity of experimental

formulations was compared to three commercial formulations (Hibiscrub© 4% w/v CHG, purchased from Boots, lot – 42K, expiry – 12/2019; Laboratory Antibacterial Moisturising Hand Wash, lot – 627014B7, expiry – 05/2019 and Milton Hand Gel, purchased from a local pharmacy, lot – 125082, expiry – 09/2018). The spindle was placed in 50 mL of the formulation and left for 3 min to prevent a false measurement occurring from disruption of the formulation. Formulations were covered as much as possible using Parafilm® (PF) without disturbing the spindle to minimise ethanol evaporation. Temperature was recorded as 20.3 °C.

2.3.4 Characterising experimental gel formulations

2.3.4.1 pH measurement of gel formulations

Gel was weighed (0.1 g), placed inside a glass beaker and dispersed evenly within 10 mL of distilled water by swirling the beaker. pH measurements were taken in triplicate from each formulation using a digital Hanna Instruments pH 209 pH meter. The pH meter was calibrated using standards with known pH values (4, 7 and 9) before use. The temperature was recorded as 20.1 °C.

2.3.4.2 CHG content of formulations

CHG formulations were diluted (0.1 mL diluted to 100 µg/mL) using HPLC grade distilled water. Drug content was measured using HPLC to examine if there was any loss of drug following formulation. According to the British Pharmacopoeia (2019a), “the preparation complies with the test if not more than one individual content is outside the limits of 85-115% of the average content and none is outside the limits of 75-125% of the average content”.

2.3.4.3 Antimicrobial susceptibility testing

Antimicrobial susceptibility testing was carried out according to the EUCAST disk diffusion method guidelines (Version 7.0 – January 2019). The British Pharmacopeia was not used as the test is advised for assessing sterility of formulations when a preservative is added rather than assessment of the efficacy of the active ingredient in the formulation.

Agar was prepared with a level depth of 4.0 ± 0.5 mm. Plates were stored in house prior to use in a laboratory fridge and allowed to rise to room temperature prior to susceptibility testing. An overnight culture of the chosen organisms (*S. aurus* and *E. coli*) was also prepared on agar prior to antimicrobial susceptibility testing.

The following morning, cotton swabs were used to remove an even colony layer from the overnight culture and the direct colony suspension method was used to make a suspension of the chosen organisms to 0.5 McFarland turbidity standard density. The suspension was mixed thoroughly on a vortex mixer and the density of the suspension was checked in a spectrophotometer with a 1 cm light path and matched cuvettes. The absorbance was measured at 625 nm and the density was within the correct range at a reading of 0.08-0.13.

The agar plates were checked visually for any signs of moisture. Assuming they passed this test, a sterile cotton swab was dipped into the suspension and plates were inoculated by swabbing evenly over the entire agar surface in three different directions, ensuring that there were no gaps between streaks. This was completed within 15 min of the suspension preparation in accordance with the EUCAST guidelines.

Within 15 min of suspension application to the agar plate, a circular paper plate was submerged within the specific formulation for 10 seconds. The paper plate was then carefully placed in the centre of the agar plate. Formulations (solutions and gels) were tested in the presence and absence of CHG (control), and in the presence of absence of the PAMAM dendrimer.

Plates were allowed to stand for 10 min so that the formulation could settle into the agar. Following this time, the agar plates were incubated at 37 ±1 ^{o}C for 24hr. After 24 hr, the zone of inhibition diameter (mm) was measured using a Duratool 150 mm digital calliper to two decimal places. Following zone of inhibition measurements, agar plates were disposed of in an autoclave waste bin.

2.3.5 Statistical analysis of data

Means and standard error were calculated in Microsoft Excel. Statistical analysis was completed using IPM SPSS 24 and in this chapter, a One-Way ANOVA was used to determine if there was any statistically significant differences between the formulation utilised and the zone of inhibition recorded (Section 2.3.4.3). A One-Way ANOVA was used after finding there was no outliers (determined by a boxplot) and data passed both the test for normality (Shapiro-Wilk) and homogeneity of variance test (Levene's).

2.4 Results

2.4.1 CHG adsorption onto glass surfaces

CHG is understood to adsorb onto glass surfaces (Denton 2001). Beakers were silanised to ascertain whether silanising glassware would decrease CHG adsorption onto glass.

Table 2.2. Percentage recovery of a CHG solution and experimental CHG gels from untreated and silanised glassware, *n=3 ± SE*.

CHG Concentration	Mean (± SEM) percentage recovery of dose spiked onto glassware	
	Untreated	**Silanised**
4% w/v CHG solution	83.59 ± 6.79	83.68 ± 1.07
4% w/v CHG gel	87.27 ± 0.96	83.21 ± 2.75
4% w/v CHG-1 mM PAMAM gel	78.74 ± 3.28	82.62 ± 4.20

The % recovery of CHG was similar across each group. This suggests that CHG adsorption onto glass is not concentration dependent but surface area dependent, confirming the results reported by Holmes *et al.* (2017).

Gel formulations were also tested to determine if there was any discernible difference between CHG glass adsorption when formulated as a solution and CHG and as a gel. This experiment was novel as CHG glass absorption form the gel formulation had never before been characterised. Similarly to the previous experiment, CHG loss was not adversely affected by time or CHG concentration within the gel formulation. Glassware pre-treatment did not improve CHG recovery. It seems there was no difference in glass adsorption between CHG solutions and CHG gels. There was a slight reduction in CHG recovery from untreated glassware containing the PAMAM dendrimer, although when considering the standard error the result was not dissimilar to the 4% w/v CHG solution. Silanising glassware did not improve the recovery of CHG, for this reason all glassware used in the Franz-type diffusion cell experiments and tape stripping

experiments were not silanised prior to use; as this method was not found to reliably improve CHG adsorption onto glassware.

2.4.2 Co-formulation Development

2.4.2.1 Ethanol Concentration

CHG is insoluble in absolute ethanol (Denton 2001). In addition, Direct mixing of CHG and the PAMAM dendrimer results in formation of a precipitate (Judd 2013a). Judd was able to stabilise CHG and PAMAM dendrimer in an 50:50 ethanol:water solution, thus prior mixing of the drug and dendrimer in an ethanol:water mixture before combining the two provided stability to the formulation. Formulations varied ethanol concentration to determine the specific point at which CHG was no longer soluble in the formulation, characterised by the formulation turning from transparent to cloudy.

Formulations including 75% ethanol and above immediately turned cloudy when CHG was added to the formulation. The cloudy formulations were mixed overnight in an attempt to solubilise the drug in the ethanol. No formulations that were observed to be cloudy had become transparent after mixing overnight. Therefore, an optimal concentration of 60% ethanol in all further formulations was chosen to be taken forward. 60% ethanol was comparable to commercial gel formulations tested whilst still allowing effective dissolution of other formulation components, without presenting stability concerns with ingredients which are known to be incompatible with ethanol absolute, such as HEC and CHG (Denton 2001, Harwood 2006).

2.4.2.2 HEC Concentration – apparent viscosity measurements

Measuring the apparent viscosity was a simple method of characterising the semisolid in comparison to other commercial gels currently available for simple skin antisepsis.

Table 2.3. Viscosity measurements (±SE) of various experimental and commercial formulations – *spindle 63 (lowest available), n=20 ± SE.*

	Viscosity (mPas) ± standard error							
Speed (rpm)	**0.5% HEC**	**1% HEC**	**2% HEC**	**3% HEC**	**4% HEC**	**Hibiscrub 4%**	**Laboratory Hand Wash**	**Milton Hand Gel**
0.3	11333.33 ±666.67	15656.67 ±1016.30	391733.33 ±134346.00	1142666.67 ±17676.00	-	3866.67 ±874.33	10000.00 ±692.82	19466.67 ±2182.80
0.5	6476.67 ±264.34	7736.67 ±373.56	356866.67 ±126392.00	1000000.00 ±20033.00	-	1933.33 ±290.59	7000.00 ±152.75	12933.33 ±1737.20
0.6	4376.67 ±53.65	5426.67 ±185.50	341400.00 ±121177.00	929333.33 ±18550.00	-	1266.67 ±66.67	6666.67 ±240.37	10800.00 ±2023.20
1	3336.67 ±288.12	4840.00 ±309.89	286466.67 ±101476.00	-	-	833.33 ±33.33	6266.67 ±233.33	6933.33 ±1707.20
1.5	2840.00 ±128.58	4056.67 ±393.38	244960.00 ±86448.00	-	-	606.67 ±24.04	5993.33 ±213.02	4800.00 ±1531.20
2	2096.67 ±54.87	3776.67 ±374.00	206401.33 ±88299.00	-	-	506.67 ±17.64	5760.00 ±240.00	4020.00 ±1115.00
3	1963.33 ±128.11	3466.67 ±349.73	-	-	-	406.67 ±14.53	5593.33 ±273.39	3263.33 ±1106.70
4	1666.00 ±47.43	3140.00 ±219.32	-	-	-	336.67 ±12.01	5480.00 ±280.00	2653.33 ±1179.50
5	1563.33 ±32.83	2633.33 ±69.60	-	-	-	310.00 ±10.00	5416.67 ±262.06	2190.00 ±997.40
6	853.333 (±29.059)	2440.00 ±69.28	-	-	-	246.67 ±13.33	5276.67 ±214.68	1876.67 ±872.93
10	833.33 ±33.33	2133.33 ±53.65		-	-	216.67 ±8.82	5240.00 ±221.21	1646.67 ±767.01
12	780.00 ±15.28	2016.67 ±43.72	-	-	-	203.33 ±8.82	5223.33 ±189.06	1203.33 ±553.85
20	763.33 ±8.82	1750.00 ±23.58	-	-	-	166.67 ±8.82	5193.33 ±173.24	1073.33 ±507.85

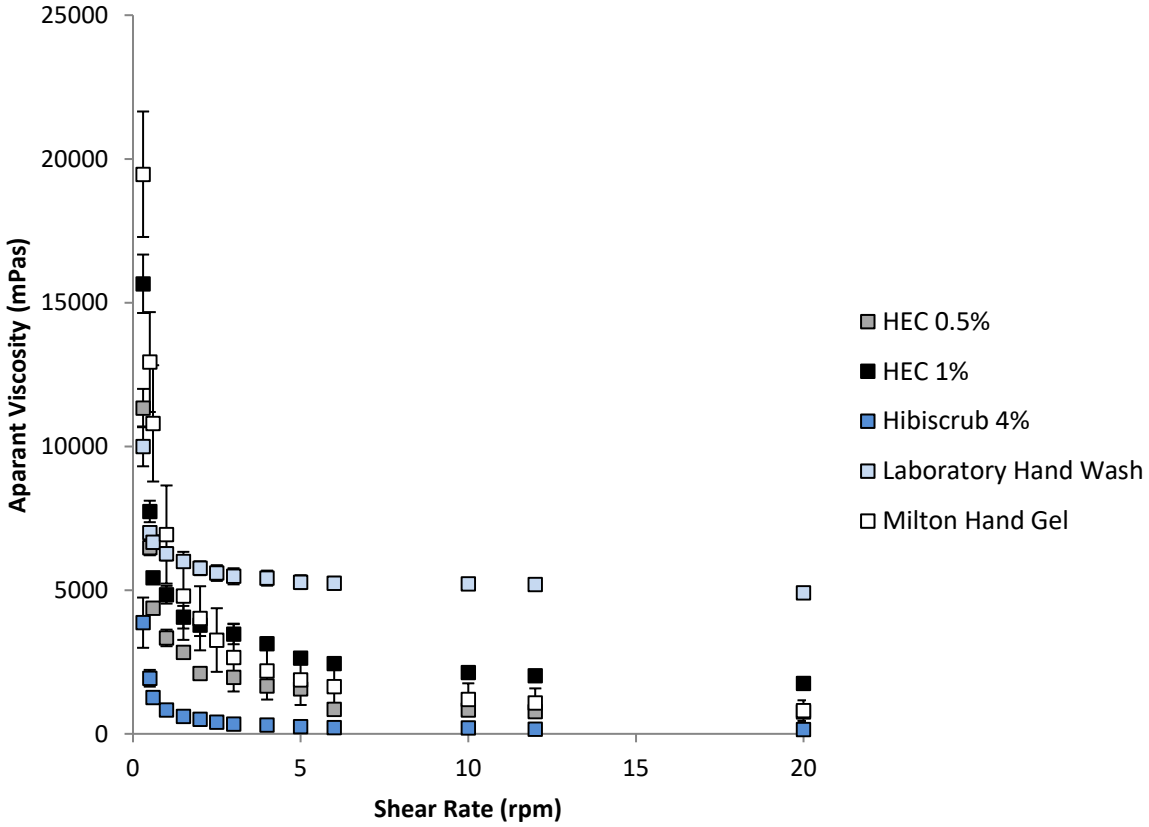

Figure 2.2. Apparent viscosity measurements of experimental and commercial formulations with increasing spindle speed ± SE. *n=20 ± SE.*

All formulations exhibited non-Newtonian, pseudoplastic behaviour (Marriott 2002) whereby increasing the shear rate decreases the viscosity of the formulation. This is consistent with the expectations of the British Pharmacopeia for gel preparations (2019a). As the spindle speed increased from 0.3-1 rpm the apparent viscosity rapidly declined; increasing spindle speed further decreased the apparent viscosity, but at a much slower rate.

The blank sections in the tabulated results indicate that an error message appeared on the viscometer at the specified speed of the spindle. This indicates that the percentage torque readings exceeded 100%. It is clear from Table 2.3 and Figure 2.2 that the experimental formulations containing 0.5% w/v and 1% w/v HEC are the closest reflection of the commercial alcohol-based hand washes and gels tested. The expected trend was observed where a higher

concentration of gelling agent in the experimental formulation caused an increase in apparent viscosity.

2.4.2.3 Appearance

The gels which appeared stable (i.e. which were not cloudy from excess ethanol) were transparent with a strong alcohol odour. Formulations containing 0.5%-1% HEC spread across the skin easily and there appeared to be no change in physical stability upon first application.

A previous study noted that upon addition of CHG to a G3 PAMAM-NH_2 dendrimer solution, CHG precipitates out (Judd 2013a). This was confirmed experimentally in this study, and is further explored in Section 3.4.7. Stabilising the CHG and dendrimer in separate ethanol:water solutions prior to mixing together appeared to prevent precipitation before formulation application to the skin (Figure 2.1).

2.4.2.4 pH

Table 2.4. Measured pH for experimental formulations with and without the addition of PAMAM dendrimer following a 1:50 dilution using purified water. *n=3 ± SE.*

Formulation	Mean pH measurement ± standard error
1% CHG	7.7 ± 0.12
2% CHG	7.8 ± 0.06
3% CHG	8.0 ± 0.07
4% CHG	8.0 ± 0.03
4% CHG-0.5 mM PAMAM	8.7 ± 0.06
4% CHG-1 mM PAMAM	8.9 ± 0.04

A Kruskal Wallis ANOVA indicated that there was no statistically significant difference between the formulation and pH measurement ($p>0.05$).

2.4.2.5 CHG content of experimental formulations

Table 2.5. CHG recovery from experimental formulations after dissolving 1mL of formulation to create a 10µg/mL solution - n=*3/4 ± SE depending on formulation, see table.*

Formulation	Percentage Recovery ± standard error (%)
1% CHG *(n=3)*	89.07 ± 4.53
2% CHG *(n=3)*	90.85 ± 2.79
3% CHG *(n=3)*	92.63 ± 3.12
4% CHG *(n=3)*	93.15 ± 2.98
4% CHG-0.5 mM PAMAM *(n=4)*	86.69 ± 2.35
4% CHG-1 mM PAMAM *(n=4)*	87.22 ± 2.38

A One-Way ANOVA indicated that there was no statistically significant difference between the formulation and CHG recovery ($p>0.05$). The results also pass the uniformity of content test specified by the British Pharmacopoeia (2019a). The test specifies that "the preparation complies with the test if not more than one individual content is outside the limits of 85-115% of the average content and none is outside the limits of 75-125% of the average content".

2.4.2.6 Antimicrobial efficacy of formulations

The zone of inhibition readings can be found in Table 2.6 and Table 2.7. Initially, specific volumes (10 µL, 50 µL and 100 µL) of formulation were placed within the centre of the agar plate and left in the incubator for 24 hr. However, the formulations were not viscous enough to retain the initial position within the centre of the agar plate, and many plates showed evidence of the

formulation running across the agar, distorting the "circular" zone of inhibition (data not shown). Submerging a paper disc within the formulation for 10 seconds was found to better retain the circular shape of the zone of inhibition, allowing for greater accuracy when taking diameter readings.

Table 2.6. Zone of inhibition of experimental formulations and commercial benchmarks against Gram positive *S. aureus* at 37 °C after 24 hr, *n = 3 ± SE.*

	Zone of inhibition (mm)			
	Solution		Gel	
Formulation	**Mean**	**Standard Error**	**Mean**	**Standard Error**
Control	11.04	0.21	11.99	0.53
Hibiscrub® (4% CHG)	19.12	1.11	-	-
4% CHG	21.01	2.05	23.87	1.05
4% CHG-0.5 mM PAMAM	22.48	1.64	23.01	0.26
4% CHG-1 mM PAMAM	18.10	0.69	22.54	1.84

Table 2.7. Zone of inhibition of experimental formulations and commercial benchmarks against Gram negative *E. coli* at 37 °C after 24 hr, *n = 3 ± SE.*

	Zone of inhibition (mm)			
	Solution		Gel	
Formulation	**Mean**	**Standard Error**	**Mean**	**Standard Error**
Control	10.59	0.71	11.18	0.63
Hibiscrub® (4% CHG)	19.51	0.51	-	-
4% CHG	17.18	0.13	20.25	0.58
4% CHG-0.5 mM PAMAM	18.36	0.76	20.79	0.98
4% CHG-1 mM PAMAM	18.84	0.43	19.54	0.21

Table 2.6 and Table 2.7 indicate confirms that CHG was active within the formulations, as all formulations containing CHG resulted in a significantly larger zone of inhibition than the control ($p < 0.05$). Furthermore, the co-formulation still exhibits antimicrobial efficacy. The efficacy from the co-formulation is comparable to the commercial benchmark, which is expected given that both formulations contain 4% w/v CHG and the paper disc placed on the agar plate was submerged in the respective formulation for the same amount of time. There was no increased zone of inhibition when comparing the co-formulation to the experimental formulation with PAMAM dendrimer, unlike results previously published by Holmes *et al.* (2019) indicated that PAMAM dendrimers exhibit antimicrobial properties. There was a general decrease in zone of inhibition when comparing *S. aureus* agar plates and *E. coli* agar plates across all formulations.

A One-Way ANOVA indicated that there was no significant difference in antimicrobial efficacy between formulations when applied to an agar plate colonised with *S. aureus* ($p>0.05$). There was a significant difference noted in the zone of inhibition between formulations when applied to an agar plate colonised with *E. coli* ($p <0.05$). Table 2.8 reports the pairwise comparisons which were statistically significant –

Table 2.8. One-Way ANOVA data analysis to determine whether formulations with and without PAMAM dendrimer, and the commercial benchmark Hibiscrub significantly affect the zone of inhibition following 24hr incubation with *S. aureus* or *E. coli.* Pairwise comparisons are arranged so that the formulation which developed the highest concentration of CHG is given first. *OWA – One-Way ANOVA, n=3.*

Bacterial culture	Analytical Test	Statistically Significant Result	Pairwise Comparisons	
			F1	F2
S. aureus	OWA	N	-	-
E. coli	OWA	Y	4% CHG gel	4% CHG solution
			4% CHG-0.5 mM PAMAM gel	4% CHG solution

2.5 Discussion

As discussed in Section 2.2, the purpose of this chapter was to develop a physically stable, clinically acceptable and efficacious co-formulation containing both CHG and a G3 PAMAM-NH_2 dendrimer for enhanced deposition of CHG into the skin for improved topical antisepsis. This study builds upon the results published by Holmes *et al.* (2017), where a G3 PAMAM-NH_2 dendrimer pre-treatment enhanced the depth permeation of CHG within porcine skin. The development of a drug-dendrimer co-formulation would ultimately be more practical and convenient to use and therein lies the rationale for this study.

The concentrations of PAMAM dendrimer chosen for the co-formulations were based on previously reported findings (Holmes *et al.* 2017). The study used 0.5 mM-10 mM concentrations of the PAMAM dendrimer in the pre-treatment but found that the penetration enhancement effect of the dendrimer was not concentration-dependent – a similar enhancement effect occurred over the concentration range examined (0.5 mM-10 mM) relative to control. Therefore, this study used PAMAM dendrimer concentrations of 0.5 mM and 1 mM (equivalent to 3.45 mg/mL and 6.91 mg/mL), which was within the range of concentrations used in other topical dendrimer studies (Moghimi *et al.* 2010; 1, 4 and 6 mg/mL); (Chauhan *et al.* 2003; 2 mg/mL) and so was thought to be within normal limits for clinical use.

Following justification of the use of a PAMAM dendrimer for CHG mediated permeation enhancement, it was imperative to determine the type of formulation appropriate for enhanced delivery of CHG via co-formulation with the PAMAM dendrimer. NICE (2019) recommends that either an alcohol or aqueous based solution of CHX is used as a topical antiseptic, dependent on whether the site is next to a mucous membrane, and specifically names Hibiscrub® as an aqueous based solution. Antimicrobial formulations are also commercially available as gels which contain large amounts of ethanol due to its antimicrobial properties (Ali *et al.* 2001). An

ethanol-based gel was ultimately chosen as the formulation in this study, for numerous reasons. Ethanol-based hand gels are fast acting, economical and convenient to use (Rotter 2001, Traore *et al.* 2007, Bolon 2016). They apply to the skin smoothly, are aesthetically pleasing, and the ethanol smell is associated with cleanliness. Gels may be preferred over other topically available formulations (Dunlap *et al.* 1998, Hol 2010a, 2010b). For example, (Lambert, Hol and Vink (2015) found patients preferred using a betamethasone dipropionate gel rather than ointment due to the convenience and ease of application, despite the equal effectiveness of both formulations. Therefore, an antimicrobial gel was chosen as this replicated commercially available products which are available and acceptable (in the majority) to patients. In addition to the predicted consumer acceptability associated with such a formulation (which was considered due to the progression of the study from a pre-treatment study (completed by [Holmes *et al.* 2017]) to a convenient one-step product), a formulation which contained ethanol was found to be the most appropriate when considering formulation stability.

Direct mixing of CHG and the PAMAM dendrimer results in formation of a precipitate (Judd 2013a). Judd was able to stabilise CHG and PAMAM dendrimer in an 50:50 ethanol:water solution, thus prior mixing of the drug and dendrimer in an ethanol:water mixture before combining the two provided stability to the formulation. The results obtained previously were developed further in this study by increasing the concentration of volatile solvent within the formulation, to replicate commercially available antimicrobial gels which typically contain ≥ 60% ethanol (Boyce and Pittet 2002); with the additional knowledge that ethanol exhibits antimicrobial properties (Ali *et al.* 2001) and thus would be a useful addition into an antimicrobial formulation. Moreover, the PAMAM dendrimer is considered more stable in ethanol than water (Sigma Aldrich 2019a). However, it was imperative not to increase the concentration of ethanol within the formulation higher than necessary, firstly because CHG is insoluble in absolute ethanol (Denton 2001, Kaiser *et al.* 2009) and secondarily because this

would no longer reflect commercial products. Additionally, high concentrations of ethanol may cause irritation via lipid extraction (Kai *et al.* 1990, Kownatzki 2003), which has the potential to reduce consumer acceptance, although this is reportedly uncommon. For example, the frequency of skin irritation and dryness was found to be significantly lower in nurses when using an alcoholic hand gel in comparison to traditional soap and water ($p < 0.05$) (Boyce *et al.* 2000, Löffler and Kampf 2008), potentially due to excipients producing an occlusive effect.

A range of ethanol-based gel candidates were formulated which contained 50-100% ethanol. Formulations that contained ≥ 75% ethanol immediately appeared cloudy upon addition of CHG. There was no improvement in the appearance of the formulation following mixing overnight. Thus, 60% ethanol was utilised in all further formulations. This allowed effective dissolution and stability of formulation components, without causing precipitation of CHG and HEC which are known to be incompatible with ethanol absolute (Denton 2001, Harwood 2006), whilst maintaining a formulation which was comparable to commercial antimicrobial gels.

HEC was utilised in this study as a gelling agent primarily due to its safety profile (non-toxic and non-irritant; [Liebert, 1986]), established use in topical preparations, compatibility with CHG, and with the potential to create a film on the skin surface which could maximise drug contact with the desired site of action. HEC has been used successfully in a gel formulation containing CHX as an endodontic irrigant (Ferraz *et al.* 2001), and therefore there were no concerns regarding potential incompatibilities between the two compounds. A patent secured by Khan and Hoang (1997) detailed the invention of an antimicrobial film containing HEC and CHG. The film produced was tack free, flexible, and its retention on the skin surface enhanced contact with the antimicrobial throughout a surgical procedure. HEC is hygroscopic (Harwood 2006) and the increasing *stratum corneum* hydration in topical formulations has already been well established as a method of enhancing drug delivery into the skin (McKenzie and Stoughton 1962, Behl *et al.* 1980, Roberts and Walker 1993). This mechanism held the potential for further

enhancement of CHG permeation into the skin similarly to a secondary benefit of utilising ethanol in the formulation, however this was not the primary use of the gelling agent and it was proposed that film-forming properties would be a greater contributor to enhancement of CHG depth permeation within porcine skin. Interactions between HEC and CHG have previously reported an interaction whereby CHG acts as a plasticiser, (White 1991, Sine *et al.* 2000) which was considered to be useful for retaining a flexible film on the skin surface without cracking (Wypych 2017), ultimately increasing drug residence time on the skin surface.

Glycerol was included in the topical formulation primarily for its emollient properties (Price 2006). Typically, consumers prefer topical preparations to feel less "greasy" (Feldman and Housman 2003, Bewley and Page 2011) and so a minimal amount of glycerol was added to the formulations to establish a balance between enhancing "smoothness" but preventing the formulation from feeling greasy, which could reduce consumer acceptance. Furthermore, glycerol is understood to act as a plasticiser (Pedersen and Jemec 1999). With the understanding that CHG may also act as a plasticiser due to interactions with HEC (White 1991, Sine *et al.* 2000), which may make the drug less available for interaction with the *stratum corneum*, glycerol may be added to the formulation as a plasticiser to support film formation and "saturate" the role, allowing CHG to be readily available for partitioning into the skin. Glycerol has also been attributed to permeation enhancement effects through hydrating the *stratum corneum* (Hara and Verkman 2003, Atrux-Tallau *et al.* 2010), though this was not the primary reason for including the compound in the gel. Furthermore, the minimal amounts formulated in the co-treatment were thought to have minimal occlusive properties, although these effects may become more dominant following evaporation of the ethanolic vehicle.

In summary, the excipients added to the formulation were considered primarily for stability because of the numerous incompatibilities associated with CHG (McCarthy 1969, Yousef *et al.* 1973, McCarthy and Myburgh 1974, Denton 2001). Secondarily, it was imperative to create a

formulation which could be considered similar to commercially available antimicrobial formulations given that this study focused on developing a co-treatment from a previous pre-treatment study (Holmes *et al.* 2017), ultimately creating a more convenient, practical and acceptable product.

The purpose of characterising the experimental formulations was to benchmark its characteristics against commercially used ethanol based antimicrobial gels, the commercial benchmark (Hibiscrub®), and against British Pharmacopoeia standards where appropriate. The British Pharmacopoeia (2019a) suggests that topical dosage forms should be characterised by their rheological properties, uniformity of content, ability to be withdrawn from a suitable container and sterility where appropriate. In addition to the tests above, the International Pharmacopoeia (2018) suggests that topical dosage forms should be characterised by inspecting physical stability, and the uniformity of consistency. Furthermore, the pHs of the formulations were measured to determine the effects on drug ionisation and potential for skin irritation.

All formulations (with the exception of those discounted such as formulations which included >75% ethanol) showed no visible signs of drug precipitation when initially formulated. Formulations were transparent and had a strong alcohol scent. Following formulation of candidates with a range of HEC concentrations, the use of higher HEC concentrations (2-4%) resulted in formulations that were excessively viscous, and in the case of 3-4% HEC, gritty in texture. This suggested incomplete dissolution of HEC. All other formulations appeared to spread easily and evaporation of the vehicle began at around 1 minute after application. This left behind a thin, flexible film. This supports clinical acceptability of the formulation, which was not sticky or greasy, spread easily across the skin and was visually acceptable and therefore fulfils many of the requirements for increasing patient compliance when using topically applied formulations (Brown *et al.* 2006).

The apparent viscosity was measured to benchmark the candidate formulations rheological behaviour against commercially available antimicrobial gels and the commercial benchmark. Topically applied formulations require flow properties so they can effectively be placed in a container, and easily removed, handled and appropriately applied to the affected area by the consumer (Mastropietro *et al.* 2013). The plot of apparent viscosity against shear rate immediately showed that the experimental gels showed pseudoplastic, non-Newtonian behaviour (Florence and Attwood 2006b), in agreement with the commercial products tested. Methyl cellulose derivatives are understood to exhibit this type of behaviour due to the entanglement of long carbon chains in an immobilised solvent or solvent blend, which become aligned when a shearing force is applied, reducing the resistance to flow (Marriott 2002). When used by the consumer, the product must be removed from the container and applied to the treatment site, thus application of the product will reduce the formulation viscosity via application of force. An initial decrease in viscosity due to formulation application onto the skin may theoretically increase the rate of drug partitioning into skin temporarily, as there will be a reduction in diffusional resistance, improving CHG contact with the *stratum corneum* surface. However, in the case of the candidate formulations created in this study, evaporation of the ethanol vehicle is likely to negate this initial decrease in viscosity by increasing the percentage of HEC in the residual formulation. However, this increase in viscosity may aid in retaining the drug on the skin surface, therefore non-Newtonian behaviour of a topically applied formulation can be considered advantageous when considering the balance required for consumer acceptance whilst promoting drug contact with the skin surface, and availablitiy for *stratum corneum* partitioning. Semi-solid formulations intended for topical use typically exhibit pseudoplastic behaviour.

Figure 2.2 illustrates the apparent viscosity measurements of commercially available antimicrobial formulations and the results indicated that the experimental formulations

containing 0.5% w/v and 1% HEC w/v were most reflective of the commercial products (formulations containing 2-4% w/v HEC were excessively viscous when compared to commercially available products). This information was utilised alongside the *in vitro* diffusion cell studies of formulations containing differing amounts of HEC (Section 3.4.2) to determine the most appropriate concentration of HEC to formulate into the drug-dendrimer co-formulation. The results in Chapter 3 concluded that 0.5% HEC was the most appropriate concentration of gelling agent to use, thus the concentration of gelling agent in the CHG-PAMAM co-formulations reflected the commercially available products in terms of rheological behaviour in addition to maximising the concentration of CHG delivered into skin (Figure 3.6).

It was important to determine whether drug content would be adversely affected by the addition of the G3 PAMAM-NH_2 dendrimer to the formulation. The results of the uniformity of content study indicated that there was no significant difference between the formulation in question and the uniformity of CHG content, therefore addition of the dendrimer did not significantly reduce the amount of CHG viable for topical skin antisepsis. Furthermore the mean percentage of drug detected in each formulation complied with British Pharmacopoeia standards (2019a) for topical semi-solid dosage forms.

The pH of the candidate formulations was measured to compare against the commercial benchmark and to determine if the addition of the PAMAM dendrimer significantly influenced the formulation pH. This pH required consideration because of the potential influence on the *stratum corneum* barrier (and thus, the likelihood of causing irritation), and the potential influence on ionisation state of the drug, i.e. the ability of the drug to permeate into the skin. The pK_a value of the drug, pH of the formulation and the pH of the skin must all be considered when understanding the effects on topical drug permeation, which is complex and not easily predictable (Surber *et al.* 2018). The effect of pH on the dermal delivery of drugs has been widely investigated (Swarbrick *et al.* 1984, Siddiqui *et al.* 1985, Neubert 1989, Valenta *et al.* 2000).

Typically, unionised drugs are better permeators than ionised ones (Shore *et al.* 1957), but in the case of CHX, the ionised salt form (CHG) is typically preferred as this form has a much higher aqueous solubility (0.008% w/v CHX, > 70% w/v CHG; [Denton, 2001]). Without sufficient solubility, a suitable concentration gradient for drug diffusion cannot be established which minimises drug permeation into skin.

The results of the study indicated that there was a general trend of increasing pH with increasing CHG concentration, and a further increase in pH upon addition of the G3 PAMAM-NH_2 dendrimer. The lowest pH measurement was 7.74 ± 0.12 (1% w/v CHG) and the highest pH measurement was 8.98 ± 0.04 (4% CHG-1 mM PAMAM). CHX is a basic drug and has two pK_a values: 10.3 and 2.2 (Hugo and Longworth 1964) which represents the formation of the monocation and dication respectively. Thus, at pH 2.2, the drug exists 100% in the monocation form, and 61% in the dication form. As the pH increases, the percentage of the dication form decreases (Hugo and Longworth, 1964; Figure 2.3).

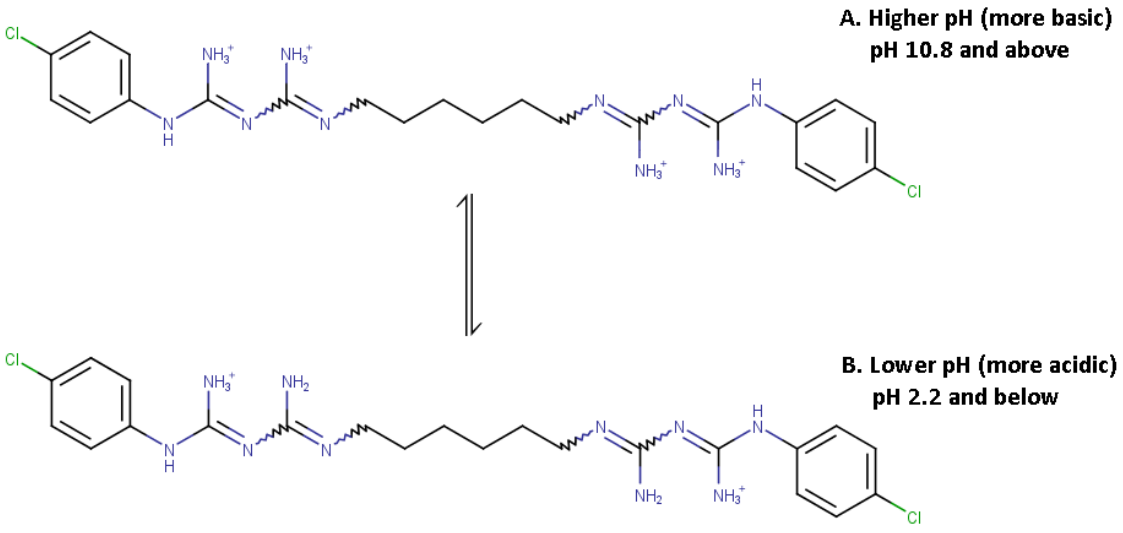

Figure 2.3. Ionisation states of CHX in A. basic and B. acidic conditions. CHG has two pK_a values representing the monocation and dication, 2.2 and 10.8 respectively (Hugo and Longworth 1964).

Thus, the drug exists in the ionised form (primarily dication) when considering the pH of the gel formulation. The pH would have to be increased above 10.8 to provide a primarily unionised form of the drug if one is hoping to manipulate the ionisation state of the drug to maximise dermal delivery. However, the likelihood of CHG precipitation increases when the pH increases above 8 in aqueous solution (Denton 2001). This supports the requirement of a permeation enhancer to deliver greater amounts of CHG into the skin. Experimentally, there were no visible signs of drug precipitation of the formulation prior to use despite some pH measurements recorded above pH 8 (maximum recorded measurement 8.98 ± 0.04 from the 4% w/v CHG-1mM PAMAM formulation).

Boonchai and Iamtharachai (2010) evaluated the pH of commonly available cleansers and alcohol gels. Fifteen cleansers were measured, and the pH was found to vary widely. The lowest measurement was 5.21 (Eucerin pH 5 Wash Lotion™), the highest was 11.69 ("Attack Concentrated™" Laundry Detergent). The gels within the list were found to exhibit a slightly acidic pH (Physiogel™, pH 5.95 and Siriraj™ hand clean 70% alcohol gel, pH 5.5), and Hibiscrub® exhibited an average pH of 5.82. Therefore, the gels formulated within this Chapter cannot be considered in line with the pH of the commercial benchmark. The shift towards a more basic pH of the co-formulations was attributed to the addition of the PAMAM dendrimer due to its numerous peripheral amine groups. It could be argued that a slightly acidic formulation pH would be preferred for topical application, as the *stratum corneum* surface exhibits a slightly acidic pH of approximately 4.5-5.3 when healthy, increasing in a gradient with increasing depth to 6.8 in the lower *stratum corneum* (Fluhr and Elias 2002).

Stratum corneum barrier function is linked to the pH of this layer, as formulation this barrier is dependent on several pH-sensitive enzymes, which function optimally at the "acid mantle" pH found in normal skin. As described in Section 1.1.4, degradation of corneodesmosomes is regulated by proteolytic cleavage of their extracellular portions, viakallikrein-regulated

peptidases and cathepsins (Kitajima 2015). β-glucocerebrosidase and acidic sphingomyelinase are two enzymes used to process lamellar lipids and work optimally at pH 5.6 and 4.7 respectively (Rippke *et al.* 2002). Activity of β-glucocerebrosidase is 10 times lower when the pH is increased from 5.5 to 7.4 (Mauro *et al.* 1998). Studies have also shown that elevating skin pH disturbs the skin barrier by increasing the activity of serine proteases (increasing the rate of desquamation) and reducing the activity of ceramide-generating enzymes (decreasing the presence of a key lipid component of the barrier, [Hachem *et al.* 2003, 2005]). Theoretically, application of a slightly basic formulation to the skin may affect the ability of enzymes to maintain the skin barrier (Hachem *et al.* 2003, 2005). However, one must consider the use of this formulation in context to other topically applied products which are typically alkaline, such as soaps (Baranda *et al.* 2002). Soaps can be used multiple times daily and sustained use of soaps over time can affect the barrier repair mechanism of skin (Fluhr *et al.* 2001, Ananthapadmanabhan *et al.* 2004). In context, a CHG-PAMAM co-formulation intended for use prior to surgery is unlikely to be used frequently enough by a single patient to cause changes to the *stratum corneum* barrier function considered comparable to other commercially used cleansers when used repeatedly. Rippke, Schreiner and Schwantiz (2002) found that hand washing with soap increased the pH of the palms by 3 units for 90 min after washing. It may be the case that the experimental co-formulation would cause an increase in skin pH, but this effect would likely be transient and therefore considered worthwhile due to the reduced risk of SSTIs caused by an enhanced deposition of CHG.

Zone of inhibition experiments were conducted to show reasonable equivalence of efficacy of the drug in the experimental formulations compared to the commercial benchmark (Hibiscrub®). As the primary aim of this thesis was to enhance CHG deposition for enhanced skin antisepsis, it was imperative to ensure the antimicrobial efficacy of the formulations created in this chapter were equivalent to formulations currently available. As mixing of CHG and a G3

PAMAM-NH_2 dendrimer has been found to cause drug precipitation (Figure 3.1; [Judd, 2013a]), and the pH of the co-formulations were found to be above pH 8 which has been reported to cause CHG precipitation (Denton 2001), it was important to establish that the formulation retained antimicrobial activity. The results indicated that there was no statistically significant difference between the experimental formulations and the commercial benchmark when assessing the zone of inhibition. It appeared that combining both the drug and dendrimer in a co-formulation did not significantly affect the antimicrobial activity of the drug. Therefore, provided that the co-formulation was able to enhance deposition of CHG within porcine skin (explored in Chapter 3), antisepsis effects equivalent to or greater than the commercial benchmark would occur in deeper skin layers, fulfilling the main aim of this thesis.

Additionally, the zone of inhibitions recorded for the gram positive (*S. aureus*) strain were greater than the gram negative (*E. coli*) strain. CHX is active against both gram positive and gram negative bacteria, though chlorhexidine salts are known to be less active against gram negative bacteria than gram positive bacteria (Owen 2006), which is consistent with the results presented in this study. There was a statistically significant increase in the zone of inhibition when comparing the 4% CHG and 4%-0.5 mM gel with the 4% CHG solution. This may suggest that gels increase the antimicrobial efficacy of a formulation applied to the skin, potentially due to the increased contact time on the biological tissue. A further reason may be due to the evaporation of the ethanolic vehicle in the gel, which would increase the % CHG saturation in the formulation (Schwarb *et al.* 1999, Intarakumhaeng and Li 2014, Woertz and Surber 2014). However, this statistical significance did not extend to the 4% CHG-1 mM PAMAM gel group and so further repeats of the test should be conducted before such conclusions are definitively made.

The suitability of the storage container was also considered in accordance with suggestions from the International Pharmacopoeia (2018). The formulations were stored in an amber glass bottle, as both CHG and the G3 PAMAM-NH_2 dendrimer should be shielded from light according to the

manufacturer (Sigma Aldrich, 2019a, 2019b). Formulations which included 0.5-2% w/v CHG were easily removed from the bottle, whereas formulations with 3-4% w/v CHG could not be removed from the formulation by pouring and had to be removed manually using a spatula. To counteract the effects this might have on the viscosity of the formulation for *in vitro* studies, as it was previously shown that increasing shear stress reduced the apparent viscosity, before application to the skin formulations containing 3-4% w/v HEC were allowed to stabilise by storage in a wider container overnight, reducing the amount of shear stress required in the process of removing formulation from the container and applying the formulation to the porcine skin surface.

In summary, the ethanol-based gel formulations created in this chapter (except those that have been discussed and omitted) appear similar to commercially available gel formulations when considering appearance, consistency, physical stability, rheological behaviour and antimicrobial efficacy. Where the properties of the formulations (such as pH) deviate from commercially available formulations, this has been justified accordingly. The gel formulations appeared stable in the container and they retained their antimicrobial activity when compared to the commercial benchmark. The development of the formulation from a pre-treatment to a co-treatment may increase consumer acceptance and adherence.

2.6 Conclusion

The aim of this chapter was to identify a formulation containing both CHG and a G3 PAMAM-NH_2 dendrimer that was physically stable, comparable to commercially available antimicrobials and acceptable to the consumer. Fulfilling these aims was considered a requirement for successful progression from the previously published PAMAM pre-treatment (Holmes *et al.* 2017) to a more convenient and acceptable co-formulation. The study selected the most appropriate formulation for the delivery of CHG into skin with the most viable excipients for assuring drug stability and acceptability of the final formulation. Furthermore, the formulation was characterised against, and found comparable to, commercially available antimicrobial formulations.

The final CHG-PAMAM co-formulations appeared stable and cosmetically acceptable, two primary concerns when developing a formulation for the end user. The zone of inhibition results indicate that co-formulation remains able to kill both gram positive and gram negative bacteria and retains its antimicrobial activity compared to the commercial benchmark. Assuming the co-formulation delivers an increased CHG concentration into deeper skin layers (investigated in Chapter 3), there may be potential for reducing the incidence of SSTIs in the patient population.

3 Chapter Three - Co-formulation of CHG with G3 PAMAM-NH2 dendrimer

3.1 Introduction

It was established in Chapter 2 that a stable and clinically viable CHG gel formulation could be created with the incorporation of a G3 PAMAM-NH_2 dendrimer. This was a development from a previous "proof of concept" study (Holmes *et al.* 2017), which found that a G3 PAMAM-NH_2 24hr pre-treatment enhanced the depth permeation of CHG within porcine skin. For clinical use, a 24hr pre-treatment step is impractical when considering CHG is used for skin antisepsis prior to surgery. It was postulated that combining CHG with a PAMAM dendrimer would increase the depth permeation to that required for targeting bacteria in deeper skin layers, but without extensive PAMAM permeation or systemic CHG absorption which has the potential to cause irritation and or toxicity and thus could prevent the formulation from being accepted by patients. This is a novel use of the dendrimer, which has not yet been successfully incorporated into a co-formulation with CHG for the topical delivery of the antimicrobial.

The use of PAMAM dendrimers for topical and transdermal drug delivery has been discussed extensively in Section 1.12, and their properties which make them viable for use in topical and transdermal drug delivery have been discussed in Section 2.1. Many studies have investigated the use of PAMAM dendrimers in a co-formulation for enhanced permeation of a drug (Chauhan *et al.* 2003, Yiyun *et al.* 2007, Venuganti and Perumal 2008, Küchler *et al.* 2009, Filipowicz and Wołowiec 2011), but the permeation of CHG from a topical gel formulation has yet to be investigated.

3.2 Aims and Objectives

The aim of this chapter was to identify an efficacious formulation containing CHG and a G3 PAMAM-NH_2 dendrimer which would deliver enhanced depth permeation of CHG compared to a commercially available benchmark (Hibiscrub®). The objectives to complete this aim were:

1. To quantify the depth permeation of the commercial benchmark Hibiscrub® (4% w/v CHG) into porcine skin *in vitro* using Franz-type diffusion cell and tape stripping studies
2. To systematically create gel formulations with varying amounts of gelling agent, drug and G3 PAMAM-NH_2 dendrimer
3. To measure subsequent CHG depth permeation from each formulation using Franz-type diffusion cell and tape stripping studies
4. To compare CHG depth permeation from experimental formulations with the commercial benchmark Hibiscrub® (4% w/v CHG) to determine if there is evidence of improved depth permeation of CHG from the experimental formulations

3.3 Materials and Methods

3.3.1 Materials

The following chemicals were purchased from Sigma Aldrich: trimethylamine (25% wt. in H_2O), HPLC grade methanol (>99.8%), glacial acetic acid (>99/7%) and HPLC grade acetonitrile (>99.8%). Sodium octane-1-sulfonate monohydrate (99+% crystalline) was purchased from Alfa Aesar. Franz-type diffusion cells were purchased from Soham Scientific (Cambridge, UK). The following were purchased from Fisher Scientific: syringe filters (0.2 µm, 15 mm diameter), HPLC vials (1.5 mL crimp neck vial, 32 × 11.6 mm) and crimper caps (1.0mm), D-squame™ tape strips (standard), blot roller for ensuring homogeneity of tape strip pressure applied to skin surface. Loctite® super glue was purchased from Lyreco (Shropshire, UK).

3.3.2 Methods

3.3.2.1 Experimental gel formulation development

To create the most efficacious CHG-PAMAM co-formulation, several parameters were systematically altered and tested in succession using Franz-type diffusion cell studies and tape stripping studies. Drug permeation was assessed via HPLC analysis of receptor fluid samples and tape strip(s) which were adjusted for the weight of *stratum corneum* removed. Ultimately the receptor fluid samples provided little information on CHG permeation as all samples were below the limit of detection (<LOD; appendix 1), consequently the tape strip data is the main focus of this chapter.

The formulation which improved skin deposition of CHG the most was taken forward into the next round of testing. All formulations were created in standard amber glass reagent bottles

with a plastic screw lid as formulated in Chapter 2. Details of formulation components can be found in Section 2.3.3. The HEC prototype formulation which delivered the most CHG into porcine skin was carried forward and four formulations were created with varying CHG content (1-4% w/v) to reflect the typical concentrations of the active ingredient found in commercial formulations. The most efficacious concentration of CHG from diffusion cell and tape stripping studies was taken forward into the CHG-PAMAM co-formulation.

3.3.3 *In vitro* diffusion cell studies and tape stripping protocols

3.3.3.1 Experimental Protocol

All *in vitro* percutaneous penetration studies conducted in this thesis follows the following protocols where possible. The protocols stated are best practice for using porcine skin as a surrogate for human skin in *in vitro* studies. Any deviations to these protocols are stated within the chapter;

(i) *OECD Test Guideline 428 (2004) – Skin absorption: In vitro method*

(ii) *OECD Guidance Document No. 28 (2004)*

(iii) Holmes et al (2017)

3.3.3.2 Preparation of porcine skin

Porcine flank skin samples were sourced from a local abattoir as a residue of the food production process but before exposure to the steam or chemical cleaning process. Excess tissue and subcutaneous fat was carefully removed from the skin with a scalpel, taking care not to damage the skin layers. Excess surface hair was trimmed using scissors, taking care to keep the *stratum corneum* intact. Other debris, such as soil, was removed from the skin surface by gently washing

the skin using minimal amounts of HPLC grade distilled water and by gently patting the skin with a paper towel to remove excess moisture. Samples were stored in a freezer at -20 °C and were fully thawed prior to use.

TEWL was measured for each skin sample to check its integrity using a Biox Aquaflux™ meter (model AF200). The TEWL probe was allowed to equilibrate for 2 min before any TEWL measurements of skin samples were taken. Any skin sample with a TEWL measurement 4 × above or below the mean TEWL measurement was discarded (Davies *et al.* 2015).

3.3.3.3 Diffusion cell studies

Diffusion cells were prepared by adding a magnetic stirrer bead to the receptor chamber of each cell, followed by placing a thin layer of Loctite® superglue around the outer rim of both the receptor and donor chamber and placing the porcine skin which had passed the integrity check between the two chambers. The cell was secured by a horseshoe clip, inverted, and the receptor compartment filled with phosphate buffered saline (PBS, approximately 3 mL per cell). The injection port was covered with PF to prevent evaporation of receptor fluid whilst in the water bath. Cells were placed in a water bath set to 37 °C to replicate a skin surface temperature of 32 ± 1 °C and allowed to equilibrate for 30 min, after which 1 mL of formulation was added to each donor chamber (surface area of Franz-type diffusion cell donor chamber – 1.03 cm^2). At specific time points – 1 hr, 2 hr, 3 hr, 4 hr, 6 hr, 8 hr, 12 hr and 24 hr, 1 mL of receptor fluid was removed from the receptor compartment and replaced with 1 mL of fresh PBS. The 1mL of fluid which was removed was syringe filtered (0.2 µm) placed inside a glass HPLC vial, sealed, and analysed immediately using HPLC to determine permeation of CHG through the porcine skin.

3.3.3.4 Tape Stripping

Following the 24 hr time point of the diffusion cell experiments, each cell was disassembled. Excess formulation was gently removed from the skin surface and was placed in a glass vial filled with 100 mL of water and homogenised using a Retsch Homogeniser. 2 mL aliquots (10 mL in total) of water were washed over the skin and donor chamber in order to determine if any excess formulation had remained on the skin surface, or if it had adsorbed onto the donor chamber. The skin was then patted with a paper towel to remove excess moisture. Skin was allowed to air dry for 2 hr in accordance with a published protocol (Al-Mayahy *et al.* 2019), then 21 D-Squame™ tape strips were taken from each piece of skin. The tape strip was weighed on a 4-point balance (OHAUS Pioneer) before and after tape stripping occurred so that strips could be adjusted for weight of *stratum corneum* removed. Tape strips 4-6, 7-10, 11-16 and 17-21 were accumulated to consider the comparative relationship between the HPLC LoD/LoQ and the poor skin permeability of CHG reported previously, particularly on deeper tape strips (Karpanen *et al.* 2008a). This specific tape stripping method was replicated from Holmes *et al.* (2017). Tape strips were placed in 20 mL vials, filled with 5 mL of mobile phase, sealed, and left overnight to allow CHG to leach from the tape strips into the mobile phase. The following morning 1 mL of sample was syringe filtered (0.2 µm) into a HPLC vial and analysed using HPLC.

Following HPLC analysis, the concentration of drug on the tape strip was normalised to account for the amount of *stratum corneum* material removed per tape strip using an equation published by Reddy *et al.* (2002).

$$C_n = m_n p_{sc} / m_{sc,n} \quad \textbf{(3)}$$

Where

C_n is the concentration of CHG on the n^{th} tape strip once accounted for the mass of *stratum corneum* material

m_n is the mass of drug on the n^{th} tape strip

p_{sc} is the density of the *stratum corneu*m (1 g/cm^3; [Pirot *et al.* 1997])

$m_{sc,n}$ is the mass of *stratum corneum* material of the n^{th} tape strip, deduced gravimetrically

3.3.3.5 Quantifying transdermal CHG delivery from Hibiscrub®

Hibiscrub® (contains 4% w/v CHG) was used as the commercial benchmark formulation as it is specifically named as a CHG containing formulation for prevention of SSTIs (NICE, 2019). The depth permeation of Hibiscrub 4% was analysed using diffusion cell and tape stripping experiments as above. Hibiscrub® is used commercially as a wash rather than "leave on" formulation, and thus experiments left Hibiscrub® on the skin surface for both 2min and 24hr, to reflect the real life use of Hibiscrub® and to act as a comparator to the experimental "leave on" gel formulation. Results from these experiments provided information on the depth permeation of CHG from a commercially accepted formulation, thus providing a benchmark and informing whether candidate formulations were superior in terms of CHG delivery into deeper skin layers.

3.3.3.6 HPLC Analysis

The British Pharmacopoeia method was used initially for the detection of CHG using HPLC, conducted on a Shimadzu Prominence HPLC system with an SPD M20 diode array detector. The British Pharmacopoeia method was unsuitable for CHG detection with a high sample quantity (explored further in Section 3.4.1). The final HPLC method was based upon the method used by Holmes *et al.* (2017), initially adjusted from Karpanen *et al.* (2008a).

The samples were run at a flow rate of 1.5 mL/min at 40 °C through a reverse-phase chromatography column (C18; dimension, 150 × 4.6 mm, 5 µM [Thermo Scientific, United Kingdom]), with UV detection at 254 nm. The isocratic mobile phase consisted of a methanol:water mixture (75:25) with 0.005 M sodium octane-1-sulfonate as an ion pairing reagent (Kudo *et al.* 2002), 0.1% w/v trimethylamine and adjusted to pH 4 with glacial acetic acid. A Thermo Scientific guard column with replaceable guard cartridges (Thermo Scientific, C18 10 mm, 5 µm) were used to ensure HPLC pressure remained stable. Cartridges were replaced when the pressure exceeded 20% of the normal pressure limits as recommended by the manufacturer.

The HPLC method was validated by analysing a series of standardised CHG concentrations and plotting a graph of peak area versus CHG concentration. The limit of detection (LoD) and limit of quantification (LoQ) were calculated from this calibration graph according to the following equations: LoD = (3 × standard deviation)/slope; LoQ = (10 × standard deviation)/slope according to the Karpanen *et al.* (2008a) method. The experimental mobile phase was used as the solvent for all CHG extractions and was validated on the Shimadzu system (R^2 value 0.9992). The LoD was calculated to be 0.362 µg/mL and the LoQ was calculated to be 1.098 µg/mL.

3.3.4 Investigating the interactions between CHG and PAMAM dendrimers using light microscopy, infra-red (IR) and X-ray diffraction (XRD)

To confirm previous observations noted by Judd (2013b), concentrations of CHG used within this thesis (1%-4% w/v) were mixed with experimental concentrations of PAMAM dendrimer (0.5 mM or 1 mM) and observed using light microscopy at 4 × and 40 × magnification on contact and

after 1 hr, 2 hr, 4 hr, 6 hr, 8 hr, 12 hr and 24 hr. The experiment was repeated, this time by adding experimental concentrations of PAMAM dendrimer to experimental concentrations of CHG in order to observe if the order of addition of experimental compounds affected the appearance of crystal formation. Following the end of the experiment, after 30hr, it was noted that the 4% CHG-1mM PAMAM and 1 mM PAMAM-4% CHG mixture had produced crystals that were visible to the naked eye on the bottom of the vial.

A glass vial containing the crystals obtained from the experiment was clamped at a 45^{o} angle with the lid left off and left for 24hr to allow for any remaining liquid to evaporate. A minimal amount of sample was then loaded onto the sample platform and using IR in an attempt to characterise the crystals. IR analysis was completed using a Thermo Nicolet iS10 IR spectrophotometer with an attached ATR (attenuated total reflectance) with a diamond window. Samples were scanned 32 times with a resolution of 4 ×.

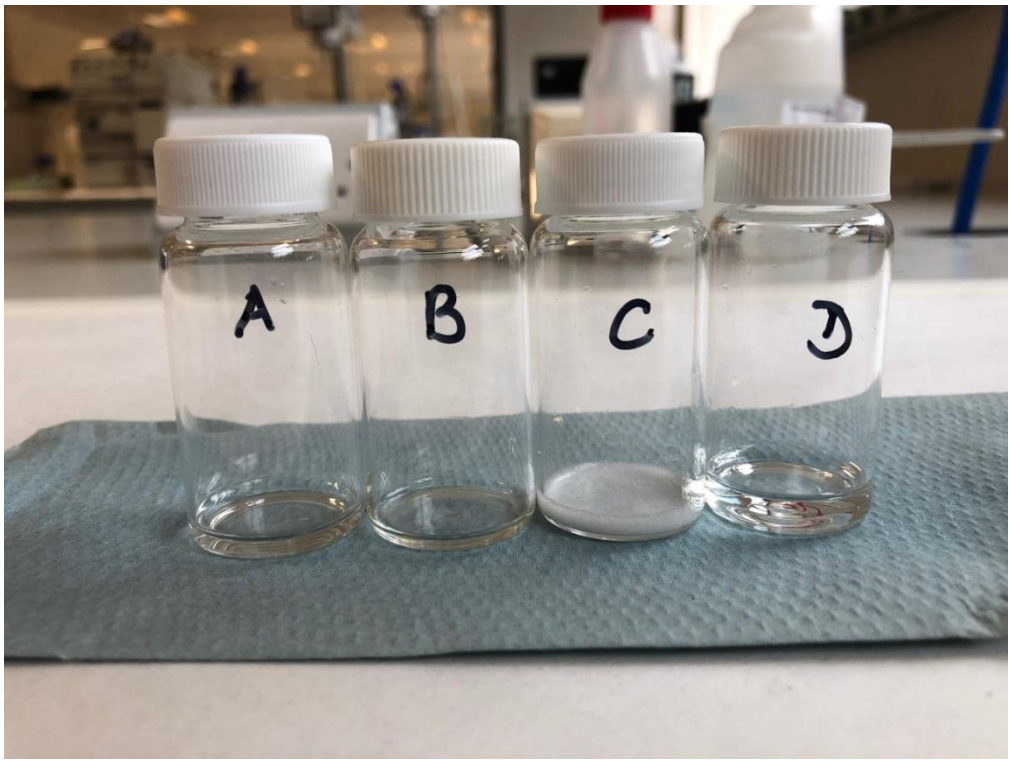

Figure 3.1. Evidence of drug-dendrimer interactions. ***A – 20% w/v CHG in water, B – 20% w/v PAMAM in methanol, C – 0.5 mL of 20% w/v PAMAM added to 0.5 mL of 20% w/v CHG, D – 0.5 mL 20% w/v PAMAM in methanol and 0.5 mL of 20% w/v CHG stabilised in a water-ethanol 50:50 solution.***

3.3.4.1 Investigating the precipitate following the end of a 24hr diffusion cell experiment

Following a 24hr Franz cell experiment, the viscosity of the co-formulation vastly increased, to the point where the co-formulation retained the cylindrical shape of the donor chamber without the presence of the donor chamber. Upon closer inspection, the formulation had become more translucent in appearance with some pearlescent white areas (Figure 3.2 and Figure 3.3).

The precipitate was removed from the skin surface using a stainless steel spatula and analysed using single crystal XRD. The diffraction data were collected on a Bruker D8 Quest ECO with graphite-monochromated Mo Kα radiation (λ = 0.71073 Å). A single crystal was mounted on a

Mitegen micromount in NVH immersion oil, and the temperature was maintained at 150 K using an Oxford cryostream. Measurements were carried out using ϕ and ω scans, with collections and data reductions carried out in the Bruker APEX-3 suite of programs.

X-ray powder diffraction was performed using a Bruker D8 Advance diffractometer with a Cu-Kα source (λ = 1.54178 Å). The sample was mounted on a zero-background silicon single crystal sample holder. All samples were measured at room temperature in the θ range 5 - 55°, and these data were compared against simulated patterns from the single crystal data collections at 150 K.

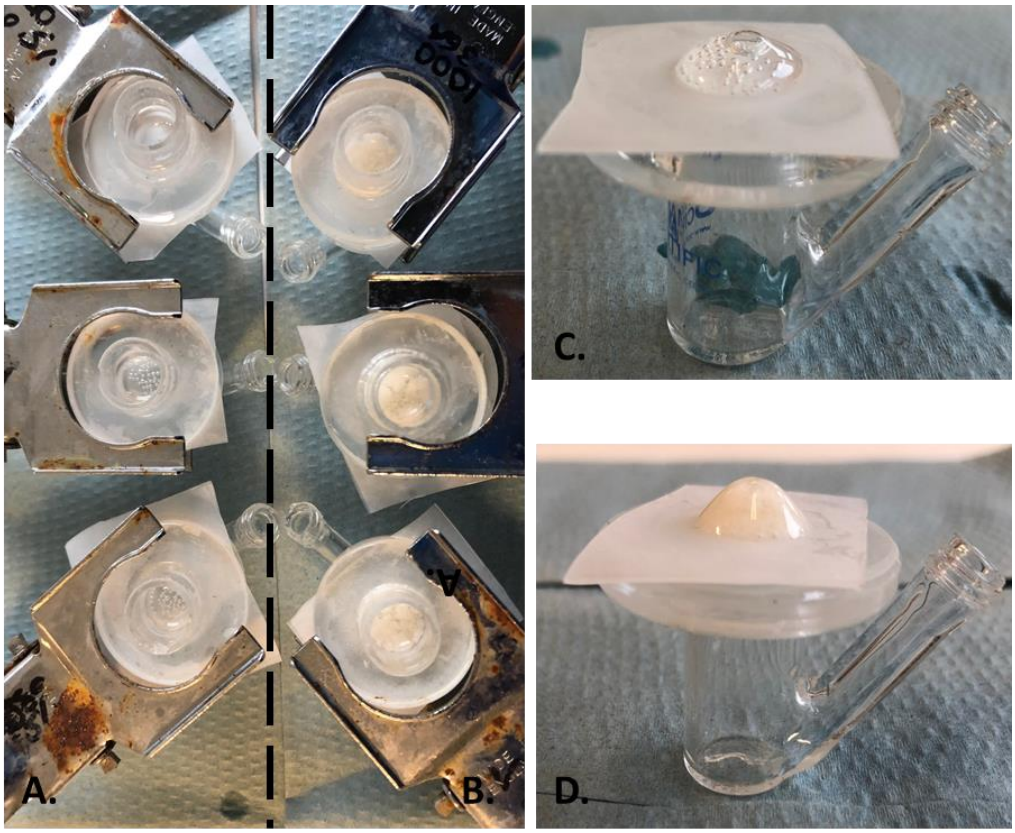

Figure 3.2. Appearance of candidate formulations following a 24 hr application onto a silicone membrane. The formulation retains the shape set by the donor chamber at the start of the experiment. ***A. 4% CHG gel formulation; B. 4% CHG-1 mM PAMAM gel formulation; C. and D. Appearance of 4% CHG gel / 4% CHG -1 mM PAMAM gel following donor chamber removal indicating ability of the gel to hold its own shape.***

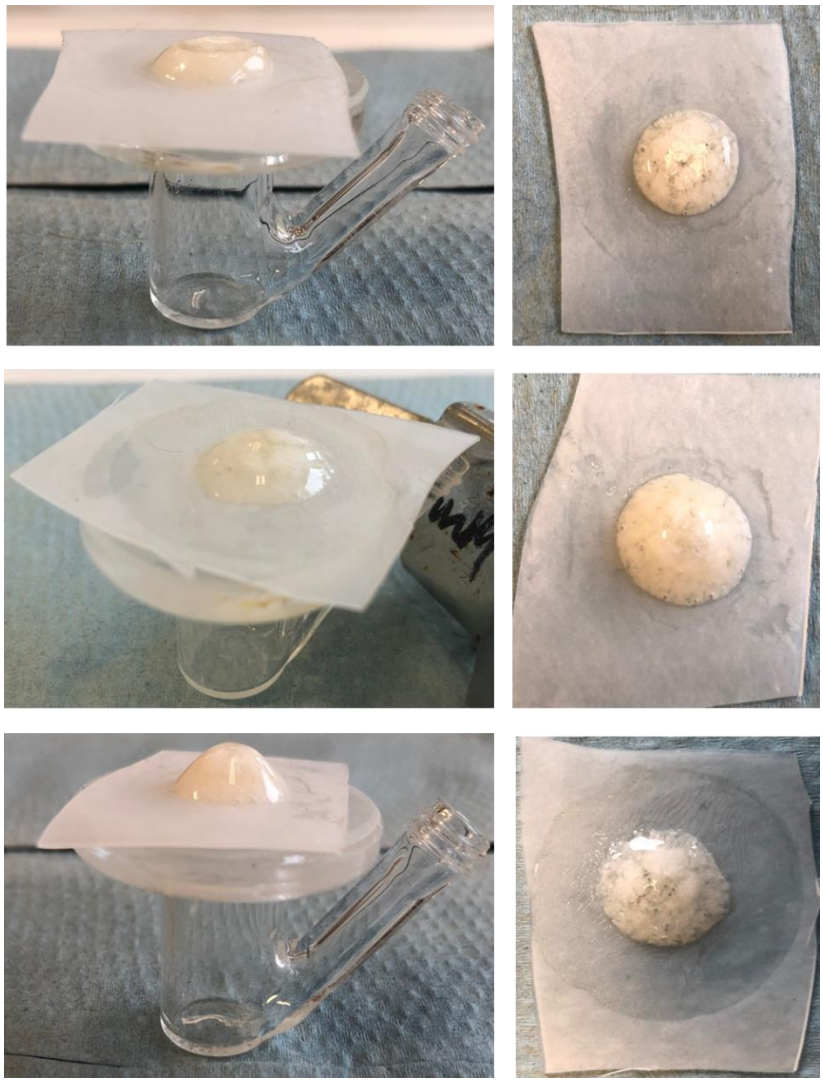

Figure 3.3. Images of a 4% CHG-1 mM PAMAM gel co-formulation illustrating the formulation of a pearlescent white precipitate at the end of a 24 hr diffusion cell experiment.

3.3.4.2 Statistical analysis of data

Means, standard deviation and standard error were all calculated in Microsoft Excel. Franz cell and tape strip HPLC data within this thesis was analysed using IBM SPSS 24 with either a One Way ANOVA (with Tukey's or Games-Howell post-hoc depending on the Levene's test result), or a Kruskal Wallis ANOVA (where the data was non-parametric). For Franz-type diffusion cell experiments and tape stripping studies, the number of replicates was a minimum of four, in accordance with OECD guidelines 428 (2004) for testing skin absorption *in vitro*.

The One-Way ANOVA was the primary choice and assumes that there are no significant outliers, data is normally distributed and the variance is equal in each group of the independent variable. Each of these parameters were assessed prior to statistical analysis. When outliers were discovered (via observation of a box plot in SPSS), only extreme outliers (indicated by an * symbol rather than a ^{o} symbol in the software) were removed. Values which are >3 interquartile ranges (IQRs) from the end of the boxplot are labelled as extreme (*), values >1.5 IQRs but <3 IQRs from the end of the boxplot are labelled as outliers (^{o}). Data was then tested for normality, and homogeneity of variance using a Shapiro-Wilk and Levene's test respectively. A Games-Howell post-hoc test was used when a One-Way ANOVA was appropriate (i.e. no outliers, normality of data), but the Levene's test failed. The flow chart below details the fulfilments for each test type. A value of $p < 0.05$ represented a statistical significant result.

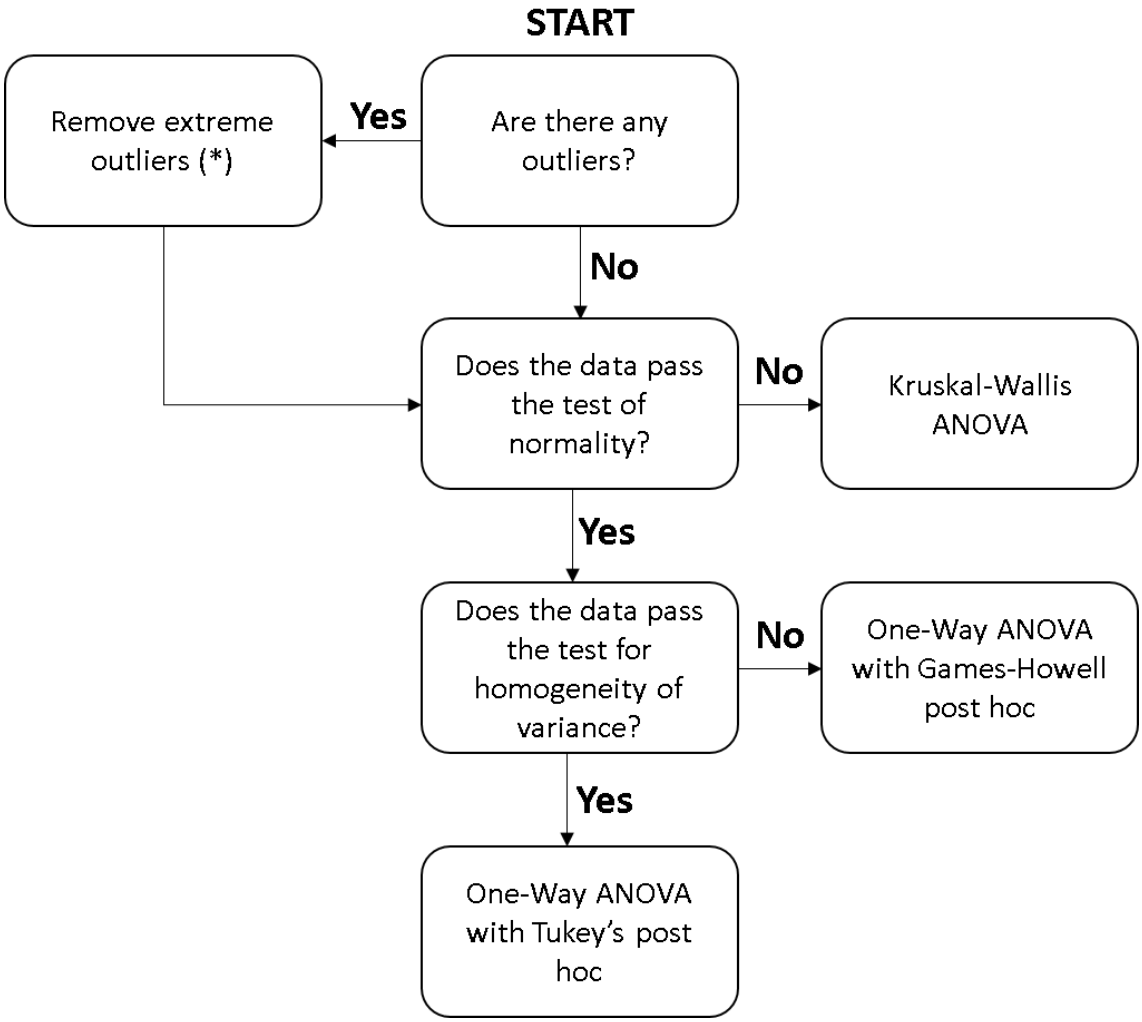

Figure 3.4. Schematic diagram of the requirements for each statistical test type utilised within this thesis.

3.4 Results

3.4.1 Analysis of CHG by HPLC

The British Pharmacopoeia (2019b) was used as the starting point for the HPLC method. Whilst the British Pharmacopoeia method gave resolved and separated peaks, consistent and prolonged use of the recommended mobile phase increased the pressure of the HPLC (>5000 psi) eventually overloading the instrument, causing splitting of the injection needle seal which resulted in leaking of mobile phase and a sudden drop in instrument pressure. In addition, the ambient temperature sometimes caused peaks to shift somewhat on the chromatogram, providing an inconsistent retention time.

It appeared that the high volume of glacial acetic acid specified in the BP method was reacting with the stationary phase of the column, resulting in a precipitate which restricted flow through the column (Teutenberg *et al.* 2009). The incompatibilities were resolved by using the HPLC method provided by Holmes *et al.* (2017). Other than the reduced volume of glacial acetic acid, the method increased the flow rate (1.5 mL/min) and set the oven temperature to 40 ^{o}C, which set the elution time of CHG to 2.5 min without the variation observed in peak elution times when the original BP method was used. Heating chlorhexidine salts does not cause decomposition of the drug into 4-chloroaniline until temperatures exceed 100 ^{o}C (Owen 2006). This method combined with the use of a guard column with regular guard cartridge changes stabilised the pressure at ~2000 psi. Prior to use the mobile phase was filtered using 55 mm filter paper.

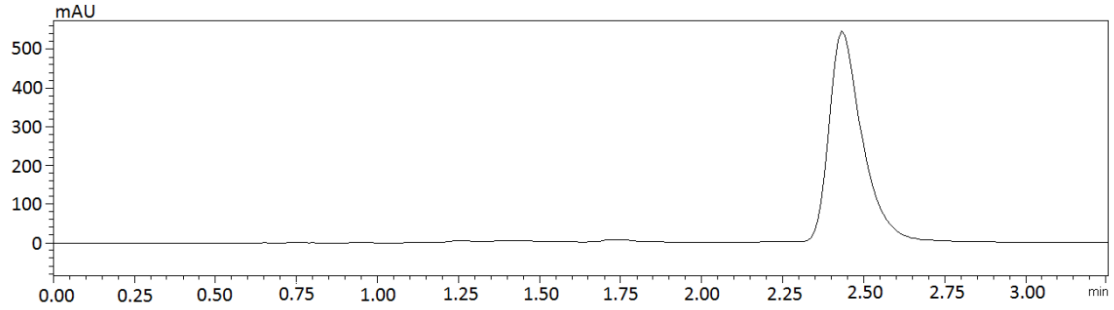

Figure 3.5. Example chromatogram obtained from a tape strip containing porcine skin material and CHG, allowed to leach from the tape into mobile phase over a 24hr period – *4% CHG-1 mM PAMAM, tape strip 4-6.*

Following each experiment the HPLC instrument was flushed through with a methanol:water gradient solution, beginning with 95% methanol, 5% water and ending in 5% methanol, 95% water for 30 min. This ensured any water soluble crystals could be dissolved and removed from the HPLC system. As a result, crystal formation and increased HPLC pressures could be delayed.

3.4.2 Effect of HEC concentration in gels on the *in vitro* skin permeation of CHG

There was no drug detectable in the receptor fluid from the 24hr experiments conducted which applied a 1% w/v CHG gel formulation with varying concentrations of HEC onto the skin (<LoD, appendix 1) indicating no drug flux through full thickness porcine skin.

Figure 3.6 illustrates the concentration of CHG calculated per mg of *stratum corneum* material removed on the corresponding tape strips. The equation used to account for the weight of *stratum corneum* material per tape strip can be found in Section 3.3.3.4.

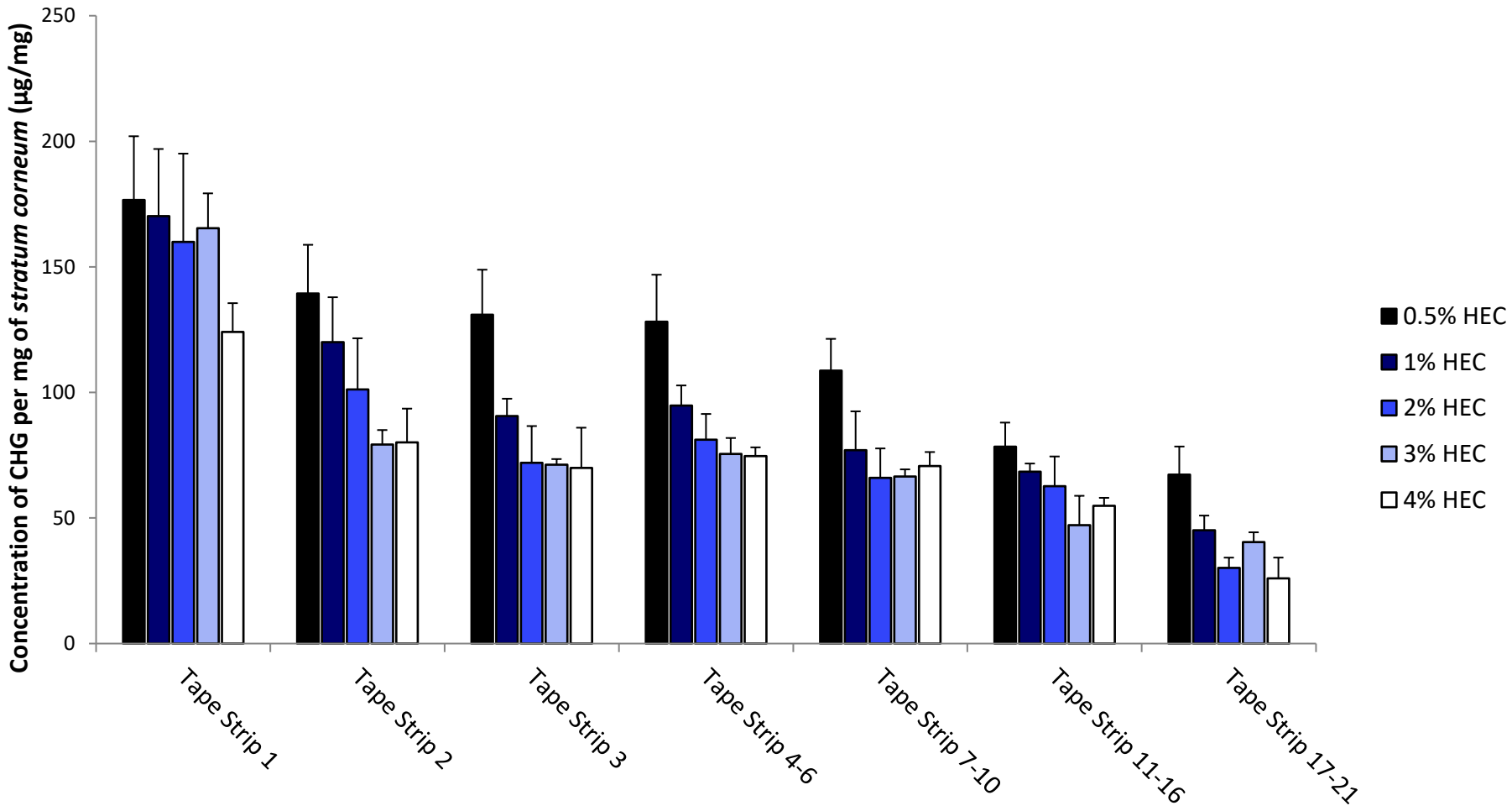

Figure 3.6. Concentration profile of CHG detected on tape strips 1-21 following treatment with an experimental 1% CHG gel formulation with varying concentrations of HEC (0.5-4%). *n=6 ± SE.*

The permeation profile showed some irregularities, however there was a general trend of decreasing CHG concentration on each tape strip with increasing HEC concentration. The experimental formulation which contained the least HEC (0.5% w/v) delivered the highest concentration of drug onto tape strips 1-21.

The first tape strip showed the delivery of the highest CHG concentration, however the first layer of skin is considered to have adsorbed drug rather than absorbed it, and as a result some studies discount this layer (Sheth 1987, Surber *et al.* 1999, Lademann *et al.* 2009). However, this information is still presented in Figure 3.6 as it allowed statistical analysis of total CHG concentration removed from the *stratum corneum* between groups.

The amount of CHG delivered to lower layers of the *stratum corneum* decreased as further tape strips were collected. For example, the concentration of CHG detected on the first tape strip was 176.68 ± 25.33 µg/mg, 170.17 ± 26.77 µg/mg, 159.95 ± 35.15 µg/mg, 165.34 ± 13.92 µg/mg and 124.05 ± 11.49 µg/mg for formulations 0.5%, 1%, 2%, 3% and 4% w/v HEC respectively. The concentration of CHG detected on tape strips 17-21 was 67.24 ± 11.21 µg/mg, 45.17 ± 5.80 µg/mg, 30.15 ± 4.07 µg/mg, 40.40 ± 3.89 µg/mg and 25.92 ± 8.30 µg/mg for formulations 0.5%, 1%, 2%, 3% and 4% w/v HEC respectively. The decrease in CHG deposition between tape strip 1 and tape strips 17-21 is approximately 5 fold.

The results in Table 3.1 indicated pairwise comparisons which were statistically significant ($p < 0.05$). Whilst a directional trend was seen, not all the comparisons are statistically different.

Table 3.1. Analytical tests chosen to determine whether formulations with differing concentration of HEC (0.5-4%) significantly affect the depth permeation of CHG within porcine skin and the resulting pairwise comparisons which resulted in a statistically significant result ($p < 0.05$). Pairwise comparisons are arranged so that the formulation which developed the highest concentration of CHG is given first (F1). ***KW – Kruskal Wallis; OWA – One-Way ANOVA, n=6.***

Tape Strip Number	Analytical Test	Statistically Significant Result	Pairwise Comparisons	
			F1	F2
Tape Strip 1	KW	N	-	-
Tape Strip 2	OWA	N	-	-
Tape Strip 3	KW	Y	4% HEC	0.5% HEC
Tape Strip 4-6	KW	N	-	-
Tape Strip 7-10	OWA	N	-	-
Tape Strip 11-16	OWA	N	-	-
Tape Strip 17-21	KW	Y	2% HEC	0.5% HEC
Total Tape Strips	OWA	N	-	-

3.4.3 Effect of CHG concentration in gels on the *in vitro* skin permeation of CHG

There was no drug detectable in the receptor fluid from the 24 hr experiments conducted (<LoD, appendix 1).

Figure 3.7 illustrates the concentration of CHG calculated per mg of *stratum corneum* material removed on the corresponding tape strips.

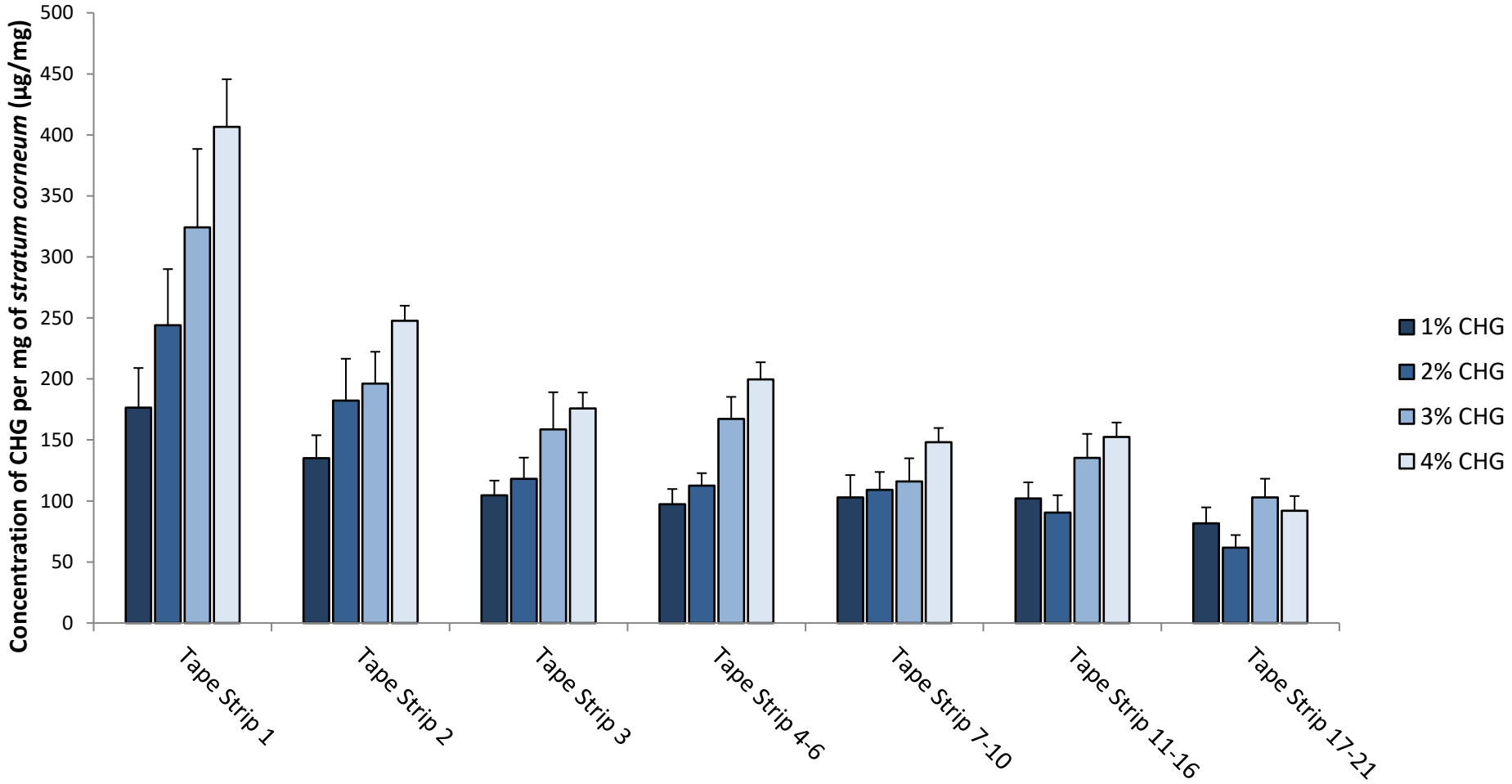

Figure 3.7. Concentration profile of CHG detected on tape strips 1-21 following treatment with an experimental gel formulation with varying concentrations of CHG (1-4%). *n=9 ± SE.*

Similar to the previous experiment, there was a general trend of decreasing CHG concentration with increasing tape strip number. For example, the concentration of CHG detected on the first tape strip was 176.46 ± 32.50 µg/mg, 244.02 ± 45.99 µg/mg, 324.21 ± 64.26 µg/mg and 406.65 ± 38.96 µg/mg for formulations 1%, 2%, 3% and 4% w/v CHG respectively. The concentration of CHG detected on tape strips 17-21 was 81.71 ± 13.05 µg/mg, 61.84 ± 10.24 µg/mg, 102.84 ± 15.40 µg/mg and 92.07 ± 11.96 µg/mg for formulations 1%, 2%, 3% and 4% w/v CHG respectively.

With increasing tape strip number, the difference in CHG concentration delivered between each formulation diminished. For instance, there was a 230.18 µg/mg difference in the concentration of CHG delivered to tape strip 1 when comparing the CHG 1% and 4% gel formulations, but only a 10.36 µg/mg difference in the concentration of CHG delivered to tape strip 17-21 when comparing the same formulations. The decrease in CHG deposition between tape strip 1 and tape strips 17-21 was approximately between 2-5 fold.

An increase in CHG concentration on the skin surface generally increased the concentration of CHG in each tape strip. The gel formulation which contained 4% w/v CHG delivered the highest concentration of CHG to tape strips 1-16, reflected both in Figure 3.7. The results in Table 3.2 indicated pairwise comparisons which were statistically significant ($p < 0.05$). In the majority, 4% w/v CHG delivered significantly more CHG onto tape strips than 1% w/v CHG and in some instances, 3% w/v CHG also delivered significantly more CHG than 1% w/v CHG.

Table 3.2. Analytical tests chosen to determine whether formulations with differing concentration of CHG (1-4%) significantly affect the depth permeation of CHG within porcine skin and the resulting pairwise comparisons which resulted in a statistically significant result ($p < 0.05$). Pairwise comparisons are arranged so that the formulation which developed the highest concentration of CHG is given first (F1). ***KW – Kruskal Wallis; OWA – One-Way ANOVA, n=9.***

Tape Strip Number	Analytical Test	Statistically Significant Result	Pairwise Comparisons	
			F1	F2
Tape Strip 1	KW	Y	4% CHG	1% CHG
Tape Strip 2	KW	Y	4% CHG	1% CHG
Tape Strip 3	KW	Y	4% CHG	1% CHG
Tape Strip 4-6	OWA	Y	4% CHG	1% CHG
			4% CHG	2% CHG
			3% CHG	1% CHG
			3% CHG	2% CHG
Tape Strip 7-10	OWA	N	N/A	N/A
Tape Strip 11-16	OWA	Y	4% CHG	2% CHG
Tape Strip 17-21	OWA	N	N/A	N/A
Total Tape Strips	OWA	Y	4% CHG	1% CHG
			4% CHG	2% CHG
			3% CHG	1% CHG

3.4.4 Effect of G3 PAMAM-NH_2 concentration in gels on the *in vitro* skin permeation of CHG

Application of a 4% w/v CHG gel formulation combined with either 0.5 mM or 1 mM of a G3 PAMAM-NH_2 did result in minimal amounts of drug detectable in the receptor fluid samples, but they were all <LoD (appendix 1). This is a clear indication of poor CHG permeation and thus highlights the requirement of tape stripping studies in order to provide valuable data in this study.

The cumulative concentration of CHG detected in receptor fluid was compared after 24hr using an independent t-test. There was no statistically significant difference found between the concentration of PAMAM dendrimer applied to the skin surface in the co-formulation and the cumulative concentration of CHG detected in receptor fluid after 24hr ($p>0.05$).

The depth permeation profile of CHG of the co-formulations containing either 0.5 mM or 1 mM G3 PAMAM-NH_2 dendrimer can be found in Figure 3.8).

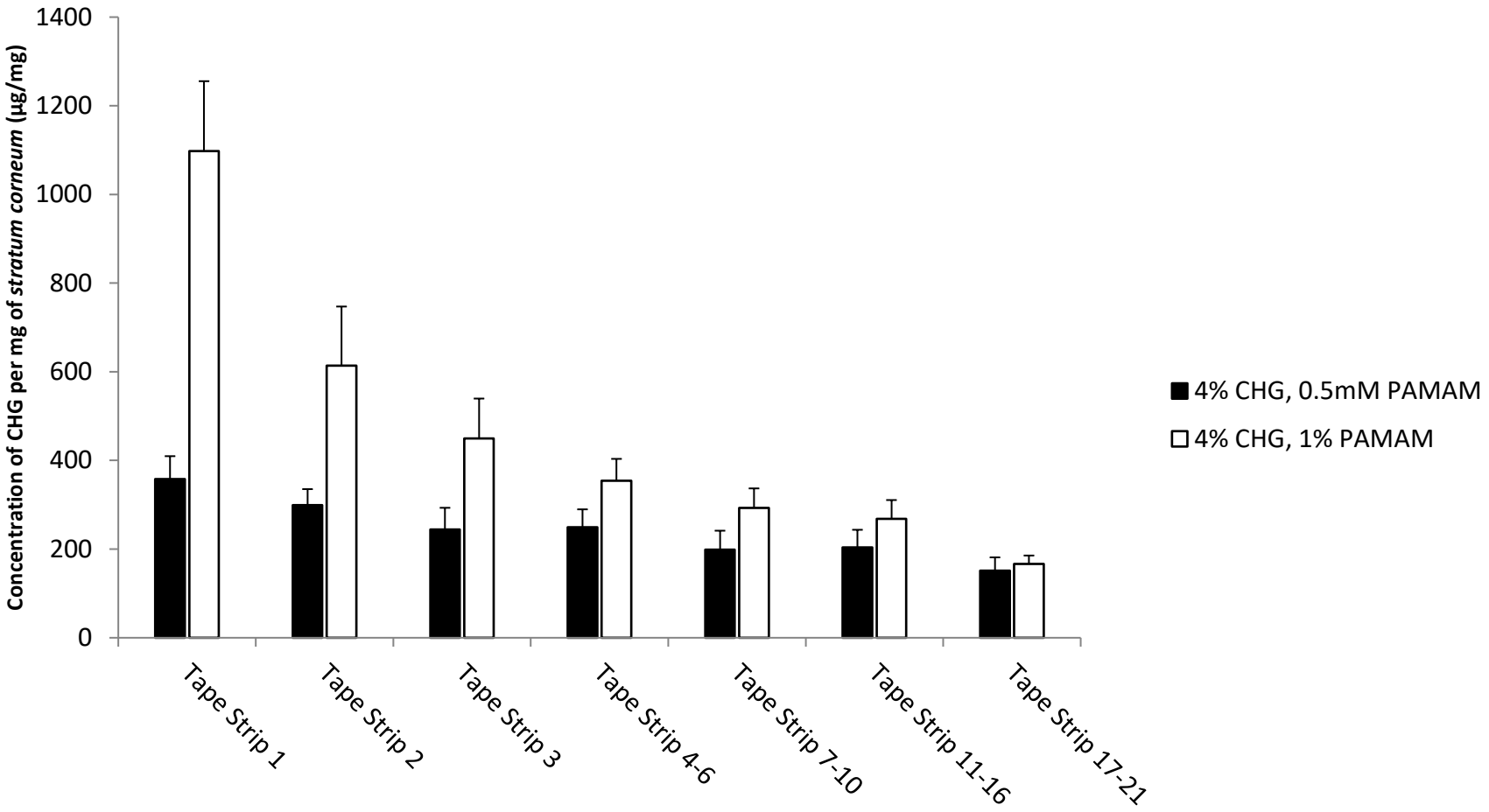

Figure 3.8. Concentration profile of CHG detected on tape strips 1-21 following treatment with an experimental gel formulation with varying concentrations of PAMAM dendrimer. *n=13 ± SE.*

The trend of decreasing CHG concentration with increasing tape strip number was observed. Similar to previous *in vitro* experiments, the increase in CHG concentration on each tape strip between the two variables decreased with increasing tape strip number. The difference in CHG concentration delivered to tape strip 1 when comparing the 4% CHG-0.5 mM PAMAM and 4% CHG-1 mM PAMAM co-formulations was 739.928 µg/mg, but only a 15.151 µg/mg difference in the concentration of CHG delivered to tape strip 17-21 when comparing the same formulations.

Increasing the PAMAM dendrimer concentration in the formulation from 0.5 mM to 1 mM increased the concentration of drug in all tape strips. For example, the concentration of CHG detected on tape strip 1 was 358.079 ± 51.51 µg/mg and 1098.01 ± 157.50 µg/mg for 4% CHG-0.5 mM PAMAM and 4% CHG-1 mM PAMAM respectively. The concentration of CHG detected on tape strips 17-21 was 151.47 ± 29.83 µg/mg and 166.62 ± 18.85 µg/mg for 4% CHG-0.5 mM PAMAM and 4% CHG- 1mM PAMAM respectively.

An independent t-test indicated that the 4% CHG-1 mM PAMAM significantly increased the deposition of CHG into tape strips 1, 3 and 4-6 when compared to the 4% CHG-0.5 mM PAMAM formulation. This result was statistically significant ($p < 0.05$). Furthermore, an independent t-test was used to determine whether there was a statistically significant difference between the treatment groups and the total CHG concentration extracted from tape strips 1-21. The 4%-1 mM PAMAM treatment group significantly increased the concentration of CHG delievered to tape strips 1-21 compared to the 4%-0.5 mM PAMAM treatment group ($p < 0.05$).

3.4.5 Commercial benchmark – *in vitro* permeation studies

Hibiscrub® was used as the commercial benchmark in this study as it is a common CHG containing preparation used for topical skin antisepsis and is recommended by NICE for the

prevention of SSTIs (NICE, 2019). The formulation also contains 4% w/v CHG which is comparable to the co-formulations utilised in this study. However, Hibiscrub® is advertised as a skin wash, rather than a "leave on" formulation which the experimental gel formulations used in this thesis more closely represents. Therefore, the permeation profile of Hibiscrub® was measured after a 2 min and 24 hr application time to reflect its commercial use and to compare against the experimental leave on formulation.

There was no drug detectable in the receptor fluid from the 24hr experiments conducted which applied Hibiscrub® for a 2 min and 24 hr application time.Figure 3.9 illustrates the concentration of CHG calculated per mg of *stratum corneum* material removed on the corresponding tape strips.

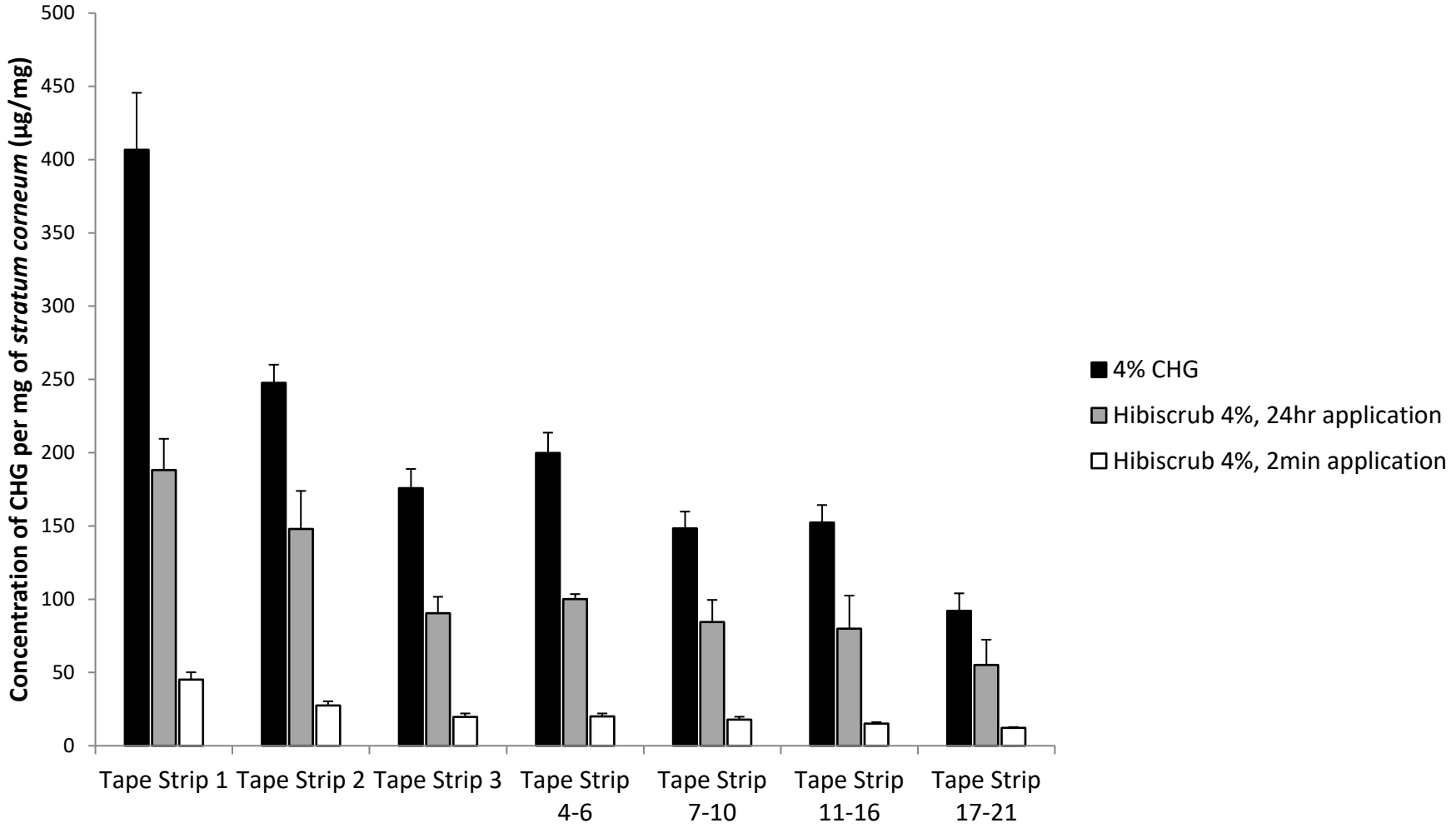

Figure 3.9. Concentration profile of Hibiscrub® 4% detected on tape strips 1-21 following a 2 min or 24 hr application time following 24hrs. *n=4* for Hibiscrub® 4%, *n= 9* for 4% CHG, ± SE.

There was a decrease in CHG concentration with increasing tape strip number, and the 24 hr application of Hibiscrub® delivered an increased concentration of CHG to each tape strip compared to the Hibiscrub 2 minute application.

For example, the concentration of CHG detected on tape strip 1 was 85.56 ± 20.89 µg/mg and 188.20 ± 21.30 µg/mg for Hibiscrub® 2 min and Hibiscrub® 24 hr respectively. The concentration of CHG detected on tape strips 17-21 was 29.53 ± 4.96 µg/mg and 55.15 ± 17.23 µg/mg for Hibiscrub® 2 min and Hibiscrub® 24 hr respectively.

Table 3.3. Analytical tests chosen to determine whether the duration of application of the commercial benchmark significantly affected the depth permeation of CHG within porcine skin and the resulting pairwise comparisons which resulted in a statistically significant result (p <0.05). Pairwise comparisons are arranged so that the formulation which developed the highest concentration of CHG is given first (F1). *KW – Kruskal Wallis; OWA – One-Way ANOVA, n=4* for Hibiscrub® 4%, *n= 9* for 4% CHG.

Tape Strip Number	Analytical Test	Statistically Significant Result	Pairwise Comparisons	
			F1	F2
Tape Strip 1	KW	Y	Hibiscrub, 24hr	Hibiscrub, 2 min
Tape Strip 2	OWA	Y	Hibiscrub, 24hr	Hibiscrub, 2 min
Tape Strip 3	OWA	Y	Hibiscrub, 24hr	Hibiscrub, 2 min
Tape Strip 4-6	OWA	Y	Hibiscrub, 24hr	Hibiscrub, 2 min
Tape Strip 7-10	OWA	Y	Hibiscrub, 24hr	Hibiscrub, 2 min
Tape Strip 11-16	OWA	Y	Hibiscrub, 24hr	Hibiscrub, 2 min
Tape Strip 17-21	OWA	Y	Hibiscrub, 24hr	Hibiscrub, 2 min
Total Tape Strips	KW	Y	Hibiscrub, 24hr	Hibiscrub, 2 min

3.4.6 Comparative Data

The *in vitro* diffusion cell studies above were used to create the most efficacious ethanol based gel formulation for enhancement of CHG into porcine skin. To understand whether the 4% CHG-1 mM PAMAM co-formulation was more efficacious than an ethanol based gel formulation without the addition of the PAMAM dendrimer and the commercial benchmark, the concentrations of drug per mg of *stratum corneum* material were plotted and analysed statistically using a Kruskal Wallis ANOVA. The results are shown in Figure 3.10.

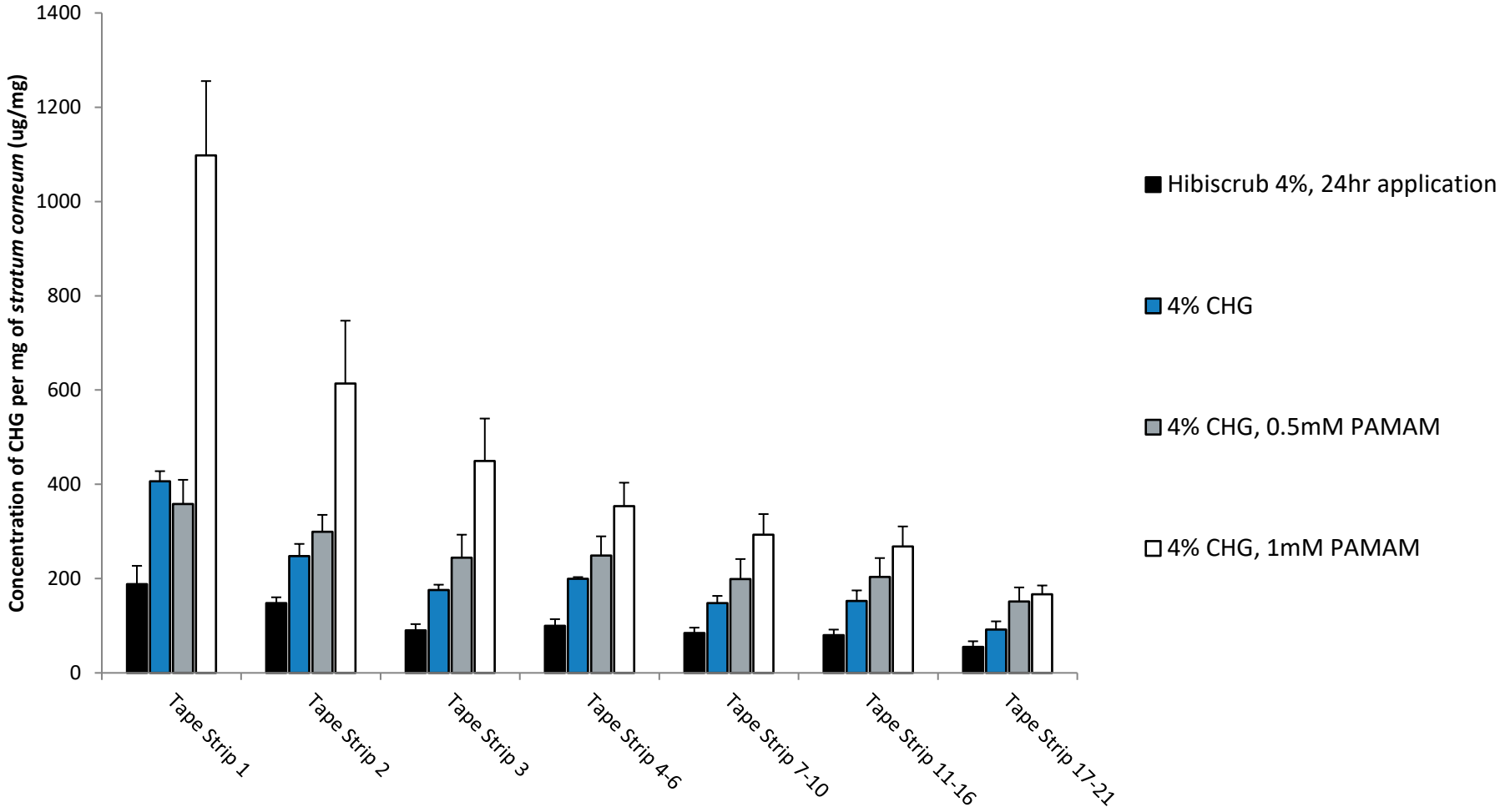

Figure 3.10. Comparative data of concentration of CHG permeated onto tape strips 1-21 from various experimental and commercial formulations. *n=4* for Hibiscrub® 4%, *n=9* for 4% CHG, *n=13* for 4% CHG-0.5mM PAMAM and 4% CHG-1mM PAMAM, ± SE.

The graph clearly shows that the addition of a G3 PAMAM-NH_2 dendrimer enhances the deposition of CHG within porcine skin. The formulation containing 1 mM PAMAM considerably enhanced the deposition of CHG when compared to the formulation containing 0.5 mM PAMAM, however further investigation with additional dendrimer concentrations would be required to determine whether this effect was concentration dependent.

Statistical results for this dataset can be found in Table 3.4. Statistically significant pairwise comparisons which were within groups (i.e. 4%-0.5 mM PAMAM-4%-1 mM PAMAM) are not displayed in the table as these comparisons have already been presented in Table 3.1, Table 3.2 and Table 3.3.

Table 3.4. Analytical tests chosen to determine whether formulations with and without PAMAM dendrimer, and with the commercial benchmark Hibiscrub® significantly affect the depth permeation of CHG within porcine skin. The table reports the resulting pairwise comparisons which resulted in a statistically significant result ($p < 0.05$). Pairwise comparisons are arranged so that the formulation which developed the highest concentration of CHG is given first. ***KW – Kruskal Wallis; OWA – One-Way ANOVA. n=4 for Hibiscrub® 4%, n=9 for 4% CHG, n=13 for 4% CHG-0.5mM PAMAM and 4% CHG-1mM PAMAM.***

Tape Strip Number	Analytical Test	Statistically Significant Result	Pairwise Comparisons	
			F1	F2
Tape Strip 1	KW	Y	4% CHG-1mM PAMAM	Hibiscrub 4%, 24hr
Tape Strip 2	OWA	Y	4% CHG-1mM PAMAM	4% CHG
			4% CHG-1mM PAMAM	Hibiscrub 4%, 24hr
Tape Strip 3	KW	Y	4% CHG-1mM PAMAM	Hibiscrub 4%, 24hr
Tape Strip 4-6	OWA	Y	4% CHG-0.5mM PAMAM	Hibiscrub 4%, 24hr
			4% CHG-1mM PAMAM	4% CHG
			4% CHG-1mM PAMAM	Hibiscrub 4%, 24hr
			4% CHG	Hibiscrub 4%, 24hr
Tape Strip 7-10	OWA	Y	4% CHG-0.5mM PAMAM	Hibiscrub 4%, 24hr
			4% CHG-1mM PAMAM	4% CHG
			4% CHG-1mM PAMAM	Hibiscrub 4%, 24hr
Tape Strip 11-16	OWA	Y	4% CHG-1mM PAMAM	Hibiscrub 4%, 24hr
Tape Strip 17-21	OWA	Y	4% CHG-1mM PAMAM	4% CHG
			4% CHG-1mM PAMAM	Hibiscrub 4%, 24hr
Total Tape Strips	OWA	Y	4% CHG-0.5mM PAMAM	Hibiscrub 4%, 24hr
			4% CHG-1mM PAMAM	4% CHG
			4% CHG-1mM PAMAM	Hibiscrub 4%, 24hr
			4% CHG	Hibiscrub 4%, 24hr

The results from these studies conclude that the 4% CHG-1 mM PAMAM dendrimer co-formulation delivers significantly more CHG into porcine skin than the market leading product Hibiscrub® (which contains the same concentration of CHG), and that the 4% CHG-1 mM PAMAM gel formulation enhances delivery of CHG more so that 4% w/v CHG without dendrimer, but the significance of this is limited to the upper layers of skin only. Interestingly, the 4% w/v CHG experimental formulation (without PAMAM) delivered a higher concentration of CHG into porcine *stratum corneum* compared to the commercial benchmark (containing 4% w/v CHG); however this difference was only statistically

significant on tape strips 4-6 and when comparing the total amount of CHG on tape strips 1-21. This highlights the importance of the vehicle and how this may affect drug deposition within skin.

This is the first time that a CHG-PAMAM gel co-formulation has been made which has been shown to enhance the deposition of CHG within porcine skin compared to a commercial benchmark.

3.4.7 Investigating the interactions between CHG and PAMAM dendrimers using light microscope and infra-red (IR)

Experimental concentrations of CHG (1%-4% w/v) were mixed with experimental concentrations of PAMAM dendrimer (0.5 mM or 1 mM) and vice versa and observed using light microscopy at 4 × and 40 × magnification to confirm the results first found by Judd (2013b), i.e. that precipitation would occur without stabilising both the drug and dendrimer in an ethanol:water vehicle prior to mixing. This was shown to be the case, as observed in Figure 3.1.

A general trend was observed in which increasing the concentration of either the PAMAM dendrimer or CHG resulted in an increased quantity of crystals. Crystal formation increased with time and large crystal fragments were observable at around 4-6 hr. Contrary to a previous study (Judd, 2013b), it seems that crystal shape was not entirely dependent on the order of addition as per the previous study, although in general, addition of CHG to PAMAM dendrimer resulted in crystal shards emanating from a focal point, whereas addition of PAMAM dendrimer to CHG resulted in rod shaped shards.

IR spectra were acquired of CHG 20% w/v in water, 20% G3 PAMAM-NH_2 in methanol, and the combination of both CHG and PAMAM without prior stabilisation in an ethanol-water vehicle in an attempt to view potential interactions between the drug and dendrimer.

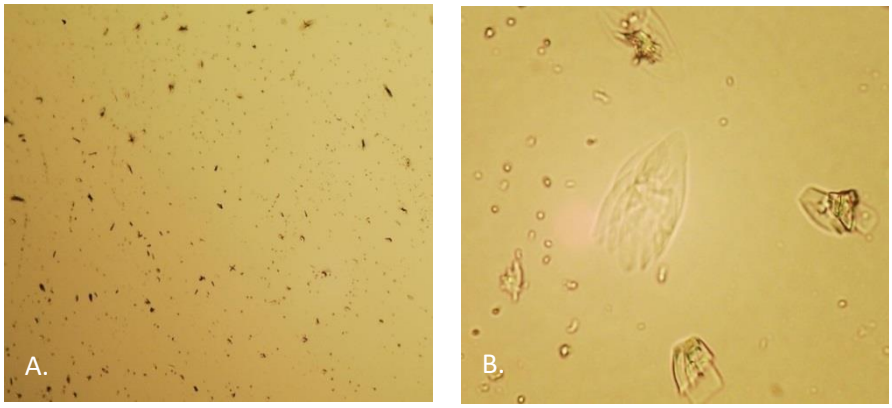

Figure 3.11. Photograph of shard crystals produced on addition of 0.5 mM PAMAM dendrimer to 4% CHG after 24hr *A. 4* × *magnification, B. 40* × *magnification.*

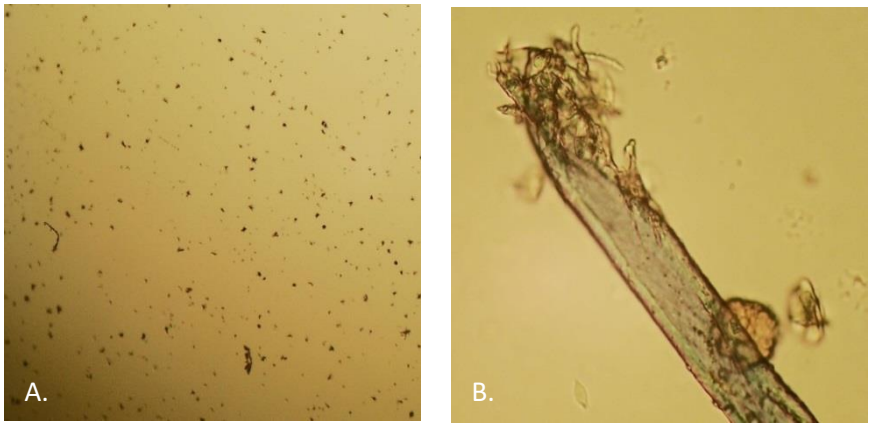

Figure 3.12. Photograph of shard crystals produced on addition of 4% CHG to 1 mM PAMAM dendrimer after 24hr *A. 4* × *magnification, B. 40* × *magnification.*

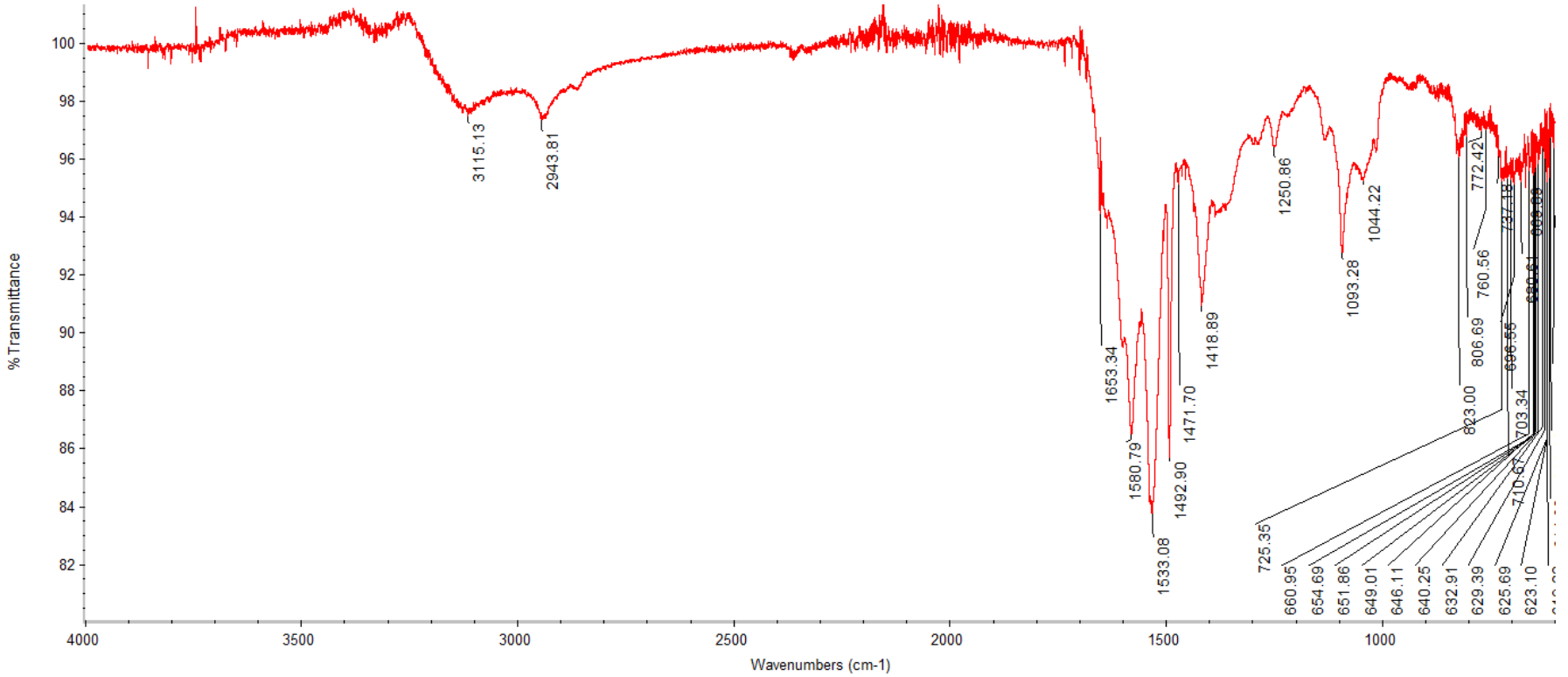

Figure 3.13. IR spectra of CHG 20% w/v in water.

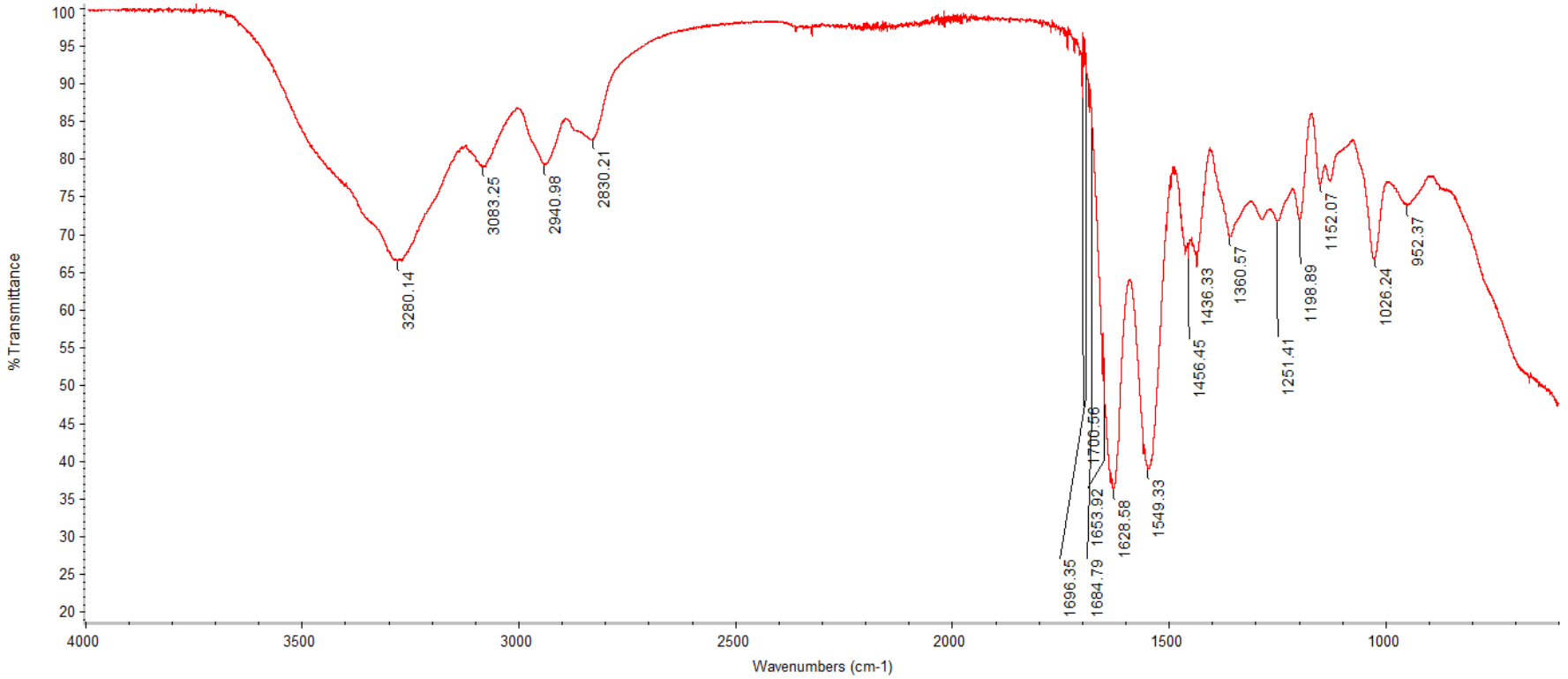

Figure 3.14. IR spectra of G3 PAMAM-NH_2 PAMAM 20% w/v in methanol.

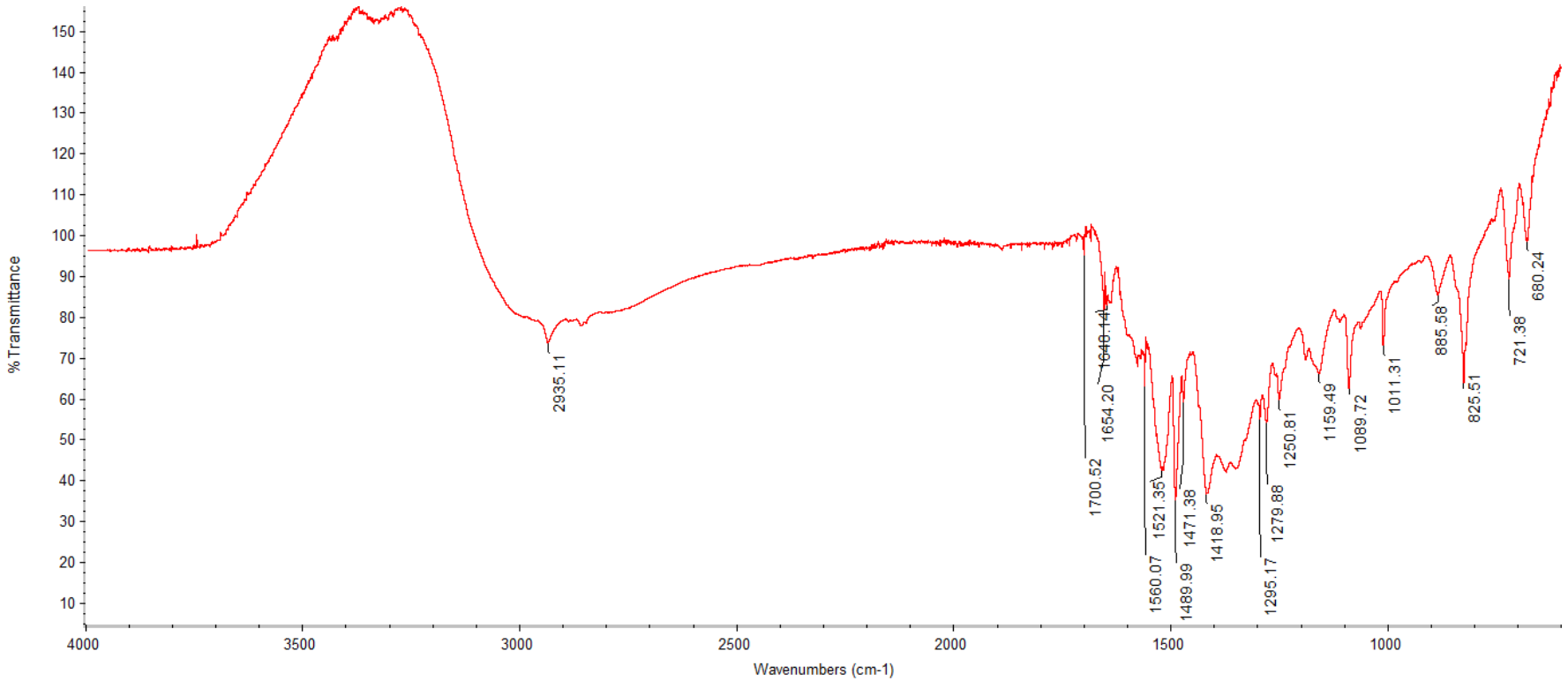

Figure 3.15. IR spectra of 4% CHG-1 mM PAMAM crystals.

Table 3.5. IR spectroscopy absorptions and associated functional groups of CHG (20% w/v in water).

Frequency (cm^{-1})	Type of Bond	Functional Group
2943	CH (b)	Alkane
1653	$R_2C{=}*N{-}R$	Iminium
1580	C=C benzene (str)	Benzene
1533	COO^-	Caboxylate
1471	C=C benzene (str)	Benzene
1044	C-O-H (str)	Alcohol
823	CH (b)	Para-substituted benzene
710	CH_2 (b)	Alkane
703	C-Cl	Carbon-Halogen bond

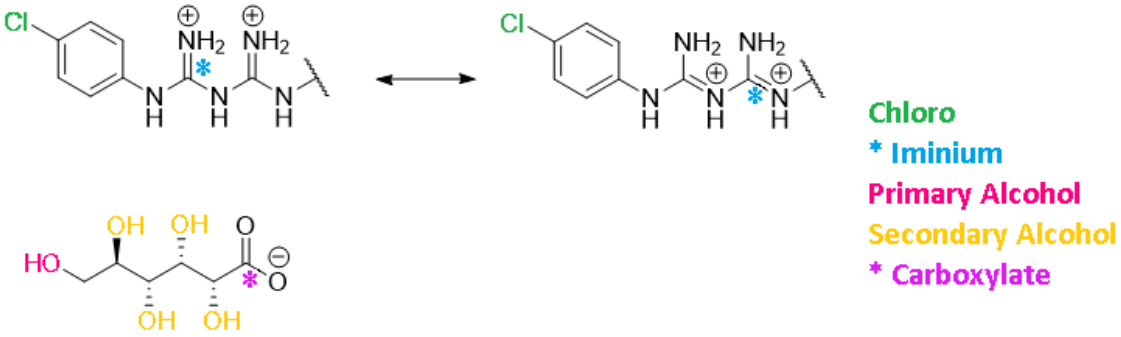

Figure 3.16. Annotated diagram indicating functional groups indicative of CHG.

Table 3.6. IR spectroscopy absorptions and associated functional groups of G3 PAMAM-NH_2 (20% w/v in methanol).

Frequency (cm^{-1})	Type of Bond	Functional Group
3280	NH (str)	Amide
2940	C-H (str)	Alkane
1653	C=O (str)	Amide
1628	N-H (b)	Amide
1549	N-H (b)	Amine
1198	C-N (str)	Amine

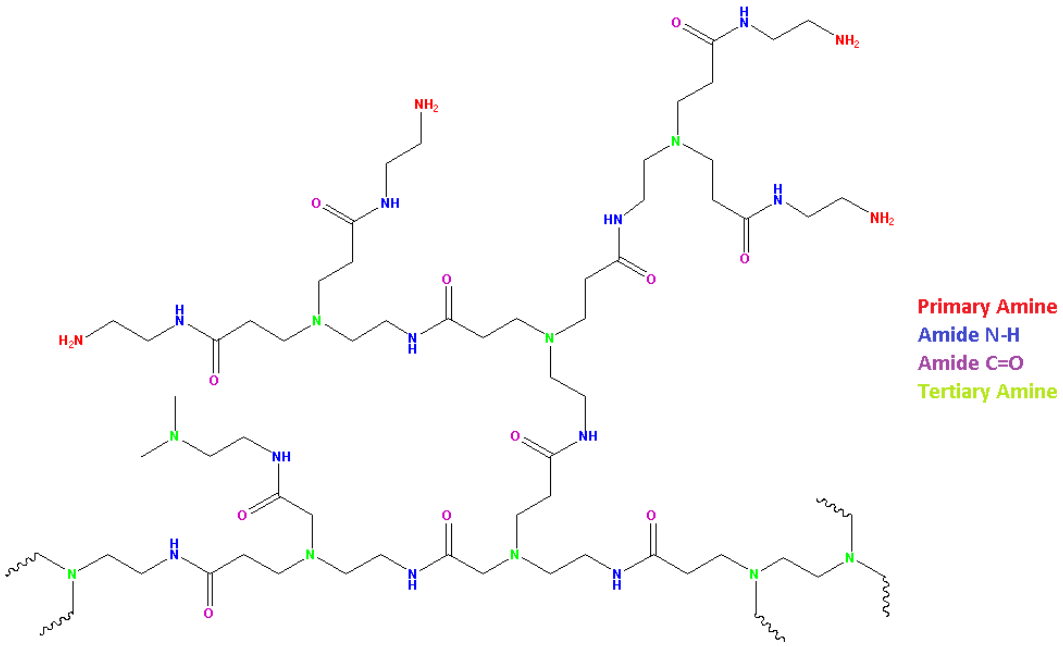

Figure 3.17. Annotated diagram indicating function groups indicative of G3-PAMAM NH_2. Note that this figure does not include the entirety of the G3 PAMAM-NH_2 structure, but includes a branch that allows identification of the groups indicated by IR.

Table 3.7. IR spectroscopy absorptions and associated functional groups of CHG (20% w/v in water)-G3 PAMAM-NH_2 (20% w/v in methanol) mixture.

Frequency (cm^{-1})	Characterisation	Functional Group
2935	CH (str)	Alkane
1700	CH (b)	Benzene
1654	RHN-C=O (str)	Amide
1640	RHC=N-R (str)	Imine
1560	NH (b)	Amide
1521	NH (b)	Amine
1159	C-N (str)	Alkyl
1089	C-OH (str)	Alcohol
825	C-H (b)	Para-substituted benzene
721	C-Cl (str)	Carbon-halogen bond

Table 3.8. Table indicating shifts in IR frequency (cm^{-1}) upon mixing 20% w/v CHG and 20% w/v PAMAM dendrimer together.

Type of Bond	Functional Group	Frequency before CHG-PAMAM mixed (cm^{-1})	Frequency after CHG-PAMAM mixed (cm^{-1})	Shift in frequency (cm^{-1})
N-H (b)	Amine	1628	1560	-68
		1549	1521	-28
N-H (b)	Iminium	1653	1640	-13
R_2C=*N-R (str)	Alcohol	1044	1089	45
C-Cl (str)	Carbon-halogen bond	703	721	18

The IR data presented in Table 3.5 and Table 3.6 indicate that functional groups associated with CHG and the G3 PAMAM-NH_2 dendrimer can be readily identified (such as the C-Cl group

associated with CHG and the numerous amide bonds associated with the G3 PAMAM-NH_2 dendrimer). The IR data presented in Table 3.7 shows that the CHG can still be identified by the presence of the C-Cl group and para-substituted benzene ring.

Table 3.8 indicates shifts in IR frequency for specific functional groups, which may provide evidence of interactions between the drug and dendrimer. The greatest frequency shifts were the amide N-H (b) (shift of 68 cm^{1}), alcohol C-OH (str) (shift of 45 cm^{-1}) and the amine N-H (b) (shift of -27cm^{-1}). The functional groups associated with the carboxylate ion/carboxylic acid are not recorded here, as it was difficult to ascertain the nature of the functional group given that the group was aligned with the digluconate in water prior to mixing with the PAMAM dendrimer. The presence of the carboxylate ion is supported by Taylor and Chu (2018). The authors found a shift in the peak associated with napthenic acid when transforming into its calcium salt (from 1709 to 1543 cm^{-1}). Further, a loss of band at 1265 cm^{-1} was consistent with salt formation. The size of the peak at 1250 cm^{-1}, and peak at 1533 cm^{-1} in Figure 3.13 confirms the CHX is in its salt form, CHG. However, the nature of the interaction between CHG and PAMAM is unknown, and cannot be readily recognised from Figure 3.15, although shifts in the spectrum indicate an interaction has taken place. Hence, the requirement for a secondary analytical method to determine the nature of the precipitate (Section 3.4.8).

3.4.8 X-ray diffraction (XRD) analysis of unknown precipitate

Table 3.9. Crystal data obtained from XRD analysis.

Empirical formula	$C_{22.85}H_{40.15}Cl_2N_{10}O_{7.15}P_{0.15}$
Formula weight (g/mol)	644.94
Crystal system	Monoclinic
Crystal size (mm^3)	0.44 × 0.11 × 0.03

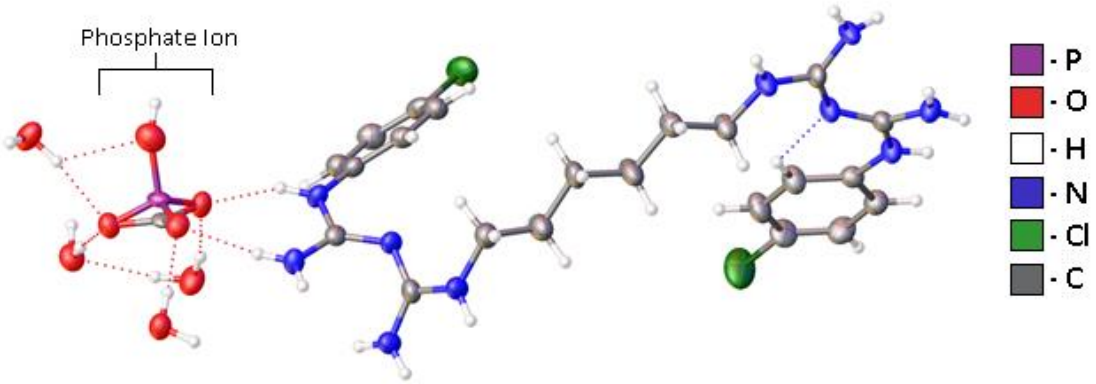

Figure 3.18. Chemical structure obtained from XRD analysis of a single crystal of the unknown precipitate.

The XRD analysis revealed a mixture, the majority of which was found to be a CHX salt (Cattaneo *et al.* 2016). No PAMAM dendrimer was found in the XRD precipitate but was believed to be a component of the mixture.

3.5 Discussion

The purpose of this chapter was to determine whether a CHG-G3 PAMAM NH_2 dendrimer co-formulation was able to enhance the depth permeation of CHG into porcine skin for improved skin antisepsis compared to the commercial benchmark. This was a development of a previous pre-treatment study (Holmes *et al.* 2017) into a more practical drug-dendrimer co-formulation. It was proposed that co-formulating the drug and dendrimer would improve dermal deposition of CHG compared to that delivered from the commercial benchmark and market leading product Hibiscrub® (contains 4% w/v CHG), a liquid wash recommended by NICE, which is used prior to surgery as a preventative measure against SSTIs. The permeation of CHG into skin is poor (Karpanen *et al.* 2008a), and the concentrations of drug reaching deeper skin layers (Nakatsuji *et al.* 2013) and follicles (where bacteria reservoirs reside with the ability to cause SSTIs [Touitou, Meidan and Horwitz, 1998]) is unlikely to kill bacteria without aid of a permeation enhancer. The 4% CHG-1 mM PAMAM co-formulation (containing 0.5% w/v HEC and 60% w/v ethanol) was found to significantly increase the concentration of drug delivered onto all tape strips when compared to the commercial benchmark, and further statistical significance was observed in the deeper tape strips 4-6, 7-10 and 17-21 between 4% CHG-1 mM PAMAM and 4% w/v CHG ($p < 0.05$).

The Franz-type diffusion cell experiments indicated that, in general, an increase in viscosity decreased the concentration of CHG which was delivered into deeper skin layers. This is in accord with the Stokes-Einstein equation (Equation 4, Einstein and Fürth, 1956), which illustrates the inverse relationship between the diffusion coefficient (a measure of how easily a drug may traverse through a tissue) and viscosity, among other properties.

$$\boldsymbol{D = \frac{RT}{6\pi\eta a N_A}} \quad \textbf{(4)}$$

Where

D is the diffusion coefficient (of a spherical particle)

R is Boltzmann's constant,

T is temperature (K),

η is viscosity

α is the radius of the diffusing molecule

N_A is Avogadro's Number.

An increase in viscosity reduces the diffusion coefficient because it reduces or prevents free movement of drug particles within the formulation, thereby reducing the incidence in which a drug particle is able to come into contact with the skin surface, interact with it, and diffuse through the barrier (Kriwet and Müller-Goymann 1995).

The increase in CHG delivered with increasing CHG concentration in the formulation (Figure 3.7) was also expected, consistent with Fick's law of diffusion (Equation 1). An increase in concentration applied to the skin surface increases the concentration gradient and therefore increases the spontaneous movement of particles from an area of high concentration (the skin surface) to an area of low concentration (deeper skin layers). However, the differences between groups are not as large as one might expect, especially when taking into account the variance in results. This is reflected in the statistical analysis where the significant differences generally are present only between the highest and lowest applied CHG concentration (i.e. between 4% w/v and 1% w/v CHG). This may be due to the inherent variation in skin samples, limited treatment area of the Franz type-diffusion cell donor chamber (1.03 cm^2) and a lack of surface wettability.

The delivery of a permeant into and across the skin is proportional to diffusional surface area (Higuchi 1960, Flynn 1992, Sietsema 2012). Guy and Hadgraft (1992) investigated the role of the vehicle and the membrane in an attempt to determine where the rate of permeation is controlled. They compared the amount of drug released from a delivery system alone with the amount of drug released from the delivery system in contact with the skin. This study was repeated to include four different transdermal systems. The results found that neither the membrane nor the drug device controlled flux, but that the surface area of the drug in contact with the skin was the most important parameter. Increasing the concentration of drug is likely to increase the partitioning of drug into the skin; however eventually the surface becomes saturated with drug molecules, and increasing the applied concentration further simply "stacks" the drug above this saturated layer in the donor chamber where it is unavailable for contact with the *stratum corneum* surface (and thus is unavailable for partitioning into the skin) until the drug molecules directly adjacent to the skin surface are able to penetrate. Therefore the rate of permeation is directed by the ability of molecules adjacent to the skin surface to penetrate (Williams 2003b). This effect may have been further perpetuated by the small surface area of the donor chamber (1.03 cm^2) limiting the amount of CHG able to be in contact with the skin surface at any one time. This may also be influenced by the "aqueous diffusion" or "aqueous boundary" layer, i.e. an unstirred water layer adjacent to the membrane surface (Díez-Sales *et al.* 1991, Flynn 1992) which may limit drug diffusion into the skin (Woolfson and McCafferty 1993, Cross and Roberts 2000). However, this may influence the ability of lipophilic molecules to diffuse more than hydrophilic molecules and thus may not be considered a significany limitation when discussing the ability of CHG to permeate into the skin (Potts and Guy 1992).

In addition to the surface area of the donor chamber, the surface tension and wettability of the drug in the formulation may also have contributed to a lack of significant difference between CHG concentration and CHG permeability. The ability of a molecule to absorb into the skin may

depend on the surface activity of the interacting molecule(s) (Fathi-Azarbayjani *et al.* 2009). The surface tension of human skin is 27-28 dyne/cm (Ginn *et al.* 1968), although this may differ with body site due to the distribution of sebum (Elkhyat *et al.* 2017). According to Ginn, Noyes and Jungermann (1968), for good adherence to the skin surface, the surface tension measurement should be equal to or less than that of human skin. The surface tension of CHG 4% w/v in water has been reported in Table 5.5 as 0.0466 Newton/metre (equal to 46 dyne/cm). This supports the idea that a reduction in surface tension may be required for CHG permeation enhancement as the surface tension of CHG 4% w/v in water is not lower than the surface tension of human skin, despite the fact that CHG is moderaly surface active (Heard and Ashworth, 1968; Denton, 2001).

The influence of wettability on drug permeation into skin has been demonstrated in the literature. Azarbayjani *et al.* (2010) found that cyclodextrin vehicles that increased the wettability of haloperidol resulted in significantly greater drug permeation across human epidermis *in vitro*. The permeability of a hydroxypropyl methylcellulose diclofenac formulation was found to be greater than the same drug in a polyvinylpyrrolidone formulation across rat and human skin (Fang *et al.* 1999b). The presence of both hydrophilic and hydrophobic groups in hydroxypropyl methylcellulose was thought to reduce the surface tension of the aqueous formulation, increasing the spreading of drug on the skin surface, resulting in a higher permeability. Hydroxypropyl-β-cyclodextrins have also been used for the transdermal delivery of ketoprofen (Sridevi and Diwan 2002). In addition to enhanced wettability, the increased solubility of the drug was attributed to the enhanced permeation of ketoprofen.

Surfactants are able to reduce the surface tension and thus increase the spreading of a drug on the skin surface and have been explored as a method of permeation enhancement for many years. They have successfully acted as permeation enhancers in many instances (Cappel and Kreuter 1991, Shokri *et al.* 2001, Nokhodchi *et al.* 2003), although their mechanism of action

cannot solely be attributed to increased wettability of the drug, as many (particularly ionic) surfactants may also act on the skin lipids, fluidising and extracting them and in doing so, reducing the pertinent *stratum corneum* barrier (Scheuplein and Ross 1970, Dugard and Scheuplein 1973). The influence of surface tension on the topical permeation of CHG is explored further in Chapter 5.

The 4% CHG-1 mM PAMAM co-formulation successfully enhanced CHG deposition into porcine skin. This enhancement effect was considered statistically significant across all tape strips compared to the commercial benchmark ($p < 0.05$). The delivery of CHG from the 1 mM co-formulation into the first tape strip layer was almost 6 × that of Hibiscrub®. This 6 fold increase in permeation enhancement was not consistent across all tape strips and was found to decrease as tape strip number increased, so that when analysing tape strips 17-21, the delivery of CHG from the 1 mM co-formulation was found to be 3 × that of Hibiscrub®. This general trend was seen across all formulations tested in this study, and in previous studies investigating CHG permeation enhancement (Karpanen *et al.* 2010; Holmes *et al.* 2017).

CHG permeation through full thickness porcine skin was <LoD (appendix 1). This is advantageous for this particular setting, whereby permeation enhancement was successful, and the lack of permeation through full thickness skin indicates a reduced risk of systemic absorption and potential adverse drug reactions (ADRs). This is also advantageous in comparison to the G3 PAMAM-NH_2 24 hr pre-treatment study (Holmes *et al.* 2017), which found 1.169 ± 0.438%, 0.601 ± 0.154% and 1.053 ± 0.212% of an applied 2% w/v CHG solution was delivered into receptor fluid by the 0.5 mM, 1 mM and 10 mM pre-treatment respectively. The two studies are not directly comparable due to the differences in applied dose (2% w/v pre-treatment vs. 4% w/v co-treatment) and thickness of skin (epidermal membrane in the pre-treatment study, full thickness porcine skin in the co-treatment study). Regardless, the results from this study indicate that an efficacious co-formulation was successfully created, a development from the previous

pre-treatment study by removing the need for the impractical pre-treatment step whilst still enhancing CHG depth permeation for improved skin antisepsis, without permeation through full thickness porcine skin.

Whilst the 0.5 mM PAMAM co-formulation delivered an increased concentration of CHG to tape strips 1-21 compared to Hibiscrub®, this was only considered statistically significant in tape strips 4-6 and 7-10. These tape strips likely represent the *stratum dysjunctum*, the outermost region of *stratum corneum*, in which adherence between corneocytes are weakened due to degradation of corneodesmosomes. As the adherence between these cells are reduced, it is likely that permeation enhancement of CHG by the PAMAM dendrimer at 0.5mM concentration into the more superficial layers of the *stratum corneum* is more easily achieved than permeation into the *stratum compactum*, where adjacent corneocytes are held firmly in place by intact corneodesmosomes.

The results from this study suggest that the permeation enhancement of CHG is not dependent on PAMAM dendrimer concentration, agreeable with previous studies (Venuganti and Perumal 2009, Holmes *et al.* 2017), as increasing the concentration of PAMAM dendrimer does not appear to proportionally increase the concentration of CHG which permeates into porcine skin. However, only two concentrations of PAMAM dendrimer were tested in this study, therefore an *in vitro* study utilising a wider range of formulations with differing concentrations of G3 PAMAM-NH_2 dendrimer is required to confirm this possibility. It was suggested by both studies cited above that an aggregation of PAMAM dendrimer at high concentrations may be the reasoning behind this lack of concentration dependent effect (Klajnert and Epand 2005).

It was found that the experimental gel formulation containing 4% w/v CHG was able to deliver more CHG into the *stratum corneum* than Hibiscrub® (4% w/v CHG), when applied to the skin for 24 hr (although this increase was only considered statistically significant on tape strips 4-6

and when comparing total CHG permeation across all tape strips). This result indicates that development of the vehicle improved the ability of CHG to permeate into porcine skin, independent of co-formulating the drug with a G3 PAMAM-NH_2 dendrimer. The ability of simple vehicles to influence the permeation of drugs into and through skin has been discussed extensively in the literature (Møllgaard and Hoelgaard 1983, Wotton *et al.* 1985, Hoelgaard *et al.* 1988, Francoeur *et al.* 1990, Bonina *et al.* 1993, Megrab *et al.* 1995a), however it is often difficult to determine what effects are likely to occur from mixtures of several vehicles (Karande and Mitragotri 2009, Karadzovska *et al.* 2013, Roberts 2013) where covariance and synergy should be considered. The ability of the co-formulation to enhance CHG deposition compared to Hibiscrub® may be attributed to the increased film formation effects resulting in increased residency time of the drug on the skin, drug saturation following ethanol evaporation, and possibly occlusive and surface tension effects, each of which are discussed below.

Film formation occurs following drug application to the skin in a suitable volatile vehicle and film-forming excipients (such as HEC [White, 1991; Khan and Hoang, 1997; Sine *et al.* 2000]). Following application to the skin, the volatile component of the vehicle (in this study, ethanol) evaporates, leaving behind a drug containing film. Understanding drug permeation from film-forming systems is challenging given that the degree of drug saturation will change as the solvent evaporates, the rate of evaporation may be altered by non-volatile solvents in the system, and excipients may also influence the rate of drug permeation (McAuley and Caserta 2015).

Evaporation of the volatile vehicle component increases drug saturation, which in turn promotes drug flux through increasing the thermodynamic activity of the drug in the formulation without compromising the barrier function of the *stratum corneum* (Kalia and Guy 2001, Moser *et al.* 2001). Increasing drug delivery to the skin without affecting the skin's barrier integrity reduces the risk of irritation and therefore should be considered highly advantageous, particularly within

this study as the patient acceptability of the formulation is of great significance. Increasing the drug saturation in the vehicle and causing supersaturation (i.e. the permeant exceeds its solubility but remains in solution) has been attributed to increasing topical and transdermal drug permeation extensively within the literature (Megrab *et al.* 1995b, Pellett *et al.* 1997, Iervolino *et al.* 2000, 2001, Reid *et al.* 2009). Li *et al.* (2014) developed a film-forming hydrogel that sustained the release of rotigotine. The delivery of the drug increased with increasing concentration, however at drug concentrations >3%, rotigotine began to precipitate "by crystallization because of a large amount of ethanol evaporation". Supersaturated systems are physically unstable and may result in drug precipitation and crystallisation of the drug from the vehicle (Coldman *et al.* 1969, Stinchcomb *et al.* 1999, Hou and Siegel 2006), though this may be reduced by the addition of excipients which stabilise the formulation (Fang *et al.* 1999a). In particular, cellulose derivatives (i.e. HEC) have been found to stabilise supersaturated systems (Megrab *et al.* 1995b, McAuley and Caserta 2015). For example, Raghavan *et al.* (2001) found that hydroxypropyl cellulose was more effective in stabilising hydrocortisone acetate than polyvinyl pyrollidone. This could support the theory that drug precipitation from the CHG-PAMAM co-formulation did not rapidly occur following solvent evaporation due to the presence of HEC which may have stabilised the supersaturated formulation, allowing enhanced CHG deposition for a greater time period. This mechanism may have also worked alongside the increase in viscosity that inevitably occurred with solvent evaporation, slowing particle movement and thus the ability of the CHG and PAMAM to interact with one another.

In addition to enhancing the thermodynamic activity of the drug in the formulation, increasing contact time of a drug on the skin surface typically provides a greater opportunity for drug partitioning into the skin, as partitioning into the *stratum corneum* is dependent on direct contact between the drug and the skin surface (Williams 2003b). It is proposed that in this study that film formation increased CHG residency time on the skin, aided by the plasticiser (glycerol;

[Pedersen and Jemec, 1999]). An interaction between CHG and HEC may also have occurred in which CHG may act as a plasticiser, previously found by Khan and Hoang (1997) and Judd (2013b), thus further increasing the flexibility of the film. Judd (2013b) compared CHG 2% w/v solution against a mixture of CHG and PAMAM in ethanol-water with the addition of hydroxyl propyl cellulose (formulation "F_a") using ATR-FTIR. Peak shifts were found which corresponded to the C=N stretch – 1633 cm^{-1} for 2% w/v CHG which shifted to 1647 cm^{-1} in formulation F_a; the chlorophenyl functional group appeared at 1492-1533 cm^{-1} for CHG 2% w/v but shifted to 1380 cm^{-1} in formulation F_a. Furthermore, Judd found a peak corresponding to a C-H stretch at 2975 cm^{-1} in the F_a spectrum that was missing from the 2% CHG w/v spectrum. In addition, C-H bending due to the aromatic ring on CHG was observed at 878 cm^{-1} within F_a that was not present in the CHG 2% w/v spectrum.

Other preparation types, such as liquids (Hibiscrub®), creams and ointments may not form films, or may form weak films. Thus, any film present may not exhibit persistent contact with the skin surface. They can also be easily removed, unlike films, which are somewhat resistant to being wiped off by the patient, although can usually be easily removed by running the contact site under water as HEC is water soluble (Harwood 2006, Kathe and Kathpalia 2017). Hibiscrub® may form a film following application to the skin due to the inclusion of glycerol and a surfactant (Poloxamer 237) in the formulation (Bodratti and Alexandridis 2018). However, this film may not be as well developed as the film produced by the experimental formulation, or the film may dry out if suitable excipients are not included which retain enough moisture. A lack of developed film is suggested due to the lack of vehicle evaporation when compared to the experimental formulations (a loss of 0.51 ± 0.02 g; 0.48 ± 0.05 g; 0.13 ± 0.01 g occurred after 24 hr for 4% w/v CHG, 4% CHG-1 mM PAMAM and Hibiscrub® 4% respectively). If the film-forming effects are less pronounced, so too may the ability of the drug to partition into the skin (assuming that the film does not dry out and thus immobilise the drug). This may provide a reason for why the

experimental gel formulation was able to deliver a higher concentration of CHG into porcine skin compared to the commercial benchmark.

Whilst film-forming systems do not have inherent occlusive properties (Kathe and Kathpalia 2017), film-forming systems may increase hydration via occlusion, and inclusion of specific excipients into the experimental formulation may have promoted occlusive effects, despite not being the primary purpose for inclusion into the formulation. Excipients that hydrate the skin may also hydrate the film, preventing it from drying out and thus preventing drug immobilisation. Occlusion is also an established mechanism of drug permeation enhancement in skin (Shelmire 1960, Roberts and Walker 1993, Wester and Maibach 1995). Glycerol has humectant properties (Barr *et al.* 1988, Atrux-Tallau *et al.* 2010), and the presence of both glycerol and water may contribute to hydratation of the skin surface (Behl *et al.* 1980, Roberts and Walker 1993, Bouwstra *et al.* 2003). This does not necessarily guarantee enhanced drug permeation, as conflicting results on the effects of occlusion have been reported. For example, Treffel *et al.* (1992) found that occlusion did not enhance the rate of caffeine (ampiphilic drug) delivery, but did enhance the rate of citropten (lipophilic drug) delivery. Thus, occlusive mechanisms may contribute to enhanced CHG deposition, but this may not be the predominant driving force for enhanced CHG deposition in this system.

A potential mechanism that may have reduced the permeation of CHG is that of increasing formulation viscosity due to vehicle evaporation. Increasing the viscosity decreases the diffusion coefficient of CHG, decreasing its permeation into porcine skin (Equation 4). Increase in formulation viscosity was evidenced by the reduced mass of the formulation on the diffusion cell donor chamber after 24hr (a loss of 0.51 ± 0.02 g; 0.48 ± 0.05 g; 0.13 ± 0.01 g for 4% w/v CHG, 4% CHG-1 mM PAMAM and Hibiscrub® 4% respectively). However, inclusion of excipients that may secondarily act to occlude the skin may aid in keeping CHG dissolved in formulation via hydration of the skin, thereby allowing the drug to continually partition into the skin, albeit at a

slower rate due to the changes in viscosity. It is proposed that the increase in viscosity slowed the process of drug precipitation alongside the presence of HEC as a stabilising excipient. For example, Tsai *et al* (1999) found that permeation of berberine through rat skin was inversely related to ointment viscosity, and Potter *et al* (1999) found that topical permeation of radiolabelled benzo(a)pyrene skin was inversely related to viscosity.

The gelling agent used in this study, HEC (alongside other cellulose derivatives), has also been attributed to surface tension effects (Chang and Gray 1978, Hu *et al.* 1991, Nahringbauer 1995, Olorunsola and Adedokun 2014). The presence of HEC within the gel formulation may have reduced the surface tension of the formulation, allowing CHG to reside on the skin surface with a lower contact angle than that reported in Table 5.4 (CHG 4%-water), and thereby allowing the drug to exhibit a greater contact with the skin surface, resulting in better partitioning of the drug into the skin.

In summary, the results obtained herein would suggest that film formation, drug supersaturation, increased contact time, occlusion and surface tension effects are likely to have contributed to the enhanced delivery of CHG from a gel formulation compared to Hibiscrub®. Upon application of the gel formulation to the skin, the ethanol component of the formulation evaporated, leaving behind a film. This resulted in supersaturation of the drug in the formulation (Figure 3.2 and Figure 3.3), enhancing drug permeation through enhanced contact with the skin surface and increasing the thermodynamic activity of the drug in the formulation. Evaporation of the ethanolic vehicle would increase the proportion of gelling agent in the system, increasing viscosity which would slow CHG permeation, but the inclusion of compounds in the formulation which may act to occlude the skin and stabilise the system may have prevented CHG permeation from halting completely. This is a secondarily important mechanism for ensuring prolonged CHG delivery into skin over the course of an *in vitro* experiment.

The co-formulation containing 1 mM PAMAM significantly enhanced the deposition of CHG into tape strips 2, 4-6, 7-10 and 17-21 when compared to the experimental formulation containing 4% w/v CHG (no PAMAM dendrimer). This illustrates the ability of the G3 PAMAM-NH_2 dendrimer to act as a permeation enhancer of CHG and that CHG permeation enhancement in this study compared to the commercial benchmark was not simply limited to improvement of the formulation as discussed above. The mechanism of G3 PAMAM-NH_2 mediated CHG permeation enhancement is discussed in Chapter 5.

Although the co-formulation significantly enhanced CHG depth permeation compared to Hibiscrub®, it failed to enhance the permeation of CHG to the same extent as a 24 hr G3 PAMAM-NH_2 skin pre-treatment followed by a 2% w/v CHG 24 hr application to the skin found by Holmes *et al.* (2017). For example, the study states that in tape strips 7-10, the mean concentration of CHG extracted was 179.182 ± 63.057 µg/mL for the 1 mM PAMAM dendrimer pre-treatment, a 20 fold decrease from tape strip 1. For the 4% CHG-1 mM PAMAM dendrimer co-formulation, the mean concentration of CHG extracted from tape strips 7-10 was 114.589 ± 16.453 µg/mL which is comparable to the pre-treatment, however the concentration of CHG from the co-formulation detected on tape strip 1 was 325.355 ± 50.263 µg/mL, an approximate 3 fold difference in CHG concentration. This difference is more profound when considering the pre-treatment used 2% w/v CHG solution whereas the co-formulation used a gel containing a greater drug concentration (4% w/v CHG). It appears, from a mechanistic perspective, that a PAMAM dendrimer pre-treatment may be able to deliver a greater concentration of drug into skin because of the increased contact time of only the dendrimer on the skin, allowing the dendrimer to exert its effects prior to application of the drug (e.g. via occlusion or lipid disruption [Sun *et al.* 2012; Judd, 2013b]), as opposed to dendrimer application to the skin alongside the active and excipients. This observation further demonstrates the advantages of the co-formulation as opposed to a PAMAM dendrimer pre-treatment (in addition to creating a simple

one-step application), as permeation enhancement effects from the co-formulation still occurred, increasing the concentration of drug in deeper skin layers, without significant permeation through full thickness porcine skin. Furthermore, the concentrations of CHG delivered into deeper skin layers from the co-formulation still reached concentrations considered to be bactericidal.

Staphylococci and *Streptococci* are some of the most common bacteria which make up normal skin flora (Somerville 1969). In the co-formulation that contained 4% CHG and 1 mM G3-NH_2 PAMAM, the average concentration of CHG found in tape strips 17-21 was 49.18 ± 4.67 µg/mL. The 2 minute application of Hibiscrub® gave a CHG concentration of 3.68 ± 0.15 µg/mL in tape strips 17-21. The minimum inhibitory concentration (MIC) of *Staphylococcus aureus* and *Streptococcus pyogenes* were given as 1-4 µg/mL and 1-8 µg/mL respectively (Denton 2001). Therefore the co-formulation, despite its stability issues has shown to deliver the drug at a concentration, which exceeds the MIC, and as a result, it is likely to be bactericidal against skin flora that is commonly found in deeper skin layers. Hibiscrub® may be able to inhibit the growth of the *Staphylococcus aureus* and *Streptococcus pyogenes* bacteria, but would be unlikely to be able to kill the bacteria. Tape strips 17-21 ideally represent 5 layers of skin. If it is assumed that the CHG concentration was spread equally in these skin layers (although it is more likely that there would be more CHG in tape strip 17 than tape strip 21 due to the trends observed in the *in vitro* permeation studies), we can estimate that the concentration of CHG in tape strip 21 would be 9.84 µg/mL from the 4% CHG-1 mM PAMAM co-formulation and 0.74 µg/mL for Hibiscrub®. The co-formulation still provides a CHG concentration in the deepest skin layer that is above the MIC for the specified bacterium, but the Hibiscrub® does not. The co-formulation delivers CHG concentrations into each tape strip that are bactericidal, which would likely reduce the rate of SSTIs.

Many studies have compared the ability of permeants to be enhanced via pre-treatment or co-formulation with a PAMAM dendrimer. Studies are cited in the introduction of this thesis (Section 1.12.1) and several have illustrated the ability of a dendrimer pre-treatment to enhance drug penetration, but failure of the co-formulation to enhance drug penetration into the skin to the same extent or at all. For example, interactions between furfural and a PAMAM dendrimer - either by covalent interactions with dendrimer surface groups or by encapsulation of the drug within the dendrimer core – decreased flux in a concentration dependent manner (Moghimi, Varshochian et al. 2010). Wang *et al.* (2003a) found that a G3 PAMAM-NH_2 dendrimer pre-treatment enhanced tamsulosin permeation through shed snake skin, but a co-formulation of drug and dendrimer failed to have an enhancement effect. The lack of permeation enhancement when delivered as a co-formulation was thought to be due to interactions between the drug and dendrimer, preventing drug permeation into the skin. A further study sought to characterise this mechanism of enhancement (Wang *et al.* 2003b) and found that drug crystallisation occurred, which unexpectedly encouraged drug release by promoting unidirectional drug diffusion. Penetration of ketoprofen through snake skin was also studied alongside clonidine (using G3-NH_2 and G2.5-COOH) as a co-treatment, however little permeation enhancement effect was noted when combined with a PHA matrix which contained the dendrimer.

It is important to express that many of the studies that investigate PAMAM-mediated drug delivery enhancement do not use porcine skin as a surrogate for human skin. Porcine skin is considered to be the best surrogate for human skin, discussed in more detail in Section 1.7. The results of studies published which do not use porcine skin as an alternative to human skin should be considered critically with the understanding that the results may not necessarily reflect the permeation profile that would result from application of the formulation to porcine or human skin. Nonetheless, studies which utilise PAMAM dendrimers as topical and transdermal

permeation enhancers are limited, therefore these studies should not be discounted when considering the wider body of topical and transdermal permeation enhancement research.

Venuganti and Perumal (2008) investigated the effects of a PAMAM dendrimer on the enhancement of 5FU in three different vehicles: PBS, MO and IPM. The dendrimer either was used as a pre-treatment (up to 24 hr) or was delivered simultaneously with 5FU. When used as a pre-treatment, the dendrimer was able to enhance 5FU flux by 4 × and 2.5 × for the MO and IPM vehicle respectively. When used as a co-formulation, the dendrimer was able to enhance 5FU flux by 1.77 × and 1.38 × for the MO and IPM vehicle respectively. Flux was not increased when PBS was used as a vehicle. This study is of particular interest because 5FU was used as a model hydrophilic drug as previously the literature had focused on PAMAM-mediated enhancement of lipophilic drugs (attributed to drug solubility enhancement via drug encapsulation inside the dendrimer core [D'Emanuele and Attwood, 2005]), and therefore shares some similarities with CHG, such as its high aqueous solubility and low log P (-0.089 and 0.0133 for 5FU and CHG respectively).

The study found that when the skin was pre-treated with the PAMAM dendrimer, there was an increase in TEWL and decrease in skin resistance compared to the control (blank buffer), insinuating that the dendrimer was able to interact with skin lipids and disrupt the *stratum corneum* barrier. This is consistent with results published by (Judd *et al.* 2013b), who visualised changes in the *stratum corneum* barrier by differing concentrations of a G3 PAMAM-NH_2 dendrimer using optical coherence tomography (OCT). Furthermore, Venuganti and Perumal (2008) suggested hydration as an additional cause of 5FU permeation enhancement when the dendrimer was applied as a pre-treatment, as the 24hr dendrimer contact time provides a greater time period available for skin hydration, a mechanism understood to enhance drug deposition into skin (McKenzie and Stoughton 1962, Behl *et al.* 1980, Roberts and Walker 1993).

In the presence of the PAMAM dendrimer, 5FU solubility significantly increased in PB and decreased in the lipophilic vehicles (IPM and MO) and the IPM vehicle showed the largest increase in drug flux for both the dendrimer pre-treatment and co-formulation groups. (Sherertz *et al.* 1987) found an inverse relationship between solubility and permeability coefficient for 5FU, i.e., the vehicle with the closest solubility parameter to the drug increases the drugs solubility, decreasing its permeability coefficient. The IPM had the solubility parameter farthest from 5FU and was therefore the vehicle that resulted in the highest drug permeation. Addition of the dendrimer to the IPM vehicle further shifted the solubility parameter away from the drug, closer to the skin, decreasing the drugs solubility in the vehicle but increasing the permeability coefficient. Therefore, dendrimer mediated reduction in drug solubility increased its permeability coefficient and thus its rate of permeation into the skin when applied as a co-formulation.

The relatively lesser flux enhancement seen in the co-formulation study in comparison to the pre-treatment study may be attributed to drug-dendrimer interactions. The authors found that the addition of the PAMAM dendrimer to the formulation resulted in an increase in pH to 9, which results in ionisation of 5FU and thus reduces the ability of the drug to permeate across the non-polar *stratum corneum*. The authors also postulated the potential for salt formation between 5FU and the dendrimer, though there was no experimental proof of this.

In summary, it is likely that a G3 PAMAM-NH_2 was able to enhance CHG to a greater extent when applied as a pre-treatment (Holmes *et al.* 2017) because the increased contact time of the dendrimer alone likely allowed disruption of *stratum corneum* lipids, and potentially increased hydration of the skin. When applied in a co-formulation, the dendrimer must compete with other formulation components to become adjacent to the skin surface and therefore the opportunities for such interactions are fewer. There were suggestions of CHG salt formation at

the end of a 24 hr diffusion cell experiment, which may further provide evidence of reduced CHG permeation when comparing a PAMAM dendrimer pre-treatment and co-formulation.

Formulations were stored at 4 ^{o}C in an amber glass bottle and were stable in the bottle with no visible signs of drug crystallisation. However, evidence of drug precipitation was apparent at the end of a 24 hr diffusion cell experiment (Figure 3.2 and Figure 3.3). The co-formulation was transparent when first applied, but following the 24 hr *in vitro* experiment, evidence of pearlescent white particulates were visible by eye. Evidence of drug precipitation following the end of a 24 hr diffusion cell study was only found for the co-formulations (i.e. formulations with the G3 PAMAM-NH_2 dendrimer) and was thought to be caused by interactions between the drug and dendrimer, which has previously been shown to prevent drug permeation into skin (Wang *et al.* 2003a; Wang *et al.* 2003b; Moghimi *et al.* 2010).

Judd (2013b) previously found that within 12 hr contact, CHG and a G3 PAMAM-NH_2 dendrimer formed crystals in aqueous solution. Crystals were analysed using light microscopy, Matrix Assisted Laser Desorption Ionization Time of Flight (MALDI-ToF) spectrometry and XRD. The XRD data provided by the author showed that the digluconic acid was missing from the CHG structure and in its place were four water molecules and an oxocarbon anion. It is possible that the polycationic PAMAM dendrimer had scavenged the gluconic acid resulting in precipitation of the CHX base due to a lack of solubility in aqueous solution (solubility; 0.008% w/v in water, [Farkas *et al.* 2007]).

It was of interest in this study to characterise the crystal structure formed to confirm whether the structure found in this study matched the structure characterised by Judd (2013b). This study confirmed that crystals were formed when directly mixing the drug and dendrimer together, which were characterised by light microscopy. Results thus far were in agreement with the previous study (Judd 2013a). Next, crystals formed from mixing the drug and dendrimer

together were characterised using IR. There were shifts on the IR spectra that may be attributed to interactions between the drug and dendrimer (Table 3.8). Of particular interest was the N-H (b) amide peak, which shifted by 68 cm^{-1}, the N-H (b) amine peak, which shifted by 27 cm^{-1}, and the C-OH (str), where there was a 45 cm^{-1} shift when comparing the drug-dendrimer precipitate to their individual components. Judd (2013a) speculated that the interaction between the drug and dendrimer was an electrostatic interaction between the amine groups of the dendrimer and the carboxyl group of the gluconic acid. The IR shifts found in Table 3.8 support this theory. A study completed by Kolhe *et al.* (2003) investigated the drug-dendrimer interactions between ibuprofen and a G3 and G3 PAMAM-NH_2 dendrimer. Similarly to CHG, interactions were found to occur between the carboxyl group on the ibuprofen and the peripheral amine groups of the dendrimers. This was characterised by FTIR and there was a characteristic shift in the C=O (of the carboxylic acid) for both generations of dendrimer when complexed via ionic interactions to ibuprofen (66.5 $cm^{-1}$for the G3 PAMAM and 54 cm^{-1} for the G4 PAMAM). Prajapati *et al.* (2009) attributed solubility enhancement of piroxicam to electrostatic complexation with a G3 PAMAM-NH_2 dendrimer, where a downward shift in the N-H amide stretch at 1650 cm^{-1} was observed in the FTIR spectrum.

Although the IR data appeared to support an occurrence of an interaction between CHG and the PAMAM dendrimer, the exact nature of the interaction and the composition of the precipitate remained unknown. Thus, a second analytical method (XRD) was required for determining the chemical composition of the crystal precipitate.

The XRD data indicated that the precipitate was a phosphate salt of CHX. There was no PAMAM dendrimer present in the XRD sample, but this was believed to be part of the amorphous mixture, which cannot be analysed using XRD. Whilst not exactly the same as the XRD structure previously characterised by Judd, (2013a), the mechanism of CHX precipitation may still be similar. It may be possible that the PAMAM dendrimer scavenged the gluconic acid (supported

by the COOH (str) shift on the IR spectrum), resulting in the formation of a phosphate salt of the drug, which had a lower aqueous solubility than CHG, causing drug precipitation. Misra (1994) characterised the interactions between CHG and hydroxyapatite (an essential component of bone and teeth). The author found that interactions generated a CHX phosphate salt, which was sparingly soluble in aqueous solution (0.5mM, equal to 0.007% w/v aqueous solubility). This is comparable to the poor aqueous solubility of CHX (0.008% w/v [Denton, 2001]) and so it is plausible for the phosphate salt of CHX to precipitate out of the formulation.

In summary, it appears that upon application of the gel formulation to the skin surface, vehicle evaporation occurred, resulting in film formation. CHG permeation into the skin was able to continue due to increased saturation and potentially due to excipients exhibiting occlusive and stabilising effects, keeping the drug in solution despite the increase in viscosity. For the co-formulation, there was found to be an interaction between the drug and dendrimer (likely accelerated by the solvent evaporation) over the course of a 24 hr experiment, whereby the dendrimer scavenged the gluconic acid of CHG, leaving CHX to form a new phosphate salt which is sparingly soluble in aqueous solution, causing precipitation of the drug.

The primary purpose of this study was met – a co-formulation was identified which enhanced the depth permeation of CHG into deeper skin layers when compared to the commercial benchmark. The amounts detected in these deeper layers were large enough to be bactericidal and therefore it could be postulated that utilising this formulation for skin antisepsis prior to surgery would result in fewer SSTIs.

3.6 Conclusion

The aim of this chapter was to determine whether a CHG-PAMAM co-formulation could enhance the permeation of CHG within porcine skin compared to the commercial benchmark (Hibiscrub®). The study demonstrated that this was possible - the 4% CHG-1 mM PAMAM co-formulation delivered clinically relevant concentrations of CHG into deeper skin layers with increased efficacy when compared to application of the commercial benchmark. This is the first time that a CHG-PAMAM gel co-formulation has been designed which has successfully enhanced CHG permeation into the skin, compared to the commercial benchmark and market leader, Hibiscrub™. The enhanced skin antisepsis from a convenient one-step co-formulation may have significant benefit to the health care sector via a reduction in SSTIs.

The chapter established some stability issues with the co-formulation use after 24 hr at 32 ^{o}C. It is important to further understand the mechanism of action of the PAMAM dendrimer, as this may allow for more successful coupling with specific drugs where permeation enhancement may be guaranteed and reduce pairings which may result in drug precipitation (explored in Chapter 5).

4 Chapter Four – Characterisation of skin deposition of CHG by Time-of-Flight Secondary Ion Mass Spectrometry (ToF-SIMS)

4.1 Introduction

In Chapter 3, the "gold standard" technique of tape stripping (Kezic 2008, Ho *et al.* 2016) was used to quantify the depth permeation of CHG from various formulations into porcine skin. Although the technique is a robust and simple method of quantifying depth permeation of drugs within skin, the procedure suffers from some drawbacks that require consideration.

The disadvantages of the tape stripping technique were discussed in detail in Section 1.7. Briefly, the technique assumes that a single tape strip removes a single, even layer of corneocytes (van der Molen *et al.* 1997, Breternitz *et al.* 2007), which is often not the case (Lademann *et al.* 2009). The amount of cells removed and their depth are dependent on numerous factors such as site of application (Machado *et al.* 2010), vehicle (Jacobi *et al.* 2003), adhesive strength (Jui-Chen *et al.* 1991) and velocity of tape removal (Loffler, Dreher and Maibach, 2004). Results may also be skewed by the incorporation of sebum or interstitial fluid on the tape (Weigmann *et al.* 1999, 2003, Alikhan and Maibach 2010). Where drug permeation into the skin is particularly poor, as is the case for CHG (Karpanen *et al.* 2008a), the LoD of the HPLC prevents the ability to accurately quantify the depth permeation of the drug on each skin layer, as later tape strips must be pooled to reach the LoD of this analytical technique.

Time-of-Flight Secondary Ion Mass Spectrometry (ToF-SIMS) offers some notable advantages for characterisation of the surface chemistry of a sample, many of which could be considered complimentary to the traditional tape stripping technique (Section 1.8.1). Briefly, it is a highly sensitive technique with a high mass resolution and wide mass range (Bich *et al.* 2015). Furthermore, a drug which has permeated into the skin can be co-localised alongside other

tissue components (Belu *et al.* 2003), potentially allowing identification of the route of permeation and mechanism of action. For permeation enhancers such as PAMAM dendrimers, where the mechanism of CHG mediated permeation enhancement is currently not well understood, understanding the mechanism of action could allow the permeation enhancer to be more successfully coupled with drugs where a permeation enhancement effect would be more likely. Current studies estimate that PAMAM dendrimer permeation within skin is unlikely due to its high molecular weight and ionisation state (Sun *et al.* 2012) and therefore permeation enhancement effects are likely to be limited to the skin surface, but these speculations have yet to be proven. Alongside the active and permeation enhancer, it may also be useful to map the distribution of excipients within a formulation. Information on excipient penetration may aid the understanding of problems with a formulation, such as irritation which is often a causative factor of topical product non-compliance (Pittet 2001).

ToF-SIMS can analyse individual tape strips due to its low LoD compared to HPLC, removing the requirement for pooling as was required in this study for quantification of CHG on deeper tape strips using HPLC. ToF-SIMS is able to differentiate between tape and skin by selecting regions and or ions of interest, ensuring only drug absorbed within skin tissue is analysed. The instrument's ability to accurately image the depth permeation of CHG has previously been explored by Judd *et al.* (2013b), who found a unique CHG fragment ($C_7H_4N_2Cl^-$) which corresponds to an aromatic branch of CHG. The ion was chosen for its high ion intensity and high chemical specificity.

The purpose of this study was to enhance the depth permeation of CHG, preferably to 400-700 µm below the skin surface, which nominally relates to the depth at which bacterial reservoirs reside in the skin, both in the dermis and hair follicle structures (Selwyn and Ellis 1972, Touitou *et al.* 1998, Grice and Segre 2011, Nakatsuji *et al.* 2013). Studies in this chapter involved utilising ToF-SIMS to provide an accurate depth permeation measurement of CHG from various

experimental gel formulations (in the presence and absence of the PAMAM dendrimer) by tape strip and cross section analysis, and to compare the results to the commercial benchmark to determine which formulation was the most efficacious in terms of dose delivered at the preferable depth. Visualisation of CHG deposition from the CHG-PAMAM co-formulations created in Chapter 2 is a novel use of this method. Finally, the instrument was utilised to transform the qualitative image data into semi-quantitative data for robust statistical analysis that could also be compared to Chapter 3 analytical results, a further novel use of this method.

4.2 Aims and Objectives

With the consideration that ToF-SIMS may be able to combat the limitations of the HPLC analytical technique (notably the low LoD), and that ToF-SIMS can provide unique co-localisation information that tape stripping cannot, the aim of this study was to use ToF-SIMS alongside the tape stripping studies reported in Chapter 3 to characterise the depth permeation of CHG into skin following the topical application of gel formulations in the presence and absence of PAMAM dendrimers. This serves both as a comparison of the two analytical methods but also as a method of validating – or otherwise – the tape stripping technique with regard to the precision and accuracy of results.

Within this, an aim of this study was to co-localise the drug with endogenous skin components to understand how the drug is distributed within the skin. The ability to co-localise the drug alongside other skin structures is unique to ToF-SIMS and cannot be achieved by tape stripping experiments analysed using HPLC.

This is the first time ToF-SIMS has been used to visualise the depth permeation of CHG from the previously optimised gel formulation within porcine skin. The tape stripped ToF-SIMS CHG images were also transformed into semi-quantitative ion intensity values using the "batch statistics" tool (Section 4.3.2.6) so data can be analysed statistically.

The objectives to complete the aims of this study were –

(i) To characterise the depth permeation and localisation of CHG into porcine skin from the commercial benchmark and from formulations in the presence and absence of PAMAM dendrimer, using ToF-SIMS via analysis of tape strips and cross sections.

(ii) To transform the skin images into semi-quantitative ion intensity values and to compare these results to the HPLC quantitative data to determine whether the HPLC

and ToF-SIMS could be considered complimentary techniques for quantification of drug permeation into skin.

The mechanism of action of the PAMAM dendrimer in enhancing skin permeation (in this case, of CHG) is currently unknown and an improved understanding of the distribution of the drug within the *stratum corneum* could allow for contributions to be made towards elucidating the mechanism of action. Thus, a secondary aim of this chapter was to visualise the localisation and distribution of the G3 PAMAM-NH_2 dendrimer within porcine skin using ToF-SIMS.

The objectives to complete the aims of this study were –

(i) To analyse a G3 PAMAM-NH_2 dendrimer alone and within porcine skin using ToF-SIMS in an attempt to identify a unique PAMAM dendrimer fragment which is distinguishable from endogenous skin components.

(ii) Retrospectively image the permeation (if any) of the unique PAMAM dendrimer fragment from porcine skin treated with CHG-PAMAM co-formulations.

4.3 Materials and Methods

4.3.1 Materials

Chlorhexidine digluconate (CHG) 20% w/v in water was purchased from Alfa Aesar. G3 PAMAM-NH_2 dendrimer 20% w/v in methanol was purchased from Sigma Aldrich. Tape stripping was performed using D-Squame™ standard discs purchased from Fisher Scientific, USA. Optimal cutting temperature material (OCT material) was purchased from VWR International Ltd. Belgium. OCT Compound is a water-soluble blend of glycols and resins that provides a convenient specimen matrix for cryostat sectioning at temperatures of -10˚C and below.

4.3.2 Methods

4.3.2.1 Identification of fragment ions characteristic of G3-PAMAM-NH_2 dendrimer

To determine whether a unique fragment ion existed which was characteristic of the G3-PAMAM-NH_2 dendrimer, a minimal volume of the G3 PAMAM-NH_2 dendrimer (20% w/v in methanol) was placed on a glass microscope slide and left for a few minutes to encourage methanol evaporation. The sample was analysed in the negative spectra using ToF-SIMS to find ion peaks that may be considered characteristic of the dendrimer. Furthermore, porcine flank skin was dosed with 1 mL of either 0.5 mM PAMAM dendrimer, 1 mM PAMAM dendrimer or 20% w/v PAMAM in methanol using the protocol outlined in Section 3.3.3. An untreated piece of porcine skin was used as a negative control. After 24 hr, excess formulation was removed from the skin surface, six tape strips were taken from each skin sample and samples were analysed immediately using ToF-SIMS.

The G3 PAMAM-NH_2 dendrimer was drawn in the application ChemDraw Prime 15.1. The "mass fragmentation" tool was used to mimic the molecular fragmentation that may occur in the ToF-SIMS instrument, thus providing m/z values that would be expected from ToF-SIMS analysis of porcine skin treated with the G3 PAMAM-NH_2 dendrimer. Fragments were predicted under the assumption that the synthesis of dendrimer via the addition of branches would reflect the way in which fragments were removed from the dendrimer by ToF-SIMS analysis (Esfand and Tomalia 2001).

4.3.2.2 Skin preparation and diffusion cell study

Preparation of porcine flank skin and assembly of the diffusion cells follows OECD guidelines 428 (2004b) and the protocol in Sections 3.3.3.2-3.3.3.4.

4.3.2.3 Sample preparation for cryosectioning

Cryosectioning porcine skin for ToF-SIMS analysis followed the method published by Al-Mayahy *et al.* (2019). For cryosectioning, porcine skin samples were removed from the diffusion cell apparatus at the end of the 24hr experiment. Excess formulation was removed from the skin surface using an absorbent sponge, and excess skin that was not part of the treatment site was removed using a sharp scalpel blade. The scalpel blade was cleaned using acetone and absorbent paper between samples. Base moulds were labelled with the sample name at the bottom, and an asterisk on the left edge to indicate the *stratum corneum* of interest.

An aluminium block was placed into the centre of a polystyrene box and liquid nitrogen was poured into the box, ensuring the aluminium block was not wholly submerged. The lid was placed on top of the box for 15 min to allow the liquid nitrogen bath to stabilise (indicated by no vapour or mist rising from the box). Skin samples were placed in the base moulds, on top of

the aluminium block and covered until frozen. This process was observed as the skin slowly changing from pink to white from the outside in. This process was complete after approximately 10 min.

Skin samples were temporarily removed from the base moulds. OCT material was placed in the base mould to fill the mould approximately by half, which was enough to support the skin section but did not submerge the skin sample. Then forceps were used to turn the skin upright on its side (ensuring the *stratum corneum* of interest was facing the asterisk marked on the mould) and placed in the OCT material. The skin treatment area was not embedded by the OCT material and was only used to ensure the skin stayed upright. The moulds were quickly returned to the liquid nitrogen bath to solidify the OCT material. Once frozen, the samples were stored at -80 ^{o}C until cryosectioning occurred.

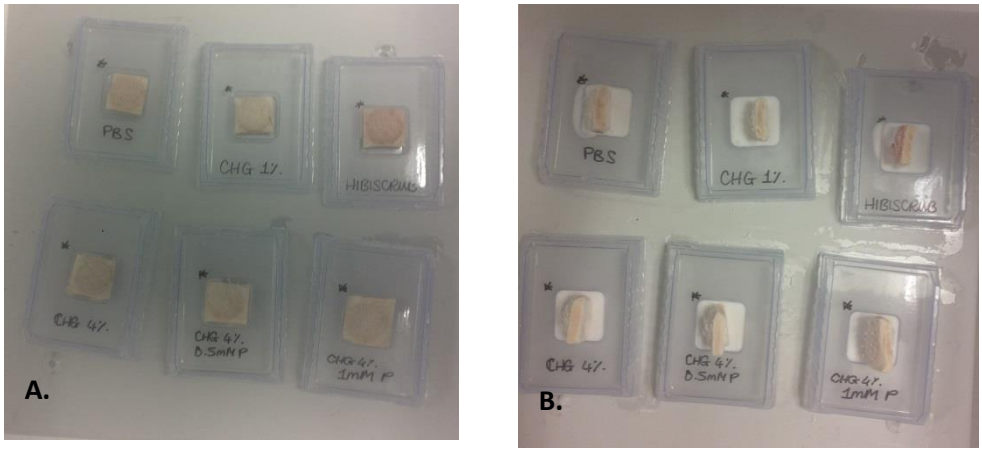

Figure 4.1. Images of skin samples A. in the process of freezing in liquid nitrogen, B. skin samples following partial embedding in OCT material.

Cryosectioning was completed using a Leica CM3050 Research Cryostat. The sample holder temperature was set to -30^{o}C and the chamber temperature was set to -24 ^{o}C. The temperature of the chamber was warmer than the sample holder to minimise rolling which could lead to loss of information during sample collection. The cryostat was set to collect skin sections that were 20 µm thick.

A generous layer of OCT material was spread onto a metal chuck and the skin sample was removed from the base mould and placed on the chuck. The chuck was mounted on the cryostat stage and the cryostat wheel located outside of the chamber was rotated clockwise to slowly move the skin sample towards the blade. Skin layers were trimmed from the sample until a whole skin cross section was clear. The glass anti-roll plate was placed over the blade to ensure skin layers would not curl upon slicing. For each skin sample, 12 cross sections were taken and transferred onto a microscope slide for histological examination and ToF-SIMS analysis. Skin slices that passed the histological integrity check were analysed using ToF-SIMS.

Once analysis was complete, the ion indicative of CHG ($C_7H_4N_2Cl^-$, green colour), phosphite (PO_3^-, red colour) and cholesterol ($C_{27}H_{45}SO_4^-$, blue colour) were overlaid to visualise the depth permeation of CHG in relation to the *stratum corneum* and epidermis.

4.3.2.4 Tape stripping study

Double-sided Sellotape™ was placed on three pieces of glass microscope slides. D-Squame™ tape strips were cut in half – this still covered the entirety of the sample area and doubled the number of strips available for use. Tape strips were taken from a skin sample in accordance with the protocol in Section 3.3.3.4; however the centre of the non-sticky side of the tape strip was marked with a black dot using a permanent marker prior to placement on the skin. This was to direct the ToF-SIMS probe towards the correct 4 mm × 4 mm area which was to be analysed. 21 tape strips were taken from a single piece of treated skin, and tape strips 1, 2, 3, 6, 9, 12, 15, 18 and 21 were placed onto the microscopic slides so that the skin cell faced upwards.

4.3.2.5 ToF-SIMS Analysis

Samples were analysed using the "SurfaceLab 6" (IONTOF GmbH) software (mass spectrometry and image analysis) with a Bi_3^+ cluster source in the negative spectra, "high current, bunched" mode. The mounted samples were exposed to a primary ion energy of 25 kV and were maintained at $< 1 \times 10^{12}$ per cm^2 in order to maintain static conditions. Images were acquired at a resolution of 100 pixels/mm over a 4 mm × 4 mm area (tape strips) and 1.5 mm × 3 mm area (cryosections). Charge compensation of the sample was achieved using a low energy (<20 eV) electron flood gun. All exported peak ion intensities were normalised to the total ion count of the spectra.

A unique CHG fragment has already been identified in the negative spectra (Judd *et al.* 2013b). The ion identified as $C_7H_4N_2Cl^-$, m/z 151 corresponded to an aromatic branch of CHX. Starr *et al.* (2016) identified CN^- as a generic tissue marker and $C_{25}H_{47}SO_4^-$ as a marker for cholesterol sulphate. Schaepe *et al.* (2017) identified PO_3^- as a marker indicative of phospholipids. There are no phospholipids present in healthy *stratum corneum* (Wertz and van den Bergh 1998) and cholesterol sulphate is an abundant molecule present in the *stratum corneum* (Sjövall *et al.* 2014), therefore the combination of both ion fragments were used to co-localise CHG within porcine skin epidermis.

4.3.2.6 Data processing and analysis using the "Batch Statistics", "Line Scan" and "Measurement Editor" functions

Prior to image analysis, images were calibrated and processed to select only biological tissue for analysis and to remove ions indicative of adhesive tape from the image. This was completed by thresholding the image against the CN^- ion, which is indicative of biological tissue. Images were rebuilt using the software and ions were normalised to the total ion intensity within this CN^-

region of interest (ROI; biological tissue only). The ToF-SIMS images in this chapter are all presented following selection of the ROI, which represents biological material, and are normalised for total ion intensity.

The IONTOF software is able to assign an ion intensity value to indicate the ion intensity of a specific ROI (also known as "batch statistics"). This was used to provide semi-quantitative data alongside the tape strip images so ion intensity values could be compared between treatment groups, a novel use of the ToF-SIMS technology. The CHG ion of interest ($C_7H_4N_2Cl^-$), following CN^- ROI selection, was further divided into four equal sized squares (2 mm × 2 mm) and the ion intensity values of the selected ion of interest were exported for each 2 mm × 2 mm ROI. Ion intensity values were compared between treatment groups.

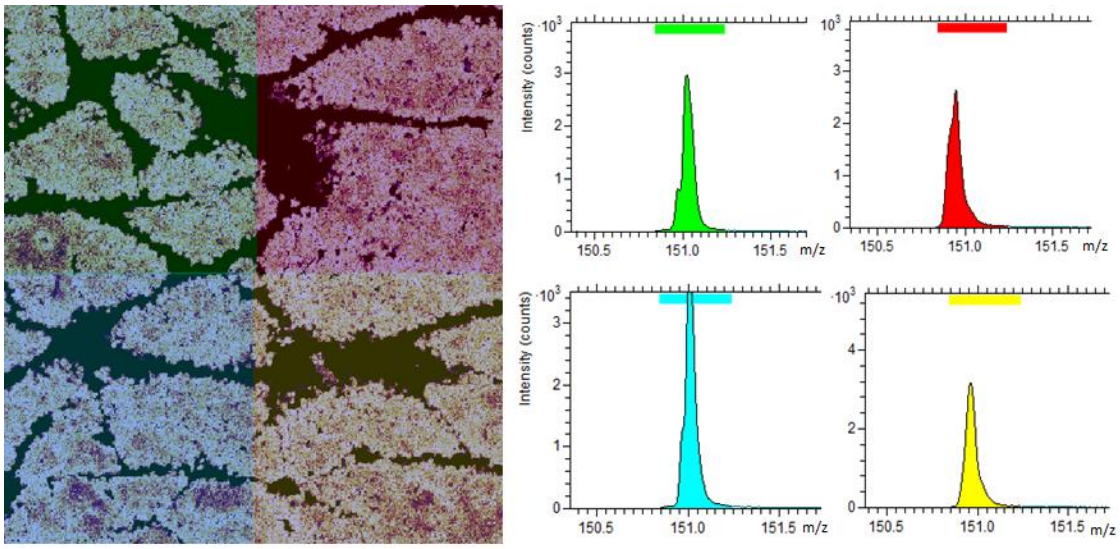

Figure 4.2. ToF-SIMS corneocyte image data; ion intensity processing (following CN^- thresholding) to produce four 2 mm × 2 mm regions of interest (ROI).

Ion intensities were analysed using a One-Way ANOVA with either Tukey's or Games-Howell post-hoc test, or using a Kruskal Wallis ANOVA (where data was non-parametric) using the method detailed in Section 3.3.4.2. A value of $p < 0.05$ represented a statistical significant result.

A further method of viewing semi-qualitative data is by utilising the IONTOF software to produce depth permeation data ("line scan" and "measurement editor" tool). Line scans produce a graph from the chosen cross sectional image which provides information on how the ion intensity value changes with increasing depth within the sample (in this case, within porcine skin). Line scan measurements were transformed from cross sections of blank skin and skin treated with Hibiscrub® 4% w/v, 1% w/v CHG, 4% w/v CHG, 4% CHG-0.5 mM PAMAM and 4% CHG-1 mM PAMAM.

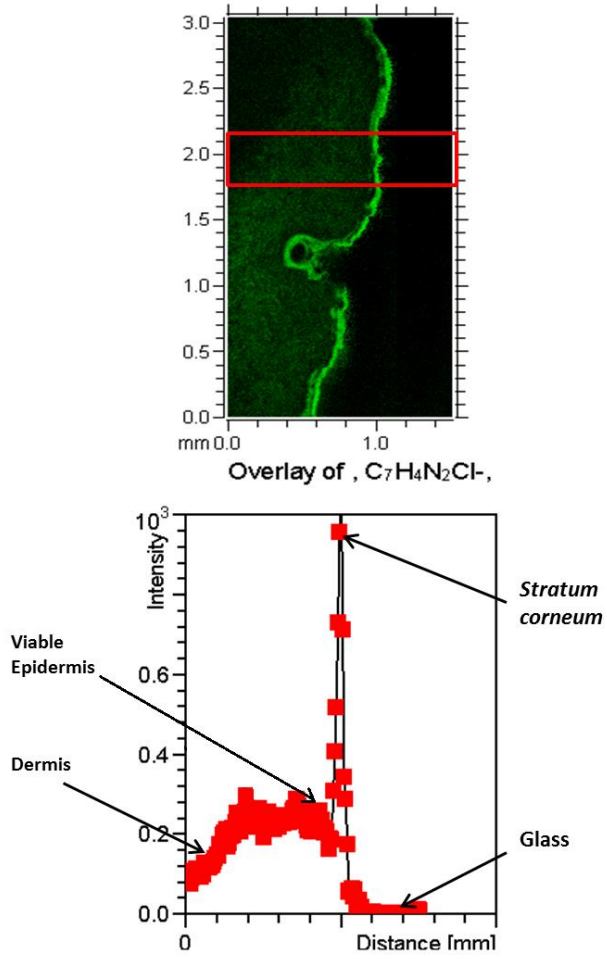

Figure 4.3. Image illustrating how the CHG ion intensity changes across the cross section (section manually chosen indicated by the red box). Intensity of CHG ion spikes indicating CHG resides mainly in the *stratum corneum*.

The “measurement editor” tool allows the depth permeation of a chosen ion to be measured manually across the depth of the cross section (µm). The $C_7H_4N_2Cl^-$ ion was used as a marker of the drug and was utilised to manually measure the depth permeation of the ion. 20 measurements were taken systematically across the entire width of each cross section sample for each formulation to account for differing epidermal thickness across the skin cross sections and the numerous wrinkles and furrows in the skin.

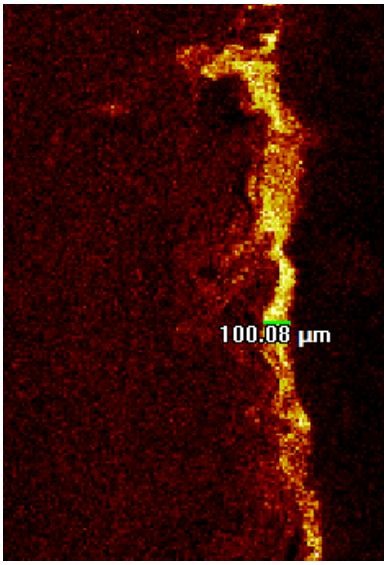

Figure 4.4. Illustration of the “Measurement Editor” feature using the IONTOF software. Depth permeation of the $C_7H_4N_2Cl^-$ ion within porcine skin cross sections are measured manually and are illustrated by the green line.

4.4 Results

4.4.1 Identification of fragment ions characteristic of G3-PAMAM-NH_2 dendrimer

The PAMAM dendrimer was initially analysed alone to identify ions which may be considered unique to the structure. Following this, porcine skin was treated with different concentrations of PAMAM dendrimer used in the co-formulation and as provided by the manufacturer (20% w/v) to determine if the same peaks were evident within porcine skin or if ions indicative of biological tissue obscured these potential fragments.

Several peaks of interest are presented when analysing the overlaid spectra. For example, it was common to identify a PAMAM dendrimer fragment which was clearly visible without application to skin, however once applied to skin, the peak is no longer visible (Figure 4.5 A, B m/z 26.01 and 101.08 respectively, and Figure 4.6 D, m/z 241.22). A peak was also present for the 20% w/v PAMAM dendrimer (untreated skin) at m/z 179.06 (Figure 4.6 C), and this peak was further translated to the 20% w/v PAMAM dendrimer treated skin (although this peak was not well resolved). However, once the PAMAM was applied to skin at the clinically relevant concentrations selected for the co-formulation, no peak was visible which was distinguishable from blank porcine skin. The overlaid mass spectra images can be found in Figure 4.5 and Figure 4.6. No fragments were found which were considered to be indicative of a G3 PAMAM-NH_2 dendrimer fragment according to the theoretical fragments found by utilising the mass fragmentation tool in ChemDraw Prime 15.1 (Figure 4.7).

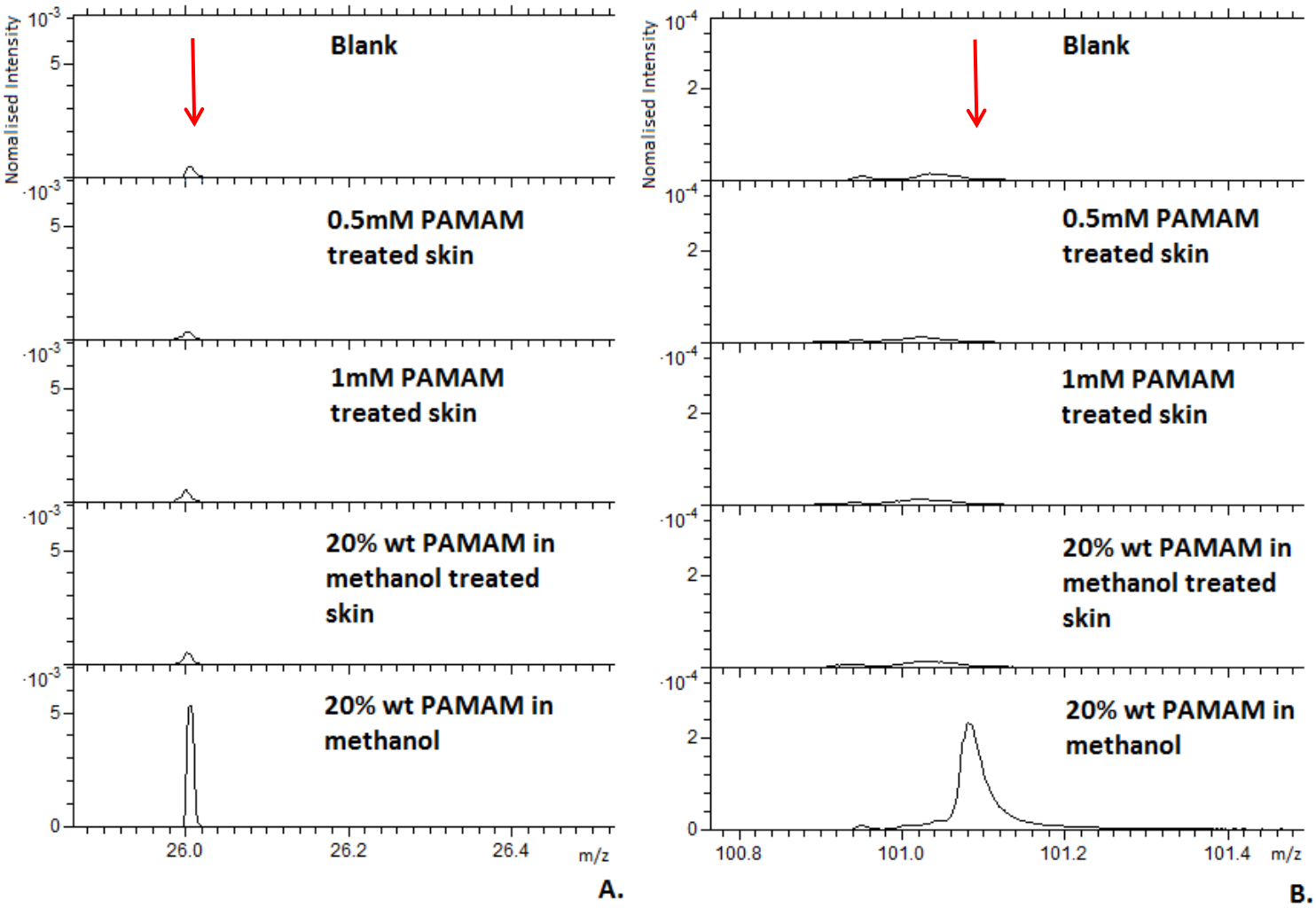

Figure 4.5. m/z values of interest, A. 26.01 and B. 101.08. All mass spectra represent tape strip 3 from porcine skin.

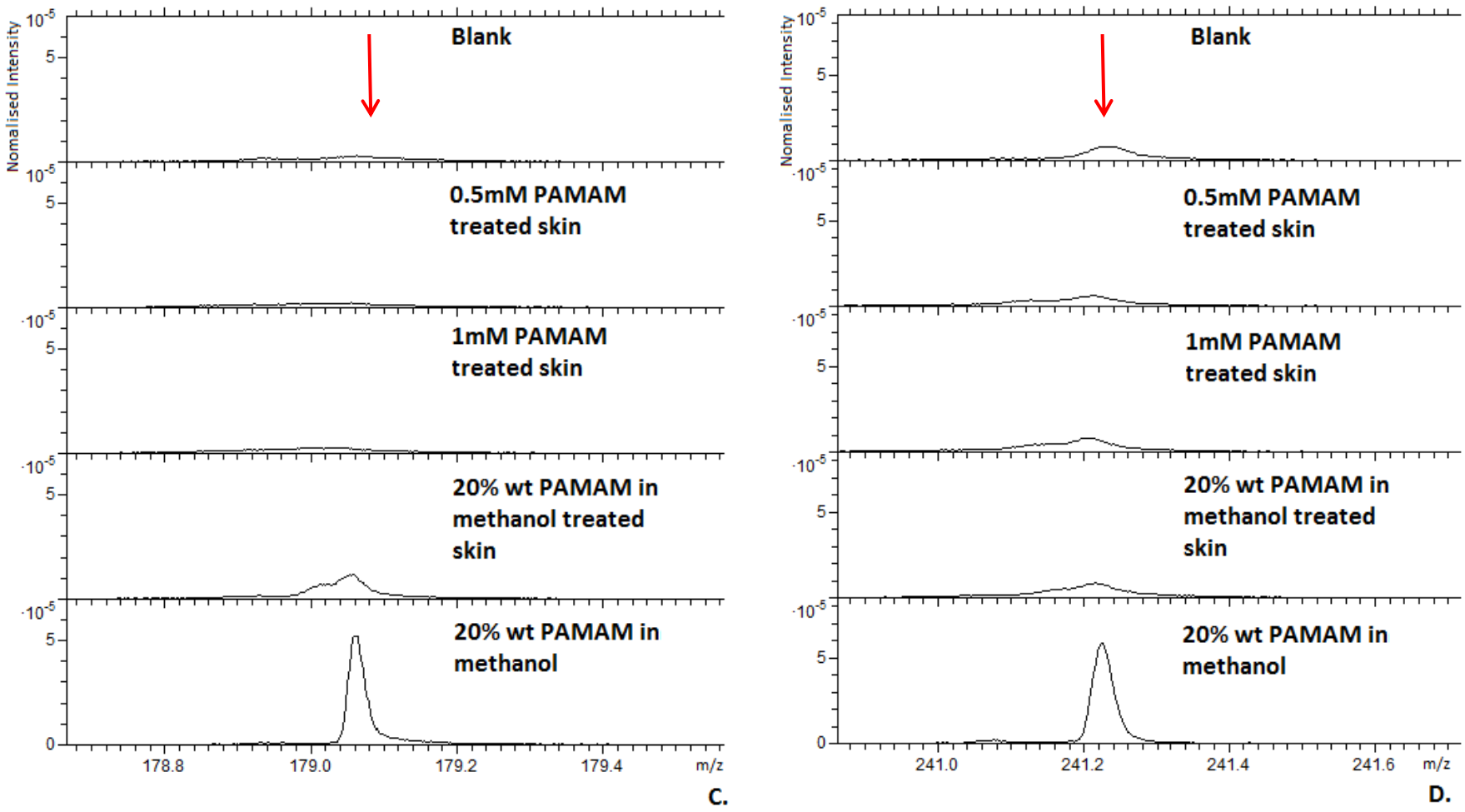

Figure 4.6. m/z values of interest, C. 179.06 and D. 241.22 All mass spectra represent tape strip 3 from porcine skin.

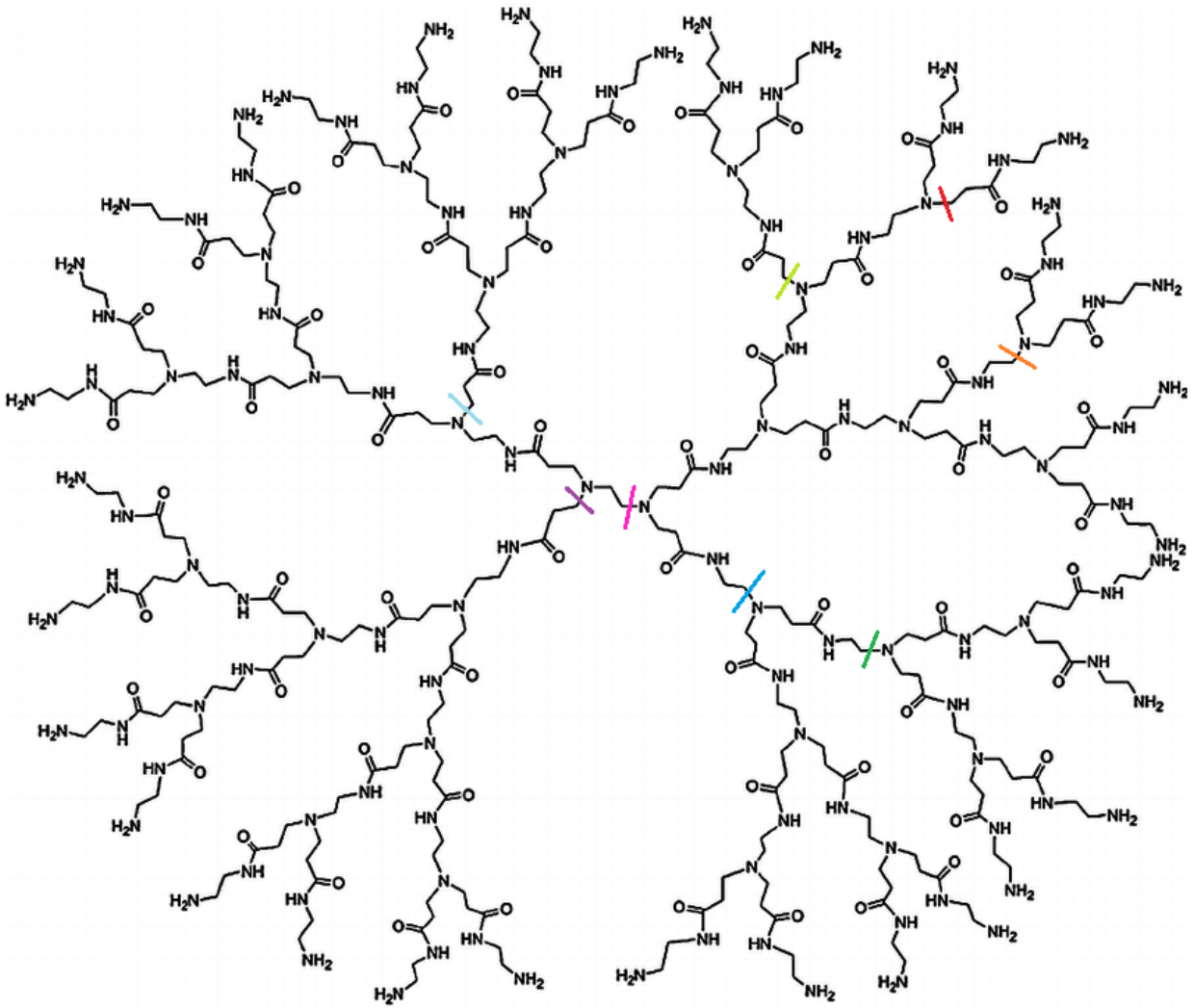

Colour	Fragment	m/z
	$C_5H_{11}N_2O$	115.09
	$C_{10}H_{22}N_5O_2$	244.18
	$C_{15}H_{31}N_6O_3$	343.25
	$C_{30}H_{62}N_{13}O_6$	700.49
	$C_{35}H_{71}N_{14}O_7$	799.56
	$C_{70}H_{142}N_{29}O_{14}$	1613.13
	$C_{75}H_{151}N_{30}O_{15}$	1712.20
	$C_{150}H_{302}N_{61}O_{30}$	3438.40

Figure 4.7. Theoretical mass fragmentation sites of the G3 PAMAM-NH_2 dendrimer and the associated m/z values.

4.4.2 ToF-SIMS analysis of CHG treated porcine tape strips

CHG depth permeation from commercial and experimental formulations (with and without co-formulation with the G3 PAMAM-NH_2 dendrimer) were analysed using ToF-SIMS to generate images indicating the depth permeation and co-localisation of the drug within porcine skin.

The chemical distribution of the CHG ion ($C_7H_4N_2Cl^-$) was mapped within untreated porcine skin and porcine skin treated with 4% w/v CHG gel formulation to indicate the specificity and ion intensity of the chosen ion which was indicative of the drug (Figure 4.8 and Figure 4.9). The untreated tape strips confirm $C_7H_4N_2Cl^-$ as the unique CHG ion previously found by Judd *et al.* (2013b) as only background noise was visible when visualising this ion from the untreated strips.

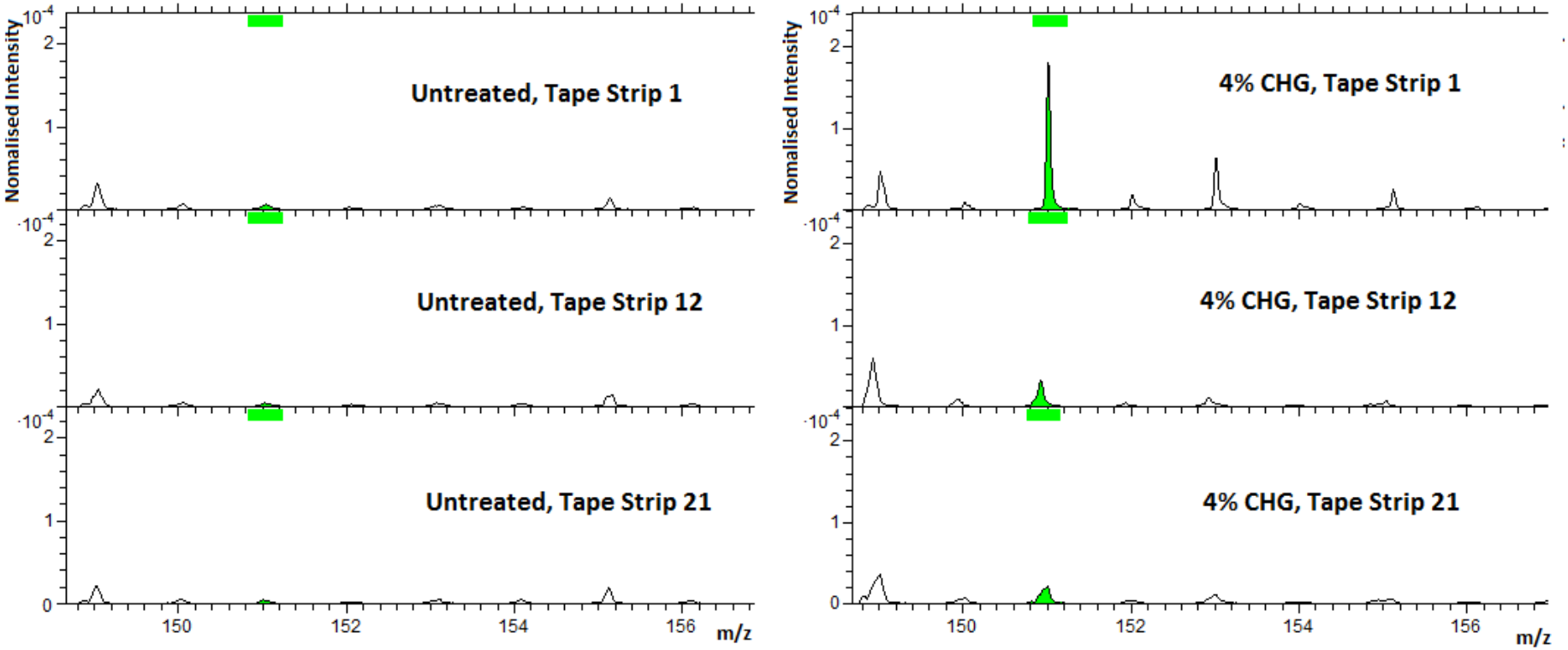

Figure 4.8. Mass spectra images indicating specificity of $C_7H_4N_2Cl^-$ ion to CHG.

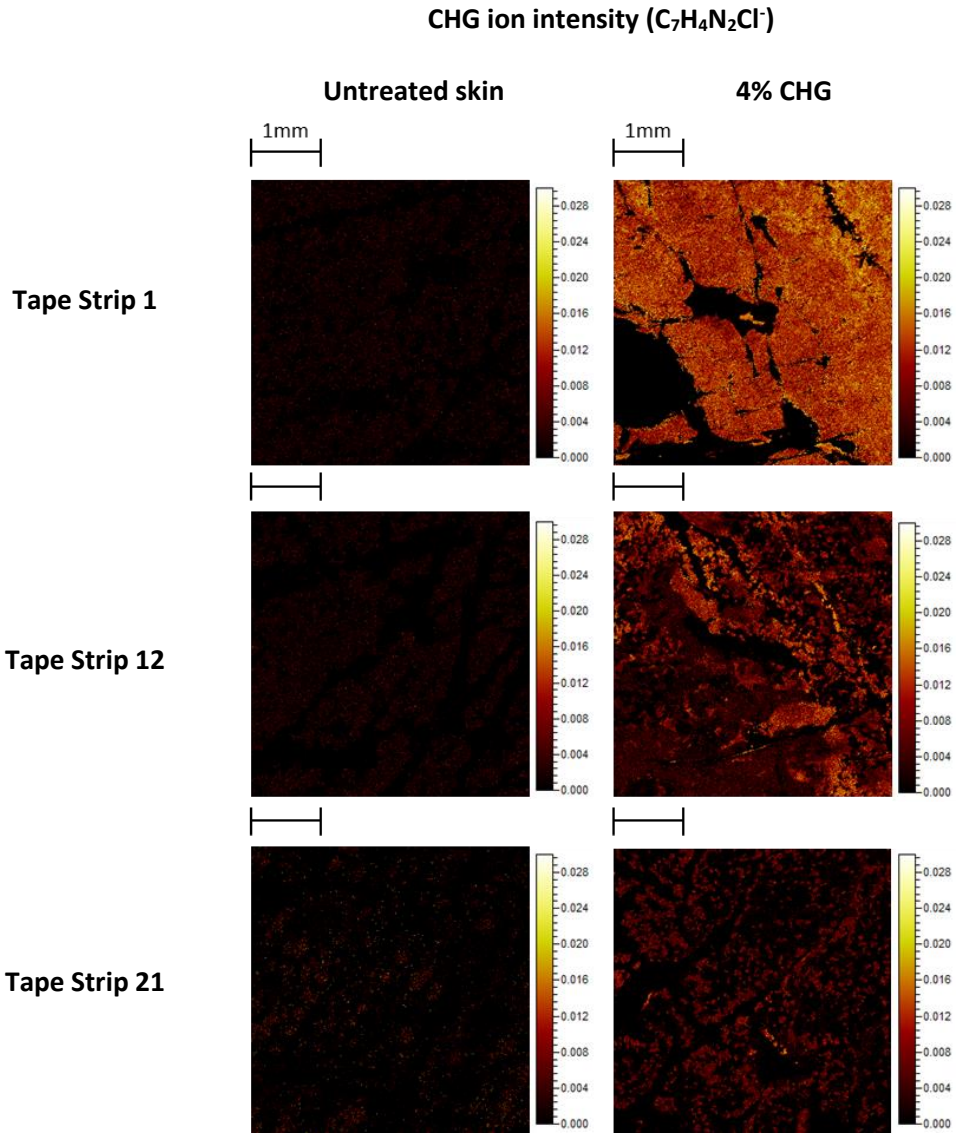

Figure 4.9. Tape strip images indicating specificity of $C_7H_4N_2Cl^-$ ion to CHG. Each image represents a 4 mm × 4 mm area.

Three ions were chosen to aid co-localisation of the drug within the biological tissue. $C_7H_4N_2Cl^-$ represented the drug, PO_3^- represented the lower epidermis and dermis and $C_{27}H_{45}SO_4^-$ represented the *stratum corneum*. Together these ions provided information on the depth permeation of the drug within porcine skin. Plotting these ions as a function of tape strip number provided some noteworthy trends. Within this results section, key images will be shown to support the important trends discovered.

Firstly, there was a general trend of increasing PO_3^- ion intensity (m/z 79) with increasing tape strip number, indicative of removal of cells from the viable epidermis. This trend was generally apparent around tape strip 9-12, however with some treatment groups, this increase in intensity occurred much earlier. For example, in the majority of cases, the PO_3^- did not significantly increase in intensity until approximately tape strip 12 (Figure 4.10, 4% w/v CHG treatment group). However, there was a great increase in PO_3^- ion intensity for the 2% w/v CHG and 3% w/v CHG treatment group after tape strip 2. This supports the previously noted limitations of tape stripping, where a single tape strip does not necessarily correlate to a single layer of skin cells of the same depth (Sheth, McKeough and Spruance, 1987; Lademann *et al.* 2009) as it is clear from Figure 4.10 that tape strip 2 represents the *stratum corneum* according to the intensity of the PO_3^- ion for the 4% w/v group, but for the 2% w/v and 3% w/v group, the same tape strip represents lower epidermal layers due to the intensity of the PO_3^- ion. This information can also be used in conjunction with the CHG ion ($C_7H_4N_2Cl^-$) to estimate where the drug is localised within the upper skin strata.

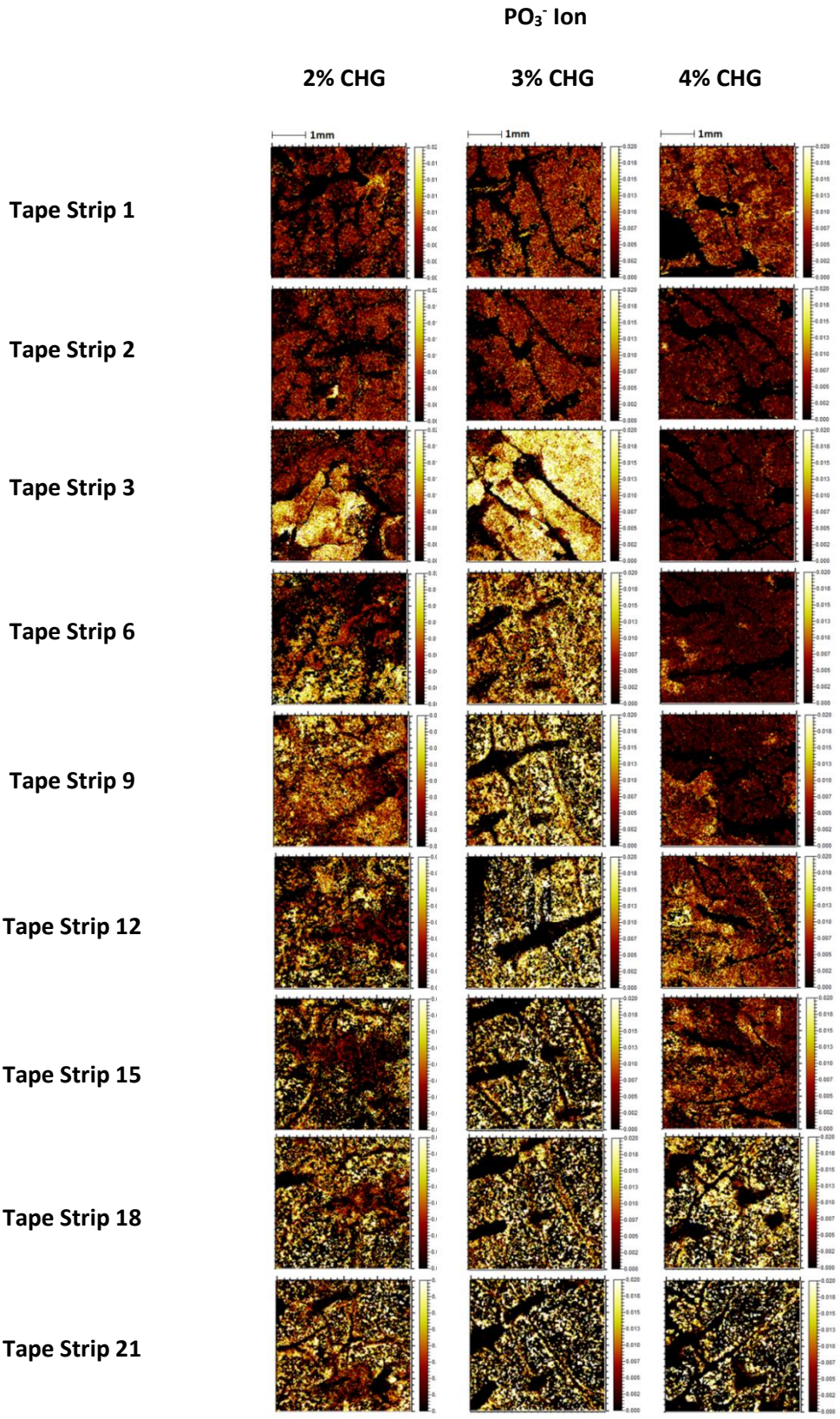

Figure 4.10. Tape strip images indicating ion intensity of PO_3^- on the same tape strips of different treatment groups. Each image represents a 4 mm × 4 mm area.

A second notable trend was that increasing the tape strip number decreases the mass of *stratum corneum* material removed from the skin. Thresholding the data for the CN^- ion as an indicator of biological tissue confirmed that the distribution profile was representative of the removed skin cells. This decrease in *stratum corneum* material with increasing tape strip number is evident in Figure 4.9 and Figure 4.10 and likely represents corneocyte removal from the *stratum dysjunctum* layer. Thirdly, the distribution of the CHG ion ($C_7H_4N_2Cl^-$) generally decreased in intensity with increasing tape strip number. The CHG ion images were isolated and tabulated (Figure 4.11) to visualise the differences in CHG depth permeation across all treatment groups.

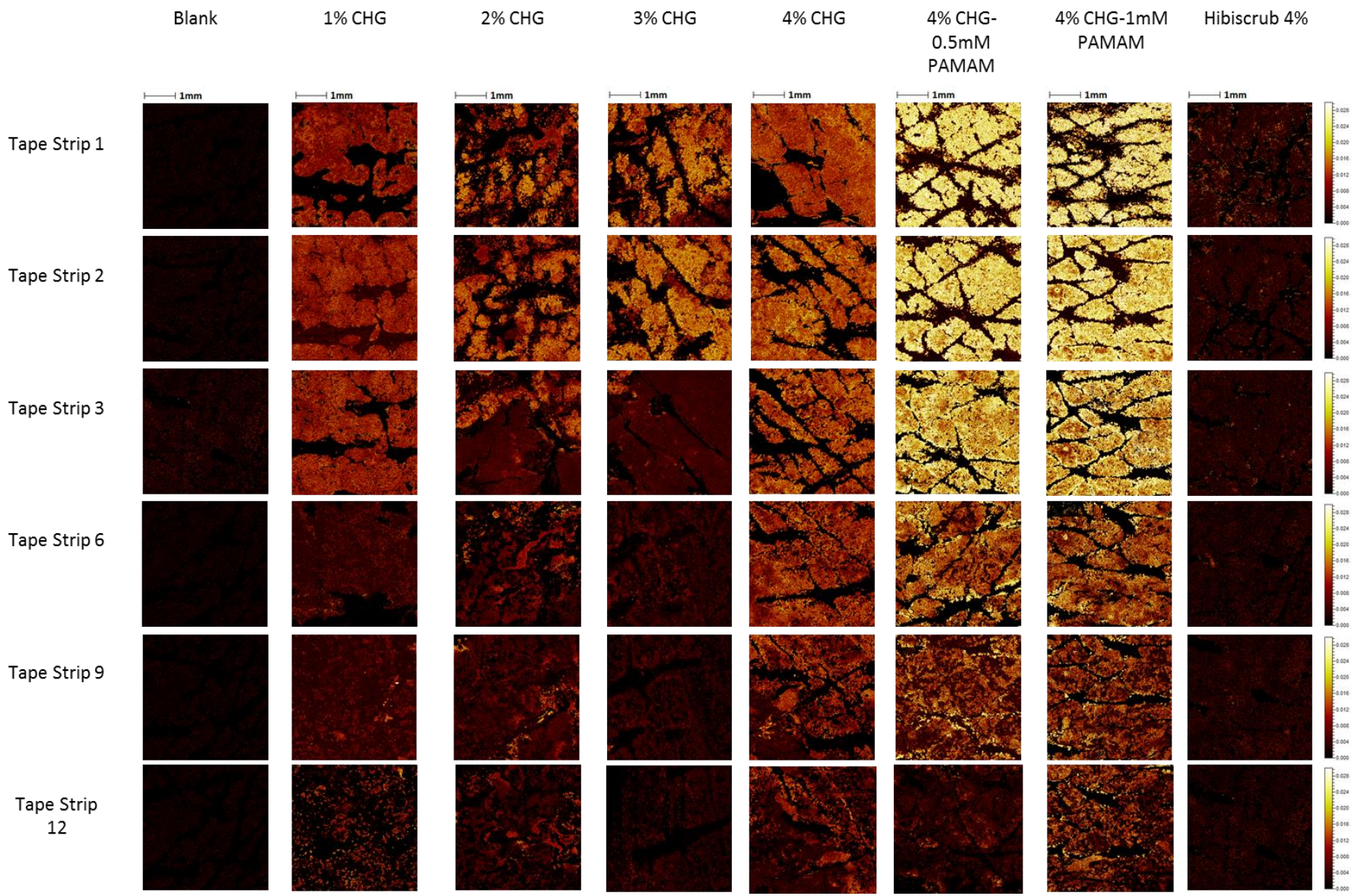
Blank
1% CHG
2% CHG
3% CHG
4% CHG
4% CHG-0.5mM PAMAM
4% CHG-1mM PAMAM
Hibiscrub 4%
Tape Strip 1
Tape Strip 2
Tape Strip 3
Tape Strip 6
Tape Strip 9
Tape Strip 12
1mm

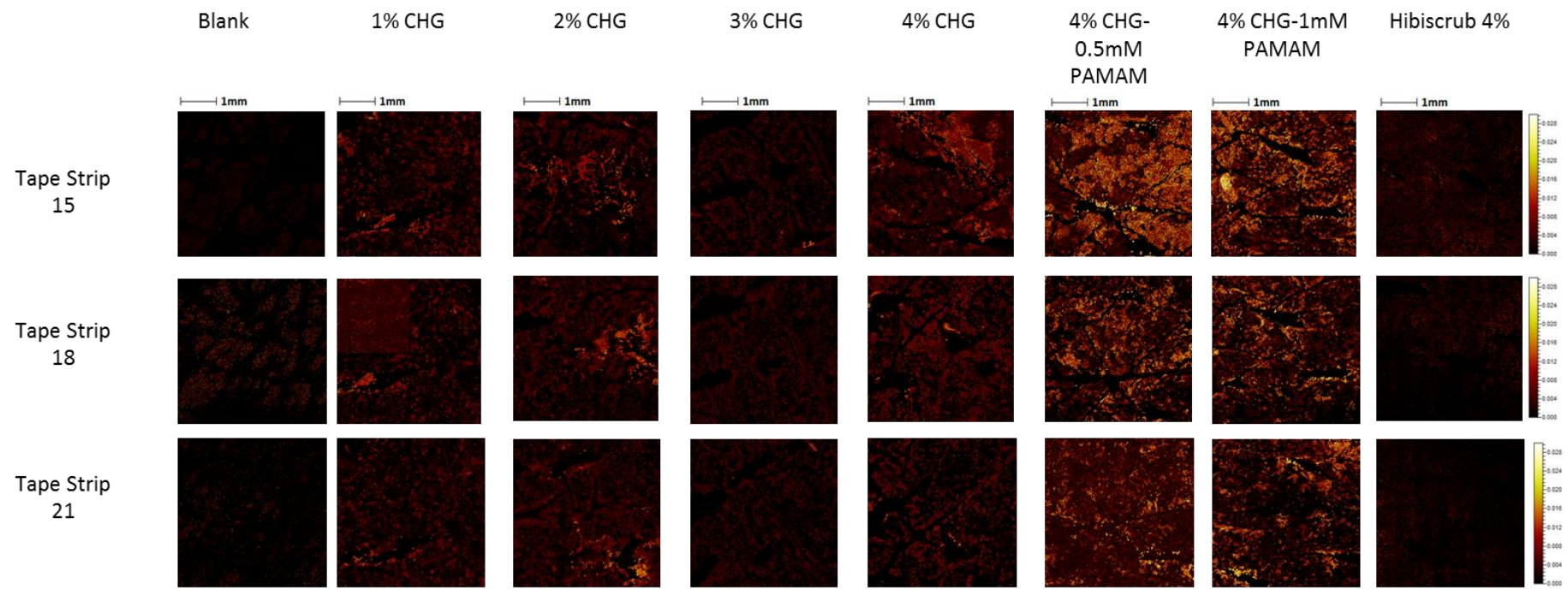

Figure 4.11. CHX ion $C_7H_4N_2Cl^-$ ion intensity across Hibiscrub® 4%, formulations 1-4% CHG, 4% CHG-0.5 mM PAMAM and 4% CHG-1 mM PAMAM. Each image represents a 4 mm × 4 mm area.

The distribution of the CHG ion ($C_7H_4N_2Cl^-$) generally increased with increasing CHG concentration applied to the skin. Further CHG ion intensity enhancement was visible when the PAMAM dendrimer was co-formulated with the drug. The enhancement effect was highly visible in upper tape strips. For example, from tape strip 1-6, the difference in ion intensities was obvious between 4% w/v CHG and 4% CHG-1 mM PAMAM, whereas on tape strips 12-15 onwards the ion intensities appeared fairly similar across the treatment groups.

CHG ion intensity did not appear to be consistent across individual tape strips. For example, on tape strips 3-21 from the 2% w/v CHG group, 9, 12 and 18 from the 4% w/v CHG group and tape strip 21 from the 4% CHG-1 mM PAMAM group there appeared to be spots of higher ion intensity in unspecified areas of the tape strip.

4.4.3 Ion intensity analysis of CHG treated porcine tape strips

The tape strip images were processed by dividing the images into four 2 mm × 2 mm squares (Figure 4.2) and by using the "batch statistics" tool to produce ion intensity values. This transformed the tape strip images into semi-quantitative data with means and standard error values. The resulting semi-quantitative data was then used to determine whether there was an increase in CHG ion intensity on the same tape strip in different treatment groups, a novel use of the tool. Distinguishing these differences visually (from the ToF-SIMS images) was subject to interpretation (for example the 4% CHG-0.5mM/1 mM PAMAM co-formulation CHG ion intensity appeared similar between tape strips). The exported ion intensity values defined the differences that were not inherently obvious and hence this tool was particularly useful for determining which formulation had the highest CHG ion intensity on deeper tape strips.

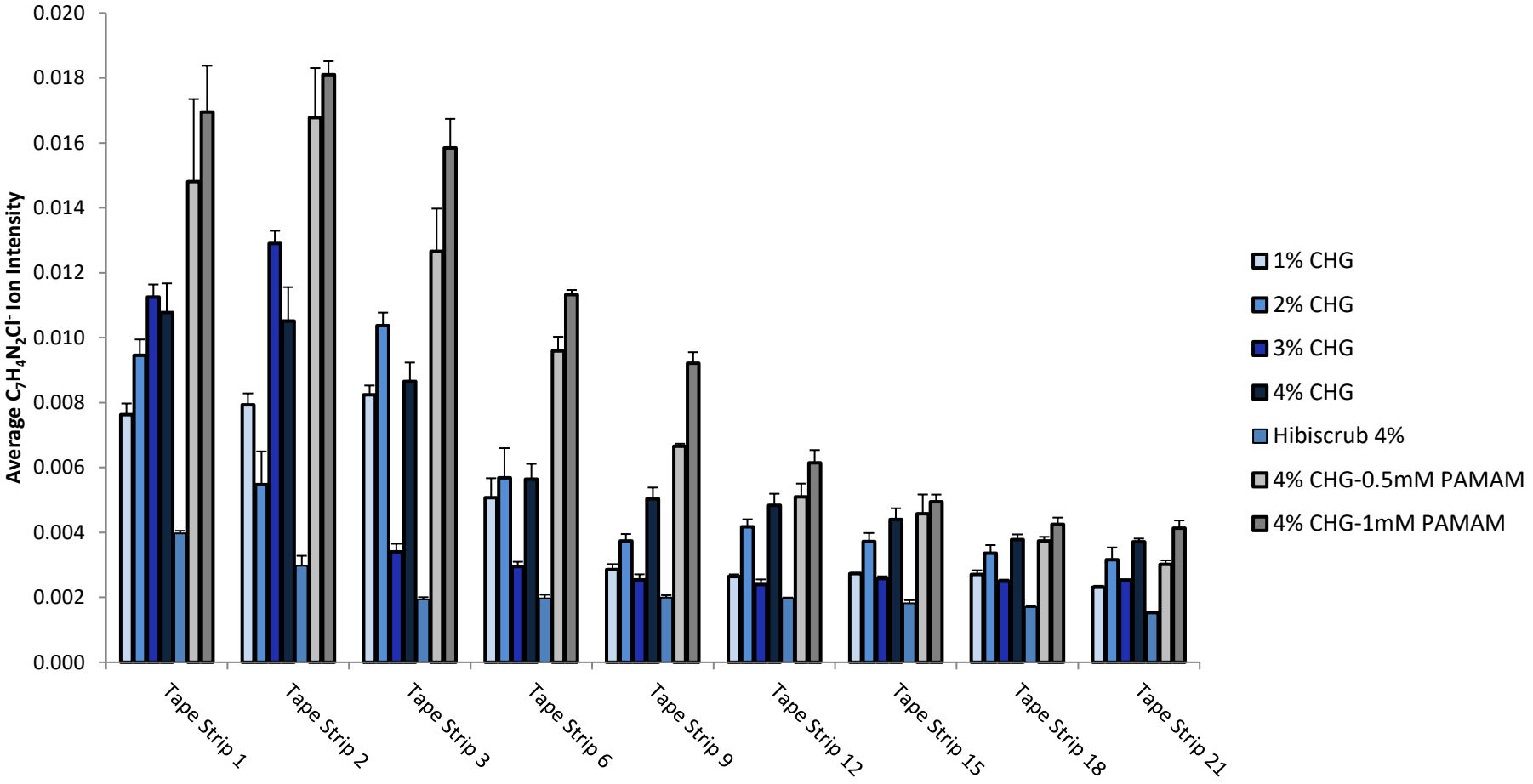

Figure 4.12. Quantified $C_7H_4N_2Cl^-$ ion intensity values for tape strips 1, 2, 3, 6, 9, 12, 15, 18, 21 from treatment groups 1-4% CHG, Hibiscrub™ 4%, 4% CHG-0.5 mM PAMAM and 4% CHG-1 mM PAMAM. Areas normalised by total ion intensity, *n=4 ± SE*.

The general trend of decreasing CHG ion intensity with increasing tape strip number is apparent from the transformed ion intensity data. Increasing CHG concentration generally increased CHG ion intensity; however a major stipulation to this generalisation is the lack of CHG permeation from the 3% w/v treatment group in tape strip 3 onwards compared to 2% w/v CHG. The reasoning for this is discussed in Section 4.5.

It is clear that the ion intensity of the CHG ion increased greatly, specifically in tape strips 1-9, when CHG was applied in combination with the PAMAM dendrimer compared to formulations without the dendrimer. This difference in ion intensity is limited to upper tape strips. Hibiscrub® 4% w/v consistently had the lowest ion intensity values across all tape strips, even compared to the 1% w/v CHG experimental formulation which contained a lower concentration of drug. The data is consistent with HPLC data collected in Chapter 3 and the ToF-SIMS tape strip images. The shape of the graph and the trends associated supports the HPLC data in Chapter 3 (Figure 3.10) Collating the tape strips (Chapter 3) or choosing selective tape strips (Figure 4.11) is sufficient for identifying and comparing trends with the data sets for the purpose of this study.

4.4.4 ToF-SIMS analysis of CHG treated porcine cryosections

Cross sections were viewed using light microscopy to ensure all skin layers were intact prior to ToF-SIMS analysis. An example histological sample and associated ToF-SIMS analysis is presented in Figure 4.13.

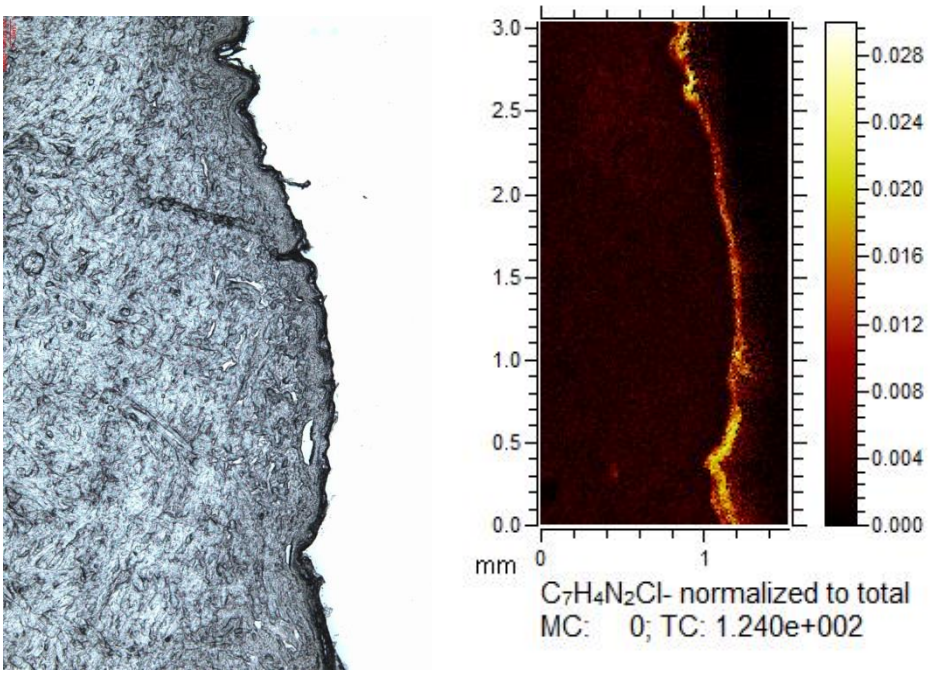

Figure 4.13. Histology analysis of a 20µm thick porcine skin cross section prior to ToF-SIMS analysis and associated ToF-SIMS analytical image of the unique CHG fragment ion.

Chemical distribution maps were created, again $C_7H_4N_2Cl^-$ represented the drug, PO_3^- represented the viable epidermis and $C_{27}H_{45}SO_4^-$ represented the *stratum corneum*. The cross sections of the drug included all skin layers as opposed to the tape stripping study which focused on the *stratum corneum* and to some extent the viable epidermis. This technique of skin visualisation avoids the issue of pooling tape strips or selection of specific tape strips required to determine the trends observed, as the cross section provides images of the entirety of the skin sample treated. Using the supporting ions readily allowed the distribution and co-localisation of CHG to be mapped within the skin.

Once chemical distribution maps were created, the three ions of interest were overlaid and coloured to allow the drug to be easily co-localised within the skin. Green colour resented the $C_7H_4N_2Cl^-$ ion, red colour represented the PO_3^- ion and blue colour represented the $C_{27}H_{45}SO_4^-$ (cholesterol) ion.

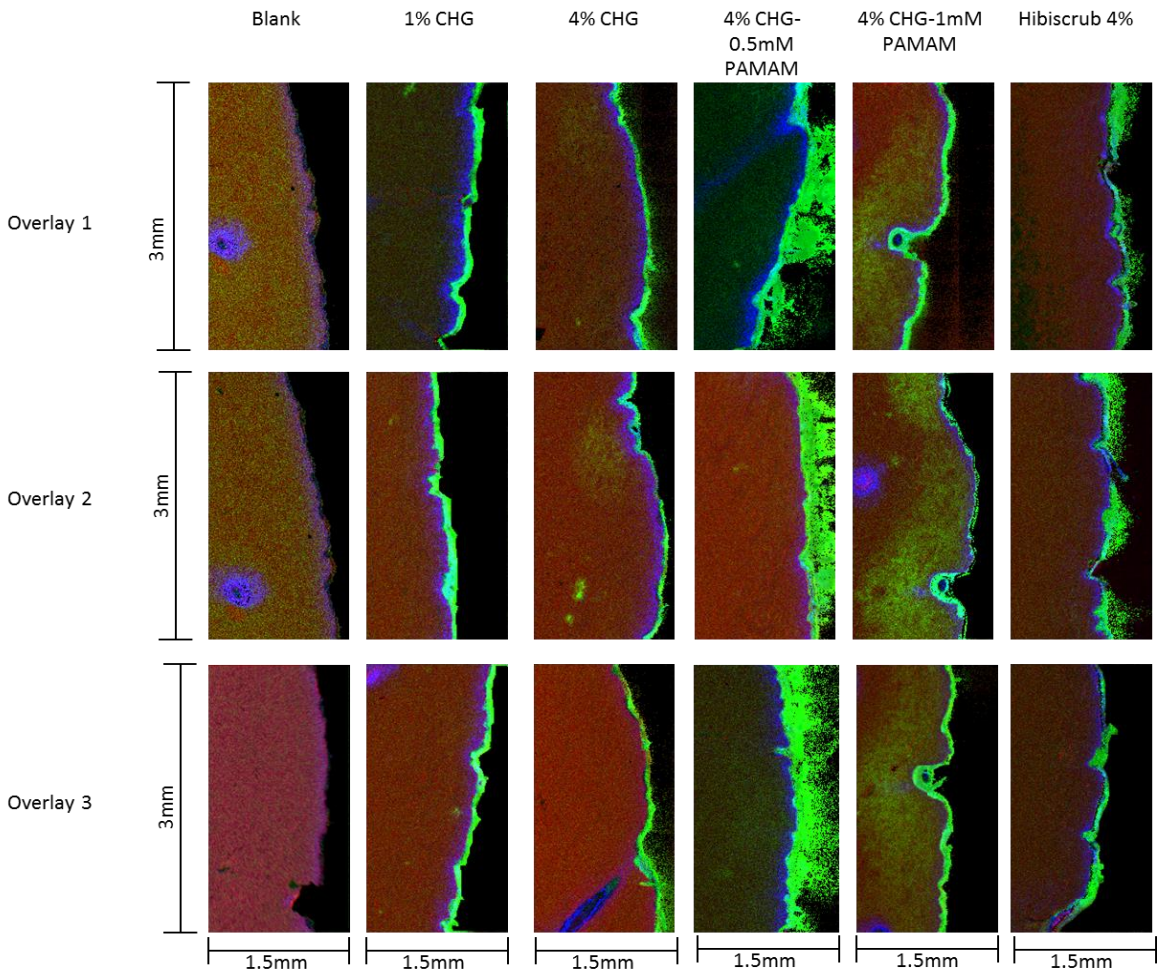

Figure 4.14. Comparative ion intensity overlaid chemical distribution maps illustrating the chemical distribution of $C_7H_4N_2Cl^-$ (drug, green) PO_3^- (phosphite, red) and $C_{27}H_{45}SO_4^-$ (cholesterol sulphate, blue), *n=3*.

The ToF-SIMS analysis of CHG treated cross sections provides information on ion distribution throughout the entirety of the porcine skin layer, building upon the *stratum corneum* information provided by the tape strip images (Figure 4.11).

Untreated skin showed no intensity for the CHG ion ($C_7H_4N_2Cl^-$, green colour). The PO_3^- ion successfully showed the viable epidermis and below (red colour), with a clear darker band above which indicated the presence of the *stratum corneum* where there was little PO_3^- ion intensity. The addition of the cholesterol ion ($C_{27}H_{45}SO_4^-$, blue colour) which has a high intensity in the *stratum corneum* (but also shows lower ion intensity in the lower epidermal layers) indicated the presence of the *stratum corneum.* Together, the combination of the PO_3^- ion and $C_{27}H_{45}SO_4^-$ ion indicated the *stratum corneum*-viable epidermal junction. This is clear when viewing the untreated skin samples without interference from the unique CHG ion fragment ($C_7H_4N_2Cl^-$). For that reason the depth penetration of the CHG ion could be assessed from the successful co-localisation of these components.

For all groups treated with the CHG containing formulation, CHG appears to be localised in the majority to the *stratum corneum* with similar intensities, however the intensity of the green colour indicating the CHG ion ($C_7H_4N_2Cl^-$) may be subject to interpretation between the groups without PAMAM dendrimer. The most obvious change is apparent when comparing the formulations with and without the PAMAM dendrimer. For formulations without the addition of the permeation enhancer, there appears to be very little CHG intensity within the lower epidermis as the PO_3^- ion (red colour) is still clearly visible from the overlay images (indicating the viable epidermis). However, particularly with the co-formulation that contained 1 mM PAMAM, there appears to be a clearer CHG ion intensity gradient that permeates into the epidermis and is even present deeper in the skin towards the dermis.

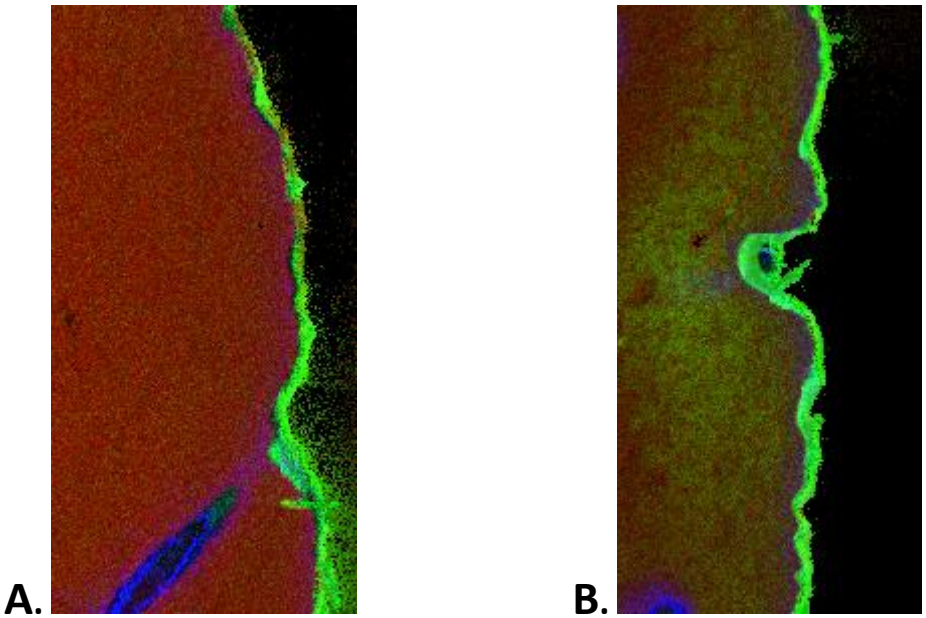

Figure 4.15. Magnified image of A. 4% CHG treatment group and B. 4% CHG-1 mM PAMAM treatment group. $C_7H_4N_2Cl^-$ ion indicative of CHG (green colour) has permeated past the *stratum corneum* in the 4% CHG-1 mM PAMAM treatment group.

The cross section images following a 24hr treatment with Hibiscrub® 4% w/v and 4% CHG-0.5 mM PAMAM dendrimer co-formulation (Figure 4.14) appear to show a large area of green colouration indicating the CHG ion. It should be noted that this is not representative of CHG permeation into the *stratum corneum*, but is unfortunately caused by smearing of the cross section when transferring the sample from the OCT machine onto a microscope slide for ToF-SIMS analysis. This highlights the need for the PO_3^- and $C_{27}H_{45}SO_4^-$ ion to co-localise the CHG ion that has specifically permeated into the *stratum corneum*.

Certain skin appendages are visible from the ToF-SIMS analysis of porcine skin cross sections. For example, a sweat gland appears to be visible in Figure 4.16 and the remnant of a hair follicle shaft appears to be visible in Figure 4.17. There appears to be no ion intensity indicative of CHG permeation in either figure. A skin furrow also appears visible on Figure 4.18. In contrast to the skin appendage images, the CHG ion intensity is bright within this skin furrow.

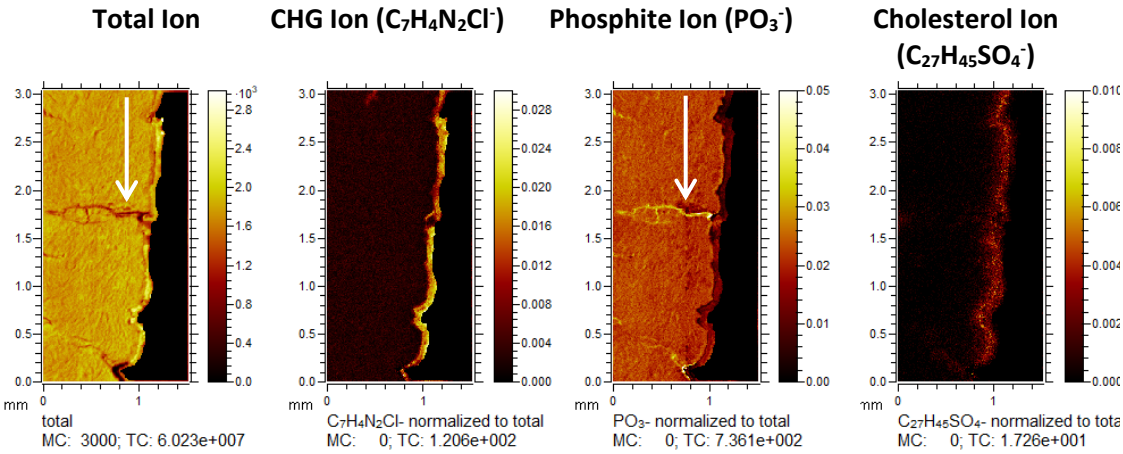

Figure 4.16. Suggestion of a sweat gland, apparent from the total ion count and phosphite ion chemical distribution map indicated by the white arrows. There appears to be no evidence of the CHG ion ($C_7H_4N_2Cl^-$) within the gland.

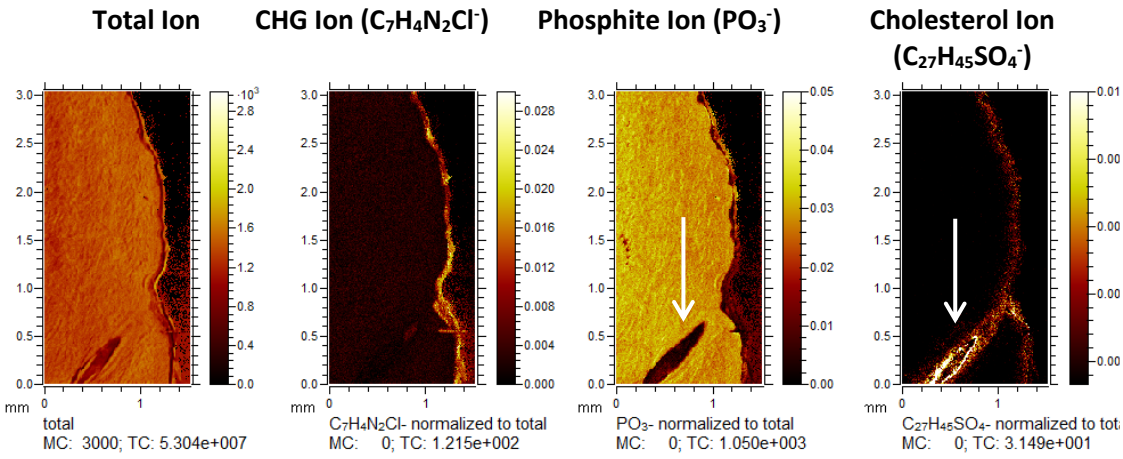

Figure 4.17. Suggestion of a hair follicle, apparent from the phosphite ion and cholesterol sulphate ion chemical distribution map, indicated by the white arrows. There appears to be no evidence of the CHG ion ($C_7H_4N_2Cl^-$) within the hair follicle shaft.

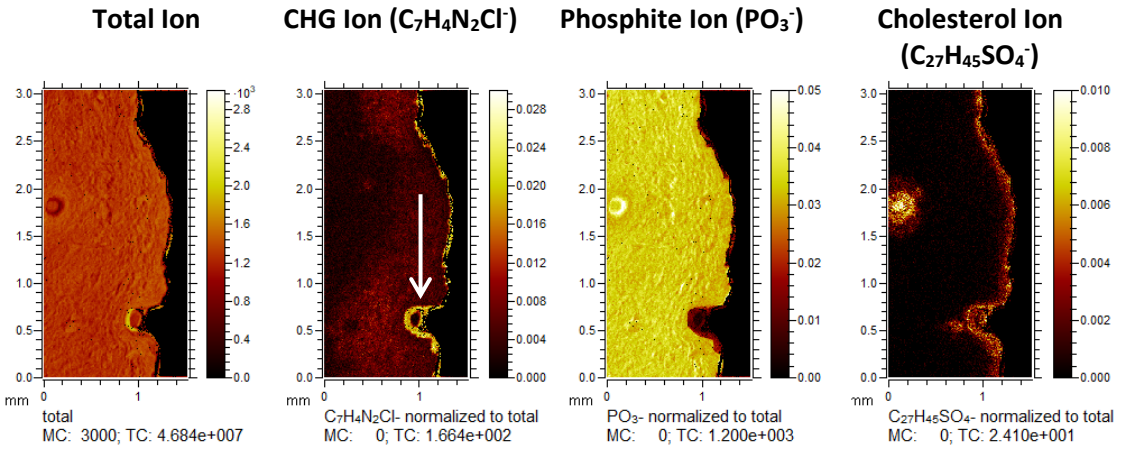

Figure 4.18. Suggestion of a skin furrow, apparent from the CHG ion ($C_7H_4N_2Cl^-$) chemical distribution map indicated by the white arrow. The CHG ion ($C_7H_4N_2Cl^-$) appears to accumulate within the furrow.

The cross sections could be transformed using the "line scan" function. This function allows a horizontal section of the cross section image to be selected (Figure 4.3), which is then plotted as a measure of ion intensity over distance (Figure 4.19). This provides semi-quantitative information on the intensity of the selected ion and the distance (mm) ingress into the skin where this ion intensity eventually drops off. This is particularly useful where there is subjectivity in the "brightness" of the CHG ion colour and as such its depth permeation into porcine skin from viewing the cross section images.

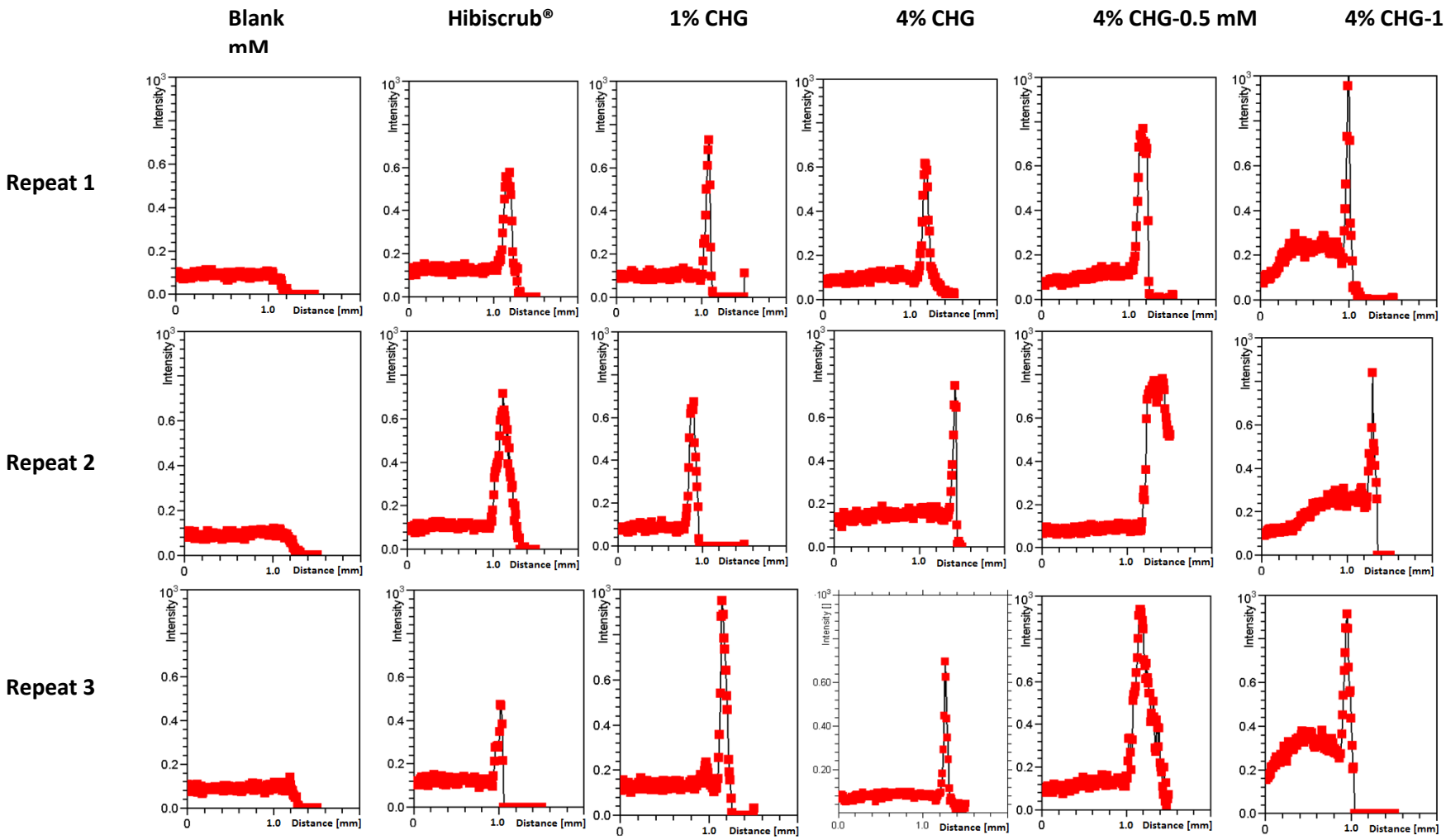

Figure 4.19. Line scan images illustrating the changes in ion intensity with depth permeation (mm) of CHG within porcine skin from various skin treatments, *n=3.*

The depth analysis images show that CHG ion intensity is largely localised to the *stratum corneum*. The ion intensity of the untreated porcine skin samples provides a useful baseline, from which the treatment groups can be compared to. For the Hibiscrub®, 1% w/v CHG, 4% w/v CHG and 4% CHG-0.5 mM PAMAM treatment groups, CHG ion intensity is localised to the *stratum corneum* and almost immediately drops to the baseline, indicating CHG retention within the *stratum corneum* without further drug permeation. The ion intensity spike indicative of the stratum corneum is generally greater for the CHG formulations that are co-formulated with the PAMAM dendrimer. The 4% CHG-1 mM PAMAM treatment group shares the spike in ion intensity indicative of CHG present in the stratum corneum. However, the ion intensity does not immediately drop to the baseline established by the untreated sample as distance within skin increases. This follows the colour gradient established by the cross section images for this treatment group (Figure 4.15B), indicating the permeation enhancement effect of the PAMAM dendrimer at the 1 mM concentration.

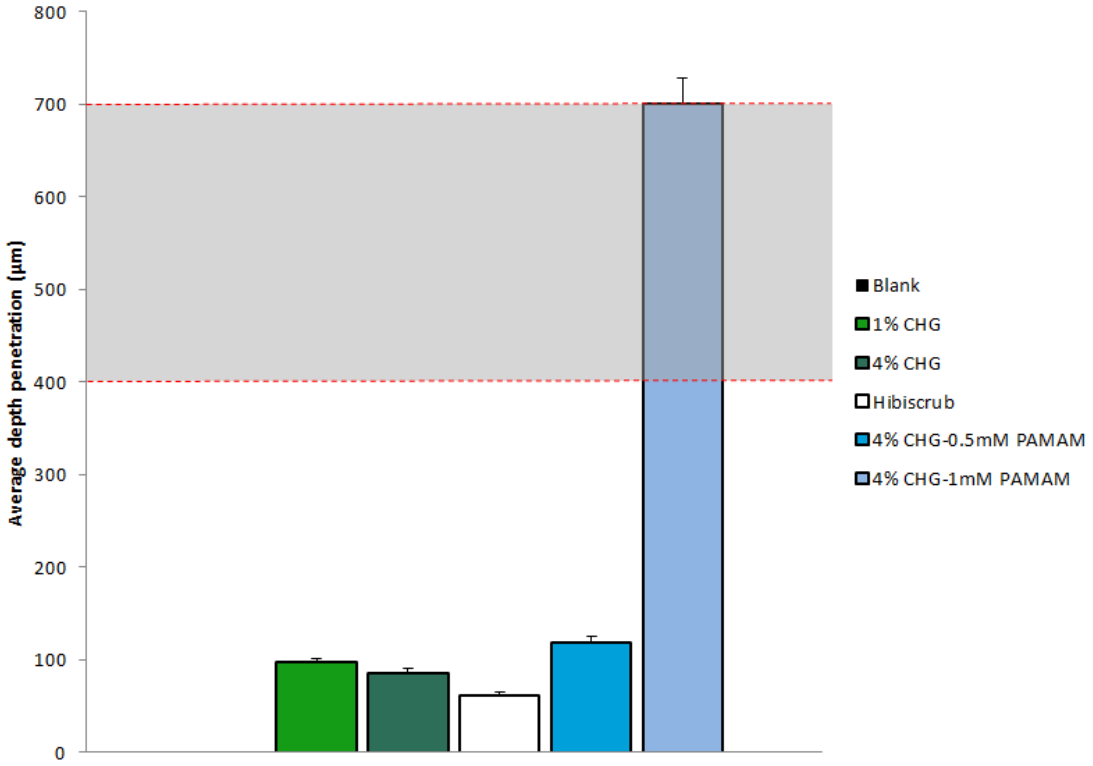

Figure 4.20. Depth permeation of CHG ($C_7H_4N_2Cl^-$ ion) according to the "Measurement Editor" software from various formulations. The translucent grey box indicates the 400-700 µm depth target of CHG permeation (Selwyn and Ellis 1972, Touitou *et al.* 1998, Grice and Segre 2011, Nakatsuji *et al.* 2013), *n=20 ± SE*.

The measurement tool was used to transform the cross section data into a quantitative measurement of the depth permeation of CHG from various formulations following a 24hr treatment. The untreated porcine skin section showed no depth permeation of CHG. The permeation of 1% w/v, 4% w/v CHG, Hibiscrub® 4% w/v, 4% CHG-0.5 mM PAMAM and 4% CHG-1 mM PAMAM into porcine skin was 96.53 ± 4.05µm; 85.44 ± 3.75 µm; 60.84 ± 3.12 µm; 117.77 ± 3.74 µm and 699.84 ± 18.58 µm respectively.

The 4% CHG-1 mM PAMAM was found to deliver CHG into the 400-700 µm zone cited by Touitou, Meidan and Horwitz (1998) indicative of appendages which have been thought to hold reservoirs of bacteria (Reybrouck 1986).

4.5 Discussion

The main purpose of this chapter was to characterise the depth permeation and co-localisation of CHG from various formulations (commercial and experimental, in the presence and absence of the PAMAM dendrimer) from tape strips and cryosections using ToF-SIMS. A further aim was to compare this data to the quantitative results in Chapter 3, to determine whether HPLC and ToF-SIMS provide complimentary datasets that could be used in the future to provide information on the drug deposition and co-localisation for topically applied compounds.

The main findings of this chapter indicate that ToF-SIMS can be utilised to visualise trends in drug depth permeation within porcine skin and drug co-localisation with endogenous skin components by analysing selective tape strips and cross sections respectively. Data can be transformed to produce semi-quantitative ion intensity values (using the "batch statistics" tool), and compared to the HPLC data given in Chapter 3 for complimentary qualitative and quantitative datasets. The drug-dendrimer co-formulation at a concentration of 1 mM delivered CHG past the *stratum corneum* barrier to a depth which is within the ideal range of 400-700 µm as detailed by Touitou, Meidan and Horwitz (1998) for enhanced antisepsis effects, indicated by the "measurement editor" feature (although it should be stated that this result may only act as support for other types of data due to the manual application of the tool and thus the subjectivity of depth permeation) . A unique ion fragment indicative of the G3 PAMAM-NH_2 dendrimer could not be confirmed, suggesting that permeation of the enhancer into porcine skin is likely to be minimal which supports previous studies (Venuganti *et al.* 2011, Sun *et al.* 2012).

The G3 PAMAM-NH_2 dendrimer was analysed using ToF-SIMS alone (after solvent evaporation) and following a 24hr skin treatment at various concentrations. Assuming a unique PAMAM fragment could be found which was distinguishable from untreated skin, the potential

mechanism of action of the PAMAM dendrimer could be established via visualisation of its permeation pathway. Sun *et al.* (2012) proposed that the PAMAM dendrimer may enhance drug delivery into the skin by accelerating drug release from the dendrimer into the vehicle, maximising the concentration gradient which is a driving force for drug permeation into skin (Williams 2003b). Venuganti and Perumal (2008) suggested that PAMAM-mediated permeation enhancement of 5FU was caused by a reduction of drug solubility into the vehicle, encouraging drug partitioning into the skin. Both postulated mechanisms suggest *stratum corneum* permeation of PAMAM dendrimers is low, due to their high molecular weight and the numerous ionisable terminal groups, neither of which are favourable for *stratum corneum* permeation (Naik *et al.* 2000). If a unique PAMAM dendrimer fragment could be detected within porcine skin tape strips, this postulated mechanism could be supported or disputed.

It is clear from Figure 4.5, Figure 4.6 and Figure 4.7 that there were no definitive fragments identified which corresponded with those found through ToF-SIMS analysis of PAMAM treated skin. Upon searching for the fragments identified from Figure 4.5 and Figure 4.6 in the ToF-SIMS IONTOF spectra programme, either peaks were found which were almost identical to those found in untreated skin or peaks were found which were indistinguishable from untreated skin when applied at the clinically relevant concentrations used to create the drug-dendrimer co-formulation. It was imperative to analyse porcine skin treated with clinically relevant concentrations of the PAMAM dendrimer to reflect the concentrations used in the co-formulation. For example, ethanol works through different mechanisms dependent on the concentration. At low concentrations, permeant solubility is enhanced, but at higher concentrations *stratum corneum* lipid extraction occurs (Williams and Barry 2012). Therefore, if a PAMAM dendrimer fragment was visible only at higher concentrations than those used in the co-formulation, it could not be guaranteed that any mechanism derived from the ToF-SIMS data was applicable to the co-formulation data analysis because it has previously found with other

permeation enhancers, such as ethanol, that the mechanism of permeation enhancement may be dependent on concentration applied.

As a result, permeation of the PAMAM dendrimer into porcine skin could not be identified and thus other methods were required to understand the mechanism of PAMAM dendrimer permeation (if the dendrimer permeation into skin occurs at all). Understanding the permeation pathway of the PAMAM dendrimer would be a useful contribution to the question of how the PAMAM dendrimer mediates enhancement of drugs across skin and was investigated further in Chapter 5. Considering the results of this study and the physicochemical properties of the PAMAM dendrimer (i.e. high molecular weight and ionisation), PAMAM dendrimer permeation into the skin is considered highly unlikely. The results within this study agree with those published by Sun *et al.* (2012) which also argue that PAMAM dendrimer permeation into the skin is unlikely. However, it should be stressed that the conclusion derived from this study is purely speculative as no ToF-SIMS fragment indicative of the PAMAM dendrimer was found.

The analysis of tape strips using ToF-SIMS was undertaken in order to overcome some of the limitations associated with the use of HPLC, primarily a high LoD which dictated the need to pool tape strips (Holmes *et al.* 2017); secondarily the inability to distinguish between drug adsorbed onto and absorbed into skin, and to compare the two techniques to determine whether their complimentary nature (i.e. quantitative data from HPLC, semi-quantitative depth permeation data from ToF-SIMS) resulted in the same conclusions surrounding the improvement of CHG depth permeation when the drug is co-formulated with the G3-PAMAM-NH_2 dendrimer. Additionally, ToF-SIMS analysis of tape strips provided images that detailed the distribution of CHG on each skin cell layer.

Samples analysed using ToF-SIMS were calibrated, normalised to total ion intensity to allow comparison between samples and were thresholded for biological tissue so ions indicative of

adhesive tape were removed from the tissue. Processing the data in this way increased the accuracy of the conclusions formed from the drug deposition images. This further improves the accuracy of the ion intensity values produced from the drug deposition images using the batch statistics tool, by including drug ion data which is present only in biological tissue, a feature which is lacking from HPLC analysis which may skew data from the initial tape strips where drug is adsorbed onto skin so is viable for removal by tape stripping, but the drug has not absorbed into the skin (Sheth 1987, Lademann *et al.* 2009).

The tape strip images created by the IONTOF software generally concur with the results from the tape strip study in Chapter 3. The most positive result from tape strip analyses in both chapters was that the 4% CHG-1mM PAMAM co-formulation significantly enhanced CHG depth permeation compared to the commercial benchmark, Hibiscrub® ($p < 0.05$). This was the case for all tape strips analysed, and the total amount of CHG delivered for both methods of analysis. The use of two different analytical methods provides confidence in the conclusion that 1mM PAMAM is able to significantly enhance CHG deposition within skin, which has wider implications for prevention of SSTIs in the healthcare sector.

There was a general trend of decreasing CHG ion intensity with increasing tape strip number but increasing CHG ion intensity on each comparable tape strip when the concentration of CHG applied to the skin surface was increased. For both data sets (Chapter 3 and 4 tape strips), higher concentrations of CHG applied to the skin resulted in a significantly higher concentration of CHG delivered into the skin. There are some inconsistencies with this trend – although in the majority 4% CHG delivered significantly more CHG than 1% CHG according to the statistical analysis from both Chapter 3 and 4, tape strips 2, 3, 6, 9 and 12 from the 2% w/v CHG group had a significantly higher CHG ion intensity than the 3% w/v CHG group when analysed by ToF-SIMS, indicating that significantly more CHG was delivered to these tape strips. This can be explained by viewing the PO_3^- ion for each group – the intensity of this ion vastly increases at tape strip 3 for the 3% w/v

CHG group, but does not increase as sharply until deeper strips for the 2% w/v CHG group. A high PO_3^- indicates that the skin layers that are being removed represent the deeper layers of the epidermis as phospholipids are largely absent in the *stratum corneum* (Wertz and van den Bergh 1998, Williams 2003a). This may be due to factors such as force of tape strip removal (Loffler, Dreher and Maibach, 2004), adhesive strength (Jui-Chen *et al.* 1991) or inherent variability between skin samples. The results from Chapter 3 did not indicate that there was any statistically significant difference between the concentrations of CHG on tape strips 6-21 when comparing CHG 2% w/v and 3% w/v, so it is possible that the difference observed in this chapter was due to inherent variance between skin samples (Southwell *et al.* 1984, Williams 2003c). Therefore, the tape strips from the 3% w/v CHG group reached the lower epidermal layers faster than the tape strips from the 2% w/v group and so it is expected that the 3% w/v CHG group would show decreased ion intensity more readily because permeation of CHG past the *stratum corneum* layer into the viable epidermis is poor. This highlights the advantages of detecting the PO_3^- and $C_{27}H_{45}SO_4^-$ ion alongside the $C_7H_4N_2Cl^-$ (drug) ion so the drug can be co-localised within the *stratum corneum*. Furthermore, this emphasises the disadvantages of tape stripping already discussed in Section 1.7, primarily the fact that a single layer of cells removed by a tape strip does not necessarily equal a layer of cells from the same depth within the *stratum corneum* (Lademann *et al.* 2009).

As with the tape strip study in Chapter 3, increasing tape strip number decreased the amount of *stratum corneum* material removed from the skin. This is to be expected, as increasing the depth in skin tissues increases the number of intact corneodesmosomes which rivet the corneocyte cells together, thereby making cells more difficult to remove using the tape adhesive as well as an increased incidence of orthorhombically packed lipid bilayers which also contribute towards the tightly packed structure (Elias *et al.* 1983, Garson *et al.* 1991).

The ToF-SIMS tape strip images provided additional data compared to that provided by HPLC analysis in Chapter 3. For example, the tape strip images illustrated the ability of CHG to strongly bind to the upper layers of the *stratum corneum* and the lack of ability to permeate into the deeper layers of skin after 24 hr. Even when the concentration of CHG was increased and a PAMAM dendrimer co-formulated with the drug, permeation enhancement appeared limited to the upper tape strips where the differences in ion intensity were obvious by eye (Figure 4.11 and Figure 4.12). The ion intensities appeared similar across all groups on the latter tape strips, indicating similar CHG concentration on these deeper tape strips. Limiting the permeation enhancement within upper skin layers is advantageous by reducing the risk of systemic absorption and possible toxicity whilst still providing enhanced antisepsis effects. For hydrophilic drugs such as CHG, the rate-limiting step for permeation into the skin is permeation across the highly hydrophobic *stratum corneum* (Naik *et al.* 1999). Therefore it was a concern that once this barrier was bypassed, the drug would be able to permeate easily through the hydrophilic dermis and be viable for uptake into the systemic circulation. A balance was required whereby the drug permeated past the *stratum corneum* barrier, but was still retained within skin tissue without permeation through full thickness skin. The *in vitro* experiments completed in Chapter 3 and the cross section images within this chapter appear to show that this balance was fulfilled; permeation of CHG through full thickness porcine skin after 24 hr was <LoD (appendix 1) of the HPLC when a CHG-PAMAM co-formulation was applied to the skin surface and Figure 4.14 and Figure 4.15B shows little to no ion intensity for CHG at the edge of the full thickness cross section, indicated by the lack of green colouration.

The images also provided information on the homogeneity of permeation across the tape strip. Cross section images appear to show a homogeneous layer of CHG within the *stratum corneum,* however, tape strip analysis by ToF-SIMS allows visualisation of the corneocytes on a magnified scale. In deeper tape strips, the ion intensity is not spread equally across the tape strip, indicating

that the permeation of the drug is not consistent between layers of skin. From the tape strip images, it was impossible to tell whether spots of higher ion intensity was indicative of CHG accumulation within specific skin sites e.g. hair follicles and sebaceous glands. Inconsistent CHG delivery across deeper skin layers may be a cause for concern as this suggests that antisepsis may be incomplete on deeper skin layers. The poor permeation of CHG within skin has been confirmed by other studies (Lafforgue *et al.* 1997; Karpanen *et al.* 2008a).

The tape strip images clearly show improvement in CHG depth permeation in the presence of the PAMAM dendrimer. Unlike the HPLC data, the 4% CHG-0.5 mM PAMAM and 4% CHG-1 mM PAMAM co-formulations appear to enhance the depth permeation of CHG almost equally when viewing the ion intensity values graph (Figure 4.12), although the images are subject to interpretation. In Chapter 3, 4% CHG-0.5mM PAMAM was not able to deliver significantly more CHG into skin compared to the 4% CHG formulation on any tape strips, but in Chapter 4, 4% CHG-0.5mM PAMAM delivered significantly more CHG into skin on tape strips 3, 6 and 9. Previous studies have found that the enhancement effect was not concentration dependent (Venuganti and Perumal 2009, Holmes *et al.* 2017), potentially due to aggregation of dendrimers at high concentrations (Klajnert and Epand 2005) but this could not be confirmed in this study without application of the co-formulation with numerous difference concentrations of PAMAM dendrimer.

The images presented in Figure 4.11 do not contain the complete set of 1-21 tape strips. This was a conscious decision following results published by Holmes *et al.* (2017). The results were published to visualise the depth permeation of a 2% w/v CHG solution. The ToF-SIMS images clearly show a gradual decrease in CHG ion intensity with increasing tape strip number as expected, and this is still visible when selecting tape strips 1, 2, 3, 6, 12, 15, 18 and 21. Furthermore, this study existed to visualise trends in CHG treatment groups and to visualise generalised differences between groups, rather than differences on specific tape strips.

Therefore, visualisation of a chosen selection of tape strips, rather than the entire data set, was sufficient for data comparison. Where depth permeation of CHG was to be specifically measured, the cross section images were used which provides information of CHG permeation across the skin as a whole, rather than just the *stratum corneum*.

The "batch statistics" tool allowed the ToF-SIMS images to be transformed into semi-quantitative ion intensity values whereby each image was given an intensity value according to the intensity of each ion detected on the analysis area. This novel technology was used to compare the HPLC and ToF-SIMS CHG permeation data and to determine whether HPLC and ToF-SIMS provide complimentary results.

The trends observed in Figure 4.12 appear similar to those in Figure 3.10. The general trends of increasing ion intensity with increasing CHG concentration and decreasing CHG concentration with increasing tape strip number is consistent with the trends seen in Figure 4.12, however this is much less consistent than Figure 3.10, potentially due to the fact the ion intensities were unable to be adjusted according to mg of *stratum corneum* material removed as they were in Chapter 3.

HPLC data and ToF-SIMS ion intensity value data were found to agree in the majority of cases – for the HPLC data sets the primary statistically significant pairing was 4% w/v CHG and 1% w/v CHG, followed by 4% CHG-1 mM PAMAM-Hibiscrub® (Table 3.4). Ion intensity value data also showed the same trends (Figure 4.12). The HPLC data also found that 4% w/v CHG delivered significantly more CHG into certain tape strips compared to lower CHG concentrations (Table 3.2). The ion intensity data also observed this, although significance was often paired with 4% w/v CHG and 3% w/v CHG rather than the 1% w/v CHG gel formulation.

The ToF-SIMS ion intensity data also showed on numerous occasions that the 4% CHG-0.5 mM PAMAM delivered significantly more CHG than the 4% w/v CHG formulation (tape strips 3, 6

and 9, and Hibiscrub® 4% w/v, 24hr (tape strips 2, 3, 6, 9, 12, 15). For the HPLC data in Table 3.4, 4% CHG-0.5 mM PAMAM showed statistical significance compared to Hibiscrub® 4% w/v, 24hr (tape strips 4-6 and 7-10; $p < 0.05$), but no statistical significance was observed between 4% CHG-0.5 mM PAMAM and 4% w/v CHG. This difference was also noticeable from the tape strip and cross section images compared to the HPLC data presented in Chapter 3 – in Chapter 4, the 4% CHG-0.5 mM PAMAM co-formulation appeared to provide a similar enhancement effect compared to the 4% CHG-1 mM PAMAM co-formulation, however in Chapter 3, the 4% CHG-0.5 mM PAMAM co-formulation appeared to provide a lesser enhancement effect which was more similar to 4% w/v CHG without addition of the permeation enhancer. Variability in skin samples (Southwell *et al.* 1984) may have contributed to the discrepancies between the 4%-0.5 mM PAMAM formulation and the CHG deposition results from both chapters and it is suggested that the experiment is repeated in the future with a larger sample size with various different PAMAM dendrimer concentrations to determine whether a concentration dependent effect does exist.

ToF-SIMS analysis of tape strips has removed the requirement to pool tape strips to reach the limit of detection, a requirement of the HPLC method when the permeation of drugs into and through skin is poor (Gamer *et al.* 2006, Holmes *et al.* 2017). Furthermore, the images provided detailed information on the homogeneity of drug permeation within the *stratum corneum* and, when the PO_3^- ion intensity increases, deeper layers of the epidermis (Wertz and van den Bergh, 1998). The addition of the batch statistics tool is able to transform the images into semi-quantitative ion intensity values. The use of a second technique that confirms the quantitative results gained from the HPLC data confirms that HPLC analysis of tape strips should still be considered the gold standard technique for quantification of the depth permeation of exogenous chemicals applied to the skin.

Despite this conclusion, the tape stripping technique has some limitations which cannot be overcome by using a different analytical technique (ToF-SIMS), such as removal of unequal layers of *stratum corneum* (illustrated by 2% w/v and 3% w/v CHG vs 4% w/v CHG tape strips in Figure 4.10), adhesive strength (Jui-Chen *et al.* 1991), duration of application pressure (Reed *et al.* 1995) and velocity of tape strip removal (Loffler *et al.* 2004). Porcine skin cross sections treated with experimental formulations and Hibiscrub® were analysed alongside the tape strips to remove the disadvantages of the tape stripping technique. Cross sections provide spatial information of the entirety of the skin rather than being limited to the *stratum corneum* alone, providing a better representation of drug depth permeation within the entirety of skin. The identification of ions indicative of the *stratum corneum*-viable epidermal junction (PO_3^- and $C_{27}H_{45}SO_4^-$) from cross sectional data also allowed the drug to be co-localised within the epidermis, providing a more accurate picture of the depth permeation of the drug in relation to different skin layers.

The cross section images further support the results obtained from the tape stripping study – CHG without the addition of a permeation enhancer strongly binds to the upper skin layers (Aki and Kawasaki 2004) with poor permeation into deeper tissues. A clear gradient is visible from the 4% CHG-1 mM PAMAM co-formulation treated skin where the CHG is able to permeate past the *stratum corneum* into deeper skin tissues, albeit, at a much lower concentration (Figure 4.14). Interestingly, the cross section images of the 4% CHG-0.5 mM PAMAM co-formulation appear to support the results obtained from the HPLC analysis of tape strips rather than the ToF-SIMS analysis of tape strips and associated ion intensity values. Upon visual inspection, the cross section images of the 4% CHG-0.5 mM PAMAM co-formulation do not appear to enhance the deposition of CHG any more so than the 4% w/v CHG experimental formulation which did not contain the PAMAM dendrimer (although this result is limited to differences visible bye eye and subjectivity of image interpretation). The 4% CHG-1 mM PAMAM co-formulation does appear

to enhance the depth permeation of CHG into deeper skin layers, where the intensity of the CHG ion (green) remains bright in colour past the *stratum corneum* layer and the gradient does not appear to diminish until much deeper in the skin tissue compared to other samples (Figure 4.15B).

In addition to providing a clearer image of depth permeation across the entirety of skin than tape strip images, cross section images of the skin can also provide data on the permeation route of a drug. The CHG ion increased in intensity where skin furrows are clear (Figure 4.18). However, there did not appear to be any CHG visible within porcine skin appendages (Figure 4.16 and Figure 4.17). The conclusions taken from this may only be speculated because of the small sample size, but the results are interesting nonetheless. The physicochemical properties of the drug dictate that the drug is more likely to permeate into skin via the transcellular and or transappendageal routes (i.e. low log P of 0.0133 [Farkas *et al.* 2007], molecular weight >500 Da and ionisation). As discussed in Section 1.3, the role of follicles in transdermal drug delivery is contentious. It is argued that polar molecules, such as CHG, may be able to diffuse dermally via the appendages (Meidan *et al.* 2005, Wosicka and Cal 2010). However, this does not take into account the fact that follicles are lined with cornified cells, and follicles are often filled with sebum (Figure 1.4, [Chilcott 2008]). Therefore, a lack of CHG permeation into the hair follicle may be attributed to the extension of the *stratum corneum* into the follicle, and potentially the presence of sebum in the follicle, providing a lipophlic environment in which CHG would struggle to permeate into. The presence of “open” and “closed” follicles was confirmed by Otberg *et al.* (2004a), where plugs of shed corneocytes pushed out of the follicle orifices by growing hairs or emerging sebum prevented could prevent the ingress of exogenous chemicals (Lademann *et al.* 2001).

It is possible for the drug to permeate across the thin aqueous pathway between the polar head groups of the lipid lamellae, so it is possible this route was also utilised by the drug for

partitioning into skin. This route avoids the requirement of repeated partitioning between lipid and aqueous phases required by the transcellular route, so is usually preferred where possible even though the route is more tortuous.

The depth analysis data tools ("line scan" and "measurement editor") supported the cross section images by demonstrating that the 4% CHG-1 mM PAMAM was able to deliver a concentration of CHG past the *stratum corneum* barrier that was above the baseline indicated by the untreated sample. The line scan graphs supported the subjective assumptions made by visualising the cross section data by plotting the intensity of the CHG ion ($C_7H_4N_2Cl^-$) as a function of depth within porcine skin. The most important point to take away from the line scan data is the intensity of the ion from the 4% CHG-1 mM PAMAM dendrimer group immediately proceeding the *stratum corneum*. Rather than immediately returning to the baseline ion intensity established by the blank sample as was observed with the other treatment groups, the intensity of the CHG ion was depleted but not immediately to the baseline level, therefore establishing the use of the G3 PAMAM-NH_2 dendrimer at 1 mM concentration as a permeation enhancer of CHG.

The measurement editor tool allowed a quantitative value to be assigned to the depth permeation of the CHG ion that was identified by the cross section images. The main drawback to this technique is the fact that the depth permeation line is placed manually, so the accurate depth permeation of a drug may be subject to interpretation, especially when the permeation is a gradient – when should the measurement line be stopped? The decision was made to stop the measurement when the line reached an area of skin that visually showed as much CHG ion intensity as the blank cross section. Visual inspection is not reliable and so the results from this technique were only used as supportive data. The results show that the depth permeation of CHG from the 4% CHG-1 mM PAMAM co-formulation was within the cited desirable range of 400-700 µm (indicated by the translucent grey box, Figure 4.20), confirming that this co-

formulation may be able to target opportunistic bacteria which reside deeper within skin, thus acting as a more efficacious antimicrobial formulation that the commercial benchmark and formulations which did not include the PAMAM dendrimer.

Potentially the most important outcome from Chapter 3 and 4 is that each analytical technique suffers from limitations. The limitations of tape stripping and HPLC have been discussed at length in the general introduction and the introduction to this chapter. ToF-SIMS is dependent on the identification of a fragment unique to that compound, which is not always possible. Further limitations of ToF-SIMS include the price of instrumentation and lack of widespread availability. Matrix effects prevent the technique from being considered fully qualitative (Benninghoven 1994). Thus, alone, the techniques provide information on the depth permeation of the drug, but with caveats attached. When HPLC and ToF-SIMS data are combined, the two complimentary techniques produce unparalleled quantitative and qualitative information on the concentration, depth permeation and spatial distribution of a chosen drug. The two techniques unanimously found that the addition of 1 mM PAMAM to the 4% w/v CHG containing gel formulation enhanced the deposition of the drug within porcine skin, thereby increasing the concentration of drug available in deeper skin tissues that reduces the potential for SSTIs in the healthcare setting.

4.6 Conclusion

In conclusion, this study effectively demonstrated that ToF-SIMS has a useful role in accurately imaging the depth permeation and co-localisation of a drug within skin tissue, providing a unique secondary ion fragment indicative of the drug can be found. As an analytical tool, ToF-SIMS was able to visualise CHG drug deposition on individual tape strips due to its low LoD when compared to HPLC analysis conducted in Chapter 3, increasing the accuracy when determining the drugs depth permeation. Furthermore, the tape strip images provided detailed drug distribution information on the 4mm × 4mm area analysed, imperative for understanding whether antisepsis effects could be considered homogenous across the upper skin layers. Analysis of porcine skin cross sections treated with CHG in the presence and absence of the PAMAM dendrimer removed the disadvantages associated with tape strip analysis, summarised in the introduction of this chapter and thus improving the accuracy of results. Furthermore, the ability to co-localise the drug against other ions indicative of specific skin layers provided unique insights into the distribution of CHG within porcine skin. This may allow development of a theoretical permeation pathway specific to the analysed compound, and potentially its mechanism of action where there is currently a lack of understanding.

Within this study, the capabilities of ToF-SIMS were demonstrated firstly by illustrating the drug distribution within each skin layer, co-localised to the *stratum corneum* and epidermis, secondly by illustrating that 4% w/v CHG in the presence of 1mM PAMAM was able to significantly enhance CHG skin deposition compared to the commercial benchmark, and finally by confirming the majority the conclusions of the study completed in Chapter 3 with the aid of statistical analysis from transformed datasets. The development of the ToF-SIMS qualitative images into semi-quantitative data is novel and encourages the use of this technology to further describe topical drug distribution in the future. The technology is somewhat limited by the need to

identify a unique fragment which can be distinguished from skin structures (illustrated by the inability to locate a unique PAMAM fragment), however the technology may be exploited to detect metal elements from topically applied drugs and cosmetics, which should be theoretically simple because one is searching for an element rather than a unique fragment

Further investigations are required to understand the relationship between PAMAM concentration and permeation enhancement effect, as the results from Chapter 3 and 4 are conflicting with respect to 4% CHG-0.5mM PAMAM. Repeating *in vitro* permeation studies with a wider range of PAMAM concentrations co-formulated with CHG may provide a greater insight into the effect of PAMAM concentration on the proportion of CHG enhancement. Additionally, an inability to identify a unique PAMAM dendrimer fragment illustrated that ToF-SIMS could not be used to determine the mechanism of action of the PAMAM dendrimer. This was investigated further with alternative methods in Chapter 5.

5 Chapter 5 – Investigating the mechanism of G3 PAMAM-NH_2 dendrimer skin permeation enhancement

5.1 Introduction

Chemical permeation enhancers may exhibit their permeation enhancement effect through single or multiple mechanisms, and synergistic or covariate responses may be observed. Where multiple mechanisms occur, one mechanism may predominate over another, or one might require another mechanism to occur first before enhancement can take place.

Katz and Poulsen (1972) proposed that the ideal permeation enhancer should be –

(i) Pharmacologically inert

(ii) Non-toxic, irritating or allergenic

(iii) Able to prove immediate onset of penetration enhancement upon application

(iv) Able to allow the skin to recover immediately and fully its barrier function upon removal

(v) Compatible with a wide range of drugs and excipients

(vi) Able to solubilise drugs

(vii) Compliant

(viii) Inexpensive

(ix) Odourless, colourless and tasteless, thus cosmetically acceptable

No such permeation enhancer currently exists and this demonstrates to a certain extent why the field of topical and transdermal drug delivery has failed to be as successful as drug delivery by other routes (e.g. oral) – many enhancers are able to cause permeation enhancement effects but at cost of unacceptable levels of skin irritation, vastly reducing the likelihood of patient

acceptance and compliance (Wiedersberg and Guy 2014). For example, DMSO has been used to enhance permeation of numerous penetrants, but the concentrations used for a permeation enhancement effect can cause erythema, scaling, burning and stinging (Kligman 1965). Ionic surfactants have proven to enhance the permeation of penetrants through skin, but have powerful irritating properties (Tupker *et al.* 1990). Non-ionic surfactants are better tolerated by users because their effects on the skin barrier are less pronounced, but as a result, permeation enhancement effects are reduced (Shokri *et al.* 2001). The disadvantages of chemical permeation enhancers are reflected in the lack of commercial products found in the BNF that use chemical permeation enhancers, other than basic solvents such as PG and urea.

Without an understanding of the mechanism of action of these permeation enhancers, it cannot be reasonably predicted whether the permeation enhancer will cause a detectable enhancement in permeation of a specific drug either into or through the skin, nor can it be known if the penetration enhancer may cause unacceptable levels of irritation. Understanding the mechanism of action of a permeation enhancer may aid in successful pairing with a specific drug, increasing the likelihood that a permeation enhancement effect will occur.

It was observed in Chapter 2 that the addition of a G3 PAMAM-NH_2 dendrimer significantly enhanced the depth permeation of CHG into porcine skin, though the mechanism of this enhancement is unknown. The PAMAM dendrimer may have contributed to the enhancement of CHG through occlusive effects as PAMAM dendrimers are highly hygroscopic (Uppuluri *et al.* 1998) so are able to extract water from the environment, increasing the water content adjacent to the *stratum corneum*. Increasing hydration in this manner is believed to cause permeation enhancement effects by disrupting lipid packing by interacting with the polar section of the lipid bilayer (Barry 1987).

A reduction of surface tension has been suggested as a potential PAMAM dendrimer mechanism by Sayed-Sweet *et al.* (1997); Kirton *et al.* (1998) and Tully and Fréchet (2001). A reduction in surface tension would reduce the contact angle of the formulation on the skin surface, providing a greater surface area across which the drug can make contact with, and partition into, the skin.

A review by Sun *et al.* (2012) postulated three possible mechanisms of action for the PAMAM dendrimer. They are discussed in more detail in Section 1.12.2, but briefly, the authors suggested firstly that the drug might act as a drug release modifier by rapidly releasing encapsulated drug into the vehicle, increasing the concentration of drug in the vehicle and thus promoting the thermodynamic driving force which is required for favourable diffusion across the skin barrier. Secondly, the authors suggested a vehicle dependent penetration enhancement effect. By pairing the dendrimer (with drug encapsulated) with a penetration enhancer that is known to fluidise skin lipids, for example IPM, the *stratum corneum* barrier is effectively removed allowing the PAMAM dendrimer to diffuse across the minimised barrier. Finally, the authors suggested accumulation of dendrimer nanoparticles within follicular openings where they may act as a depot for drug release.

The mechanistic effects of the PAMAM dendrimer are likely to be contained to the skin surface and the enhancer is unlikely to permeate across the *stratum corneum* barrier due to the compound's high molecular weight and extensive surface charge, which do not align with physicochemical parameters which are considered ideal for topical and transdermal drug delivery (a molecular weight <500 g/mol and unionised permeants are preferred for topical and transdermal drug delivery [Naik, Kalia and Guy, 2000]). This theory was supported by Venuganti *et al.* (2011) who found that fluorescently labelled PAMAM dendrimers were limited to the *stratum corneum* and deposition was only enhanced when using iontophoresis (2 hr) to drive the dendrimer into the skin using a voltage gradient. These results must be interpreted with the understanding that labelling topical and transdermal permeants using fluorescent tags may limit

their permeation because of their large size (Seto *et al.* 2012). The results from Chapter 4 suggest that PAMAM dendrimer permeation into skin is unlikely. A unique PAMAM dendrimer fragment could not be identified due to the lack of unique fragments that would allow it to be distinguished from the background (skin). However, given the physicochemical properties of the dendrimer investigated in Chapter 4, it is highly unlikely that they were able to permeate the skin intact via the intercellular or intracellular routes.

5.2 Aims and Objectives

It is clear from the diffusion cell and tape stripping studies completed in Chapter 3 and 4, drug delivery of CHG into porcine skin can be increased by co-formulation with a G3 PAMAM-NH_2 dendrimer. The mechanism of this enhancement, however, remains unclear. The aim of this chapter was to elucidate the mechanism of action of the PAMAM dendrimer as a permeation enhancer of CHG within the gel formulations created in Chapter 2 for topical and transdermal drug delivery. Proposed mechanisms include disruption of *stratum corneum* lipid bilayers, a reduction in surface tension and occlusive effects.

The objectives required to meet this aim are:

- Measure TEWL of skin samples over a 24hr time period following a 4% CHG-0.5mM/1 mM PAMAM dendrimer solution or gel application to porcine skin to measure time-dependent changes in skin barrier integrity
- Use OCT to visualise changes in porcine skin barrier integrity in a time-dependent manner
- Measure the surface tension of a CHG gel formulation with and without the G3 PAMAM-NH_2 dendrimer, in order to determine the dendrimer is responsible for a change in surface tension, and thereby permeation enhancement effects
- Use the information gathered to postulate a mechanism of action of the dendrimer

5.3 Materials and Methods

5.3.1 Materials

Details of the components which were used to create the CHG-PAMAM co-formulation can be found in Chapter 2. All surfactants (Tween 40, Tween 80, Tween 85, Span 80) were purchased from Sigma Aldrich. PG was purchased from Fisher Scientific.

5.3.2 Methods

5.3.2.1 Transepidermal water loss (TEWL) Measurements

Previously, the barrier integrity of porcine skin was measured after dosing porcine skin with a G3 PAMAM-NH_2 dendrimer for 24hr (Judd 2013b)**.** However, it was of interest to understand whether PAMAM dendrimer mediated changes in TEWL were time-dependent. This study measured TEWL at various time points over the course of a 24hr study (1 hr, 2 hr, 4 hr, 6 hr, 8 hr, 12 hr and 24 hr).

Skin was dosed with either a 4% CHG-0.5 mM/1 mM PAMAM solution or gel formulation (Table 2.1). 1mL of each formulation was placed on porcine skin set up in a Franz type diffusion cell apparatus in accordance with the protocol outlined in Section 3.3.3. A blank skin sample was used as a control and 1mL of SDS (5% w/v) was used as a positive control. All samples were unoccluded.

At specific time points over a 24 hr period, excess formulation was washed from the skin surface using minimal amounts of distilled water. Excess moisture was immediately removed from the skin surface using a paper towel and once all moisture was removed, TEWL was measured in triplicate. TEWL was measured using a Biox Aquaflux TEWL meter (model AF200). The TEWL

meter was gently placed on the skin surface and allowed to equilibrate for 2 minutes before TEWL reading was recorded (g/m^2/h). The humidity and temperature was recorded alongside the TEWL measurement.

5.3.2.2 Optical Coherence Tomography (OCT)

This method was based upon the method previously used by Judd *et al.* (2013a) for delineation of the interactions between PAMAM dendrimers and the porcine skin surface skin samples were either left untreated or treated with 1-4% w/v CHG or CHG 4% w/v co-formulated with 0.5 mM/1 mM G3 PAMAM-NH_2 and set up in the diffusion cell apparatus, following the protocol in Section 3.3.3. After 30 min, 1 hr, 4 hr, 8 hr and 24 hr excess formulation was removed from the cell using an absorbent paper towel. Following each time point, skin samples were analysed using a spectral domain optical coherence tomograph (TELESTO-II, Thorlabs, USA). The OCT utilised centre wavelength at 1300 nm providing approximately 3.5 mm imaging penetration in the highly scattered skin samples. A superluminescence diode generated light beam is split in two and directed at the sample and an internal reference mirror, which measures light backscattering in the horizontal (or axial) and vertical (or depth) position when both sources are combined. After source combination, signal interference is measured and an image is produced based on the extent of signal interference from the internal reference mirror (Arevalo *et al.* 2009).

5.3.2.3 Surface Tension Measurements

The surface tension of water, 4% w/v CHG gel formulation, 4% CHG-0.5 mM PAMAM co-formulation and 4% CHG-1 mM PAMAM co-formulation was measured using a Torsion Balance OS White model obtained from Torsion Balance Supplies. The experimental gel formulations

created in Chapter 2 were utilised to compare the surface tension of the gel system with and without the presence of the PAMAM dendrimer. 5 mL of the sample was placed in a concave glass dish on a platform below the platinum ring. The platform was slowly raised until the platinum ring touched the surface of the liquid sample. The platform was then gradually lowered and at the same time the index pointer on the balance was moved in an anticlockwise direction. This continued until the platinum ring was pulled apart from the liquid. At this point, the value indicated on the torsion balance was provided as the surface tension measurement.

5.3.2.4 Reformulation of CHG without G3 PAMAM-NH_2 dendrimer

Following the results of the surface tension measurement study, further formulation development was undertaken. CHG was formulated with a number of different surfactants at different concentrations, replicating the methods from two previous studies (Shokri *et al.* 2001, Nokhodchi *et al.* 2003), which investigated the effect of various surfactants on the skin permeation of diazepam and lorazepam, respectively. These studies used a surfactant concentration of 0.5%, 1%, 2.5% or 5% w/v in a water-PG 50:50 vehicle. The CHG-Span formulation however used an ethanol-water 50:50 vehicle, as CHG was insufficiently soluble in the former solvent.

Table 5.1. Hydrophilic-Lipophilic Balance (HLB) values for surfactants used in this study.

Surfactant	HLB Value
Tween 40	15.6
Tween 80	15.0
Tween 85	11.0
Span 80	4.3

Table 5.2. Cricical micellar concentrations (CMCs) of surfactants utilised in this study.

Surfactant	Critical Micellar Concentration (CMC) (M)
Tween 40	2.30×10^{-05}
Tween 80	1.00×10^{-05}
Tween 85	2.9×10^{-07}
Span 80	N/A

Table 5.3. CHG-surfactant formulation ingredients. The vehicle used for formulations containing Tween surfactant was water-PG 50:50; the vehicle used for the formulation containing Span surfactant was water-ethanol 50:50.

	CHG Concentration (w/v %)	Surfactant Concentration (w/v %)	Vehicle volume (mL)
Tween 40	4	0.5	To 50mL
	4	1	To 50mL
	4	2.5	To 50mL
	4	5	To 50mL
Tween 80	4	0.5	To 50mL
	4	1	To 50mL
	4	2.5	To 50mL
	4	5	To 50mL
Tween 85	4	0.5	To 50mL
	4	1	To 50mL
	4	2.5	To 50mL
	4	5	To 50mL
Span 80	4	0.5	To 50mL
	4	1	To 50mL
	4	2.5	To 50mL
	4	5	To 50mL
No Surfactant	4	0	To 50mL

The CHG permeation into and through porcine skin from the CHG-surfactant formulations was measured using the protocol provided in Chapter 3 (Section 3.3.3; *n=4)*.

5.4 Results

5.4.1 TEWL Measurements

The difference in TEWL measurements between pre and post dose of the chosen formulations over the course of 24 hr is illustrated in Figure 5.1. The difference in TEWL measurements after 24 hr is illustrated in Figure 5.2.

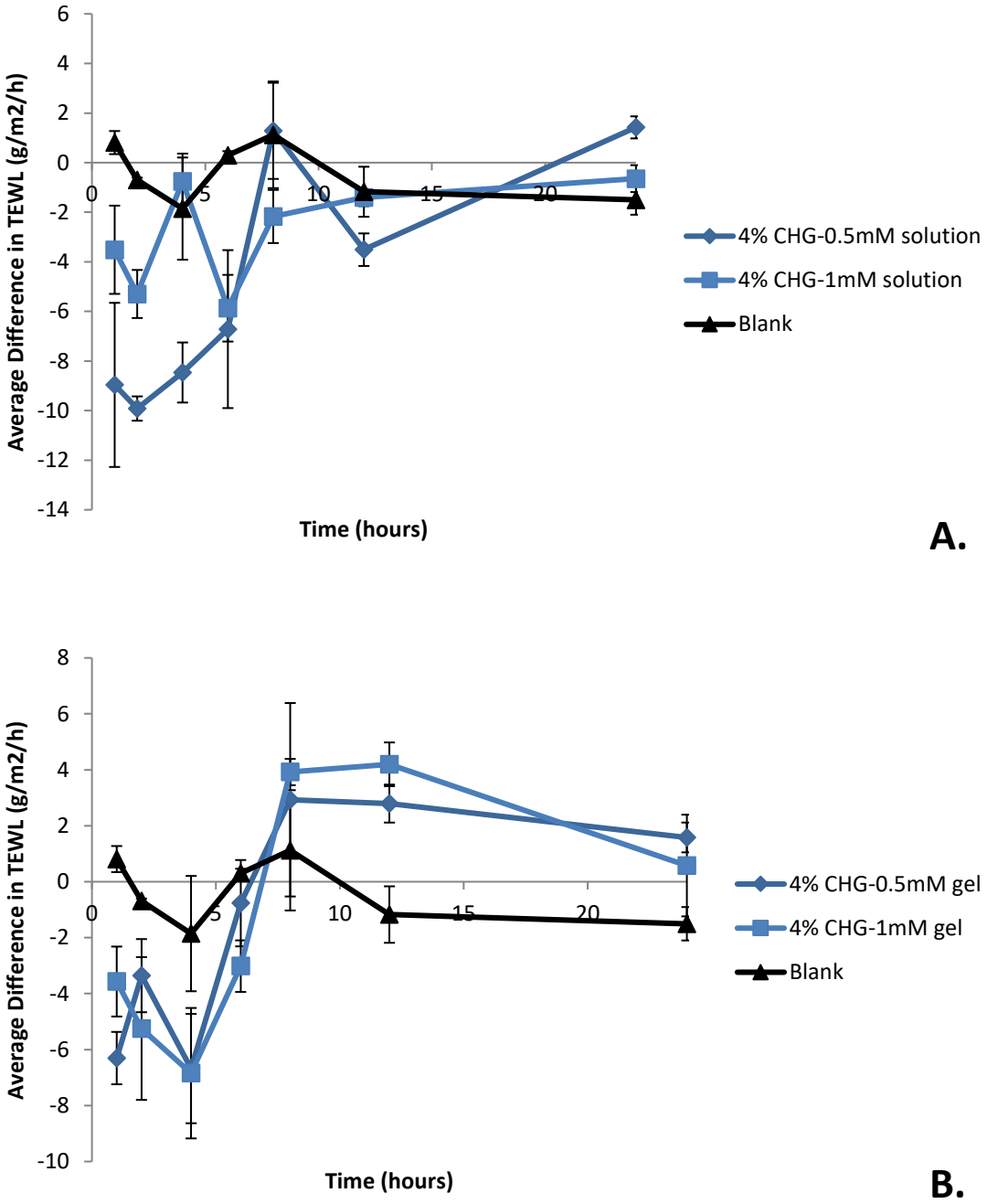

Figure 5.1. Measurement of skin barrier integrity, as determined by TEWL, over the course of 24 hr, following dosing with G3 PAMAM-NH_2 dendrimer (A) solutions and (B) gels, *n=3*. *Mean temperature 19.7 ± 0.4 °C; mean humidity 35.50 ± 2.50%, n=3 ± SE.*

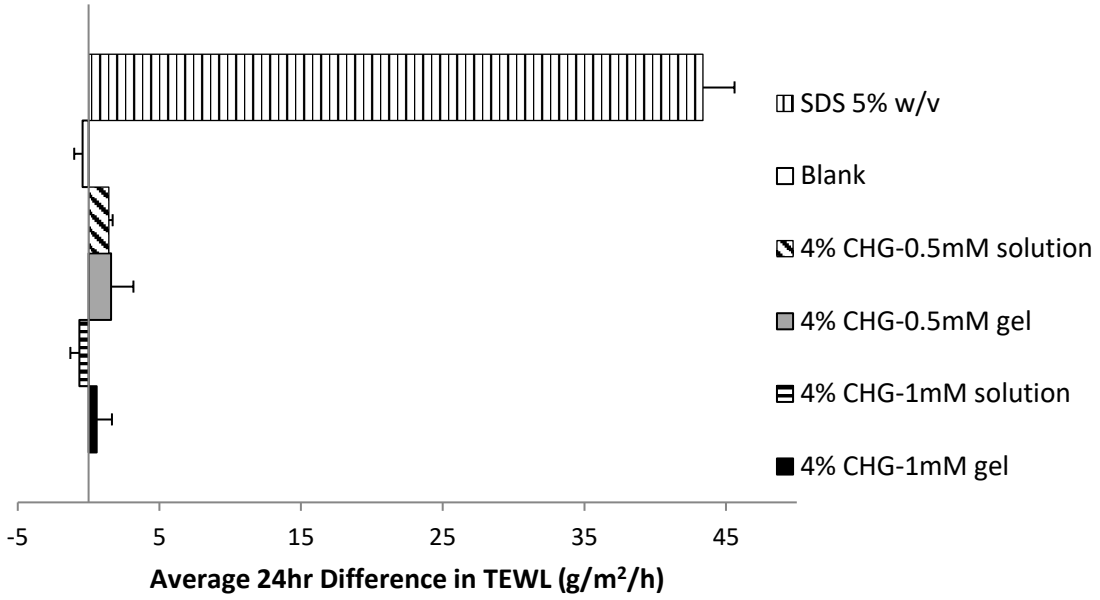

Figure 5.2. Measurement of skin barrier integrity, as determined by TEWL, before and after dosing with G3 PAMAM-NH_2 dendrimer solutions and gels, *n=3 ± SE*. *Mean temperature 19.7 ± 0.4 °C; mean humidity 35.50 ± 2.50%.*

The TEWL of skin samples treated with experimental formulations were measured after 1, 2, 4, 6, 8, 12 and 24hr. Minimal changes in TEWL were observed over the course of the 24hr experiment; therefore the 24hr difference in TEWL is presented in Figure 5.2. Both gels and solutions followed the same pattern of an initial increase in TEWL, which slowly decreased over the course of the experiment, although the correlation was weak for each group. The changes in TEWL for the co-formulations were minimal; with the maximum increase in TEWL of 4.20 g/m^2/hr (4% CHG-1 mM PAMAM gel, 12 hr). This is considerably lower than the changes exhibited by SDS 5% w/v solution which is clear from Figure 5.2.

In addition to the experimental formulations, the TEWL measurements of untreated skin and skin treated with a 5% w/v SDS solution were also compared pre and post dose (after 24 hr, *n=4*) and were used as a blank and positive control respectively. There was a reported increase in average TEWL for the blank samples (0.36 ± 0.59 g/m^2/hr) after 24 hr and a large increase in

average TEWL for the skin samples treated with a 5% w/v SDS solution for 24hr (43.38 ± 2.23 g/m^2/hr).

TEWL measurements indicated that upon initial application of the gel formulation to porcine skin, TEWL decreased (by 6.30 g/m^2/h for the 4% CHG-0.5 mM gel and by 3.57 g/m^2/h for the 4% CHG-1 mM gel). From that point onwards, the TEWL increased. By the end of the experiment, TEWL had increased by a maximum of 2.93 g/m^2/h for the 4% CHG-0.5 mM gel and by 4.20 g/m^2/h for the 4% CHG-1 mM gel. The average change in TEWL to the negative control (blank skin) was a decrease by 0.36 g/m^2/h after 24hr. The average change in TEWL to the positive control (skin treated with 1 mL of 5% w/v SDS) was an increase by 43.38 g/m^2/h after 24 hr. The changes in TEWL associated with the formulations tested compared to the positive control, were minimal. There was no statistically significant difference between any of the experimental gel formulations when considering the average 24 hr difference in TEWL ($p>0.05$). A Kruskal Wallis ANOVA indicated that 5% w/v SDS significantly increased TEWL compared to all other treatment groups ($p <0.05$). Because the differences in TEWL were minimal, OCT was utilised in an attempt to characterise changes to the *stratum corneum* surface in more detail.

5.4.2 Optical Coherence Tomography (OCT) to determine time-dependent interactions between G3 PAMAM-NH_2 dendrimers and porcine skin

OCT images are generated according to how polarised light reflects off skin structures, such as keratin and collagen (Babalola *et al.* 2014, Hussain *et al.* 2017). The keratin in the *stratum corneum* in particular is believed to reflect a large amount of polarised light (Pircher *et al.* 1991, Sun *et al.* 2003) and therefore OCT was utilised in this study in an attempt to visualise changes to the *stratum corneum* surface band of light when a CHG-PAMAM co-formulation was applied

to the skin surface, as some penetration enhancers are believed to exert their permeation enhancement effects via *stratum corneum* disruption (Moser *et al.* 2001). OCT measurements of skin were taken at various time points in order to view whether changes to the *stratum corneum* surface were time-dependent.

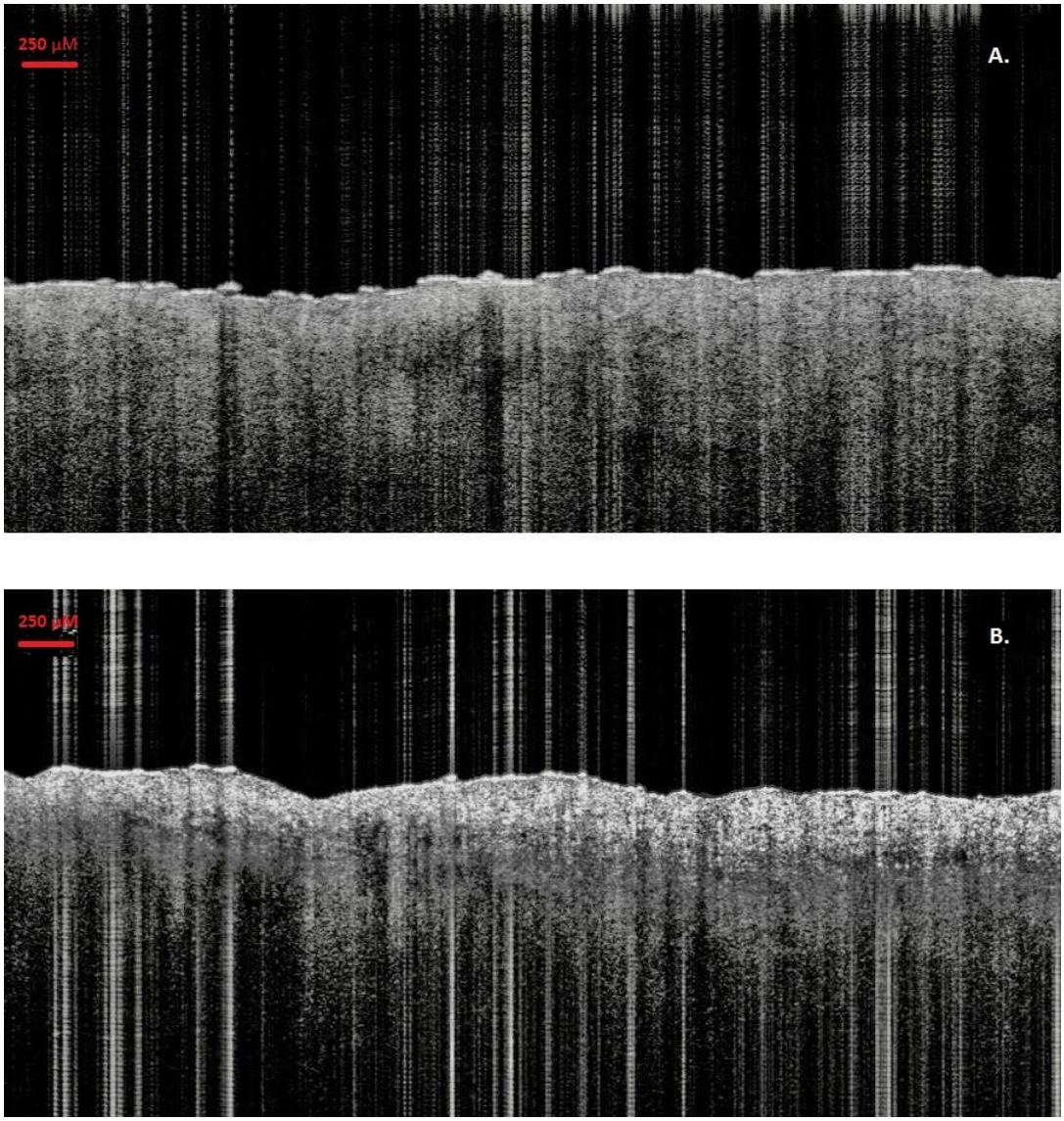

Figure 5.3. OCT images of untreated porcine ear skin at *A. 30 min* and *B. 24 hr. Red line 250 µm scale bar.*

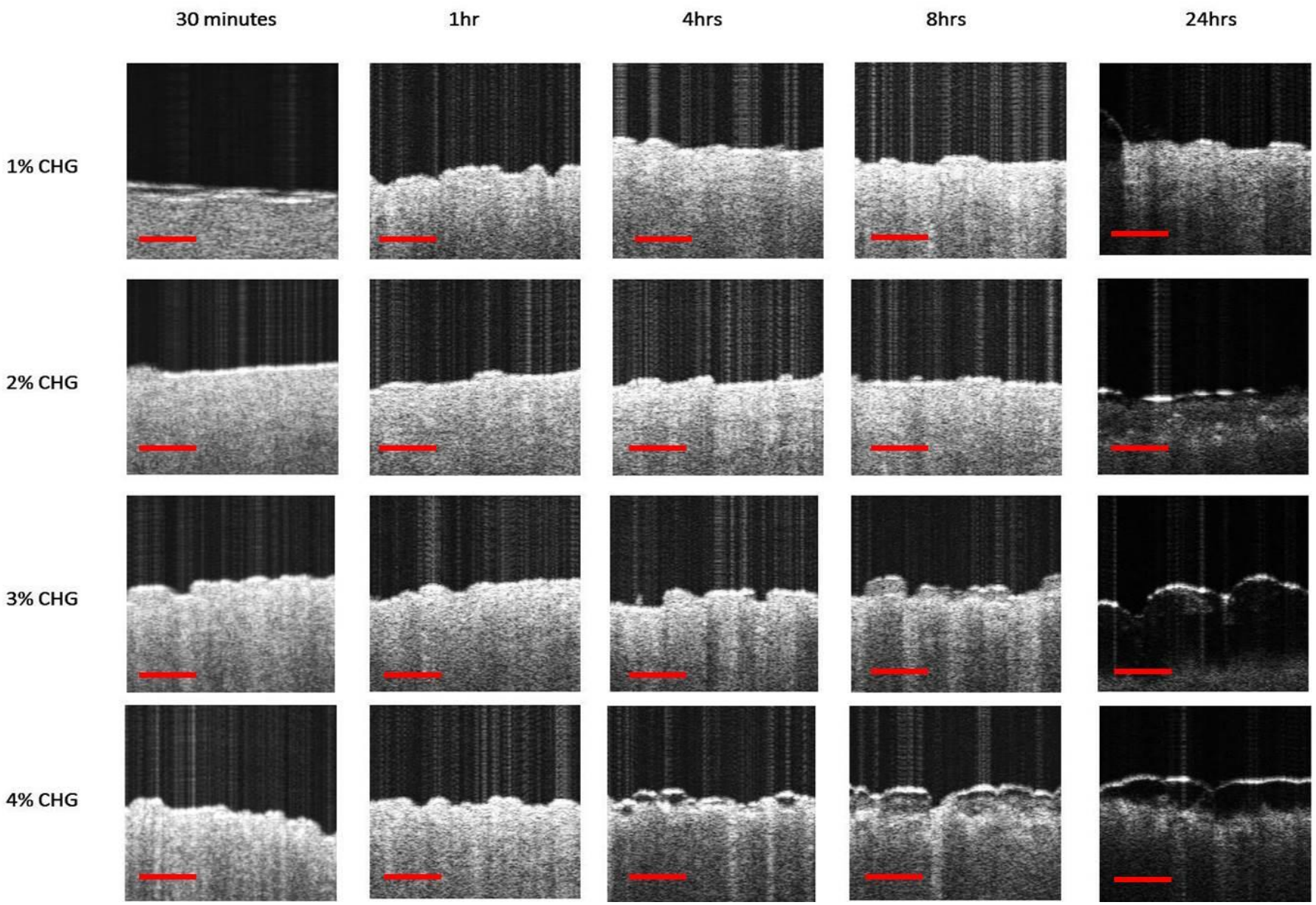
30 minutes
1hr
4hrs
8hrs
24hrs
1% CHG
2% CHG
3% CHG
4% CHG

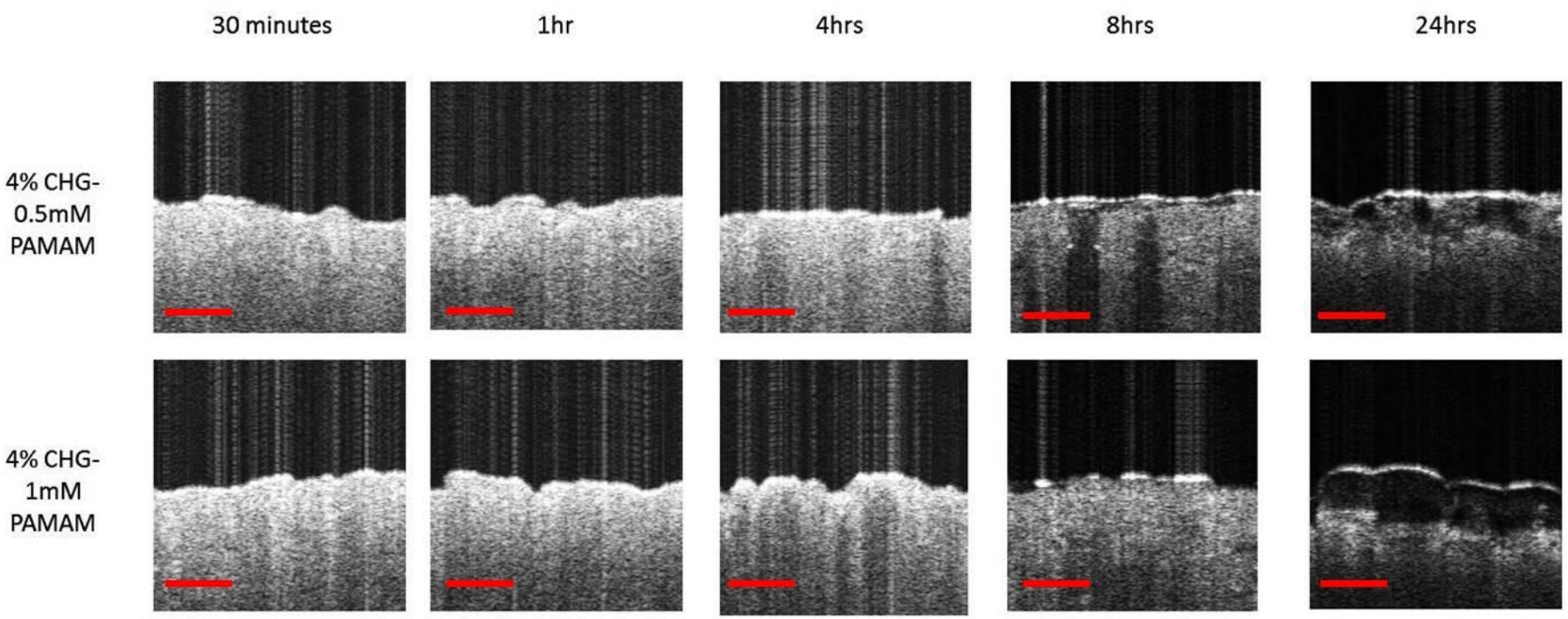

Figure 5.4. OCT images of porcine ear skin dosed with a either 1%, 2%, 3% 4% CHG gel formulation or 4% CHG-0.5 mM or 4% CHG-1 mM PAMAM gel co-formulation taken over a 24 hr time period. ***Red line - 250 µm scale bar.***

There appears to be minimal differences between the formulations and the appearance of the reflective band over time, specifically compared to the results published by Judd *et al.* (2013a) which investigated the interactions of PAMAM dendrimers with the surface of porcine skin. There appears to be a slight increase in reflective band disruption from 8hr onwards when comparing formulations that did contain the PAMAM dendrimer and those that did not. For all formulations tested, there appears to be a consistent disruption in the reflective band at the 24 hr time point, which is not isolated to the formulations that contained PAMAM dendrimer. An OCT image of a basal cell carcinoma lesion above the eyebrow appears to show similar disruption in certain areas of skin to those visualised at 24 hr within this study (Hussain *et al.* 2017). The hypo-reflective streak stretching from the surface was attributed to a hair casting a shadow. The author notes that areas of tissue such as fluid and air are hypo-reflective and as a result appear black in the OCT image. In contrast to the other time point images, there is often a dark patch between the hyper-reflective band indicating the *stratum corneum* and the lower skin structures. This may be indicative of air or fluid trapped between the *stratum corneum* and skin structures below, which may be indicative of skin hydration. This is supported by studies that have found the application of glycerol to reduce the refractive index of the skin (Vargas *et al.* 1999, Welzel 2001, Knüttel *et al.* 2003). Alternatively, this may be indicative of bacterial degradation to give a gas, given that the skin was present in a diffusion cell for 24 hr. However, it is difficult to find supportive evidence of this as most OCT studies focus on diseases *in vivo*. Where *in vitro* studies are completed, the duration of the experiment rarely exceeds an hour (Zhong *et al.* 2010, Wen *et al.* 2012). Nevertheless, the potential air or fluid trapped between the *stratum corneum* and structures below is present in skin samples that have been treated with the gel formulation that does not contain the PAMAM dendrimer, therefore it is unlikely that the PAMAM dendrimer contributed towards this change and more likely components of the gel formulation resulted in this effect.

In accordance with the TEWL measurement results, there appears to be little to no OCT reflective band disruption for the first half of the experiment for any formulation. This may suggest that occlusive effects are more pronounced than disruption of the *stratum corneum* layer. However, when occluding the skin surface one might expect to see a "thickening" of the hyper-reflective band indicative of the *stratum corneum*. Such a phenomena is absent in these studies. Therefore, it may be the case that occlusion of the skin surface contributes towards the PAMAM dendrimer mechanism of action, but it is not the predominant mechanism.

5.4.3 G3 PAMAM-NH_2 surface tension measurements

The surface tension of the experimental 4% w/v CHG gel formulation with and without addition of PAMAM dendrimer was measured. Twenty measurements were taken of each formulation on three separate occasions and the average temperature in each case noted. The results can be found in Table 5.4 and Figure 5.5.

Table 5.4. Surface tension measurements of various co-formulations with and without the addition of a G3 PAMAM-NH_2 dendrimer at clinically relevant concentrations, *n = 20 ± SE*. Mean temperature 20.0 ± 2 °C

Formulation	Surface Tension Measurement (Newton/metre) ± SE
4% CHG	$3.23 \times 10^{-2} \pm 6.67 \times 10^{-5}$
4% CHG, 0.5 mM PAMAM	$3.17 \times 10^{-2} \pm 5.25 \times 10^{-5}$
4% CHG, 1 mM PAMAM	$3.09 \times 10^{-2} \pm 7.41 \times 10^{-5}$

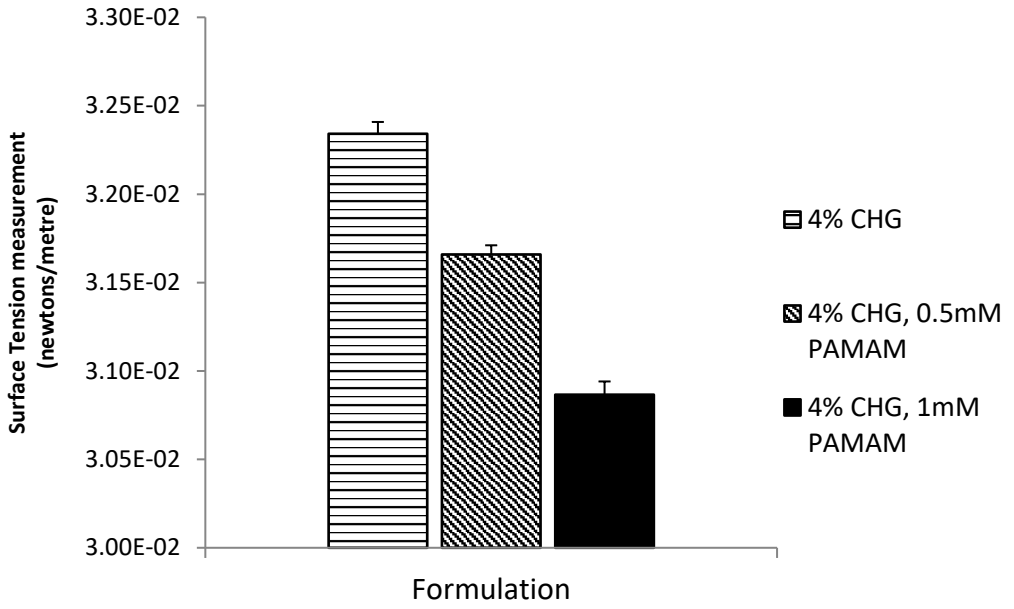

Figure 5.5. PAMAM-dendrimer-mediated change in surface tension, *n=20 ± SE.*

A Kruskal Wallis ANOVA indicated a statistically significant difference between all pairwise comparisons ($p < 0.05$). The formulations that contained the PAMAM dendrimer had a significantly lower surface tension than the formulations that did not contain the PAMAM dendrimer, and the 4% CHG-1 mM PAMAM co-formulation had a significantly lower surface tension than the 4% CHG-0.5 mM PAMAM co-formulation. This may indicate that there is an inverse relationship between the concentration of PAMAM dendrimer in the formulation and the surface tension. However, this would suggest that permeation enhancement effects of the dendrimer are concentration dependent, but this has been disputed (Venuganti and Perumal 2009, Holmes *et al.* 2017).

The surface tension measurements of formulations provided in Table 5.4 are shown in Table 5.5. Ten measurements of each formulation were recorded.

Table 5.5. Surface tension measurements of various co-formulations with and without the addition of a non-ionic surfactant at clinically relevant concentrations, *n=10 ± SE*. Mean temperature 20.5 ±2 °C.

Formulation		Surface Tension Measurement (Newton/metre) ± SE
Water	-	$6.90 \times 10^{-2} \pm 2.0 \times 10^{-4}$
CHG 4% in water	-	$4.66 \times 10^{-2} \pm 2.0 \times 10^{-4}$
CHG 4% in water-PG 50:50	-	$5.01 \times 10^{-2} \pm 1.0 \times 10^{-4}$
CHG 4% - Tween 40	0.5%	$4.15 \times 10^{-2} \pm 1.0 \times 10^{-4}$
	1%	$4.14 \times 10^{-2} \pm 1.0 \times 10^{-4}$
	2.5%	$4.14 \times 10^{-2} \pm 1.0 \times 10^{-4}$
	5%	$4.14 \times 10^{-2} \pm 1.0 \times 10^{-4}$
CHG 4% - Tween 80	0.5%	$4.14 \times 10^{-2} \pm 1.0 \times 10^{-4}$
	1%	$4.10 \times 10^{-2} \pm 1.0 \times 10^{-4}$
	2.5%	$4.10 \times 10^{-2} \pm 1.0 \times 10^{-4}$
	5%	$4.10 \times 10^{-2} \pm 1.0 \times 10^{-4}$
CHG 4% - Tween 85	0.5%	$3.87 \times 10^{-2} \pm 2.0 \times 10^{-4}$
	1%	$3.82 \times 10^{-2} \pm 1.0 \times 10^{-4}$
	2.5%	$3.82 \times 10^{-2} \pm 1.0 \times 10^{-4}$
	5%	$3.82 \times 10^{-2} \pm 1.0 \times 10^{-4}$
CHG 4% - Span 80	0.5%	$3.43 \times 10^{-2} \pm 1.0 \times 10^{-4}$
	1%	$3.42 \times 10^{-2} \pm 1.0 \times 10^{-4}$
	2.5%	$3.35 \times 10^{-2} \pm 1.0 \times 10^{-4}$
	5%	$3.35 \times 10^{-2} \pm 1.0 \times 10^{-4}$

The data from Table 5.4 and Table 5.5 indicates that, when compared to water, the 4% CHG-1 mM PAMAM co-formulation resulted in the greatest reduction in surface tension.

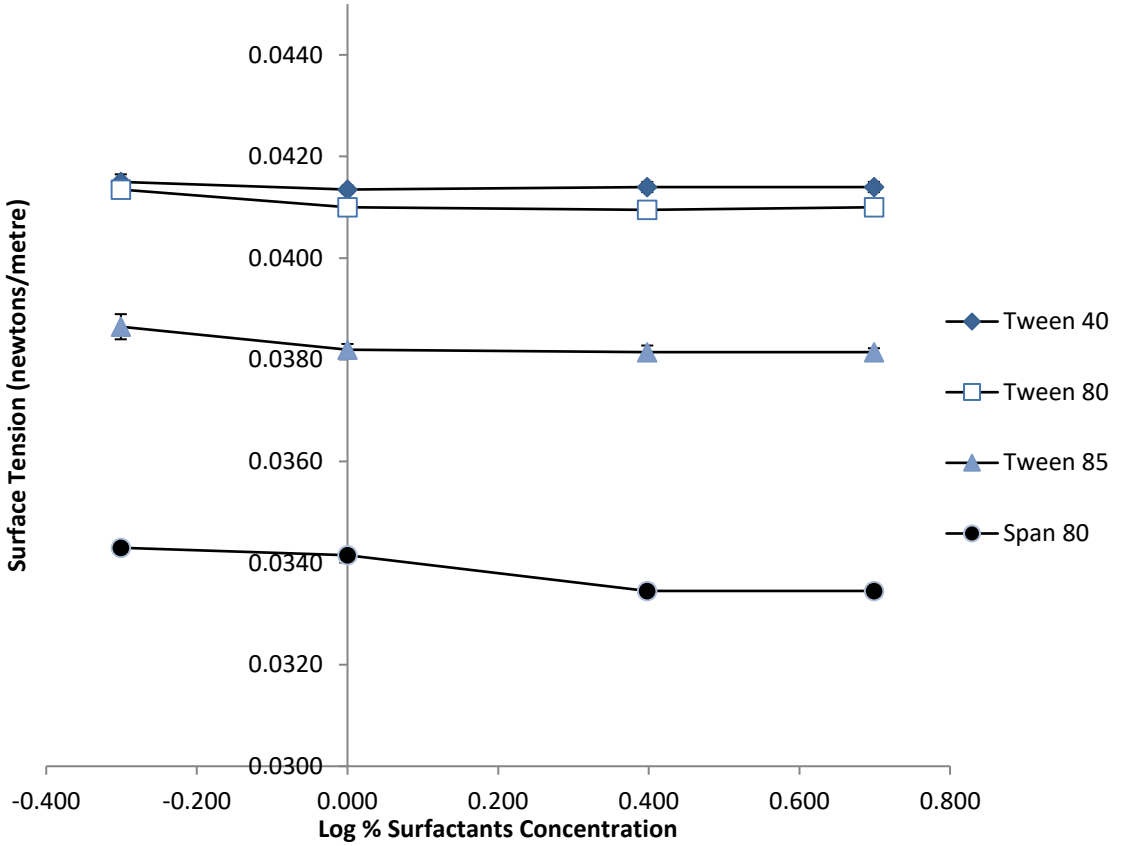

Figure 5.6. Scatter plot illustrating the change in surface tension with increasing surfactant concentration, *n=10 ± SE*.

Generally, for each surfactant, there was very little difference between concentration and surface tension. For all Tween based formulations, there is a small decrease in surface tension between 0.5% w/v and 1% w/v of the surfactant. Further increase in surfactant concentration did not decrease the surface tension. For the Span based formulation, there is a small decrease in surface tension between 0.5% w/v and 1% w/v of the surfactant, and a further, greater decrease in surface tension between 1% w/v and 2.5% w/v surfactant. Increasing the surfactant concentration to 5% w/v Span 80 did not decrease the surface tension any further. The minimal changes in surface tension with increasing surfactant concentration are likely to be related to the CMC's of the surfactants, as the concentrations of surfactants used in this study exceed the CMC's recorded in Table 5.2. The concentrations of CHG detected in tape strips 1-21 from each formulation is provided in Figure 5.7-5.12.

A Kruskal Wallis ANOVA indicated that there was no statistically significant difference between the concentration of Tween surfactant and surface tension measurement ($p>0.05$). A Kruskal Wallis ANOVA indicated that there was a statistically significant difference between 1% and 3%; 1% and 4%; 2% and 3% and 2% and 4% Span 80 surfactant.

5.4.4 CHG experimental formulation with Tween and Span surfactants in a water-PG/water-ethanol 50:50 vehicle

For formulations that contained Tween surfactants, there was generally an inverse relationship between surfactant concentration and concentration of CHG that had permeated into each layer. This trend is not present in the CHG-Span formulation. In this case, the concentration of CHG recovered by tape stripping generally increased with increase surfactant concentration from 0.5% to 1% w/v Span 80, but following this, increasing the concentration of Span 80 further decreases the concentration of CHG delivered into the skin. The expected trends were also present which were consistent with those noted in Chapter 2, such as decreasing CHG concentration and decreasing corneocyte weight with increasing tape strip number. All data is presented following gravimetric analysis (Reddy *et al.* 2002).

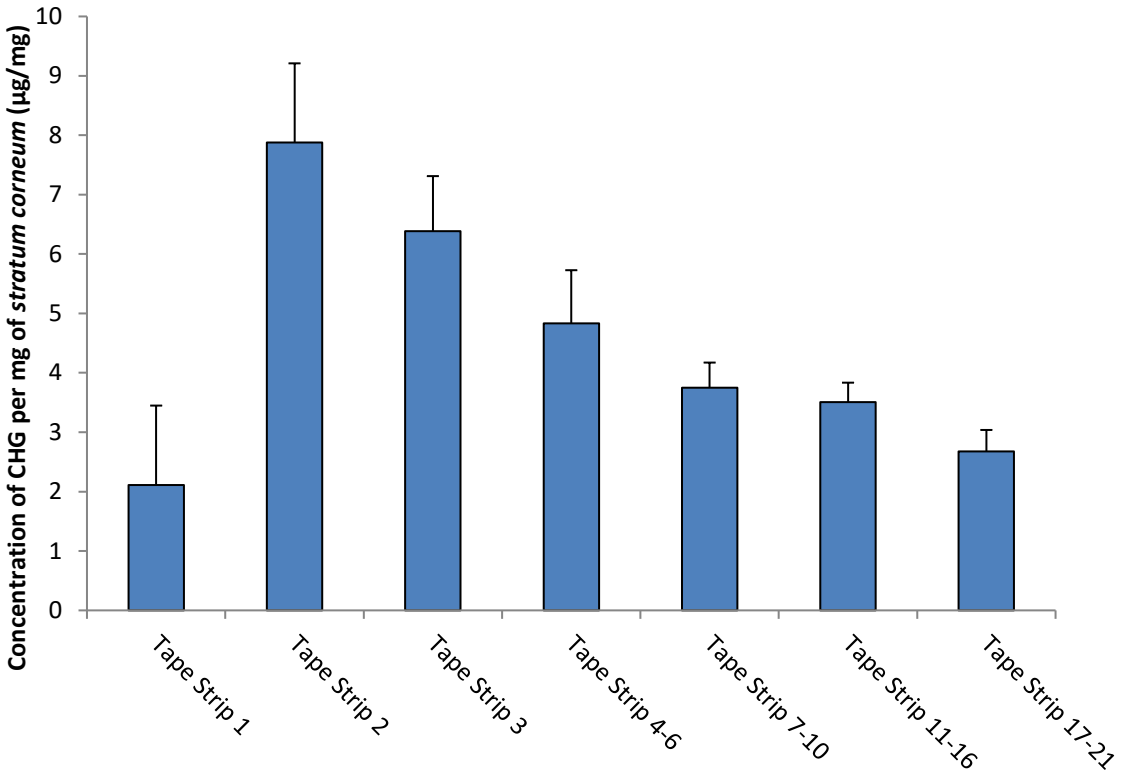

Figure 5.7. Concentration profile of CHG detected on tape strips 1-21 following treatment with a CHG 4% in a water-PG 50:50 vehicle. Concentrations are presented following gravimetric analysis. *n=4 ± SE.*

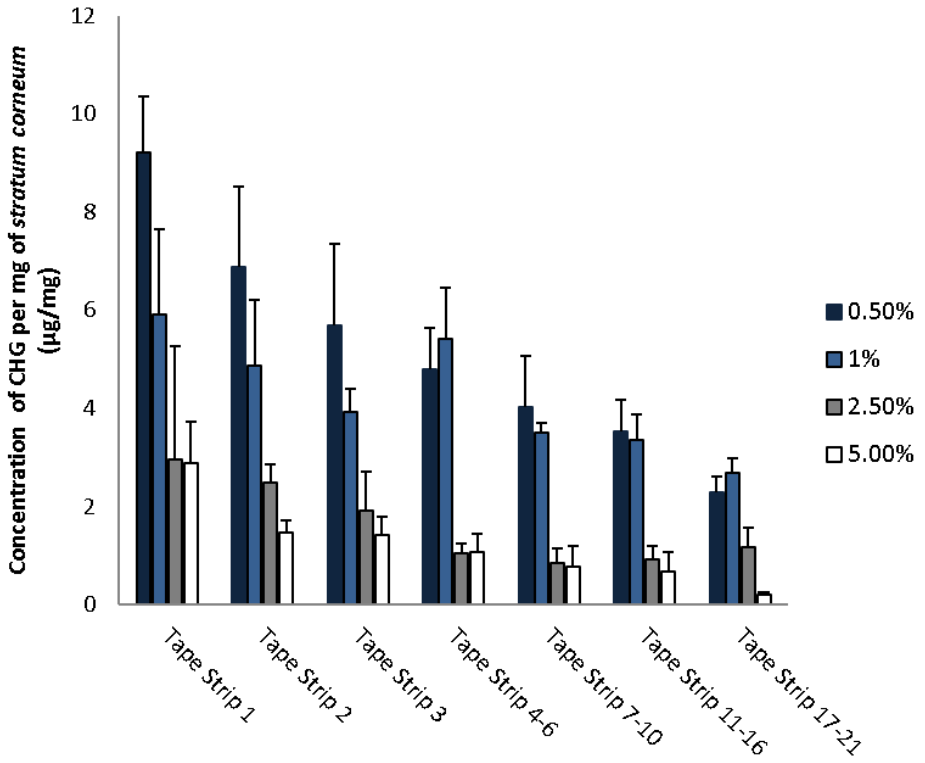

Figure 5.8. Concentration profile of CHG detected on tape strips 1-21 following treatment with CHG 4%-Tween 40 formulations containing various concentrations of surfactant (0.5%-5%) in a water-propylene glycol 50:50 vehicle. Concentrations are presented following gravimetric analysis. ***n=4± SE.***

Table 5.6. Analytical tests chosen to determine whether formulations with differing concentration of Tween 40 (0.5-5%) significantly affects the depth permeation of CHG within porcine skin. Pairwise comparisons are arranged so that the formulation which delivered the highest concentration of CHG is given first (F1). ***KW – Kruskal Wallis; OWA – One-Way ANOVA, n=4.***

Tape Strip Number	Analytical Test	Statistically Significant Result	Pairwise Comparisons	
			F1	F2
Tape Strip 1	OWA	N	-	-
Tape Strip 2	OWA	Y	0.50%	5%
Tape Strip 3	OWA	Y	0.50%	5%
Tape Strip 4-6	OWA	Y	0.50%	2.50%
			0.50%	5%
			1%	2.50%
			1%	5%
Tape Strip 7-10	OWA	Y	0.50%	2.50%
			0.50%	5%
			1%	2.50%
			1%	5%
Tape Strip 11-16	OWA	Y	0.50%	2.50%
			0.50%	5%
			1%	2.50%
			1%	5%
Tape Strip 17-21	OWA	Y	0.50%	5%
			1%	2.50%
			1%	5%
Total Tape Strips	KW	Y	0.50%	5%

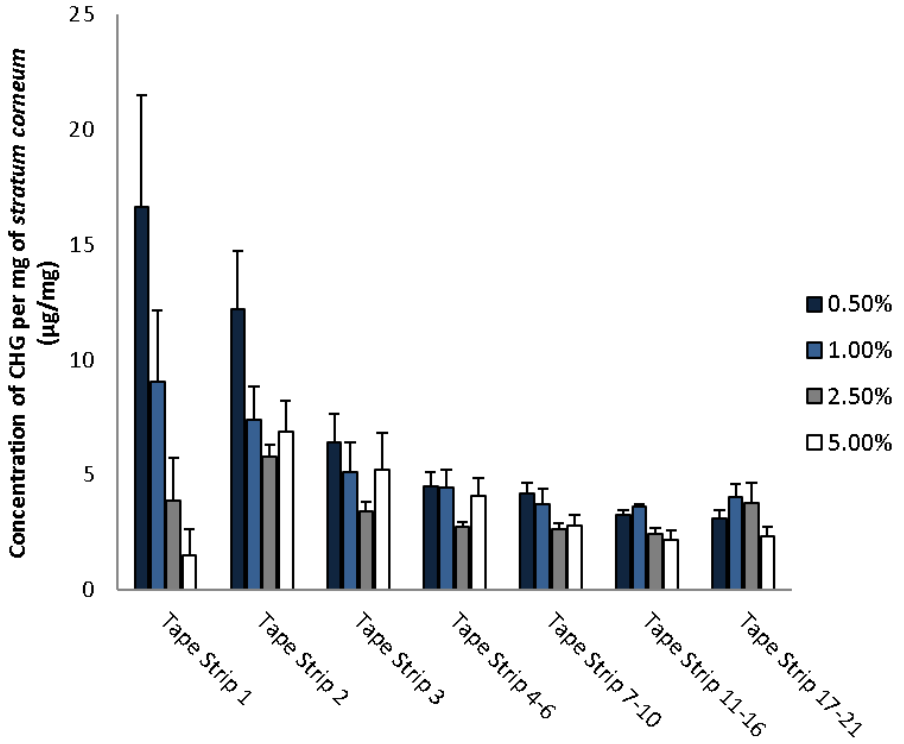

Figure 5.9. Concentration profile of CHG detected on tape strips 1-21 following treatment with CHG 4%-Tween 80 formulations containing various concentrations of surfactant (0.5%-5%) in a water-propylene glycol 50:50 vehicle. Concentrations are presented following gravimetric analysis. ***n=4± SE.***

Table 5.7. Analytical tests chosen to determine whether formulations with differing concentration of Tween 80 (0.5-5%) significantly affects the depth permeation of CHG within porcine skin. Pairwise comparisons are arranged so that the formulation which delivered the highest concentration of CHG is given first (F1). ***KW – Kruskal Wallis; OWA – One-Way ANOVA, n=4.***

Tape Strip Number	Analytical Test	Statistically Significant Result	Pairwise Comparisons	
			F1	F2
Tape Strip 1	KW	Y	0.5%	5%
Tape Strip 2	KW	N	-	-
Tape Strip 3	OWA	N	-	-
Tape Strip 4-6	OWA	N	-	-
Tape Strip 7-10	OWA	N	-	-
Tape Strip 11-16	OWA	Y	1%	5%
Tape Strip 17-21	KW	N	-	-
Total Tape Strips	OWA	Y	5%	0.5%

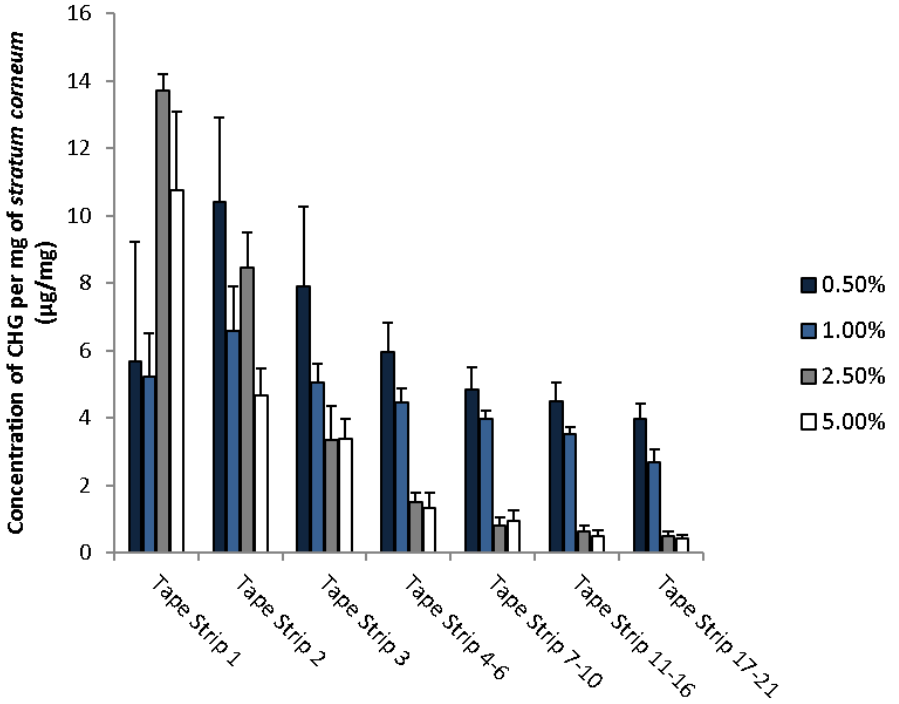

Figure 5.10. Concentration profile of CHG detected on tape strips 1-21 following treatment with CHG 4%-Tween 85 formulations containing various concentrations of surfactant (0.5%-5%) in a water-propylene glycol 50:50 vehicle. Concentrations are presented following gravimetric analysis. ***n=4± SE.***

Table 5.6. Analytical tests chosen to determine whether formulations with differing concentration of Tween 85 (0.5-5%) significantly affects the depth permeation of CHG within porcine skin. Pairwise comparisons are arranged so that the formulation which delivered the highest concentration of CHG is given first (F1). ***KW – Kruskal Wallis; OWA – One-Way ANOVA, n=4.***

Tape Strip Number	Analytical Test	Statistically Significant Result	Pairwise Comparisons	
			F1	F2
Tape Strip 1	OWA	N	-	-
Tape Strip 2	OWA	N	-	-
Tape Strip 3	OWA	N	-	-
Tape Strip 4-6	KW	Y	0.5%	5%
Tape Strip 7-10	OWA	Y	0.5%	2.5%
			0.5%	5%
Tape Strip 11-16	KW	Y	0.5%	5%
Tape Strip 17-21	OWA	Y	0.5%	5%
			2.5%	5%
Total Tape Strips	OWA	Y	0.5%	1%
			0.5%	2.5%
			0.5%	5%

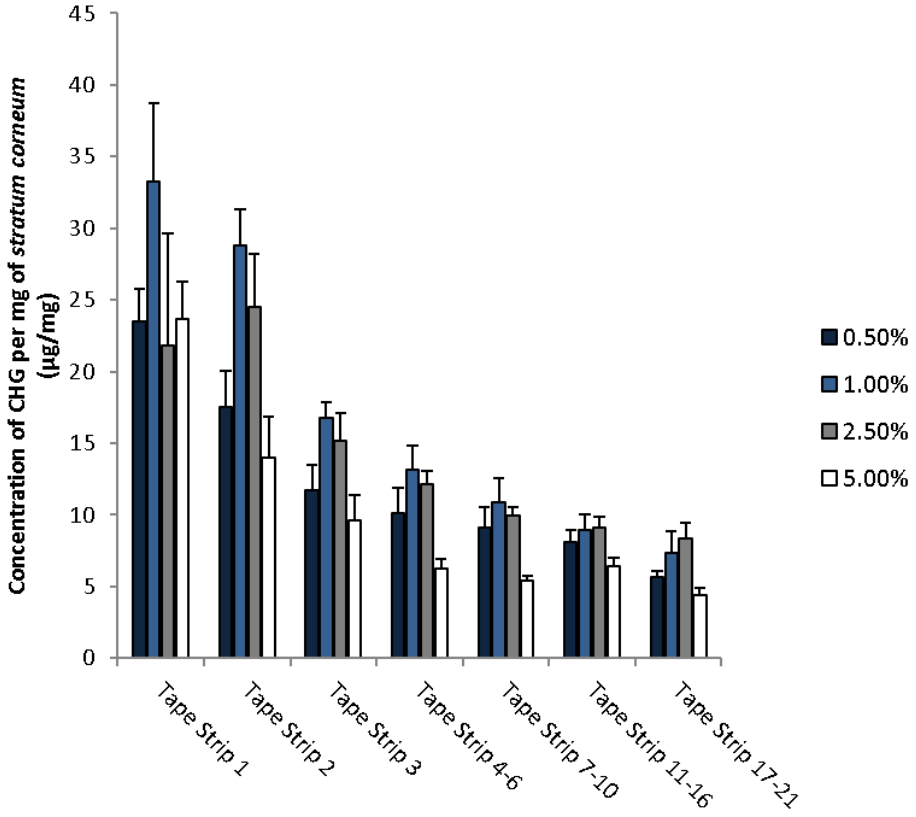

Figure 5.11. Concentration profile of CHG detected on tape strips 1-21 following treatment with CHG 4%-Span 80 formulations containing various concentrations of surfactant (0.5%-5%) in a water-ethanol 50:50 vehicle. Concentrations are presented following gravimetric analysis. ***n=4 ± SE.***

Table 5.9. Analytical tests chosen to determine whether formulations with differing concentration of Span 80 (0.5-5%) significantly affects the depth permeation of CHG within porcine skin. Pairwise comparisons are arranged so that the formulation which delivered the highest concentration of CHG is given first (F1). ***KW – Kruskal Wallis; OWA – One-Way ANOVA, n=4.***

Tape Strip Number	Analytical Test	Statistically Significant Result	Pairwise Comparisons	
			F1	F2
Tape Strip 1	OWA	N	-	-
Tape Strip 2	OWA	N	-	-
Tape Strip 3	OWA	N	-	-
Tape Strip 4-6	OWA	Y	1%	5%
Tape Strip 7-10	OWA	N	-	-
Tape Strip 11-16	OWA	N	-	-
Tape Strip 17-21	KW	Y	2.5%	5%
Total Tape Strips	OWA	Y	1%	5%

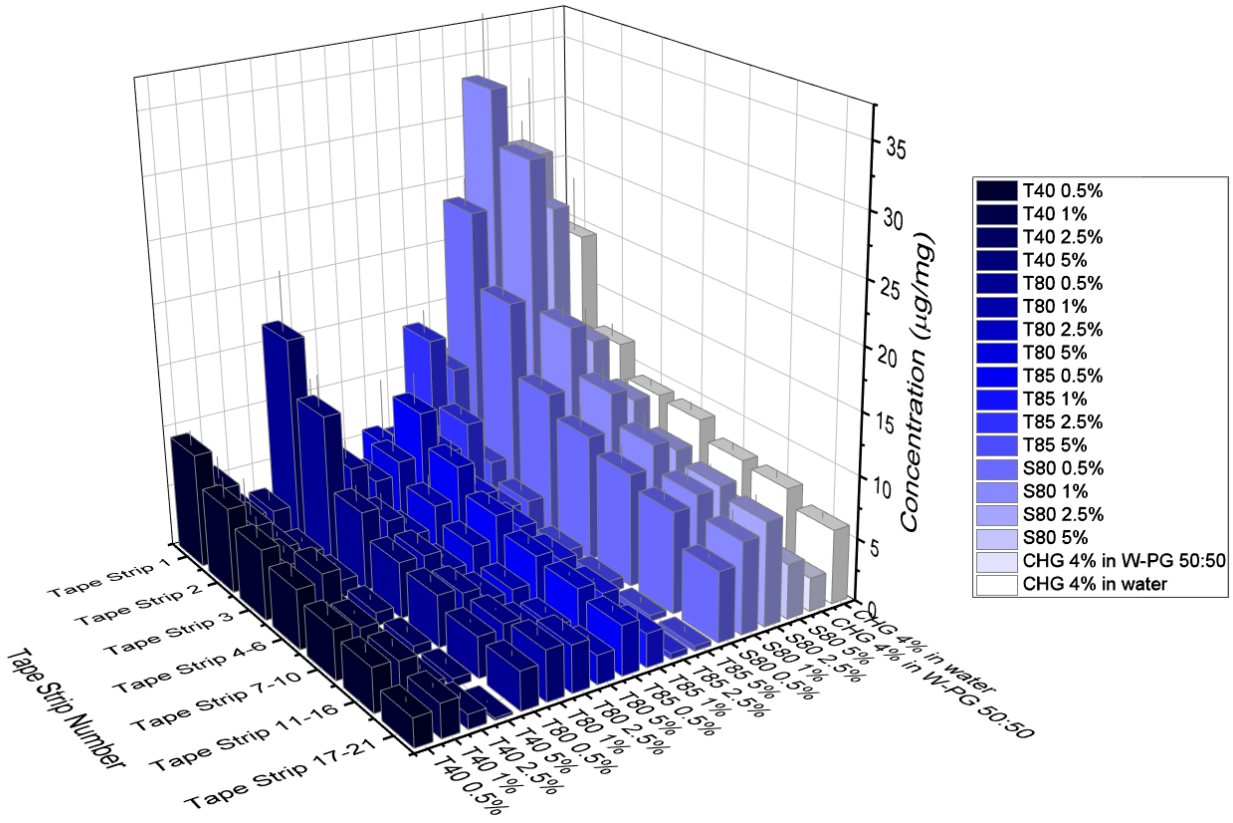

Figure 5.12. Comparative tape strip data, including controls (CHG 4% in water, CHG 4% in water-PG 50:50) and treatment groups, *n=4 ± SE*.

The comparative data graph indicates that the CHG-Tween formulations generally failed to improve CHG permeation into porcine skin when compared to CHG permeation in a water vehicle and in a water-PG 50:50 vehicle. The CHG-Span formulation was more successful in enhancing the permeation of CHG into porcine skin compared to the control.

Table.5.10. Pairwise comparisons between CHG-surfactant formulations which provided a statistically significant result (p <0.05), *n=4*.

Tape Strip Number	Analytical Test	Statistically Significant Result	Pairwise Comparisons	
			F1	F2
Tape Strip 1	KW	Y	S80 1%	T80 5%
Tape Strip 2	KW	Y	S80 0.5%	T40 5%
			S80 2.5%	T40 5%
			S80 1%	T40 5%
			S80 2.5%	T40 2.5%
			S80 1%	T40 2.5%
Tape Strip 3	KW	Y	S80 0.5%	T40 5%
			S80 2.5%	T40 5%
			S80 1%	T40 5%
			S80 2.5%	T40 2.5%
			S80 1%	T40 2.5%
Tape Strip 4-6	KW	Y	S80 0.5%	T40 5%
			S80 2.5%	T40 5%
			S80 1%	T40 5%
			S80 0.5%	T40 2.5%
			S80 2.5%	T40 2.5%
			S80 1%	T40 2.5%
			S80 2.5%	T85 5%
			S80 1%	T85 5%
			S80 2.5%	T85 2.5%
			S80 1%	T85 2.5%
Tape Strip 7-10	KW	Y	S80 0.5%	T40 5%
			S80 2.5%	T40 5%
			S80 1%	T40 5%
			S80 2.5%	T40 2.5%
			S80 1%	T40 2.5%
			S80 0.5%	T85 2.5%
			S80 2.5%	T85 2.5%
			S80 1%	T85 2.5%
			S80 0.5%	T85 5%
			S80 2.5%	T85 5%
			S80 1%	T85 5%
Tape Strip 11-16	KW	Y	S80 0.5%	T85 5%
			S80 1%	T85 5%
			S80 2.5%	T85 5%
			S80 2.5%	T40 5%
			S80 0.5%	T40 5%
			S80 1%	T40 5%
			S80 0.5%	T85 2.5%
			S80 1%	T85 2.5%
			S80 2.5%	T85 2.5%
			S80 1%	T40 2.5%
			S80 2.5%	T40 2.5%
Tape Strip 17-21	KW	Y	S80 0.5%	T40 5%
			CHG 4% in water	T40 5%
			S80 1%	T40 5%
			S80 2.5%	T40 5%
			CHG 4% in water	T85 5%
			S80 1%	T85 5%
			S80 2.5%	T85 5%
			S80 1%	T85 2.5%
			S80 2.5%	T85 2.5%
			S80 2.5%	T40 2.5%

5.5 Discussion

As discussed in Section 1.12.1, PAMAM dendrimers are able to act as dermal and transdermal permeation enhancers for several compounds, with varying speculation surrounding their mechanism. The purpose of this chapter therefore was to explore the mechanism of action of the PAMAM dendrimer in enhancing skin deposition of CHG, as shown in Chapter 3 and 4. Determining the mechanism of action of the dendrimer is important, as this may allow for more effective formulation strategies to be developed which take advantage of the specific mechanisms discovered, which may enhance drug partitioning into (and across if desired) skin for topical and transdermal drug delivery.

The study completed by Sun *et al.* (2012) has already been discussed in detail (Section 1.12.2) and it was important to design studies which could support or refute these putative mechanisms where possible.

The first possible mechanism was that the dendrimer acts as a drug release modifier (Chandrasekar *et al.* 2007, Kurtoglu *et al.* 2010). Encapsulation of drugs within the dendrimer core may increase the aqueous solubility of the drug. When drug loaded dendrimer formulations are applied to the skin, the solubilised drug is able to be released rapidly and consequently creates a high thermodynamic activity in the vehicle which is able to drive drug permeation into skin (Higuchi 1960). This was shown by Chauhan *et al.* (2003), who found that an indomethacin-PAMAM complex significantly enhanced drug deposition compared to a control aqueous drug suspension. The model drug (indomethacin) used in this study was lipophilic (log P 3.10; [Bonina *et al.* 1995]), therefore the concentration of drug available in the control aqueous formulation was unlikely to be high, hence why the PAMAM dendrimer improved drug partitioning into the skin by increasing the solubility of the drug by encapsulating it within its core. The authors found that for the G4-OH PAMAM dendrimer used in this study, encapsulation was made available due

to non-specific non-covalent interactions that were considered overwhelmingly stronger than electrostatic repulsion that would be expected at the experimental pH (pH 7).

In contrast, CHG is hydrophilic (log P 0.037, Farkas *et al.* 2007) with a high aqueous solubility (>50%; [Sigma Aldrich, 2019b]) and so it is likely that as the drug is already highly soluble in the aqueous gel formulation. Speculatively, any increase in solubility via co-formulation with the PAMAM dendrimer is unlikely to be the predominant permeation enhancement mechanism. As CHG aqueous solubility is high, it appears that the rate-limiting step to penetration into the *stratum corneum* is the lipophilic nature of this layer in comparison to the hydrophilic drug, rather than the solubility in the vehicle.

It is unknown whether the drug is encapsulated by the dendrimer or if the drug is able to interact with surface groups present on the outer dendrimer shell. A PAMAM dendrimer pre-treatment study was found to significantly enhance CHG deposition within porcine skin (Holmes *et al.* 2017). As CHG permeation was enhanced without direct contact between the drug and dendrimer in this study, it suggests that the dendrimer has an effect on the surface of the skin, which allows the drug to penetrate rather than directly interacting with the drug (i.e. occlusion, lipid disruption, reduction in surface tension). This does not necessarily mean that the drug and dendrimer do not interact, as numerous mechanisms may contribute towards permeation enhancement effects, but interactions between the drug and dendrimer may not be the predominant cause of CHG permeation enhancement.

Drug encapsulation inside the dendrimer core seems unlikely as both the drug and dendrimer exhibit cationic groups and therefore repulsive forces may predominate. Furthermore, the pK_a of the dendrimer interior is understood to be between 3-6 (Tomalia *et al.* 1985). At pH 7-8, measured in Table 2.4, this would mean the interior of the basic dendrimer would be unionised, whereas the drug (pK_a 10.3 and 2.2, representing the formation of the monocation and dication

respectively [Hugo and Longworth, 1964]) would be ionised (Figure 2.3). Additionally, IR spectra can be used to determine whether drug encapsulation or electrostatic interaction had occurred. For example, a flavonoid tetramethylscutellarein was successfully encapsulated within the core of a G4 PAMAM dendrimer, which was confirmed by viewing the difference between the IR spectra of dendrimer alone and dendrimer- tetramethylscutellarein complex (Shadrack *et al.* 2015). When the compound was complexed with the dendrimer, a new broad absorption peak appeared between 3100-2500cm^{-1}, which indicated an interaction between the dendrimer and compound. The authors suggested that the existence of this broad peak was due to the presence of an $–NH_3^+$ functionality which was a result of electrostatic interaction between the compound and the dendrimer, which is comparable to other encapsulation studies (Kolhe *et al.* 2003, Prajapati *et al.* 2009). Judd (2013b) believed interactions between the CHG and G3 PAMAM dendrimer were likely to be an electrostatic interaction between the amine groups of the PAMAM dendrimer and the carboxyl group of the gluconic acid. This is supported by Chauhan *et al.* (2003), who determined that solubility enhancement of indomethacin by a G4-NH_2 dendrimer was due to an electrostatic bond between the amino groups of the dendrimer and the carboxylic acid group of the drug. The IR data collected in Table 3.8 may provide evidence of potential electrostatic interactions or hydrogen bonding present between the drug and dendrimer (Susi 1972). These shifts have already been discussed in Chapter 3, but briefly, shifts associated with N-H (b) amine (27 cm^{-1} shift), N-H (b) amide (68 cm^{-1} shift), C-OH (str) (45 cm^{-1} shift) are indicative of hydrogen bonding or electrostatic interactions between the drug and dendrimer. These shifts indicative of drug-dendrimer interactions were supported by Kolhe *et al.* (2003), who investigated interactions between the carboxyl groups on ibuprofen and the peripheral amine groups on a G3 and G4 PAMAM-NH_2 dendrimer. Additionally, Prajapati *et al.* (2009) found that solubility enhancement of piroxicam was attributed to electrostatic complexation with a G3 PAMAM-NH_2 dendrimer, where a downward shift in the N-H amide stretch at 1650 cm^{-1} was apparent in the FTIR spectrum.

A second potential mechanism of permeation enhancement using PAMAM dendrimers was described by Sun *et al.* (2012) as "vehicle dependent effects". The mechanism suggests that co-application of a drug-dendrimer complex in a potent vehicle enhances drug permeation, as the potent vehicle (e.g. IPM) is able to disrupt lamellar lipids, essentially removing the *stratum corneum* barrier which is considered the rate limiting step for drug permeation into skin. Cationic dendrimers may aid in the perturbation of lipid bilayers – cationic PAMAM dendrimers have been found to cause changes in the lipid architecture (Gardikis *et al.* 2006, Shcharbin *et al.* 2006), thus allowing the encapsulated drug to be delivered into the *stratum corneum*. One may argue that this is not really the mechanism of the PAMAM dendrimer, but the mechanism of the penetration enhancer which is able to initially disrupt the lipid bilayers, allowing penetration of the dendrimer for further disruption. Furthermore, the results from the studies in this chapter indicate that barrier damage due to the PAMAM dendrimer is minimal, through time-dependent changes in TEWL and observation of OCT images of skin treated with the PAMAM dendrimer over time. Given the results of this study, there is a lack of evidence to support this potential mechanistic aspect of PAMAM dendrimer mediated drug permeation enhancement.

Although the drug was not considered to be applied in a vehicle capable of causing substantial disruption to the *stratum corneum* barrier (as this would have implications for clinical acceptance), potential disruption was measured. TEWL is a common method of measuring barrier integrity of the skin (Wilson and Maibach 1989, Kalia *et al.* 1996, OECD 2004b, Elkeeb *et al.* 2010, Imhof and McFeat 2014) and is one of the methods recommended by OECD (2004a) for measuring barrier integrity. TEER and or measuring the penetration characteristics of a reference material such as tritiated water are also recommended, however the use of tritiated water may hydrate the *stratum corneum*, which could adversely affect compound penetration (Nangia *et al.* 1998, Elmahjoubi *et al.* 2009). Judd (2013b) used TEWL and TEER to measure differences in skin barrier integrity after a 24 hr application of 10 mM solution of a G3

PAMAM-NH_2 dendrimer in methanol. After 24 hr, the difference in TEWL was 2.76 ± 1.46 g/m^2/hr, and the difference in TEER was 2.55 ± 0.53 kΩ. Although this provided conflicting results (a decrease in barrier integrity from TEWL, and increase in barrier integrity from TEER), neither difference was significantly different from the vehicle control. Ultimately, TEWL was chosen to measure skin barrier integrity in this study due to its established use in *in vitro* skin studies (Leveque *et al.* 1977, Murahata *et al.* 1986, Lotte *et al.* 1987, Moloney 1988, Roskos and Guy 1989, Wilson and Maibach 1989) and its ability to quickly establish the barrier integrity of porcine skin samples (Nangia *et al.* 1998).

The results from the TEWL experiment indicate that initially, the *stratum corneum* barrier function increased (TEWL decreased slightly). An increase in TEWL did not occur until 8 hr onwards, and this was minimal compared to the positive control. There was no statistically significant difference between any of the experimental gel formulations when considering the average 24 hr difference in TEWL ($p>0.05$). A Kruskal Wallis ANOVA indicated that 5% w/v SDS significantly increased TEWL compared to all other treatment groups ($p <0.05$).

It remains of interest to postulate what may have caused the fluctuations in TEWL over the course of a 24 hr experiment. One might expect an initial increase in TEWL caused by the application of a gel which contained a large proportion of ethanol, a volatile vehicle well known for causing *stratum corneum* disruption (Friend *et al.* 1988, Pershing *et al.* 1990), however it is likely that evaporation of the vehicle within the first few minutes following formation application to the skin diminished the concentration of ethanol available for *stratum corneum* disruption. Other formulation components, such as glycerol and water (and potentially the dendrimer) may have contributed to the initial decrease in TEWL via hydration and occlusion of the skin (Friend *et al.* 1988, Pershing *et al.* 1990).

If the skin surface was extensively hydrated, one might then expect a large decrease in TEWL, but this was not observed. This may be explained by the change in mobility in the formulation. Over the course of a 24hr experiment, the viscosity was understood to increase. Kreilgaard, Pedersen and Jaroszewski (2000) reported that drug flux of lidocaine and prilocaine from microemulations was dependent on drug mobility in the vehicle, although plasticisers (such as glycerol and potentially CHG) may soften the rigidity of the polymer chains in film structure by reducing the intermolecular forces (Bergo and Sobral 2007, Padula *et al.* 2007). A decrease in drug mobility from dried topical films has previously been described (Gallagher and Heard 2005, Reid *et al.* 2008, 2009). Thus, a decrease in mobility may have prevented excipients from changing the barrier properties of skin extensively in either direction, and as a result, TEWL was not adversely affected.

When comparing the results to the positive control (SDS), it is clear that the gels containing PAMAM dendrimer and PAMAM dendrimer solutions had a negligible effect on the barrier properties of the *stratum corneum*. Judd (2013a) found that there was no significant difference in TEWL and TEER measurements between PAMAM dendrimer treated skin (10 mM) and the vehicle control treated skin after 24 hr. The results from the time-dependent study concur with the results of the study completed previously (Judd, 2013a).

A secondary method of measuring skin barrier disruption was utilised in this chapter to confirm the results provided by TEWL, and following reports in the literature that TEWL is most suitable for detecting large changes in barrier function, rather than smaller changes. For example, Netzlaff *et al.* (2006) measured the TEWL of intact and perforated heat separated human epidermis (punctured with a 1 mm diameter needle and stripped with adhesive tape either 3, 7 or 15 times). The study detected no significant differences between intact and punctured human heat separated epidermis. A statistically significant difference between intact and tape stripped skin was only detected when the skin was stripped 15 times. The study concluded that TEWL

measurements were only able to detect severe damage to human heat separated epidermis, even though minimal damage (i.e. tape stripping 3 or 7 times) did result in an increased permeation of flufenamic acid, indicating barrier damage had occurred. The lack of correlation between TEWL and barrier integrity was not limited to this study - Chilcott *et al.* (2002) found no correlation between TEWL loss rate and drug permeability following 15 tape strips or 4 needle punctures. Zhang *et al.* (2018) found only a weak correlation between TEWL and fentanyl skin permeation. Nangia, Berner and Maibach (1999) found that TEWL measurements of human heat separated epidermis were not significantly different from controls, despite the 2-5 × increase in tritiated water permeation. TEWL was noted as a useful method for measuring barrier integrity when chemicals were applied which caused rapid and irreversible damage to the skin barrier, such as chloroform:methanol (2%:1% v/v) and sodium lauryl sulphate. TEWL was utilised in the study in this thesis to estimate changes in barrier function as this method was recommended by OECD guidelines (OECD 2004b) and was still useful in demonstrating that the barrier function was not effected as severely as other products which are commonly used on skin, such as SDS used in cleansing products.

OCT was used to further investigate the effects of the experimental formulation on the *stratum corneum* barrier, in the circumstance that changes in the barrier were occurring but were too small to be detected by TEWL. OCT is a fast, non-invasive technique that can be used to qualitatively measure changes in the skins barrier function, with a good resolution (approximately 15 µm) and a penetration depth of 0.5-1.5 mm (Welzel *et al.* 1997). The technique is well established in the field of skin diagnostics (Gladkova *et al.* 2000, Gambichler *et al.* 2007, Mogensen *et al.* 2009) and for microneedle insertion into skin (Donnelly, *et al.* 2010). Furthermore, a review by Antonov, Schliemann and Elsner (2016) found that non-invasive techniques which produce skin images are preferable to TEWL when determining changes to skin morphology (Czaika *et al.* 2012, Vergou *et al.* 2012, Bargo *et al.* 2013). OCT has previously

been shown to detect changes in *stratum corneum* barrier disruption where TEWL cannot. For example, (Judd, 2013b; Judd *et al.* 2013a) found no significant differences in TEWL between PAMAM treated skin (10 mM solution) however, OCT images of skin treated with the same solution showed disruption of the reflective band indicative of disruption to the *stratum corneum*.

The conclusions made from the TEWL data in this study are also largely supported by the OCT images. Similarly to the TEWL measurements, changes in the reflective band indicative of *stratum corneum* disruption (Welzel *et al.* 1997) are minimal until the 8 hr time point and there appears to be only a slight increase in reflective band disruption between formulations which did and that did not contain a PAMAM dendrimer. This further indicates that the PAMAM dendrimer used in this study is unlikely to be able to cause significant barrier disruption. These results disagree with those found by Judd *et al.* (2013a), who investigated the effects of a 5 mM and 10 mM PAMAM dendrimer solution on the skin barrier integrity using OCT. These experiments differ, as the solutions used by Judd are of a higher concentration than those used in this study (0.5 mM and 1 mM). Furthermore, the PAMAM dendrimer solutions applied to the skin in this study used a water-methanol vehicle (65:35 for $–NH_2$ terminated dendrimers, 82.5:17.5 for –COOH terminated dendrimers). The presence of the organic solvent methanol may have contributed to the disruptions in the OCT entrance signal (Vinson *et al.* 1965, Scheuplein *et al.* 1970, Abrams *et al.* 1993, Cross *et al.* 2001) in contrast to the ability of occlusive products to cause thickening of the *stratum corneum* barrier, reflected in a thicker light band on the OCT image (Welzel 2001). The study within this chapter aimed to investigate how the experimental gel co-formulation affected the *stratum corneum* barrier in order to understand the mechanism of CHG enhancement from the experimental gel co-formulation, rather than from the PAMAM dendrimer alone.

These differences in the pre-treatment and co-formulation studies may be attributed to the ability of the dendrimer to make sufficient contact with the skin surface in a solvent vehicle, which may be more likely to cause barrier disruption. The pre-treatment study applied a G3 PAMAM-NH_2 dendrimer (0.5 mM-10 mM) in an ultra-pure water vehicle (Holmes *et al.* 2017). Cationic dendrimers have previously been found to interact with negatively charged membranes (Hong *et al.* 2004) (of which skin is a primary example [Burnette and Ongpipattanakul, 1987]). For example, increased permeability of 5FU following PAMAM dendrimer pre-treatment was attributed to interactions between the cationic dendrimer and skin surface (Venuganti and Perumal 2009). This may explain why the PAMAM dendrimer pre-treatment was found using OCT to disrupt the *stratum corneum* barrier when compared to the co-treatment explored in this chapter (Judd *et al.* 2013a). The increased viscosity of the gel formulations when applied to the skin as a co-treatment may have slowed free movement of PAMAM dendrimer particles in addition to competition from other materials in the formulation, minimising the ability of the dendrimer to disrupt the *stratum corneum* barrier. This may also contribute to the understanding of how the PAMAM dendrimer pre-treatment delivered a higher concentration of CHG into the skin than the CHG-PAMAM co-formulation. On the other hand, this may be mitigated somewhat by the ability of the gelling polymer (HEC) to reduce the surface tension of the system (Fang *et al.* 1999a), potentially increasing CHG wettability on the skin surface.

The key understanding from the TEWL and OCT studies in this chapter is that that barrier damage to the skin following application of a CHG-PAMAM gel co-formulation is minimal and further focuses consideration of the mechanism of action of the PAMAM dendrimer, as enhancement occurs despite minimal barrier damage. This is highly advantageous when considering patient acceptability of the formulation, as it is likely that a lack of barrier damage correlates to a lack of irritation (Pathan and Setty 2009). A lack of barrier damage would reduce the risk of external microbes infiltrating the skin, the exact scenario to be avoided. These results add to the

numerous other advantages of the co-formulation found throughout this thesis, such as satisfactory depth permeation of CHG, able to reach MIC levels of typical skin microbes in deeper skin layers, without significant permeation through full thickness porcine skin, reducing the likelihood of adverse events from systemic uptake (Chapter 3 and 4).

Such little barrier damage also supports the theory that PAMAM dendrimer permeation into the skin is low due to its dense surface charge, ionisation state and high molecular weight. Although not proven, the results from the ToF-SIMS study in Chapter 4 indicate that PAMAM dendrimer permeation within the skin is highly unlikely and there was no evidence of a PAMAM dendrimer ion fragment found within tape-stripped skin. Furthermore, Venuganti *et al.* (2011) identified the presence of PAMAM dendrimers within porcine skin, but only after entensive (2 hr) iontophoresis. Without this, PAMAM dendrimers were limited to the *stratum corneum* surface. Thus far, the results found in the literature and within this thesis suggest that PAMAM dendrimers exhibit their mechanism without significant barrier damage.

The final proposed mechanism of action by the Sun *et al.* (2012) study was that the dendrimer may accumulate within skin appendages and furrows. Figure 4.16 and Figure 4.17 appeared to show minimal CHG penetration into appendages, which was surprising as the cationic drug is considered more likely to penetrate via this route due to its ionisation state (Higuchi 1960). However, the sample size is too small to definitively conclude that this is the case. OECD (2004a) suggests at least four replicates per test preparation; however this focuses on permeation through bulk skin rather than specifically detailing follicular penetration. Otberg *et al.* (2004b) measured hair follicle density of seven difference body sites in six healthy volunteers. With the exception of forehead skin, the regions measured (back, thorax, upper arm, forearm, thigh and calf) provided a hair follicle density of between 14-32 follicles per cm^2 on average. This is somewhat comparable to adult porcine skin used in this study (10.16 follicles per cm^2 [Ferry, Argentieri and Lochner, 1995]). Furthermore, the ToF-SIMS images suggest that CHG

permeation did not occur in the appendages, but this does not necessarily mean that the PAMAM dendrimer follows the diffusion path of the drug. This would assume that the dendrimer is conjugated with the drug in some way, for example by entrapment or electrostatic interaction. This may not be the case, although shifts in the IR spectra appear to show hydrogen bonding or electrostatic interactions between the drug and dendrimer to be more likely (Table 3.7).

Two further mechanisms postulated for PAMAM dendrimers-mediated permeation enhancement into the skin were investigated. Occlusion has been suggested as a mechanism of PAMAM dendrimer action by Judd (2013a) and the results from the study in Chapter 3 support this mechanism. The co-formulation was observed visually to increase in viscosity over the course of the 24hr diffusion cell experiment and this may occlude and possibly hydrate the skin surface, allowing drug permeation to continue despite the increase in viscosity, reducing drug mobility (Reid *et al.* 2008). PAMAM dendrimers are highly hygroscopic (Uppuluri *et al.* 1998, Topp *et al.* 1999) and it is possible that they contributed to the permeation enhancement effect via occlusion of the skin surface. However, it may also be the case that other excipients within the formulation known to be hydrate the *stratum corneum* (i.e. water, glycerol) may have also contributed (and to a greater extent given their larger proportion in the formulation compared to the dendrimer), so it would not be fair to suggest that the entirety of the occlusive effects were due to the PAMAM dendrimer. The lack of barrier damage noted by the TEWL and OCT studies certainly does not rule out this potential mechanism.

The reflective band at the top of the skin on the OCT images represents the *stratum corneum*. Occlusion prevents water loss from the skin surface, resulting in swelling of corneocytes and water uptake into lipid domains (Bucks *et al.* 1989, 1991). Occlusive effects may manifest as a thickening of the reflective band on the OCT images (Welzel 2001). This was not seen and may suggest that the relative contribution of occlusion as a mechanism of CHG permeation enhancement is smaller than PAMAM dendrimer mediated surface tension effects.

It is proposed that the PAMAM dendrimer exerts its mechanism at least partially through surface tension effects. A reduction of surface tension has been suggested as a potential PAMAM dendrimer mechanism by Kirton *et al.* (1998) and Tully and Fréchet, (2001). A study completed by Sayed-Sweet *et al.* (1997) investigated the properties of hydrophobically modified PAMAM dendrimers at the air-water interface. They speculated two potential mechanisms for how the dendrimer might behave at the air-water interface. Firstly, they believed that the hydrophilic interior of lower generation dendrimers might associate with water, whereas the hydrophobic end groups would extend away from the water surface to integrate with neighbouring molecules. A second mechanism suggested for higher-generation dendrimers is that it may act as a hydrophobic spheroid that is able to float at the air-water interface. The presence of this flattened, oblate conformation was confirmed by Schenning *et al.* (1998), who compared dendrimer generation and molecular area of the PAMAM dendrimers.

The surface activities of dendrimers are further discussed more recently by Astruc, Boisselier and Ornelas (2010), however their potential for surface reduction as a mechanism for topical skin permeation enhancement does not appear to be explicitly stated within the literature. It seems therefore, that the finding that G3 PAMAM-NH_2 dendrimer reduces surface tension at the skin-air interface is a novel one. Incorporation of the dendrimer within the gel formulation may have reduced the contact angle of the formulation, allowing a higher concentration of CHG to be in contact with the skin at any one time. As previously stated, the surface tension of human skin is 27-28 dyne/cm, or 0.027-0.028 Newton/metre (Ginn *et al.* 1968) and the surface tension of the applied compound should be below this for appropriate adhesion to the skin for partitioning. Of all formulations tested, the dendrimer reduced the surface tension by the greatest amount, a reduction considered to be statistically significant compared to the gel formulation without the dendrimer ($p < 0.05$), suggesting the dendrimer was the most suitable addition to the formulation for CHG adhesion to the skin surface. Formulation of CHG with a

compound that exhibits surface active effects would allow this effect to be tested in order to determine if co-formulation with a product with the same mechanism as that theorised for the dendrimer would result in similar permeation enhancement effects. Furthermore, Chapter 3 identified some stability issues with the drug and dendrimer, resulting in drug precipitation (Section 3.4.7-3.4.8) and thus reformulating the drug with an alternative surface-active agent may have avoided these stability issues.

Ionic surfactants are generally considered to be more effective permeation enhancers than non-ionic surfactants via interactions with keratin present in corneocytes, fluidising the structure and increasing the ability of permeants to permeate into the structure (Pandey 2014). Fluidisation of the lamellar lipids is also thought to contribute to the ionic surfactant mechanism of permeation enhancement (Gibson and Teall 1983, Rhein *et al.* 1986, Froebe *et al.* 1990). Cationic surfactants, in particular, may interact with anionic components of the *stratum corneum* to stimulate the transfer of an anionic drug into the skin (Kitagawa *et al.* 2000). However, it has been established in the literature (Pesonen *et al.* 1995, Kaiser *et al.* 2009) and experimentally as part of this thesis that CHG is incompatible with anionic materials and therefore it was unsuitable for CHG to be formulated with an anionic surfactant. Cationic surfactants are thought to be more irritating and potentially damaging to the skin, as evidenced by the large increase in drug flux (Kushla *et al.* 1993, Nokhodchi *et al.* 2003, Seweryn 2018) which would increase the risk of systemic absorption of CHG and reduced patient acceptability due to likely increased irritation. This would also increase the risk of infection by allowing infiltration of microbes through a compromised barrier.

Non-ionic surfactants exert their mechanism of enhancing the permeation of drugs topically and transdermally by disrupting and fluidising *stratum corneum* lipids (Scheuplein *et al.* 1970). Furthermore, the surfactant may also penetrate into the intercellular matrix, binding to keratin filaments to disrupt the corneocyte (Nokhodchi *et al.* 2003). Non-ionic surfactants have the

advantage of causing less irritation than anionic surfactants and are generally considered safe which is imperative for ensuring patient acceptance for topical formulations (Som *et al.* 2012). The antibacterial activity of CHX is said to be reduced in the presence of non-ionic surfactants (Kostenbauder 1983). Nicoletti *et al.* (1993) found that 3% w/v Tween 80 in 0.89% saline was not sufficient to neutralise CHG, but a solution containing 5% w/v Tween 80 and 0.75% phospholipid (azolectin) was sufficient. Conversely, Owen (2006) states that CHX salts are compatible with most cationic and non-ionic surfactants, but in high concentrations CHX activity may be reduced due to micellar binding. Commercially, cetostearyl alcohol has been used in a CHX preparation (10% w/w, Savlon™) with sufficient antimicrobial effects. Cetostearyl alcohol exhibits surfactant like properties by stabilising emulsions (Frunzi and Sarsfield 2006). There appears to be no further evidence within the literature on the ability of CHG to be inactivated by non-ionic surfactants. It was of interest to prove or disprove this experimentally given that surface tension effects are believed to be at least partially responsible for PAMAM dendrimer mediated CHG permeation enhancement *in vitro* (Kirton *et al.* 1998; Tully and Fréchet, 2001).

A mixture of PG-water was used as a vehicle for the CHG-surfactant co-formulations as it was of interest to see the effect of other solvents on CHG permeation in a simplified system. It is likely that the excipients within the gel formulation (glycerol, HEC) may have contributed to the enhancement effect of CHG (Atrux-Tallau *et al.* 2010). Vehicle and formulation components have been acknowledged as influencers of permeation of drugs through skin (Wotton *et al.* 1985, Bronaugh and Franz 1986, Hilton *et al.* 1994, Cross *et al.* 2001, Larrucea *et al.* 2001, Karande and Mitragotri 2009, Karadzovska *et al.* 2013) and the complex, often synergistic, effects they have are not always predictable. Reducing co-variances by simplifying the formulation allows such effects on CHG permeation to be decoupled and potentially isolated, yielding a greater understanding of the role of each excipient. Furthermore, PG is understood to increase the critical micellar concentration (CMC) of non-ionic surfactants (Marszall 1980) by a

factor of 10 (Aguiar and Weiner 1969, Pandey 2014). Increasing the CMC of a surfactant would increase the concentration of surfactant that can be added into the formulation before micelles form. As there is a general trend of increasing penetration of chemicals with increasing surfactant concentration until the CMC is reached, this would allow a greater concentration of surfactant to enhance percutaneous penetration to a greater extent without CMC being reached.

The HLB value associated to a surfactant is an measure of its ratio between its hydrophilic and lipophilic groups (ICI Americas Inc, 1976). Although all surfactants may be considered miscible in oil and water due to the presence of both hydrophilic and lipophilic groups, the HLB value provides an indication of whether the surfactant's affinity is toward the water phase or the oil phase. Emulsifiers with low HLB values (most Span surfactants) tend to be more "oil miscible" and emulsifiers with high HLB values (most Tween surfactants) tend to be more "water miscible" (Allen and Ansel 2014). It was initially thought that using a surfactant such as Tween with greater affinity to the water phase would be the most conducive to a stable CHG-surfactant formulation given the concerns surrounding CHG and non-ionic surfactant stability (Kostenbauder, 1983; Nicoletti *et al.* 1993) and CHG's high aqueous solubility. A Span surfactant, although more "oil miscible" compared to Tween surfactants, was utilised in this study as a comparator to the Tween surfactants to determine if the HLB value of the surfactant had any significant effects on the permeation of the drug into porcine skin. Tween and Span surfactants were formulated in water-PG 50:50 with CHG however the formulations that included Span surfactants turned cloudy immediately and later appeared to separate. This was attributed to the high oil affinity of the surfactant. Span 80 was reformulated with CHG in a water-ethanol 50:50 vehicle, which proved to be more stable than the water-PG 50:50 vehicle, with the formulation remaining transparent following preparation.

Across all formulations that included a Tween surfactant, increasing the surfactant concentration decreased CHG permeability**.** This was not as clearly mirrored with the formulation containing Span 80 – there appears to be an increase in CHG permeability when the concentration of surfactant is increased from 0.5% w/v to 1% w/v, but further increases in surfactant concentration did not result in an increase in CHG permeability. All formulations failed to enhance CHG depth permeation compared to the experimental gel formulation containing CHG-PAMAM, and even compared to the experimental gel formulation containing CHG alone, without the addition of the dendrimer.

The trend of increasing surfactant concentration resulting in decreased CHG permeation into skin was likely due to the fact that concentrations of the surfactants used were above their CMC stated in the literature (Table 5.2), resulting in micelle formation. Increasing the concentration of surfactant beyond its CMC is understood to reduce the permeation enhancement effect due to encapsulation of the drug by micelles, reducing the thermodynamic activity of the drug (Scheuplein *et al.* 1970, Sarpotdar and Zatz 1986, Cappel and Kreuter 1991). However, the CMCs of surfactants are known to be increased in the presence of PG (Marszall and Van Valkenburg 1982), so this was thought to potentially reduce the incidence of micelle formation by a factor of 10. Sarpotdar and Zatz, (1986a) investigated the permeation of lidocaine from non-ionic surfactants in the presence of proplyene glycol. The study illustrated that increasing the PG concentration increased the CMC of each surfactant. This is supported by other studies which found that CMC is increased in the presence of PG, approximately by a factor of 10 (Aguiar and Weiner 1969, Pandey 2014). However, the evidence in Figure 5.6 and Figure 5.7-5.12 suggests micelle formation occurred in this study.

This does not necessarily mean that increasing the concentration of surfactant above its CMC will definitely result in reduced drug permeation, despite this being a known phenomenon. For example, Sarpotdar and Zatz, (1986a) reported enhanced permeation of lidocaine in the

presence of 1% Tween 20 and 40% PG. Furthermore, two studies (Shokri *et al.* 2001, Nokhodchi *et al.* 2003) illustrated that increasing concentrations of surfactant (0.5-5%) in the presence of a water:PG 50:50 vehicle increased the permeation of diazepam and lorazepam, respectively. One may attibute the increased drug delivery in these studies to the high concentration of PG. It's permeation enhancement effects are attributed to its co-solvent properties, ability to work synergistically with other permeation enhancers (Williams 2003e, Williams and Barry 2012) and interactions with *stratum corneum* lipids (Bouwstra, *et al.* 1991b). However, CHG was delivered to the skin in this study using a water:PG 50:50 vehicle (in the presence and absence of varying surfactant concentrations), therefore, one would expect the same permeation profile as the previous studies cited given that similar concentrations of PG were utilised. This was not the case. The physicochemical properties of the drugs may allow one to understand why the permeation enhancement of CHG was not increased in the presence of high concentrations of PG (in the presence and absence of surfactant), but the permeation of lidocaine, lorazepam and diazepam were all increased in similar vehicles (i.e., vehicles which included a high concentration of PG and in the presence of surfactants above their CMCs).

Table 5.11. Table indicating the log P and aqueous solubility of – CHG (Farkas *et al.* 2007, Sigma Aldrich 2019b), diazepam (Newton *et al.* 1981, Kempe, Metz and Mäder, 2008), lidocaine (Nakano 1979, Padula *et al* 2013) and lorazepam (Nokhodchi *et al.* 2003, van der Vossen *et al.* 2017, PubChem 2019c).

	Log P	**Aqueous Solubility**
CHG	0.0133	>70 %
Diazepam	2.92	0.004 %
Lidocaine	2.60	0.059 %
Lorazepam	2.40	0.008 %

Table 5. indicates that diazepam, lidocaine and lorazepam are drugs with low aqueous solubility and reasonaly high log P's, indicating that they may be considered reasonably liophilic, in

contrast to CHG. PG is understood to improve the solubility of topically applied drugs (Shokri *et al.* 2001, Trottet *et al.* 2004, Watkinson *et al.* 2009), and this may explain why permeation of the lipophilic drugs was enhanced by the inclusion of PG in the formulation, but not CHG.

It is proposed that PG enhanced the aqueous solubility of CHG, discouraging its partition into the *stratum corneum*. In Section 1.6 the role of thermodynamics in skin permeation was discussed. Briefly, a molecule will generally diffuse from a region of high concentration to a region of low concentration in accordance with Fick's Law (Equation 1). However, the molecules fugacity is influenced by its surrounding environment. For skin permeation studies, the partition coefficient plays a large role and aids in understanding how a molecule may permeate within the *stratum corneum* and into deeper skin layers.

Aqueous solubility is a desirable property of topically applied drugs when the applied vehicle is also aqueous, as a lack of aqueous solubility would correspond to minimal concentrations of drug solubilised in the vehicle available for diffusion into skin. Permeation enhancers such as PG that increase a drug's solubility are therefore useful where the drugs aqueous solubility is low. A lipophilic drug (such as diazepam, lidocaine or lorazepam) with an increased aqueous solubility due to the presence of PG is therefore able to partition into the *stratum corneum* in greater concentrations required for passive diffusion.

However, if the drug already exhibits a high aqueous solubility (such as CHG), increasing its aqueous solubility further may discourage the drug from partitioning away from the vehicle into an area of low aqueous solubility (*stratum corneum*). Thus, the thermodynamic gradient would be reduced (Section 1.6) and so would drug partitioning between the aqueous vehicle and the lipophilic *stratum corneum*. This theory is supported by Venuganti and Perumal (2008), who found that PAMAM-mediated permeation enhancement of a model hydrophilic drug (5FU) was governed by the partition coefficient. The enhancement in partition coefficient was greatest

from vehicles where the drug was least soluble (lipophilic vehicles), thus providing the thermodynamic driving force for drug partitioning into the skin.

If one assumes that this PG increases the aqueous solubility of CHG, increasing the solubility of CHG in the vehicle would further decrease the tendency of CHG to partition into the lipid *stratum corneum*, reducing the rate of percutaneous penetration. The presence of a more "water miscible" surfactant, Tween, may have further discouraged the drug from partitioning away from the vehicle where its solubility is high into the lipid *stratum corneum*. Upon the addition of a more "oil miscible" surfactant, Span, the drug may be more likely to partition away from this vehicle (than the CHG-Tween formulation) and into the *stratum corneum*. However, the *stratum corneum* is still highly likely to be the most lipophilic between the two phases (Span based formulation and *stratum corneum*); therefore permeation from this vehicle is still poor and hence why the permeation enhancement of CHG from this formulation is small.

This theory is supported by studies in the literature that indicate PG causes minimal permeation enhancement effects of hydrophilic drugs. For example, Touitou and Abed (1985) found that PG decreased the flux of 5FU when increasing concentrations were added to the aqueous system. Goodman and Barry (1988) found that PG was unable to enhance 5FU permeation from saturated aqueous solutions, without co-formulation with other permeation enhancers such as Azone and oleic acid. A later study (Goodman and Barry 1989) found that PG was able to enhance 5FU permeation when applied in a finite dose, and this was attributed to the fact that the previous study utilised a full hydrated *stratum corneum*, thus the effects of water may have masked the enhancement effects of PG. Nonetheless, PG was more effective when combined with other permeation enhancers than when used alone.

Non-ionic surfactants are belived to exert their permeation enhancement mechanism through fluidising and extraction of skin lipid components. Secondly, interaction within keratin filaments

may disrupt corneocyte cells (Breuer 1979, Walters 1990). Disruption of corneocyte cells may suggest the inability of cells to sufficiently adhere to tape strips, manifesting as a decreased mass of *stratum corneum* material removed on each tape strip, but this was found not to be the case. This suggests that, as the concentration of surfactants used in this study was above the CMC, insuficcient *stratum corneum* disruption occurred, potentially preventing CHG permeation enhancement. Whilst ideal from a patient perspective (as discussed previously in this chapter via TEWL and OCT data), the lack of CHG permeation enhancement from the CHG-surfactant systems prevents this from being a viable formulation.

There are several other possible reasons why the combination of CHG with the non-ionic surfactants may have failed to enhance the permeation of drug into the skin. The lack of permeation enhancement may be attributed to the fact that non-ionic surfactants are less able to enhance the permeation of drugs compared to their ionic counterparts. Yu *et al.* (1988) explored the effects of a number of vehicles on the percutaneous absorption of nicardipine and ketorolac in rhesus monkeys. The addition of Tween 20 to formulations did not enhance permeation of either drug. The use of rhesus monkeys as models for human skin in this study is acceptable as previous studies have shown that absorption of various compounds is similar across human and rhesus monkey skin (Wester and Maibach 1975, 1976). The legs, trunk and arms of rhesus monkeys are relatively hairless, similarly to humans and the same anatomical site can be used in both species (Wester and Maibach 1993). The use of rhesus monkeys as substitutes for human skin is limited due to the extra facilities and care required for experimentation with monkeys (Bronaugh *et al.* 1982).

Goodman and Barry (1989) investigated the permeation of 5FU using the various vehicles such as Azone® and decylmethyl sulphoxide in PG, water and oleic acid. They found that permeation of 5FU through human and snake skin was not enhanced by 0.1% w/v Tween 20 in saline. Aungst, Rogers and Shefter (1986) explored the effects of various adjuvants (non-ionic and ionic) in 10%

v/v PG on the flux of naloxone through human skin. Of 29 non-ionic adjuvants tested, three (Tween 20, Laureth 23 and Oleth 20) failed to enhance the flux of the drug compared to the control. The authors questioned how the mechanisms of action differ between adjuvants and whether skin penetration effects are selective for certain drugs. Cappel and Kreuter (1991) found that Tween surfactants only minimally increased the permeability of methanol, a hydrophilic permeant. Furthermore, the permeability of octanol decreased with increasing Tween 20, 21, 80 and 81 concentrations, believed to be due to a decrease in thermodynamic activity as a result of micelle formation.

CHG itself is moderately surface active and forms micelles in solution (Heard and Ashworth, 1968; Denton, 2001). The presence of surfactants may increase the rate of saturation at the interface and cause micelles to form. Interestingly, lidocaine also exhibits surfactant-like properties. (Leor *et al.* 1990). Speculatively, the presence of surfactants in addition to drugs which exhibit surfactant-like properties may increase the rate of saturation at the oil-water interface, thereby reducing the systems CMC. A mixed amphiphilic system can exhibit surface properties different from those of pure individual components (Azum *et al.* 2014). Where a mixed ampiphile system results in a lower CMC than that of pure components is so called a synergistic mixed micelle (Bakshi and Singh 2005, Kabir-ud-Din *et al.* 2012).

Finally, the lack of CHG permeation enhancement may be supporting evidence that CHG is incompatible, or its activity is reduced in the presence of non-ionic surfactants (Kostenbauder 1983, Nicoletti *et al.* 1993), however the formulations appeared stable throughout creation and use in *in vitro* experiments, unlike when combining the drug with SDS where the solution immediately turned cloudy. Owen (2006) states that CHX salts are compatible with most cationic and non-ionic surfactants, but in high concentrations CHX activity may be reduced due to micellar binding, but no specific concentration was provided in this study.

In conclusion, it appears that the permeation enhancement of CHG using non-ionic surfactants was limited by the formulation discouraging partitioning from the formulation into the skin surface, limiting drug diffusion across the *stratum corneum*. Furthermore, incompatibilities associated with CHG limited the choice of surfactants to those which are non-ionic, which are already understood to have only mild enhancement effects. Although the reduction in surface tension appears to be one of the main potential mechanisms of PAMAM dendrimer mediated CHG permeation enhancement, it appears that the reduction in surface tension exhibited by the surfactants used in this study was limited by micelle formation. This may be explored in the future by utilising concentrations of surfactant above and below the CMC to determine if there is a positive correlation between increasing surfactant concentration and CHG permeation (up to the point of CMC), although the concentrations of Tween/Span for this study would be minimal and practically difficult to include in formulations accurately. However, measurement of TEWL and OCT imaging would be required to compare these formulations to the CHG-PAMAM co-formulation, as a great advantage of the CHG-PAMAM co-formulation is its lack of barrier damage, which may not necessarily be the case with CHG-surfactant formulations due to the mechanism of non-ionic permeation enhancement.

CHG partitioning may have also been limited by enhanced drug solubility in the vehicle via inclusion of PG into the formulation, discouraging drug partitioning across the lipophilic *stratum corneum*. This does not necessarily mean dendrimer-mediated permeation enhancement is not due to surface tension effects. More likely, these surface tension effects are more pronounced than those given by non-ionic surfactants. Non-ionic surfactants appear to exert their mechanism *via* interaction with lipid bilayers and targeting keratin fibrils; from the OCT images it appears that a dendrimers-mediated decrease in surface tension does not focus on *stratum corneum* lipid disruption, moreover the solubilisation of the aqueous layer is more likely which could result in a change of the partition coefficient of this region of skin (Barry 1983). This is

agreeable with PAMAM dendrimer mediated enhancement of drugs delivered orally, where the PAMAM dendrimer increases the aqueous solubility of the drug to allow it to diffuse across intestinal epithelia.

5.6 Conclusion

The results of this study contributed towards the understanding of G3 PAMAM-NH_2 PAMAM dendrimer mediated CHG permeation enhancement into porcine skin. It appeared as though the dendrimer exerted its effects through a physical effect on the skin surface, and does not appear to encapsulate the drug but rather associates with it electrostatically.

Building upon previous studies (Sun *et al.* 2012, Judd 2013b), it appears that a synergistic reduction in surface tension and occlusion of the *stratum corneum* surface most likely influenced the permeation enhancement ability of the PAMAM dendrimer, though a lack of *stratum corneum* thickening in OCT images would suggest that a reduction in surface tension is the predominant mechanism. Disruption of the *stratum corneum* layer was minimal and so this was unlikely to contribute to the PAMAM dendrimers' mechanism of action. This is highly advantageous when considering that this formulation would have a low risk of skin irritation, often a contributing factor towards patient non-compliance (Pittet *et al.* 1999, Hugonnet *et al.* 2002, Pessoa-Silva *et al.* 2005). This suggests that the formulation would be clinically acceptable for clinical use for skin antisepsis prior to surgery.

There is a large scope for further investigation on how surfactants affect CHG permeation within skin. Although the surfactant is limited to the non-ionic type as CHG is incompatible with ionic materials, the vehicle in which the surfactant is formulated may be altered in an attempt to encourage CHG permeation from the vehicle into the *stratum corneum*. This study appeared to show that CHG permeation was limited by increased solubility via formulation with PG, which discouraged partitioning away from the aqueous vehicle into the *stratum corneum*. Therefore it may be of interest to formulate CHG in vehicles where it is exhibits lower aqueous solubility (such as IPM and MO, similarly to the Venuganti and Perumal (2008) study), to determine if this encourages drug partitioning into the *stratum corneum*.

6 Chapter 6 – Investigating the use of microneedles as a physical method of drug permeation enhancement

6.1 Introduction

In Chapter 3 and 4 it was shown that the skin permeation of CHG was enhanced by co-formulating the drug with a G3 PAMAM-NH_2 dendrimer. A 4% CHG-1 mM PAMAM co-formulation was found to significantly enhance the depth and amount of CHG permeating into porcine skin compared to Hibiscrub® (4% w/v), the commercial benchmark used in this study.

Chemical permeation enhancers should exhibit numerous properties in order to be considered "ideal" for use as an enhancer. These properties are listed in Section 1.11. Unfortunately, no permeation enhancer currently exists which fulfil all of these ideal criteria and as a result compromises must be made to ensure the compound-enhancer combination is efficacious whilst still considered acceptable for patient use. One of the ideal properties, that an enhancer is "compatible with numerous excipients and drugs" was not fulfilled by the PAMAM dendrimer, as precipitation of the drug following a 24 hr diffusion cell experiment (see Figure 3.2 and Figure 3.3) was observed. Whilst this precipitate did not prevent CHG penetration into skin and therefore is not considered an issue from an efficacy standpoint, the gritty texture and pearlescent appearance may be unpleasant from a patient perspective.

It was of interest to compare a physical method of permeation enhancement against the chemical method utilised within this thesis, particularly because utilising a physical method of permeation enhancement avoids the potential for incompatibilities with CHG. CHG has numerous incompatibilities, such as soaps, insoluble powders, insoluble compounds of zinc, magnesium and calcium and suspending agents such as tragacanth and alginates (McCarthy 1969, Yousef *et al.* 1973, McCarthy and Myburgh 1974) and is a useful model drug for comparing

chemical and physical methods of enhancement to determine if the two are directly comparable in terms of depth permeation of drug and homogeneity of permeation across the skin surface.

Microneedles (MNs) are a physical method of permeation enhancement. MNs create temporary holes within the skin through which the drug may bypass the major *stratum corneum* barrier. They have numerous advantages, explored in Section 1.13. In particular, MNs may be manufactured to a specific length, resulting in a specific depth permeation of a drug (Yan *et al.* 2010). MNs have yet to be used for the enhancement of CHG into deeper layers of porcine skin. This chapter aimed to use a solid MN pre-treatment step to enhance the permeation of CHG into porcine skin for the first time and to determine whether the permeation enhancement offered by MNs was comparable to the PAMAM dendrimer in terms of depth permeation of the drug and homogeneity of permeation enhancement.

6.2 Aims and Objectives

The aim of this study was to assess whether a solid MN pre-treatment was able to enhance the permeation of CHG into porcine skin. A secondary aim of this chapter was to assess whether the use of MNs as a physical method of permeation enhancement was comparable to the chemical method of permeation enhancement utilised in Chapter 3 in terms of depth permeation and homogeneity of drug delivery across the skin.

The objectives to complete this study were to:

1. Determine the most appropriate MN insertion device and needle length for CHG permeation
2. Investigate the effects of MN pre-treatment on the permeation of CHG into porcine skin using HPLC and ToF-SIMS
3. Determine the effects of MN array on CHG permeation into porcine skin using HPLC and ToF-SIMS
4. Compare HPLC and ToF-SIMS data from data gathered in Chapter 3 and 4 to determine if the physical and chemical methods of CHG permeation enhancement were considered comparable

6.3 Materials and Methods

6.3.1 Materials

Details of all formulation materials can be found in Section 2.3.3. Materials required for HPLC analysis and the HPLC method can be found in Section 3.3.3.6. Gentian violet 1% w/v solution was obtained from De La Cruz products, USA. A Derma stamp in the form of an electric pen (Dermapen®, TBPHP) was used to pierce the skin by vibrational motion prior to the application of the CHG based gel formulation. 12A and 36A MNs were purchased separately (TBPHP, Lot NC000513-4). A dermal manual stamp (Dermastamp™, 40A) was used to determine homogeneity of MN diameter and depth penetration compared to the Dermapen®. This was also purchased from TBPHP. PF used in the penetration depth study was purchased from Bemis, USA.

6.3.2 Methods

6.3.2.1 Homogeneity of MN diameter and depth penetration – gentian violet study

To determine the penetration of the Dermapen® in relation to the needle length selected, and to compare the needle depth penetration from a Dermpen® and Dermastamp™, skin was stained with 200 µL gentian violet 1% w/v solution post MN insertion (10 seconds). The dye was left on the skin surface for 50 min, after which excess dye was removed using a 70% alcohol wipe, following a staining protocol published by Al-Mayahy *et al*. (2019). Following gentian violet staining, samples were prepared for OCT using the protocol outlined in Section 4.3.2.3.

Cross sections were visualised using a Zeta Profilometer and the depth of the gentian violet permeation was measured.

6.3.2.2 Homogeneity of MN diameter and depth penetration – Parafilm® study

A study published by Larrañeta *et al.* (2014) detailed a method of estimating the diameter of MN holes. This method was replicated due to the potential for MN channel diameters to be overestimated by the gentian violet method (Coulman *et al.* 2011, Lutton *et al.* 2015). A sheet of PF was folded to give eight layers. PF was then placed upon a cork sheet for support and the Dermapen® was inserted into the PF for 10 seconds (green light, lowest setting). Following removal of the Dermapen® from the PF layers, each layer was separated, labelled and viewed under a light microscope. The diameters of five holes created by the MNs were measured on each layer to determine the consistency of holes created.

6.3.2.3 Permeation of CHG formulations with MN pre-treatment

The permeation of CHG from 1% w/v and 4% w/v CHG experimental gel formulations and Hibiscrub 4% w/v following MN pre-treatment (12A and 36A) was investigated. Skin samples were prepared in accordance with the protocol in Chapter 3. Prior to samples being mounted in the diffusion cell apparatus, samples were placed on a cork board for support and the Dermapen® was applied vertically to the skin at the lowest intensity (green light) for 10 seconds. After removal of the Dermapen®, the skin was immediately placed in between the diffusion cell apparatus and the formulation applied to the skin.

Diffusion cell experiments continued in accordance with the protocol outlined in Section 3.3.3. Samples were taken from the Franz cell receptor at specific time points over 24hr. Following the end of the diffusion cell experiment, tape stripping studies were completed for both HPLC and ToF-SIMS analysis (Sections 3.3.3.4 and 4.3.2.4). Samples were also set aside for cross section studies as outlined by the protocol in Section 4.3.2.3.

The *in vitro* diffusion cell experiments were repeated and this time horizontal cross sections were taken from the skin. There were two reasons for adopting this approach. Firstly, specific cross section images provided reason to doubt the ability of MNs to deliver a homogeneous layer of drug across the skin. Therefore horizontal cross sections would allow distribution of drug to be investigated on a magnified scale. Secondly, horizontal cross sections were taken in an attempt to view evidence of drug lateral diffusion, which has been debated amongst scientists (Johnson *et al.* 1997, Mitragotri 2003, Schicksnus and Müller-Goymann 2004, Gee *et al.* 2012). ToF-SIMS has never been used in this context and so if the technology could be used to find evidence of lateral diffusion, this would be a novel use of the ToF-SIMS imaging capabilities.

6.3.2.4 Statistical analysis of data

Means, standard deviation and standard error were all calculated in Microsoft Excel. Data within this chapter was analysed using either a One Way ANOVA (with Tukey's or Games-Howell post-hoc depending on the Levene's test result), or a Kruskal Wallis ANOVA (where the data was non-parametric) as outlined by the method detailed in Section 3.3.4.2. A value of $p < 0.05$ represented a statistical significant result.

6.4 Results

6.4.1 Homogeneity of MN depth penetration – gentian violet study

The depth permeation of MN channels stained with gentian violet was measured from each MN device (Dermapen® vs Dermastamp™) with differing needle lengths and needle arrays.

Table 6.1. Skin treatments for determining the effect of MN length and array on penetration. *n=3.*

Treatment	Array size
Dermapen® 750 µm	12
Dermapen® 750 µm	36
Dermapen® 1000 µm	12
Dermapen® 1000 µm	36
Dermastamp™ 1000 µm	40

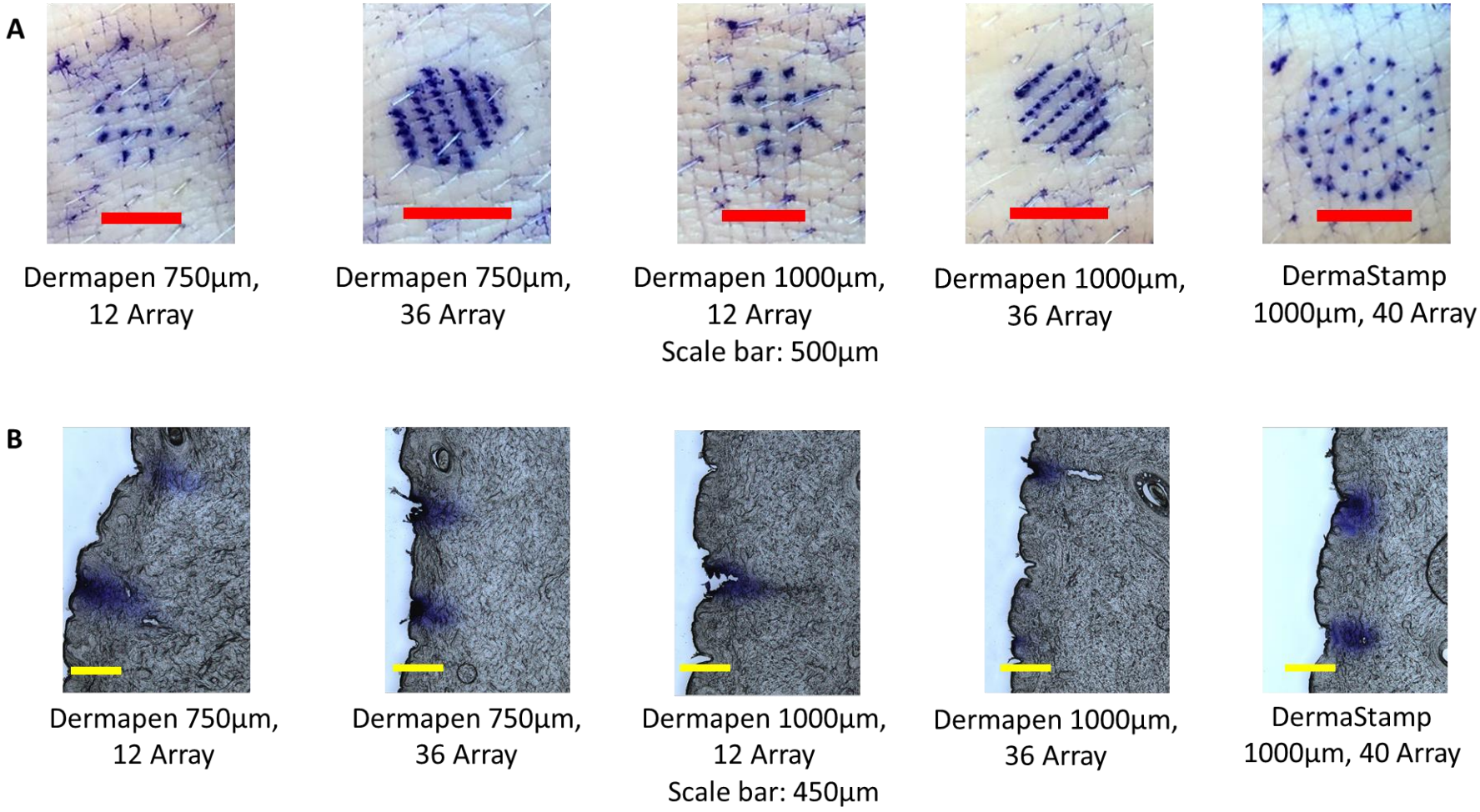

Figure 6.1. A. Appearance of skin samples following application of various MN devices. B. Appearance of gentian violet stained MN channels following application of various MN devices. *n=3.*

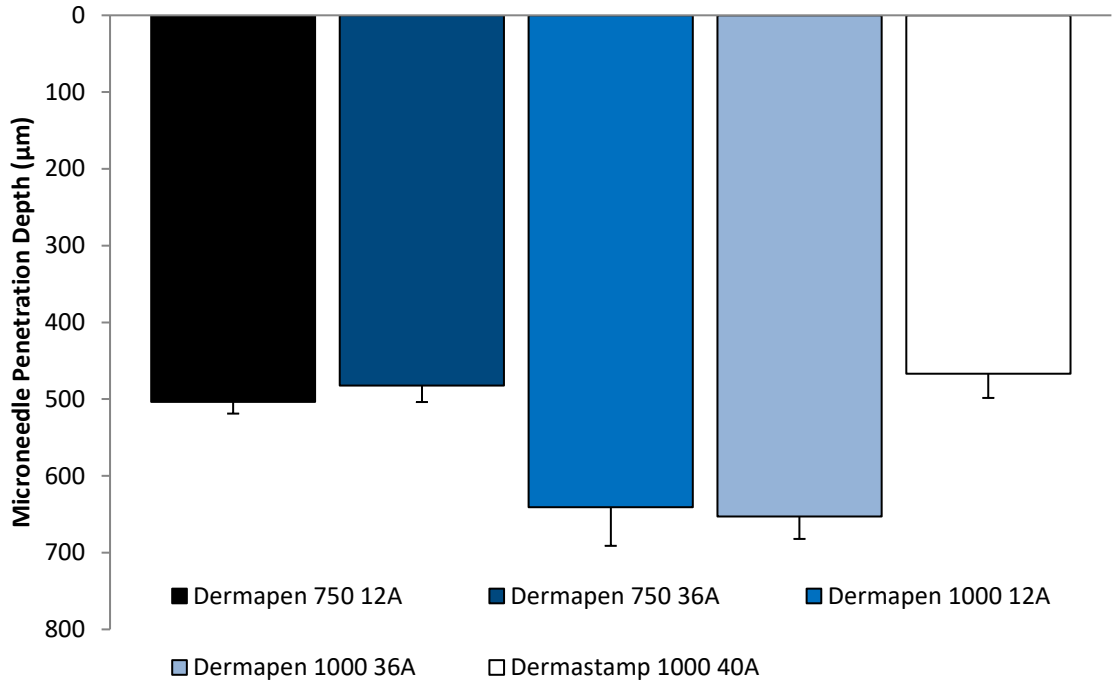

Figure 6.2. Depth penetration of MN channels from various MN devices, MN depth settings and MN arrays. "Zero" value is considered to be the outermost layer of skin, the *stratum corneum n=10 ± SE.*

The mean depth penetration was 503.42 ± 15.44 µm; 482.38 ± 21.39 µm; 640.95 ± 50.18 µm; 652.91 ± 29.24 µm; for the Dermapen® 750 µm 12A; Dermapen® 750 µm 36A; Dermapen® 1000 µm 12A and the Dermapen® 1000 µm 36A respectively. The mean MN channel depth was recorded as 467.06 ± 31.39 µm for the Dermastamp™ 1000 µm 40A. There was a noticeable increase of MN channel depth when the length of needle was increased from 750 µm to 1000 µm. There was no notable change in MN depth when the MN array was increased from 12A to 36A. Increasing MN channel depth with increasing needle length (750 µm vs 1000 µm) is expected, however both needle lengths failed to penetrate the dye to the depth specified. Despite this, the Dermapen® outperformed the Dermastamp™ - the 1000 µm 12A stamp delivered needles to a depth of 467.06 ± 31.39 µm, 532.94 µm lower than anticipated, whereas the 1000 µm 12A oscillating pen delivered needles to a depth of 640.95 ± 50.18 µm, 359.05 µm lower than anticipated. This was attributed to the ability of the oscillating pen to somewhat overcome the elastic nature of the skin.

A Kruskal Wallis ANOVA indicated that there was no statistically significant difference between the MN array (12A vs 36A) and the depth penetration of MNs ($p>0.05$), but there was a statistically significant difference between the MN length (750 µm vs 1000 µm) and the depth penetration of MNs ($p <0.05$).

6.4.2 Homogeneity of MN diameter and depth penetration – Parafilm® study

The diameter of the MN channel holes were measured by following a method outlined by Larrañeta *et al.* (2014). The Dermapen® was applied to 8 sheets of PF for 10 seconds (green light, lowest intensity setting). The study was repeated to include measurements from 250 µm, 500 µm, 750 µm and 1000 µm needle lengths at both 12 and 36 array. The diameter of MN channels was measured using a light microscope at 10 × magnification. 5 MN channels were measured on each layer to provide a mean measurement.

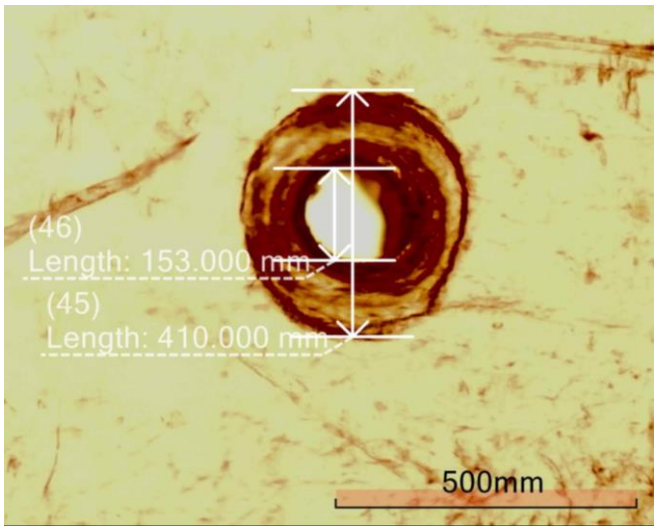

Figure 6.3. Visualisation of a MN channel viewed using light microscope at 10 × magnification. The inner diameter was measured (153 mm) for the graphs created for Figure 6.4. Inner diameters were measured from the widest point. ***MN channel from a Dermapen®, 750 µm, 12A, PF sheet 1.***

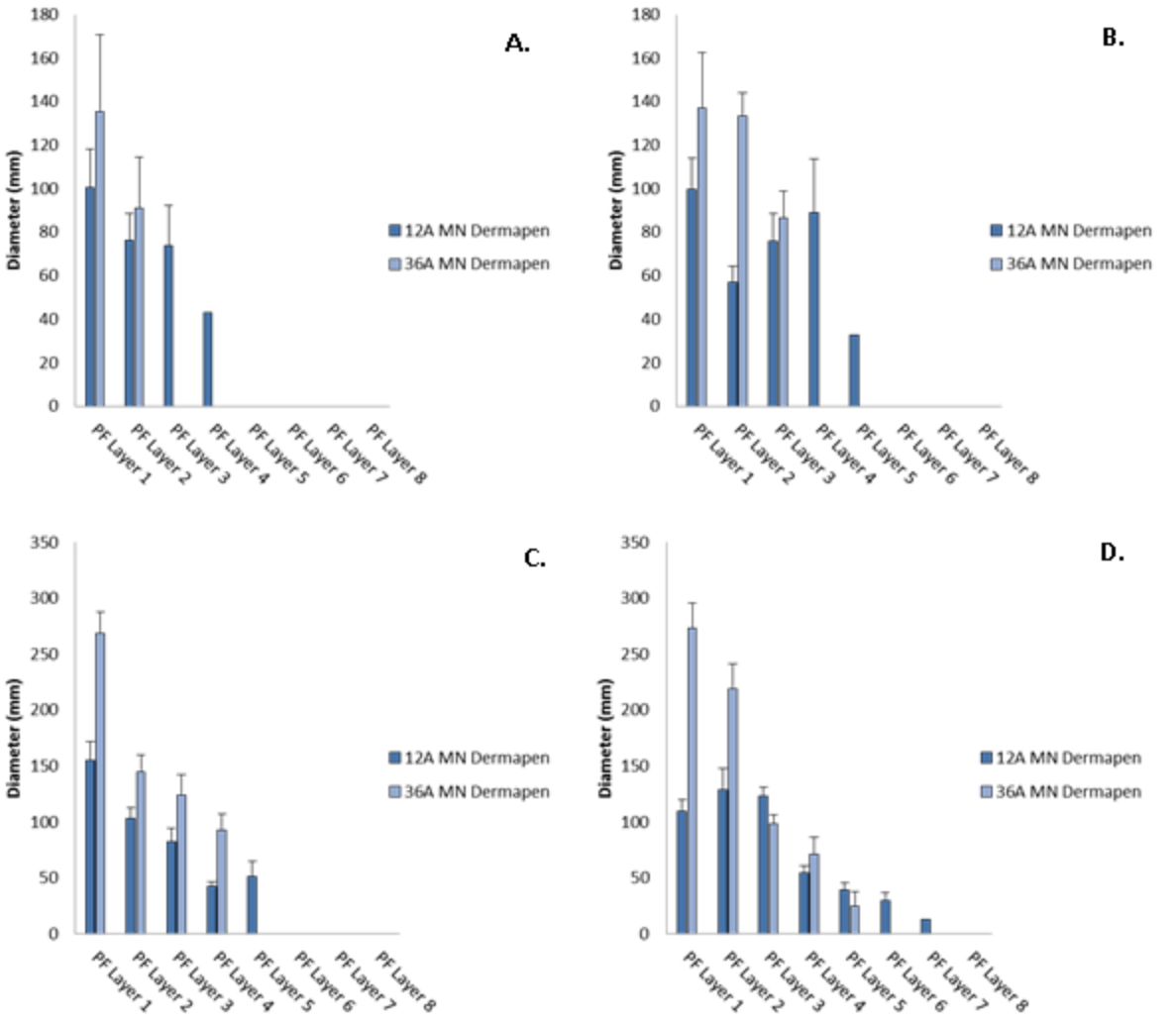

Figure 6.4. MN diameter measurements on each PF layer from a Dermapen® MN device with varying needle length. A. 250 µm, B. 500 µm, C. 750 µm, D. 1000 µm, *n=4 ± SE*.

The mean diameter for the 250 µm MN length on PF layer 1 was 100.5 ± 17.5 mm and 135.6 ± 35.3 mm for the 12A and 36A respectively. The mean diameter of the MN channel on the final PF layer which was detectable was 43.2 ± 10.5 mm (PF layer 4) and 90.9 ± 23.6 mm (PF layer 2) for the 12A and 36A respectively. The mean diameter for the 500 µm MN length on PF layer 1 was 99.8 ± 14.2 mm and 137.2 ± 25.4 mm for the 12A and 36A respectively. The mean diameter of the MN channel on the final PF layer which was detectable was 33.0 ± 3.0 mm (PF layer 5) and 86.5 ± 12.5 mm (PF layer 3) for the 12A and 36A respectively. The mean diameter for the 750 µm MN length on PF layer 1 was 154.6 ± 16.6 mm and 268.5 ± 18.9 mm for the 12A and 36A respectively. The mean diameter of the MN

channel on the final PF layer which was detectable was 51.1 ± 13.8 mm (PF layer 5) and 93.9 ± 13.6 mm (PF layer 4) for the 12A and 36A respectively. The mean diameter for the 1000 µm MN length on PF layer 1 was 109.6 ± 10.2 mm and 273.1 ± 22.7 mm for the 12A and 36A respectively. The mean diameter of the MN channel on the final PF layer which was detectable was 12.3 ± 0.0 mm (PF layer 7) and 24.66 ± 12.5 mm (PF layer 5) for the 12A and 36A respectively.

There was a general trend of decreasing MN diameter with increasing PF layer. There was also a general trend observed whereby increasing the MN length increased the appearance of MN perforation on deeper PF layers. For each graph, the diameter of the MN channel was wider from the 36A MN array than the 12A MN array on the first few layers of PF. Following the first 1-2 PF layers, the diameter of the MN channels appeared similar for both MN arrays.

In addition to MN diamater measurements, the PF study provided MN depth penetration measurements. The depth permeation of MNs from both the PF and gentian violet study were compared to determine whether the PF study was a useful predictor of MN depth penetration.

Table 6.2. Approximate depth permeation of 12A and 36A MNs of differing lengths (250-1000µm) according to the number of PF layers permeated, assuming a single PF layer is equal to 127µm thickness, *n=4*.

	Mean depth permeation (µm)	
MN needle Length (µm)	**12A**	**36A**
250	508	254
500	635	381
750	635	508
1000	889	635

Table 6.3. Depth permeation of 12A and 36A MNs of differing lengths (750-1000 µm) – comparison of gentian violet dyed porcine skin and the eight layer PF study, assuming a single PF layer is equal to 127 µm thickness, *n=4*.

	Mean Depth Permeation (µm)			
	12A		36A	
MN needle Length (µm)	Porcine Skin	Parafilm®	Porcine Skin	Parafilm®
750	503.4	635.0	482.4	508.0
1000	641.0	889.0	652.9	635.0

The depth penetration of the MN channels was somewhat comparable between the porcine skin study and the PF study, however unlike a previous study (Larrañeta *et al.* 2014) which noted that MN channels created by piercing PF presented slightly lower penetration depths compared to neonatal porcine skin, the majority of the MN channels created in this study by piercing PF presented higher penetration depths when compared to the channels measured from gentian violet stained porcine skin. There was a statistically significant difference in the MN depth permeation between porcine skin and PF for both the 750 µm 12A and 1000 µm 12A needle lengths and arrays ($p < 0.05$)

6.4.3 Permeation of CHG from gel formulations following MN pre-treatment

Franz-type diffusion cell studies were performed to determine how the MN array affected the permeation of experimental and commercial CHG gel formulations into porcine skin. The results were collected and compared to the "no MN" datasets, which can be found in Chapter 3. Firstly, the patterns within groups were interpreted (all 12A groups compared, then all 36A groups compared), finally all MN data was compared to the "no MN" datasets.

The permeation of CHG from the 4% w/v, 12A MN pre-treatment group was greater from tape strips 1-2, but the permeation of CHG from both 1% w/v CHG 12A and 4% w/v CHG 12A MN pre-treatment groups was found to be similar from tape strip 3 onwards. Similarly when comparing CHG permeation within 36A MN groups, the permeation of CHG from the 4% w/v 36A MN pre-treatment group is

superior to the 1% w/v CHG 36A MN pre-treatment group on tape strips 1 and 2 only. Following this, the permeation of CHG from both 1% w/v and 4% w/v formulations was found to be similar, with both experimental formulations delivering significantly more CHG onto all tape strips compared to the Hibiscrub 4% w/v 36A MN pre-treatment.

When comparing the MN datasets to the "no MN" data in Chapter 3, in general the addition of a 12A MN pre-treatment enhanced the depth permeation of CHG from each group (experimental and commercial), and increasing the MN array from 12A to 36A further increased the depth permeation of CHG. However, there are some inconsistencies with this trend. For example, in deeper tape strips (> tape strips 3) for the 4% w/v CHG and Hibiscrub 4% w/v datasets, there appears to be minimal difference between the "no MN" data and the 12A MN pre-treatment. It is not until the use of 36A MN is employed that the depth permeation of CHG largely increases across all tape strips. This is reflected in the statistical data which can be found in Table 6.4.

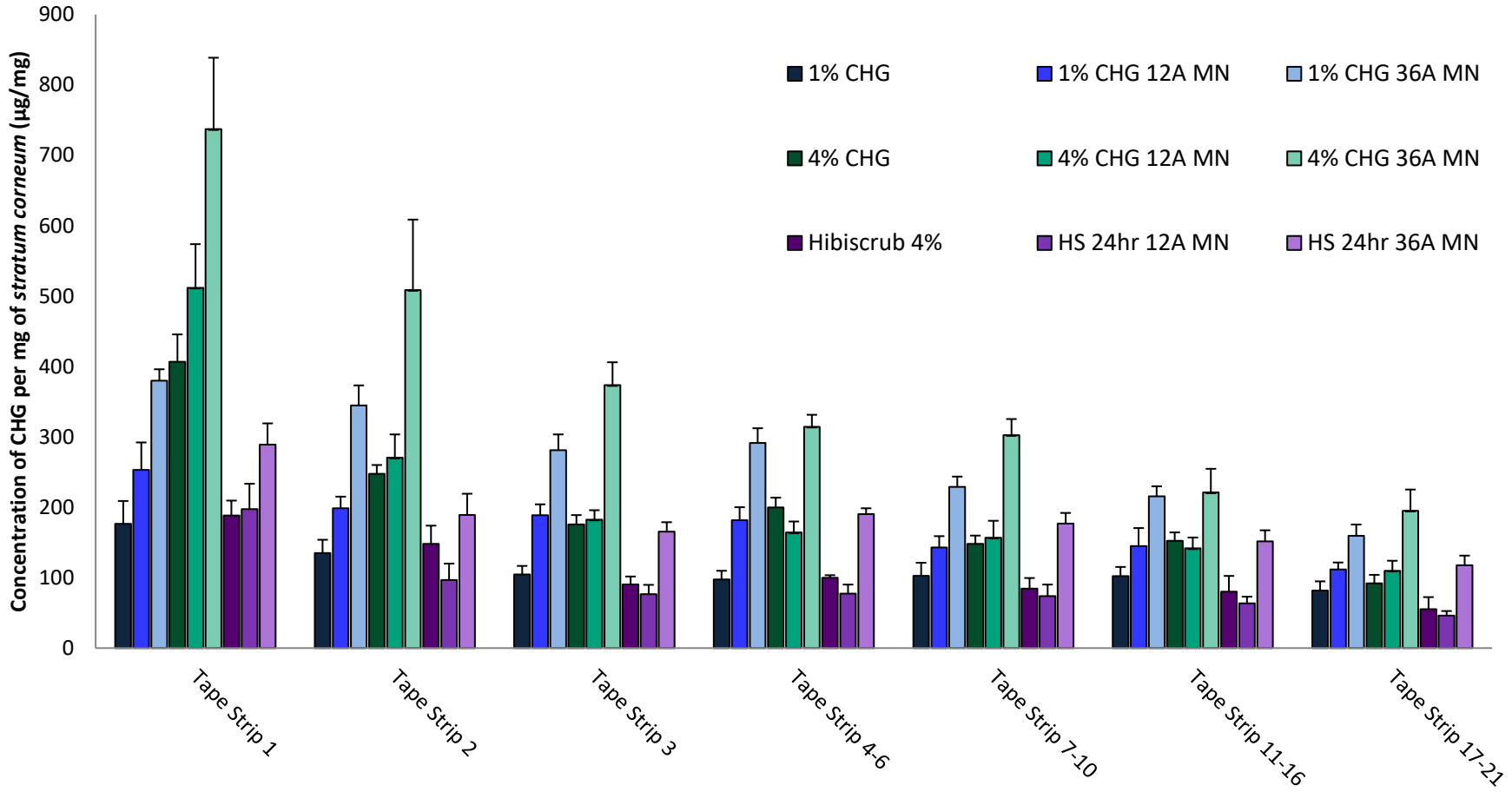

Figure 6.5. Comparative graphical data illustrating the concentration of CHG found in tape strips 1-21 from treatment groups 1% and 4% CHG, Hibiscrub 4%. Data compares the CHG concentration from porcine skin treated with formulation only, formulation following a 12A 750 µm solid MN pre-treatment or formulation following a 36A 750 µm solid MN pre-treatment, *n=4 ± SE*.

Table 6.4. Analytical tests chosen to determine whether formulations significantly affect the depth permeation of CHG within porcine skin – HPLC data – comparing no MN, 12A MN and 36A MN treatment groups and reporting the resulting pairwise comparisons which resulted in a statistically significant result ($p < 0.05$). Pairwise comparisons are arranged so that the formulation which developed the highest concentration of CHG is given first. ***KW – Kruskal Wallis; OWA – One-Way ANOVA, n=4.***

Tape Strip Number	Analytical Test	Statistically Significant Result	Pairwise Comparisons	
			F1	F2
Tape Strip 1	KW	Y	4% CHG, 12A	Hibiscrub 4%, 12A
			4% CHG, 36A	Hibiscrub 4%, 36A
			4% CHG, 12A	1% CHG
			4% CHG, 12A	1% CHG
			4% CHG, 36A	1% CHG
			4% CHG, 36A	Hibiscrub 4%, 12A
			4% CHG, 36A	Hibiscrub 4%
Tape Strip 2	KW	Y	4% CHG, 12A	Hibiscrub 4%, 12A
			4% CHG, 36A	Hibiscrub 4%, 36A
			1% CHG, 36A	1% CHG
			1% CHG, 36A	Hibiscrub 4%, 12A
			4% CHG, 36A	1% CHG
			4% CHG, 36A	Hibiscrub 4%
			4% CHG, 36A	Hibiscrub 4%, 12A

Tape Strip Number	Analytical Test	Statistically Significant Result	Pairwise Comparisons	
			F1	F2
Tape Strip 3	OWA	Y	4% CHG, 12A	Hibiscrub 4%, 12A
			1% CHG, 12A	Hibiscrub 4%, 12A
			4% CHG, 36A	Hibiscrub 4%, 36A
			4% CHG, 36A	1% CHG, 36A
			1% CHG, 36A	Hibiscrub 4%, 36A
			4% CHG, 12A	Hibiscrub 4%
			1% CHG, 12A	1% CHG
			1% CHG, 36A	1% CHG
			1% CHG, 36A	4% CHG
			1% CHG, 36A	Hibiscrub 4%
			1% CHG, 36A	4% CHG, 12A
			1% CHG, 36A	Hibiscrub 4%, 12A
			4% CHG, 36A	1% CHG
			4% CHG, 36A	4% CHG
			4% CHG, 36A	Hibiscrub 4%
			4% CHG, 36A	1% CHG, 12A
			4% CHG, 36A	4% CHG, 12A
			4% CHG, 36A	Hibiscrub 4%, 12A
			Hibiscrub 4%, 36A	Hibiscrub 4%, 12A

Tape Strip Number	Analytical Test	Statistically Significant Result	Pairwise Comparisons	
			F1	F2
Tape Strips 4-6	OWA	Y	4% CHG, 12A	Hibiscrub 4%, 12A
			1% CHG, 12A	Hibiscrub 4%, 12A
			4% CHG, 36A	Hibiscrub 4%, 36A
			1% CHG, 36A	Hibiscrub 4%, 36A
			4% CHG	Hibiscrub 4%, 12A
			1% CHG, 12A	1% CHG
			4% CHG, 12A	1% CHG
			1% CHG, 36A	1% CHG
			1% CHG, 36A	4% CHG
			1% CHG, 36A	Hibiscrub 4%
			1% CHG, 36A	1% CHG, 12A
			1% CHG, 36A	4% CHG, 12A
			1% CHG, 36A	Hibiscrub 4%, 12A
			4% CHG, 36A	1% CHG
			4% CHG, 36A	4% CHG
			4% CHG, 36A	Hibiscrub 4%
			4% CHG, 36A	1% CHG, 12A
			4% CHG, 36A	4% CHG, 12A
			4% CHG, 36A	Hibiscrub 4%, 12A
			Hibiscrub 4%, 36A	1% CHG
			Hibiscrub 4%, 36A	Hibiscrub 4%
			Hibiscrub 4%, 36A	Hibiscrub 4%, 12A

Tape Strip Number	Analytical Test	Statistically Significant Result	Pairwise Comparisons	
			F1	F2
Tape Strip 7-10	OWA	Y	4% CHG, 36A	Hibiscrub 4%, 36A
			4% CHG, 36A	1% CHG, 36A
			4% CHG	Hibiscrub 4%, 36A
			1% CHG, 36A	1% CHG
			1% CHG, 36A	4% CHG
			1% CHG, 36A	Hibiscrub 4%
			1% CHG, 36A	1% CHG, 12A
			1% CHG, 36A	4% CHG, 12A
			1% CHG, 36A	Hibiscrub 4%, 12A
			4% CHG, 36A	1% CHG
			4% CHG, 36A	4% CHG
			4% CHG, 36A	Hibiscrub 4%
			4% CHG, 36A	1% CHG, 12A
			4% CHG, 36A	4% CHG, 12A
			4% CHG, 36A	Hibiscrub 4%, 12A
			Hibiscrub 4%, 36A	1% CHG
			Hibiscrub 4%, 36A	Hibiscrub 4%
			Hibiscrub 4%, 36A	Hibiscrub 4%, 12A

Tape Strip Number	Analytical Test	Statistically Significant Result	Pairwise Comparisons	
			F1	F2
Tape Strips 11-16	OWA	Y	4% CHG, 12A	Hibiscrub 4%, 12A
			1% CHG, 12A	Hibiscrub 4%, 12A
			4% CHG, 36A	Hibiscrub 4%, 36A
			1% CHG, 36A	Hibiscrub 4%, 36A
			4% CHG	Hibiscrub 4%, 12A
			1% CHG, 36A	1% CHG
			1% CHG, 36A	Hibiscrub 4%
			1% CHG, 36A	Hibiscrub 4%, 12A
			4% CHG, 36A	1% CHG
			4% CHG, 36A	Hibiscrub 4%
			4% CHG, 36A	4% CHG, 12A
			4% CHG, 36A	Hibiscrub 4%, 12A
			Hibiscrub 4%, 36A	Hibiscrub 4%, 12A

Tape Strip Number	Analytical Test	Statistically Significant Result	Pairwise Comparisons	
			F1	F2
Tape Strips 17-21	KW	Y	4% CHG, 12A	Hibiscrub 4%, 12A
			1% CHG, 12A	Hibiscrub 4%, 12A
			1% CHG, 36A	1% CHG
			1% CHG, 36A	Hibiscrub 4%, 12A
			4% CHG, 36A	1% CHG
			4% CHG, 36A	Hibiscrub 4%
			4% CHG, 36A	Hibiscrub 4%, 12A
Total Tape Strips	KW	Y	4% CHG, 12A	Hibiscrub 4%, 12A
			4% CHG, 36A	Hibiscrub 4%, 36A
			4% CHG	Hibiscrub 4%, 12A
			1% CHG, 36A	1% CHG
			1% CHG, 36A	Hibiscrub 4%
			1% CHG, 36A	Hibiscrub 4%, 12A
			4% CHG, 12A	1% CHG
			4% CHG, 12A	Hibiscrub 4%
			4% CHG, 36A	1% CHG
			4% CHG, 36A	4% CHG
			4% CHG, 36A	Hibiscrub 4%
			4% CHG, 36A	1% CHG, 12A
			4% CHG, 36A	Hibiscrub 4%, 12A
			Hibiscrub 4%, 36A	Hibiscrub 4%, 12A

6.4.4 Permeation of CHG from experimental gel formulations following MN pre-treatment – tape strip study analysed using ToF-SIMS

The tape strip images (Figure 6.6 and Figure 6.7) followed the trends already established in Chapter 4. For example, the blank tape showed no evidence of CHG permeation; there was a general observed trend of decreasing CHG ion intensity with increasing tape strip number and decreasing amount of *stratum corneum* on each tape strip with increasing tape strip number. The cholesterol Ion ($C_{27}H_{45}SO_4^-$) and phosphite ion (PO_3^-) were analysed alongside the CHG ion ($C_7H_4N_2Cl^-$) to indicate the *stratum corneum* and the viable epidermal junction respectively. There is an overall trend of increasing evidence of the PO_3^- ion with increasing tape strip number, likely indicating that the tape strips of increasing number are removing cells that are closer to the epidermis. There appears to be no real relationship between tape strip number and cholesterol ion – the intensity of this ion appears similar across all tape strips, indicating that the tape strips contain cells that are indicative of upper skin layers. The visualisation of these secondary ion fragments helps to identify which region of skin each tape strip is removing cells from.

Ions indicative of biological tissue (indicated by the CN^- ion) were used to threshold the image against the tape strip adhesive, ensuring only drug that had absorbed into biological tissue was analysed. The ToF-SIMS images in this chapter are all presented following selection of the ROI that represents *stratum corneum* material and normalisation according to total ion intensity.

When considering trends for this specific data set, the tape strip images appear in the majority to agree with the HPLC data (Figure 6.5 vs. Figure 6.7). Visually, there appears to be little difference in CHG permeation on each tape strip between the 1% w/v CHG and 1% w/v CHG MN 12A, and again between 4% w/v CHG and 4% w/v CHG 12A, however there is a clear visual increase in CHG ion intensity when the MN array is increased to 36 needles. Furthermore, both experimental formulations appear to deliver more CHG onto each tape strip than the Hibiscrub 4% w/v group, even with MN pre-

treatment. The 4% w/v CHG 36A MN pre-treatment group appears to deliver more CHG onto tape strips 6, 9 and 12 compared to the same tape strips in the 1% w/v CHG MN 36A pre-treatment group, but this conclusion could not be confirmed without the use of the "batch statistics" tool to transform the data into ion intensity values. The tape strip images provided information on the distribution of the CHG ion within each tape strip. It appeared that distribution was mostly homogeneous, however there were bright spots particularly visible in the 1% w/v CHG 36A group (tape strips 6-12), and indicating that CHG distribution following a solid MN pre-treatment was not necessarily homogeneous in deeper layers of the skin.

In accordance with the protocol in Chapter 4, the tape strip images were divided into four ROI's (Figure 4.2) and the ion intensity values for each ROI were plotted as a function of tape strip number. This allowed the qualitative tape strip images to be transformed into semi-quantitative ion intensity data that could be compared to the quantitative HPLC data in Section 3.4.6.

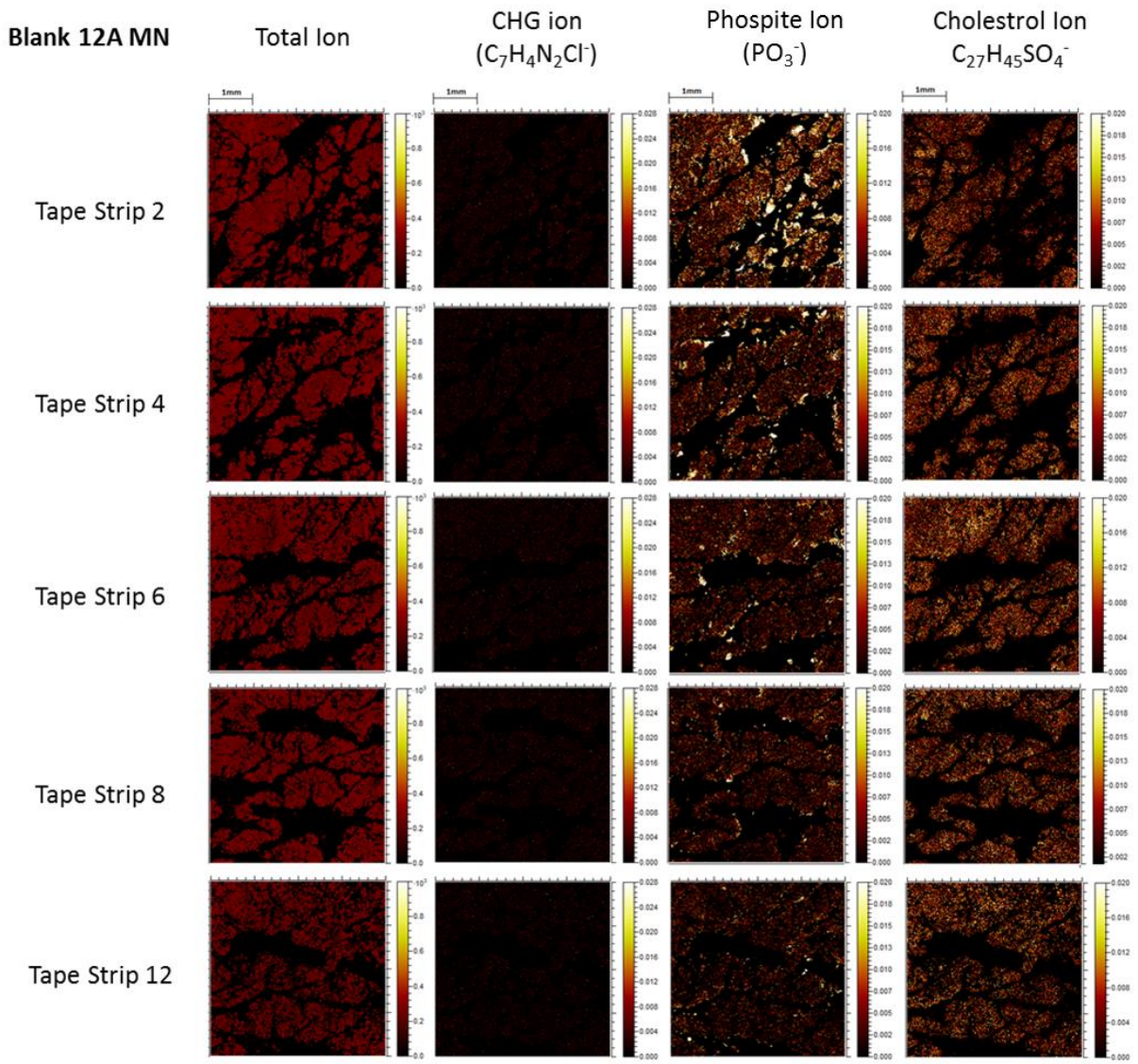

Figure 6.6. Distribution of ions $C_7H_4N_2Cl^-$ (drug), PO_3^- (phosphite) and $C_{27}H_{45}SO_4^-$ (cholesterol) in untreated skin. Images were rebuilt to account for *stratum corneum* material only and the ion intensity was normalised to the total ion within the region of interest to ensure ion intensity was representative of *stratum corneum* material.

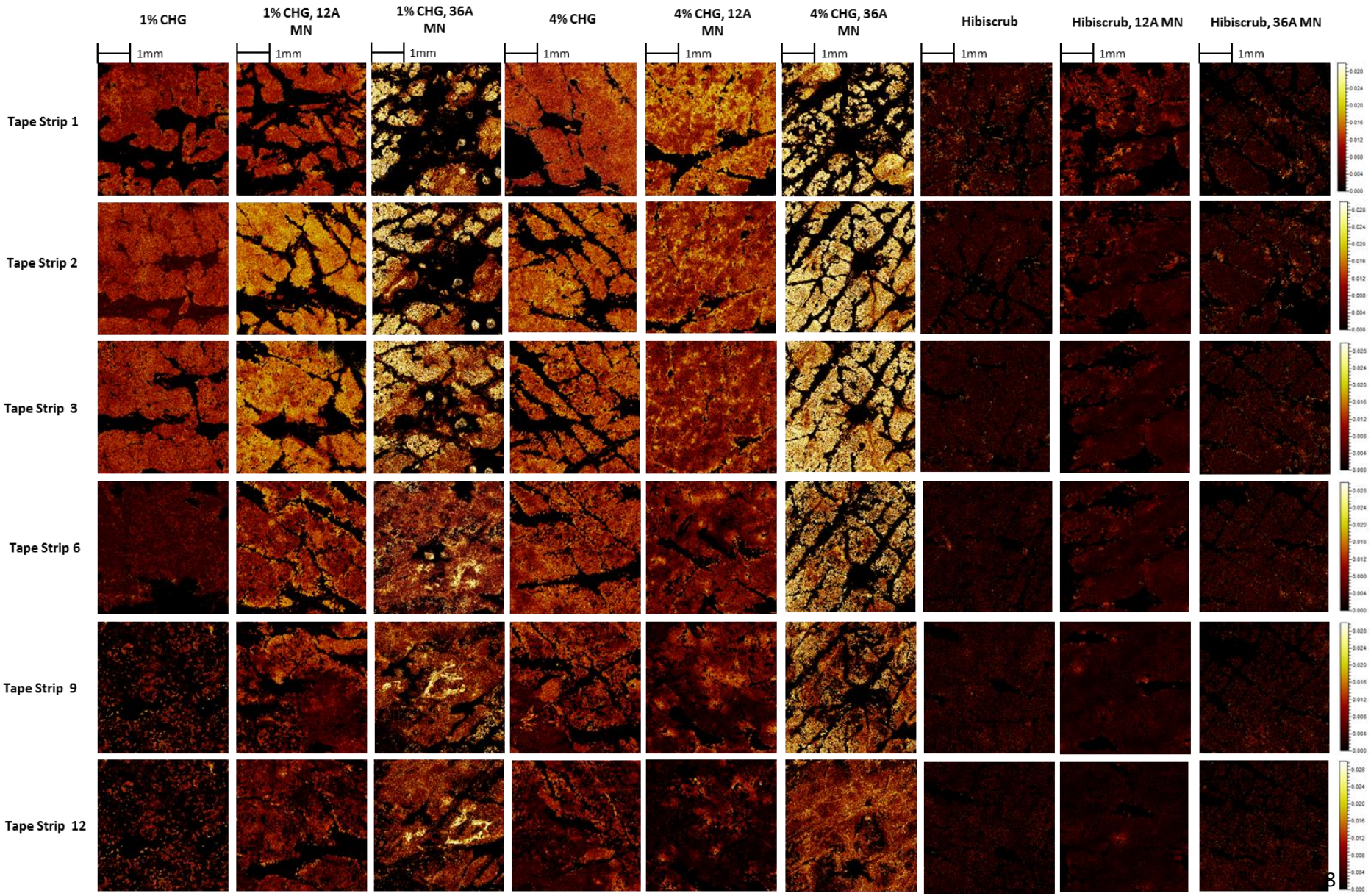
1% CHG
1% CHG, 12A MN
1% CHG, 36A MN
4% CHG
4% CHG, 12A MN
4% CHG, 36A MN
Hibiscrub
Hibiscrub, 12A MN
Hibiscrub, 36A MN
1mm
Tape Strip 1
Tape Strip 2
Tape Strip 3
Tape Strip 6
Tape Strip 9
Tape Strip 12

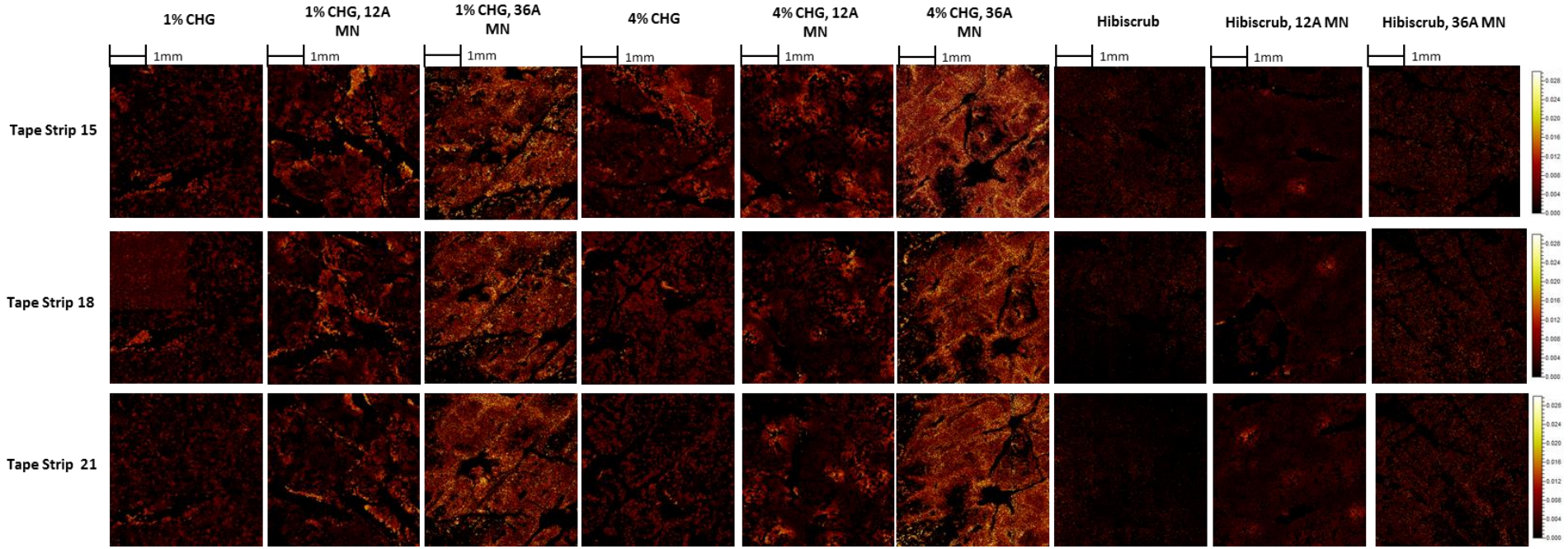

Figure 6.7. CHX ion $C_7H_4N_2Cl^-$ ion intensity across porcine skin treated with either experimental 1% or 4% CHG formulations, or the commercial benchmark Hibiscrub. Data compares the CHG ion intensity from porcine skin treated with formulation only, formulation following a 12A 750 µm solid MN pre-treatment or formulation following a 36A 750 µm solid MN pre-treatment.

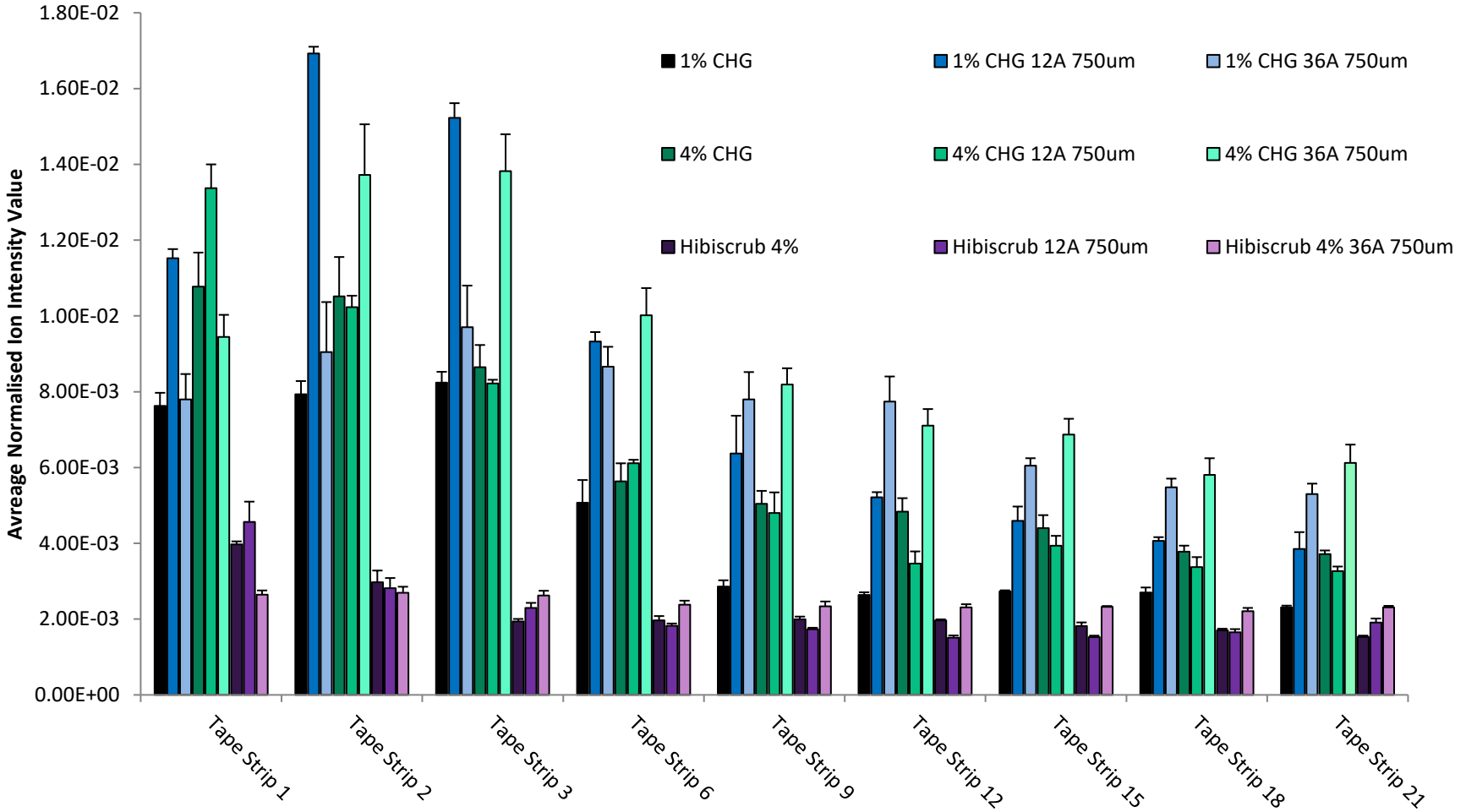

Figure 6.8. Quantified mean ion intensity values for tape strips 1, 2, 3, 6, 9, 12, 15, 18, 21 from treatment groups 1% and 4% CHG, Hibiscrub 4%. Areas normalised by total ion intensity. Data compares the CHG ion intensity from porcine skin treated with formulation only, formulation following a 12A 750 µm solid MN pre-treatment or formulation following a 36A 750 µm solid MN pre-treatment, *n=4± SE*.

The ion intensity value data and associated statistics also agreed with the preceding datasets in general. Increasing tape strip number decreased CHG ion intensity, and adding a 12A MN pre-treatment step minimally enhanced CHG ion intensity compared to the "no MN" datasets, however increasing the needle array to 36 needles had a more significant impact on CHG ion intensity. The commercial benchmark remained a poor competitor to the experimental formulations tested, even compared to the 1% w/v CHG experimental formulation which applied a lower concentration of drug to the skin surface than the commercial product.

The statistical data largely supported the HPLC statistical data and showed that ultimately, the 4% w/v CHG 36A MN group delivered the most CHG onto tape strips and generally, a MN pre-treatment step enhanced CHG depth permeation compared to no MN pre-treatment. At times, no MN pre-treatment enhanced CHG permeation to a greater extent than a MN pre-treatment. For example, the ion intensity value data indicated that 4% w/v CHG (no MN pre-treatment) delivered significantly more CHG onto tape strip 9 than Hibiscrub 12A or 36A. This again indicates the poor permeation of CHG from the commercial benchmark.

6.4.5 Permeation of CHG from gel formulations following MN pre-treatment – cross section study analysed using ToF-SIMS

The data reported in Figure 6.9 provides a typical cross section from each group to allow visual comparisons to be made. Similarly to Chapter 4, the cross section images followed the trend whereby the CHG ion intensity was largely limited to the *stratum corneum* with minimal permeation past these upper skin layers. There appeared to be little visual difference in CHG permeation between the 1% w/v and 4% w/v 12A MN pre-treatment groups, however there was a clear difference when comparing the 1% w/v and 4% w/v 12A MN pre-treatment groups to the Hibiscrub 4% w/v pre-treatment group. The thickness of the CHG ion band appeared to be

thinner for the Hibiscrub 4% w/v 12A MN pre-treatment group. Furthermore, the CHG ion band across the *stratum corneum* for the 1% w/v and 4% w/v 12A MN pre-treatment group appeared clear, without any gaps in intensity, whereas there appeared to be gaps in CHG ion intensity for the Hibiscrub 4% w/v 12A MN pre-treatment group.

In general, the cryosection images from the 36A MN group appeared less clear than those from the 12A MN pre-treatment group. This is particularly obvious when viewing the Hibiscrub 4% w/v 36A MN cross section, where there was no clear green line of CHG ion intensity that was visible in the Hibiscrub 4% w/v 12A MN cross section. There appeared to be some accumulation of CHG in skin furrows (Figure 6.9, 1% w/v CHG, 36A MN cross section). The 4% w/v CHG 36A MN pre-treatment group cross sections showed a definite lack of homogeneity of the CHG ion. Bright spots of CHG ion intensity appeared within the dermis of the 4% w/v CHG, 36A cross section. This is important to consider in view of the potential for incomplete antisepsis if areas of skin are left without sufficient CHG permeation to provide an adequate antiseptic effect. In light of this, depth permeation data was not provided using the "Line Scan" function as in Chapter 4, as the results would not be consistent depending on which horizontal section (which is chosen manually) of the cross section image was analysed.

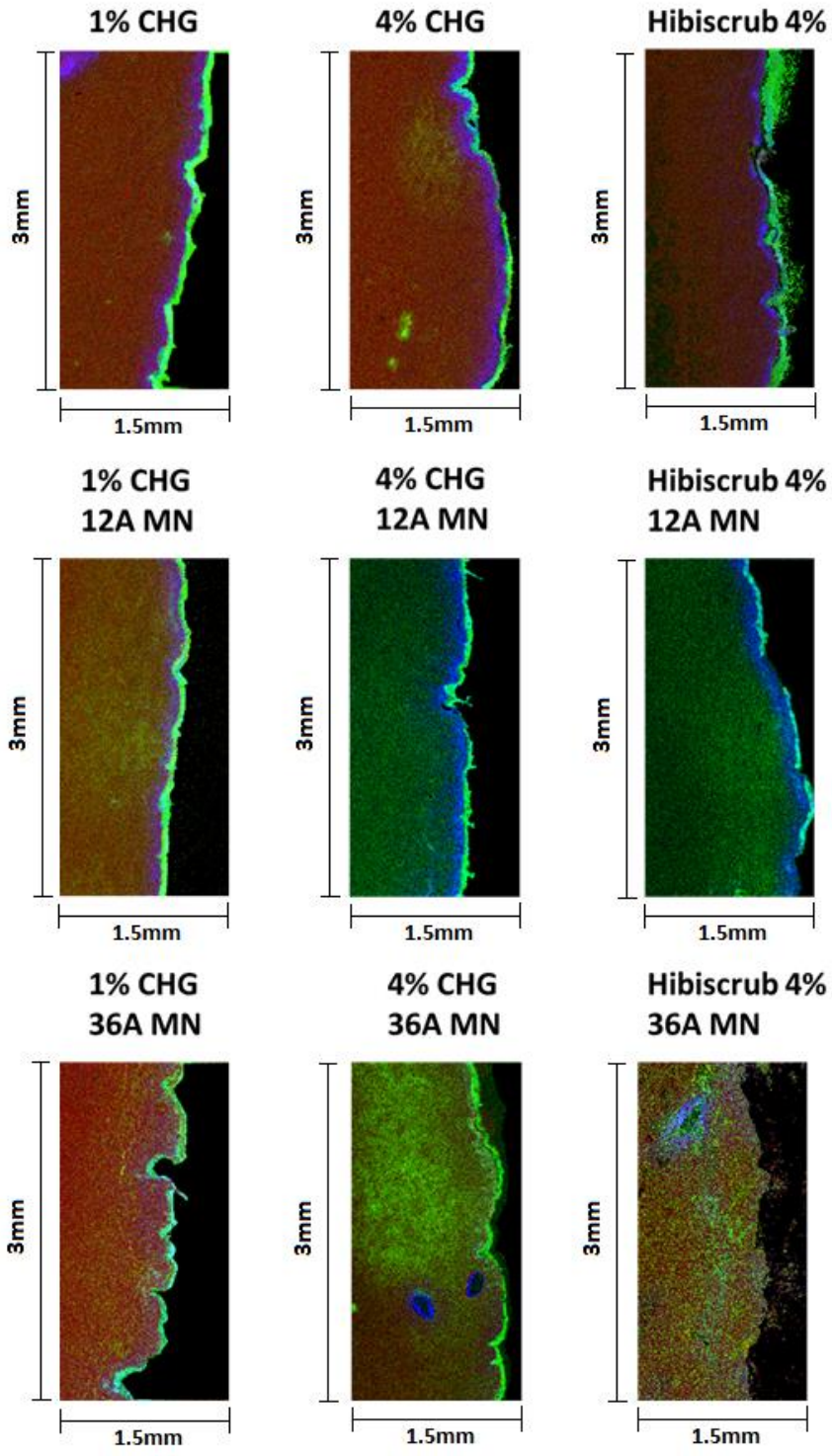

Figure 6.9. ToF-SIMS images of CHG ($C_7H_4N_2Cl^-$, green colour), phosphite (PO_3^-, red colour) and cholesterol ($C_{27}H_{45}SO_4^-$, blue colour) overlaid to indicate CHG depth permeation within porcine skin treated following various 24 hr formulation treatments with and without the use of solid MNs as a skin pre-treatment.

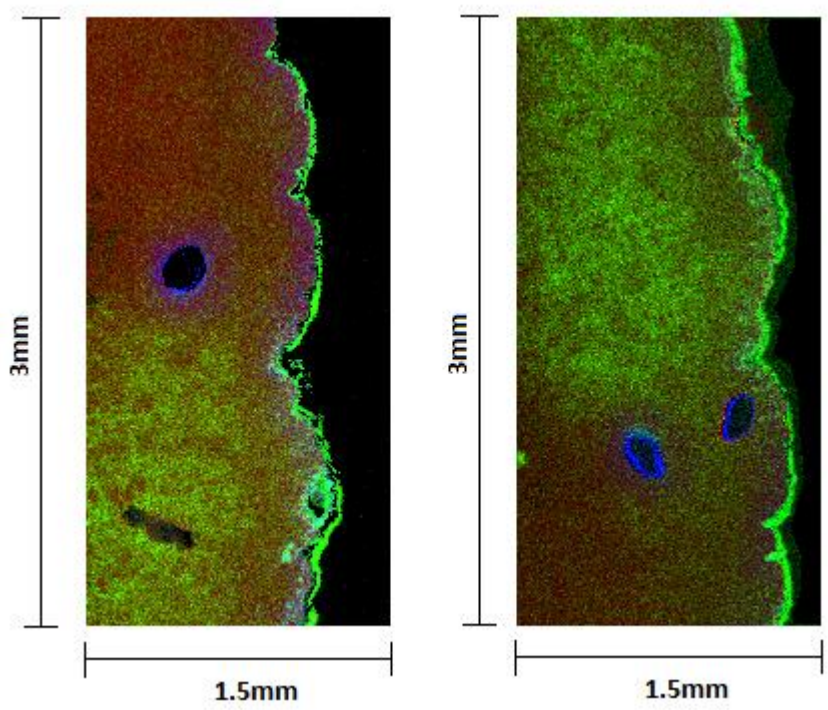

Figure 6.10. Porcine skin treated with 4% CHG following a 36A solid MN pre-treatment. Figure indicates inconsistent CHG permeation in deeper skin layers.

The combination of HPLC data, tape strip images supported by batch statistics data and cross section images provides a clear illustration of how the concentration of CHG was affected by the use of solid MNs of different arrays as a pre-treatment prior to formulation application to the skin. Furthermore, the images produced by ToF-SIMS gave an idea of how drug distribution was affected across the skin when a solid MN pre-treatment was used.

In summary, the tape strip data analysed by HPLC appeared to support the tape strip data analysed by ToF-SIMS. There was a general trend of increasing drug permeation into porcine skin with the addition of a solid MN pre-treatment step, and again when the MN array was increased from 12A to 36A; however this latter difference was more pronounced. For example, the Hibiscrub 4% w/v HPLC data again indicated very little difference between the no MN and 12A MN treatment group. In most cases, the Hibiscrub 12A MN group did not improve the CHG permeation when compared to the group without MN pre-treatment. This was also reflected in

the batch statistics data. This trend was not always consistent within the first few tape strips, however it has been shown previously that the first few strips may be discounted to account for drug adsorption rather than absorption within the skin (Sheth *et al.* 1987, Surber *et al.* 1999, Lademann *et al.* 2009).

Finally, the cross section data supported the notion that the use of a solid MN pre-treatment enhanced the depth permeation of CHG compared to no MN pre-treatment, however it was difficult to distinguish by eye whether there was a large difference between the 12A and 36A groups when viewing the cross section images alone. There appeared to be some inconsistent bright spots of green evidenced deeper in the skin for the 36A treatment group compared to the 12A treatment group, indicating enhanced CHG depth permeation from the 36A group, which was consistent with the HPLC and ToF-SIMS tape strip data. This gives some cause for concern if delivery of CHG is heterogeneous, as this may have implications for incomplete antisepsis within certain areas of skin if delivery is poor.

Statistical data from both HPLC (Table 6.4) and ToF-SIMS (**Error! Reference source not found.**) a nalysed tape strips supported the visual trends presented. It was interesting to find that on some tape strips, the no MN treatment groups delivered significantly more CHG compared to MN treatment groups. This was usually the case when comparing experimental formulations without a MN pre-treatment with the commercial benchmark (Hibiscrub®) with a solid MN pre-treatment (12A or 36A). This further illustrates that the experimental formulations within this thesis are considered superior to the commercial benchmark.

It is important to note that there was no clear evidence from the cross section images that the drug is retained at a high concentration within MN channels. The cross section images appeared to show a relatively homogeneous distribution of CHG ions across the majority of the *stratum*

corneum after a 24hr diffusion cell experiment. This may indicate the ability of the drug to diffuse laterally across the skin layers. This was investigated further.

6.4.6 Horizontal cross sections

Particular cross section images (Figure 6.10) indicated that CHG ion distribution across skin may not be homogeneous; this was of interest to explore further as incomplete antisepsis may result from a lower distribution of CHG within skin. Furthermore, the use of MNs essentially places large deposits of drug within the MN channels and it was of interest to explore whether the drug was able to diffuse laterally across the skin. Horizontal cross sections provide different information to tape strips, as tape strips are limited to the removal of the *stratum corneum* only, whereas the horizontal cross sections (15 µm thick) are able to remove layers of the viable epidermis and potentially the dermis, providing drug distribution information in deeper skin layers. Additionally, horizontal cross sections are able to identify MN bores unlike tape strips. Furthermore, tape strips are used to remove the *stratum corneum* cells but may also remove interstitial fluid which may skew the data when normalising for total weight removed, as interstitial fluid will increase this weight difference (Weigmann *et al.* 1999, Lademann *et al.* 2009). Cross sectioning does not suffer from these limitations.

In an attempt to determine whether there was evidence of lateral diffusion following solid MN pre-treatment prior to CHG gel formulation application to the skin, porcine skin was treated in accordance with the protocol in Section 3.3.3, however horizontal cross sections were removed from the skin rather than the typical vertical cross sections. 10 cross sections (10 µm × 15 µm) were taken sequentially from the porcine skin surface and were analysed using ToF-SIMS to track the diffusion pathways of the drug, originating from a MN bore. For the comparative purposes, selective cross sections of interest are reported in this chapter.

Figure 6.11. Histological examination of porcine skin following 12A solid MN pre-treatment (MN channels shown in red circles). ***Red scale bar - 150µm.***

Horizontal cross sections of blank porcine skin and skin treated with 1% w/v CHG and 4% w/v CHG following a 12A solid MN pre-treatment step were analysed using ToF-SIMS. Images were thresholded to the biological tissue marker (CN^-) in accordance with previous studies in this thesis. This allowed identification of the MN channels, as there was an obvious dark spot indicative of no biological tissue where the MN had created the bore through the skin (Figure 6.12). $C_7H_4N_2Cl^-$ was used as a marker for the drug and the ion previously used as an identifier for cholesterol ($C_{27}H_{45}SO_4^-$) was used alongside the CN^- marker to identify the MN channels. In the vertical cross section studies within this thesis, it is apparent that this unique ion is localised to the upper layers of skin and is primarily found in the *stratum corneum* (Starr *et al.* 2016). The horizontal cross sections provide images within the viable epidermis and below and therefore should show a low intensity for the cholesterol ion. However, when MNs are inserted into the

skin, it is suggested that the cholesterol present in the *stratum corneum* is pushed downwards with the needle and this is why a ring of high $C_{27}H_{45}SO_4^-$ ion intensity was apparent surrounding the MN channel.

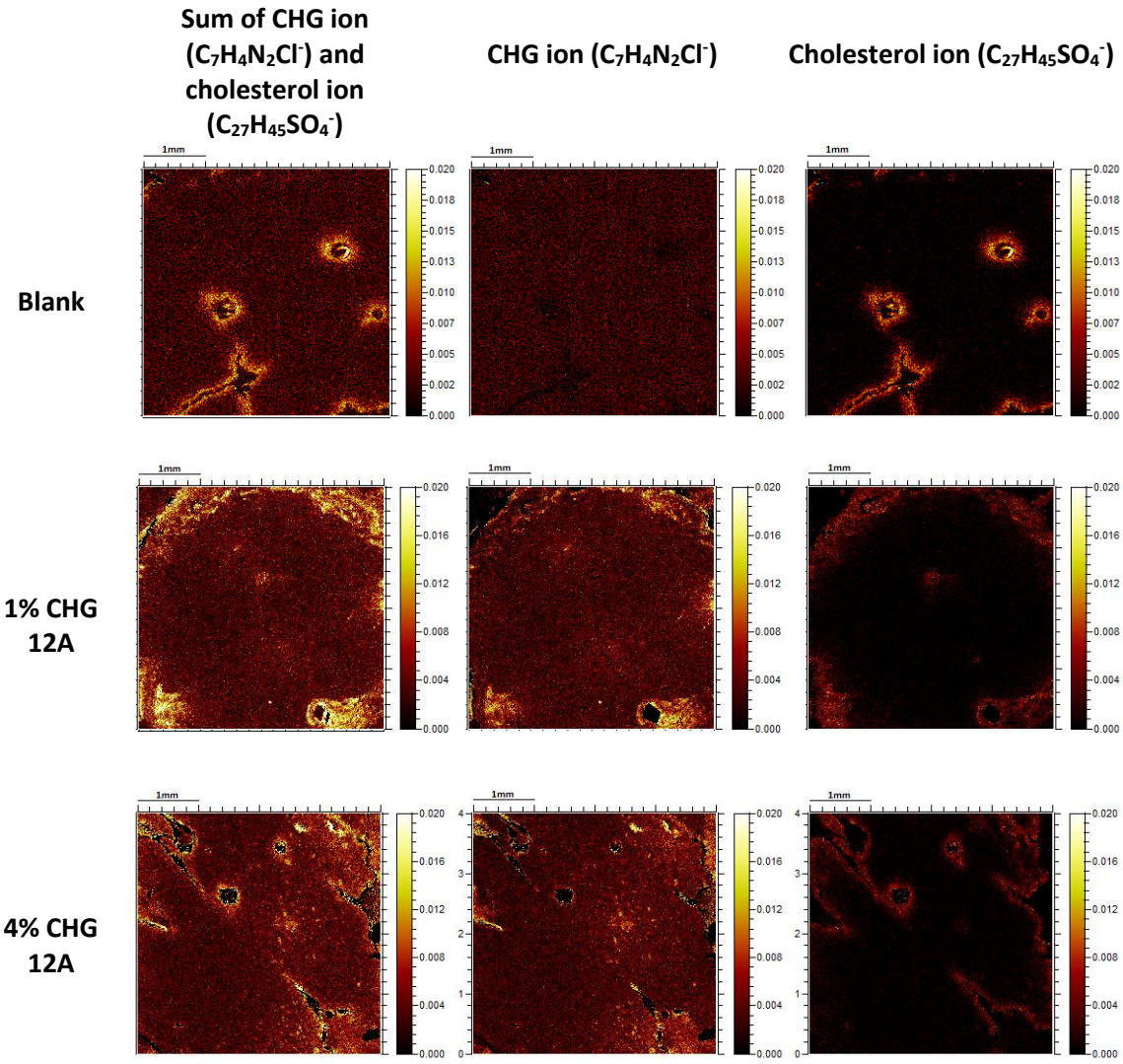

Figure 6.12. ToF-SIMS images of horizontal porcine skin cross sections. Images indicate the bores created by the Dermapen® using the ion indicative of cholesterol ($C_{27}H_{45}SO_4^-$) and the drug using the unique CHG fragment ion ($C_7H_4N_2Cl^-$).

It appeared from the images in Figure 6.12 that after a 24hr diffusion cell experiment whereby porcine skin was pre-treated with a 12A MN prior to formulation application on the skin, diffusion occurred laterally across the *stratum corneum*. This is because the CHG ion intensity in the 1% w/v and 4% w/v CHG treatment group appeared higher than the control group across

the bulk of the 4 mm × 4 mm area analysed and the increase in ion intensity appeared not to be limited to the area immediately surrounding the MN channels. Figure 6.13 illustrates the changes in ion intensity within the area immediately surrounding the MN bore.

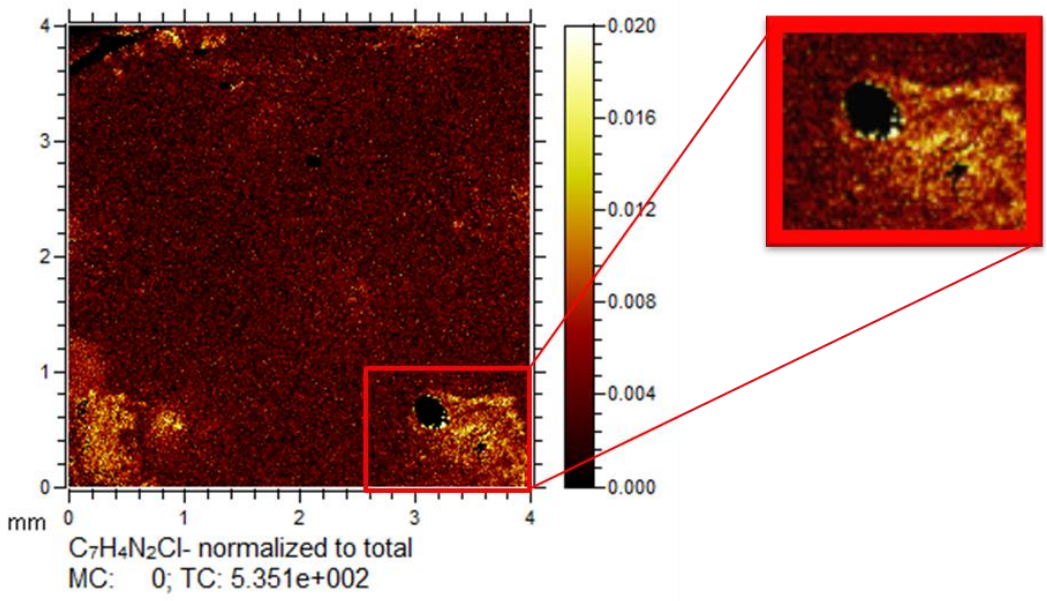

Figure 6.13. ToF-SIMS image of CHG diffusion within a porcine skin cross section, illustrating higher ($C_7H_4N_2Cl^-$) ion intensity in the area immediately surrounding the MN bore.

Lateral diffusion appeared evident as areas of *stratum corneum* not specifically pierced with a 12A MN continue to show elevated CHG ion intensity compared to the negative control, illustrating that the drug had diffused from the application site (MN bore) into these areas of "bulk" skin. However, it is understood that image interpretation is subjective. To compare the difference in ion intensity at specific sites within the horizontal cross sections (immediately surrounding the MN bore and within "bulk" skin) the average ion intensity values were plotted for each group and are presented in Figure 6.14.

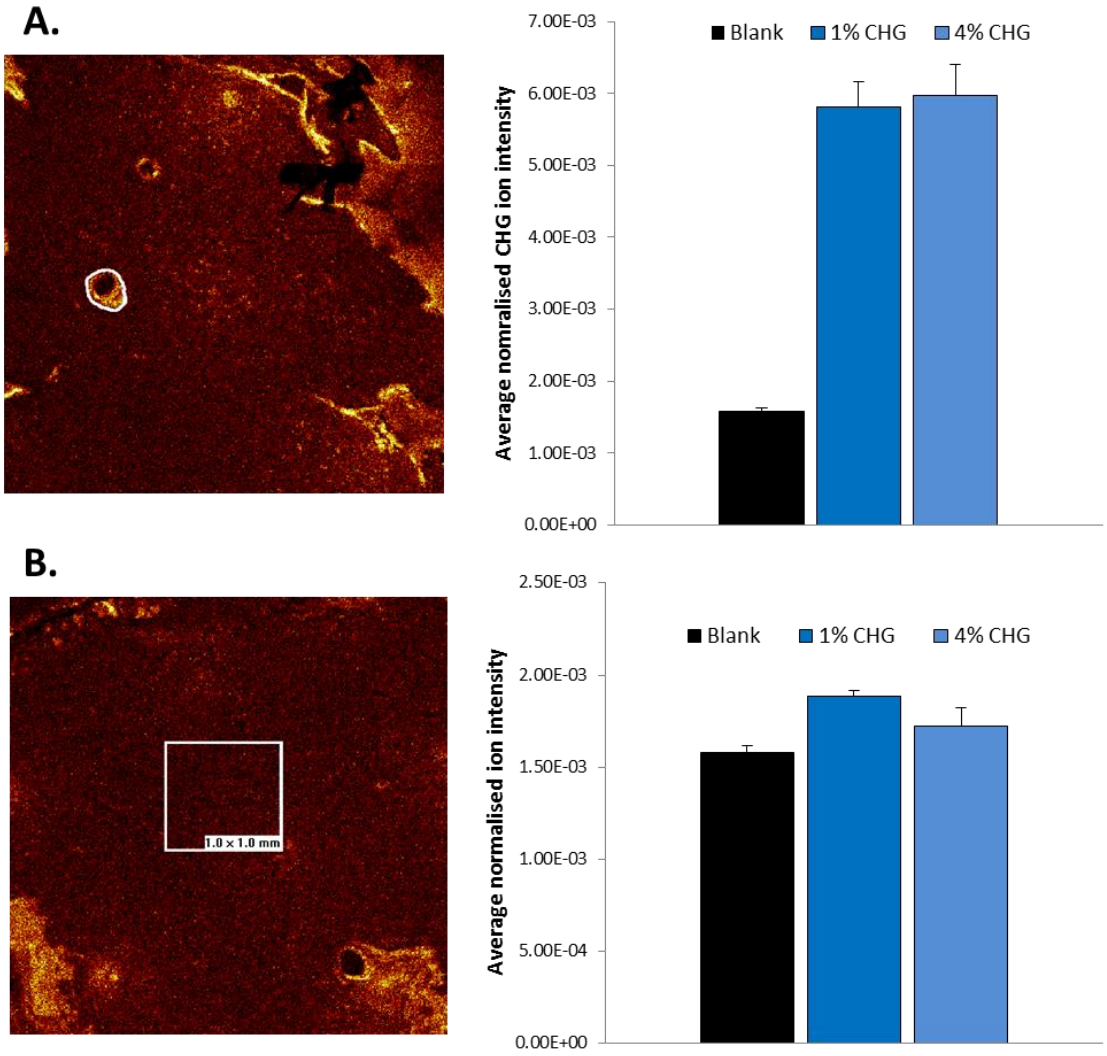

Figure 6.14. Example ToF-SIMS image of CHG distribution within porcine skin treated with 4% CHG following a 12A solid MN pre-treatment. Area indicated on ToF-SIMS images provides an example of the ion intensity values plotted to compare CHG ion distribution between groups A. area immediately surrounding the MN bore, B. 1 mm × 1 mm area in "bulk" skin. All values normalised for total ion intensity, *n=3 ± SE*.

The ion intensity values in Figure 6.14 show that the CHG ion intensity in the area immediately surrounding the MN bore is higher for the skin treated with CHG than for the blank sample, which is expected. Interestingly, there is little difference in average ion intensity between the 1% w/v CHG and 4% w/v CHG group despite the concentration increase of drug applied to the skin. A Kruskal Wallis ANOVA indicated that there was a significant difference in the average ion

intensity values between both 1% w/v CHG, 4% w/v CHG and the blank sample ($p < 0.05$). This is unsurprising as there was no CHG applied to the negative control.

There is less difference between the ion intensity values for the 1 mm × 1 mm area of "bulk" skin. Theoretically, if lateral diffusion was apparent, the average ion intensity value for the treatment groups (1% w/v and 4% w/v CHG) would be higher than the average ion intensity value for the blank control, as this would indicate drug diffusion into "bulk" skin. This certainly appeared to be the case when visualising the 1% CHG ion intensity (Figure 6.14). However, the difference in ion intensity values appeared to be minimal. A One-Way ANOVA with Tukey's post hoc showed a statistical significant difference in the average ion intensity value between 1% w/v CHG and the control, and between 1% w/v CHG and 4% w/v CHG. Interestingly there was no significant difference between 4% w/v CHG and the control.

Therefore, there is some evidence of lateral diffusion from the 1% w/v CHG group, but not the 4% w/v CHG group. Further investigation with an increased number of repeats would be required, as it would be expected that the 4% w/v CHG group would also exhibit this trend, however this was found not to be the case.

6.4.7 Comparisons of a chemical (G3 PAMAM-NH_2 dendrimer) and physical (12A/36A solid MN pre-treatment) as a method of enhancing the dermal deposition of CHG within porcine skin

Comparison of the chemical and physical methods of enhancing dermal deposition of CHG within this thesis can be found in Table 6.5 and Figure 6.15. It was important to compare the two methods of enhancing dermal deposition of CHG to determine if one method was more successful than another, not only in terms of drug deposition of the active drug, but when

determining other factors which need to be considered in order to create a commercially successful product, such as stability of the product and patient acceptability.

Table 6.5. Concentration of drug adjusted per mg of *stratum corneum* material (µg/mg) detected using HPLC on tape strips 1-21 from various treatment groups. All formulations contained 4% CHG and permeation enhancement was detected by chemical methods (co-formulation with a G3 PAMAM-NH_2 dendrimer) or by physical methods (solid MN pre-treatment), *n=6 for 4% CHG, n=13 for 4% CHG-0.5mM PAMAM and 4% CHG-1mM PAMAM, n=4 for 4% CHG 12A and 4% CHG 36A, ± SE.*

	Concentration following gravimetric analysis (µg/mg)									
	4% CHG		4% CHG-0.5 mM PAMAM		4% CHG-1 mM PAMAM		4% CHG, 12A MN 750µm		4% CHG, 36A MN 750µm	
Tape Strip Number	Mean	Standard Error	Mean	Standard Error	Mean	Standard Error	Mean	Standard Error	Mean	Standard Error
Tape Strip 1	406.65	38.96	358.08	51.51	1098.01	157.50	511.93	61.86	737.08	101.57
Tape Strip 2	247.66	12.39	299.34	35.92	614.04	133.11	270.46	33.08	508.58	100.10
Tape Strip 3	175.81	13.10	244.42	48.75	449.59	89.98	182.45	13.43	373.41	32.59
Tape Strip 4-6	199.74	13.93	249.03	40.63	353.96	49.53	164.05	15.76	314.36	17.09
Tape Strip 7-10	148.24	11.57	198.76	42.74	293.14	43.76	156.77	24.05	302.44	22.89
Tape Strip 11-16	152.40	11.89	203.50	40.08	268.38	42.27	141.72	15.34	220.91	33.75
Tape Strip 17-21	92.07	11.96	151.47	29.83	166.62	18.85	109.91	14.15	195.12	30.09

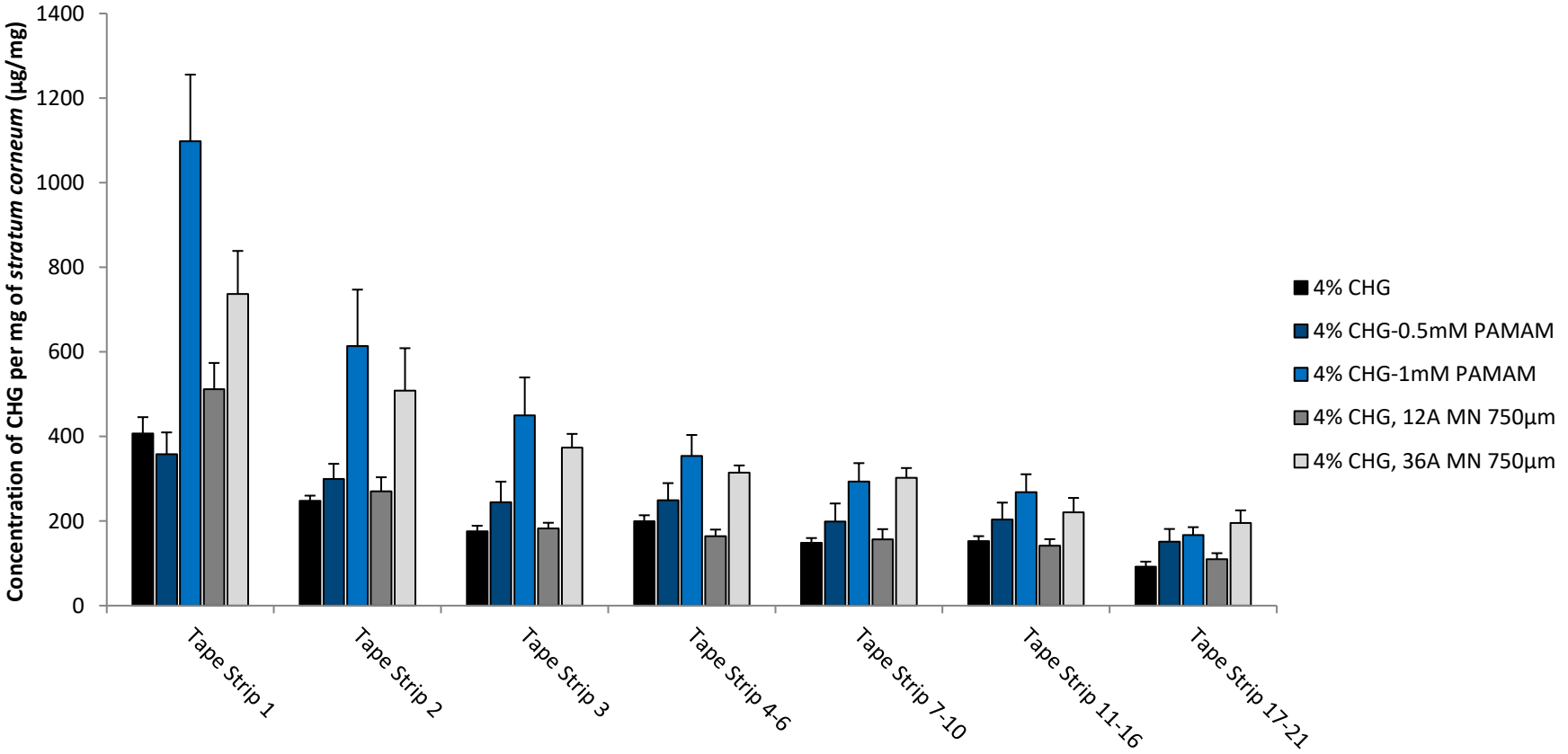

Figure 6.15. Graphical illustration of the tabulated data found in Table 6.5. Concentration of drug adjusted per mg of *stratum corneum* material (µg/mg) detected using HPLC on tape strips 1-21 from various treatment groups. All formulations contained 4% CHG and permeation enhancement was detected by chemical methods (co-formulation with a G3 PAMAM-NH2 dendrimer) or by physical methods (solid MN pre-treatment)- Concentration of drug adjusted per mg of *stratum corneum* material (µg/mg) detected using HPLC on tape strips 1-21 from various treatment groups. All formulations contained 4% CHG and permeation enhancement was detected by chemical methods (co-formulation with a G3 PAMAM-NH_2 dendrimer) or by physical methods (solid MN pre-treatment), *n=6 for 4% CHG, n=13 for 4% CHG-0.5mM PAMAM and 4% CHG-1mM PAMAM, n=4 for 4% CHG 12A and 4% CHG 36A, ± SE*.

Statistical results for this dataset can be found in Table 6.6. Statistically significant pariwise comparisons which were within groups (i.e. 1% w/v CHG-4% w/v CHG, 4% w/v CHG 1mM-Hibiscub 4% w/v) are not displayed in the table as these comparisons have already been presented in Chapter 3 (within PAMAM groups) and tables in this chapter (within MN groups).

Table 6.6. Analytical tests chosen to determine whether formulations significantly affect the depth permeation of CHG within porcine skin – HPLC data – comparing CHG without permeation enhance, CHG-PAMAM co-formulation and CHG with MN pre-treatment, and reporting the resulting pairwise comparisons which resulted in a statistically significant result (p <0.05). Pairwise comparisons are arranged so that the formulation which developed the highest concentration of CHG is given first. ***KW – Kruskal Wallis; OWA – One-Way ANOVA, n=6 for 4% CHG, n=13 for 4% CHG-0.5mM PAMAM and 4% CHG-1mM PAMAM, n=4 for 4% CHG 12A and 4% CHG 36A***

Tape Strip Number	Analytical Test	Statistically Significant Result	Pairwise Comparisons	
			F1	F2
Tape Strip 1	KW	Y	4% CHG 36A	4% CHG-0.5mM PAMAM
Tape Strip 2	OWA	Y	4% CHG-1mM PAMAM	4% CHG 12A
Tape Strip 3	KW	N*	N/A	N/A
Tape Strip 4-6	OWA	Y	4% CHG-1mM PAMAM	4% CHG 12A
			4% CHG 36A	4% CHG-0.5mM PAMAM
			4% CHG 36A	4% CHG 12A
Tape Strip 7-10	OWA	Y	4% CHG-1mM PAMAM	4% CHG 12A
			4% CHG 36A	4% CHG-0.5mM PAMAM
Tape Strip 11-16	OWA	Y	4% CHG-1mM PAMAM	4% CHG 12A
			4% CHG 36A	4% CHG-0.5mM PAMAM
Tape Strip 17-21	OWA	N*	N/A	N/A
Total Tape Strips	KW	Y	4% CHG 36A	4% CHG-0.5mM PAMAM

*Note that there were statistically significant pairwise comparisons within this group; however such comparisons were within groups (i.e. no PAMAM vs PAMAM, 12A vs 36A) rather than between groups. Statistically significant pairwise comparisons within groups are detailed elsewhere.

The comparative results indicate that the 12A solid MN pre-treatment provided similar levels of enhancement compared to the 4% CHG-0.5 mM PAMAM co-formulation, whereas the 36A solid MN pre-treatment provided similar levels of enhancement compared to the 4% CHG-1 mM PAMAM co-formulation. Therefore, these methods of chemical and physical enhancement have resulted in relatively similar pairings of CHG deposition within porcine skin. The implications for this are explored in further detail in the discussion.

6.5 Discussion

The main purpose of this chapter was to determine whether a physical method of permeation enhancement (MNs) was comparable to a chemical method of permeation enhancement (G3 PAMAM-NH_2 dendrimer) in terms of depth of drug permeated and homogeneity of permeation across the skin. The results in this chapter determined that the use of a 750 µm 36A MN pre-treatment step was comparable to a 4% CHG-1 mM G3 PAMAM-NH_2 dendrimer co-formulation when considering concentration of drug detected on each tape strip layer. However, there were some concerns when exploring the homogeneity of drug delivery across the skin from the MN treatment group which are discussed further.

The use of MNs has developed significantly since they were first explored as a drug delivery device in the 1970's (Gerstel and Place 1971). Today MNs exist as a variety of insertion devices (stamp, pen or roller), needle lengths, arrays and delivery types (solid, coated, dissolving, hollow). It was imperative to choose the correct device that would provide the most accurate and reproducible data in this study, as a central theme of this thesis is the creation of a clinically acceptable product. The devices considered in this study were a Dermaroller®, manual Dermastamp™ and an oscillating Dermastamp (Dermapen®).

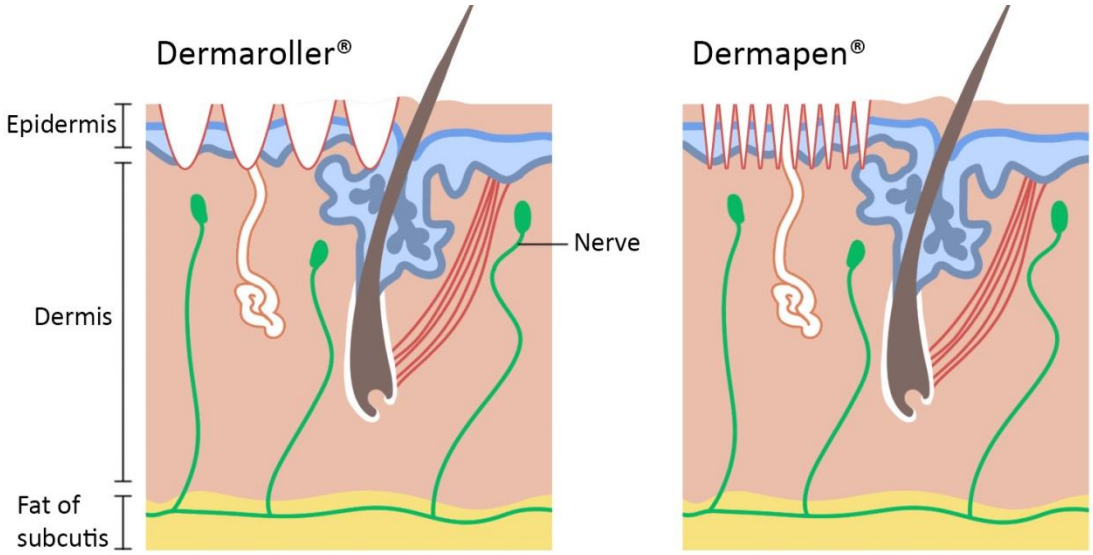

Figure 6.16. MN channels created from a. Dermaroller®; b. Dermapen®.

A Dermaroller® has the advantage of being able to cover a large surface area in a short period of time, but the needle enters and leaves the skin at an angle, which is likely to create larger holes that are different sizes. They will take longer to naturally repair, increasing the risk of infection (Gupta *et al.* 2011), and this method increases the risk of contact with nerves, potentially increasing the risk of pain sensation. The Dermastamp™/Dermapen® does not cover such a large area quickly; however the holes created are more controlled, reproducible and may potentially be less painful due to a decreased risk of nerve contact (Figure 6.16). The depth of MN penetration is adjustable and the MN array can be changed when using an oscillating Dermapen®. The Dermaroller® and Dermastamp™ have no such advantage. Additionally, the force of needle application may also vary with a Dermastamp™ in comparison to a Dermapen®, which is instead controlled by electronic oscillation. For large treatment areas, it seems that the Dermaroller® is preferred, whereas for small areas, a manual Dermastamp™ or oscillating Dermapen® is preferred (Doddaballapur 2009, Fertig *et al.* 2018).

For the delivery of CHG for skin antisepsis prior to surgery, a large area would not usually be required. Whilst CHG is used as a whole body scrub prior to surgery, deeper penetration of CHG is only required

where a surgical incision will occur, thus where the risk of infection would be the highest. To determine whether a Dermastamp™ or Dermapen® would be preferred for the *in vitro* studies, the ability of the each device to overcome skin elasticity was determined. Needle lengths for the Dermapen® chosen were 750 µm to reflect the length used in *in vitro* permeation studies and 1000 µm to allow direct comparison to the manual Dermastamp™ (the needle length of the manual stamp was 1000 µm and could not be altered). A secondary aim of this study was to determine the effects of MN array on CHG permeation into porcine skin, therefore 12A and 36A MNs were utilised when using the Dermapen® in the gentian violet study.

The gentian violet study was used to demonstrate the ability of the Dermastamp™ and Dermapen® to successfully pierce the skin, and to demonstrate the ability of the oscillating Dermapen® to overcome the skin's elasticity which otherwise may prevent a homogeneous depth of MN penetration. The light microscopy images (Figure 6.1) show that the gentian violet dye was able to penetrate into the skin through the MN channels, where they are retained. This demonstrates the capability of the MN devices to pierce the skin.

The Dermapen® needles set to a length of 750µm penetrated the needles to a depth of 503.4 ± 15.4 µm (12 needles) / 482.4 ±21.4 µm (36 needles), and the Dermapen® needles set to a length of 1000 µm penetrated the needles to a depth of 641.0 ± 50.2 µm (12 needles) / 652.9 ±29.2 µm (36 needles). Although the needles fell short of penetrating to the 750 µm depth specified, the Dermapen® outperformed the Dermastamp™, which had a needle length of 1000 µm (non-adjustable), but penetrated the needles to an average depth of 467.1 ± 31.4 µm, less than the Dermapen® with a needle length of 750 µm. The Dermastamp™ was placed only once onto the skin surface and held in place for 10 seconds, whereas the Dermapen® uses oscillating vibrations to move the needles up and down for the 10 second duration of skin contact (Dermapen, 2019). The efficiency and ability of the Dermapen® to penetrate needles deeper than the Dermastamp™ was attributed to the oscillation mechanism of the pen, which counteracted the elasticity of the porcine skin. These findings are

supported by (Verbaan *et al.* 2008), who found that using an electronic applicator to insert 300 µm solid metal MNs into the skin at a velocity of 1 or 3 m/s was more successful than manual piercing. Additionally, the pressure of application is more variable with manual application of a stamp than an oscillating pen; so the obvious choice for precision of results moving forward was the oscillating Dermapen®. A notable advantage of the Dermapen® over the Dermastamp™ is the fact that needle cartridges from the pen device are disposable and are intended for a single use. The Dermastamp™ needles cannot be removed from the stamp device. Therefore, the use of single use MNs which are manufactured in a sterile environment further decreases the risk of infection, and potential physical problems such as blunting or breaking of the MNs from repeated use (Daugimont *et al.* 2010).

One reported disadvantage of the gentian violet study is the potential for overestimation of the diameter of MN channels due to lateral diffusion of the dyes (Coulman *et al.* 2011, Lutton *et al.* 2015). Thus, it was of interest to determine the diameter of the MN channels using an alternative method.

The purpose of the PF study was to measure the diameter of the needle holes to ensure homogeneity of MN diameter. The homogeneity of MN hole diameter (in addition to MN hole depth) is important to ensure a formulation is able to move through the holes in equal amounts, which will correlate to the homogeneity of drug distribution across the entirety of the treated skin layer. It must be stressed that this experiment could only approximate needle diameters due to the fact that living human skin is able to repair the holes after the device is removed from the skin surface (Gupta *et al.* 2011). The MN channel diameter decreased with increasing PF layer. The error bars on Figure 6.2 indicate that the diameter of all MN channels measured were relatively similar which could be attributed to the consistent velocity from the oscillating pen. It appeared that the diameters were homogeneous across the treatment area.

As the PF study also provided depth permeation data, the data was used to validate whether PF could be used as a predictor of MN channel depth by comparing the depth permeation data from the PF

study with that collected from the gentian violet study. Porcine skin is one of the best available substitutes for human skin for *in vitro* studies due to its similarities to human skin (Bronaugh *et al.* 1982, Jacobi *et al.* 2007, Barbero and Frasch 2009), however biological tissue is heterogeneous and is more difficult to obtain than an artificial membrane such as PF (Williams 2003c). If a suitable artificial membrane could be identified that could be used as a predictor for MN depth permeation in biological tissue, such a membrane could be used in quality control applications. This is imperative for commercial development of MN devices, as there is currently a lack of commercial MN devices available and this is attributed at least in part to the lack of Good Manufacturing Practice (GMP) standards for the insertion of MNs into skin (Lutton *et al.* 2015). Therefore it was useful to determine whether the PF study could be used to accurately predict depth penetration of the MNs in comparison to histological assessment.

Unfortunately, the PF study was not found to be comparable to the traditional gentian violet study used to estimate depth permeation of MNs. The PF study may be useful where disadvantages of biological tissue such as its heterogeneous nature may prevent the development of a standard, routine quality control method for MNs. However, for the purposes of this study, the accuracy of the gentian violet study for the depth permeation of MNs was deemed more important and true to life than the potential reproducibility by using PF rather than porcine skin. The PF study appeared to overestimate the depth permeation of the needles compared to the gentian violet study. This disagrees with the initial study published by Larrañeta *et al.* (2014), who found that the insertion depths were slightly lower (especially for higher insertion forces) for PF compared to skin. Larrañeta *et al.* (2018) utilised this same method to study the force of insertion of hyaluronic acid hydrogel MNs, however no comparison was made against porcine or human skin to determine the accuracy of the study. The same method was used again by Larrañeta *et al.* (2015) to compare MN insertion into skin following different methods to prepare the MNs. Again, no comparison was made to porcine or human skin. The differences found between this study and the initial published PF study may be attributed to force

of application, which is different between subjects and is difficult to control as patients cannot "calibrate" their force of application (Donnelly 2018), and potentially the site of porcine skin used, which may have been a different thickness to the type used in this published study. The force of MN application was controlled as much as possible by the researcher being the only person to apply the device to the chosen membrane; however the exact force of application could not be controlled. Furthermore, the PF study can only approximate depths (thickness of 127 µm). For example, if a needle pierced through PF layer 3 but not through layer 4, there was often a needle indentation on layer 4 but this was not enough to pierce through the next PF layer. Furthermore, the PF study could only be used to estimate the depth permeation to three significant figures, whereas the gentian violet stained porcine skin MN studies could estimate the depth of the MN channels to 5 significant figures, a more accurate result.

It was interesting to note that the "bed of nails" effect was apparent in the gentian violet and Parailm® study, but appears more pronounced in the PF study. The 12A MN arrays were able to penetrate slightly deeper into PF layers across all needle lengths compared to the 36A MN array (Figure 6.4). The "bed of nails" effects has been documented by Teo *et al.* (2006), who found that the permeation enhancement effects were much lower than a previous study (Henry *et al.* 1998). This was attributed to the reduced sharpness of the MN tips and the increase in MN density. More recently, Yung *et al.* (2012) designed a method for fabrication of sharp tipped plastic hollow MN arrays, and determined that the distance between the MN holes was one of the vial design considerations in order to avoid the "bed of nails" effect.

Following selection of the appropriate MN device and needle length, the penetration of CHG from experimental formulations (created in Chapter 2) following a solid MN pre-treatment was measured and compared to CHG-PAMAM dendrimer treated skin (Chapter 3 and 4). Experimental formulations, rather than simple CHG solutions, were used in this study because this allowed direct comparisons to be made between the chemical and physical methods of permeation enhancement used in this thesis.

The results of the permeation studies indicate that, in general, the use of a solid MN pre-treatment enhanced the depth permeation of CHG within porcine skin. This conclusion is a result of a combination of diffusion cell studies and associated tape strips, and ToF-SIMS analysis of cross sections and tape strips, which were transformed into semi-quantitative ion intensity values using the "batch statistics" tool (Section 4.3.2.6). This appears to be the first time that skin has been imaged using ToF-SIMS following treatment with MNs to determine the depth permeation of CHG and the first time that MNs have been used to enhance topical deposition of CHG. This discussion will briefly review interesting observations made between MN groups (i.e. no permeation enhancement vs 12A vs 36A) before discussing the usefulness of this physical method of permeation enhancement compared to the chemical method explored in chapters 3 and 4.

The HPLC data which compared CHG permeation within MN groups (Figure 6.5) illustrated that solid MN pre-treatment significantly enhanced 4% w/v CHG deposition within skin compared to Hibsicrub 4% w/v ($p < 0.05$), similarly to 4% CHG-1 mM PAMAM vs Hibiscrub 4% w/v. On specific tape strips (3, 4-6, 11-16, 17-21 in the 12A group and 3, 4-6 and 11-16 in the 36A group) 1% w/v CHG gel delivered significantly more CHG than Hibiscrub 4% w/v ($p < 0.05$), highlighting the importance of vehicle development for permeation enhancement alongside coupling with a permeation enhancer (discussed in Section 2.5). The ToF-SIMS tape strip images follow the pattern observed previously (Chapter 4) of decreasing CHG concentration and *stratum corneum* content with increasing tape strip number and there is a clear increase in CHG ion intensity between the 12A and 36A groups for the 1% w/v and 4% w/v CHG treatment group. Also similarly to Chapter 4, Hibiscrub® 4% w/v (12A and 36A) fails to deliver a concentration of CHG comparable to the 1% w/v experimental formulation. Between groups, both the HPLC data and transformed ToF-SIMS tape strip data show that the 36A MN was more effective than the 12A MN for delivering an increased concentration of drug into the skin.

This result was often statistically significant, particularly when comparing 4% w/v CHG 36A and Hibiscrub 12A, although the diameter of the MN channels was found to be lower from the 36A MN

array when compared to the 12A MN array according to the PF study. It is likely that the 36A MN array improved CHG permeation onto each tape strip because increasing MN array presents more channels in the skin that the drug may diffuse through, thereby resulting in an increased concentration of CHG on each tape strip layer. This is consistent with other studies such as Li *et al.* (2009) who found that increasing the number of MNs increased the transdermal penetration of therapeutic antibodies. It has also been reported that increasing the number of MNs in the array does not cause an increase in pain and still remained less painful than a traditional hypodermic needle (Gill *et al.* 2008) which is important when considering clinical use of MNs.

The data within this chapter was compared to the data obtained from Chapters 3 and 4 to determine whether a solid 750 µm MN pre-treatment step could be considered comparable to chemical enhancement of permeation (via a co-formulation with a G3 PAMAM-NH_2 dendrimer). Figure 6.15 compared the depth permeation of CHG from 4% w/v CHG gel, 4%-0.5 mM PAMAM, 4%-1 mM PAMAM and 4% w/v CHG following either a 12A or 36A 750 µm MN pre-treatment step. Generally, it appeared that the 4% CHG-0.5 mM PAMAM and 12A 750 µm MN pre-treatment steps were comparable, and the 4% CHG-1 mM PAMAM and 36A 750 µm MN pre-treatment steps were comparable in terms of drug concentration per mg of *stratum corneum* material delivered onto each tape strip layer. The result suggest that the concentrations of drug detected on each layer are within the MIC provided for the most common pathogen associated with SSTIs – *S. aureus* as reported in more detail in Section 2.5 (Denton 2001, McCaig *et al.* 2006).

Whilst it has been shown that the two methods of permeation enhancement are comparable in terms of permeation onto each tape strip, this does not provide detailed information on the exact location and distribution of drug permeation, specifically within regions of skin which harbour bacteria with the potential to become pathogenic (Grice and Segre 2011). The structure of human skin is such that bacteria reside mainly within the skin surface and within the epidermis, but reservoirs of bacteria also exist within skin furrows and appendages which remain undetected by traditional skin sampling

methods such as skin swabbing (Reybrouck 1986). Given the low density of hair follicles within the skin (Schaefer and Redelmeier 1996, Otberg *et al.* 2004b), it is unlikely that a MN pre-treatment step is able to effectively target these follicular reservoirs; it is more likely that drug would be delivered through MN bores into bulk skin which would then diffuse throughout the skin layer. Follicular diffusion would rely upon passive diffusion following formulation application to the skin, rather than diffusion specifically through MN bores. Diffusion of CHG into bulk skin is not undesirable, as bacteria exist deep within the epidermis (Zeeuwen *et al.* 2012) which has previously been shown to be unreachable at concentrations considered to be bactericidal by application of a simple 2% w/v CHG aqueous solution (Karpanen *et al.* 2008a). Furthermore, it has been shown in more recent studies that bacteria exist deeper within the epidermis and even subepidermally (Nakatsuji *et al.* 2013). This discovery has likely been overlooked by previous studies due to the methods utilised to sample the skin. For example, Alexeyev and Jahns (2012) compared swabbing, scraping, cyanoacrylate strips and skin biopsies as methods for detecting *Propionbacterium acnes*. Bacteria detected were dependent upon the method used. The study completed by Nakatsuji *et al.* (2013) used several methods (quantitative PCR, Gram staining, immunofluorescence and in situ hybridization) to confirm that bacteria was consistently detectable within the dermis.

Therefore, the use of MN's may still be considered relevant for removal of bacteria within the epidermis and dermis unable to be targeted by bactericidal concentrations of CHG by application of simple aqueous solutions of CHG to the skin (Karpanen *et al.* 2008a). However, it is unlikely that delivery of CHG by this method is able to target appendages that have been understood to act as reservoirs of bacteria. For example, Selwyn and Ellis (1972) found that up to 20% of total skin flora was beyond reach of routine sampling and disinfection methods and was located in skin appendages and furrows. Furthermore, there was a direct positive association between the number of skin appendages and microbial colonisation found by Bojar and Holland (2002). It is likely that drug diffusion into the hair follicles would be associated with a lower incidence of SSTIs, because of the

proportion of bacteria residing within these appendages. Application of CHG co-formulated with a PAMAM dendrimer is more likely to lead to enhanced depth permeation of drug across the entirety of skin, including the appendages rather than depositing greater concentrations of drug in holes created by MNs, through which diffusion must occur to create an even layer of CHG permeation for antisepsis within bulk skin. CHG is a large, polar molecule and for these reasons it is considered more likely to permeate into the skin via the transappendageal route rather than the intercellular route (Section 1.3).

Many studies in the literature that have demonstrated the use of solid MNs as a physical method of permeation enhancement. However, the majority of studies focus on an increase in transdermal drug delivery, i.e. across skin rather than deeper into skin (Kearney *et al.* 2016, Hutton *et al.* 2018, Migdadi *et al.* 2018, Ramöller *et al.* 2019). There is evidence of MN use for enhanced topical delivery, but the proportion of studies is comparatively smaller than those focusing on transdermal drug delivery. Silicone MNs were used to enhance the skin penetration of 5-aminolevulinic acid into the upper regions of excised porcine skin for photodynamic therapy of skin tumours (Donnelly *et al.* 2008). Further exploration into MNs for the delivery of anticancer agents for skin tumours was completed by (Tham *et al.* 2018). The authors developed a nanovehicle loaded with photosensitisers and clinically relevant drugs for combination therapy of melanomas. The therapy was contained mainly within the epidermis. A polymer MN was successfully created which enhanced the delivery of tranexamic acid into skin for the treatment of melasma (irregular coloured patches of skin which are usually exposed to UV light; [Machekposhti *et al.* 2017]). The study found 34% of the released drug was retained within the skin and the rest was systemically absorbed. This would be unacceptable for this study due to the potential for toxicity issues associated with systemic uptake, despite these being rare occurrences and usually requiring large volumes of tranexamic acid to induce (Quinn and Bini 1989, Chan 1994). MNs have also been utilised to enhance the topical delivery of anaesthetics (Li *et al.* 2010, Ornelas *et al.* 2016), vaccines (Li *et al.* 2017) and steroids (Shin *et al.* 2018).

To summarise, although the chemical method and physical method of permeation enhancement can be considered comparable in terms of CHG depth permeation, this does not take into account the fact that MNs are unlikely to be able to target skin appendages which hold a large proportion of bacteria which may be able to cause SSTIs. Follicular diffusion would rely upon passive diffusion following formulation application to the skin, rather than diffusion specifically through MN bores. An absence of clear evidence of lateral diffusion surrports this view that MNs are not well placed for enhancement of CHG permeation due to a lack of targeting bacteria reservoirs. MNs have clear advantages and should be explored further for drug delivery enhacement across the skin, however when specifically considering CHG, it appears as though the chemical method of permeation enhancement is the most well suited for drug delivery to the relevant areas of skin.

The physical method of permeation enhancement should not be overlooked as a method of delivering increased amounts of a drug into skin, particularly when the drug has numerous chemical incompatibilities which may impede drug stability, and as a result, patient acceptability. Furthermore, MNs hold the advantage of being able to deliver drug into a specific depth within skin and can be controlled by altering MN length. Chemical permeation enhancers offer no such advantage and the extent of depth permeation may be subject to several trial and error diffusion cell and tape stripping studies with differing concentrations of a single permeation enhancer, or by testing several different permeation enhancers. The use of MNs as a permeation enhancer of a drug with numerous chemical incompatibilities still provides a contribution to the body of topical and transdermal research by comparing physical and chemical methods of permeation enhancement of a model drug (CHG). Comparisons of chemical and permeation enhancers for a single drug are limited within the literature and it is of interest to determine whether chemical and physical methods of permeation enhancement are comparable when deciding upon the most suitable method for permeation enhancement.

Artusi *et al.* (2004) investigated a chemical (lauric acid) and physical (iontophoresis) method of enhancing the transdermal delivery of thiocolchicoside, a muscle relaxing agent with physicochemical

properties which make it a poor transdermal permeator (high molecular weight, low log P), similarly to CHG. The results of the study found that both chemical and physical methods were able to enhance the transdermal permeation of thiocochicoside; however lauric acid was more successful in enhancing drug permeation than iontophoresis. Iontophoresis led to an enhancement factor of 60, whereas lauric acid produced enhancement factors of 200 and 300 for concentrations of 2% w/v and 4% w/v, respectively. This suggests that the enhanced partition coefficient (via co-formulation with lauric acid) had a greater effect on drug permeation than electroosmosis exhibited by iontophoresis. These results may also allude to the mechanism by which permeation enhancement of a specific drug is most effective, as enhancing the partition coefficient had a greater effect on the flux of this drug than the flux obtained from electroosmosis.

Nicoli *et al.* (2001) investigated the effects of lauric acid and iontophoresis on the enhancement of triptorelin, an analogue of the luteinizing hormone-releasing hormone for the treatment of sex hormone-dependent tumours. Transdermal delivery was considered as a practical alternative to the current method of implanting microparticles containing the drug. The study found that permeation enhancement occurred in both instances; however iontophoresis was preferred as the presence of lauric acid affected the stability of the drug and was considered potentially unacceptable for patient use due to anecdotal evidence of skin irritation.

Pillai and Panchagnula (2003) investigated the transdermal delivery of insulin from poloxamer gels with menthone, linoleic acid and/or iontophoresis. Both linoleic acid and menthone in combination with iontophoresis showed a synergistic enhancement of insulin permeation. The plasma insulin concentration was highest with linoleic acid pre-treatment, in agreement with ex vivo permeation studies, but the reduction in plasma glucose levels was comparable to iontophoresis. A combination of the chemical enhancers and iontophoresis caused greater skin irritation than when either method was used alone.

These studies illustrate that it is not always possible to predict which method of permeation enhancement may deliver the highest concentration of drug into and across skin. In the three studies cited, many outcomes were shown (chemical enhancement preferred, physical enhancement preferred, and synergism of chemical and physical methods). Therefore it is useful to determine which method delivers the highest concentration of drug and from this, decide which method is most likely to succeed from a clinical perspective. It would be of interest in the future to compare the chemical method of enhancing CHG depth permeation (co-formulation with a G3 PAMAM-NH_2 dendrimer) alongside iontophoresis, given that CHG is cationic and iontophoresis has been used successfully to drive ionic permeants into follicles (Guy *et al.* 2000, Essa *et al.* 2002), the site of bacteria reservoirs. Currently, iontophoresis is only used clinically for hyperhidrosis (excessive sweating).

In addition to comparing the depth penetration of CHG from a physical and chemical method of permeation enhancement, homogeneity of drug distribution was also compared, as skin bacteria resides across the entirety of the skin surface and deeper into the epidermis, which cannot be targeted with sufficient bactericidal concentrations of CHG by application of aqueous solutions of 2% w/v CHG to the skin surface (Karpanen *et al.* 2008a). To visualise whether CHG permeation continued to be enhanced from the MN pre-treatment groups in viable epidermal skin layers, cross sections of porcine skin pre-treated with MNs were analysed, which built upon the information provided by ToF-SIMS images of tape strips indicating drug distribution throughout the *stratum corneum*.

The vertical cross sections indicated, in accordance with the HPLC data and ToF-SIMS images of tape strips, that a MN pre-treatment enhanced the depth permeation of CHG. However, there were some bright spots of CHG ion intensity visible on specific porcine skin cross sections (Figure 6.10), which was not spread evenly across the entirety of the cross section. This was a concern because uneven distribution of the drug across the deeper skin layers may be correlated to a reduced antisepsis effect, negating the entire purpose of enhancement of CHG deposition within skin. This could be viewed as a disadvantage of the MN technique when compared to the chemical permeation enhancer utilised

within this thesis. Use of a chemical permeation enhancer appeared to provide a more even distribution of drug across the deeper skin layers, potentially resulting in a more complete level of antisepsis across the treatment site.

The evidence of uneven drug distribution (Figure 6.10) was explored further by analysing horizontal cross sections of porcine skin treated a 4% w/v CHG gel following MN pre-treatment. Furthermore, visualisation of drug distribution within each horizontal cross section was thought to potentially provide evidence of lateral diffusion, a concept which is often cited as the main method of intercellular delivery of drugs which are less likely to permeate across the corneocytes, and preferentially diffuse through the lipid bilayers (Barry 2002a, Tanner and Marks, 2008).

The lateral diffusion of ibuprofen in human skin was studied by Schicksnus and Müller-Goymann (2004). This was of particular interest due to the log P value of the drug indicating lipophilicity, hence it was postulated that the drug might be retained in the *stratum corneum*, resulting in a drug depot for sustained ibuprofen release. The authors found that the drug distribution profile could be divided into two parts, one where the drug accumulates until the drug concentration reaches its maximum, followed by a redistribution phase where lateral diffusion occurs. The addition of permeation enhancers increased both the accumulation and redistribution of drug. Tape stripping was used by Jacobi *et al.* (2004) to examine the lateral spreading of topically applied UV filter substances. The authors found the lateral spreading of the UV filter substances to be symmetrical and that the emulsion vehicle was the main component (rather than the lipophilicity of the actives) which was responsible for lateral transport. Johnson *et al.* (1996) measured the lateral diffusion coefficients of nine fluorescent probes in two model lipid bilayer systems. Molecular weight was found to be an important factor affecting the ability of the probe to diffuse laterally – smaller probes diffused faster than the larger ones. There is currently no published data on the use of ToF-SIMS as a method of imaging lateral diffusion.

Horizontal cross sections were taken of porcine skin following a "poke and patch" solid MN (750 µm, 12A) pre-treatment. The horizontal cross section images provided some evidence of lateral diffusion. When comparing the ion intensity of the treated groups to the ion intensity of the untreated groups it appears that the drug was able to diffuse away from the immediate MN bore area as the areas of skin analysed which had not been pierced by a MN still exhibited a higher ion intensity than the negative skin control. There was also evidence of a small "depot" of drug surrounding the MN bore from the skin samples treated with CHG, which showed a high CHG ion intensity in the area immediately surrounding the MN bore. Assuming this cross section is from the *stratum corneum* or viable epidermis, it is understandable that a highly hydrophilic drug would struggle to diffuse laterally within the highly hydrophobic environment as permeation through the *stratum corneum* is the rate limiting step for hydrophilic drugs such as CHG (Williams 2003b). This was demonstrated by Sznitowska, Janicki and Williams (1998) who found that removal of intercellular lipids dramatically increased the flux of the hydrophilic drug baclofen. The statistical tests which compared ion intensity values in the area immediately surrounding the MN bore and a 1 mm × 1 mm area within bulk skin indicated that lateral diffusion was apparent from the 1% w/v CHG group as there was a statistically significant difference in CHG ion intensity in bulk skin between 1% w/v CHG and the negative control, indicating CHG had diffused from the MN bore to the bulk of skin. However, there was no significant difference in ion intensity between the 4% w/v CHG group and blank skin, which is surprising given the high concentration of drug applied to the skin.

Therefore the horizontal cross section images did provide some semi-quantitative evidence of lateral diffusion (Figure 6.14); however there were some inconsistencies in the trends noted. One major limitation of this study was the fact that the "poke and patch" method did not deliver CHG through the MN channels exclusively – moreover, the drug was applied to the entirety of the skin surface rather than limiting the delivery to the MN channels. The drug was allowed to diffuse not only from the MN channels but also from the intact areas of *stratum corneum*. To determine if lateral diffusion of the

drug from the MN channels is evident in the future, the delivery of the drug should be limited to the MN channels only, by using an alternative MN delivery method such as a the “coat and poke” method whereby the MNs are coated with the drug, rather than the drug being applied to the entirety of the skin surface. Cross sections should be taken shortly after formulation application to the skin and thereafter at specific time points in order to visualise time-dependent changes in CHG intensity in “bulk” skin.

The initial results from this study were promising, however there may be potential for the study to provide robust conclusions if the method was developed further. In addition to the suggestions above, increasing the MN array (12A was used in this study) would increase the likelihood of MN channels being visible across the cross section area analysed by ToF-SIMS. Furthermore, numerous repeats should be taken to reduce the likelihood of false positive results from differences in the quality of skin samples and or potential human error from angled insertion of the MN. Furthermore, the drug used in this study has a high aqueous solubility and low log P (Farkas *et al.* 2007), indicating that permeation into the skin is more likely to follow the transcellular pathway. It would be of interest to view the diffusion pathway of a lipophilic drug, whereby horizontal diffusion through the tortuous lipid bilayer pathways is more likely (Moss 2015).

Despite the drawbacks of this study, further development of the method may allow for more robust conclusions to be made regarding the potential for lateral diffusion of drugs from MN channels, a novel use of the ToF-SIMS technology. A method published by Gee *et al.* (2012) would be useful to replicate in the future when attempting to elucidate the lateral diffusion of CHG from MN channels. The authors developed a novel concentric tape strip design, whereby the innermost tape strip segment represented the application site and outer segments became further removed from this site. The largest concentric tape strip had an outer diameter of 32mm. This is preferable to the 4 mm × 4 mm site analysed using ToF-SIMS as it is more representative of the sample. The study used contour plots to demonstrate the lateral diffusion of three drugs with differing lipophilicities, caffeine (log P -

0.07 [Leo, Hansch and Elkins, 1971]); hydrocortisone (log P 1.43 [El-Kattan *et al.* 2001]) and ibuprofen (log P 3.51 [El-Kattan *et al.* 2001]). The results showed that drugs with a lower log P form a "flat and shallow" reservoir with more lateral than vertical diffusion. The opposite is the case for drugs with a higher log P, a "narrow and deep" diffusion gradient is visible whereby the tendency to spread laterally was reduced but penetration vertically is increased. Therefore it is likely that lateral diffusion occurred, most likely following the pattern established by the hydrophilic drug caffeine in the Gee *et al.* (2012) study, however the ToF-SIMS study was underdeveloped and as a result failed to appropriately show evidence of lateral diffusion of CHG from the holes created by the solid MN pre-treatment.

There appears to be no literature available that has captured the initial stage of drug distribution from the solid MN channel into the surrounding dermal tissue using imaging techniques. A study completed by Wang *et al.* (2015) investigated the mechanism of drug diffusion inside dissolving MNs in an attempt to improve drug delivery efficiency. The proportion of drug loading from each needle was measured following several changes to the system, ultimately evaporation of base solvent was found to be the most important factor that improved drug loading. However the study does not image drug release from the dissolving MNs. Drug distribution from dissolving MNs has been investigated in depth as this can be controlled by altering the polymer type used for MN manufacture as well as the mixing method of the polymer and drug (Waghule *et al.* 2019). Literature could not be found which visualised drug diffusion from MN holes created from solid MNs. OCT has been widely used to visualise MN insertion into skin (Donnelly, *et al.* 2010, Coulman *et al.* 2011), however no studies could be found which expanded on this technology to visualise immediate drug release and diffusion from the MN holes. Therefore, further development of the ToF-SIMS method could be utilised in the future to image drug diffusion over time following MN insertion into skin, specifically a time-course ToF-SIMS study if possible.

6.6 Conclusion

This chapter demonstrated the ability of a solid MN pre-treatment to enhance the deposition of CHG to the same depth as the chemical permeation enhancer explored in chapters 3 and 4. The MN length of 750 µm was sufficient for delivery of CHG into deeper epidermal and dermal layers where bacteria reside with the ability to cause a skin infection if the barrier is compromised, without resulting in CHG permeation across full thickness porcine skin. Using CHG as a model drug has shown that the chemical and physical methods of enhancing drug delivery examined in this study can be considered equivalent in terms of the amount of enhancement each method offers. This is a positive result as this increases the number of viable options available for enhancement of a drug into and across skin. This is the first study of its kind to demonstrate CHG mediated permeation enhancement using a solid microneedle pre-treatment.

However, it was found that the MN pre-treatment would be unlikely to target skin appendages, the predominant site of bacteria reservoirs. For CHG specifically, it appears that the PAMAM dendrimer may be more suitable for enhancement of the drug within skin due to homogeneity of drug distribution within porcine epidermis and dermis.

The combination of HPLC and ToF-SIMS has again demonstrated (alongside results from Chapters 3 and 4) that the two analytical techniques provide complimentary information on the drug deposition and distribution within skin. The 36A MN pre-treatment has been proven as effective as the 4% CHG-1 mM PAMAM co-formulation, without the stability issues demonstrated with the co-formulation in Chapter 3.

ToF-SIMS was used for the first time in an attempt to visualise lateral diffusion across horizontal skin cross sections. The results were inconclusive and further method development is required before robust conclusions can be made.

7 General Conclusion

The purpose of this thesis was to enhance the dermal deposition of CHG for enhanced topical skin antisepsis. Application of CHG to the skin is sufficient for surface antisepsis, however bacteria reside within deeper skin layers and in appendages which harbour the ability to become pathogenic if the skin barrier is breached, such as at the site of a surgical incision. It was of interest to enhance CHG deposition within skin to target these opportunistic bacteria that are unable to be targeted by simple CHG solutions. This chapter will summarise the findings of importance, the implications of these findings and future work to be undertaken.

A key finding of the thesis includes the development and optimisation of a CHG-PAMAM co-formulation that is able to enhance the depth permeation of CHG within porcine skin. This is a progression from a previous study that found that a PAMAM dendrimer pre-treatment was able to enhance CHG deposition within skin. It was of interest to co-formulate the drug and dendrimer into a one-step application for practical purposes and to produce a clinically relevant formulation. The ethanol-based gel co-formulation successfully enhanced CHG depth permeation into skin – this increase was considered statistically significant when comparing the 4% w/v CHG-1 mM PAMAM co-formulation alongside Hibiscrub® (contains 4% CHG), the commercial benchmark. This is the first time an ethanol-based CHG-PAMAM gel co-formulation has been found to successfully enhance CHG permeation into porcine skin compared to a commercially established antiseptic product. Antisepsis in deeper layers of skin would reduce the bacterial load of the skin and thus may potentially reduce the incidence of SSTIs.

The assessment of drug permeation across skin is traditionally achieved using Franz-type diffusion cells. Where assessment of dermal deposition is also required, tape stripping is an accepted method of elucidating the concentration of drug on each skin layer. Despite these techniques being commonplace in the realm of topical and transdermal drug delivery, both tape stripping and

subsequent analysis using HPLC suffers from several drawbacks. These drawbacks are summarised in Sections 1.7 and 4.1. For the reasons discussed, ToF-SIMS was utilised as a complimentary technique to confirm the results initially found when completing traditional *in vitro* permeation studies. Furthermore, the technique has a low limit of detection (in relation to HPLC) and was thought to be able to detect low concentrations of CHG in deeper skin layers where HPLC may not. The technique also produces semi-quantitative images of skin providing information on the spatial distribution and co-localisation of CHG.

The ToF-SIMS images supported the initial observations from the quantitative Franz-type diffusion cell experiments in that the PAMAM dendrimer was able to enhance CHG depth permeation when co-formulated with the drug. Although identification of a unique PAMAM fragment was attempted for determination of the route of PAMAM permeation into skin, the structure was deemed too similar to endogenous skin components. Results suggested that the PAMAM was unable to permeate into porcine skin, although this could not be confirmed.

PAMAM dendrimers have been found to enhance the topical and transdermal deposition of both hydrophilic and lipophilic drugs; however the mechanism of this permeation enhancement is not well understood. In Chapter 5, the mechanism of PAMAM-mediated CHG permeation enhancement from the co-formulation was investigated. Contrary to previous studies, it was found that barrier disruption was minimal via TEWL and OCT experiments. This difference was attributed to comparison of a formulation with occlusive properties as opposed to a solution of the dendrimer in methanol. A novel discovery was made whereby it was found that the addition of the PAMAM dendrimer to ethanol-based gel formulation significantly reduced the surface tension of the formulation. Therefore it is postulated that PAMAM-mediated enhancement in CHG is primarily due to surface tension effects, and potentially also due to occlusive effects.

The final chapter within this thesis investigated a solid microneedle pre-treatment to compare chemical and physical methods of permeation enhancement, with CHG being utilised as the model drug. It was found that a solid MN pre-treatment step was able to enhance CHG dermal deposition. A 12A MN pre-treatment step was found to be comparable to a 4% w/v CHG-0.5 mM PAMAM co-formulation. A 36A MN pre-treatment step was found to be comparable to a 4% w/v CHG-1 mM PAMAM co-formulation. This is the first time CHG deposition has been enhanced using a solid MN pre-treatment. ToF-SIMS analysis of porcine skin cryosections following a solid MN pre-treatment and CHG application found areas of inhomogeneous drug distribution, which may have implications for complete skin antisepsis in deeper skin layers. This was investigated further by the novel characterisation of CHG permeation in horizontal porcine skin cross sections. Experimental findings suggested a higher concentration of drug in MN bores compared to bulk skin; however the method requires further development.

7.1 Implications of research and future work

The results presented within this thesis identify two methods of enhanced CHG delivery for improved topical antisepsis. Although the vast microflora of skin can exist symbiotically with the host, at risk patients (such as the elderly or immunocompromised) would benefit from greater skin antisepsis that should reduce the risk of SSTIs. The unpopularity of developing new antimicrobials due to a potential lack of investment return when resistance inevitably develops means that optimisation of formulations currently available is crucial for delaying the looming antibiotic crisis. The successful permeation enhancement of CHG within this study demonstrates that formulation optimisation can be achieved, which has considerable benefits in the healthcare sector for patients who are at risk of developing SSTIs.

In Chapter 3 in this thesis, *in vitro* permeation studies using porcine skin were utilised to demonstrate that the CHG-PAMAM co-formulation improves CHG dermal deposition. The next clear step would be to complete the experiments using *ex vivo* human skin to confirm that CHG permeation enhancement still occurs using the best available model, and to compare this against the commercial benchmark. Furthermore, the long-term stability of the formulation should be investigated further, utilising accelerated stability tests to provide a cautious estimation on shelf life.

A positive outcome from this thesis was the inference that the PAMAM dendrimer does not permeate into skin, as no unique fragment could be identified within the skin using ToF-SIMS. This would infer that the PAMAM dendrimer cannot permeate into skin at a large enough concentration to cause adverse events, although this could only be inferred using ToF-SIMS rather than confirmed, as no unique fragment indicative of the dendrimer could be found. To develop this further, one may utilise other techniques that may be able to identify the dendrimer with greater specificity. Despite the high mass resolution of ToF-SIMS, it is still possible that unique PAMAM fragment ions could not be distinguished due to their likely high mass (as the ToF-SIMS resolution decreased with increasing mass). The use of developing technologies with a greater mass resolution, such as OrbiSIMS, may help combat this limitation. Furthermore, it may be possible, if a unique PAMAM fragment can be found, to understand the mechanism of action of the dendrimer by imaging its permeation pathway using SIMS. This may allow for more accurate pairing between a drug and permeation enhancer according to the mechanism of enhancement required.

The use of ToF-SIMS for the determination of dermal deposition of drugs is still relatively new. In the future, the technique may be particularly useful for delineating the permeation of metals into the skin, which is a continued concern in occupational settings such as the manufacturing industry where exposure is high. ToF-SIMS would be well placed for such studies as a unique fragment would not be required – one would simply search for the elemental ion in the skin.

For the first time in this thesis, a solid MN pre-treatment step was used to enhance the dermal deposition of CHG. This physical method of permeation enhancement was utilised to compare whether a physical method could be considered comparable to the chemical method of co-formulating the drug with a PAMAM dendrimer. The use of a physical and chemical method to compare the permeation of the same drug has not been extensively published within the literature, but an understanding of which method is preferred for topical and transdermal drug delivery in terms of efficacy, stability and safety is clearly useful for formulating a drug for clinical use. As the study in this thesis could be considered a "proof of concept" study, there now opens potential for formulation development by altering the MN type (dissolving, coated, hydrogel) for a more simple, "one step" process.

ToF-SIMS was utilised for the first time in this study to visualise lateral drug diffusion from MN bores into bulk skin. This novel method could be developed and improved to provide more robust conclusions in the future. For example, horizontal cross sections could be taken of skin over the course of a 24 hr experiment to visualise how the diffusion gradient changes over time. It would also be useful to pair this with a developed tape strip method cited previously (Gee *et al.* 2012, 2014), to provide complimentary quantitative and qualitative data as has been found in chapters 2 and 3 of this thesis. The use of the novel concentric tape strip design cited above would also cover a larger area than that available for ToF-SIMS analysis (4 mm × 4 mm in this study). The use of the two methods would allow mapping of a contour plot to map the change in drug concentration across the skin area over time.

The results within this thesis have found two methods of enhancing the dermal deposition of CHG. When developed further, this finding could prove to be of great use, reducing the burden, both clinically and economically, in the healthcare sector. Future work would aid in the development of strategies for topical and transdermal drug delivery enhancement, particularly in the understanding of mechanistic aspects which would serve to provide more acceptable formulations by maximising efficacy and reducing adverse events.

References

Abrams, K., Harvell, J.D., Shriner, D., Wertz, P., Maibach, H., Maibach, H.I., and Rehfeld, S.J., 1993. Effect of Organic Solvents on In Vitro Human Skin Water Barrier Function. *Journal of Investigative Dermatology*, 101 (4), 609–613.

Adlhart, C. and Baschong, W., 2011. Surface distribution and depths profiling of particulate organic UV absorbers by Raman imaging and tape stripping. *International Journal of Cosmetic Science*, 33 (6), 527–534.

Aguiar, A.J. and Weiner, M.A., 1969. Percutaneous Absorption Studies of Chloramphenicol Solutions. *Journal of Pharmaceutical Sciences*, 58 (2), 210–215.

Aki, H. and Kawasaki, Y., 2004. Thermodynamic clarification of interaction between antiseptic compounds and lipids consisting of stratum corneum. *Thermochimica Acta*, 416 (1–2), 113–119.

Al-Mayahy, M.H., Sabri, A.H., Rutland, C.S., Holmes, A., McKenna, J., Marlow, M., and Scurr, D.J., 2019. Insight into imiquimod skin permeation and increased delivery using microneedle pre-treatment. *European Journal of Pharmaceutics and Biopharmaceutics*, 139, 33–43.

Alexander, A., Dwivedi, S., Ajazuddin, Giri, T.K., Saraf, S., Saraf, S., and Tripathi, D.K., 2012. Approaches for breaking the barriers of drug permeation through transdermal drug delivery. *Journal of Controlled Release*, 164, 26–40.

Alexeyev, O.A. and Jahns, A.C., 2012. Sampling and detection of skin Propionibacterium acnes: Current status. *Anaerobe*, 18 (5), 479-483.

Ali, Y., Dolan, M.J., Fendler, E.J., and Larson, E.L., 2001. Alcohols. *In*: S.S. Block, ed. *Disinfection, Sterilization, and Preservation*. Philadelphia: Lippincott Williams and Wilkins, 229–254.

Alikhan, A. and Maibach, H.I., 2010. Biology of stratum corneum: Tape stripping and protein quantification. *In*: *Textbook of Aging Skin*. Springer Berlin Heidelberg, 401–407.

Alkilani, A.Z., McCrudden, M.T.C., and Donnelly, R.F., 2015. Transdermal Drug Delivery: Innovative Pharmaceutical Developments Based on Disruption of the Barrier Properties of the Stratum Corneum. *Pharmaceutics*, 7 (4), 438–470.

Allen, L. V. and Ansel, H.C., eds., 2014. Liquid Dosage Forms - Disperse Systems. *In*: *Ansel's Pharmaceutical Dosage Forms and Drug Delivery Systems*. Philadelphia: Lippincott Williams and Wilkins, 445–507.

Alvarez-Román, R., Naik, A., Kalia, Y.N., Fessi, H., and Guy, R.H., 2004. Visualization of skin penetration using confocal laser scanning microscopy. *European Journal of Pharmaceutics and Biopharmaceutics*, 58 (2), 301–316.

Aly, R. and Maibach, H.I., 1979. Comparative study on the antimicrobial effect of 0.5% chlorhexidine gluconate and 70% isopropyl alcohol on the normal flora of hands. *Applied and Environmental Microbiology*, 37 (3), 610–613.

Amstalden van Hove, E., Smith, D., and Heeren, R., 2010. A concise review of mass spectrometry imaging. *Journal of Chromatography A*, 1217 (25), 3946–3954.

Ananthapadmanabhan, K.P., Moore, D.J., Subramanyan, K., Misra, M., and Meyer, F., 2004. Cleansing without compromise: the impact of cleansers on the skin barrier and the technology of mild cleansing. *Dermatologic Therapy*, 17 (S1), 16–25.

Anigbogu, A.N.C., Williams, A.C., Barry, B.W., and Edwards, H.G.M., 1995. Fourier transform raman spectroscopy of interactions between the penetration enhancer dimethyl sulfoxide and human stratum corneum. *International Journal of Pharmaceutics*, 125 (2), 265–282.

Antonov, D., Schliemann, S., and Elsner, P., 2016. Methods for the Assessment of Barrier Function. *Current Problems in Dermatology*, 49, 61–70.

Arevalo, J.F., Krivoy, D., and Fernandez, C.F., 2009. How Does Optical Coherence Tomography Work? Basic Principles. *In*: *Retinal Angiography and Optical Coherence Tomography*. New York: Springer, 217–222.

Artusi, M., Nicoli, S., Colombo, P., Bettini, R., Sacchi, A., and Santi, P., 2004. Effect of chemical enhancers and iontophoresis on thiocolchicoside permeation across rabbit and human skin in vitro. *Journal of Pharmaceutical Sciences*, 93 (10), 2431–2438.

Astruc, D., Boisselier, E., and Ornelas, C., 2010. Dendrimers Designed for Functions: From Physical, Photophysical, and Supramolecular Properties to Applications in Sensing, Catalysis, Molecular Electronics, Photonics, and Nanomedicine. *Chemical Reviews*, 110 (4), 1857–1959.

Atrux-Tallau, N., Romagny, C., Padois, K., Denis, A., Haftek, M., Falson, F., Pirot, F., and Maibach, H.I., 2010. Effects of glycerol on human skin damaged by acute sodium lauryl sulphate treatment. *Archives of Dermatological Research*, 302 (6), 435–441.

Augustin, M., Holland, B., Dartsch, D., Langenbruch, A., and Radtke, M.A., 2011. Adherence in the Treatment of Psoriasis: A Systematic Review. *Dermatology*, 222 (4), 363–374.

Aungst, B.J., J. Rogers, N., and Shefter, E., 1986. Enhancement of naloxone penetration through human skin in vitro using fatty acids, fatty alcohols, surfactants, sulfoxides and amides. *International Journal of Pharmaceutics*, 33 (1–3), 225–234.

Azarbayjani, A.F., Lin, H., Yap, C.W., Chan, Y.W., and Chan, S.Y., 2010. Surface tension and wettability in transdermal delivery: a study on the in-vitro permeation of haloperidol with cyclodextrin across human epidermis. *Journal of Pharmacy and Pharmacology*, 62 (6), 770–778.

Azum, N., Rub, M.A., and Asiri, A.M., 2014. Analysis of surface and bulk properties of amphiphilic drug ibuprofen and surfactant mixture in the absence and presence of electrolyte. *Colloids and Surfaces B: Biointerfaces*, 121, 158–164.

Babalola, O., Mamalis, A., Lev-Tov, H., and Jagdeo, J., 2014. Optical coherence tomography (OCT) of collagen in normal skin and skin fibrosis. *Archives of Dermatological Research*, 306 (1), 1–9.

Badia, J.M., Casey, A.L., Petrosillo, N., Hudson, P.M., Mitchell, S.A., and Crosby, C., 2017. Impact of surgical site infection on healthcare costs and patient outcomes: a systematic review in six European countries. *Journal of Hospital Infection*, 96 (1), 1–15.

Bako, J., Szepesi, M., Veres, A.J., Borbely, Z.M., Hegedus, C., and Borbely, J., 2006. Chlorhexidine Release from Nanocomposite Hydrogels. *Polmeric Materials: Science and Engineering Preprints*, 94, 367–368.

Bako, J., Szepesi, M., Veres, A.J., Cserhati, C., Borbely, Z.M., Hegedus, C., and Borbely, J., 2008. Synthesis of biocompatible nanocomposite hydrogels as a local drug delivery system. *Colloid and Polymer Science*, 286 (3), 357–363.

Bakshi, M.S. and Singh, K., 2005. Synergistic interactions in the mixed micelles of cationic gemini with zwitterionic surfactants: Fluorescence and Krafft temperature studies. *Journal of Colloid and Interface Science*, 287 (1), 288–297.

Bal, S.M., Caussin, J., Pavel, S., and Bouwstra, J.A., 2008. In vivo assessment of safety of microneedle arrays in human skin. *European Journal of Pharmaceutical Sciences*, 35 (3), 193–202.

Baleeiro, R.B., Wiesmüller, K.H., Reiter, Y., Baude, B., Dähne, L., Patzelt, A., Lademann, J., Barbuto, J.A., and Walden, P., 2013. Topical vaccination with functionalized particles targeting dendritic cells. *Journal of Investigative Dermatology*, 133 (8), 1933–1941.

Banks, S.L., Pinninti, R.R., Gill, H.S., Paudel, K.S., Crooks, P.A., Brogden, N.K., Prausnitz, M.R., and Stinchcomb, A.L., 2010. Transdermal Delivery of Naltrexol and Skin Permeability Lifetime after Microneedle Treatment

in Hairless Guinea Pigs. *Journal of Pharmaceutical Sciences*, 99 (7), 3072–3080.

Banning, T.P. and Heard, C.M., 2002. Binding of doxycycline to keratin, melanin and human epidermal tissue. *International Journal of Pharmaceutics*, 235 (1–2), 219–227.

Baranda, L., González-Amaro, R., Torres-Alvarez, B., Alvarez, C., and Ramírez, V., 2002. Correlation between pH and irritant effect of cleansers marketed for dry skin. *In*: *International Journal of Dermatology*, 41 (8), 494–499.

Barbero, A.M. and Frasch, H.F., 2009. Pig and guinea pig skin as surrogates for human in vitro penetration studies: A quantitative review. *Toxicology in Vitro*, 23 (1), 1–13.

Bargo, P.R., Walston, S.T., Chu, M., Seo, I., and Kollias, N., 2013. Non-invasive assessment of tryptophan fluorescence and confocal microscopy provide information on skin barrier repair dynamics beyond TEWL. *Experimental Dermatology*, 22 (1), 18–23.

Baroni, A., Buommino, E., De Gregorio, V., Ruocco, E., Ruocco, V., and Wolf, R., 2012. Structure and function of the epidermis related to barrier properties. *Clinics in Dermatology*, 30 (3), 257–262.

Barr, M.D., Favid, W.B., Fairhurst, E., Gerrard, W.A., and Ridge, B.D., 1988. Changes in the physical properties of the stratum corneum following treatment with glycerol. *Journal of the Society of Cosmetic Chemists*, 39, 367–381.

Barry, B.W., 1983. *Dermatological formulations: Percutaneous absorption, drugs and pharmaceutical sciences*. New York: Marcel Dekker.

Barry, B.W., 1987. Penetration Enhancers. Mode of action in human skin. *In*: B. Shroot and H. Schaefer, eds. *Pharmacology of the Skin*. Basel: Karger, 121–137.

Barry, B.W., 2002a. Drug delivery routes in skin: a novel approach. *Advanced Drug Delivery Reviews*, 54, S31–S40.

Barry, B.W., 2002b. Transdermal Drug Delivery. *In:* M.E. Aulton, ed. *Pharmaceutics. The Science of Dosage Form Design.* New York: Churchill Livingstone, 499-533.

Barry, B. W., 2004. Breaching the skin's barrier to drugs. *Nature Biotechnology,* 22 (2), 165-167.

Beezer, A.., King, A.S.., Martin, I.., Mitchel, J.., Twyman, L.., and Wain, C.., 2003. Dendrimers as potential drug carriers; encapsulation of acidic hydrophobes within water soluble PAMAM derivatives. *Tetrahedron*, 59 (22), 3873–3880.

Behl, C.R., Flynn, G.L., Kurihara, T., Harper, N., Smith, W., Higuchi, W.I., Ho, N.F., and Pierson, C.L., 1980. Hydration and percutaneous absorption: I. Influence of hydration on alkanol permeation through hairless mouse skin. *Journal of Investigative Dermatology*, 75 (4), 346–352.

Belu, A.M., Graham, D.J., and Castner, D.G., 2003. Time-of-flight secondary ion mass spectrometry: techniques and applications for the characterization of biomaterial surfaces. *Biomaterials*, 24 (21), 3635–3653.

Benabdellah, F., Seyer, A., Quinton, L., Touboul, D., Brunelle, A., and Laprévote, O., 2010. Mass spectrometry imaging of rat brain sections: nanomolar sensitivity with MALDI versus nanometer resolution by TOF–SIMS. *Analytical and Bioanalytical Chemistry*, 396 (1), 151–162.

Benninghoven, A., 1994. Chemical Analysis of Inorganic and Organic Surfaces and Thin Films by Static Time-of-Flight Secondary Ion Mass Spectrometry (TOF-SIMS). *Angewandte Chemie International Edition*, 33 (10), 1023–1043.

Benson, H.A.E., 2012. Skin Structure, Function, and Permeation. *In*: H.A.E. Benson and A.C. Watkinson, eds. *Transdermal and Topical Drug Delivery: Principles and Practice*. New Jersey: John Wiley and Sons, 3–22.

Bergo, P. and Sobral, P.J.A., 2007. Effects of plasticizer on physical properties of pigskin gelatin films. *Food*

Hydrocolloids, 21 (8), 1285–1289.

Bernard, D., Méhul, B., Thomas-Collignon, A., Simonetti, L., Remy, V., Bernard, M.A., and Schmidt, R., 2003. Analysis of Proteins with Caseinolytic Activity in a Human Stratum Corneum Extract Revealed a Yet Unidentified Cysteine Protease and Identified the So-Called "Stratum Corneum Thiol Protease" as Cathepsin L2. *Journal of Investigative Dermatology*, 120 (4), 592–600.

Bewley, A. and Page, B., 2011. Maximizing patient adherence for optimal outcomes in psoriasis. *Journal of the European Academy of Dermatology and Venereology*, 25, 9–14.

Bich, C., Touboul, D., and Brunelle, A., 2014. Cluster TOF-SIMS imaging as a tool for micrometric histology of lipids in tissue. *Mass Spectrometry Reviews*, 33 (6), 442–451.

Bich, C., Touboul, D., and Brunelle, A., 2015. Biomedical studies by TOF-SIMS imaging. *Biointerphases*, 10 (1), 018901–7.

Boas, U., Karlsson, A.J., de Waal, B.M.F., and Meijer, E.W., 2001. Synthesis and Properties of New Thiourea-Functionalized Poly(propylene imine) Dendrimers and Their Role as Hosts for Urea Functionalized Guests. *The Journal of Organic Chemistry*, 66 (6), 2136–2145.

Boas, U. and Heegaard, P.M.H., 2004. Dendrimers in drug research. *Chemical Society Reviews*, 33, 43–63.

Bodratti, A.M. and Alexandridis, P., 2018. Formulation of poloxamers for drug delivery. *Journal of Functional Biomaterials*, 9 (1), 11-24.

Bojar, R.A. and Holland, K.T., 2002. The human cutaneous microflora and factors controlling colonisation. *World Journal of Microbiology and Biotechnology*, 18 (9), 889-903.

Bojar, R.A. and Holland, K.T., 2004. Acne and propionibacterium acnes. *Clinics in Dermatology*, 22 (5), 375–379.

Bolon, M.K., 2016. Hand Hygiene: An Update. *Infectious Disease Clinics of North America*, 30 (3), 591–607.

Bond, J.R. and Barry, B.W., 1988a. Hairless Mouse Skin is Limited as a Model for Assessing the Effects of Penetration Enhancers in Human Skin. *Journal of Investigative Dermatology*, 90, 810–813.

Bond, J.R. and Barry, B.W., 1988b. Limitations of Hairless Mouse Skin as a Model for In Vitro Permeation Studies Through Human Skin: Hydration Damage. *Journal of Investigative Dermatology*, 90 (4), 486–489.

Bonina, F.P., Carelli, V., Di Colo, G., Montenegro, L., and Nannipieri, E., 1993. Vehicle effects on in vitro skin permeation of and stratum corneum affinity for model drugs caffeine and testosterone. *International Journal of Pharmaceutics*, 100 (1–3), 41–47.

Bonina, F.P., Montenegro, L., De Caprariis, P., Palagiano, F., Trapani, G., and Liso, G., 1995. In vitro and in vivo evaluation of polyoxyethylene indomethacin esters as dermal prodrugs. *Journal of Controlled Release*, 34 (3), 223–232.

Bonnel, D., Legouffe, R., Eriksson, A.H., Mortensen, R.W., Pamelard, F., Stauber, J., and Nielsen, K.T., 2018. MALDI imaging facilitates new topical drug development process by determining quantitative skin distribution profiles. *Analytical and Bioanalytical Chemistry*, 410 (11), 2815–2828.

Boonchai, W. and Iamtharachai, P., 2010. The pH of Commonly Available Soaps, Liquid Cleansers, Detergents and Alcohol Gels. *Dermatitis*, 21 (3), 154–156.

Borowska, K., Wołowiec, S., Rubaj, A., Głowniak, K., Sieniawska, E., and Radej, S., 2012. Effect of polyamidoamine dendrimer G3 and G4 on skin permeation of 8-methoxypsoralene—In vivo study. *International Journal of Pharmaceutics*, 426 (1–2), 280–283.

Bos, J.D. and Meinardi, M.M.H.M., 2000. The 500 Dalton rule for the skin penetration of chemical compounds and drugs. *Experimental Dermatology*, 9 (3), 165–169.

Bourne, N., Stanberry, L.R., Kern, E.R., Holan, G., Matthews, B., and Bernstein, D.I., 2000. Dendrimers, a new class of candidate topical microbicides with activity against herpes simplex virus infection. *Antimicrobial Agents and Chemotherapy*, 44 (9), 2471–2474.

Bouwstra, J.A., Gooris, G.S., van der Spek, J.A., and Bras, W., 1991a. Structural Investigations of Human Stratum Corneum by Small-Angle X-Ray Scattering. *Journal of Investigative Dermatology*, 97 (6), 1005–1012.

Bouwstra, J.A., de Vries, M.A., Gooris, G.S., Bras, W., Brussee, J., and Ponec, M., 1991b. Thermodynamic and structural aspects of the skin barrier. *Journal of Controlled Release*, 15 (3), 209–219.

Bouwstra, J.A., Dubbelaar, F.E.R., Gooris, G.S., and Ponec, M., 2000. The Lipid Organisation in the Skin Barrier. *Advances in Dermatology and Venerology*, S208, 23–30.

Bouwstra, J.A., de Graaff, A., Gooris, G.S., Nijsse, J., Wiechers, J.W., and van Aelst, A.C., 2003. Water Distribution and Related Morphology in Human Stratum Corneum at Different Hydration Levels. *Journal of Investigative Dermatology*, 120 (5), 750–758.

Bouwstra, J.A. and Ponec, M., 2006. The skin barrier in healthy and diseased state. *Biochimica et Biophysica Acta - Biomembranes*, 1758 (12), 2080–2095.

Boyce, J.M., Kelliher, S., and Vallande, N., 2000. Skin Irritation and Dryness Associated With Two Hand-Hygiene Regimens: Soap-and-Water Hand Washing Versus Hand Antisepsis With an Alcoholic Hand Gel. *Infection Control & Hospital Epidemiology*, 21 (7), 442–448.

Boyce, J.M. and Pittet, D., 2002. Guideline for Hand Hygiene in Health-Care Settings: Recommendations of the Healthcare Infection Control Practices Advisory Committee and the HICPAC/SHEA/APIC/IDSA Hand Hygiene Task Force. *Infection Control & Hospital Epidemiology*, 23 (S12), 3–40.

Brazdaru, L., Micutz, M., Staicu, T., Albu, M., Sulea, D., and Leca, M., 2015. Structural and rheological properties of collagen hydrogels containing tannic acid and chlorhexidine digluconate intended for topical applications. *Comptes Rendus Chimie*, 18 (2), 160–169.

Breternitz, M., Flach, M., Präßler, J., Elsner, P., and Fluhr, J.W., 2007. Acute barrier disruption by adhesive tapes is influenced by pressure, time and anatomical location: integrity and cohesion assessed by sequential tape stripping; a randomized, controlled study. *British Journal of Dermatology*, 156 (2), 231–240.

Breuer, M.M., 1979. The interation between surfactants and keratinous tissues. *Journal of the Society of Cosmetic Chemists*, 30, 41–64.

British Pharmacopoeia, 2019a. Topical Semi-solid Preparations. Available from: https://www.pharmacopoeia.com/bp-2020/formulated-general/topical-semi-solid-preparations-of-the-british-pharmacopoeia.html?published-date=2019-08-01&text=topical+. Accessed [7 July 2019].

British Pharmacopoeia, 2019b. Chlorhexidine Gluconate Eye Drops. Available from: https://www.pharmacopoeia.com/bp-2019/formulated-specific/chlorhexidine-gluconate-eye-drops.html?date=2019-07-01&text=chlorhexidine+chromatography. Accessed [7 July 2019].

Bronaugh, R.L., Stewart, R.F., and Congdon, E.R., 1982. Methods for in vitro percutaneous absorption studies II. Animal models for human skin. *Toxicology and Applied Pharmacology*, 62 (3), 481–488.

Bronaugh, R.L. and Franz, T.J., 1986. Vehicle effects on percutaneous absorption: in vivo and in vitro comparisons with human skin. *British Journal of Dermatology*, 115 (1), 1–11.

Bronaugh, R.L., Stewart, R.F., and Simon, M., 1986. Methods for in vitro percutaneous absorption studies VII: Use of excised human skin. *Journal of Pharmaceutical Sciences*, 75 (11), 1094–1097.

Brooks, S.E., Walczak, M.A., Hameed, R., and Coonan, P., 2002. Chlorhexidine Resistance in Antibiotic-Resistant Bacteria Isolated From the Surfaces of Dispensers of Soap Containing Chlorhexidine. *Infection Control & Hospital Epidemiology*, 23 (11), 692–695.

Brown, K.K., Rehmus, W.E., and Kimball, A.B., 2006. Determining the relative importance of patient motivations for nonadherence to topical corticosteroid therapy in psoriasis. *Journal of the American Academy of Dermatology*, 55 (4), 607–613.

Bucks, D., Maibach, H.I., and Guy, R.H., 1989. Occlusion Does Not Uniformly Enhance Penetration In Vivo. *In*: R.L. Bronaugh and H.I. Maibach, eds. *Percutaneous absorption: mechanisms, methodology, drug delivery*. New York: Marcel Dekker, 77–93.

Bucks, D., Guy, R., and Maibach, H.I., 1991. Effects of Occlusion. *In*: R.L. Bronaugh and H.I. Maibach, eds. *In Vitro Percutaneous Absorption: Principles, Fundamentals and Applications*. Boca Raton: CRC Press, 85–114.

Bui, L.N., Swan, J.T., Shirkey, B.A., Olsen, R.J., Long, S.W., and Graviss, E.A., 2018. Chlorhexidine bathing and Clostridium difficile infection in a surgical intensive care unit. *Journal of Surgical Research*, 228, 107–111.

Bunch, J., Clench, M.R., and Richards, D.S., 2004. Determination of pharmaceutical compounds in skin by imaging matrix-assisted laser desorption/ionisation mass spectrometry. *Rapid Communications in Mass Spectrometry*, 18 (24), 3051–3060.

Bunge, A.L. and Cleek, R.L., 1995. A New Method for Estimating Dermal Absorption from Chemical Exposure: 2. Effect of Molecular Weight and Octanol-Water Partitioning. *Pharmaceutical Research,* 12 (1), 88–95.

Burnette, R.R. and Ongpipattanakul, B., 1987. Characterization of the permselective properties of excised human skin during iontophoresis. *Journal of Pharmaceutical Sciences*, 76 (10), 765–773.

Calabretta, M.K., Kumar, A., McDermott, A.M., and Cai, C., 2007. Antibacterial Activities of Poly(amidoamine) Dendrimers Terminated with Amino and Poly(ethylene glycol) Groups. *Biomacromolecules*, 8 (6), 1807–1811.

Campbell, C.S.J., Contreras-Rojas, L.R., Delgado-Charro, M.B., and Guy, R.H., 2012. Objective assessment of nanoparticle disposition in mammalian skin after topical exposure. *Journal of Controlled Release*, 162 (1), 201–207.

Cappel, M.J. and Kreuter, J., 1991. Effect of nonionic surfactants on transdermal drug delivery: I. Polysorbates. *International Journal of Pharmaceutics*, 69 (2), 143–153.

Cattaneo, D., McCormick, L.J., Cordes, D.B., Slawin, A.M.Z., and Morris, R.E., 2016. Crystal structure resolution of two different chlorhexidine salts. *Journal of Molecular Structure*, 1121, 70–73.

Chakrabarti, S., 2014. What's in a name? Compliance, adherence and concordance in chronic psychiatric disorders. *World Journal of Psychiatry*, 4 (2), 30.

Chan, T.Y.K., 1994. Poisoning due to Savlon (Cetrimide) Liquid. *Human & Experimental Toxicology*, 13 (10), 681–682.

Chandrasekar, D., Sistla, R., Ahmad, F.J., Khar, R.K., and Diwan, P. V., 2007. The development of folate-PAMAM dendrimer conjugates for targeted delivery of anti-arthritic drugs and their pharmacokinetics and biodistribution in arthritic rats. *Biomaterials*, 28 (3), 504–512.

Chang, S.A. and Gray, D.G., 1978. The surface tension of aqueous hydroxypropyl cellulose solutions. *Journal of Colloid And Interface Science*, 67 (2), 255–265.

Chauhan, A.S., 2018. Dendrimers for Drug Delivery. *Molecules*, 23 (4), 938.

Chauhan, A.S., Jain, N.K., and Diwan, P.V., 2010. Pre-clinical and behavioural toxicity profile of PAMAM dendrimers in mice. *Proceedings of the Royal Society A: Mathematical, Physical and Engineering Sciences*, 466 (2117), 1535–1550.

Chauhan, A.S., Sridevi, S., Chalasani, K.B., Jain, A.K., Jain, S.K., Jain, N.., and Diwan, P. V., 2003. Dendrimer-mediated transdermal delivery: enhanced bioavailability of indomethacin. *Journal of Controlled Release*, 90 (3), 335–343.

Cheng, Y., Qu, H., Ma, M., Xu, Z., Xu, P., Fang, Y., and Xu, T., 2007. Polyamidoamine (PAMAM) dendrimers as biocompatible carriers of quinolone antimicrobials: An in vitro study. *European Journal of Medicinal Chemistry*, 42 (7), 1032–1038.

Chilcott, R.P., Dalton, C.H., Emmanuel, A.J., Allen, C.E., and Bradley, S.T., 2002. Transepidermal Water Loss Does Not Correlate with Skin Barrier Function In Vitro. *Journal of Investigative Dermatology*, 118 (5), 871–875.

Chilcott, R.P., 2008. Cutaneous anatomy and function. *In*: R.P. Chilcott and S. Price, eds. *Principles and Practice of Skin Toxicology*. Chichester: John Wiley and Sons, 1–17.

Climo, M.W., Yokoe, D.S., Warren, D.K., Perl, T.M., Bolon, M., Herwaldt, L.A., Weinstein, R.A., Sepkowitz, K.A., Jernigan, J.A., Sanogo, K., and Wong, E.S., 2013. Effect of Daily Chlorhexidine Bathing on Hospital-Acquired Infection. *New England Journal of Medicine*, 368 (6), 533–542.

Coldman, M.F., Poulsen, B.J., and Higuchi, T., 1969. Enhancement of percutaneous absorption by the use of volatile: Nonvolatile systems as vehicles. *Journal of Pharmaceutical Sciences*, 58 (9), 1098–1102.

Cornwell, P.A. and Barry, B.W., 1993. The routes of penetration of ions and 5-fluorouracil across human skin and the mechanisms of action of terpene skin penetration enhancers. *International Journal of Pharmaceutics*, 94 (1–3), 189–194.

Costello, E.K., Lauber, C.L., Hamady, M., Fierer, N., Gordon, J.I., and Knight, R., 2009. Bacterial community variation in human body habitats across space and time. *Science*, 326 (5960), 1694–1697.

Coulman, S.A., Birchall, J.C., Alex, A., Pearton, M., Hofer, B., O'Mahony, C., Drexler, W., and Považay, B., 2011. In Vivo, In Situ Imaging of Microneedle Insertion into the Skin of Human Volunteers Using Optical Coherence Tomography. *Pharmaceutical Research*, 28 (1), 66–81.

Crank, J., 1975. *The Mathematics of Diffusion*. 2nd ed. Oxford, UK: Clarendon Press.

Crosby, C., Elliott, T., Lambert, P., and Adams, D., 2009. Preoperative skin preparation: a historical perspective. *British Journal of Hospital Medicine*, 70 (10), 579–582.

Cross, S.E. and Roberts, M.S., 1993. Subcutaneous Absorption Kinetics and Local Tissue Distribution of Interferon and Other Solutes. *Journal of Pharmacy and Pharmacology*, 45 (7), 606–609.

Cross, S.E. and Roberts, M.S., 2000. The effect of occlusion on epidermal penetration of parabens from a commercial allergy test ointment, acetone and ethanol vehicles. *Journal of Investigative Dermatology*, 115 (5), 914–918.

Cross, S.E., Pugh, W.J., Hadgraft, J., and Roberts, M.S., 2001. Probing the effect of vehicles on topical delivery: Understanding the basic relationship between solvent and solute penetration using silicone membranes. *Pharmaceutical Research*, 18 (7), 999–1005.

Czaika, V., Alborova, A., Richter, H., Sterry, W., Vergou, T., Antoniou, C., Lademann, J., and Koch, S., 2012. Comparison of transepidermal water loss and laser scanning microscopy measurements to assess their value in the characterization of cutaneous barrier defects. *Skin Pharmacology and Physiology*, 25 (1), 39–46.

D'Emanuele, A. and Attwood, D., 2005. Dendrimer–drug interactions. *Advanced Drug Delivery Reviews*, 57 (15), 2147–2162.

Van Damme, P., Oosterhuis-Kafeja, F., Van der Wielen, M., Almagor, Y., Sharon, O., and Levin, Y., 2009. Safety and efficacy of a novel microneedle device for dose sparing intradermal influenza vaccination in healthy adults. *Vaccine*, 27 (3), 454–459.

Darouiche, R.O., Wall, M.J., Itani, K.M.F., Otterson, M.F., Webb, A.L., Carrick, M.M., Miller, H.J., Awad, S.S., Crosby, C.T., Mosier, M.C., Al-Sharif, A., and Berger, D.H., 2010. Chlorhexidine–Alcohol versus Povidone–Iodine for Surgical-Site Antisepsis. *New England Journal of Medicine*, 362 (1), 18–26.

Daugimont, L., Baron, N., Vandermeulen, G., Pavselj, N., Miklavcic, D., Jullien, M.C., Cabodevila, G., Mir, L.M., and Préat, V., 2010. Hollow microneedle arrays for intradermal drug delivery and DNA electroporation. *Journal of Membrane Biology*, 236 (1), 117–125.

Davies, D.J., Heylings, J.R., McCarthy, T.J., and Correa, C.M., 2015. Development of an in vitro model for studying the penetration of chemicals through compromised skin. *Toxicology in Vitro*, 29 (1), 176–181.

Davis, S.P., Landis, B.J., Adams, Z.H., Allen, M.G., and Prausnitz, M.R., 2004. Insertion of microneedles into skin: measurement and prediction of insertion force and needle fracture force. *Journal of Biomechanics*, 37 (8), 1155–1163.

Delaney, J.S., 2005. Predicting aqueous solubility from structure. *Drug Discovery Today*, 10 (4), 289–295.

Dendritech, 2017. PAMAM Dendrimers. Available: http://www.dendritech.com/pamam.html. Accessed [1 Feb 2019].

Denton, G.W., 2001. Chlorhexidine. *In*: S.S. Block, ed. *Disinfection, Sterlization and Preservation*. Philadelphia: Lippincott Williams and Wilkins, 321–333.

Derici, L., Harcup, J.P., Hill, S.P., and Khoshdel, E., 2010. Hair care composition comprising a dendritic macromolecule . Patent Number: WO2010072527A1.

Dermapen, 2019. Safe, Effective Dermapen Leads the Way. Available from: https://dermapen.com/2013/11/13/safe-effective-dermapen-leads/ [Accessed 19 Aug 2019].

Devarakonda, B., Hill, R.A., and De Villiers, M.M., 2004. The effect of PAMAM dendrimer generation size and surface functional group on the aqueous solubility of nifedipine. *International Journal of Pharmaceutics*, 284 (1–2), 133–140.

Díez-Sales, O., Copoví, A., Casabó, V.G., and Herráez, M., 1991. A modelistic approach showing the importance of the stagnant aqueous layers in in vitro diffusion studies, and in vitro-in vivo correlations. *International Journal of Pharmaceutics*, 77 (1), 1–11.

Doddaballapur, S., 2009. Microneedling with dermaroller. *Journal of Cutaneous and Aesthetic surgery*, 2 (2), 110–1.

Donnelly, R.F., 2018. Clinical Translation and Industrial Development of Microneedle-based Products. *In*: R.F. Donnelly, T.R.R. Singh, E. Larrañeta, and M.T.C. McCrudden, eds. *Microneedles for Drug and Vaccine Delivery and Patient Monitoring*. New Jersey: John Wiley and Sons, Ltd, 307–322.

Donnelly, R.F., Singh, T.R.R., and Woolfson, A.D., 2010. Microneedle-based drug delivery systems: Microfabrication, drug delivery, and safety. *Drug Delivery*, 17 (4), 187–207.

Donnelly, R.F., Morrow, D.I.J., McCarron, P.A., Woolfson, A.D., Morrissey, A., Juzenas, P., Juzeniene, A., Iani, V., McCarthy, H.O., and Moan, J., 2008. Microneedle-mediated intradermal delivery of 5-aminolevulinic acid: Potential for enhanced topical photodynamic therapy. *Journal of* Donnelly, R.F., Garland, M.J., Morrow, D.I.J., Migalska, K., Singh, T.R.R., Majithiya, R., and Woolfson, A.D., 2010. Optical coherence tomography is a valuable tool in the study of the effects of microneedle geometry on skin penetration characteristics and in-skin dissolution. *Journal of Controlled Release*, 147 (3), 333–341.

Donnelly, R.F., Singh, T.R.R., Tunney, M.M., Morrow, D.I.J., McCarron, P.A., O'Mahony, C., and Woolfson, A.D., 2009. Microneedle Arrays Allow Lower Microbial Penetration Than Hypodermic Needles In Vitro. *Pharmaceutical Research*, 26 (11), 2513–2522.

Donnelly, R.F., Singh, T.R.R., Garland, M.J., Migalska, K., Majithiya, R., McCrudden, C.M., Kole, P.L., Mahmood, T.M.T., McCarthy, H.O., and Woolfson, A.D., 2012a. Hydrogel-Forming Microneedle Arrays for Enhanced Transdermal Drug Delivery. *Advanced Functional Materials*, 22 (23), 4879–4890.

Donnelly, R.F., Thakur, R.R.S., Morrow, D.I.J., and Woolfson, D.A., eds., 2012b. Microneedles: Design, Microfabrication and Optimization. *In*: *Microneedle-mediated Transdermal and Intradermal Drug Delivery*.

Sussex: John Wiley and Sons, 20–56.

Donnelly, R.F., Singh, T.R.R., Alkilani, A.Z., McCrudden, M.T.C., O'Neill, S., O'Mahony, C., Armstrong, K., McLoone, N., Kole, P., and Woolfson, A.D., 2013. Hydrogel-forming microneedle arrays exhibit antimicrobial properties: Potential for enhanced patient safety. *International Journal of Pharmaceutics*, 451 (1–2), 76–91.

Donnelly, R.F., Moffatt, K., Alkilani, A.Z., Vicente-Pérez, E.M., Barry, J., McCrudden, M.T.C., and Woolfson, A.D., 2014. Hydrogel-Forming Microneedle Arrays Can Be Effectively Inserted in Skin by Self-Application: A Pilot Study Centred on Pharmacist Intervention and a Patient Information Leaflet. *Pharmaceutical Research*, 31 (8), 1989–1999.

Downing, D.T., 1992. Lipid and protein structures in the permeability barrier of mammalian epidermis. *Journal of Lipid Research*, 33, 301–313.

Dryden, M.S., 2009. Skin and soft tissue infection: microbiology and epidemiology. *International Journal of Antimicrobial Agents*, 34 (S1), 2-7.

Dugard, P.H. and Scheuplein, R.J., 1973. Effects of ionic surfactants on the permeability of human epidermis: an electrometric study. *The Journal of investigative dermatology*, 60 (5), 263–269.

Duncan, R. and Izzo, L., 2005. Dendrimer biocompatibility and toxicity. *Advanced Drug Delivery Reviews*, 57 (15), 2215–2237.

Dunlap, Mills, Tuley, Baker, and Plott, 1998. Adapalene 0·1% gel for the treatment of acne vulgaris: its superiority compared to tretinoin 0·025% cream in skin tolerance and patient preference. *British Journal of Dermatology*, 139 (S52), 17–22.

Einstein, A., 1959. *Investigations on the Theory of the Brownian Movement*. Oxford, UK: Dove Publications.

Ekholm, I.E., Brattsand, M., and Egelrud, T., 2000. Stratum Corneum Tryptic Enzyme in Normal Epidermis: a Missing Link in the Desquamation Process? *Journal of Investigative Dermatology*, 114 (1), 56–63.

El-Kattan, A.F., Asbill, C.S., Kim, N., and Michniak, B.B., 2001. The effects of terpene enhancers on the percutaneous permeation of drugs with different lipophilicities. *International Journal of Pharmaceutics*, 215 (1–2), 229–240.

Elias, P.M., 1983. Epidermal Lipids, Barrier Function, and Desquamation. *Journal of Investigative Dermatology*, 80 (S6), 44–49.

Elias, P.M. and Friend, D.S., 1975. The permeability barrier in mammalian epidermis. *The Journal of Cell Biology*, 65 (1), 180–91.

Elias, P.M., Bonar, L., Grayson, S., and Baden, H.P., 1983. X-ray Diffraction Analysis of Stratum Corneum Membrane Couplets. *Journal of Investigative Dermatology*, 80 (3), 213–214.

Elkeeb, R., Hui, X., Chan, H., Tian, L., and Maibach, H.I., 2010. Correlation of transepidermal water loss with skin barrier properties in vitro: comparison of three evaporimeters. *Skin Research and Technology*, 16 (1), 9–15.

Elkhyat, A., Fanian, F., Abdou, A., Amarouch, H., and Humbert, P., 2017. Influence of the Sebum and the Hydrolipidic Layer in Skin Wettability and Friction. *In*: P. Humbert, F. Fanian, H.I. Maibach, and P. Agache, eds. *Agache's Measuring the Skin*. Cham: Springer, 191–202.

Elmahjoubi, E., Frum, Y., Eccleston, G.M., Wilkinson, S.C., and Meidan, V.M., 2009. Transepidermal water loss for probing full-thickness skin barrier function: Correlation with tritiated water flux, sensitivity to punctures and diverse surfactant exposures. *Toxicology in Vitro*, 23 (7), 1429–1435.

Enthaler, B., Pruns, J.K., Wessel, S., Rapp, C., Fischer, M., and Wittern, K-P., 2012. Improved sample preparation for MALDI–MSI of endogenous compounds in skin tissue sections and mapping of exogenous active

compounds subsequent to ex-vivo skin penetration. *Analytical and Bioanalytical Chemistry*, 402 (3), 1159–1167.

Enthaler, B., Trusch, M., Fischer, M., Rapp, C., Pruns, J.K., and Vietzke, J-P., 2013. MALDI imaging in human skin tissue sections: focus on various matrices and enzymes. *Analytical and Bioanalytical Chemistry*, 405 (4), 1159–1170.

Esfand, R. and Tomalia, D.A., 2001. Poly(amidoamine) (PAMAM) dendrimers: from biomimicry to drug delivery and biomedical applications. *Drug Discovery Today*, 6 (8), 427–436.

Essa, E.A., Bonner, M.C., and Barry, B.W., 2002. Human skin sandwich for assessing shunt route penetration during passive and iontophoretic drug and liposome delivery. *Journal of Pharmacy and Pharmacology*, 54 (11), 1481–1490.

Essendoubi, M., Gobinet, C., Reynaud, R., Angiboust, J.F., Manfait, M., and Piot, O., 2016. Human skin penetration of hyaluronic acid of different molecular weights as probed by Raman spectroscopy. *Skin Research and Technology*, 22 (1), 55–62.

European Committee on Antimicrobial Susceptibility Testing, 2019. *Antimicrobial susceptibility testing EUCAST disk diffusion method*. Available from: http://www.eucast.org/fileadmin/src/media/PDFs/EUCAST_files/Disk_test_documents/2019_manuals/Manual_v_7.0_EUCAST_Disk_Test_2019.pdf. Accessed [3 Feb 2019].

Fabin, B. and Touitou, E., 1991. Localization of lipophilic molecules penetrating rat skin in vivo by quantitative autoradiography. *International Journal of Pharmaceutics*, 74 (1), 59–65.

Fahlén, A., Engstrand, L., Baker, B.S., Powles, A., and Fry, L., 2012. Comparison of bacterial microbiota in skin biopsies from normal and psoriatic skin. *Archives of Dermatological Research*, 304 (1), 15–22.

Fang, J.Y., Kuo, C.T., Huang, Y. Bin, Wu, P.C., and Tsai, Y.H., 1999a. Transdermal delivery of sodium nonivamide acetate from volatile vehicles: Effects of polymers. *International Journal of Pharmaceutics*, 176 (2), 157–167.

Fang, J.Y., Sung, K.C., Lin, H.H., and Fang, C.L., 1999b. Transdermal iontophoretic delivery of diclofenac sodium from various polymer formulations: in vitro and in vivo studies. *International Journal of Pharmaceutics*, 178 (1), 83–92.

Farkas, E., Kiss, D., and Zelko, R., 2007. Study on the release of chlorhexidine base and salts from different liquid crystalline structures. *International Journal of Pharmaceutics*, 340 (1–2), 71–75.

Fathi-Azarbayjani, A., Jouyban, A., and Chan, S.Y., 2009. Impact of surface tension in pharmaceutical sciences. *Journal of Pharmacy and Pharmaceutical Sciences*, 12 (2), 218-228.

Feldman, S.R. and Housman, T.S., 2003. Vehicle Preference for Corticosteroid Treatments of Scalp Psoriasis. *American Journal of Clinical Dermatology*, 4 (4), 221–224.

Fenner, J. and Clark, R.A.F., 2016. Anatomy, Physiology, Histology, and Immunohistochemistry of Human Skin. *In*: M. Albanna and J.H. Holmes, eds. *Skin Tissue Engineering and Regenerative Medicine*. London: Elsevier, 1–18.

Ferraz, C.C.R., de Almeida Gomes, B.P.F., Zaia, A.A., Teixeira, F.B., and de Souza-Filho, F.J., 2001. In Vitro Assessment of the Antimicrobial Action and the Mechanical Ability of Chlorhexidine Gel as an Endodontic Irrigant. *Journal of Endodontics*, 27 (7), 452–455.

Ferry, L.L., Argentieri, G., and Lochner, D.H., 1995. The comparative histology of porcine and guinea pig skin with respect to iontophoretic drug delivery. *Pharmaceutica Acta Helvetiae*, 70 (1), 43–56.

Fertig, R.M., Gamret, A.C., Cervantes, J., and Tosti, A., 2018. Microneedling for the treatment of hair loss? *Journal of the European Academy of Dermatology and Venereology*, 32 (4), 564–569.

Fierer, N., Hamady, M., Lauber, C.L., and Knight, R., 2008. The influence of sex, handedness, and washing on the diversity of hand surface bacteria. *Proceedings of the National Academy of Sciences of the United States of America*, 105 (46), 17994–17999.

Filipowicz, A. and Wołowiec, S., 2011. Solubility and in vitro transdermal diffusion of riboflavin assisted by PAMAM dendrimers. *International Journal of Pharmaceutics*, 408 (1–2), 152–156.

Florence, A.T. and Attwood, D., 2006a. Physicochemical properties of drugs in solution. *In*: A.T. Florence and D. Attwood, eds. *Physicochemical Principles of Pharmacy*. London: Pharmaceutical Press, 56–90.

Florence, A.T. and Attwood, D., eds., 2006b. Emulsions, suspensions and other disperse systems. *In*: *Physicochemical Principles of Pharmacy*. London: Pharmaceutical Press, 229–272.

Fluhr, J.W. and Elias, P.M., 2002. Stratum corneum pH: Formation and Function of the 'Acid Mantle'. *Exogenous Dermatology*, 1 (4), 163–175.

Fluhr, J.W., Kao, J., Jain, M., Ahn, S.K., Feingold, K.R., and Elias, P.M., 2001. Generation of free fatty acids from phospholipids regulates stratum corneum acidification and integrity. *Journal of Investigative Dermatology*, 117 (1), 44–51.

Flynn, G.L., 1992. Physicochemical determinants of skin absorption. *In*: T.R. Gerrity and C.J.. Henry, eds. *Principles of Route-to-Route Extrapolation for Risk Assessment*. New York: Elsevier, 93–127.

Francoeur, M.L., Golden, G.M., and Potts, R.O., 1990. Oleic Acid: Its Effects on Stratum Corneum in Relation to (Trans)Dermal Drug Delivery. *Pharmaceutical Research*, 7 (6), 621–627.

Franz, T.J., 1975. Percutaneous Absorption. On the Relevance of in Vitro Data. *Journal of Investigative Dermatology*, 64 (3), 190–195.

Friend, D., Catz, P., Heller, J., Reid, J., and Baker, R., 1988. Transdermal delivery of levonorgestrel I: Alkanols as permeation enhancers in vitro. *Journal of Controlled Release*, 7 (3), 243–250.

Fritz, S.A., Hogan, P.G., Camins, B.C., Ainsworth, A.J., Patrick, C., Martin, M.S., Krauss, M.J., Rodriguez, M., and Burnham, C-A.D., 2013. Mupirocin and chlorhexidine resistance in Staphylococcus aureus in patients with community-onset skin and soft tissue infections. *Antimicrobial Agents and Chemotherapy*, 57 (1), 559–568.

Froebe, C.L., Simion, F.A., Rhein, L.D., Cagan, R.H., and Kligman, A., 1990. Stratum corneum Lipid Removal by Surfactants: Relation to in vivo Irritation. *Dermatology*, 181 (4), 277–283.

Frunzi, G. and Sarsfield, B., 2006. Cetostearyl Alcohol. *In*: R.C. Rowe, P.J. Sheskey, and S.C. Owen, eds. *Handbook of Pharmaceutical Excipients*. London: Pharmaceutical Press, 150–151.

Fry, D.E., 2006. The Surgical Infection Prevention Project: Processes, Outcomes, and Future Impact. *Surgical Infections*, 7 (S1), 17-26.

Gallagher, S.J. and Heard, C.M., 2005. Solvent content and macroviscosity effects on the in vitro transcutaneous delivery and skin distribution of ketoprofen from simple gel formulations. *Skin Pharmacology and Physiology*, 18 (4), 186–194.

Gambichler, T., Orlikov, A., Vasa, R., Moussa, G., Hoffmann, K., Stücker, M., Altmeyer, P., and Bechara, F.G., 2007. In vivo optical coherence tomography of basal cell carcinoma. *Journal of Dermatological Science*, 45 (3), 167–173.

Gamer, A.O., Leibold, E., and van Ravenzwaay, B., 2006. The in vitro absorption of microfine zinc oxide and titanium dioxide through porcine skin. *Toxicology in Vitro*, 20 (3), 301–307.

Gao, Z., Tseng, C.H., Pei, Z., and Blaser, M.J., 2007. Molecular analysis of human forearm superficial skin bacterial biota. *Proceedings of the National Academy of Sciences of the United States of America*, 104 (8), 2927–2932.

Gardikis, K., Hatziantoniou, S., Viras, K., Wagner, M., and Demetzos, C., 2006. A DSC and Raman spectroscopy study on the effect of PAMAM dendrimer on DPPC model lipid membranes. *International Journal of Pharmaceutics*, 318 (1–2), 118–123.

Garson, J-C., Doucet, J., Lévêque, J-L., and Tsoucaris, G., 1991. Oriented Structure in Human Stratum Corneum Revealed by X-Ray Diffraction. *Journal of Investigative Dermatology*, 96 (1), 43–49.

Gautam, S.P., Gupta, A.K., Wani, S.U.D., Malviya, N., Gautam, T., and Sharma, A.K., 2015. PAMAM Dendrimers mediated solubility enhancement of poorly soluble drugs: a concise review. *International Journal of Pharmaceutics and Drug Analysis*, 3 (4), 105–110.

Gee, C.M., Nicolazzo, J.A., Watkinson, A.C., and Finnin, B.C., 2012. Assessment of the lateral diffusion and penetration of topically applied drugs in humans using a novel concentric tape stripping design. *Pharmaceutical Research*, 29 (8), 2035–2046.

Gee, C.M., Watkinson, A.C., Nicolazzo, J.A., and Finnin, B.C., 2014. The effect of formulation excipients on the penetration and lateral diffusion of ibuprofen on and within the stratum corneum following topical application to humans. *Journal of Pharmaceutical Sciences*, 103 (3), 909–919.

Gerstel, M.S. and Place, V.A., 1971. Drug Delivery Device. Patent Number: US3964482A.

Gibbs, B.M. and Stuttard, L.W., 1967. Evaluation of Skin Germicides. *Journal of Applied Bacteriology*, 30 (1), 66–77.

Gibson, W.T. and Teall, M.R., 1983. Interactions of C12 surfactants with the skin: Changes in enzymes and visible and histological features of rat skin treated with sodium lauryl sulphate. *Food and Chemical Toxicology*, 21 (5), 587–594.

Gill, H.S., Denson, D.D., Burris, B.A., and Prausnitz, M.R., 2008. Effect of microneedle design on pain in human volunteers. *The Clinical Journal of Pain*, 24 (7), 585–594.

Gilmore, I.S. and Seah, M.P., 2002. Electron flood gun damage in the analysis of polymers and organics in time-of-flight SIMS. *Applied Surface Science*, 187 (1–2), 89–100.

Ginn, M.E., Noyes, C.M., and Jungermann, E., 1968. The contact angle of water on viable human skin. *Journal of Colloid And Interface Science*, 26 (2), 146–151.

Gladkova, N.D., Petrova, G.A., Nikulin, N.K., Radenska-Lopovok, S.G., Snopova, L.B., Chumakov, Y.P., Nasonova, V.A., Gelikonov, V.M., Gelikonov, G. V., Kuranov, R. V., Sergeev, A.M., and Feldchtein, F.I., 2000. In vivo optical coherence tomography imaging of human skin: Norm and pathology. *Skin Research and Technology*, 6 (1), 6–16.

Godin, B. and Touitou, E., 2004. Mechanism of bacitracin permeation enhancement through the skin and cellular membranes from an ethosomal carrier. *Journal of Controlled Release*, 94 (2–3), 365–379.

González, S., Zonios, G., Nguyen, B.C., Gillies, R., and Kollias, N., 2000. Endogenous Skin Fluorescence is a Good Marker for Objective Evaluation of Comedolysis. *Journal of Investigative Dermatology*, 115 (1), 100–105.

Goodman, M. and Barry, B.W., 1988. Action of penetration enhancers on human skin as assessed by the permeation of model drugs 5-fluorouracil and estradiol. I. Infinite dose technique. *Journal of Investigative Dermatology*, 91 (4), 323–327.

Goodman, M. and Barry, B.W., 1989. Lipid-protein-partitioning (LPP) theory of skin enhancer activity: finite dose technique. *International Journal of Pharmaceutics*, 57 (1), 29–40.

Gould, I.M. and Bal, A.M., 2013. New antibiotic agents in the pipeline and how they can help overcome microbial resistance. *Virulence*, 4 (2), 185–191.

Grams, J., Góralski, J., and Szczepaniak, B., 2007. Time-of-flight secondary ion-mass spectrometry as a new technique for the investigations of the deactivation process of hydrodechlorination catalysts. *Russian*

Journal of Physical Chemistry A, 81 (9), 1515–1520.

Gray, G.M. and Yardley, H.J., 1975. Lipid compositions of cells isolated from pig, human, and rat epidermis. *Journal of Lipid Research*, 16 (6), 434–40.

Green, K.J. and Simpson, C.L., 2007. Desmosomes: New Perspectives on a Classic. *Journal of Investigative Dermatology*, 127 (11), 2499–2515.

Grice, E.A., Kong, H.H., Renaud, G., Young, A.C., Bouffard, G.G., Blakesley, R.W., Wolfsberg, T.G., Turner, M.L., and Segre, J.A., 2008. A diversity profile of the human skin microbiota. *Genome Research*, 18 (7), 1043–50.

Grice, E.A., Kong, H.H., Conlan, S., Deming, C.B., Davis, J., Young, A.C., Bouffard, G.G., Blakesley, R.W., Murray, P.R., Green, E.D., Turner, M.L., and Segre, J.A., 2009. Topographical and temporal diversity of the human skin microbiome. *Science*, 324 (5931), 1190–1192.

Grice, E.A. and Segre, J.A., 2011. The skin microbiome. *Nature Reviews Microbiology*, 9 (4), 244–253.

Gupta, J., Felner, E.I., and Prausnitz, M.R., 2009. Minimally Invasive Insulin Delivery in Subjects with Type 1 Diabetes Using Hollow Microneedles. *Diabetes Technology & Therapeutics*, 11 (6), 329–337.

Gupta, J., Gill, H.S., Andrews, S.N., and Prausnitz, M.R., 2011. Kinetics of skin resealing after insertion of microneedles in human subjects. *Journal of Controlled Release*, 154 (2), 148–155.

Gupta, V. and Trivedi, P., 2018. In vitro and in vivo characterization of pharmaceutical topical nanocarriers containing anticancer drugs for skin cancer treatment. *In*: *Lipid Nanocarriers for Drug Targeting*. Elsevier, 563–627.

Guy, R.H. and Hadgraft, J., 1987. Transdermal drug delivery: A perspective. *Journal of Controlled Release*, 4 (4), 237–251.

Guy, R.H. and Hadgraft, J., 1992. Rate control in transdermal drug delivery? *International Journal of Pharmaceutics*, 82 (3), R1–R6.

Guy, R.H., Kalia, Y.N., Delgado-Charro, M.B., Merino, V., López, A., and Marro, D., 2000. Iontophoresis: Electrorepulsion and electroosmosis. *In*: *Journal of Controlled Release*, 64 (1-3), 129–132.

Haake, A., Scott, G.A., and Holbrook, K.A., 2001. Structure and function of the skin: overveiw of the epidermis and dermis. *In*: R.K. Freinkel and D.T. Woodley, eds. *The Biology of the Skin*. New York: The Parthenon Publishing Group, 19–45.

Hachem, J.-P., Crumrine, D., Fluhr, J., Brown, B.E., Feingold, K.R., and Elias, P.M., 2003. pH directly regulates epidermal permeability barrier homeostasis, and stratum corneum integrity/cohesion. *The Journal of investigative dermatology*, 121 (2), 345–53.

Hachem, J.P., Man, M.Q., Crumrine, D., Uchida, Y., Brown, B.E., Regiers, V., Roseeuw, D., Feingold, K.R., and Elias, P.M., 2005. Sustained serine proteases activity by prolonged increase in pH leads to degradation of lipid processing enzymes and profound alterations of barrier function and stratum corneum integrity. *Journal of Investigative Dermatology*, 125 (3), 510–520.

Haigh, J.M., Meyer, E., Smith, E.W., and Kanfer, I., 1997. The human skin blanching assay for in vivo topical corticosteroid assessment. *International Journal of Pharmaceutics*, 152 (2), 179–183.

Haq, M.I., Smith, E., John, D.N., Kalavala, M., Edwards, C., Anstey, A., Morrissey, A., and Birchall, J.C., 2009. Clinical administration of microneedles: skin puncture, pain and sensation. *Biomedical Microdevices*, 11 (1), 35–47.

Hara, M. and Verkman, A.S., 2003. Glycerol replacement corrects defective skin hydration, elasticity, and barrier function in aquaporin-3-deficient mice. *Proceedings of the National Academy of Sciences of the United States of America*, 100 (12), 7360–7365.

Harding, C.R., 2004. The stratum corneum: structure and function in health and disease. *Dermatologic Therapy*, 17 (S1), 6–15.

Harding, C.R., Watkinson, A., Rawlings, A. V, and Scott, I.R., 2000. Dry skin, moisturization and corneodesmolysis. *International journal of Cosmetic Science*, 22 (1), 21–52.

Hart, P.J., Francese, S., Claude, E., Woodroofe, M.N., and Clench, M.R., 2011. MALDI-MS imaging of lipids in ex vivo human skin. *Analytical and Bioanalytical Chemistry*, 401 (1), 115–125.

Harwood, R.J., 2006. Hydroxyethyl cellulose. *In*: R.C. Rowe, P.J. Sheskey, and S.C. Owen, eds. *Handbook of Pharmaceutical Excipients*. Washington: Pharmaceutical Press, 330–333.

Hashmi, S., Ling, P., Hashmi, G., Reed, M., Gaugler, R., and Trimmer, W., 1995. Genetic transformation of nematodes using arrays of micromechanical piercing structures. *BioTechniques*, 19 (5), 766–770.

Heard, D.D. and Aashworth, R.W., 1968. The colloidal properties of chlorhexidine and its interaction with some macromolecules. *Journal of Pharmacy and Pharmacology*, 20 (7), 505–512.

Heard, C.M. and Screen, C., 2008. Probing the permeation enhancement of mefenamic acid by ethanol across full-thickness skin, heat-separated epidermal membrane and heat-separated dermal membrane. *International Journal of Pharmaceutics*, 349 (1–2), 323–325.

Hendry, E.R., Worthington, T., Conway, B.R., and Lambert, P.A., 2009. Antimicrobial efficacy of eucalyptus oil and 1,8-cineole alone and in combination with chlorhexidine digluconate against microorganisms grown in planktonic and biofilm cultures. *Journal of Antimicrobial Chemotherapy*, 64 (6), 1219–1225.

Henry, S., McAllister, D. V., Allen, M.G., and Prausnitz, M.R., 1998. Microfabricated Microneedles: A Novel Approach to Transdermal Drug Delivery. *Journal of Pharmaceutical Sciences*, 87 (8), 922–925.

Hibbard, J.S., Mulberry, G.K., and Brady, A.R., 2002. A clinical study comparing the skin antisepsis and safety of ChloraPrep, 70% isopropyl alcohol, and 2% aqueous chlorhexidine. *Journal of Infusion Nursing*, 25 (4), 244–249.

Higuchi, T., 1960. Physical chemical analysis of percutaneous absorption process from creams and ointments. *Journal of the Society of Cosmetic Chemists*, 11, 85–97.

Hilton, J., Woollen, B.H., Scott, R.C., Auton, T.R., Trebilcock, K.L., and Wilks, M.F., 1994. Vehicle Effects on in Vitro Percutaneous Absorption Through Rat and Human Skin. *Pharmaceutical Research: An Official Journal of the American Association of Pharmaceutical Scientists*, 11 (10), 1396–1400.

Ho, D., Kraeva, E., Jagdeo, J., and Levenson, R.M., 2016. Spectral Imaging in Dermatology. *In*: M.R. Hamblin, P. Avci, and G.K. Gupta, eds. *Imaging in Dermatology*. London: Elsevier, 217–236.

Hoelgaard, A., Møllgaard, B., and Baker, E., 1988. Vehicle effect on topical drug delivery. IV. Effect of N-methylpyrrolidone and polar lipids on percutaneous drug transport. *International Journal of Pharmaceutics*, 43 (3), 233–240.

Hol, K., 2010a. Patient preference for topical psoriasis formulations. *In*: *19th Congress of the European Academy of Dermatology and Venereology(EADV)*. Gothenburg, Sweden, 572.

Hol, K., 2010b. European study into the opinions of psoriasis patients andphysicians. *In*: *19th Congress of the European Academy of Dermatologyand Venereology (EADV)*. Gothenburg, Sweden, 573.

Holbrook, K.A. and Odland, G.F., 1974. Regional Differences in the Thickness (Cell Layers) of the Human Stratum Corneum: An Ultrastructural Analysis. *Journal of Investigative Dermatology*, 62 (4), 415–422.

Holmes, A.M., Scurr, D.J., Heylings, J.R., Wan, K-W., and Moss, G.P., 2017. Dendrimer pre-treatment enhances the skin permeation of chlorhexidine digluconate: Characterisation by in vitro percutaneous absorption studies and Time-of-Flight Secondary Ion Mass Spectrometry. *European Journal of Pharmaceutical Sciences*, 104, 90–101.

Holmes, A.M., Heylings, J.R., Wan, K-W., and Moss, G.P., 2019. Antimicrobial efficacy and mechanism of action of poly(amidoamine) (PAMAM) dendrimers against opportunistic pathogens. *International Journal of Antimicrobial Agents*, 53 (4), 500–507.

Hong, S., Bielinska, A.U., Mecke, A., Keszler, B., Beals, J.L., Shi, X., Balogh, L., Orr, B.G., Baker, J.R., and Banaszak Holl, M.M., 2004. Interaction of poly(amidoamine) dendrimers with supported lipid bilayers and cells: Hole formation and the relation to transport. *Bioconjugate Chemistry*, 15 (4), 774–782.

Hou, H. and Siegel, R.A., 2006. Enhanced permeation of diazepam through artificial membranes from supersaturated solutions. *Journal of Pharmaceutical Sciences*, 95 (4), 896–905.

Hu, R.Y.Z., Wang, A.T.A., and Hartnett, J.P., 1991. Surface tension measurement of aqueous polymer solutions. *Experimental Thermal and Fluid Science*, 4 (6), 723–729.

Hugo, W.B. and Longworth, A.R., 1964. Some aspects of the mode of action of chlorhexidine. *Journal of Pharmacy and Pharmacology*, 16 (10), 655–662.

Hugonnet, S., Perneger, T. V., and Pittet, D., 2002. Alcohol-based handrub improves compliance with hand hygiene in intensive care units. *Archives of Internal Medicine*, 162 (9), 1037–1043.

Hussain, A.A., Themstrup, L., Mogensen, M., and Jemec, G.B.E., 2017. Optical Coherence Tomography Imaging of the Skin. *In*: *Agache's Measuring the Skin*. Cham: Springer, 493–502.

Hutton, A.R.J., Quinn, H.L., McCague, P.J., Jarrahian, C., Rein-Weston, A., Coffey, P.S., Gerth-Guyette, E., Zehrung, D., Larrañeta, E., and Donnelly, R.F., 2018. Transdermal delivery of vitamin K using dissolving microneedles for the prevention of vitamin K deficiency bleeding. *International Journal of Pharmaceutics*, 541 (1–2), 56–63.

ICI Americas Inc, 1976. *The HLB System - A time saving guide to emulsifier selection*. Available from: http://www.firp.ula.ve/archivos/historicos/76_Book_HLB_ICI.pdf Accessed [12 Jun 2019].

Iervolino, M., Cappello, B., Raghavan, S.L., and Hadgraft, J., 2001. Penetration enhancement of ibuprofen from supersaturated solutions through human skin. *International Journal of Pharmaceutics*, 212 (1), 131–141.

Iervolino, M., Raghavan, S.L., and Hadgraft, J., 2000. Membrane penetration enhancement of ibuprofen using supersaturation. *International Journal of Pharmaceutics*, 198 (2), 229–238.

Imhof, B. and McFeat, G., 2014. Evalulation of the Barrier Function of Skin Using Transepidermal Water Loss (TEWL). A Critical Overview. *In*: A.O. Barel, M. Paye, and H.I. Maibach, eds. *Handbook of Cosmetic Science and Technology*. Boca Raton: CRC Press, 131–139.

Inoue, K., 2000. Functional dendrimers, hyperbranched and star polymers. *Progress in Polymer Science*, 25 (4), 453–571.

Intarakumhaeng, R. and Li, S.K., 2014. Effects of solvent on percutaneous absorption of nonvolatile lipophilic solute. *International Journal of Pharmaceutics*, 476 (1–2), 266–276.

International Pharmacopoeia, 2018. Topical semi-solid dosage forms. Available from: http://apps.who.int/phint/pdf/b/6.2.1.8.Topical-semi-solid-dosage-forms.pdf. Accessed [2 Jult 2019].

Ito, Y., Hirono, M., Fukushima, K., Sugioka, N., and Takada, K., 2012. Two-layered dissolving microneedles formulated with intermediate-acting insulin. *International Journal of Pharmaceutics*, 436 (1–2), 387–393.

Jacobi, U., Meykadeh, N., Sterry, W., and Lademann, J., 2003. Effect of the vehicle on the amount of stratum corneum removed by tape stripping. *Journal of the German Society of Dermatology*, 1 (11), 884–889.

Jacobi, U., Weigmann, H-J., Baumann, M., Reiche, A.-I., Sterry, W., and Lademann, J., 2004. Lateral Spreading of Topically Applied UV Filter Substances Investigated by Tape Stripping. *Skin Pharmacology and Physiology*, 17 (1), 17–22.

Jacobi, U., Weigmann, H-J., Ulrich, J., Sterry, W., and Lademann, J., 2005. Estimation of the relative stratum corneum amount removed by tape stripping. *Skin Research and Technology*, 11 (2), 91–96.

Jacobi, U., Kaiser, M., Toll, R., Mangelsdorf, S., Audring, H., Otberg, N., Sterry, W., and Lademann, J., 2007. Porcine ear skin: an in vitro model for human skin. *Skin Research and Technology*, 13 (1), 19–24.

Jang, W.D., Kamruzzaman Selim, K.M., Lee, C.H., and Kang, I.K., 2009. Bioinspired application of dendrimers: From bio-mimicry to biomedical applications. *Progress in Polymer Science*, 34 (1), 1-23.

Jansen, J.F.G.A., Meijer, E.W., and de Brabander-van den Berg, E.M.M., 1995. The Dendritic Box: Shape-Selective Liberation of Encapsulated Guests. *Journal of the American Chemical Society*, 117 (15), 4417–4418.

Jarnik, M., Simon, M.N., and Steven, A.C., 1998. Cornified cell envelope assembly: a model based on electron microscopic determinations of thickness and projected density. *Journal of Cell Science*, 111, 1051–1060.

Jepps, O.G., Dancik, Y., Anissimov, Y.G., and Roberts, M.S., 2013. Modeling the human skin barrier — Towards a better understanding of dermal absorption. *Advanced Drug Delivery Reviews*, 65 (2), 152–168.

Jevons, M.P., 1961. "Celbenin" - resistant Staphylococci. *British Medical Journal*, 1 (5219), 124.

Johnson, M.E., Berk, D.A., Blankschtein, D., Golan, D.E., Jain, R.K., and Langer, R.S., 1996. Lateral diffusion of small compounds in human stratum corneum and model lipid bilayer systems. *Biophysical Journal*, 71 (5), 2656–2668.

Johnson, M.E., Blankschtein, D., and Langer, R., 1997. Evaluation of Solute Permeation through the Stratum Corneum: Lateral Bilayer Diffusion as the Primary Transport Mechanism. *Journal of Pharmaceutical Sciences*, 86 (10), 1162–1172.

Johnson, A., Kapadia, B., Daley, J., Molina, C., and Mont, M., 2013. Chlorhexidine Reduces Infections in Knee Arthroplasty. *Journal of Knee Surgery*, 26 (3), 213–218.

Jonca, N., Guerrin, M., Hadjiolova, K., Caubet, C., Gallinaro, H., Simon, M., and Serre, G., 2002. Corneodesmosin, a component of epidermal corneocyte desmosomes, displays homophilic adhesive properties. *The Journal of Biological Chemistry*, 277 (7), 5024–5029.

Jones, C.G., 1997. Chlorhexidine: is it still the gold standard? *Periodontology 2000*, 15 (1), 55–62.

Jones, E.A., Lockyer, N.P., and Vickerman, J.C., 2007. Mass spectral analysis and imaging of tissue by ToF-SIMS—The role of buckminsterfullerene, C60+, primary ions. *International Journal of Mass Spectrometry*, 260 (2–3), 146–157.

Jorgensen, W.L. and Duffy, E.M., 2002. Prediction of drug solubility from structure. *Advanced Drug Delivery Reviews*, 54 (3), 355–366.

Judd, A.M., 2013a. An investigation into the co-formulation of a PAMAM dendrimer-CHG skin treatment and the development and optimisation of a suitable topical formulation that will ultimately deliver an increased concentration of CHG within the skin. Keele University.

Judd, A.M., 2013b. Elucidation of the interaction between PAMAM dendrimers and porcine skin. Keele University.

Judd, A.M., Moss, G.P., Heylings, J., Wan, K-W., and Yang, Y., 2013a. Optical coherence tomography to delineate the interactions of PAMAM dendrimers with the porcine skin surface. *In*: *Dynamics and Fluctuations in Biomedical Photonics X*. SPIE, 85800G.

Judd, A.M., Scurr, D.J., Heylings, J.R., Wan, K-W., and Moss, G.P., 2013b. Distribution and Visualisation of Chlorhexidine Within the Skin Using ToF-SIMS: A Potential Platform for the Design of More Efficacious Skin Antiseptic Formulations. *Pharmaceutical Research*, 30 (7), 1896–1905.

Jui-Chen, T., Weiner, N.D., Flynn, G.L., and Ferry, J., 1991. Properties of adhesive tapes used for stratum corneum

stripping. *International Journal of Pharmaceutics*, 72 (3), 227–231.

Jung, E.C. and Maibach, H.I., 2015. Animal models for percutaneous absorption. *Journal of Applied Toxicology*, 35 (1), 1–10.

Kabir-ud-Din, Abdul Rub, M., and Naqvi, A.Z., 2012. Micellization of mixtures of amphiphilic drugs and cationic surfactants: A detailed study. *Colloids and Surfaces B: Biointerfaces*, 92, 16–24.

Kai, T., Mak, V.H.W., Potts, R.O., and Guy, R.H., 1990. Mechanism of percutaneous penetration enhancement: effect of n-alkanols on the permeability barrier of hairless mouse skin. *Journal of Controlled Release*, 12 (2), 103–112.

Kaiser, N., Klein, D., Karanja, P., Greten, Z., and Newman, J., 2009. Inactivation of chlorhexidine gluconate on skin by incompatible alcohol hand sanitizing gels. *American Journal of Infection Control*, 37 (7), 569–573.

Kalia, Y.N. and Guy, R.H., 2001. Modeling transdermal drug release. *Advanced Drug Delivery Reviews*, 48 (2-3), 159-172.

Kalia, Y.N., Nonato, L.B., and Guy, R.H., 1996. The Effect of Iontophoresis on Skin Barrier Integrity: Non-invasive Evaluation by Impedance Spectroscopy and Transepidermal Water Loss. *Pharmaceutical Research*, 13 (6), 957–960.

Kampf, G., 2016. Acquired resistance to chlorhexidine – is it time to establish an 'antiseptic stewardship' initiative? *Journal of Hospital Infection*, 94 (3), 213-227.

Kannan, R.M., Perumal, O.P., and Kannan, S., 2007. Dendrimers and Hyperbranched Polymers for Drug Delivery. *In*: V. Labhasetwar and D.L. Leslie-Pelecky, eds. *Biomedical applications of nanotechnology*. Wiley-Interscience, 105–126.

Karadzovska, D., Brooks, J.D., Monteiro-Riviere, N.A., and Riviere, J.E., 2013. Predicting skin permeability from complex vehicles. *Advanced Drug Delivery Reviews*, 65 (2), 265–277.

Karande, P. and Mitragotri, S., 2009. Enhancement of transdermal drug delivery via synergistic action of chemicals. *Biochimica et Biophysica Acta (BBA) - Biomembranes*, 1788 (11), 2362–2373.

Karas, M. and Hillenkamp, F., 1988. Laser Desorption Ionization of Proteins with Molecular Masses Exceeding 10 000 Daltons. *Analytical Chemistry*, 60 (20), 2299-2301.

Karpanen, T.J., Worthington, T., Conway, B.R., Hilton, A.C., Elliott, T.S.J., and Lambert, P.A., 2008a. Penetration of chlorhexidine into human skin. *Antimicrobial agents and chemotherapy*, 52 (10), 3633–3636.

Karpanen, T.J., Worthington, T., Hendry, E.R., Conway, B.R., and Lambert, P.A., 2008b. Antimicrobial efficacy of chlorhexidine digluconate alone and in combination with eucalyptus oil, tea tree oil and thymol against planktonic and biofilm cultures of Staphylococcus epidermidis. *Journal of Antimicrobial Chemotherapy*, 62 (5), 1031–1036.

Karpanen, T.J., Worthington, T., Conway, B.R., Hilton, A.C., Elliott, T.S.J., and Lambert, P.A., 2009. Permeation of chlorhexidine from alcoholic and aqueous solutions within excised human skin. *Antimicrobial Agents and Chemotherapy*, 53 (4), 1717–1719.

Karpanen, T.J., Conway, B.R., Worthington, T., Hilton, A.C., Elliott, T.S., and Lambert, P.A., 2010. Enhanced chlorhexidine skin penetration with eucalyptus oil. *BMC Infectious Diseases*, 10 (1), 1–6.

Kassakian, S.Z., Mermel, L.A., Jefferson, J.A., Parenteau, S.L., and Machan, J.T., 2011. Impact of Chlorhexidine Bathing on Hospital-Acquired Infections among General Medical Patients. *Infection Control & Hospital Epidemiology*, 32 (3), 238–243.

Kathe, K. and Kathpalia, H., 2017. Film forming systems for topical and transdermal drug delivery. *Asian Journal*

of Pharmaceutical Sciences, 12 (6), 487–497.

Katsumi, H., Liu, S., Tanaka, Y., Hitomi, K., Hayashi, R., Hirai, Y., Kusamori, K., Quan, Y., Kamiyama, F., Sakane, T., and Yamamoto, A., 2012. Development of a Novel Self-Dissolving Microneedle Array of Alendronate, a Nitrogen-Containing Bisphosphonate: Evaluation of Transdermal Absorption, Safety, and Pharmacological Effects After Application in Rats. *Journal of Pharmaceutical Sciences*, 101 (9), 3230–3238.

Katz, M. and Poulsen, B.J., 1972. Corticoid, vehicle and skin interactions in percutaneous absorption. *Journal of the Society of Cosmetic Chemists*, 23, 565–590.

Kaushik, S., Hord, A.H., Denson, D.D., McAllister, D. V., Smitra, S., Allen, M.G., and Prausnitz, M.R., 2001. Lack of Pain Associated with Microfabricated Microneedles. *Anesthesia and Analgesia*, 92 (2), 502–504.

Kearney, M.C., Caffarel-Salvador, E., Fallows, S.J., McCarthy, H.O., and Donnelly, R.F., 2016. Microneedle-mediated delivery of donepezil: Potential for improved treatment options in Alzheimer's disease. *European Journal of Pharmaceutics and Biopharmaceutics*, 103, 43–50.

Kempe, S., Metz, H., and Mäder, K., 2008. Do situ forming PLG/NMP implants behave similarly *in vitro* and *in vivo*? A non-invasive and quantitative EPR investigation on the mechanisms of the implant formation process. *Journal of Controlled Release*, 130 (3), 220-225.

Kezic, S., 2008. Methods for measuring in-vivo percutaneous absorption in humans. *Human and Experimental Toxicology*, 27 (4), 289–295.

Kezutyte, T., Desbenoit, N., Brunelle, A., and Briedis, V., 2013. Studying the penetration of fatty acids into human skin by ex vivo TOF-SIMS imaging. *Biointerphases*, 8 (1), 1–8.

Khan, M.A. and Hoang, M.Q., 1997. Film-forming composition containing chlorhexidine gluconate. Patent Number: US5763412A.

Kim, Y-C., Park, J-H., and Prausnitz, M.R., 2012. Microneedles for drug and vaccine delivery. *Advanced Drug Delivery Reviews*, 64 (14), 1547–1568.

Kiremitçi, A.S., Çiftçi, A., Özalp, M., and Gümüşderelioğlu, M., 2007. Novel chlorhexidine releasing system developed from thermosensitive vinyl ether-based hydrogels. *Journal of Biomedical Materials Research Part B: Applied Biomaterials*, 83 (2), 609–614.

Kirkland, K.B., Briggs, J.P., Trivette, S.L., Wilkinson, W.E., and Sexton, D.J., 1999. The Impact of Surgical-Site Infections in the 1990s: Attributable Mortality, Excess Length of Hospitalization, And Extra Costs. *Infection Control & Hospital Epidemiology*, 20 (11), 725–730.

Kirton, G., Brown, A., Hawker, C., Reynolds, P., and White, J., 1998. Surface activity of modified dendrimers at high compression. *Physica B: Condensed Matter*, 248 (1–4), 184–190.

Kitagawa, S., Kasamaki, M., and Ikarashi, A., 2000. Effects of n-alkyltrimethylammonium on skin permeation of benzoic acid through excised guinea pig dorsal skin. *Chemical & Pharmaceutical Bulletin*, 48 (11), 1698–701.

Kitajima, Y., 2015. Implications of normal and disordered remodelling dynamics of corneodesmosomes in stratum corneum. *Dermatologica Sinica*, 33 (2), 58-63.

Klajnert, B. and Epand, R.M., 2005. PAMAM dendrimers and model membranes: Differential scanning calorimetry studies. *International Journal of Pharmaceutics*, 305 (1–2), 154–166.

Kligman, A.M., 1965. Topical Pharmacology and Toxicology of Dimethyl Sulfoxide. *Journal of the American Medical Association*, 193 (10), 796–804.

Knorr, F., Lademann, J., Patzelt, A., Sterry, W., Blume-Peytavi, U., and Vogt, A., 2009. Follicular transport route--research progress and future perspectives. *European Journal of Pharmaceutics and Biopharmaceutics*, 71

(2), 173–80.

Knüttel, A., Bonev, S., and Knaak, W., 2003. Scattering and refractive index properties of skin obtained with OCT. *In*: W. Dexter, ed. *Optical Coherence Tomography and Coherence Techniques*. Washington: OSA Publishing, 5140-5178.

Kolhe, P., Misra, E., Kannan, R.M., Kannan, S., and Lieh-Lai, M., 2003. Drug complexation, in vitro release and cellular entry of dendrimers and hyperbranched polymers. *International Journal of Pharmaceutics*, 259 (1–2), 143–160.

Kollias, N., Gillies, R., Moran, M., Kochevar, I.E., and Anderson, R.R., 1998. Endogenous Skin Fluorescence Includes Bands that may Serve as Quantitative Markers of Aging and Photoaging. *Journal of Investigative Dermatology*, 111 (5), 776–780.

Kong, H.H., Andersson, B., Clavel, T., Common, J.E., Jackson, S.A., Olson, N.D., Segre, J.A., and Traidl-Hoffmann, C., 2017. Performing Skin Microbiome Research: A Method to the Madness. *Journal of Investigative Dermatology*, 137 (3), 561-568.

Kostenbauder, H.B., 1983. Physical Factors influencing the activity of antimicrobial agents. *In*: S.S. Block, ed. *Disinfection, Sterlization and Preservation*. Philadelphia: Lea and Febiger, 811–828.

Kownatzki, E., 2003. Hand hygiene and skin health. *Journal of Hospital Infection*, 55 (4), 239-245.

Krautheim, A.B., Jermann, T.H.M., and Bircher, A.J., 2004. Chlorhexidine anaphylaxis: case report and review of the literature. *Contact Dermatitis*, 50 (3), 113–116.

Kreilgaard, M., Pedersen, E.J., and Jaroszewski, J.W., 2000. NMR characterisation and transdermal drug delivery potential of microemulsion systems. *Journal of Controlled Release*, 69 (3), 421–433.

Krejci-Manwaring, J., Tusa, M.G., Carroll, C., Camacho, F., Kaur, M., Carr, D., Fleischer, A.B., Balkrishnan, R., and Feldman, S.R., 2007. Stealth monitoring of adherence to topical medication: Adherence is very poor in children with atopic dermatitis. *Journal of the American Academy of Dermatology*, 56 (2), 211–216.

Kriwet, K. and Müller-Goymann, C.C., 1995. Diclofenac release from phospholipid drug systems and permeation through excised human stratum corneum. *International Journal of Pharmaceutics*, 125 (2), 231–242.

Küchler, S., Radowski, M.R., Blaschke, T., Dathe, M., Plendl, J., Haag, R., Schäfer-Korting, M., and Kramer, K.D., 2009. Nanoparticles for skin penetration enhancement – A comparison of a dendritic core-multishell-nanotransporter and solid lipid nanoparticles. *European Journal of Pharmaceutics and Biopharmaceutics*, 71 (2), 243–250.

Kudo, K., Ikeda, N., Kiyoshima, A., Hino, Y., Nishida, N., and Inoue, N., 2002. *Toxicological Analysis of Chlorhexidine in Human Serum using HPLC on a Polymer-Coated ODS Column*. Journal of Analytical Toxicology, 26 (2), 119-122.

Kurtoglu, Y.E., Mishra, M.K., Kannan, S., and Kannan, R.M., 2010. Drug release characteristics of PAMAM dendrimer–drug conjugates with different linkers. *International Journal of Pharmaceutics*, 384 (1–2), 189–194.

Kushla, G.P., Zatz, J.L., Mills, O.H., and Berger, R.S., 1993. Noninvasive Assessment of Anesthetic Activity of Topical Lidocaine Formulations. *Journal of Pharmaceutical Sciences*, 82 (11), 1118–1122.

Kuyyakanond, T. and Quesnel, L.B., 1992. The mechanism of action of chlorhexidine. *FEMS Microbiology Letters*, 100 (1–3), 211–215.

Labieniec, M., Ulicna, O., Vancova, O., Glowacki, R., Sebekova, K., Bald, E., Gabryelak, T., and Watala, C., 2008. PAMAM G4 dendrimers lower high glucose but do not improve reduced survival in diabetic rats. *International Journal of Pharmaceutics*, 364 (1), 142–149.

Lademann, J., Otberg, N., Richter, H., Weigmann, H-J., Lindemann, U., Schaefer, H., and Sterry, W., 2001.

Investigation of Follicular Penetration of Topically Applied Substances. *Skin Pharmacology and Physiology*, 14 (1), 17–22.

Lademann, J., Jacobi, U., Surber, C., Weigmann, H-J., and Fluhr, J.W., 2009. The tape stripping procedure – evaluation of some critical parameters. *European Journal of Pharmaceutics and Biopharmaceutics*, 72 (2), 317–323.

Lademann, J., Meinke, M.C., Schanzer, S., Richter, H., Darvin, M.E., Haag, S.F., Fluhr, J.W., Weigmann, H-J., Sterry, W., and Patzelt, A., 2012. In vivo methods for the analysis of the penetration of topically applied substances in and through the skin barrier. *International Journal of Cosmetic Science*, 34 (6), 551–559.

Lafforgue, C., Carret, L., Falson, F., Reverdy, M.E., and Freney, J., 1997. Percutaneous absorption of a chlorhexidine digluconate solution. *International Journal of Pharmaceutics*, 147 (2), 243–246.

Lamagni, T., Elgohari, S., and Harrington, P., 2015. Trends in surgical site infections following orthopaedic surgery. *Current Opinion in Infectious Diseases*, 28 (2), 125-132.

Lambert, J., Hol, C.W., and Vink, J., 2015. Real-life effectiveness of once-daily calcipotriol and betamethasone dipropionate gel vs. ointment formulations in psoriasis vulgaris: Final analysis of the 52-week PRO-long study. *Journal of the European Academy of Dermatology and Venereology*, 29 (12), 2349–2355.

Lampe, M.A., Williams, M.L., and Elias, P.M., 1983. Human epidermal lipids: characterization and modulations during differentiation. *Journal of Lipid Research*, 24 (2), 131–40.

Lange-Asschenfeldt, B., Marenbach, D., Lang, C., Patzelt, A., Ulrich, M., Maltusch, A., Terhorst, D., Stockfleth, E., Sterry, W., and Lademann, J., 2011. Distribution of bacteria in the epidermal layers and hair follicles of the human skin. *Skin Pharmacology and Physiology*, 24 (6), 305–311.

Larrañeta, E., Moore, J., Vicente-Pérez, E.M., González-Vázquez, P., Lutton, R., Woolfson, A.D., and Donnelly, R.F., 2014. A proposed model membrane and test method for microneedle insertion studies. *International Journal of Pharmaceutics*, 472 (1–2), 65–73.

Larrañeta, E., Lutton, R.E.M., Brady, A.J., Vicente-Pérez, E.M., Woolfson, A.D., Thakur, R.R.S., and Donnelly, R.F., 2015. Microwave-Assisted Preparation of Hydrogel-Forming Microneedle Arrays for Transdermal Drug Delivery Applications. *Macromolecular Materials and Engineering*, 300 (6), 586–595.

Larrañeta, E., Henry, M., Irwin, N.J., Trotter, J., Perminova, A.A., and Donnelly, R.F., 2018. Synthesis and characterization of hyaluronic acid hydrogels crosslinked using a solvent-free process for potential biomedical applications. *Carbohydrate Polymers*, 181, 1194–1205.

Larrucea, E., Arellano, A., Santoyo, S., and Ygartua, P., 2001. Combined effect of oleic acid and propylene glycol on the percutaneous penetration of tenoxicam and its retention in the skin. *European Journal of Pharmaceutics and Biopharmaceutics*, 52 (2), 113–119.

Lavrijsen, A.P.M., Higounenc, I.M., Weerheim, A., Oestmann, E., Tuinenburg, E.E., Bnddé, H.E., and Ponec, M., 1994. Validation of an in vivo extraction method for human stratum corneum ceramides. *Archives of Dermatological Research*, 286 (8), 495–503.

Lazar, A.N., Bich, C., Panchal, M., Desbenoit, N., Petit, V.W., Touboul, D., Dauphinot, L., Marquer, C., Laprévote, O., Brunelle, A., and Duyckaerts, C., 2013. Time-of-flight secondary ion mass spectrometry (TOF-SIMS) imaging reveals cholesterol overload in the cerebral cortex of Alzheimer disease patients. *Acta Neuropathologica*, 125 (1), 133–144.

Lboutounne, H., Chaulet, J.-F., Ploton, C., Falson, F., and Pirot, F., 2002. Sustained ex vivo skin antiseptic activity of chlorhexidine in poly(ϵ-caprolactone) nanocapsule encapsulated form and as a digluconate. *Journal of Controlled Release*, 82 (2–3), 319–334.

Lboutounne, H., Faivre, V., Falson, F., and Pirot, F., 2004. Characterization of transport of chlorhexidine-loaded nanocapsules through hairless and wistar rat skin. *Skin Pharmacology and Physiology*, 17 (4), 176–182.

Leaper, D.J., Tanner, J., Kiernan, M., Assadian, O., and Edmiston, C.E., 2015. Surgical site infection: poor compliance with guidelines and care bundles. *International Wound Journal*, 12 (3), 357–362.

Lee, H.J., Jeong, S.E., Lee, S., Kim, S., Han, H., and Jeon, C.O., 2018. Effects of cosmetics on the skin microbiome of facial cheeks with different hydration levels. *Microbiology Open*, 7 (2), 1-14.

Leo, A., Hansch, C., and Elkins, D., 1971. Partition coefficients and their uses. *Chemical Reviews*, 71 (6), 525–616.

Leor, R., Feinstein, M., Hod, H., Rabinowitz, B., and Kaplinsky, E., 1990. The influence of pH on the intravenous delivery of lidocaine solutions. *European Journal of Clinical Pharmacology*, 39 (5), 521–523.

Leveque, J.L., Leveque, J.L., Garson, J.C., and De Rigal Groupe De, J., 1977. Transepidermal water loss from dry and normal skin. *Journal of the Society of Cosmetic Chemists* , 30, 333–343.

Levin, J. and Maibach, H., 2005. The correlation between transepidermal water loss and percutaneous absorption: an overview. *Journal of Controlled Release*, 103 (2), 291–299.

Leyden, J.J., McGinley, K.J., Mills, O.H., and Kligman, A.M., 1975. Age-related changes in the resident bacterial flora of the human face. *The Journal of Investigative Dermatology*, 65 (4), 379–81.

Li, G., Badkar, A., Nema, S., Kolli, C.S., and Banga, A.K., 2009. In vitro transdermal delivery of therapeutic antibodies using maltose microneedles. *International Journal of Pharmaceutics*, 368 (1–2), 109–115.

Li, X., Zhao, R., Qin, Z., Zhang, J., Zhai, S., Qiu, Y., Gao, Y., Xu, B., and Thomas, S.H., 2010. Microneedle pretreatment improves efficacy of cutaneous topical anesthesia. *The American Journal of Emergency Medicine*, 28 (2), 130–134.

Li, X., Zhang, R., Liang, R., Liu, W., Wang, C., Su, Z., Sun, F., and Li, Y., 2014. Preparation and characterization of sustained-release rotigotine film-forming gel. *International Journal of Pharmaceutics*, 460 (1–2), 273–279.

Li, J., Zeng, M., Shan, H., and Tong, C., 2017. Microneedle Patches as Drug and Vaccine Delivery Platform. *Current Medicinal Chemistry*, 24 (22).

Liebert, M., 1986. Final Report on the Safety Assessment of Hydroxyethylcellulose, Hydroxypropylcellulose, Methylcellulose, Hydroxypropyl Methylcellulose, and Cellulose Gum. *Journal of the Americal College of Toxicology*, 5 (3), 1–59.

Lim, K.-S. and Kam, P.C.A., 2008. Chlorhexidine - pharmacology and clinical applications. *Anaesthesia and Intensive Care*, 36, 502–512.

Liu, M. and Fréchet, J.M.J., 1999. Designing dendrimers for drug delivery. *Pharmaceutical Science & Technology Today*, 2 (10), 393–401.

Livermore, D.M., 2000. Antibiotic resistance in staphylococci. *International Journal of Antimicrobial Agents*, 16 (S1), 3–10.

Loffler, H., Dreher, F., and Maibach, H.I., 2004. Stratum corneum adhesive tape stripping: influence of anatomical site, application pressure, duration and removal. *British Journal of Dermatology*, 151 (4), 746–752.

Löffler, H. and Kampf, G., 2008. Hand disinfection: How irritant are alcohols? *Journal of Hospital Infection*, 70, 44–48.

Lotte, C., Rougier, A., Wilson, D.R., and Maibach, H.I., 1987. In vivo relationship between transepidermal water loss and percutaneous penetration of some organic compounds in man: effect of anatomic site. *Archives of Dermatological Research*, 279 (5), 351–356.

Lovell, D.L., 1945. Skin Bacteria -Their Location with Reference to Skin Sterilization. *Surgery, Genecology and Obstetrics with International Abstracys of Surgery*, 80, 174-177.

Lowbury, E.J. and Lilly, H.A., 1973. Use of 4% chlorhexidine detergent solution (Hibiscrub) and other methods of

skin disinfection. *British Medical Journal*, 1 (5852), 510–515.

Lowbury, E.J., Lilly, H.A., and Ayliffe, G.A., 1974. Preoperative disinfection of surgeons' hands: use of alcoholic solutions and effects of gloves on skin flora. *British Medical Journal*, 4 (5941), 369–372.

Lu, C., Wucher, A., and Winograd, N., 2011. Molecular Depth Profiling of Buried Lipid Bilayers Using C 60 - Secondary Ion Mass Spectrometry. *Analytical Chemistry*, 83 (1), 351–358.

Lutton, R.E.M., Moore, J., Larrañeta, E., Ligett, S., Woolfson, A.D., and Donnelly, R.F., 2015. Microneedle characterisation: the need for universal acceptance criteria and GMP specifications when moving towards commercialisation. *Drug Delivery and Translational Research*, 5 (4), 313–331.

Machado, M., Salgado, T.M., Hadgraft, J., and Lane, M.E., 2010. The relationship between transepidermal water loss and skin permeability. *International Journal of Pharmaceutics*, 384 (1–2), 73–77.

Machekposhti, S.A., Soltani, M., Najafizadeh, P., Ebrahimi, S.A., and Chen, P., 2017. Biocompatible polymer microneedle for topical/dermal delivery of tranexamic acid. *Journal of Controlled Release*, 261, 87–92.

Maibach, H.I. and Feldmann, R.J., 1969. Effect of applied concentration on percutaneous absorption in man. *Journal of Investigative Dermatology*, 52, 382.

Maiti, P.K., Çağın, T., Wang, G., and Goddard, W.A., 2004. Structure of PAMAM Dendrimers: Generations 1 through 11. *Macromolecules*, 37 (16), 6236–6254.

Majoros, I.J., Myc, A., Thommey Thomas, Mehta, C.B., and James R. Baker, J., 2006. PAMAM Dendrimer-Based Multifunctional Conjugate for Cancer Therapy: Synthesis, Characterization, and Functionality. *Biomacromolecules*, 7 (2), 572–579.

Malik, N., Wiwattanapatapee, R., Klopsch, R., Lorenz, K., Frey, H., Weener, J.W., Meijer, E.W., Paulus, W., and Duncan, R., 2000. Dendrimers: Relationship between structure and biocompatibility in vitro, and preliminary studies on the biodistribution of 125I-labelled polyamidoamine dendrimers in vivo. *Journal of Controlled Release*, 65 (1–2), 133–148.

Mangram, A.J., Horan, T.C., Pearson, M.L., Silver, L.C., and Jarvis, W.R., 1999. Guideline for Prevention of Surgical Site Infection, 1999. *Infection Control & Hospital Epidemiology*, 20 (4), 247–280.

Mao, G., Flach, C.R., Mendelsohn, R., and Walters, R.M., 2012. Imaging the Distribution of Sodium Dodecyl Sulfate in Skin by Confocal Raman and Infrared Microspectroscopy. *Pharmaceutical Research*, 29 (8), 2189–2201.

Maricich, S.M., Wellnitz, S.A., Nelson, A.M., Lesniak, D.R., Gerling, G.J., Lumpkin, E.A., and Zoghbi, H.Y., 2009. Merkel cells are essential for light-touch responses. *Science*, 324 (5934), 1580–1582.

Marples, R.R., 1982. Sex, constancy, and skin bacteria. *Archives of Dermatological Research*, 272 (3–4), 317–320.

Marriott, C., 2002. Rheology. *In*: M.E. Aulton, ed. *Pharmaceutics. The Science of Dosage Form Design*. New York: Churchill Livingstone, 41–58.

Marszall, L., 1980. Effective hydrophile-lipophile balance and micelle formation of non-ionic surfactants in the presence of short-chain glycol ethers. *International Journal of Pharmaceutics*, 6 (3–4), 253–260.

Marszall, L. and Van Valkenburg, J.W., 1982. The effect of glycols on the hydrophile-lipophile balance and the micelle formation of nonionic surfactants. *Journal of the American Oil Chemists' Society*, 59 (2), 84–87.

Martanto, W., Davis, S.P., Holiday, N.R., Wang, J., Gill, H.S., and Prausnitz, M.R., 2004. Transdermal Delivery of Insulin Using Microneedles in Vivo. *Pharmaceutical Research*, 21 (6), 947–952.

Martindale: The Complete Drug Reference, 2010. Chlorhexidine. Available from: https://www.medicinescomplete.com/#/search/martindale/chlorhexidine?offset=0. [Accessed 16 July 2019].

Mastropietro, D.J., Nimroozi, R., and Omidian, H., 2013. Rheology in Pharmaceutical Formulations-A Perspective. *Journal of Developing Drugs,* 2 (2), 1-6.

Mauro, T., Grayson, S., Gao, W.N., Man, M.Q., Kriehuber, E., Behne, M., Feingold, K.R., and Elias, P.M., 1998. Barrier recovery is impeded at neutral pH, independent of ionic effects: Implications for extracellular lipid processing. *Archives of Dermatological Research*, 290 (4), 215–222.

Mavon, A., Redoules, D., Humbert, P., Agache, P., and Gall, Y., 1998. Changes in sebum levels and skin surface free energy components following skin surface washing. *Colloids and Surfaces B: Biointerfaces*, 10 (5), 243–250.

McAllister, D. V., Wang, P.M., Davis, S.P., Park, J-H., Canatella, P.J., Allen, M.G., and Prausnitz, M.R., 2003. Microfabricated needles for transdermal delivery of macromolecules and nanoparticles: fabrication methods and transport studies. *Proceedings of the National Academy of Sciences of the United States of America*, 100 (24), 13755–60.

McAuley, W.J. and Caserta, F., 2015. Film-Forming and Heated Systems. *In*: R.F. Donnelly and T.R.R. Singh, eds. *Novel Delivery Systems for Transdermal and Intradermal Drug Delivery*. Sussex: John Wiley and Sons, 97–124.

McBride, M.E., Duncan, W.C., and Knox, J.M., 1977. The environment and the microbial ecology of human skin. *Applied and Environmental Microbiology*, 33 (3), 603–8.

McCaig, L.F., McDonald, L.C., Mandal, S., and Jernigan, D.B., 2006. Staphylococcus aureus-associated skin and soft tissue infections in ambulatory care. *Emerging Infectious Diseases*, 12 (11), 1715–1723.

McCarthy, T.J., 1969. The influence of insoluble powders on preservatives in solution. *Journal of Mondern Pharmacy*, 12, 321–328.

McCarthy, T.J. and Myburgh, J.A., 1974. The effect of tragacanth gel on preservative activity. *Pharmaceutisch Weekblad*, 109, 265–268.

McCrudden, M.T.C., Alkilani, A.Z., McCrudden, C.M., McAlister, E., McCarthy, H.O., Woolfson, A.D., and Donnelly, R.F., 2014. Design and physicochemical characterisation of novel dissolving polymeric microneedle arrays for transdermal delivery of high dose, low molecular weight drugs. *Journal of Controlled Release*, 180, 71–80.

McDonnell, G.. and Russell, A.D., 1999. Antiseptics and Disinfectants: Activity, Action, and Resistance. *Clinical Microbiology Reviews*, 12 (1), 147–179.

McKenzie, A.W. and Stoughton, R.B., 1962. Method for Comparing Percutaneous Absorption of Steroids. *Archives of Dermatology*, 86 (5), 608–610.

Medicines and Healthcare products Regulatory Agency, 2012. *All medical devices and medicinal product containing chlorhexidine - Risk of anaphylactic reaction due to chlorhexidine allergy*. Available from: https://www.gov.uk/drug-device-alerts/medical-device-alert-all-medical-devices-and-medicinal-products-containing-chlorhexidine-risk-of-anaphylactic-reaction-due-to-chlorhexidine-allergy. [Accessed 8 March 2019].

Medicines and Healthcare products Regulatory Agency, 2015. *Letters sent to healthcare professionals since November 2014*. Available from: https://www.gov.uk/drug-safety-update/letters-sent-to-healthcare-professionals-since-november-2014. Accessed [3 Nov 2018].

Megrab, N.A., Williams, A.C., and Barry, B.W., 1995a. Oestradiol permeation across human skin, silastic and snake skin membranes: The effects of ethanol/water co-solvent systems. *International Journal of Pharmaceutics*, 116 (1), 101–112.

Megrab, N.A., Williams, A.C., and Barry, B.W., 1995b. Oestradiol permeation through human skin and silastic membrane: effects of propylene glycol and supersaturation. *Journal of Controlled Release*, 36 (3), 277–

294.

Meidan, V.M., Bonner, M.C., and Michniak, B.B., 2005. Transfollicular drug delivery—Is it a reality? *International Journal of Pharmaceutics*, 306 (1–2), 1–14.

Mendelsohn, R., Flach, C.R., and Moore, D.J., 2006. Determination of molecular conformation and permeation in skin via IR spectroscopy, microscopy, and imaging. *Biochimica et Biophysica Acta - Biomembranes*, 1758 (7), 923–933.

Menon, G. and Ghadially, R., 1997. Morphology of lipid alterations in the epidermis: A review. *Microscopy Research and Technique*, 37 (3), 180–192.

Menon, G.K., 2002. New insights into skin structure: scratching the surface. *Advanced Drug Delivery Reviews*, 54 (S1), 3–17.

Mess, A., Enthaler, B., Fischer, M., Rapp, C., Pruns, J.K., and Vietzke, J-P., 2013. A novel sampling method for identification of endogenous skin surface compounds by use of DART-MS and MALDI-MS. *Talanta*, 103, 398–402.

Micali, G., Lacarrubba, F., Bongu, A., and West, D.P., 2001. The skin barrier. *In*: R.K. Freinkel and D.T. Woodley, eds. *The Biology of the Skin*. New York: CRC Press, 219–232.

Migdadi, E.M., Courtenay, A.J., Tekko, I.A., McCrudden, M.T.C., Kearney, M.C., McAlister, E., McCarthy, H.O., and Donnelly, R.F., 2018. Hydrogel-forming microneedles enhance transdermal delivery of metformin hydrochloride. *Journal of Controlled Release*, 285, 142–151.

Milhem, O.M., Myles, C., McKeown, N.B., Attwood, D., and D'Emanuele, A., 2000. Polyamidoamine Starburst® dendrimers as solubility enhancers. *International Journal of Pharmaceutics*, 197 (1–2), 239–241.

Milstone, L.M., 2004. Epidermal desquamation. *Journal of Dermatological Science*, 36 (3), 131-140.

Misra, D.N., 1994. Interaction of chlorhexidine digluconate with and adsorption of chlorhexidine on hydroxyapatite. *Journal of Biomedical Materials Research*, 28 (11), 1375–1381.

Mitragotri, S., 2003. Modeling skin permeability to hydrophilic and hydrophobic solutes based on four permeation pathways. *Journal of Controlled Release*, 86 (1), 69–92.

Mittal, A., Raber, A.S., Schaefer, U.F., Weissmann, S., Ebensen, T., Schulze, K., Guzmán, C.A., Lehr, C.M., and Hansen, S., 2013. Non-invasive delivery of nanoparticles to hair follicles: A perspective for transcutaneous immunization. *Vaccine*, 31 (34), 3442–3451.

Mogensen, M., Thrane, L., Joergensen, T.M., Anderson, P.E., and Jemec, G.B.E., 2009. Optical Coherence Tomography for Imaging of Skin and Skin Diseases. *Seminars in Cutaneous Medicine and Surgery*, 28, 196–202.

Moghimi, H.R., Varshochian, R., Kobarfard, F., and Erfan, M., 2010. Reduction of percutaneous absorption of toxic chemicals by dendrimers. *Cutaneous and Ocular Toxicology*, 29 (1), 34–40.

van der Molen, R.G., Spies, F., van 't Noordende, J.M., Boelsma, E., Mommaas, A.M., and Koerten, H.K., 1997. Tape stripping of human stratum corneum yields cell layers that originate from various depths because of furrows in the skin. *Archives of Dermatological Research*, 289 (9), 514–518.

Møllgaard, B. and Hoelgaard, A., 1983. Vehicle effect on topical drug delivery. II. Concurrent skin transport of drugs and vehicle components. *Acta Pharmaceutica Suecica*, 20 (6), 443–50.

Moloney, S.J., 1988. Effect of exogenous lipids on in vitro transepidermal water loss and percutaneous absorption. *Archives of Dermatological Research*, 280 (1), 67–70.

Montenegro, L., Ademola, J.I., Bonina, F.P., and Maibach, H.I., 1996. Effect of application time of betamethasone-17-valerate 0.1% cream on skin blanching and stratum corneum drug concentration.

International Journal of Pharmaceutics, 140 (1), 51–60.

Montes, L.F. and Wilborn, W.H., 1970. Anatomical Location of Normal Skin Flora. *Archives of Dermatology*, 101 (2), 145–159.

Moser, K., Kriwet, K., Naik, A., Kalia, Y.N., and Guy, R.H., 2001. Passive skin penetration enhancement and its quantification in vitro. *European Journal of Pharmaceutics and Biopharmaceutics*, 52 (2), 103–112.

Moss, G.P., 2015. Introduction. *In*: R.F. Donnelly and T.R.R. Singh, eds. *Novel Delivery Systems for Transdermal and Intradermal Drug Delivery*. Sussex: John Wiley and Sons, 1–30.

Mukherjee, S.P. and Byrne, H.J., 2013. Polyamidoamine dendrimer nanoparticle cytotoxicity, oxidative stress, caspase activation and inflammatory response: Experimental observation and numerical simulation. *Nanomedicine: Nanotechnology, Biology, and Medicine*, 9 (2), 202–211.

Mura, S., Pirot, F., Manconi, M., Falson, F., and Fadda, A.M., 2007. Liposomes and niosomes as potential cariers for dermal delivery of minoxidil. *Journal of Drug Targeting*, 15 (2), 101–108.

Murahata, R.I., Crowe, D.M., and Roheim, J.R., 1986. The use of transepidermal water loss to measure and predict the irritation response to surfactants. *International Journal of Cosmetic Science*, 8 (5), 225–231.

Nacht, S., Yeung, D., Beasley, J.N., Anjo, M.D., and Maibach, H.I., 1981. Benzoyl peroxide: Percutaneous penetration and metabolic disposition. *Journal of the American Academy of Dermatology*, 4 (1), 31–37.

Nahringbauer, I., 1995. Dynamic Surface Tension of Aqueous Polymer Solutions, I: Ethyl(hydroxyethyl)cellulose. *Journal of Colloid And Interface Science*, 176 (2), 318–328.

Naik, A., Kalia, Y.N., Pirot, F., and Guy, R.H., 1999. Characterization of Molecular Transport Across Human Stratum Corneum In Vivo. *In*: R.L. Bronaugh and H.I. Maibach, eds. *Percutaneous Absorption: Drugs – Cosmetics – Mechanisms – Methodology1*. New York: Marcel Dekker, 149–175.

Naik, A., Kalia, Y.N., and Guy, R.H., 2000. Transdermal drug delivery: overcoming the skin's barrier function. *Pharmaceutical Science and Technology Today*, 3 (9), 318–326.

Nakano, N.I., 1979. Temperature-dependent aqueous solubilities of lidocaine, mepivacaine, and bupivacaine. *Journal of Pharmaceutical Sciences,* 68 (5), 667-668.

Nakatsuji, T., Chiang, H-I., Jiang, S.B., Nagarajan, H., Zengler, K., and Gallo, R.L., 2013. The microbiome extends to subepidermal compartments of normal skin. *Nature Communications*, 4, 1–8.

Nangia, A., Berner, B., and Maibach, H.I., 1999. Transepidermal water loss measurements for assessing skin barrier function during in vitro percutaneous absorption experiments. *In*: R.L. Bronaugh and H.I. Maibach, eds. *Percutaneous Absorption: Drugs, Cosmetics, Mechanisms, Methodology*. New York: Marcel Dekker, 587–594.

Nangia, A., Patil, S., Berner, B., Boman, A., and Maibach, H., 1998. In vitro measurement of transepidermal water loss: a rapid alternative to tritiated water permeation for assessing skin barrier functions. *International Journal of Pharmaceutics*, 170 (1), 33–40.

National Institute for Health and Care Excellence, 2019. Surgical site infections: prevention and treatment. Available from: https://www.nice.org.uk/guidance/ng125/chapter/Recommendations. Accessed [19 Aug 2019].

Netzlaff, F., Kostka, K.-H., Lehr, C.-M., and Schaefer, U.F., 2006. TEWL measurements as a routine method for evaluating the integrity of epidermis sheets in static Franz type diffusion cells in vitro. Limitations shown by transport data testing. *European Journal of Pharmaceutics and Biopharmaceutics*, 63 (1), 44–50.

Neubert, R., 1989. Ion Pair Transport Across Membranes. *Pharmaceutical Research*, 6 (9), 743-747.

Newton, D.W., Driscoll, D.F., Goudreau, J.L., and Ratanamaneichatara, S., 1981. Solubility characteristics of

diazepam in aqueous admixture solutions: theory and practice. *American journal of hospital pharmacy*, 38 (2), 179–82.

Ng, S.-F., Rouse, J.J., Sanderson, F.D., Meidan, V., and Eccleston, G.M., 2010. Validation of a Static Franz Diffusion Cell System for In Vitro Permeation Studies. *AAPS PharmSciTech*, 11 (3), 1432–1441.

Nguyen, H.X., Puri, A., Bhattaccharjee, S.A., and Banga, A.K., 2018. Qualitative and quantitative analysis of lateral diffusion of drugs in human skin. *International Journal of Pharmaceutics*, 544 (1), 62–74.

Nicoletti, G., Boghossian, V., Gurevitch, F., Borland, R., and Morgenroth, P., 1993. The antimicrobial activity in vitro of chlorhexidine, a mixture of isothiazolinones ('Kathon' CG) and cetyl trimethyl ammonium bromide (CTAB). *Journal of Hospital Infection*, 23 (2), 87–111.

Nicoli, S., Rimondi, S., Colombo, P., and Santi, P., 2001. Physical and chemical enhancement of transdermal delivery of triptorelin. *Pharmaceutical Research*, 18 (11), 1634–1637.

Nokhodchi, A., Shokri, J., Dashbolaghi, A., Hassan-Zadeh, D., Ghafourian, T., and Barzegar-Jalali, M., 2003. The enhancement effect of surfactants on the penetration of lorazepam through rat skin. *International Journal of Pharmaceutics*, 250 (2), 359–369.

Norlén, L., 2001. Skin Barrier Structure and Function: The Single Gel Phase Model. *Journal of Investigative Dermatology*, 117 (4), 830–836.

Norman, J.J., Arya, J.M., McClain, M.A., Frew, P.M., Meltzer, M.I., and Prausnitz, M.R., 2014. Microneedle patches: Usability and acceptability for self-vaccination against influenza. *Vaccine*, 32 (16), 1856–1862.

Noto, M.J., Domenico, H.J., Byrne, D.W., Talbot, T., Rice, T.W., Bernard, G.R., and Wheeler, A.P., 2015. Chlorhexidine Bathing and Health Care–Associated Infections. *Jounal of the American Medical Association*, 313 (4), 369–378.

Nygren, H., Malmberg, P., Kriegeskotte, C., and Arlinghaus, H.F., 2004. Bioimaging TOF-SIMS: localization of cholesterol in rat kidney sections. *Federation of European Biochemical Societies Letters*, 566 (1–3), 291–293.

Nygren, H., Börner, K., Hagenhoff, B., Malmberg, P., and Månsson, J-E., 2005. Localization of cholesterol, phosphocholine and galactosylceramide in rat cerebellar cortex with imaging TOF-SIMS equipped with a bismuth cluster ion source. *Biochimica et Biophysica Acta - Molecular and Cell Biology of Lipids*, 1737 (2–3), 102–110.

O'Regan, G.M., Sandilands, A., McLean, W.H.I., and Irvine, A.D., 2008. Filaggrin in atopic dermatitis. *Journal of Allergy and Clinical Immunology*, 122 (4), 689–693.

Obata, Y., Takayama, K., Maitani, Y., Machida, Y., and Nagai, T., 1993. Effect of ethanol on skin permeation of nonionized and ionized diclofenac. *International Journal of Pharmaceutics*, 89 (3), 191–198.

Odland, G.F., 1991. Structure of the Skin. *In*: L.A. Goldsmith, ed. *Physiology, Biochemistry and Molecular Biology of the Skin*. New York: Oxford University Press, 3–62.

Organisation for Economic Co-operation and Development, 2004a. Guideline 208: Skin absorption: In vitro method.

Organisation for Economic Co-operation and Development, 2004b. Guidance Notes on Dermal Absorption. Available from: https://pubchem.ncbi.nlm.nih.gov/compound/Lorazepam [Accessed 12 Oct 2019].

Ohyama, M., Terunuma, A., Tock, C.L., Radonovich, M.F., Pise-Masison, C.A., Hopping, S.B., Brady, J.N., Udey, M.C., and Vogel, J.C., 2006. Characterization and isolation of stem cell-enriched human hair follicle bulge cells. *Journal of Clinical Investigation*, 116, 249–260.

Olorunsola, E.O. and Adedokun, M.O., 2014. Surface activity as basis for pharmaceutical applications of hydrocolloids: A review. *Journal of Applied Pharmaceutical Science*, 4 (10), 110–116.

Ornelas, J., Foolad, N., Shi, V., Burney, W., and Sivamani, R.K., 2016. Effect of Microneedle Pretreatment on Topical Anesthesia. *JAMA Dermatology*, 152 (4), 476.

Osterberg, L. and Blaschke, T., 2005. Adherence to Medication. *New England Journal of Medicine*, 353 (5), 487–497.

Ostrenga, J., Steinmetz, C., and Poulsen, B., 1971. Significance of Vehicle Composition I: Relationship between Topical Vehicle Composition, Skin Penetrability, and Clinical Efficacy. *Journal of Pharmaceutical Sciences*, 60 (8), 1175–1179.

Otberg, N., Richter, H., Knuttel, A., Schaefer, H., Sterry, W., and Lademann, J., 2004a. Laser spectroscopic methods for the characterization of open and closed follicles. *Laser Physics Letters*, 1 (1), 46–49.

Otberg, N., Richter, H., Schaefer, H., Blume-Peytavi, U., Sterry, W., and Lademann, J., 2004b. Variations of Hair Follicle Size and Distribution in Different Body Sites. *Journal of Investigative Dermatology*, 122 (1), 14–19.

Owen, S.C., 2006. Chlorhexidine. *In*: R.C. Rowe, P.J. Sheskey, and S.C. Owen, eds. *Handbook of Pharmaceutical Excipients*. London: Pharmaceutical Press, 163–167.

Padula, C., Nicoli, S., Colombo, P., and Santi, P., 2007. Single-layer transdermal film containing lidocaine: Modulation of drug release. *European Journal of Pharmaceutics and Biopharmaceutics*, 66 (3), 422–428.

Padula, C., Pozzetti, L., Traversone, V., Nicoli, S., and Santi, P., 2013. *In vitro* Evaluation of Mucoadhesive FIlms for Gingival Administration of Lidocaine. *AAPS Pharm SciTech*, 14 (4), 1279-1283.

Palmer, C.N.A., Irvine, A.D., Terron-Kwiatkowski, A., Zhao, Y., Liao, H., Lee, S.P., Goudie, D.R., Sandilands, A., Campbell, L.E., Smith, F.J.D., O'Regan, G.M., Watson, R.M., Cecil, J.E., Bale, S.J., Compton, J.G., DiGiovanna, J.J., Fleckman, P., Lewis-Jones, S., Arseculeratne, G., Sergeant, A., Munro, C.S., El Houate, B., McElreavey, K., Halkjaer, L.B., Bisgaard, H., Mukhopadhyay, S., and McLean, W.H.I., 2006. Common loss-of-function variants of the epidermal barrier protein filaggrin are a major predisposing factor for atopic dermatitis. *Nature Genetics*, 38 (4), 441–446.

Pandey, A., 2014. Role of Surfactants as Penetration Enhancer in Transdermal Drug Delivery System. *Journal of Molecular Pharmaceutics & Organic Process Research*, 2 (2), 2-7.

Paradiso, P., Galante, R., Santos, L., Alves de Matos, A.P., Colaço, R., Serro, A.P., and Saramago, B., 2014. Comparison of two hydrogel formulations for drug release in ophthalmic lenses. *Journal of Biomedical Materials Research Part B: Applied Biomaterials*, 102 (6), 1170–1180.

Park, J-H., Allen, M.G., and Prausnitz, M.R., 2005. Biodegradable polymer microneedles: Fabrication, mechanics and transdermal drug delivery. *Journal of Controlled Release*, 104 (1), 51–66.

Pathan, I.B. and Setty, C.M., 2009. Chemical penetration enhancers for transdermal drug delivery systems. *Tropical Journal of Pharmaceutical Research*, 8 (2), 173-179.

Patri, A., Majoros, I., and Baker, J., 2002. Dendritic polymer macromolecular carriers for drug delivery. *Current Opinion in Chemical Biology,* 6 (4), 466-471.

Patzelt, A. and Lademann, J., 2013. Drug delivery to hair follicles. *Expert Opinion on Drug Delivery*, 10 (6), 787–797.

Patzelt, A., Richter, H., Dähne, L., Walden, P., Wiesmüller, K.H., Wank, U., Sterry, W., and Lademann, J., 2011. Influence of the vehicle on the penetration of particles into hair follicles. *Pharmaceutics*, 3 (2), 307–314.

Pearton, M., Saller, V., Coulman, S.A., Gateley, C., Anstey, A. V., Zarnitsyn, V., and Birchall, J.C., 2012. Microneedle delivery of plasmid DNA to living human skin: Formulation coating, skin insertion and gene expression. *Journal of Controlled Release*, 160 (3), 561–569.

Pedersen, L. and Jemec, G.B., 1999. Plasticising effect of water and glycerin on human skin in vivo. *Journal of Dermatological Science*, 19 (1), 48–52.

Pellett, M.A., Castellano, S., Hadgraft, J., and Davis, A.F., 1997. The penetration of supersaturated solutions of piroxicam across silicone membranes and human skin in vitro. *Journal of Controlled Release*, 46 (3), 205–214.

Pendlington, R.U., 2008. In vitro percutaneous absorption measurements. *In*: R.P. Chilcott and S. Price, eds. *Principles and Practice of Skin Toxicology*. Chichester: John Wiley and Sons, 129–149.

Pershing, L.K., Lambert, L.D., and Knutson, K., 1990. Mechanism of Ethanol-Enhanced Estradiol Permeation Across Human Skin in Vivo. *Pharmaceutical Research*, 7 (2), 170–175.

Pesonen, T., Kanerva, H., Hirvonen, J., Nuuja, T., Pohjola, J., and Rhodes, T., 1995. The Incompatibilities Between Chlorhexidine Diacetate and Some Tablet Excipients. *Drug Development and Industrial Pharmacy*, 21 (6), 747–752.

Pessoa-Silva, C.L., Posfay-Barbe, K., Pfister, R., Touveneau, S., Perneger, T. V., and Pittet, D., 2005. Attitudes and Perceptions Toward Hand Hygiene Among Healthcare Workers Caring for Critically Ill Neonates. *Infection Control & Hospital Epidemiology*, 26 (3), 305–311.

Piddock, L.J., 2012. The crisis of no new antibiotics—what is the way forward? *The Lancet Infectious Diseases*, 12 (3), 249–253.

Pillai, O. and Panchagnula, R., 2003. Transdermal delivery of insulin from poloxamer gel: Ex vivo and in vivo skin permeation studies in rat using iontophoresis and chemical enhancers. *Journal of Controlled Release*, 89 (1), 127–140.

Pimenta, A.F.R., Ascenso, J., Fernandes, J.C.S., Colaço, R., Serro, A.P., and Saramago, B., 2016. Controlled drug release from hydrogels for contact lenses: Drug partitioning and diffusion. *International Journal of Pharmaceutics*, 515 (1–2), 467–475.

Pinzauti, S., La Porta, E., and Papeschi, G., 1984. Chlorhexidine loss from simulated contact lens solutions stored in glass and plastic packages. *Journal of Pharmaceutical and Biomedical Analysis*, 2 (1), 101–105.

Pircher, M., Goetzinger, E., Leitgeb, R., Hitzenberger, C.K., Huang, D., Swanson, E.A., Lin, C.P., Schuman, J.S., Stinson, W.G., Chang, W., Hee, M.R., Flotte, T., Gregory, K., Puliafito, C.A., Fujimoto, J.G., Saxer, C.E., De Boer, J.F., Park, B.H., Zhao, Y., Chen, C., and Nelson, J.S., 1991. *Three dimensional polarization sensitive OCT of human skin in vivo*. *Optics Express*, 12, 3236-3244.

Pirot, F., Kalia, Y.N., Stinchcomb, A.L., Keating, G., Bunge, A., and Guy, R.H., 1997. Characterization of the permeability barrier of human skin in vivo. *Proceedings of the National Academy of Sciences of the United States of America*, 94 (4), 1562–7.

Pittet, D., 2001. Improving adherence to hand hygiene practice: a multidisciplinary approach. *Emerging infectious diseases*, 7 (2), 234–40.

Pittet, D., Mourouga, P., and Perneger, T. V., 1999. Compliance with handwashing in a teaching hospital. *Annals of Internal Medicine*, 130 (2), 126–130.

Piwowar, A., Fletcher, J., Lockyer, N., and Vickerman, J., 2011. Investigating the effect of temperature on depth profiles of biological material using ToF-SIMS. *Surface and Interface Analysis*, 43 (1–2), 207–210.

Potter, D., Booth, E. D., Brandt, H. C. A., Loose, R. W., Priston, R. A. J., Wright, A. S., and Watson, W. P., 1999. Studies on the dermal and systemic bioavailability of polycyclic aromatic compounds in high viscosity oil products. *Toxicokinetics and Metabolism*, 73, 129-140.

Potts, R. O. and Guy, R. H., 1992. Predicting Skin Permeability. *Pharmaceutical Research,* 9 (5), 663-669.

Potts, R.O. and Guy, R.H., 1995. A Predictive Algorithm for Skin Permeability: The Effects of Molecular Size and Hydrogen Bond Activity. *Pharmaceutical Research*, 12 (11), 1628–1633.

Pourianazar, N.T., Mutlu, P., and Gunduz, U., 2014. Bioapplications of poly(amidoamine) (PAMAM) dendrimers

in nanomedicine. *Journal of Nanoparticle Research*, 16 (4), 1–38.

Prajapati, R.N., Tekade, R.K., Gupta, U., Gajbhiye, V., and Jain, N.K., 2009. Dendimer-mediated solubilization, formulation development and in vitro-in vivo assessment of piroxicam. *Molecular Pharmaceutics*, 6 (3), 940–950.

Prausnitz, M.R., 2004. Microneedles for transdermal drug delivery. *Advanced Drug Delivery Reviews*, 56 (5), 581–587.

Prausnitz, M.R., Mikszta, J.A., Cormier, M., and Andrianov, A.K., 2009. Microneedle-Based Vaccines. *In*: R. Compans and W. Orenstein, eds. *Vaccines for Pandemic Influenza*. Berlin: Springer, 370–393.

Price, J.C., 2006. Glycerin. *In*: R.C. Rowe, P.J. Sheskey, and S.C. Owen, eds. *Handbook of Pharmaceutical Excipients*. London: Pharmaceutical Press, 301–303.

Proksch, E., Brandner, J.M., and Jensen, J-M., 2008. The skin: an indispensable barrier. *Experimental Dermatology*, 17 (12), 1063–1072.

Public Health England, 2018a. *Staphylococcus aureus (MRSA and MSSA) bacteraemia: mandatory surveillance 2017/18 Summary of the Mandatory Surveillance Annual Epidemiological Commentary 2017/18*. Available from: https://assets.publishing.service.gov.uk/government/uploads/system/uploads/attachment_data/file/724361/S_aureus_summary_2018.pdf. [Accessed 8 Jan 2019].

Public Health England, 2018b. *Surveillance of surgical site infections in NHS hospitals in England: 2017 to 2018*. Available from: https://assets.publishing.service.gov.uk/government/uploads/system/uploads/attachment_data/file/765967/SSI_annual_report_NHS_hospitals_2017_18.pdf. [Accessed 5 Feb 2019].

Pugh, W.J. and Chilcott, R.P., 2008. Principles of Diffusion and Thermodynamics. *In*: R.P. Chilcott and S. Price, eds. *Principles and Practice of Skin Toxicology2*. Sussex: John Wiley and Sons, 93–107.

Pugh, W.J., Roberts, M.S., and Hadgraft, J., 1996. Epidermal permeability - penetrant structure relationships: 3. The effect of hydrogen bonding interactions and molecular size on diffusion across the stratum corneum. *International Journal of Pharmaceutics*, 138 (2), 149–165.

Puhvel, S.M., Reisner, R.M., and Amirian, D.A., 1975. Quantification of bacteria in isolated pilosebaceous follicles in normal skin. *Journal of Investigative Dermatology*, 65 (6), 525–531.

Pyatski, Y., Zhang, Q., Mendelsohn, R., and Flach, C.R., 2016. Effects of permeation enhancers on flufenamic acid delivery in ex vivo human skin by confocal Raman microscopy. *International Journal of Pharmaceutics*, 505 (1–2), 319–328.

Quinn, M.W. and Bini, R.M., 1989. Bradycardia associated with chlorhexidine spray. *Archives of Disease in Childhood*, 64 (6), 892–893.

Raghavan, S.L., Kiepfer, B., Davis, A.F., Kazarian, S.G., and Hadgraft, J., 2001. Membrane transport of hydrocortisone acetate from supersaturated solutions; the role of polymers. *International Journal of Pharmaceutics*, 221 (1–2), 95–105.

Rajadhyaksha, M., Grossman, M., Esterowitz, D., Webb, R.H., and Rox Anderson, R., 1995. In Vivo Confocal Scanning Laser Microscopy of Human Skin: Melanin Provides Strong Contrast. *Journal of Investigative Dermatology*, 104 (6), 946–952.

Ramöller, I.K., Tekko, I.A., McCarthy, H.O., and Donnelly, R.F., 2019. Rapidly dissolving bilayer microneedle arrays – A minimally invasive transdermal drug delivery system for vitamin B12. *International Journal of Pharmaceutics*, 566, 299–306.

Raufast, V., and Mavon, A., 2006. Transfollicular delivery of linoleic acid in human scalp skin: permeation study and microautoradiographic analysis. *International Journal of Cosmetic Science*, 28 (2), 117-123.

Rawlings, A. V., 2010. Recent advances in skin 'barrier' research. *Journal of Pharmacy and Pharmacology*, 62 (6), 671–677.

Rawlings, A.V. and Harding, C.R., 2004. Moisturiation and skin barrier function. *Dermatologic Therapy*, 17 (S1), 43–48.

Rawlings, A. V and Matts, P.J., 2005. Stratum Corneum Moisturization at the Molecular Level : An Update in Relation to the Dry Skin Cycle. *Journal of Investigative Dermatology*, 124 (6), 1099–1110.

Reddy, M.B., Stinchcomb, A.L., Guy, R.H., and Bunge, A.L., 2002. Determining Dermal Absorption Parameters in Vivo from Tape Strip Data. *Pharmaceutical Research*, 19 (3), 292–298.

Reed, J.T., Ghadially, R., and Elias, P.M., 1995. Skin Type, but Neither Race nor Gender, Influence Epidermal Permeability Barrier Function. *Archives of Dermatology*, 131 (10), 1134.

Reid, M.L., Brown, M.B., and Jones, S.A., 2008. Manipulation of corticosteroid release from a transiently supersaturated topical metered dose aerosol using a residual miscible co-solvent. *Pharmaceutical Research*, 25 (11), 2573–2580.

Reid, M.L., Jones, S.A., and Brown, M.B., 2009. Transient drug supersaturation kinetics of beclomethasone dipropionate in rapidly drying films. *International Journal of Pharmaceutics*, 371 (1–2), 114–119.

Restek Corporation, 2013. *Deactivating Glassware with DMDCS.* Available from: https://www.restek.com/pdfs/400-00-003.pdf. Accessed [4 Nov 2018].

Reybrouck, G., 1986. Handwashing and hand disinfection. *Journal of Hospital Infection*, 8 (1), 5–23.

Rhein, L.D., Robbins, C.R., Fernee, K., and Cantore, R., 1986. *Surfactant structure effects on swelling of isolated human stratum corneum*. *Journal for the Society of Cosmetic Chemists,* 37, 125-139.

Ripolin, A., Quinn, J., Larrañeta, E., Vicente-Perez, E.M., Barry, J., and Donnelly, R.F., 2017. Successful application of large microneedle patches by human volunteers. *International Journal of Pharmaceutics*, 521 (1–2), 92–101.

Rippke, F., Schreiner, V., and Schwantiz, H.J., 2002. The acidic milieu of the horny layer: New findings on the physiology and pathophysiology of skin pH. *American Journal of Clinical Dermatology*, 3, 261–272.

Roberts, M.S., 2013. Solute-vehicle-skin interactions in percutaneous absorption: The principles and the people. *Skin Pharmacology and Physiology*, 26 (4–6), 356–370.

Roberts, M. and Walker, M., 1993. Water. The most natural penetration enhancer. *Drugs and the Pharmaceutical Sciences*, 59, 1–30.

Roberts, M.S. and Walters, K.A., 1998. The relationship between structure and barrier function of skin. *In*: *Dermal Absorption and Toxicity Assessment*. New York: Marcel Dekker, 1–42.

Roberts, M.S., Pugh, W.J., Hadgraft, J., and Watkinson, A.C., 1995. Epidermal permeability-penetrant structure relationships: 1. An analysis of methods of predicting penetration of monofunctional solutes from aqueous solutions. *International Journal of Pharmaceutics*, 126 (1–2), 219–233.

Roberts, J.C., Bhalgat, M.K., and Zera, R.T., 1996. Preliminary biological evaluation of polyamidoamine (PAMAM) Starburst™ dendrimers. *Journal of Biomedical Materials Research*, 30 (1), 53–65.

Roskos, K. V. and Guy, R.H., 1989. Assessment of Skin Barrier Function Using Transepidermal Water Loss: Effect of Age. *Pharmaceutical Research*, 6 (11), 949–953.

Roth, R.R. and James, W.D., 1988. Microbial ecology of the skin. *Annual Reviews in Microbiology*, 42, 441–464.

Rotter, M., 1999. Hand washing and hand disinfection. *In*: C.G. Mayhall, ed. *Hospital epidemiology and infection control*. Philadelphia: Lippincott Williams and Wilkins, 1339–1355.

Rotter, M.L., 2001. Arguments for alcoholic hand disinfection. *Journal of Hospital Infection*, 48, S4–S8.

Russell, A.D. and Path, F.R.C., 1986. Chlorhexidine: Antibacterial action and bacterial resistance. *Infection*, 14 (5), 212–215.

Saar, B.G., Contreras-Rojas, L.R., Xie, X.S., and Guy, R.H., 2011. Imaging Drug Delivery to Skin with Stimulated Raman Scattering Microscopy. *Molecular Pharmaceutics*, 8 (3), 969–975.

Sandby-Møller, J. and Wulf, H.C., 2003. Epidermal Thickness at Different Body Sites: Relationship to Age, Gender, Pigmentation, Blood Content, Skin Type and Smoking Habits. *Advances in Dermatology and Venerology*, 83, 410–413.

Sandilands, A., Sutherland, C., Irvine, A.D., and McLean, W.H.I., 2009. Filaggrin in the frontline: role in skin barrier function and disease. *Journal of Cell Science*, 122 (9), 1285–1294.

Siddiqui, O., Roberts, M.S., and Polack, A.E., 1985. The effect of iontophoresis and vehicle pH on the in-vitro permeation of lignocaine through human stratum corneum. *Journal of Pharmacy and Pharmacology,* 37 (10), 732-735.

Van De Sandt, J.J.M., Van Burgsteden, J.A., Cage, S., Carmichael, P.L., Dick, I., Kenyon, S., Korinth, G., Larese, F., Limasset, J.C., Maas, W.J.M., Montomoli, L., Nielsen, J.B., Payan, J.P., Robinson, E., Sartorelli, P., Schaller, K.H., Wilkinson, S.C., and Williams, F.M., 2004. In vitro predictions of skin absorption of caffeine, testosterone, and benzoic acid: A multi-centre comparison study. *Regulatory Toxicology and Pharmacology*, 39 (3), 271–281.

Sarpotdar, P. and Zatz, J.L., 1986. Evaluation of Penetration Enhancement of Lidocaine by Nonionic Surfactants Through Hairless Mouse Skin In Vitro. *Journal of Pharmaceutical Sciences*, 75 (2), 176–181.

Saville, P.M., White, J.W., Hawker, C.J., Wooley, K.L., and Fréchet, J.M.J., 1993. Dendrimer and Polystyrene Surfactant Structure at the Air-Water Interface. *The Journal of Physical Chemistry*, 97, 293–294.

Sayed-Sweet, Y., Hedstrand, D.M., Spinder, R., and Tomalia, D.A., 1997. Hydrophobically modified poly(amidoamine) (PAMAM) dendrimers: their properties at the air–water interface and use as nanoscopic container molecules. *Journal of Materials Chemistry*, 7 (7), 1199–1205.

Schaefer, H. and Redelmeier, T.E., 1996. Structure of the Skin. *In*: *Skin Barrier: Principles of Percutaneous Absorption*. London: Karger Publishers, 18.

Schaefer, U.F., Hansen, S., Schneider, M., Contreras, J.L., and Lehr, C-M., 2008. Models for Skin Absorption and Skin Toxicity Testing. *In*: C. Ehrhardt and K-J. Kim, eds. *Drug Absorption Studies: In Situ, In Vitro and In Silico Models*. Boston: Springer, 3–33.

Schaepe, K., Werner, J., Glenske, K., Bartges, T., Henss, A., Rohnke, M., Wenisch, S., and Janek, J., 2017. ToF-SIMS study of differentiation of human bone-derived stromal cells: new insights into osteoporosis. *Analytical and Bioanalytical Chemistry*, 409 (18), 4425–4435.

Schenning, A.P.H.J., Elissen-Roman, C., Weener, J.W., Baars, M.W.P.L., van der Gaast, S.J., and Meijer, E.W., 1998. Amphiphilic Dendrimers as Building Blocks in Supramolecular Assemblies. *Journal of the American Chemical Society*, 120 (32), 8199–8208.

Scheuplein, R. and Ross, L., 1970. Effects of Surfactants and Solvents on the Permeability of Epidermis. *Journal of the Society of Cosmetic Chemists*, 21, 853–873.

Scheuplein, R.J. and Blank, I.H., 1971. Permeability of the Skin. *Physiological Reviews*, 51 (4), 702–747.

Schicksnus, G. and Müller-Goymann, C.C., 2004. Lateral Diffusion of Ibuprofen in Human Skin during Permeation Studies. *Skin Pharmacology and Physiology*, 17 (2), 84–90.

Schwarb, F.P., Imanidis, G., Smith, E.W., Haigh, J.M., and Surber, C., 1999. Effect of Concentration and Degree of Saturation of Topical Fluocinonide Formulations on In Vitro Membrane Transport and In Vivo Availability

on Human Skin. *Pharmaceutical Research*, 16 (6), 909–915.

Selwyn, S. and Ellis, H., 1972. Skin bacteria and skin disinfection reconsidered. *British Medical Journal*, 1 (5793), 136–140.

Selzer, D., Abdel-Mottaleb, M.M.A., Hahn, T., Schaefer, U.F., and Neumann, D., 2013. Finite and infinite dosing: Difficulties in measurements, evaluations and predictions. *Advanced Drug Delivery Reviews*.

Seto, J.E., Polat, B.E., Vanveller, B., Lopez, R.F.V., Langer, R., and Blankschtein, D., 2012. Fluorescent penetration enhancers for transdermal applications. *Journal of Controlled Release*, 158 (1), 85–92.

Seweryn, A., 2018. Interactions between surfactants and the skin – Theory and practice. *Advances in Colloid and Interface Science*, 256, 242–255.

Shadrack, D.M., Mubofu, E.B., and Nyandoro, S.S., 2015. Synthesis of Polyamidoamine Dendrimer for Encapsulating Tetramethylscutellarein for Potential Bioactivity Enhancement. *International Journal of Molecular Sciences*, 16, 26363–26377.

Shcharbin, D., Drapeza, A., Loban, V., Lisichenok, A., and Bryszewska, M., 2006. The breakdown of bilayer lipid membranes by dendrimers. *Cellular and Molecular Biology Letters*, 11 (2).

Shelmire, J.B., 1960. Factors Determining the Skin-Drug-Vehicle Relationship. *Archives of Dermatology*, 82 (1), 24–31.

Sherertz, E.F., Sloan, K.B., and McTiernan, R.G., 1987. Use of theoretical partition coefficients determined from solubility parameters to predict permeability coefficients for 5-fluorouracil. *Journal of Investigative Dermatology*, 89 (2), 147–151.

Sheth, N. V., McKeough, M.B., and Spruance, S.L., 1987. Measurement of the Stratum Corneum Drug Reservoir to Predict the Therapeutic Efficacy of Topical Iododeoxyuridine for Herpes Simplex Virus Infection. *Journal of Investigative Dermatology*, 89 (6), 598–602.

Shin, J.U., Kim, J.D., Kim, H.K., Kang, H.K., Joo, C., Lee, J.H., Jeong, D.H., Song, S., Chu, H., Lee, J.S., Lee, H., and Lee, K.H., 2018. The use of biodegradable microneedle patches to increase penetration of topical steroid for prurigo nodularis. *European Journal of Dermatology*, 28 (1), 71–77.

Shokri, J., Nokhodchi, A., Dashbolaghi, A., Hassan-Zadeh, D., Ghafourian, T., and Barzegar Jalali, M., 2001. The effect of surfactants on the skin penetration of diazepam. *International Journal of Pharmaceutics*, 228 (1–2), 99–107.

Shore, P.A., Brodie, B.B., and Hogben, C.A.M., 1957. The Gastric Secretion of Drugs: A pH Partition Hypothesis. *Journal of Pharmacology and Experimental Therapeutics*, 119 (3), 361–369.

Siddiqui, O., Roberts, M.S., and Polack, A.E., 1985. The effect of iontophoresis and vehicle pH on the in-vitro permeation of lignocaine through human stratum corneum. *Journal of Pharmacy and Pharmacology*, 37 (10), 732–735.

Sietsema, W.K., 2012. Regulatory Aspects of Drug Development for Dermal Products. *In*: H.A.E. Benson and A.C. Watkinson, eds. *Transdermal and Topical Drug Delivery Principles and Practice*. New Jersey: John Wiley and Sons, 217–232.

Sigma Aldrich, 2019a. PAMAM dendrimer, ethylenediamine core, generation 3.0 solution 20 wt. % in methanol. Available from: https://www.sigmaaldrich.com/catalog/product/aldrich/412422?lang=en&region=GB [Accessed 16 Aug 2019].

Sigma Aldrich, 2019b. Chlorhexidine digluconate solution. Available from: https://www.sigmaaldrich.com/catalog/substance/chlorhexidinedigluconatesolution123451847251011?lang=en&region=GB [Accessed 16 Aug 2019].

Simon, G.A. and Maibach, H.I., 2000. The Pig as an Experimental Animal Model of Percutaneous Permeation in

Man: Qualitative and Quantitative Observations – An Overview. *Skin Pharmacology and Physiology*, 13 (5), 229–234.

Sine, M.R., Wei, K.S., Jakubovic, D.A., Thomas, C.P., Dodd, M.T., and Putman, C.D., 2000. Skin sanitizing compositions. Patent Number: US6183766B1.

Sivamani, R.K., Stoeber, B., Wu, G.C., Zhai, H., Liepmann, D., and Maibach, H., 2005. Clinical microneedle injection of methyl nicotinate: stratum corneum penetration. *Skin Research and Technology*, 11 (2), 152–156.

Sjövall, P., Johansson, B., Belazi, D., Stenvinkel, P., Lindholm, B., Lausmaa, J., and Schalling, M., 2008. TOF-SIMS analysis of adipose tissue from patients with chronic kidney disease. *Applied Surface Science*, 255 (4), 1177–1180.

Sjövall, P., Greve, T.M., Clausen, S.K., Moller, K., Eirefelt, S., Johansson, B., and Nielsen, K.T., 2014. Imaging of Distribution of Topically Applied Drug Molecules in Mouse Skin by Combination of Time-of-Flight Secondary Ion Mass Spectrometry and Scanning Electron Microscopy. *Analytical Chemistry*, 86 (7), 3443–3452.

Sjövall, P., Skedung, L., Gregoire, S., Biganska, O., Clément, F., and Luengo, G.S., 2018. Imaging the distribution of skin lipids and topically applied compounds in human skin using mass spectrometry. *Scientific Reports*, 8 (1), 1–14.

Smith, G.P.S., McGoverin, C.M., Fraser, S.J., and Gordon, K.C., 2015. Raman imaging of drug delivery systems. *Advanced Drug Delivery Reviews*, 89, 21–41.

Sodhi, R.N.S., 2004. Time-of-flight secondary ion mass spectrometry (TOF-SIMS):—versatility in chemical and imaging surface analysis. *The Analyst*, 129 (6), 483–487.

Solon, E.G., Schweitzer, A., Stoeckli, M., and Prideaux, B., 2010. Autoradiography, MALDI-MS, and SIMS-MS imaging in pharmaceutical discovery and development. *AAPS Journal*, 12, 11-26.

Som, I., Bhatia, K., and Yasir, M., 2012. Status of surfactants as penetration enhancers in transdermal drug delivery. *Journal of Pharmacy & Bioallied Sciences*, 4 (1), 2–9.

Somerville, D.A., 1969. The Normal Flora of the Skin in Different Age Groups. *British Journal of Dermatology*, 81 (4), 248–258.

Sørensen, I.S., Janfelt, C., Nielsen, M.M.B., Mortensen, R.W., Knudsen, N.Ø., Eriksson, A.H., Pedersen, A.J., and Nielsen, K.T., 2017. Combination of MALDI-MSI and cassette dosing for evaluation of drug distribution in human skin explant. *Analytical and Bioanalytical Chemistry*, 409 (21), 4993–5005.

Southwell, D., Barry, B.W., and Woodford, R., 1984. Variations in permeability of human skin within and between specimens. *International Journal of Pharmaceutics*, 18 (3), 299–309.

Sridevi, S. and Diwan, P.V.R., 2002. Optimized transdermal delivery of ketoprofen using pH and hydroxypropyl-beta-cyclodextrin as co-enhancers. *European journal of pharmaceutics and biopharmaceutics*, 54 (2), 151–4.

Srinivasan, B., Kolli, A.R., Esch, M.B., Abaci, H.E., Shuler, M.L., and Hickman, J.J., 2015. TEER Measurement Techniques for In Vitro Barrier Model Systems. *Journal of Laboratory Automation*, 20 (2), 107-126.

Starr, N.J., Johnson, D.J., Wibawa, J., Marlow, I., Bell, M., Barrett, D.A., and Scurr, D.J., 2016. Age-Related Changes to Human Stratum Corneum Lipids Detected Using Time-of-Flight Secondary Ion Mass Spectrometry Following in Vivo Sampling. *Analytical Chemistry*, 88 (8), 4400–4408.

Starr, N.J., Abdul Hamid, K., Wibawa, J., Marlow, I., Bell, M., Pérez-García, L., Barrett, D.A., and Scurr, D.J., 2019. Enhanced vitamin C skin permeation from supramolecular hydrogels, illustrated using in situ ToF-SIMS 3D chemical profiling. *International Journal of Pharmaceutics*, 563, 21–29.

Stefani, S., Chung, D.R., Lindsay, J.A., Friedrich, A.W., Kearns, A.M., Westh, H., and MacKenzie, F.M., 2012. Meticillin-resistant Staphylococcus aureus (MRSA): global epidemiology and harmonisation of typing methods. *International Journal of Antimicrobial Agents*, 39 (4), 273–282.

Stenn, K.S. and Cotsarelis, G., 2005. Bioengineering the hair follicle: Fringe benefits of stem cell technology. *Current Opinion in Biotechnology*, 16(5), 493-497.

Stinchcomb, A.L., Pirot, F., Touraille, G.D., Bunge, A.L., and Guy, R.H., 1999. Chemical Uptake Into Human Stratum Corneum In Vivo from Volatile and Non-Volatile Solvents. *Pharmaceutical Research*, 16 (8), 1288–1293.

Stiriba, S.-E., Frey, H., and Haag, R., 2002. Dendritic Polymers in Biomedical Applications: From Potential to Clinical Use in Diagnostics and Therapy. *Angewandte Chemie International Edition*, 41 (8), 1329–1334.

Storm, A., Andersen, S.E., Benfeldt, E., and Serup, J., 2008. One in 3 prescriptions are never redeemed: Primary nonadherence in an outpatient clinic. *Journal of the American Academy of Dermatology*, 59 (1), 27–33.

Sullivan, S.P., Koutsonanos, D.G., del Pilar Martin, M., Lee, J.W., Zarnitsyn, V., Choi, S-O., Murthy, N., Compans, R.W., Skountzou, I., and Prausnitz, M.R., 2010. Dissolving polymer microneedle patches for influenza vaccination. *Nature Medicine*, 16 (8), 915–920.

Sun, M., Fan, A., Wang, Z., and Zhao, Y., 2012. Dendrimer-mediated drug delivery to the skin. *Soft Matter*, 8 (16), 4301–4305.

Sun, Y., Su, J.-W., Lo, W., Lin, S.-J., Jee, S.-H., and Dong, C.-Y., 2003. Multiphoton polarization imaging of the stratum corneum and the dermis in ex-vivo human skin. *Optics Express*, 11 (25), 3377.

Supersaxo, A., Hein, W.R., and Steffen, H., 1990. Effect of Molecular Weight on the Lymphatic Absorption of Water-Soluble Compounds Following Subcutaneous Administration. *Pharmaceutical Research*, 7 (2), 167–169.

Surber, C., Abels, C., and Maibach, H., 2018. pH of the Skin: Issues and Challenges. *Current Problems in Dermatology*, 54, 143–151.

Surber, C., Schward, F.P., and Smith, E.W., 1999. Tape-Stripping Technique. *In*: R.L. Bronaugh and H.I. Maibach, eds. *Percutaneous Absorption: Drugs – Cosmetics – Mechanisms – Methodology*. New York: CRC Press, 395–410.

Surber, C., Smith, E.W., Schwarb, F.P., and Maibach, H.I., 1999. Drug Concentration in the Skin. *In*: R.L. Bronaugh and H.I. Maibach, eds. *Percutaneous Absorption: Drugs – Cosmetics – Mechanisms – Methodology*. New York: Marcel Dekker, 347–374.

Surber, C., Wilhelm, K.P., Bermann, D., and Maibach, H.I., 1993. In Vivo Skin Penetration of Acitretin in Volunteers Using Three Sampling Techniques. *Pharmaceutical Research*, 10 (9), 1291–1294.

Susi, H., 1972. The Strength of Hydrogen Bonding: Infrared Spectroscopy. *Methods in Enzymology*, 26, 381–391.

Svenson, S., 2009. Dendrimers as versatile platform in drug delivery applications. *European Journal of Pharmaceutics and Biopharmaceutics*, 71 (3), 445–462.

Swarbrick, J., Lee, G., Brom, J., and Gensmantel, N.P., 1984. Drug permeation through human skin II: Permeability of ionizable compounds. *Journal of pharmaceutical sciences*, 73 (10), 1352–5.

Sznitowska, M., Janicki, S., and Williams, A.C., 1998. Intracellular or Intercellular Localization of the Polar Pathway of Penetration Across Stratum Corneum. *Journal of Pharmaceutical Sciences*, 87 (9), 1109–1114.

Tanner, T. and Marks, R., 2008. Delivering drugs by the transdermal route: review and comment. *Skin Research and Technology*, 14 (3), 249–260.

Tattawasart, U., Maillard, J.Y., Furr, J.R., and Russell, A.D., 1999. Development of resistance to chlorhexidine

diacetate and cetylpyridinium chloride in Pseudomonas stutzeri and changes in antibiotic susceptibility. *The Journal of Hospital Infection*, 42 (3), 219–229.

Talyor, S.E., and Chu, H.T., 2018. Metal Ion Interactions with Crude Oil Components: Specificity of Ca^{2+} Binding to Napthenic Acid at an Oil/Water Interface. *Colloids and Interfaces*, 2 (3), 40.

Teo, A.L., Shearwood, C., Ng, K.C., Lu, J., and Moochhala, S., 2006. Transdermal microneedles for drug delivery applications. *Materials Science and Engineering: B*, 132 (1–2), 151–154.

Teutenberg, T., Hollebekkers, K., Wiese, S., and Boergers, A., 2009. Temperature and pH-stability of commercial stationary phases. *Journal of Separation Science*, 32 (9), 1262–1274.

Tham, H.P., Xu, K., Lim, W.Q., Chen, H., Zheng, M., Thng, T.G.S., Venkatraman, S.S., Xu, C., and Zhao, Y., 2018. Microneedle-Assisted Topical Delivery of Photodynamically Active Mesoporous Formulation for Combination Therapy of Deep-Seated Melanoma. *ACS Nano*, 12 (12), 11936–11948.

Thelwall, S., Harrington, P., Sheridan, E., and Lamagni, T., 2015. Impact of obesity on the risk of wound infection following surgery: Results from a nationwide prospective multicentre cohort study in England. *Clinical Microbiology and Infection*, 21 (11), 1008.e1-1008.e8.

Tomalia, D.A., Baker, H., Dewald, J., Hall, M., Kallos, G., Martin, S., Roeck, J., Ryder, J., and Smith, P., 1985. A New Class of Polymers: Starburst-Dendritic Macromolecules. *Polymer Journal*, 17 (1), 117–132.

Topp, A., Bauer, B.J., Tomalia, D.A., and Amis, E.J., 1999. Effect of Solvent Quality on the Molecular Dimensions of PAMAM Dendrimers, 32 (21), 7232-7237.

Tortora, G.J. and Derrickson, B., 2012. Structure of the Skin. *In*: *Principles of Anatomy and Physiology*. New York: John Wiley and Sons, 157–158.

Touboul, D., Roy, S., Germain, D.P., Chaminade, P., Brunelle, A., and Laprévote, O., 2007. MALDI-TOF and cluster-TOF-SIMS imaging of Fabry disease biomarkers. *International Journal of Mass Spectrometry*, 260 (2–3), 158–165.

Touitou, E. and Abed, L., 1985. Effect of propylene glycol, Azone and n-decylmethyl sulphoxide on skin permeation kinetics of 5-fluorouracil. *International Journal of Pharmaceutics*, 27 (1), 89–98.

Touitou, E., Meidan, V.M., and Horwitz, E., 1998. Methods for quantitative determination of drug localized in the skin. *Journal of Controlled Release*, 56 (1–3), 7–21.

Traore, O., Hugonnet, S., Lübbe, J., Griffiths, W., and Pittet, D., 2007. Liquid versus gel handrub formulation: A prospective intervention study. *Critical Care*, 11 (3), 1-8.

Treffel, P., Muret, P., Muret-D'aniello, P., Coumes-Marquet, S., and Agache, P., 1992. Effect of occlusion on in vitro percutaneous absorption of two compounds with different physicochemical properties. *Skin Pharmacology and Physiology*, 5 (2), 108–113.

Trottet, L., Merly, C., Mirza, M., Hadgraft, J., and Davis, A.., 2004. Effect of finite doses of propylene glycol on enhancement of in vitro percutaneous permeation of loperamide hydrochloride. *International Journal of Pharmaceutics*, 274 (1–2), 213–219.

Tsai, C-J., Hsu, L-R., Fang, J-L., and Lin, H-H., 1999. Chitosan Hydrogel as a Base for Transdermal Delivery of Berberine and Its Evaluation in Rat Skin. *Biological and Pharmaceutical Bulletin*, 22, 397-401.

Tsioris, K., Raja, W.K., Pritchard, E.M., Panilaitis, B., Kaplan, D.L., and Omenetto, F.G., 2012. Fabrication of Silk Microneedles for Controlled-Release Drug Delivery. *Advanced Functional Materials*, 22 (2), 330–335.

Tully, D.C. and Fréchet, J.M.J., 2001. Dendrimers at surfaces and interfaces: chemistry and applications. *Chemical Communications*, 1 (14), 1229–1239.

Tupker, R.A., Pinnagoda, J., and Nater, J.P., 1990. The transient and cumulative effect of sodium lauryl sulphate

on the epidermal barrier assessed by transepidermal water loss: inter-individual variation. *Acta Dermato-Venereologica*, 70 (1), 1–5.

Uppuluri, S., Keinath, S.E., Tomalia, D.A., and Dvornic, P.R., 1998. Rheology of Dendrimers. I. Newtonian Flow Behavior of Medium and Highly Concentrated Solutions of Polyamidoamine (PAMAM) Dendrimers in Ethylenediamine (EDA) Solvent. *Macromolecules*, 31 (14), 4498–4510.

Valenta, C., Siman, U., Kratzel, M., and Hadgraft, J., 2000. The dermal delivery of lignocaine: influence of ion pairing. *International Journal of Pharmaceutics*, 197 (1–2), 77–85.

Vandamme, T.F. and Brobeck, L., 2005. Poly(amidoamine) dendrimers as ophthalmic vehicles for ocular delivery of pilocarpine nitrate and tropicamide. *Journal of Controlled Release*, 102 (1), 23–38.

Vargas, G., Chan, E.K., Barton, J.K., Rylander, H.G., and Welch, A.J., 1999. Use of an agent to reduce scattering in skin. *Lasers in Surgery and Medicine*, 24 (2), 133–141.

Ventola, C.L., 2015. The antibiotic resistance crisis: part 1: causes and threats. *P & T*, 40 (4), 277–283.

Venuganti, V.V.K. and Perumal, O.P., 2008. Effect of poly(amidoamine) (PAMAM) dendrimer on skin permeation of 5-fluorouracil. *International Journal of Pharmaceutics*, 361 (1–2), 230–238.

Venuganti, V.V.K. and Perumal, O.P., 2009. Poly(amidoamine) dendrimers as skin penetration enhancers: Influence of charge, generation, and concentration. *Journal of Pharmaceutical Sciences*, 98 (7), 2345–2356.

Venuganti, V.V., Sahdev, P., Hildreth, M., Guan, X., and Perumal, O., 2011. Structure-Skin Permeability Relationship of Dendrimers. *Pharmaceutical Research*, 28 (9), 2246–2260.

Venuganti, V.V.K., Saraswathy, M., Dwivedi, C., Kaushik, R.S., and Perumal, O.P., 2015. Topical gene silencing by iontophoretic delivery of an antisense oligonucleotide–dendrimer nanocomplex: the proof of concept in a skin cancer mouse model. *Nanoscale*, 7 (9), 3903–3914.

Verbaan, F.J., Bal, S.M., van den Berg, D.J., Groenink, W.H.H., Verpoorten, H., Lüttge, R., and Bouwstra, J.A., 2007. Assembled microneedle arrays enhance the transport of compounds varying over a large range of molecular weight across human dermatomed skin. *Journal of Controlled Release*, 117 (2), 238–245.

Verbaan, F.J., Bal, S.M., van den Berg, D.J., Dijksman, J.A., van Hecke, M., Verpoorten, H., van den Berg, A., Luttge, R., and Bouwstra, J.A., 2008. Improved piercing of microneedle arrays in dermatomed human skin by an impact insertion method. *Journal of Controlled Release*, 128 (1), 80–88.

Vergou, T., Schanzer, S., Richter, H., Pels, R., Thiede, G., Patzelt, A., Meinke, M.C., Sterry, W., Fluhr, J.W., and Lademann, J., 2012. Comparison between TEWL and laser scanning microscopy measurements for the in vivo characterization of the human epidermal barrier. *Journal of Biophotonics*, 5 (2), 152–158.

Verma, D.D., Verma, S., Blume, G., and Fahr, A., 2003. Liposomes increase skin penetration of entrapped and non-entrapped hydrophilic substances into human skin: a skin penetration and confocal laser scanning microscopy study. *European Journal of Pharmaceutics and Biopharmaceutics*, 55 (3), 271–277.

Vernon, M.O., Hayden, M.K., Trick, W.E., Hayes, R.A., Blom, D.W., and Weinstein, R.A., 2006. Chlorhexidine gluconate to cleanse patients in a medical intensive care unit: The effectiveness of source control to reduce the bioburden of vancomycin-resistant enterococci. *Archives of Internal Medicine*, 166 (3), 306–312.

Vickerman, J.C., 2009. Molecular Surface Mass Spectrometry by SIMS. *In*: J.C. Vickerman and I.S. Gilmore, eds. *Surface Analysis: The Principal Techniques*. United Kingdom: John Wiley and Sons, 113–206.

Vinson, L.J., Singer, E.J., Koehler, W.R., Lehman, M.D., and Masurat, T., 1965. The nature of the epidermal barrier and some factors influencing skin permeability. *Toxicology and Applied Pharmacology*, 7 (S2), 7–19.

Voegeli, R. and Rawlings, A. V., 2013. Corneocare: The role of the stratum corneum and the concept of total barrier care. *Household and Personal Care Today*, 8, 7–16.

van der Vossen, A.C., van der Velde, I., Smeets, O.S.N.M., Postma, D.J., Eckhardt, M., Vermes, A., Koch, B.C.P., Vulto, A.G., and Hanff, L.M., 2017. Formulating a poorly water soluble drug into an oral solution suitable for paediatric patients; lorazepam as a model drug. *European Journal of Pharmaceutical Sciences*, 100, 205–210.

Waghule, T., Singhvi, G., Dubey, S.K., Pandey, M.M., Gupta, G., Singh, M., and Dua, K., 2019. Microneedles: A smart approach and increasing potential for transdermal drug delivery system. *Biomedicine & Pharmacotherapy*, 109, 1249–1258.

Wakefield, J.C., 2008. Glossary of main terms and abbreviations. *In*: R.P. Chilcott and S. Price, eds. *Principles and Practice of Skin Toxicology*. Chichester: John Wiley and Sons, 347–358.

Walsh, C., 2000. Molecular mechanisms that confer antibacterial drug resistance. *Nature*, 406 (6797), 775–781.

Walter, K. and Kurz, H., 1988. Binding of Drugs to Human Skin: Influencing Factors and the Role of Tissue Lipids. *Journal of Pharmacy and Pharmacology*, 40 (10), 689–693.

Walters, K.A., 1990. Surfactants and percutaneous absorption. *In*: R.C. Scott, R.H. Guy, and J. Hadgraft, eds. *Prediction of Percutaneous Penetration Methods, Measurements, Modelling*. London: IBC Technical Services, 148–162.

Walters, K.A. and Roberts, M.S., 2002. Structure and Function of Skin. *In*: K.A. Walters, ed. *Dermatological and Transdermal Formulations*. London: CRC Press, 12.

Wang, Z., Itoh, Y., Hosaka, Y., Kobayashi, I., Nakano, Y., Maeda, I., Umeda, F., Yamakawa, J., Kawase, M., and Yag, K., 2003a. Novel transdermal drug delivery system with polyhydroxyalkanoate and starburst polyamidoamine dendrimer. *Journal of Bioscience and Bioengineering*, 95 (5), 541–543.

Wang, Z., Itoh, Y., Hosaka, Y., Kobayashi, I., Nakano, Y., Maeda, I., Umeda, F., Yamakawa, J., Nishimine, M., Suenobu, T., Fukuzumi, S., Kawase, M., and Yagi, K., 2003b. Mechanism of enhancement effect of dendrimer on transdermal drug permeation through polyhydroxyalkanoate matrix. *Journal of Bioscience and Bioengineering*, 96 (6), 537–540.

Wang, B., Navath, R.S., Menjoge, A.R., Balakrishnan, B., Bellair, R., Dai, H., Romero, R., Kannan, S., and Kannan, R.M., 2010. Inhibition of bacterial growth and intramniotic infection in a guinea pig model of chorioamnionitis using PAMAM dendrimers. *International Journal of Pharmaceutics*, 395 (1–2), 298–308.

Wang, F., Cai, X., Su, Y., Hu, J., Wu, Q., Zhang, H., Xiao, J., and Cheng, Y., 2012. Reducing cytotoxicity while improving anti-cancer drug loading capacity of polypropylenimine dendrimers by surface acetylation. *Acta Biomaterialia*, 8 (12), 4304–4313.

Wang, Q., Yao, G., Dong, P., Gong, Z., Li, G., Zhang, K., and Wu, C., 2015. Investigation on fabrication process of dissolving microneedle arrays to improve effective needle drug distribution. *European Journal of Pharmaceutical Sciences*, 66, 148–156.

Watkinson, R.M., Guy, R.H., Hadgraft, J., and Lane, M.E., 2009. Optimisation of Cosolvent Concentration for Topical Drug Delivery - II: Influence of Propylene Glycol on Ibuprofen Permeation. *Skin Pharmacology and Physiology*, 22 (4), 225–230.

Weigmann, H-J., Lademann, J., Meffert, H., Schaefer, H., and Sterry, W., 1999. Determination of the Horny Layer Profile by Tape Stripping in Combination with Optical Spectroscopy in the Visible Range as a Prerequisite to Quantify Percutaneous Absorption. *Skin Pharmacology and Applied Skin Physiology*, 12 (1–2), 34–45.

Weigmann, H-J., Lademann, J., Schanzer, S., Lindemann, U., Von Pelchrzim, R., Schaefer, H., Sterry, W., and Shah, V., 2001. Correlation of the local distribution of topically applied substances inside the stratum corneum determined by tape-stripping to differences in bioavailability. *Skin Pharmacology and Applied Skin Physiology*, 14 (S1), 98–102.

Weigmann, H-J., Lindemann, U., Antoniou, C., Tsikrikas, G.N., Stratigos, A.I., Katsambas, A., Sterry, W., and Lademann, J., 2003. UV/VIS Absorbance Allows Rapid, Accurate, and Reproducible Mass Determination of

Corneocytes Removed by Tape Stripping. *Skin Pharmacology and Physiology*, 16 (4), 217–227.

Welzel, J., 2001. Optical coherence tomography in dermatology: a review. *Skin Research and Technology*, 7 (1), 1–9.

Welzel, J., Lankenau, E., Birngruber, R., and Engelhardt, R., 1997. Optical coherence tomography of the human skin. *Journal of the American Academy of Dermatology*, 37 (6), 958–963.

Wen, X., Jacques, S.L., Tuchin, V. V., and Zhu, D., 2012. Enhanced optical clearing of skin in vivo and optical coherence tomography in-depth imaging. *Journal of Biomedical Optics*, 17 (6), 066022.

Wenzel, R.P., 2004. The Antibiotic Pipeline — Challenges, Costs, and Values. *New England Journal of Medicine*, 351 (6), 523–526.

Wertz, P.W. and van den Bergh, B., 1998. The physical, chemical and functional properties of lipids in the skin and other biological barriers. *Chemistry and physics of lipids*, 91 (2), 85–96.

Wertz, P.W. and Norlén, L., 2003. 'Confidence Intervals' for the 'true' lipid compositions of the human skin barrier? *In*: B. Forslind and M. Lindbery, eds. *Skin, Hair and Nails Structure and Function*. New York: Marcel Dekker, 85–106.

Wester, R.C. and Maibach, H.I., 1975. Percutaneous absorption in the rhesus monkey compared to man. *Toxicology and Applied Pharmacology*, 32 (2), 394–398.

Wester, R.C. and Maibach, H.I., 1976. Relationship Of Topical Dose And Percutaneous Absorption In Rhesus Monkey And Man. *Journal of Investigative Dermatology*, 67 (4), 518–520.

Wester, R.C. and Noonan, P.K., 1980. Relevance of animal models for percutaneous absorption. *International Journal of Pharmaceutics*, 7 (2), 99-110.

Wester, R.C. and Maibach, H.I., 1993. Animal Models for Percutaneous Absorption. *In*: *Topical Drug Bioavailability, Bioequivalence, and Penetration*. Boston, MA: Springer US, 333–349.

Wester, R.C. and Maibach, H.I., 1995. Penetration enhancement by skin hydration. *In*: E.W. Smith and H.I. Maibach, eds. *Percutaneous Penetration Enhancers*. Florida: CRC Press, 21–28.

White, J.H., 1991. Alcohol-based antimicrobial compositions. Patent Number: US5288486A.

World Health Organisation, 2018a. *Global Guidelines for the Prevention of Surgical Site Infection*. 2nd ed. Available from: https://www.who.int/infection-prevention/publications/ssi-prevention-guidelines/en/. [Accessed 20 Aug 2019].

World Health Organisation, 2018b. Antibiotic Resistance. Available from: https://www.who.int/news-room/fact-sheets/detail/antibiotic-resistance. [Accessed 20 Aug 2019]

Wiedersberg, S. and Guy, R.H., 2014. Transdermal drug delivery: 30 + years of war and still fighting! *Journal of Controlled Release*, 190, 150–156.

Williams, A.C., 2003a. Structure and function of human skin. *In*: *Transdermal and Topical Drug Delivery*. London: Pharmaceutical Press, 1–25.

Williams, A.C., 2003b. Theoretical aspects of transdermal drug delivery. *In*: *Transdermal and Topical Drug Delivery*. London: Pharmaceutical Press, 27–49.

Williams, A.C., 2003c. Experimental Design. *In*: *Transdermal and Topical Drug Delivery*. London: Pharmaceutical Press, 51–81.

Williams, A.C., 2003d. Clinical Principles. *In*: *Transdermal and Topical Drug Delivery*. London: Pharmaceutical Press, 195–222.

Williams, A.C., 2003e. Chemical modulation of topical and transdermal permeation. *In*: *Transdermal and Topical Drug Delivery*. New York: Pharmaceutical Press, 83–117.

Williams, A.C. and Barry, B.W., 1989. Essential oils as novel human skin penetration enhancers. *International Journal of Pharmaceutics*, 57 (2), R7–R9.

Williams, A.C. and Barry, B.W., 1991. The enhancement index concept applied to terpene penetration enhancers for human skin and model lipophilic (oestradiol) and hydrophilic (5-fluorouracil) drugs. *International Journal of Pharmaceutics*, 74 (2–3), 157–168.

Williams, A.C. and Barry, B.W., 2012. Penetration enhancers. *Advanced Drug Delivery Reviews*, 64, 128–137.

Wilson, D.R. and Maibach, H.I., 1989. Transepidermal water loss: a review. *In*: J-L. Leveque, ed. *Cutaneous Investigation in Health and Disease: Noninvasive Methods and Instrumentation*. New York: Marcel Dekker, 113–133.

Woertz, K. and Surber, C., 2014. The 'Magic' Effects of Dermatologic and Cosmetic Vehicles. *In*: A.O. Barel, M. Paye, and H.I. Maibach, eds. *Handbook of Cosmetic Science and Technology*. New York: CRC Press, 175–188.

Woolfson, A.D. and McCafferty, D.F., 1993. Percutaneous local anaesthesia: drug release characteristics of the amethocaine phase-change system. *International Journal of Pharmaceutics*, 94 (1–3), 75–80.

Wosicka, H. and Cal, K., 2010. Targeting to the hair follicles: Current status and potential. *Journal of Dermatological Science*, 57 (2), 83–89.

Wotton, P.K., Møllgaard, B., Hadgraft, J., and Hoelgaard, A., 1985. Vehicle effect on topical drug delivery. III. Effect of Azone on the cutaneous permeation of metronidazole and propylene glycol. *International Journal of Pharmaceutics*, 24 (1), 19–26.

Wu, X., Griffin, P., Price, G.J., and Guy, R.H., 2009. Preparation and in vitro evaluation of topical formulations based on polystyrene-poly-2-hydroxyl methacrylate nanoparticles. *In*: *Molecular Pharmaceutics*. 1449–1456.

Wypych, G., 2017. Plasticizers in various industrial products. *In*: *Handbook of Plasticizers*. Ontario: ChemTec Publishing, 495–605.

Yan, G., Warner, K.S., Zhang, J., Sharma, S., and Gale, B.K., 2010. Evaluation needle length and density of microneedle arrays in the pretreatment of skin for transdermal drug delivery. *International Journal of Pharmaceutics*, 391 (1–2), 7–12.

Yiyun, C., Na, M., Tongwen, X., Rongqiang, F., Xueyuan, W., Xiaomin, W., and Longping, W., 2007. Transdermal Delivery of Nonsteroidal Anti-Inflammatory Drugs Mediated by Polyamidoamine (PAMAM) Dendrimers. *Journal of Pharmaceutical Sciences*, 96 (3), 595–602.

Yousef, R.T., El-Nakeeb, M.A., and Salama, S., 1973. Effects of some pharmaceutical materials on the bactericidal activities of preservatives. *Canadian Journal of Pharmaceutical Science*, 8, 54–56.

Yu, D., Sanders, L.M., Davidson III, G.W.R., Marvin, M.J., and Ling, T., 1988. Percutaneous Absorption of Nicardipine and Ketorolac in Rhesus Monkeys. *Pharmaceutical Research*, 5 (7), 457–462.

Yung, K.L., Xu, Y., Kang, C., Liu, H., Tam, K.F., Ko, S.M., Kwan, F.Y., and Lee, T.M.H., 2012. Sharp tipped plastic hollow microneedle array by microinjection moulding. *Journal of Micromechanics and Microengineering*, 22 (1), 015016.

Zavalin, A., Yang, J., Hayden, K., Vestal, M., and Caprioli, R.M., 2015. Tissue protein imaging at 1 µm laser spot diameter for high spatial resolution and high imaging speed using transmission geometry MALDI TOF MS. *Analytical and Bioanalytical Chemistry*, 407 (8), 2337–2342.

Zeeuwen, P.L., Boekhorst, J., van den Bogaard, E.H., de Koning, H.D., van de Kerkhof, P.M., Saulnier, D.M., van

Swam, I.I., van Hijum, S.A., Kleerebezem, M., Schalkwijk, J., and Timmerman, H.M., 2012. Microbiome dynamics of human epidermis following skin barrier disruption. *Genome Biology*, 13 (11), R101.

Zhang, L.W. and Monteiro-Riviere, N.A., 2012. Use of confocal microscopy for nanoparticle drug delivery through skin. *Journal of Biomedical Optics*, 18 (6), 06121–4.

Zhang, Q., Murawsky, M., LaCount, T., Kasting, G.B., and Li, S.K., 2018. Transepidermal water loss and skin conductance as barrier integrity tests. *Toxicology in Vitro*, 51, 129–135.

Zhang, Q., Saad, P., Mao, G., Walters, R.M., Mack Correa, M.C., Mendelsohn, R., and Flach, C.R., 2014. Infrared spectroscopic imaging tracks lateral distribution in human stratum corneum. *Pharmaceutical Research*, 31 (10), 2762–2773.

Zhong, H., Guo, Z., Wei, H., Zeng, C., Xiong, H., He, Y., and Liu, S., 2010. In vitro study of ultrasound and different-concentration glycerol–induced changes in human skin optical attenuation assessed with optical coherence tomography. *Journal of Biomedical Optics*, 15 (3), 036012.

Zschocke, I., Mrowietz, U., Lotzin, A., Karakasili, E., and Reich, K., 2014. Assessing adherence factors in patients under topical treatment: development of the Topical Therapy Adherence Questionnaire (TTAQ). *Archives of Dermatological Research*, 306 (3), 287–297.

Zywiel, M.G., Daley, J.A., Delanois, R.E., Naziri, Q., Johnson, A.J., and Mont, M.A., 2011. Advance pre-operative chlorhexidine reduces the incidence of surgical site infections in knee arthroplasty. *International Orthopaedics*, 35 (7), 1001–1006.

Appendix 1 – Cumulative CHG concentration detected from candidate formulations through full thickness porcine skin

Formulation	Mean 24hr Cumulative Concentration (µg/mL)	± Standard Error
0.5% w/v HEC	0.146	0.117
1% w/v HEC	0.000	0.000
2% w/v HEC	0.000	0.000
3% w/v HEC	0.000	0.000
4% w/v HEC	0.023	0.021
1% w/v CHG	0.103	0.102
2% w/v CHG	0.000	0.000
3% w/v CHG	0.000	0.000
4% w/v CHG	0.000	0.000
4% w/v CHG-0.5mM PAMAM	0.010	0.002
4% w/v CHG-1mM PAMAM	0.009	0.001

Table indicates all concentrations of CHG detected through full thickness porcine skin were <LoD (0.362µg/mL), *n=4.*